

# **Functional Molecular Building Blocks**

**M. Elbing**  
Institut für Nanotechnologie

April 2005



Forschungszentrum Karlsruhe

in der Helmholtz-Gemeinschaft

Wissenschaftliche Berichte

FZKA 7102

## **Functional Molecular Building Blocks**

Mark Elbing

Institut für Nanotechnologie

von der Fakultät für Chemie und Biowissenschaften  
der Universität Karlsruhe (TH) genehmigte Dissertation

Forschungszentrum Karlsruhe GmbH, Karlsruhe  
2005

**Impressum der Print-Ausgabe:**

**Als Manuskript gedruckt  
Für diesen Bericht behalten wir uns alle Rechte vor**

**Forschungszentrum Karlsruhe GmbH  
Postfach 3640, 76021 Karlsruhe**

**Mitglied der Hermann von Helmholtz-Gemeinschaft  
Deutscher Forschungszentren (HGF)**

**ISSN 0947-8620**

**urn:nbn:de:0005-071028**

# Functional Molecular Building Blocks

Zur Erlangung des akademischen Grades eines  
**DOKTORS DER NATURWISSENSCHAFTEN**

(Dr. rer. nat.)

von der Fakultät für Chemie und Biowissenschaften der  
Universität Karlsruhe (TH)  
genehmigte

## DISSERTATION

von

Diplom–Chemiker  
Mark Elbing  
aus Hannover

Dekan: Prof. Dr. M. M. Kappes  
Referent: Prof. Dr. M. M. Kappes  
Korreferent: Prof. Dr. S. Bräse  
Tag der mündlichen Prüfung: 15. Dezember 2004

Die vorliegende Arbeit wurde im Zeitraum von Oktober 2001 bis Oktober 2004 am Institut für Nanotechnologie, Forschungszentrum Karlsruhe GmbH unter der Leitung von Herrn Dr. M. Mayor und Herrn Prof. Dr. M. Kappes angefertigt.

Hiermit versichere ich wahrheitsgemäß, die Arbeit selbständig angefertigt, alle benutzten Hilfsmittel vollständig und genau angegeben und alles kenntlich gemacht zu haben, was aus Arbeiten anderer unverändert oder mit Änderungen übernommen wurde.

## Abstract

# Functional Molecular Building Blocks

The concept of “molecular electronics” that envisages the use of single molecules as smallest building blocks might help to further push the limit of miniaturisation of electronic devices and at the same time decrease production costs. However, the use of individual molecules as electronic active components requires the development of correlations between the structure of the molecule and its electronic transport behaviour.

It was the aim of the present work to design, synthesise and study different molecular structures to achieve distinct electronic properties. The target structures have been designed to study current–voltage characteristics of individual molecules using a mechanically controlled break junction (MCB) or of self–assembled monolayers using the mercury drop electrode. A family of oligophenylenes with increasing length has been prepared. Interruption of the  $\pi$ –system has been achieved by rotation of the phenyl–rings out of plane due to steric strain, as confirmed by x–ray analysis and by NMR studies. Besides, the barrier of rotation has been determined using DNMR. UV/Vis spectroscopy suggests that the target compounds consist of (almost) separated  $\pi$ –systems due to the rotation. The MCB measurements revealed that the current level does not depend on the number of interruptions of the  $\pi$ –system. But the onset voltage of electron transport seems to increase with increasing number of phenyl–rings.

Furthermore, two anthracene–based compounds whose molecular structure differs only in the position of the anchor–groups that bind to the gold electrodes have been synthesised. Recorded current–voltage characteristics showed that the structure with the anchor–group in *meta*–position has a resistance which is about two orders of magnitude higher than that of the compound with the anchor–groups in *para*–position.

A molecular structure consisting of two phenyl–ethynyl–phenyl  $\pi$ –systems that are separated electronically by a substituted biphenyl has been designed. As only one of both  $\pi$ –systems is substituted with fluorine, a strong electronic asymmetry is induced. By MCB measurements of this asymmetric molecule it has been shown that rectification can be an inherent function of an individual molecule. Control experiments with corresponding symmetric molecular rods further prove the molecules’ structure as the origin of rectification.

Besides, a photo–switchable azo–compound which is substituted further to allow self–assembly on a gold surface has been synthesised. Switching, that is *E*– to *Z*–isomerisation, of

such a molecular structure induced by light of two different wavelengths has been studied by UV/Vis spectroscopy in solution and on the surface of thin gold films.

# Zusammenfassung

## Funktionale Molekulare Bausteine

Das Konzept der „Molekularen Elektronik“ sieht die Verwendung von Molekülen als kleinste funktionale Bausteine elektronischer Schaltkreise vor. Damit würde die Miniaturisierung elektronischer Schaltungen weiter vorangetrieben und gleichzeitig könnten die Produktionskosten verringert werden. Allerdings setzt eine solche Anwendung ein umfassendes Verständnis der Zusammenhänge zwischen molekularer Struktur und physikalischen Eigenschaften eines Einzelmoleküls voraus.

Ziel dieser Arbeit war der Entwurf, die Synthese und die Untersuchung verschiedener molekularer Strukturen, die unterschiedliche elektronische Eigenschaften besitzen. Die Zielverbindungen wurden entworfen, um entweder Strom–Spannungs–Kennlinien von einzelnen Molekülen unter Verwendung mechanisch kontrollierter Bruchkontakte (MCB) aufzunehmen oder Untersuchungen an selbst–organisierten monomolekularen Schichten unter Verwendung der Quecksilbertropf–Elektrode zu ermöglichen.

Eine Serie von Oligophenylenen wurde synthetisiert, in denen die Anzahl der Phenylringe sukzessive erhöht wurde. Durch Rotation der Phenylringe gegeneinander aufgrund sterischer Hinderung wurde eine Unterbrechung des  $\pi$ –Systems in diesen Verbindungen erreicht, wie durch Kristallstrukturanalyse und durch NMR–Untersuchungen bestätigt werden konnte. Außerdem konnte die Rotationsbarriere in diesen Verbindungen mit Hilfe dynamischer NMR–Messungen bestimmt werden. UV/Vis–spektroskopische Untersuchungen legten nahe, dass die Zielverbindungen aufgrund der Rotation der Phenylringe aus (nahezu) getrennten  $\pi$ –Systemen bestehen. Elektronentransport–Messungen unter Verwendung von MCB zeigten, dass der Strom durch diese Strukturen unabhängig von der Anzahl der Unterbrechungen des  $\pi$ –Systems ist, aber die Spannung, bei der Stromtransport einsetzt, mit der Anzahl der Phenylringe steigt.

Weiterhin wurden zwei auf Anthracen–basierende Verbindungen, deren molekulare Struktur sich nur in der Position der Ankergruppen unterscheidet, die für die Anbindung an die Goldelektroden benutzt werden, synthetisiert. Die Aufnahme von Strom–Spannungs–Kennlinien zeigte, dass die Struktur mit den Ankergruppen in *meta*–Position einen ungefähr um zwei Größenordnungen höheren Widerstand hat als die Struktur mit den Ankergruppen in *para*–Position.

Eine molekulare Struktur bestehend aus zwei elektronisch getrennten Phenyl–ethinyl–phenyl  $\pi$ –Systemen wurde entworfen. Da nur eines der beiden  $\pi$ –Systeme mit Fluor substituiert ist, wird eine starke elektronische Asymmetrie induziert. Untersuchungen an diesem asymmetrischen Molekül unter Verwendung von MCB zeigten, dass Einzelmoleküle als Gleichrichter wirken können. Vergleichsexperimente mit entsprechenden symmetrischen Molekülen bestätigen, dass der Gleichrichtungseffekt durch die molekulare Struktur des asymmetrischen Moleküls hervorgerufen wird.

Zusätzlich wurde eine durch Licht schaltbare Azo–Verbindung dargestellt, die eine Thiol–Funktionalität zur anschließenden Befestigung auf einer Goldoberfläche aufweist. Der Schaltvorgang einer solchen molekularen Struktur, d.h. *E*–*Z*–Isomerisierung, durch Einstrahlen von Licht zwei verschiedener Wellenlängen wurde UV/Vis–spektroskopisch in Lösung und auf der Oberfläche dünner Goldfilme untersucht.

# Table of Contents

1. Aims and Objectives .....	1
2. Molecular (Scale) Electronics.....	3
2.1 Introduction.....	3
2.2 Contacting and Manipulating Molecules .....	6
2.2.1 Monomolecular Film Devices .....	7
2.2.1.1 Nanopores .....	8
2.2.1.2 Mercury Drop Electrodes.....	9
2.2.2 Single Molecule Devices.....	12
2.2.2.1 Excursus: Scanning Probe Microscopy.....	12
2.2.2.2 Molecular Junctions Using STM and AFM .....	15
2.2.2.3 Mechanically Controlled Break Junction Technique.....	17
2.2.3 Other Methods .....	22
2.3 Molecular Electronic Devices.....	24
2.3.1 Molecular Wires and Insulators.....	24
2.3.2 Molecular Rectifiers .....	28
2.3.3 Molecular Switches and Storage Elements .....	32
2.3.4 Others.....	38
2.4 Summary of Molecular (Scale) Electronics .....	38
3. Chemical and Physicochemical Methods .....	41
3.1 Metal–Catalysed Cross–Coupling Reactions.....	41
3.1.1 General Remarks .....	42
3.1.2 Kumada–Tamao–Corriu (KTC) Coupling.....	44
3.1.3 Negishi Coupling .....	46
3.1.4 Stille Coupling .....	48
3.1.5 Sonogashira Coupling .....	49
3.1.6 Suzuki–Miyaura (SM) Coupling .....	52
3.1.6.1 Preparation of Organoboron Compounds .....	52
3.1.6.2 Mechanistic Considerations and Scope of the Reaction .....	54
3.1.7 Hartwig–Buchwald (HB) Coupling .....	55
3.1.8 Summary of Metal–Catalysed Cross–Coupling Reactions .....	57
3.2 Some Aspects of Organosulphur Chemistry .....	58

3.2.1 General Remarks.....	58
3.2.2 Synthesis of Thiols, Disulphides and Acetyl-protected Thiols .....	59
3.2.3 Synthesis of Thioethers .....	61
3.2.4 Synthesis of Sulphoxides, Sulphones and Sulphonic Acids .....	63
3.2.5 Others .....	65
3.2.6 Summary of Organosulphur Chemistry .....	65
3.3 Chemistry and Physical Properties of Azo-Compounds.....	65
3.3.1 Overview of Synthetic Procedures.....	66
3.3.2 Photophysical Properties.....	68
3.3.3 Summary of Chemistry and Physical Properties of Azo-Compounds .....	71
3.4 Dynamic NMR (DNMR) Spectroscopy .....	71
3.4.1 Theoretical Background.....	73
3.4.2 Experimental Technique .....	74
3.4.3 Evaluation of Rate Constants .....	76
3.4.4 Evaluation of Activation Parameters .....	77
3.4.5 Selected Applications of DNMR .....	77
3.4.5.1 Rotation About C-C Single Bonds.....	78
3.4.5.2 Others.....	80
3.4.6 Summary of Dynamic NMR Spectroscopy.....	80
<b>4. Results and Discussion.....</b>	<b>81</b>
4.1 Molecular Wires and Insulators.....	81
4.1.1 Oligophenylenes.....	81
4.1.1.1 Synthetic Strategy.....	83
4.1.1.2 Synthesis .....	89
4.1.1.3 Characterisation and Structural Analysis .....	96
4.1.1.4 Electron Transport Measurements.....	111
4.1.2 Phenyl-ethynyl-anthracene .....	123
4.1.2.1 Synthetic Strategy .....	125
4.1.2.2 Synthesis .....	129
4.1.2.3 Characterisation and Structural Analysis .....	134
4.1.2.4 Electron Transport Measurements.....	140
4.2. Molecular Rectifiers .....	144
4.2.1 Synthetic Strategy .....	146
4.2.2 Synthesis .....	149

4.2.3 Characterisation and Structural Analysis .....	153
4.2.4 Electron Transport Measurements.....	162
4.3 Molecular Switches.....	167
4.3.1 Synthetic Strategy.....	171
4.3.2 Synthesis.....	176
4.3.3 Characterisation and Structural Analysis .....	182
5. Concluding Remarks .....	191
6. Experimental Part.....	193
6.1 General Remarks.....	193
6.2 Analytics .....	193
6.3 Synthetic Procedures.....	195
6.3.1 Oligophenylenes .....	195
6.3.2 Phenyl–ethynyl–anthracene .....	217
6.3.3 Molecular Rectifiers .....	230
5.3.4 Molecular Switches .....	238
7. Bibliography .....	251
8. Acknowledgement .....	263
9. Appendix .....	265



# 1 Aims and Objectives

The on-going miniaturisation of the silicon electronic technology will reach its physical limit in the foreseeable future<sup>[1]</sup> and hence, alternative concepts that allow to further reduce the size of electronic active components become very attractive. Especially, the visionary idea to profit from molecular structures to design electronic functions, already described in the early seventies by *Kuhn* as “molecular engineering”<sup>[2]</sup> and today known as “molecular electronics”,<sup>[3],[4]</sup> moved into the focus of interest.

Obviously for the successful development of molecular electronics a few prerequisites have to be fulfilled. The great progress in manipulating on the nanoscale, driven by the invention of scanning probe techniques,<sup>[5]</sup> allowed for the invention of several different techniques to contact and manipulate small assemblies or even single molecules. Tunnel currents through molecular films have been studied on surfaces with the STM<sup>[6]</sup> or with electrode pairs provided by crossed-wire junctions<sup>[7],[8]</sup> and mercury droplets against metallic surfaces.<sup>[9]</sup> Single molecules were addressed by STM techniques on diluted molecular films<sup>[10]</sup> and by the mechanically controlled break junction (MCB) technique.<sup>[11],[12],[13]</sup> The latter has turned out to be particularly powerful to contact single molecules, which are covalently linked to both electrodes, as has been demonstrated by the comparison of the electronic characteristics of molecules differing in spatial symmetry.<sup>[13]</sup>

Over the last years it has been reported that different organic molecules can exhibit different electronic functions when measured between two electrodes using techniques mentioned above. Compounds consisting of long delocalised  $\pi$ -systems such as oligophenylenes, oligophenylenevinylenes or oligophenylenethynylénes have been reported to act as molecular wires,<sup>[14]</sup> the conceptually simplest component of electronic circuits. A compound showing conductivity, which is three orders of magnitude lower than that of conjugated molecules, has been proposed as a single-molecule insulator.<sup>[15]</sup> Molecular counterparts of the well-known p-n junction diodes of current semiconductor devices have been published as well.<sup>[16],[17],[18]</sup> However, most of these investigations were done with monomolecular films or small packets of molecules. Only very recently, electrical rectification of a single molecule has been shown.<sup>[19]</sup> Several other studies dealing with switching and storage using molecular electronic devices have been published using both monomolecular film devices<sup>[20],[21],[22]</sup> and single molecule measurements.<sup>[23]</sup> However, in the single molecule studies, where switching was triggered by light, no reversible switching could be achieved. In studies using electrical

energy for switching the mechanism for switching is still under discussion.<sup>[24]</sup> In summary, all published data clearly show that tailor-made organic synthesis is mandatory for the development of molecular electronics and can give rise to different electronic functions.

The present work aimed to design, synthesise and study different functional organic building blocks that can fulfil different functions in molecular electronic devices. Target structures have been designed for particular experimental conditions in different physical set-ups that allow to study electron transport behaviour. These physical investigations will be done either in the group of *H. Weber* at the Institut für Nanotechnologie at the Forschungszentrum Karlsruhe GmbH or in the group of *M. Rampi* at the Università di Ferrara.

In particular, the following investigations were planned.

- The influence of the degree of  $\pi$ -conjugation on the conductance properties of the molecule was studied. For this purpose a family of oligophenylenes with a defined increase in length was designed. Thereby,  $\pi$ -conjugation was broken due to rotation of the phenyl-rings out of plane induced by steric strain.
- In another approach, bridged biphenyl compounds were used to fix the angle of rotation between the two phenyl-rings to obtain different degrees of  $\pi$ -conjugation.
- The importance of the position of the anchor-group and, thereby the influence of the coupling of the molecule to the electrodes was studied. For this purpose, two molecular rods were designed, which have the same molecular structure, but differ in the position of the anchor-group used for immobilisation of the molecule on the electrodes.
- A single molecule rectifier was designed based on the proposal by *Aviram* and *Ratner*, that is a donor- $\sigma$ -spacer-acceptor structure. This approach was used to evaluate whether rectification can be an inherent function of a single molecule.
- A compound bearing a photo-switchable subunit was designed for the study of current-voltage characteristics and light-induced switching in a device based on a self-assembled monolayer.

## 2 Molecular (Scale) Electronics

“Molecular Electronics” or “Molecular Scale Electronics” will briefly be introduced in this chapter. The main ideas and concepts of this emerging area of research will be presented from a chemist’s point of view and some key results and developments of recent years will be discussed.

### 2.1 Introduction

In 1968 *G. Moore*, one of the co-founders of *Intel Corp.*, predicted that the number of transistors per  $\text{cm}^2$  silicon would grow exponentially.<sup>[25],[26]</sup> Indeed, this guess, which became known as “*Moore’s Law*”, proved to be true over the last 35 years (Figure 2–1) mainly due to the improvement of lithographic techniques that allowed to fabricate increasingly smaller components. Nowadays, engineers in the field of information technology agree that the computational power (determined by taking into account the number of transistors, clock speed, pitch size and other factors) doubles every 18 month.<sup>[1]</sup> If this development is to be continued the current silicon-based technology would reach the molecular scale in the next 10 – 15 years facing serious technical problems and physical limitations. For example, the oxide layers used in silicon chips become poorly insulating when getting to a thickness of three atoms.<sup>[27]</sup> Furthermore, the costs of production of this top-down approach using state-of-the-

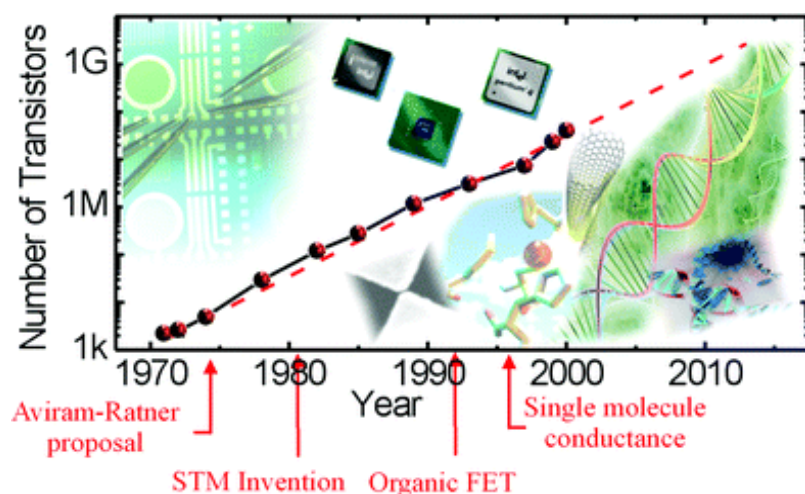


**Figure 2–1:** *Moore’s law*, number of transistors as a function of time, points refer to the various processors introduced by *Intel Corp.* Taken from ref. [26].

art lithography techniques and increasingly complex production lines will explode hindering the fabrication of ever faster and cheaper computers.<sup>[1]</sup> Hence, alternative concepts that allow to further reduce the size of electronic active components become very attractive. In particular, the visionary idea to profit from molecular structures to design electronic functions, already described in the early seventies by *Kuhn* as “molecular engineering”<sup>[2]</sup> and today known as “molecular electronics”,<sup>[28],[29],[30]</sup> moved into the focus of interest.

At present, the term molecular electronics (ME) is commonly used for two distinct branches of research (Figure 2–2).<sup>[4]</sup> The first area (2–2a) deals with bulk molecular systems. As these systems are easier to handle and process on the industrial scale, some applications have

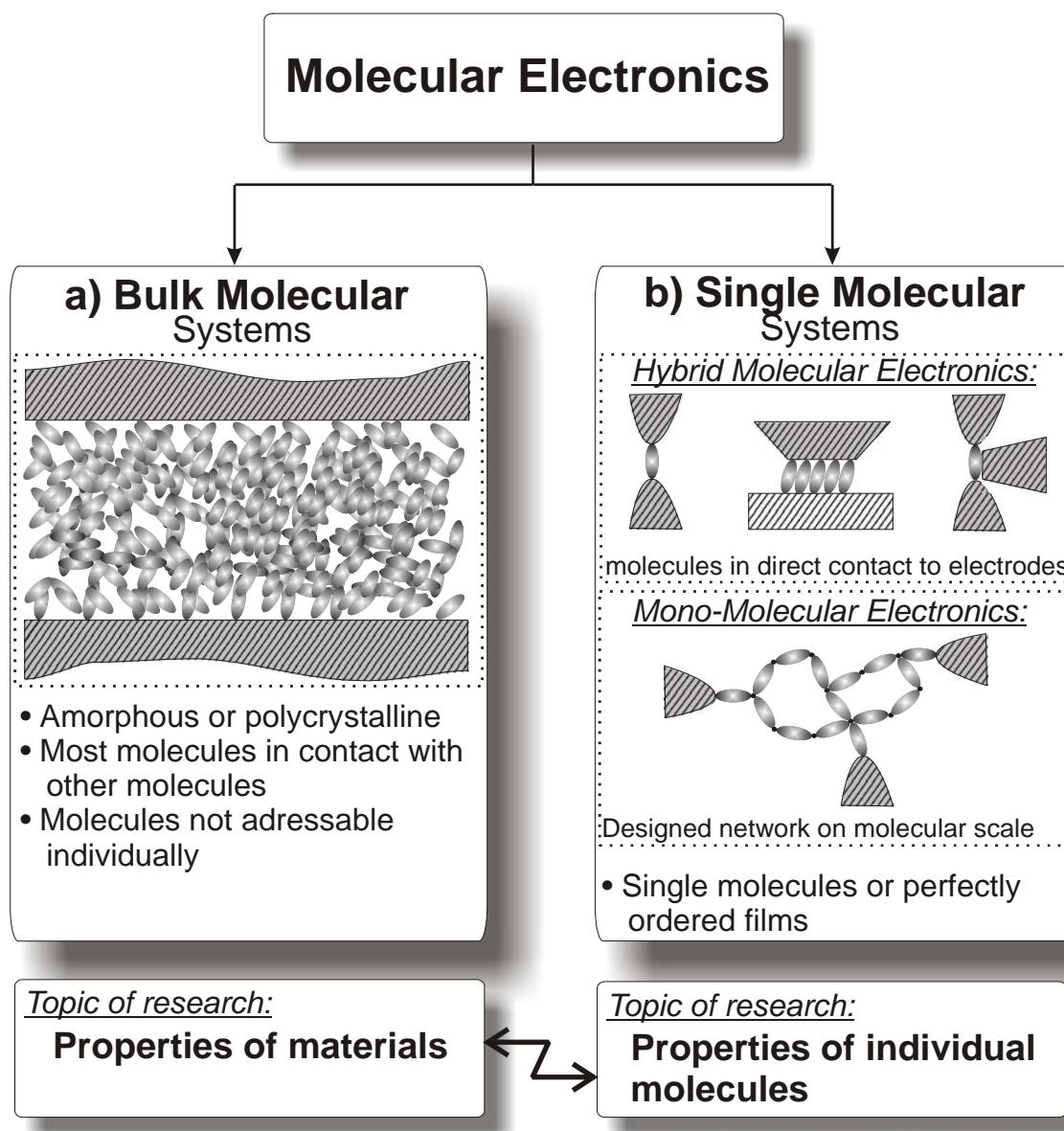


**Figure 2–2:** Currently the term of molecular electronics (ME) is used for two different areas of research, namely a) Bulk Molecular Systems and b) Single Molecular Systems. Taken and modified from ref. [4].

already been realised, for instance liquid crystal displays<sup>[31]</sup> or organic light-emitting diodes.<sup>[32]</sup> In such products mainly organic compounds, i.e. small molecules, oligomers or even polymers, are used because of their electronic properties. The characteristic dimensions in these devices are much larger than the size of individual molecules and most molecules are not directly contacted by external electrodes. The *bulk properties of materials* are the topic of research in this area. Hence, it has been suggested to rather call this branch “molecular materials for electronics”, though the definition remains problematically ambiguous.<sup>[33]</sup> Bulk properties of organic compounds are not the topic of this work, thus they will not be discussed more comprehensively.

In the context of this work, ME will be understood as the area dealing with small assemblies of molecules or even single molecular systems (Figure 2–2). In this approach the single molecule becomes the electronic component due to its intrinsic electronic properties given by the electron distribution in its structure. To contact single molecules or small packets of ordered molecules and to build nanosized electronic devices making use of the physical properties of individual molecules is the aim of this approach. Two different strategies are pursued, hybrid molecular electronics (HME) and mono–molecular electronics (MME). HME devices consist of “molecules embedded between several electrodes”<sup>[28]</sup> and are used as first test devices to exploit the potential of individual molecules as electronic devices. In MME systems, several basic electronic functions are merged in a larger molecular system consisting of numerous precisely assembled subunits for the particular electronic task resembling the modular combination of functions known from biooligomers. Though, at the moment this remains a scientific challenge. In both cases, the comprehension of *electric current through single molecules* is a crucial requirement.<sup>[4]</sup>

Obviously for such a molecular electronic to work a few prerequisites have to be fulfilled. First, it must be possible to contact and manipulate single molecules. Although the early days of this idea can be traced back to the late 1960s when *Kuhn* and *Möbius* investigated electronic properties of large numbers of organic molecules in *Langmuir–Blodgett* films absorbed on aluminium using different top electrodes, not much research was done in this field at that time.<sup>[2], [34]</sup> A little later, the seminal theoretical paper by *Aviram* and *Ratner* describing a rectifier based on an organic molecule was published.<sup>[3]</sup> But it was only in recent years that the enormous improvement in manipulation on the nanoscale mainly driven by the invention of the scanning tunnelling microscope (STM) moved this area of research in the focus of interest again. Since then, a few experiments that made it possible to actually contact and manipulate individual molecules have been described. Some of these techniques, which

are relevant for this work, will shortly be discussed. Besides, it is essential to know what kind of molecules can be employed in the production of future electronic devices, that is correlations between the structure of the molecule and its electronic transport behaviour have to be established.<sup>[35]</sup> In this regard, organic molecules have one crucial advantage compared to inorganic clusters, since organic molecules of a specific compound are absolutely identical and, therefore have identical quantum energy levels. Inorganic clusters, made for example by self-assembly, will differ slightly in the number of atoms and, consequently vary somewhat in the distribution of their energy levels. Furthermore, molecules are regarded as the smallest possible unit that can still have an inherent function. Hence, the vast knowledge of organic chemistry about the influence of different functional groups on the electronic structure of compounds, for instance the possibility to produce electron-rich and electron-poor aromatic systems by only altering the substituents, provides a quasi-unlimited toolbox to fabricate a variety of electronic materials. Experience of organic chemists to link different molecular building blocks gained by research in diverse areas such as natural product synthesis, supramolecular chemistry and materials chemistry opens up almost infinite possibilities to design and synthesise miscellaneous molecular structures. Carefully planned and performed tailor-made organic synthesis can, therefore provide a plethora of different compounds fulfilling basic functions of computing like wiring, rectification, switching or storage.<sup>[30]</sup> Some successful attempts and promising examples of ME devices will be presented below. Despite its great potential ME is unlikely to play a role in the production of electronic devices in the near future. However, the integration of devices based on molecular films on silicon might form a bridge between the fields of microelectronics on the one side and molecular electronics on the other side in the foreseeable future.

## **2.2 Contacting and Manipulating Molecules**

The small size of devices based on organic molecules is regarded as one of the advantages that ME offers compared to the current silicon-based technology. But contacting and manipulating nanometre-sized objects in a reliable and reproducible fashion is still a major scientific challenge. Consequently, all of the methods mentioned herein to contact small molecules are rather test devices for ME and not intended to be future electronic devices. That is to say, the practicability of these systems in “real-world” computing remains in dispute. However, all techniques help to gain new knowledge about electron transfer in organic

structures and, thereby to establish structure–property relationships, which are the required basis for the development of future ME devices.

## 2.2.1 Monomolecular Film Devices

Devices based on monomolecular films can be realised more easily than single-molecule devices and, hence are promising candidates for first real-life applications of ME in the near future. Such films can be prepared by a variety of methods like *Langmuir–Blodgett (LB)* films, self-assembly processes or vapour deposition techniques.<sup>[4]</sup> The latter are typically subdivided into physical vapour deposition techniques, for instance molecular beam epitaxy, pulsed laser deposition or sputter deposition, and chemical vapour deposition techniques.<sup>[36]</sup> Besides, methods for chemical solution deposition such as spin or dip coating exist. *LB* films and self-assembly processes are most widely used for the preparation of monomolecular film devices consisting of organic molecules. These will be described briefly.

Using the *LB* method mono- and multilayers of organic compounds can be deposited on hydrophilic substrates like glass, quartz or metals such as Al or Cr.<sup>[37]</sup> The organic molecules have to contain a hydrophilic group, e.g. acid or alcohol group, and a hydrophobic group, usually an aliphatic chain, to allow film formation on the surface of water (*Langmuir* film). All molecules will align in the same direction with the hydrophilic end at the water side. A continuous monolayer, which can later be transferred onto a solid substrate passing through the air–water interface, is formed by compression of the film using a movable barrier (Figure

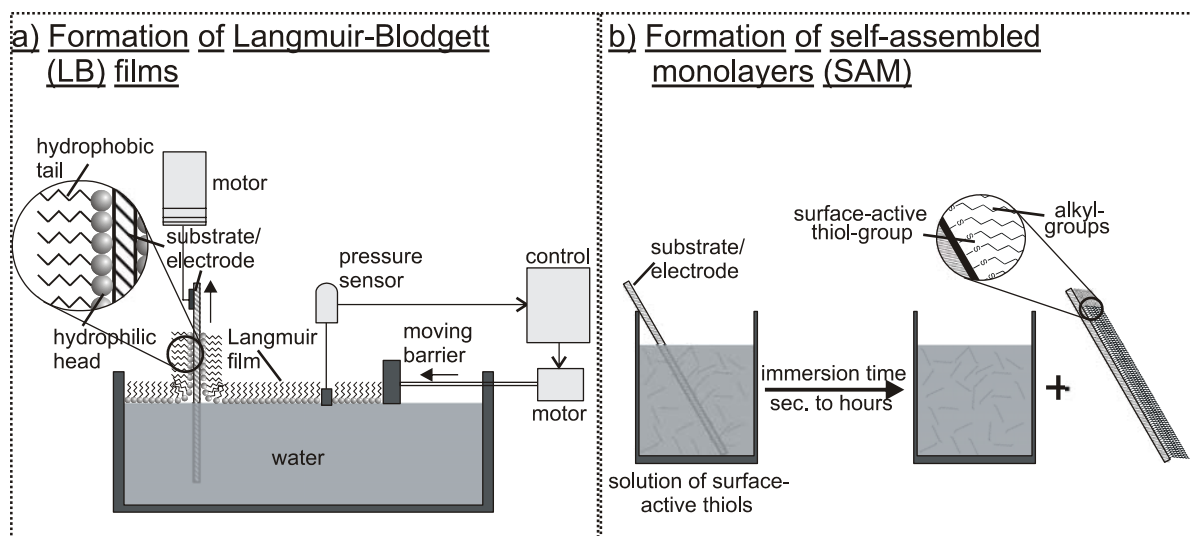


**Figure 2-3:** a) Schematic drawing of a Langmuir trough for controlled deposition of LB films; b) Schematic procedure for the self-assembly of thiol-terminated molecules on a gold substrate.<sup>[37]</sup>

2–3a). In a *Langmuir* trough the film is kept under a constant pressure using a control unit while the substrate, that is one electrode of the future monomolecular film device, is slowly removed from the bath. In this way a well-ordered monolayer of the organic molecule is formed on the surface of the substrate.

The spontaneous arrangement of (organic) molecules on a surface to almost defect-free structures is called self-assembly.<sup>[38]</sup> Formation of self-assembled monolayers (SAM) is driven by interplay of thermodynamics and kinetics. Usually SAMs are obtained by dipping the substrate, that is one electrode of the future monomolecular film device, into a diluted solution of the desired molecule (Figure 2–3b). In general, these molecules have a head-group that binds to the surface, an aliphatic or aromatic chain and a terminal end-group. Together with the properties of the surface these structural elements determine the structure of the SAM. Compared to *Langmuir–Blodgett* films SAMs have a higher chemical and mechanical stability, because they are chemisorbed on the substrate. The self-assembly of alkanethiols on a gold surface is one of the best studied and best working systems.

Both approaches require a second electrode on top of the monomolecular film to fabricate working devices. Unfortunately, evaporation of the second electrode as well as diffusion processes during usage of the device can cause defects in the structure of the film due to metal atoms penetrating the film and short-circuiting the device.<sup>[39]</sup> Nevertheless, a few functioning devices based on sandwiching molecular films between two electrodes have been demonstrated. Some of these will be discussed in the section about molecular electronic devices (chapter 2.3).

### **2.2.1.1 Nanopores**

In 1997 Zhou and Reed published an interesting method based on self-assembled monolayers that allows to limit the number of contacted organic molecules utilising tiny holes in a silicon nitride membrane (Figure 2–4).<sup>[40]</sup>

In the first step, a 50 nm thick layer of low-stress Si<sub>3</sub>N<sub>4</sub> was deposited on both sides of a polished silicon (100) wafer using standard chemical vapour deposition. After silicon had been exposed by removing the nitride in a square 400 µm by 400 µm on one side of the wafer by optical lithography and reactive ion etching (RIE), it was etched anisotropically through to the top surface to give a suspended silicon nitride membrane (about 40 µm to 40 µm). For insulation purposes 100 nm of SiO<sub>2</sub> was grown thermally on the sidewalls. Now e-beam

lithography and RIE was used to structure a single hole of about 30 to 50 nm in diameter through the membrane. The diameter of the pore at the bottom of the membrane was much smaller than the actual pattern, since the constrained geometry caused a significant reduction of the RIE rates.<sup>[41]</sup> By evaporation the bowl-shaped hole was filled with a Au contact of 200 nm thickness. Then the desired thiol-terminated organic molecule was self-assembled from solution on the gold surface inside the pore. The sample was rinsed and placed in a vacuum chamber, in which the bottom Au electrode with a thickness of 200 nm was carefully evaporated at low temperature with a rate of less than 1 Å/s. The specimen containing a small number of organic molecules (about 1000) laterally limited by the Si<sub>3</sub>N<sub>4</sub> pore between two gold electrodes was then electrically characterised. Some results of such measurements are described below.

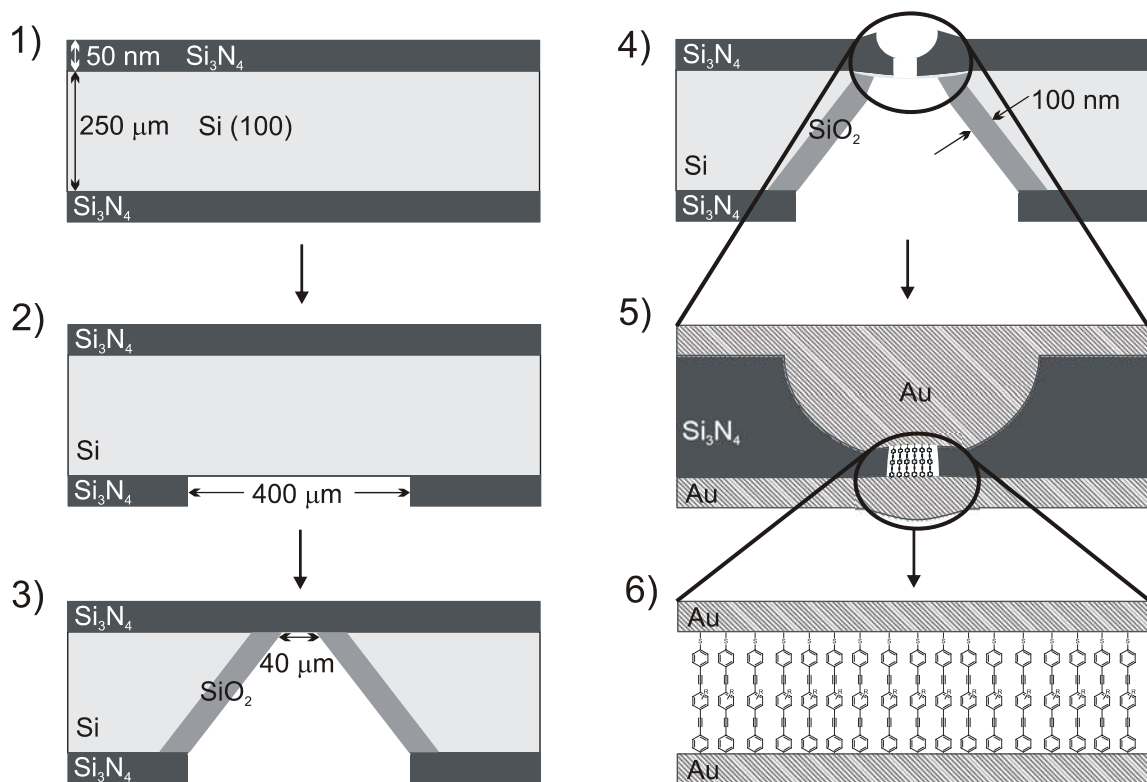


**Figure 2-4:** Schematic drawing of the nanopore fabrication process.<sup>[41]</sup>

### 2.2.1.2 Mercury Drop Electrodes

The use of mercury drop electrodes that has been presented by *Rampi* and *Whitesides* is a particularly simple method to prepare a metal-molecule-metal junction based on

monomolecular films (Figure 2–5).<sup>[42]</sup> No evaporation of the second electrode on top of the film is required.

A small mercury-drop with a diameter of ~1 mm (about 5 µl) was expressed into a 1 mM solution of hexadecanethiol (HDT) in hexadecane from a microsyringe connected to a reservoir of mercury. The SAM was allowed to form on the surface of the Hg-drop for about 10 min. The nature of the second electrode can be changed from liquid mercury<sup>[43]</sup> to freshly evaporated metal surfaces (Au, Ag, Cu), but with the latter the junction is more easy to assemble and results in fewer failures due to electrical or mechanical breakdown.<sup>[44]</sup> The molecule whose IV characteristics are to be studied has to bear a thiol anchor-group on one end to allow SAM formation on the metal surface. The SAM was formed by exposing the metal to a solution of the respective molecule in ethanol or THF (2 mM) over 24 – 48 h following standard procedures. This electrode was then placed in a beaker and covered with a solution of hexadecane containing 1 mM HDT. This ensures a higher stability of the junction probably due to healing of defects caused by the motion of the liquid surface and stabilisation of the drop against vibration. A micromanipulator was used to make contact between the SAM covered mercury drop and the solid electrode. The liquid Hg surface covered with the SAM is compliant and can, thereby adjust to the topography of the metal surface minimising the effects of irregularities of the surface on the structure. Besides, the potential for shorting is lowered. When a mercury drop that was not covered with a SAM of alkanethiol was used the metal surface was amalgamated. The area of contact was estimated to be between  $1.5 \times 10^{-3}$  and  $3 \times 10^{-3}$  cm<sup>2</sup> by means of a microscope. Then IV curves were recorded by applying a potential across the junction.

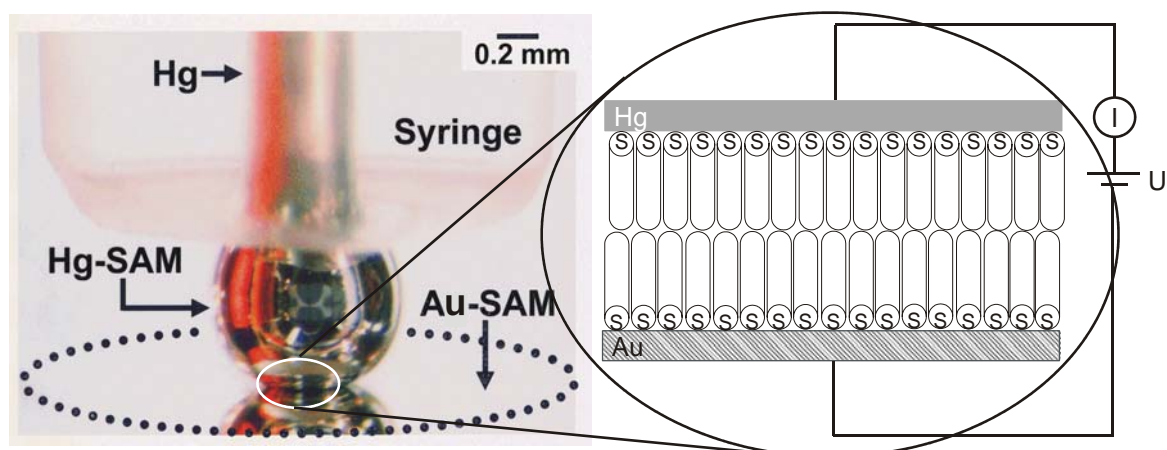
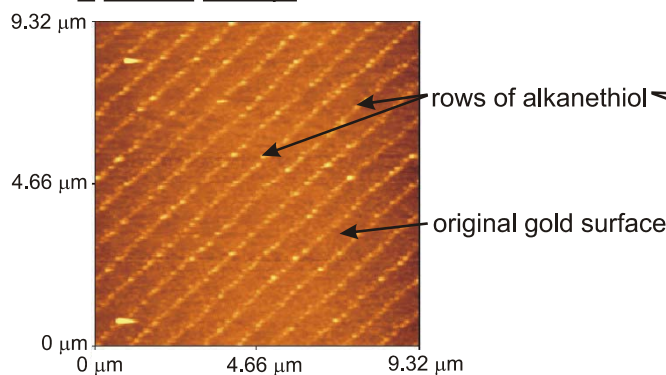


**Figure 2–5:** Photographic image of the Hg–junction with the drop of Hg on top and the counter electrode on the bottom; the schematic drawing shows the assumed molecular arrangement between the two electrodes.<sup>[44]</sup>

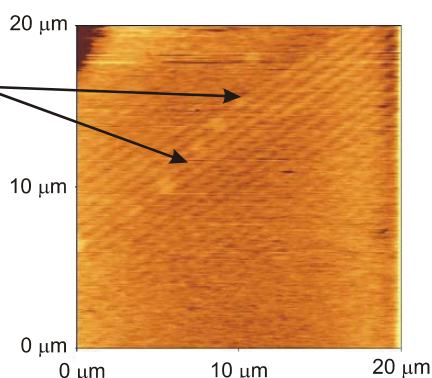
By studying a range of aliphatic and aromatic thiols, it was deduced that the magnitude of the current density decreases in the order  $\text{HS}(\text{Ph})_k\text{H} > \text{HSCH}_2(\text{Ph})_m\text{H} > \text{HS}(\text{CH}_2)_n\text{CH}_3$  for films of the same thickness. Comparison of the experimental data with a theoretical model, which assumes a) that the molecules in the monolayer act independently and b) that the electrostatic potential is determined through the combined solution of *Schrödinger* and *Poisson* equation, leads to the conclusion that electron transport occurs due to superexchange tunnelling through the molecular bridge.<sup>[9]</sup>

Recently, this approach has been developed further to enable the study of smaller numbers of molecules utilising mixed SAMs. Surface patterning on the metal surface using an elastomeric stamp of polydimethyl siloxane (PDMS) provided a SAM of alkanethiols that had a defined structure due to the shape of the stamp's protrusions (Figure 2–6).<sup>[45]</sup> In the confined space delimited by the features of the stamp a mixture of the studied molecule and biphenyl-4-thiol was self-assembled. Apart from pre-structuring the surface the SAM consisting of alkanethiol served to support the mercury drop when it was approached to the metal surface to form the junction. Because of a very thin, translucent gold surface this set-up can be used to study light-induced molecular movements (LIMM) of adequate organic molecules, for

a) Pre-structuring of gold-surface using a PDMS stamp:



b) Self-Assembly of a second SAM in the confined space



Corresponding Hg-junction set-up:

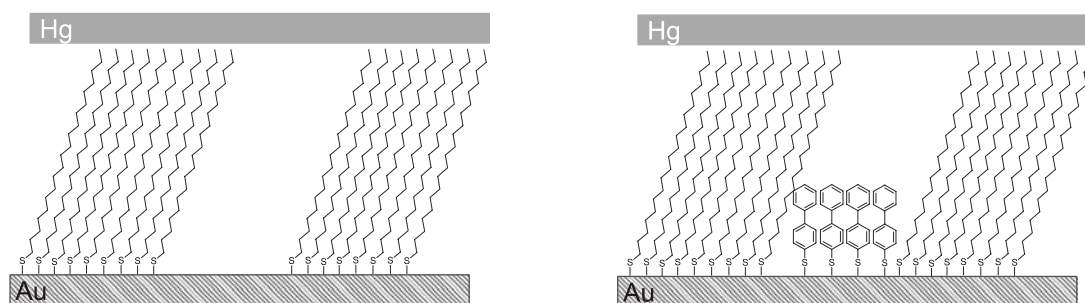


**Figure 2–6:** Modified set-up for measurement with the Hg-junction. The surface of the gold electrode was pre-structured using a PDMS stamp immersed in a solution of alkanethiol. A second SAM was deposited into the confined space delimited by the features of the stamp.<sup>[45]</sup>

example azo-compounds. For the European LIMM project a compound comprising an azo functionality substituted by a biphenyl on both sides has been synthesised during this work. To allow self-assembly on the translucent gold surface one biphenyl moiety was functionalised further with a thiol anchor-group. The synthesis of this target structure and the investigation of physical properties will be described in chapter 4.

The mercury drop electrode offers a few advantages over other methods: 1) it is very easy to assemble, and hence can be used as a quick test tool for organic compounds; 2) it is mechanically stable; 3) a range of organic structures can be studied; 4) together with the developed theory it allows to establish direct correlations between electron transport and molecular structure. The disadvantages are 1) that single molecules can not be investigated; 2) that change of the temperature is not possible; 3) that the set-up will probably not be useful to practically use microelectronic devices.<sup>[9]</sup>

## **2.2.2 Single Molecule Devices**

All methods for building ME devices that have been described so far in this chapter have certain disadvantages. Devices utilising *Langmuir–Blodgett* (LB) films lack sufficient mechanical stability.<sup>[46]</sup> Self-assembly of thiol-terminated organic molecules on a gold surface leads to higher stability, but neither the nanopore approach nor the mercury drop electrode provides the opportunity to contact a single molecule. To design future single-molecule devices it is essential, however, to get a thorough understanding of transport through individual molecules. Hence, other methods are needed that provide a (symmetric) stable test electrode pair that can be adjusted to the length of the molecule.

### **2.2.2.1 Excursus: Scanning Probe Microscopy**

Scanning probe microscopies (SPM) had a big impact on the development of nanoscience, because SPM enabled researchers to measure properties like shape, size or conductivity of individual molecules on surfaces for the first time.<sup>[4]</sup> Besides, it was now possible to manipulate single atoms or molecules and, thereby to form new artificial structures on the atomic scale.<sup>[47]</sup> In the context of the present work methods to contact single molecules using scanning tunnelling microscopy (STM) were of particular interest. Therefore, this technique

will shortly be introduced in this section followed by the description of different methods that allow to measure current–voltage characteristics of individual molecules.

In 1982 *Binning* and *Rohrer* published their first report about a new technique called scanning tunnelling microscopy (STM).<sup>[5]</sup> Since then, several methods of SPM have been developed, of which scanning tunnelling microscopy (STM) and scanning force microscopy or atomic force microscopy (AFM) are the most widely used ones. The basic principles of these techniques are very similar and will be explained by the description of STM.<sup>[48],[49]</sup>

In a standard experiment (Figure 2–7a), a voltage is applied between a fine metallic needle and the sample surface. Then the tip is moved towards the surface until the so-called tunnel current which arises from the quantum–mechanical tunnel effect, can be measured. Normally this occurs at distances of about 1 nm. While the tip is scanned over the surface in three dimensions using piezoelectric actuators, an electronic controller (a feedback loop) keeps the tunnelling current constant, but changes the distance between the tip and the sample by altering the voltage applied at the piezoelectric crystal. The variation of the applied voltage is recorded and displayed as a function of the lateral position resulting in a microscope image of the surface (a constant-current STM image). The reverse process, that is maintaining a constant distance, is also possible. In this case, a so-called current image is obtained. Either way, areas between a few nm to several  $\mu\text{m}$  can be investigated.<sup>[50]</sup>

Due to the measuring principle STM does not show the atoms directly, but rather the local

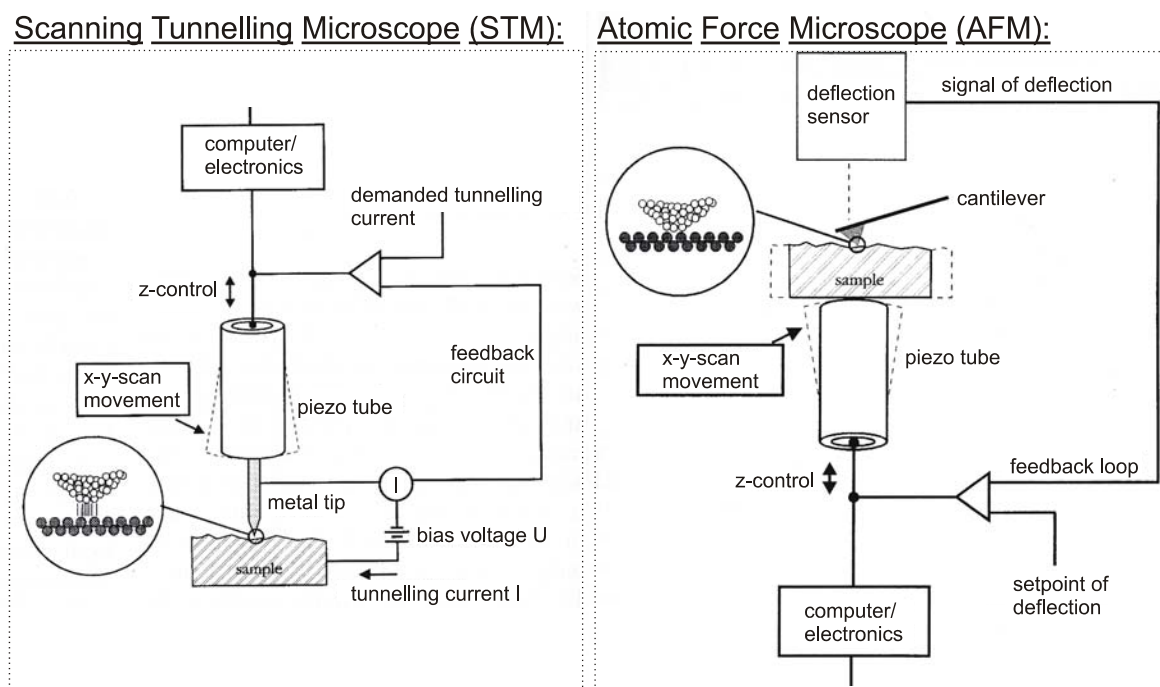


**Figure 2–7:** Schematic set-up for a) Scanning Tunnelling Microscope (STM) and b) Atomic Force Microscope (AFM) operating in the constant force imaging mode.<sup>[49]</sup>

density of states of the sample near the *Fermi* energy, as shown by a theory developed by *Tersoff* and *Hamman*.<sup>[51]</sup> According to this theory the tunnel current decreases exponentially with the tip–sample distance. Actually, as a result of this exponential dependence the STM has such a good resolution, because small changes in distance can bring about a large change in tunnel current. So if the tip has a microtip that is only 0.1 nm closer to the sample than the rest of the tip, all current will flow over this closest microtip. As a consequence, even relatively wide tips can afford atomic resolution. The main application of STM is imaging of surfaces with atomic resolution, revealing the structure of perfect crystalline surfaces as well as point defects, adsorbates and structural defects. STM is used in research areas ranging from biology to crystallography, but is only applicable to *conducting* surfaces.<sup>[48]</sup>

The design of an AFM is very similar. In this case the tip is mounted on the end of a cantilever that acts as a force sensor. Instead of the tunnelling current the deflection of the cantilever as a function of lateral position is measured using in most cases optical methods (Figure 2–7b). When the AFM is used in non–contact mode (also tapping mode), that is the distance between the tip and the sample surface is bigger than 1 nm, *van der Waals*, electrostatic, magnetic or capillary forces produce the image. In contrast, in contact mode ionic repulsion forces are more important. Assuming *Lifshits* theory the *van der Waals* forces between macroscopic bodies can be calculated and an equation describing the geometry in an AFM can be obtained. According to this equation the distance dependence in an AFM is weaker than in a STM resulting in a lower sensitivity. Nevertheless, the AFM is used more often, because on the one hand non–conducting surfaces can be used as well, and on the other hand the interacting force that is probed can be changed, for example to magnetic interaction. Apart from the ability to show individual atoms, it is possible to manipulate single atoms or molecules on a surface using SPM techniques. For instance, carbon nanotubes have been cut using an AFM<sup>[52]</sup> or even chemical reactions have been performed employing the STM, namely the *Ullmann* coupling of iodobenzene to biphenyl on a copper surface step by step.<sup>[53]</sup>

### 2.2.2.2 Molecular Junctions Using STM and AFM

The first demonstration of a single molecular wire in the solid state was done by *Bumm* and *Tour* using STM.<sup>[10]</sup> Here, the oligo(phenylene ethynylene) **1** having a thiol anchor group on one end was inserted into an insulating layer of dodecanethiol molecules attached to a gold electrode. This technique permitted to individually address and image the molecular wire (Figure 2–8). By moving the tip of the STM over the surface it was found that the conjugated molecule, although topographically higher above the surface, was more highly conducting than the alkyl chains. While this result is not surprising, it had never been demonstrated on the molecular scale before. However, tip and surface differ in shape and material. Therefore, it is not possible to establish symmetric contacts to the molecule and tunnelling, non–bonded contacts are present.

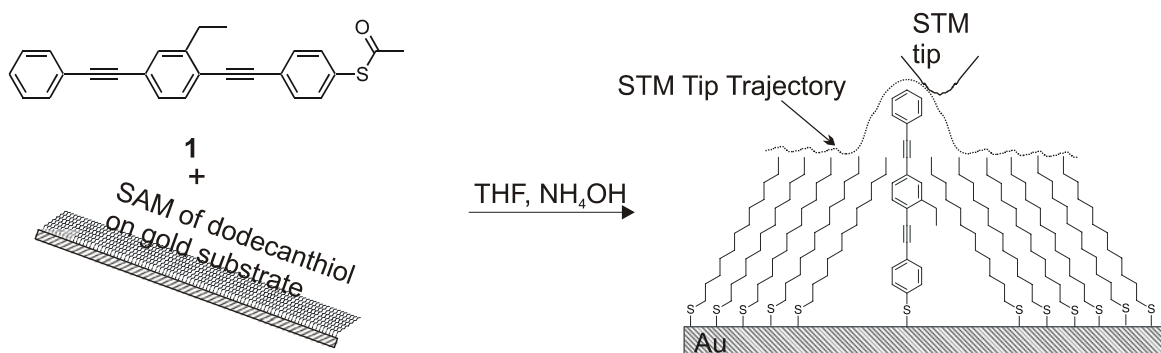


**Figure 2–8:** Formation and schematic representation of a mixed SAM of dodecanethiol and **1** on a gold surface. The trajectory of the STM tip traces out a surface of constant current allowing the measurement of single molecules.<sup>[10]</sup>

In a variation of this method the resistance of 1,8-octanedithiol has been measured repeatedly where one end is bond to a Au(111) surface via sulphur anchor-groups and the other end anchored to a gold nanoparticle.<sup>[54],[55]</sup> Since the dithiol molecules are laterally separated by a insulating monolayer of octanethiol, the investigation of individual molecules should become possible. A gold-coated AFM probe was employed to find and make contact to individual particles that had been deposited on the monolayer. The junctions have been measured hundreds of times allowing statistical analysis. It turned out that different IV curves are observed depending on the contact between the gold nanoparticle and the organic molecule. Current through bonded contacts, where the particle reacted with the second thiol group of octanedithiol, is much larger and has a different voltage dependence as opposed to non–bonded contacts, where the nanoparticle only interacts with octanethiol. Besides, bonded

contacts are highly reproducible and experimental IV curves were obtained that show a reasonable agreement with simulations. As the current–voltage characteristics of non–bonded junctions are highly governed by the properties of the non–bonding interactions, these measurements suggest that intrinsic molecular properties can only be screened when chemically bonded contacts are present. However, the measured resistance is complicated by a *Coulomb* blockade effect arising from a finite resistance between the AFM probe and the gold nanoparticle.<sup>[56]</sup>

In 2003, *Tao* and co–workers reported a method that allows the repeated formation of molecular junctions using a gold STM tip (Figure 2–9).<sup>[57]</sup> The STM tip is moved into and out of contact with a gold substrate in a solution containing the sample molecule. While pulling the tip out of contact with the substrate, a stepwise decrease of the conductance was observed. The values correspond to the well–known conductance quantisation occurring when the size of a metallic contact is decreased to a chain of gold atoms. The STM tip is retracted further from the surface while the current is monitored until at a distance equalling the length of the sample molecule 4,4’–bipyridine a new set of current plateaus is detected. This new feature, which has a two–orders of magnitude higher resistance than before, is attributed to the

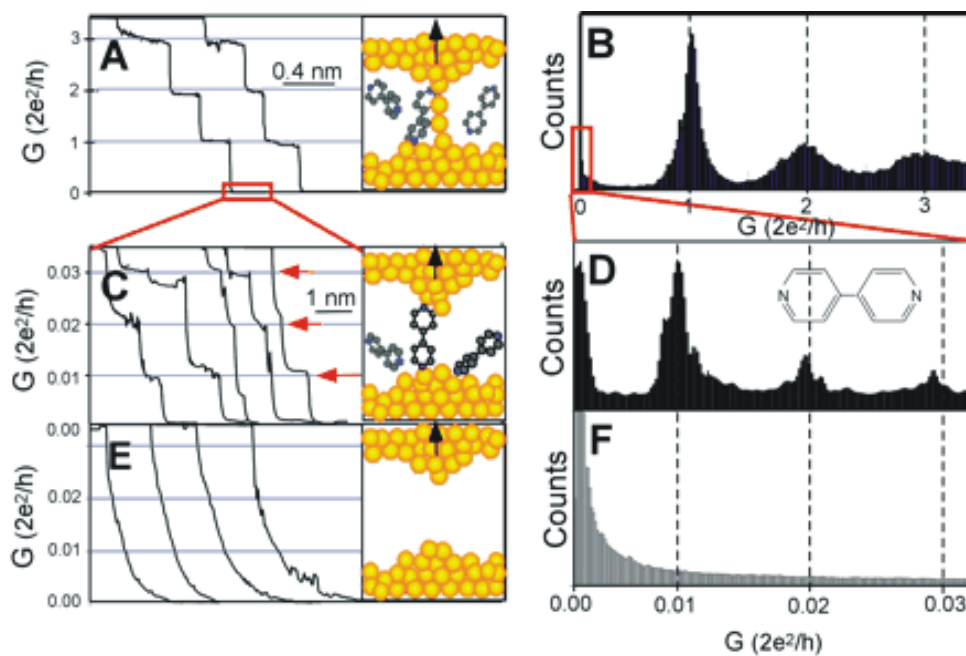


**Figure 2–9:** Method to measure the conductance of single molecules reported by *Tao* and co–workers, taken from [29]. Left: Development of the conductance as a function of distance while retracting the STM tip from the surface, a) metallic contact, c) molecular contact and e) no molecules present; right: statistical analysis done for hundreds of such junctions, b) typical pattern of a single atomic contact, d) at larger distance a peak at 0.01 is assigned to a single–molecule junction, f) an experiment without molecules does not show such conductance peaks.<sup>[29]</sup>

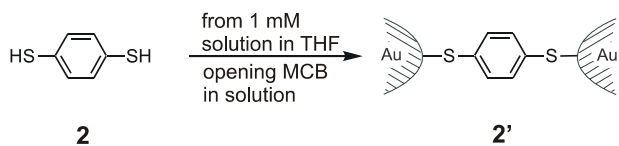
formation of a molecular junction. By statistical analysis, i.e. repeated formation and breaking of the junction, it has been shown that junctions with one, two and three molecules are obtained. The metal/molecule/metal junction can be established due to the ability of nitrogen to bind strongly to gold electrodes, because measurements with 2,2'-bipyridine do not allow the formation of reliable contacts to gold. The measurements have also been done with alkanedithiols. Hence, this method represents an interesting tool for the statistical analysis of junctions containing organic molecules, which should help to gain further insight into the electronic properties of single molecules.<sup>[29]</sup>

### 2.2.2.3 Mechanically Controlled Break Junction Technique

As explained above the use of STM allows the study of electron transport behaviour of a single or at most a few organic molecules. But these methods do not allow to establish symmetric contacts to the molecule, since tip and surface differ in shape and (often) in material. Besides, these methods lack drift stability.<sup>[4]</sup> Other methods are needed that provide a symmetric, stable test electrode pair that can be adjusted to the length of the molecule.<sup>[13]</sup> At present, metallic structures can be produced with a width of 10 to 20 nm by means of high resolution lithography and shadow mask techniques, which is still one order of magnitude too large for single molecules. Nevertheless, such metallic structures can be used as starting point to fabricate tiny voids by further controlled processing, an example is the mechanically controlled break junction (MCB) technique.<sup>[4]</sup>

In their pioneering work *Reed* and *Tour* et al. employed this technique to contact single molecules of benzene-1,4-dithiol **2** (Figure 2–10a).<sup>[11]</sup> First, a notched gold wire was glued onto a flexible substrate. Then a SAM was formed on both surfaces of the gold wire by exposing the chip to a 1 mM solution of **2** in THF under an Ar atmosphere. Now the substrate was bent in solution, until the gold wire broke giving atomically sharp contacts, as had previously been proven by conductance quantisation.<sup>[58]</sup> The THF was allowed to evaporate in the ambient Ar atmosphere. The tips were then carefully brought together again, until the onset of conductance was observed. Highly reproducible current–voltage curves could be measured. Unfortunately, at present only conductance data of the junction could be obtained, because no microscopy technique is available that is able to determine the exact number of molecules in the junction. So the final proof that only one molecule is bridging the gap is missing.

a) Experiment by Reed, Tour et al.:



### b) Experiment by Bourgoin, Joachim et al.:

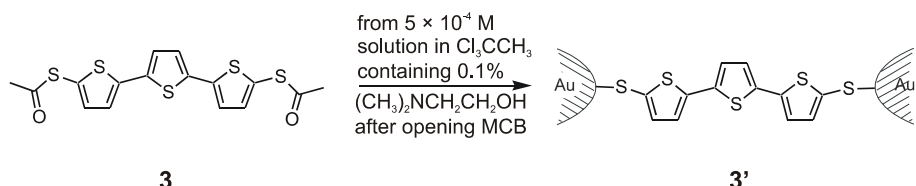


**Figure 2–10:** a) Experiment by Reed, Tour et al. with benzene-1,4-dithol **2** immobilised between two gold electrodes of a MCB.<sup>[11]</sup> b) Experiment by Bourgoin, Joachim et al. using a terthiophene **3** immobilised via sulphur anchor groups between two gold electrodes of a MCB.<sup>[12]</sup>

*Bourgoin* and co-workers used high-resolution e-beam lithography to obtain metallic structures with a predefined breaking point.<sup>[12]</sup> A rod-like molecule **3** comprising three thiophene units functionalised with thiols at both ends (Figure 2–10b) was immobilised in the gap of such advanced MCBs and reproducible IV characteristics obtained. Assuming a simple theoretical model the number of molecules in the junction was calculated to be very small or even one, though definite experimental arguments are lacking.

In order to get a better control for contacting single atoms the MCB technique was developed further by Scheer et al.<sup>[59],[60]</sup> On an elastic substrate covered with an insulating polyimide layer a gold structure consisting of two large areas connected by a thin gold bridge was fabricated lithographically (Figure 2–11). Reactive ion etching removed the upper polyimide layer around the gold and underetched the 20 to 50 nm thick gold bridge. In this way a freely suspended gold bridge was obtained. Now the chip was mounted in a three point set-up which allowed to mechanically bend the substrate in vacuum. Due to the bending the gold bridge was elongated, until it finally broke, as shown by a sudden increase in the resistance between the two big gold reservoirs. By releasing the bending tension the two atomically sharp ends of the bridge can approach each other again. Due to the extremely flat architecture this can be achieved in steps of 0.01 nm, therefore producing an electrode pair that can easily be adjusted with sub-Ångstrom resolution, that is it can be adjusted to the length of a sample molecule. This method allows the measurement of the resistance of single atoms of different materials like lead or aluminium. A further development of this set-up is now used in the group of Weber at the INT to record current–voltage characteristics of single organic molecules.

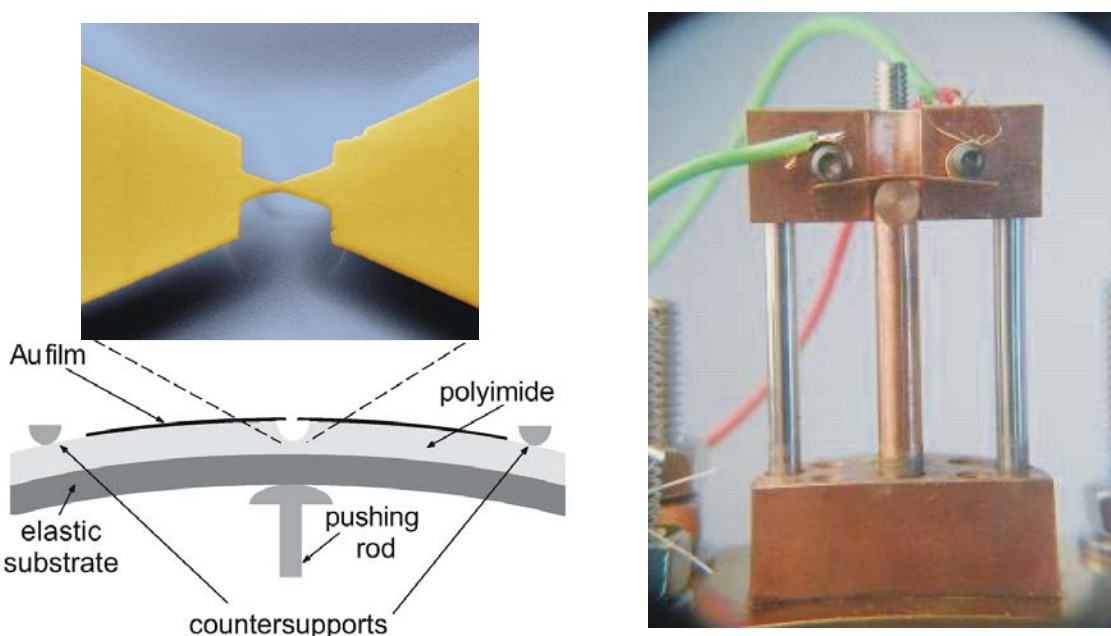


**Figure 2–11:** Set-up for the mechanically controlled break junction (MCB) technique. Left: SEM picture of a lithographically fabricated gold film on an elastic polyimide substrate and schematic drawing of the structure of the substrate. Right: The chip comprising the left structure mounted in the bending mechanism.

The molecules that bridge the structure have to fulfil a few requirements. They have to possess a polarisable, rod-like structure and anchor-groups on both ends that are needed for immobilisation on the gold surface of the electrodes. Terminal acetyl-protected sulphur groups turned out to be ideal, because the protection group splits *in situ* on a gold surface forming a defined, covalent bond between gold and sulphur.<sup>[61]</sup> The protocol for the formation of a metal–molecule–metal junction is as follows:<sup>[13]</sup> the broken MCB was opened wider than the length of the molecule (~10 nm) and a  $5 \times 10^{-4}$  solution of the molecule in THF was applied for 30 s. Due to the short application time the coverage of the surface is expected to be far below a completed monolayer. After rinsing the chip with THF under N<sub>2</sub> atmosphere, the whole setup was transferred to the sample chamber that was then pumped to  $10^{-7}$  to  $10^{-6}$  mbar. While a voltage was applied, the two electrodes were brought together again by releasing the bend. At this point individual molecules were immobilised on the gold surface of one electrode with the thiol functionality on one end, but the acetyl protection group on the other end remained intact (Figure 2–12a). The polarisable, rod-like molecules aligned themselves in the electric field towards the electrode on the opposite side. When the electrodes were driven together further, the resistance decreased exponentially with distance. Then suddenly, at a certain distance a sharp increase in current was observed that hardly changed with small alteration of the distance (Figure 2–12). This stable lock-in behaviour

was ascribed to the first molecule bridging the gap and, thereby forming a metal–molecule–metal junction. All current–voltage characteristics were recorded in this lock-in situation. Sometimes a second plateau with doubled current could be detected that was interpreted as a second molecule making contact to both electrodes. All these manipulations have been done at room temperature.

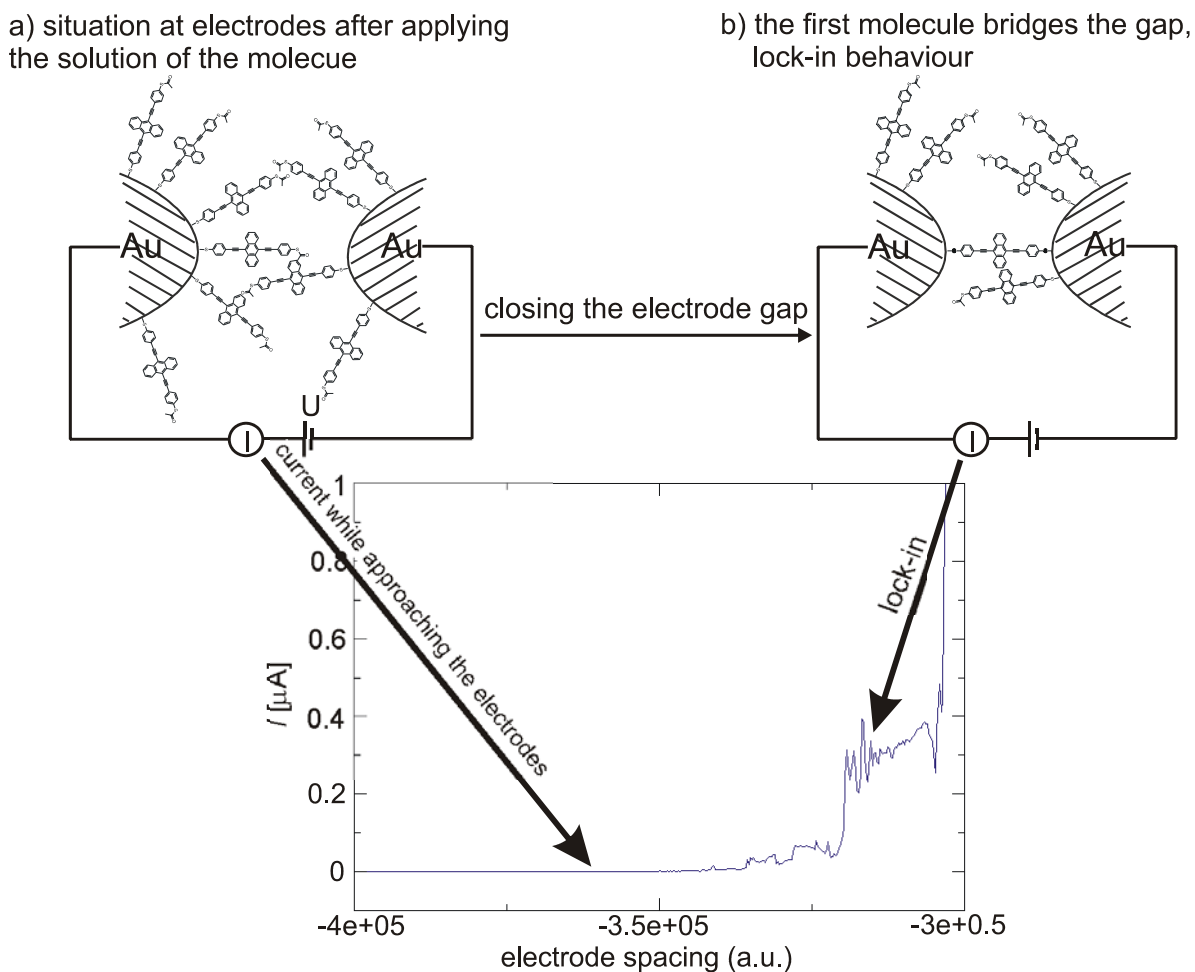


**Figure 2–12:** a) Situation at both electrodes of the MCB when driving the electrodes slowly together while applying a voltage, the observed current (arrow) which decreases exponentially with distance indicates tunnelling in this situation. b) Lock-in behaviour, that is the first molecule bridges the electrode gap giving rise to a plateau in the recorded current characteristics.<sup>[13]</sup>

As already mentioned, first experiments using the MCB to measure IV curves of organic molecules did not give clear indications about the number of molecules studied, because a systematic comparison of measurements with different organic molecules had not been done. The potential of organic chemistry to provide carefully designed, tailor-made functional building blocks that have different electronic structures was essential to clarify this issue. Therefore, a close collaboration between the organic chemistry group of *Mayor* that could

provide functional organic building blocks and the experimental physics group of *Weber* using the MCB technique was started at the INT. In the group of *Mayor* two molecules were synthesised that are very similar concerning length ( $\sim 2$  nm), functional endgroups and polarisability, but differ in their spatial symmetry (Figure 2–13). Molecular rod **4** has a symmetry plane in the centre. Therefore, the direction of the current through the molecule should not effect its conductance properties. Accordingly, the differential conductance  $dI/dV$  should be symmetric with respect to positive/negative voltages. Compound **5** bears a nitro and an acetylamino substituent on the central benzene core that break the symmetry and give rise to a dipole moment. Hence, asymmetries in the  $dI/dV$  are anticipated. Indeed, these symmetry properties of the molecules were reflected in the IV characteristics in the experiment (Figure 2–13).

These findings confirm that the junction was formed of the sample molecules and not of some undesired adsorbates. Besides, these results strongly indicate that a single molecule was

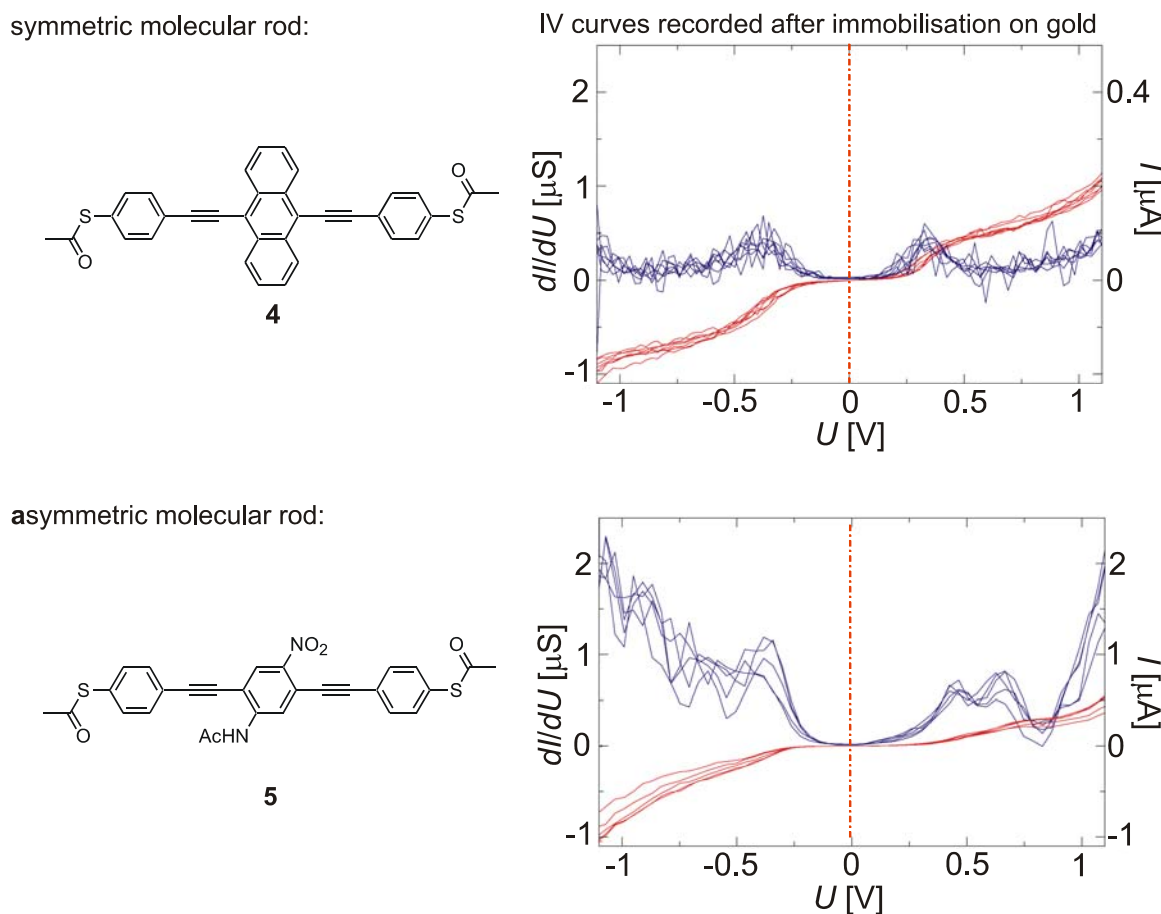


**Figure 2–13:** The spatially symmetric molecular rod **4** and the asymmetric molecule **5** were immobilised between the gold electrodes of a MCB by splitting of *in situ* the acetyl-protection groups. The red curves represent the recorded current–voltage characteristics that were measured repeatedly at room temperature, the blue curves are the differential derivatives ( $dI/dU$ ).<sup>[13]</sup>

bridging the electrode gap because a junction consisting of an ensemble of many randomly oriented molecules should give a symmetric IV curve due to averaging over all contacted molecules. Furthermore, sometimes the asymmetric shape occurred approximately mirrored with respect to the bias voltage.<sup>[13]</sup> The recorded IV characteristics can be reproduced for a stable junction, but are subject to considerable sample-to-sample fluctuations when the experiment is repeated. However, this is an expected feature of single molecule studies. Different contact realisations are one possible reason for such fluctuations, because the sulphur anchor group can chemically bind to one gold atom, but it can also bridge two or even three atoms. Due to these small changes in the atomistic electrode arrangements, the molecular wave function of the super-molecule consisting of the organic part and the gold electrodes will differ.<sup>[46]</sup>

Recently, it has been shown that the MCB technique can also be employed to conduct low temperature experiments, i.e. at about 30 K.<sup>[62]</sup> Using this slightly modified protocol the quality of the measured IV curves was considerably enhanced, in particular less sample-to-sample fluctuations were observed. Probably at low-temperature energetically favourable configurations are established more frequently. Hence, the reliability and thereby the comparability with theoretical calculations and with results obtained in other experimental set-ups could be improved.

Furthermore, a variation of the experimental set-up allowed to investigate the conductance behaviour of organic molecules in the break junction under laser illumination. For this purpose a TiSa-laser system was used, emitting either at 800 nm (continuous wave and 70 fs pulses) or frequency doubled at 400 nm (only 70 fs pulses) providing an average power between  $2 \times 10^3 - 2 \times 10^5$  W/m<sup>2</sup>. The diameter of the spot was 360 µm, that is basically the whole break junction is illuminated. During the course of the present work a molecule that absorbs light at the wavelength of the employed laser system has been synthesised, as will be described in chapter 4.

### **2.2.3 Other Methods**

First of all, electrochemical<sup>[63]</sup> and spectroscopic<sup>[64]</sup> investigations done over the last 50 years on bridged donor–acceptor molecules provide a huge database for electron transfer studies.<sup>[65]</sup> These investigations have been used to establish correlations between the structure of the organic compound and its electron transfer properties (structure–property correlations).

Furthermore, this type of bridge-mediated electronic coupling is believed to play an important role in long-range electron transfer in many biological systems such as redox proteins or nucleic acids.<sup>[66]</sup>

Crossed-wire tunnel junctions have been employed to study the effect of contact realisation<sup>[7]</sup> and bond length alternations<sup>[8]</sup> on molecular wires. In this approach a junction was formed of two 10 µm diameter gold wires, where one was modified with a SAM of the molecule of interest. The set-up was mounted to a test stage so that the wires were crossed. In an applied magnetic field the distance between the wires can be changed using a small dc current due to the *Lorentz* force generated.

A method to fabricate atom-size gaps and contacts between electrodes based on an electrochemical approach has been published by *Tao* and co-workers.<sup>[67],[68]</sup> A pair of electrodes separated by a relatively large gap is placed in an electrolyte or even pure water. When a voltage is applied between the two electrodes, metal atoms are etched off the anode and dissolved as metal ions in the electrolyte. Guided by the electric field the dissolved metal ions are deposited onto the sharpest tip of the cathode resulting in a decrease of the gap to the atomic scale. To obtain atomic gaps or contacts in a controlled fashion, the etching and deposition process must be terminated abruptly once the desired length of the gap has been reached. When one electrode is connected to an external resistor the etching-deposition-process can be self-terminated.<sup>[68]</sup> Hence, the size of the gap between the two electrodes can be adjusted by using different external resistors.

Using the so-called electromigration technique,<sup>[69]</sup> a hyphenation point in a fabricated metallic wire is opened by applying a moderate electric current. Due to the current metal atoms will start to migrate and eventually the wire will break at the bottleneck producing electrodes with a distance of 1 to 3 nm. Unfortunately, the distance between the electrodes cannot be adjusted further to the length of the molecule. But this set-up allows to introduce a gate electrode to make a nanoscale field-effect transistor, because the gap can be fabricated on a conducting substrate.

A few other techniques to study charge transport across organic molecules as a function of the molecular structure have been published, but a detailed description of all goes beyond the scope of this work.

## 2.3 Molecular Electronic Devices

ME asks for different kinds of (organic) molecules that perform different kinds of electronic functions. In contrast to the last chapters, the following paragraphs will focus mainly on the chemical structures used in the construction of ME devices employing methods described above. Thereby, the importance of tailor-made organic synthesis for the field will be highlighted.

### 2.3.1 Molecular Wires and Insulators

Wires are the conceptually simplest components of electronic circuits. In order to be considered as a “molecular wire” an organic molecule has to fulfil a number of key requirements.<sup>[14]</sup> 1) Obviously, the molecule has to be electron or hole conducting, that is provide a pathway for charge transport between two groups (molecules, electrodes or other entities) attached to its ends. To be of any use, this process should be more efficient than transport through space. 2) The wire should be linear and of a defined length to be able to bridge the gap between two components in the circuit. 3) Best results are obtained when the molecule has a rigid, rod-like structure. Molecules that are too flexible would cause problems on the molecular scale due to short-circuiting different units through space.<sup>[4]</sup>

Possible candidates for molecular wires are compounds having large delocalised  $\pi$ -systems like polyenes **6**,<sup>[70]</sup> polyynes **7**,<sup>[71]</sup> polythiophenes **8**,<sup>[72]</sup> polyphenylenes **9**,<sup>[73]</sup> polyphenylenevinylenes **10**,<sup>[74]</sup> and polyphenyleneethynylens **11** (Figure 2–14),<sup>[75]</sup> because the energy of their frontier orbitals, which are assumed to be responsible for electron transport should be close to the *Fermi* level of the electrode.<sup>[76]</sup> Typically, long molecules are prepared

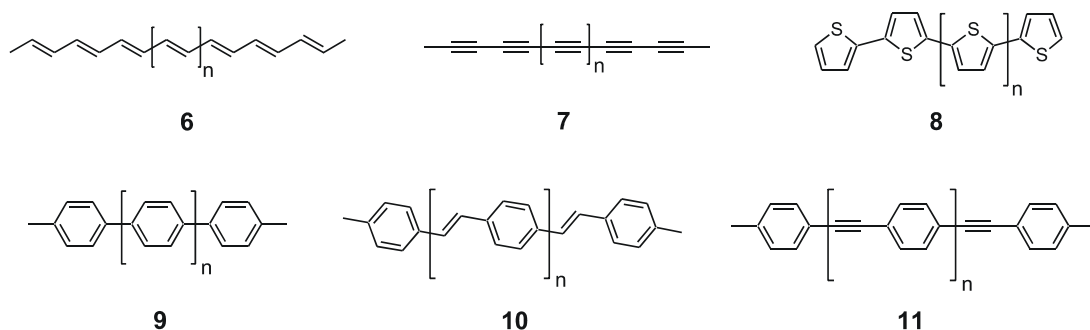


**Figure 2–14:** Possibilities for conjugation active motives (wires), taken and modified from ref [4].

by polymerisation. Unfortunately, this way of synthesis leads to mixtures that comprise molecules of different length and shape and often the isolation of the molecule of interest turns out to be tedious or even impossible. Therefore, often a series of different chain length oligomers is synthesised step by step. Thereby, the potential of different oligo(phenylene ethynylene)s<sup>[66]</sup> and oligo(phenylene vinylene)s<sup>[64]</sup> has been demonstrated by probing the properties of donor–molecular wire–acceptor systems electrochemically and spectroscopically in solution. Often in these studies the effective conjugation length can be found, that is “the extrapolation of physical properties toward infinite chain lengths and the description of a conjugated polymer in its true state”<sup>[77]</sup> becomes possible. However, structure–property relationships can only be established for physical properties that are accessible in solution. One example of such an oligomer approach in the oligophenylene series has been presented by *Schlüter* in the synthesis of rods having up to 16 phenylene rings and well-defined functional endgroups.<sup>[78]</sup> Another slightly different approach, namely the iterative divergent/convergent approach, has been used to obtain molecular wires with a length of up to 100 Å in the oligo(thiophene ethynylene) series **12** and with a length of 128 Å in the oligo(phenylene ethynylene) series **13** in both cases beginning from simple starting materials (Figure 2–15).<sup>[33]</sup> Using this method the separation of compounds is greatly facilitated, because the length of the molecule doubles with each step. Besides, using the same chemical reactions anchor–groups that allow binding to solid substrates can be put at the ends of the wires. This approach has also been shown to work on solid support.<sup>[79]</sup> While a lot of other molecular wires bearing various anchor–groups have been synthesised so far that are

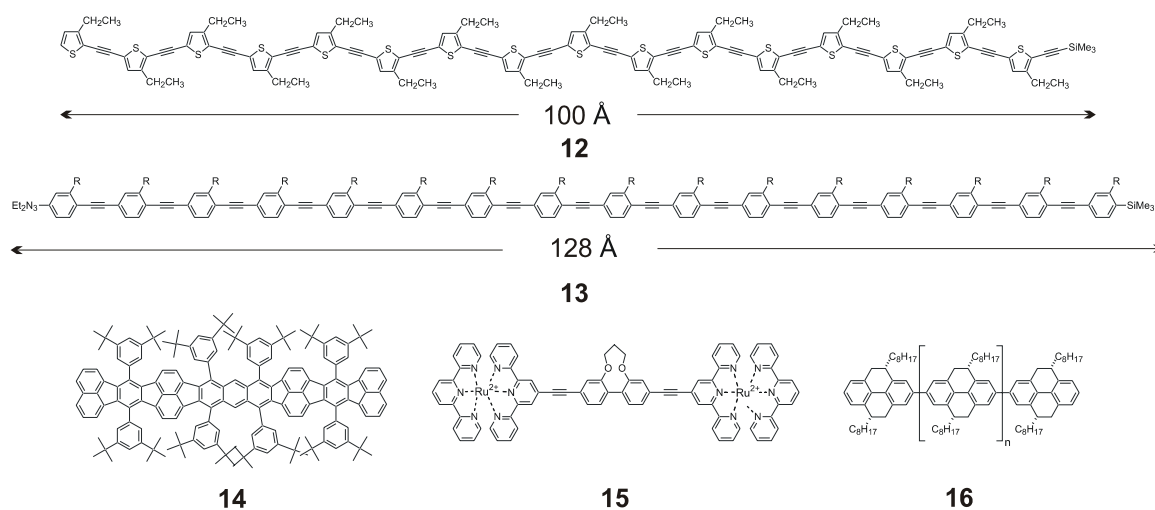


**Figure 2–15:** Some examples of molecular wire structures that have been synthesised up to date:

**12**<sup>[33]</sup> and **13**<sup>[33]</sup> are the longest known oligomers in these series so far, **14**,<sup>[28]</sup> **15**,<sup>[80]</sup> **16**<sup>[77]</sup> were chosen as illustrative examples.

interesting from a synthetic chemistry point of view,<sup>[80],[77]</sup> most of these compounds have not been designed to allow testing in full device embodiments.

All these studies provide a huge database of molecular wires in solution. However, the first demonstration of a single molecular wire in the solid state was done by *Bumm* and *Tour*,<sup>[10]</sup> which has already been described in section 2.2.2. There it has also been mentioned that current–voltage characteristics of phenyleneethynylanes (Figure 2–13)<sup>[13]</sup> and a thiol–terminated terthiophene (Figure 2–10)<sup>[12]</sup> have been recorded using a MCB device. The obtained results indicate the potential of these compounds to act as molecular wires. Besides, crossed–wired tunnel junctions have been used to study the difference between the electronic properties of oligo(phenylene ethynylene)s and oligo(phenylene vinylene)s suggesting a better conductivity for the latter.<sup>[8]</sup>

Porphyrin oligomers have also been considered as interesting molecular wire candidates, because their  $\pi$ –systems form giant supramolecular chromophores when merged together.<sup>[81]</sup> Moreover, their properties can be adjusted by substitution and introduction of different metal ions as shown in theoretical studies.<sup>[82]</sup> Apart from hydrocarbons carbon nanotubes and DNA were studied as molecular wire candidates. The applicability of DNA as molecular wire, however, remains uncertain because it is still under debate, whether DNA has insulator,<sup>[83]</sup> semi–conductor<sup>[84]</sup> or even metal<sup>[85]</sup> properties. Nevertheless, DNA can be altered by changing the base pairing and offers the unique advantage to undergo self–assembly. Carbon nanotubes can be considered as graphitic sheets with a hexagonal lattice wrapped up to form a cylinder.<sup>[86]</sup> These structures are very interesting, because single–walled carbon nanotubes are much longer (length up to  $\mu\text{m}$ ) than wide (diameter between 0.4 nm and 3 nm) and their electrical properties (metallic or semi–conducting) depend on the diameter and the wrapping angle of graphitic sheets. While this property indicates the great potential of nanotubes, it is also the biggest drawback, since it has not been possible yet to produce carbon nanotubes of only one kind in a controlled manner. But recently success has been made in separating metallic from semi–conducting tubes.<sup>[87]</sup> The difficulties in functionalising nanotubes pose another remaining problem, though progress in this type of chemistry is consistently being made.<sup>[88]</sup>

Apart from conducting molecular building blocks the opposite property, i.e. insulating behaviour, is sometimes required. For instance, the synthesis of a molecular diode based on the proposal by *Aviram* and *Ratner* relies on the connection of electronically different building blocks by an insulating linker (see below).<sup>[3]</sup> In general, such structures can be built by systems without extended  $\pi$ –conjugation (Figure 2–16). While the alkyl chain **17** is known

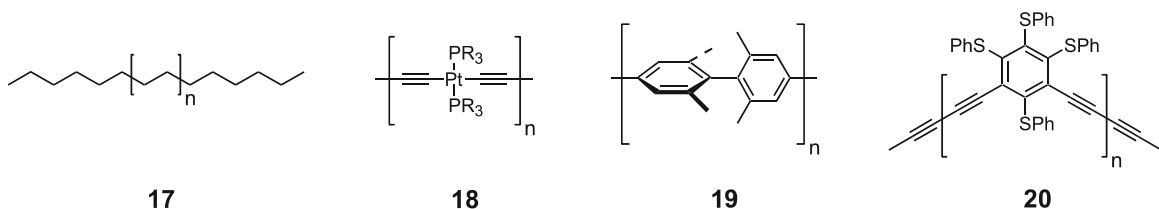


**Figure 2–16:** Possibilities for conjugation passive motives (insulators), modified from ref. [4].

to be a good insulator, it lacks the necessary rigidity and can, therefore, not be utilised in electronic devices. Metalorganic complexes like **18** may provide an opportunity to develop insulating linkers because of the  $\sigma$  character of the bond between the Pt(II) ion and the acetylene ligands.<sup>[89]</sup> Oligophenylenes consisting of ring–systems that are rotated with respect to each other like **19** are another possibility. Part of the present work was dealing with such compounds (confer chapter 4). Furthermore, compounds comprising *meta*–linkage like the structural motif **20** should act as insulators.

The potential of Pt–complexes has already been demonstrated by the investigation of complex **21** in a MCB.<sup>[15]</sup> The resistance of this metal–molecule–metal junction was determined to be three orders of magnitude higher than that of conjugated molecular wires of comparable length (Figure 2–17). However, the same complex has been investigated using a crossed–wire tunnel junction, too, and the overall resistance was found to be lower than that of oligo(phenylene ethynylene)s.<sup>[90]</sup> The marked difference between these two studies arises probably from the two different set–ups used for the measurement. In crossed–wire tunnel junctions tunnelling, which has an exponential distance dependence, is believed to be the dominant mechanism of charge transport. Therefore, the platinum–complex should show a

Pt-complex, that was immobilised via thiol anchor-groups on the gold electrodes of a MCB

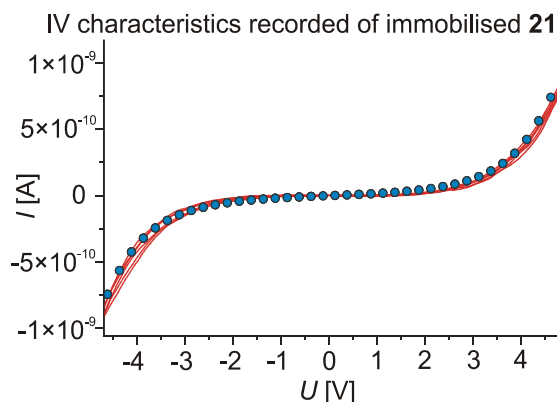
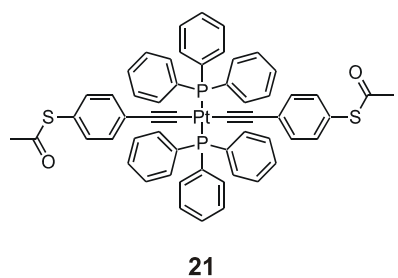


**Figure 2–17:** The symmetric molecular rod **21** was immobilised between the gold electrodes of a MCB by splitting of *in situ* the acetyl protection–groups. The red curves represent the recorded current–voltage characteristics that were measured repeatedly at room temperature, the blue dots a simulated current using a barrier height of 2.5 eV.<sup>[15]</sup>

higher conductivity as it is about 2 Å shorter than studied oligo(phenylene ethynylene)s. In MCBs electron transport through single molecules that are covalently linked to the gold electrodes is screened. Another strategy could be based on the position of the linking groups in an aromatic system. As has long been known to chemists the *meta*-position of an aromatic ring lacks conjugation and can thus reduce electronic communication.<sup>[91]</sup> This fact has already been proven by theoretical studies<sup>[92]</sup> and by electrochemical investigations of thiophenyl-substituted benzene cores **20** having acetylene bridging blocks in *meta*- or *para*-position.<sup>[63]</sup> Hence, two molecules that differ only in the position of the anchor-group on the aromatic core have been synthesised, as will be shown in more detail in chapter 4. Current-voltage characteristics recorded using a MCB revealed that the molecular rod bearing the anchor-groups in *meta*-position has a resistance which is about two order of magnitude higher than the values recorded for the *para*-compound (see also chapter 4).<sup>[93]</sup>

### 2.3.2 Molecular Rectifiers

Electronic building blocks acting as p–n junction diodes are an integral part of current semiconductor devices, and the invention of a molecular counterpart will be crucial for a successful development of ME.<sup>[94]</sup>

The use of an organic molecule as equivalent of a p–n junctions was first put forward by *Aviram* and *Ratner* in their influential paper back in 1974.<sup>[3]</sup> At that time, however, no experimental tool existed to evaluate the feasibility of this approach. By a theoretical model they predicted that molecules like **22** which have a similar structure as common silicon-based p–n junctions, namely a donor–insulator–acceptor ( $D\sigma A$ ) structure, may act as unimolecular diodes (Figure 2–18). Substitution of an aromatic core with electron–releasing groups increases the  $\pi$ –electron density and, thus, lowers the ionisation potential. Therefore such relatively electron–rich subunits were regarded as donor part. In contrast, electron–withdrawing groups decrease the  $\pi$ –electron density and generate a relatively electron–poor molecular subunit with a higher electron affinity, i.e. an electron acceptor part is formed. An insulating bridge, the  $\sigma$ –part, introduces an effective barrier for electron transfer between the donor and acceptor. The rectifier behaviour was explained as follows for a molecule of **22** in between two metal electrodes. In order to show rectifier behaviour the LUMO of the acceptor part should lie at or slightly above the *Fermi* level of the electrode and obviously above the ionising level C (HOMO) of the donor part whilst no voltage is applied (Figure 2–18). When

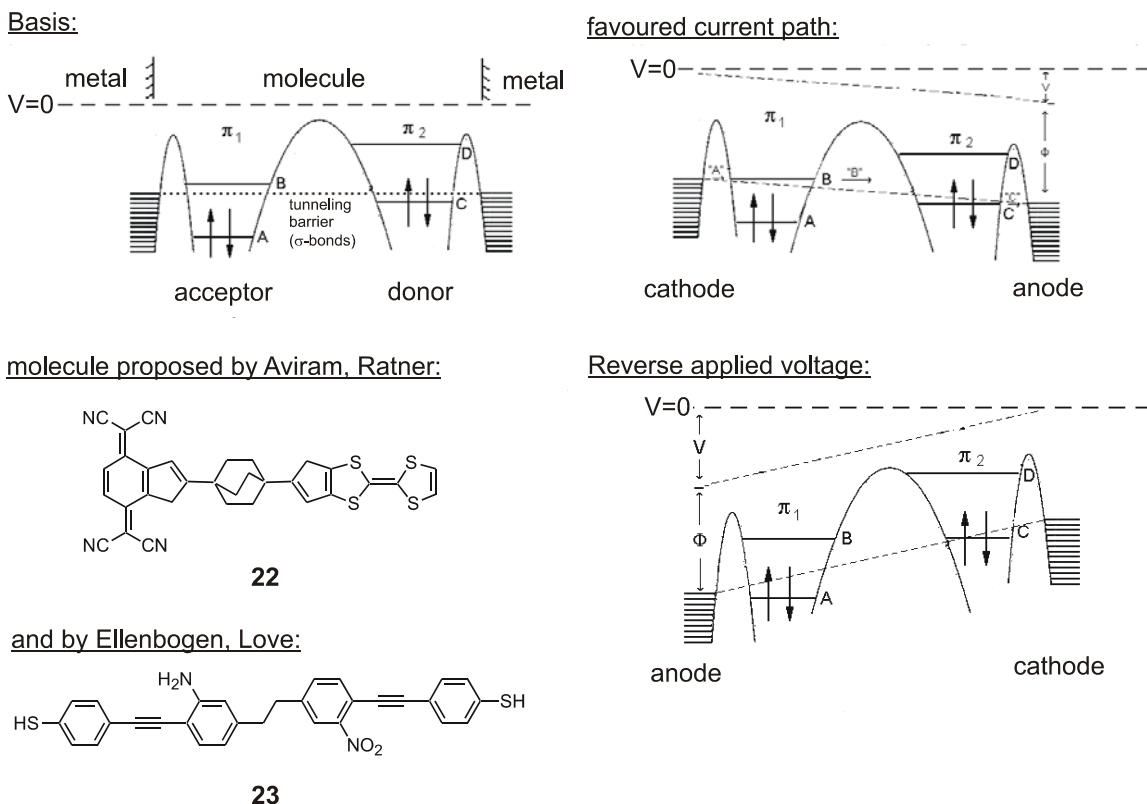


**Figure 2–18:** Left: Energy versus distance of the device (top) using the molecule **22** (below) in between two electrodes and molecular structures proposed by Aviram and Ratner<sup>[3]</sup> and Ellenbogen and Love<sup>[119]</sup> as molecular rectifier. Right: Shift of energy levels when a voltage is applied (top) employing the favoured current path and (below) the reverse applied voltage<sup>[3]</sup>

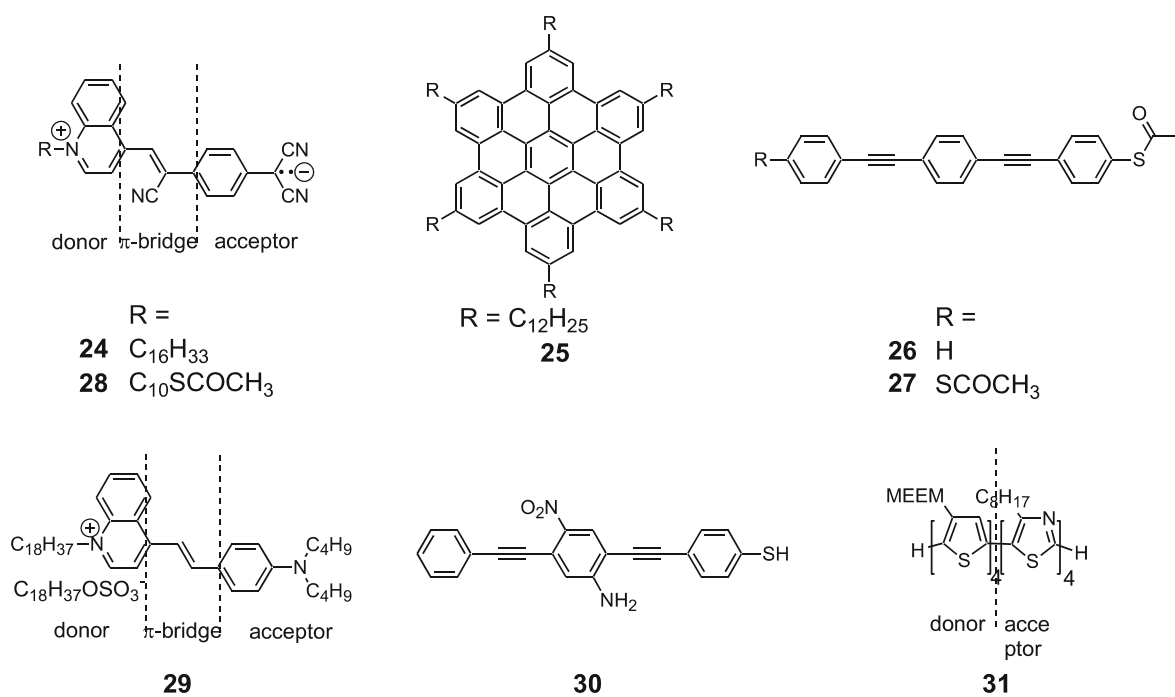
the applied field becomes large enough to cause an overlap of the cathode levels with the acceptor levels electron transfer onto the acceptor is rendered possible (Figure 2–18 top right). At the donor end a similar process is invoked, where electron transfer from the donor orbital C to the anode occurs as soon as the applied voltage V becomes greater than the ionisation potential. Of course both described processes depend also on the work function of the metal. Motion of electrons from the acceptor to the donor is made possible, because the (now occupied) LUMO and the hole on the (now ionised) donor are close in energy so that electron tunnelling will occur through the  $\sigma$ -bridge. As long as B lies above C this tunnelling is irreversible.

Figure 2–18 right explains the reverse process, that is electron transport from the donor to the acceptor, requires a higher threshold voltage. Hence, such a structure was claimed to show rectifier behaviour. Recently, it has been suggested in theoretical calculations for a different molecule **23** that “in principle the Aviram–Ratner diode can be an effective rectifier”.<sup>[94]</sup> The investigated molecule, however, did not show this electronic property, since the gap between the HOMO of the donor and the LUMO of the acceptor was too big. It should be feasible,

though, to obtain resonant conditions at smaller bias by changing the substitution pattern of the organic molecule.

First experimental indications for the validity of this concept were presented by *Ashwell* in the nineties by using *Langmuir–Blodgett* films of **24** (Figure 2–19) sandwiched between two different electrodes, namely, silver and magnesium.<sup>[95]</sup> It has been argued, however, that the different work functions of these metals can itself lead to rectification and that not the molecule is responsible for the observed effect. Therefore, in later work<sup>[16]</sup> two aluminium electrodes were used. In this case, a rectification ratio defined as (current at  $V_0$ )/(current at  $-V_0$ ) of up to 26 was determined, which diminished on repeated voltage cycles presumably due to a re-orientation of the molecules in the film. In this work a slightly modified mechanism for charge transport has been proposed as well. But still the “real proof” was lacking, because the oxides of Al or Mg might play a role in the rectification process as has been suggested by *Metzger*.<sup>[39]</sup> Therefore, only recently it could be shown that the diode behaviour is most probably due to the molecule in the *Langmuir–Blodgett* film by the use of two oxide-free gold electrodes (Figure 2–20).<sup>[17]</sup> Nevertheless, there is still on-going discussion that the rectifier behaviour can not be explained by the *Aviram–Ratner* model, but is rather caused by the asymmetric coupling of the molecule to the two electrodes due to the long alkyl chain needed for film formation.

*Rabe* and *Müllen* used hexaalkyl substituted derivatives of hexa-peri-hexabenzocoronene **25**



**Figure 2–19:** Examples of molecules that have shown rectification behaviour in different experimental set-ups.<sup>[16],[97],[98],[95],[41],[18]</sup>

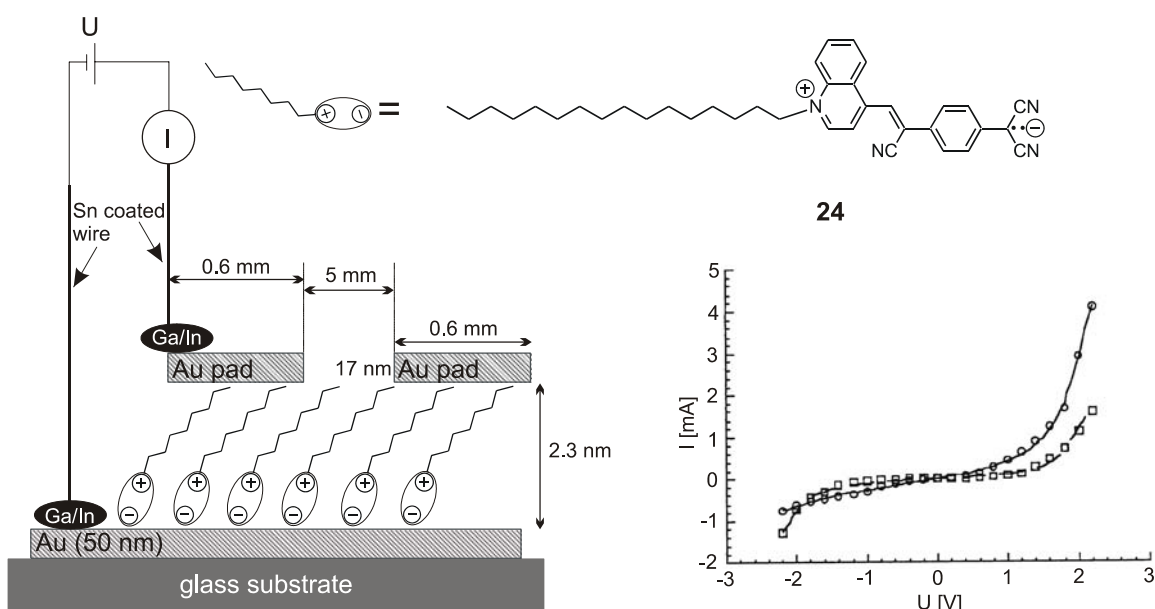


**Figure 2-20:** Left: Schematic drawing of a LB monolayer of **24** sandwiched between two gold electrodes and electrical contacts attached to the Au electrodes. Right: Current–voltage plots for one sample with a monolayer of **24** showing different cycles, the first is represented by circles and solid lines and the sixth cycle is depicted by squares and dashed lines<sup>[17]</sup>

that forms regular monomolecular patterns on a graphite surface.<sup>[96],[97]</sup> Due to the relatively large size of the discs STM investigations can be combined with scanning tunnelling spectroscopy allowing to record separate current–voltage characteristics of the aromatic and the aliphatic domains of the sample molecule. While measurements on the aliphatic chain gave rise to symmetric curves with respect to voltage inversion, placing the STM over an aromatic domain results in a diode–like response. The rectification ratio is about 10 at 1 V. This result has been ascribed mainly to the asymmetric placement of the hexabenzocoronene in between the two used electrodes, that is it is closer to the substrate than to the tip of the STM. Besides, asymmetric contact arrangements have been proven to trigger rectification by using crossed–wire tunnel junctions with oligo(phenylene ethynylene)s bearing one **26** or two **27** thiol anchor groups, respectively.<sup>[7]</sup> SAMs of oligo(phenylene ethynylene)s probed with STM as counterelectrode also showed rectification.<sup>[98]</sup> There are theoretical studies as well that hint at rectification due to asymmetric contacts.<sup>[99]</sup> In an effort to overcome the problem of re–orientation on repeated voltage cycling of the device, a SAM of **28** on a gold surface was prepared and investigated with STM.<sup>[100]</sup> This device exhibited rectification, too, while the ultimate proof due to the arguments mentioned above remains to be given.

Apart from this extensively studied zwitterionic molecule a couple of other organic molecules have been demonstrated to act as a molecular diode in different device arrangements (Figure 2–19). A closely related organic dye **29** has been investigated in LB multilayers sandwiched

between two oxide-free gold-electrodes and shown rectifier behaviour, but the effect decreases on continuous voltage cycling of the device.<sup>[101]</sup> A bis(phenylvinyl)pyridinium iodide compound showed a rectification ratio of up to 90 when contacted in a LB monolayer between two gold electrodes. But the observation is probably due to asymmetric placement of the iodide-pyridinium ion pair between the metal electrodes.<sup>[102]</sup> *Reed* and *Tour* reported diode behaviour together with an effect called negative differential resistance (NDR) at 60 K for a molecular rod **30** that had a sulphur anchor-group on one end to enable self-assembly on a gold surface.<sup>[41]</sup> Using a nanopore a small number of organic molecules (about 1000) could be contacted between two gold electrodes. However, it has not been clarified whether this interesting effect is caused by the molecule itself or by the architecture of the device. Lately, a conjugated diblock oligomer **31** consisting of a donor-like tetramer of 3-alkylthiophene covalently linked to a tetramer of acceptor-like 4-alkylthiazole has been stated to act as a molecular diode.<sup>[18]</sup> The oligomer having alkyl groups with distinct hydrophilicity/hydrophobicity properties was used to form well-defined *LB* monolayers that were studied by STM. The donor-acceptor molecule always gave rise to asymmetric current voltage characteristics while a control molecule comprising only thiophene subunits with the same alkyl substitution pattern showed only symmetric curves. Therefore, the diode effect could be assigned to the structure of the molecule. Besides, this approach offers the opportunity to alter the electronic properties of the diblock oligomer by tailor-made organic synthesis.

### 2.3.3 Molecular Switches and Storage Elements

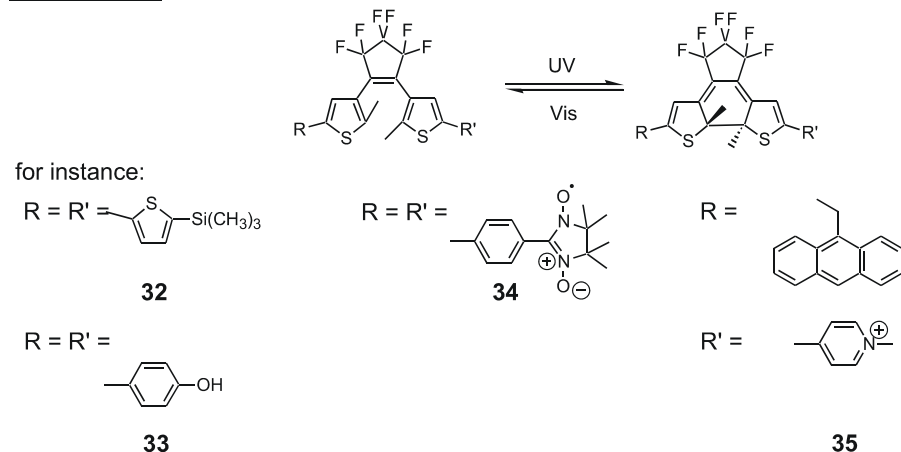
Apart from compounds that operate as wires or rectifiers, molecules that exist in two (or more) stable states are of fundamental importance to ME in order to construct building blocks that mimic switches and storage media.<sup>[4]</sup> The term “molecular-level switch” can either be assigned to an element that caused by an external driving force can reversibly interrupt the transport of electrons in a molecular wire or, more general, to any molecular-scale system that can be reversibly inter-converted between two states in response to an external stimulus. The last definition also includes elements related to storage and logic functions, for instance AND or OR gates.<sup>[103]</sup>

There are three different types of stimulus, light energy (photons), electrical energy (electrons, holes) and chemical energy (protons, metal ions etc.) that are likely to bring about switching

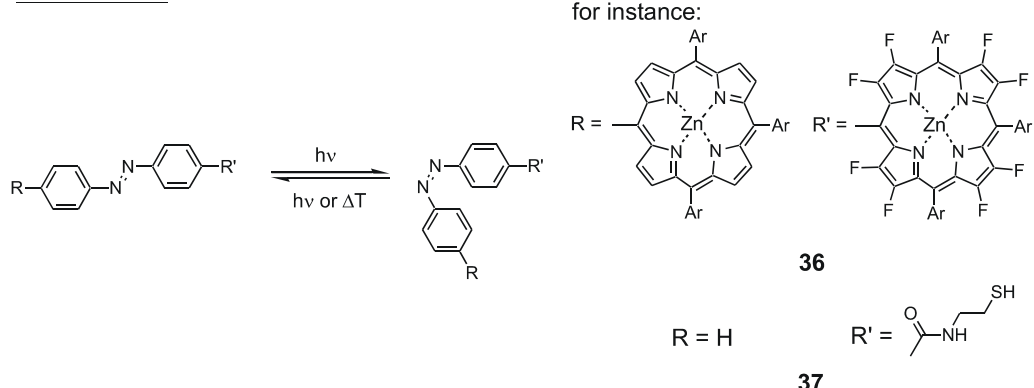
on the molecular level giving rise to both electronic and nuclear rearrangements.<sup>[104]</sup> Compared to the others, chemical stimulation is performed more difficultly and normally slower, besides chemically reading the state of the system poses problems. Photochemical stimulation involves processes based on photoisomerisation or photoinduced redox reactions and requires photochromic compounds, that is these compounds have to “reversibly change their molecular properties upon photoirradiation, such as absorption and fluorescence spectra, refractive indices, (...), oxidation/reduction potentials, and chiroptical properties”.<sup>[105]</sup> Electrochemical switching solely induces redox reactions. In more general terms, switching processes can be subdivided into processes that are done in thermodynamic equilibrium and systems that are under kinetic control.<sup>[103]</sup> System that are under thermodynamic control need permanent stimulation, since otherwise the molecule responding to the external driving force will revert slowly to its initial state. Actually, a similar scenario is also found in current silicon-based DRAM (dynamic random access memory) where two different charge storage levels representing 0 and 1 are realised using tiny capacitors.<sup>[106]</sup> Stored information needs to be refreshed periodically because of the unavoidable self-discharge of capacitors. Usually this happens at rates of fractions of a second, but shorter refresh times are desirable. Hence, ME devices that are under kinetic control might form an interesting alternative, as kinetic control allows for metastable states where the thermal back reaction to the thermodynamically stable state is inhibited because of a sufficiently high energy barrier. Systems responding to a photonic stimulus fall in this category. The de-trapping, that is switching back, can be achieved by means of a second (different) photonic input. In principle, single molecules can be addressed in systems under kinetic control which is unattainable for systems in thermodynamic equilibrium.

As for molecular wires a great number of chemical switches has been studied in solution with the most prominent examples being compounds based on diarylethenes **32 – 35**,<sup>[107]</sup> azobenzenes **36** and **37**<sup>[108]</sup> (Figure 2–21) and supramolecular rotaxanes and catenanes.<sup>[104]</sup> The switching behaviour of compounds related to the most widely used photochromic building block of 1,2-bis(2-methylthiophen-3-yl)hexafluorocyclopentene is based on the well known photocyclisation reaction of stilbene to dihydrophenanthrene.<sup>[109]</sup> In the open-ring structure the  $\pi$ -systems of the thiophene moieties are separated, while the closed-ring isomer that can be obtained by irradiation with light in the range of 200 – 380 nm has an olefinic structure and, hence a  $\pi$  system delocalised throughout the molecule.<sup>[105]</sup> The switch can be opened again somewhat depending on the substitution by using light of the wavelength between 450 – 720 nm. Such molecules can be switched reversibly having a high thermal

## Diarylethenes:



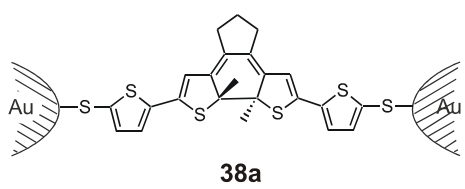
### Azobenzenes:



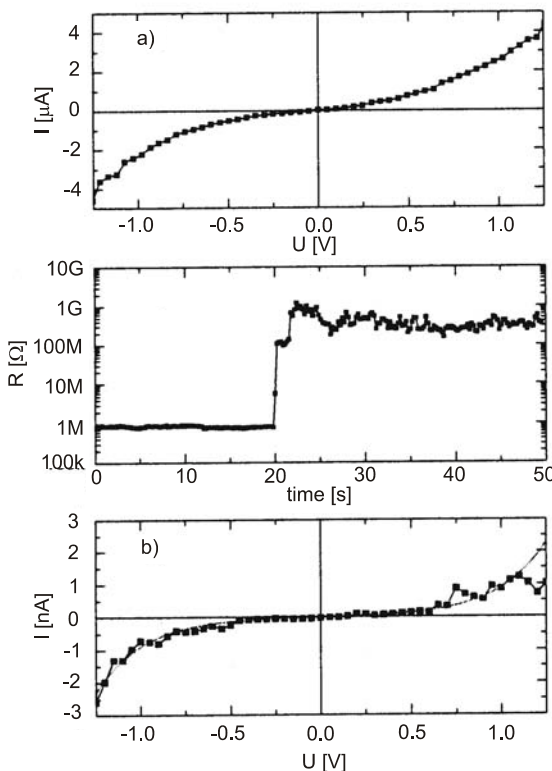
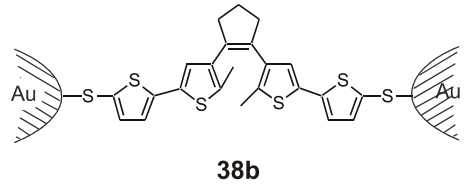
**Figure 2–21:** Examples of organic compounds whose potential for switching has already been proven in solution. Diarylethenes bearing the same substituents including thiophenyls  $32$ ,<sup>[109]</sup> hydroxyl-phenyls  $33$ ,<sup>[109]</sup> radicals  $34$ <sup>[109]</sup> and different side-groups like  $35$ <sup>[109]</sup> have been synthesised. Azobenzenes having different substituents  $36$ <sup>[108]</sup> and  $37$ <sup>[108]</sup> have been used for studies in solution.

stability and fatigue resistance and even have the potential of application as optical storage elements, as has been shown by a three-state system allowing for a write-lock-(non-destructive) read-unlock-erase cycle.<sup>[110]</sup>

Recently, molecule **38** based on this motif has been immobilised in a MCB via sulphur anchor-groups and demonstrated to switch from the closed (conducting) state to the opened (insulating) state (Figure 2–22).<sup>[23]</sup> The two states could be distinguished by their measured IV curves that showed an about three orders of magnitude larger resistance for the off-state. The back reaction, however, was not possible, which was attributed to the influence of the gold electrodes on the molecular system. This could be proven by the measurement of UV/Vis absorption spectra of the monothiol photochromic compound self-assembled on gold colloids. While switching form the closed to the open-form was possible on nanoparticles as well, the reverse process was not observed even after two days of irradiation. Theoretical

a) Closed Switch

no switching       $\lambda = 546 \text{ nm}$

b) Opened Switch

**Figure 2–22:** Left: Molecular Switch **38** based on the diarylethene structure immobilised between the gold electrodes of a MCB. Switching was only possible from the closed to the open state when the molecule is bond to a gold surface. Right: Current–voltage characteristics of a) the closed switch and b) the opened switch. The current level between these two forms differs by almost three orders of magnitude. The diagram in the middle shows the resistance versus time (at  $t=0$  a lamp is turned on) when the junction is illuminated with light of the wavelength  $\lambda=546 \text{ nm}$  (bias  $U = 1 \text{ V}$ ).<sup>[23]</sup>

calculations done in the same work suggest a quenching of the excited open state by gold preventing the closure of the ring.

The reversible photoisomerisation from the *E*– to the *Z*–form of compounds containing the azobenzene unit has long been known<sup>[111]</sup> and its applicability has been explored, for example, in studies dealing with photo–switchable host–guest systems.<sup>[112]</sup> The possibility to alter electronic properties of organic compounds comprising the azo functionality has been demonstrated, for instance, by analysing the electron–transfer processes in compound **36** upon irradiation with light.<sup>[113]</sup> Furthermore, the HOMO–LUMO gap of a quaterthiophene bridged by a bis–sulfanyl–azobenzene could be changed reversibly using light.<sup>[114]</sup> Irradiating at  $\lambda = 360 \text{ nm}$  leads to formation of the *Z*–isomer inducing a conformational change of the ring structure and at the same time a decrease of the HOMO–LUMO–gap. The electronic properties can be reverted by shining light of the wavelength  $\lambda = 480 \text{ nm}$ .

Investigation of a mixed SAM of compound **37** and n–dodecanethiol on a gold substrate using STM was used to show photoisomerisation of isolated azo molecules for the first time.<sup>[115]</sup> However, only loosely packed azo molecules like the ones absorbed at phase boundaries showed this conformational change. In addition, at applied voltages higher than +0.5 V an interesting flip–flop motion was observed that could be assigned to the rapid, reversible cis–trans isomerisation of isolated, loosely packed azo molecules under the influence of the external electric field, even when the sample is not illuminated. This effect was also observed for the first time and indicates that the conditions of the measurement, i.e. applied electric field, have some bearing on the fundamental process itself, i.e. on the isomerisation.

For electronic applications switching triggered by electrical energy is considered to be of greater interest than switching of photochromic compounds, because due to the high degree of integration of electronic components individual switching of one device using light will cause serious technical problems.<sup>[4]</sup> One of the few examples of solid–state devices presented for that kind of switches<sup>[20]</sup> utilised so–called rotaxanes and catenanes, classes of compounds known from supramolecular chemistry, where two or more macrocyclic components are interlocked in such way that no covalent bonds, but rather mechanical or topological bonds hold the units together.<sup>[112]</sup> The switching process of [2]catenane **39** has been shown in solution.<sup>[21],[116]</sup> As shown by x–ray crystallography, <sup>1</sup>H–NMR investigations and absorption spectra catenane **39** exist preferentially in a configuration, where the tetrathiafulvalene (TTF) unit is inserted through the cavity of the tetracationic cyclophane, while the naphthalene ring system resides alongside. Rotation of the TTF unit out of the cavity has been proven by different techniques including UV/Vis spectroscopy, <sup>1</sup>H–NMR investigations and cyclic voltammetry. In the NMR experiments the TTF unit was oxidised using *o*–chloroanil. The rotation of the unit was proven by the difference in chemical shifts of the 1,5–dioxynaphthalene unit before and after addition of *o*–chloroanil suggesting the movement of the naphthalene unit into the cavity. The process was reversed by reduction with Na<sub>2</sub>S<sub>2</sub>O<sub>5</sub> affording the initial <sup>1</sup>H–NMR spectrum. UV/Vis spectroscopy suggest a two–electron oxidation process upon addition of Fe(ClO<sub>4</sub>)<sub>3</sub>, as one equivalent of the oxidation agent gave rise to the characteristic absorption bands of a mono–oxidised TTF unit. According to the UV/Vis spectra higher equivalents of Fe(ClO<sub>4</sub>)<sub>3</sub> afforded the bis–oxidised form. Besides, the characteristics of a naphthalene moiety encircled by the tetracationic cyclophane were observed. After addition of two equivalents of ascorbic acid as reductant the bands of the initial TTF unit residing in the cavity of the cyclophane were completely restored, whereupon one equivalent of reducing agent afforded the TTF radical cation. Studies using cyclic

voltammetry established that the switching can also be induced by an electrochemical oxidation/reduction cycle. Hence, switching of the [2]catenane **39** in solution has been confirmed unequivocally by chemical and electrochemical stimuli.

In order to investigate the potential of catenane **39** to act as a switch in the solid state, it was sandwiched between two electrodes using *LB* monolayers. An array of crossed-wires has been employed for this purpose.<sup>[20]</sup> A series of voltage pulses between +2.0 to -2.0 V was applied and after each pulse the current through the device was read at 200 mV, a potential that does not induce switching. Figure 2–23 shows the proposed mechanism, which is somewhat different than the one in solution.<sup>[103],[20]</sup> When **39** in the starting conformation I is oxidised by applying a potential (+2 V), the TTF unit is ionised and due to coulombic repulsion inside the tetracationic cyclophane ring circumrotates affording conformation III. Note that in solution an oxidation of the naphthalene subunit has been found as well. Reducing the voltage to near-zero affords a neutral TTF unit and, hence conformation IV, which in solution spontaneously returns to conformation I.<sup>[103]</sup> In the solid state, however, the initial conformation is achieved only by going through state V where the bipyridinium entities in the cyclophane ring are reduced at negative potentials of -2 V. Since the state of the device can be read out at near-zero voltages and the current–voltage curve shows a hysteretic profile, it has been claimed to use such a device for random access memory (RAM). It should be mentioned, though, that in investigations using simpler molecules, namely eicosanoic acid, in

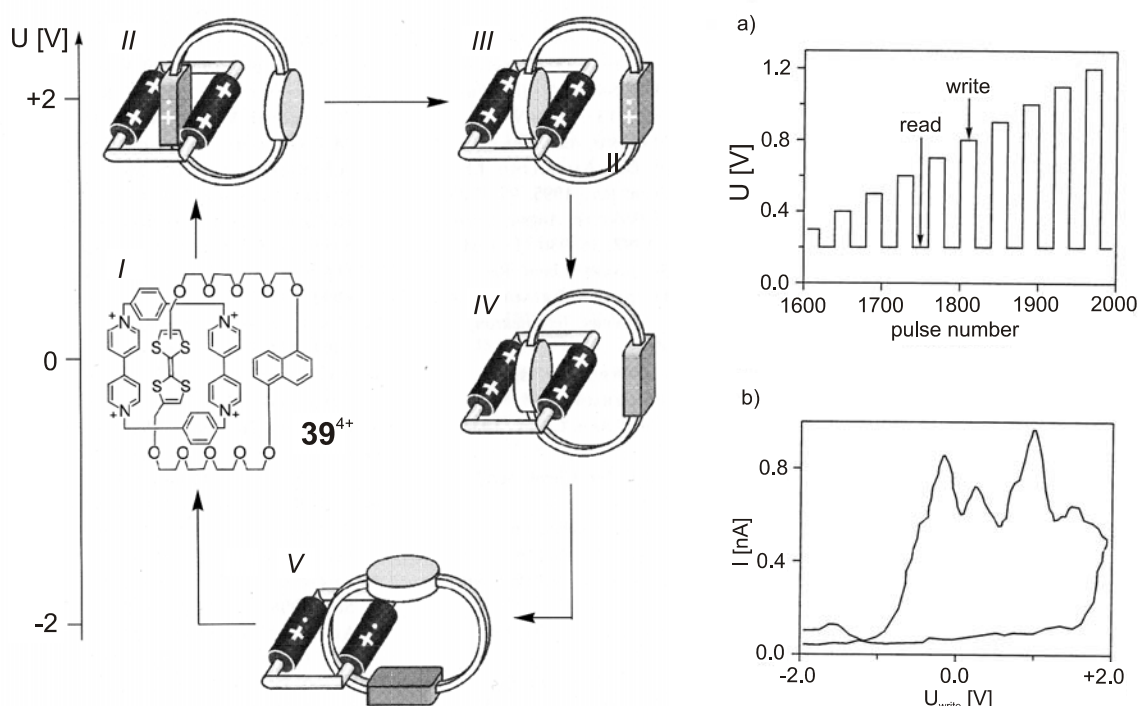


**Figure 2–23:** Proposed mechanism for switching of the device incorporating [2]catenane **39**.<sup>[20]</sup>

between the same electrode arrangement gave similar results suggesting that no supramolecular switching process is present.<sup>[24]</sup> Therefore, it has been put forward that the characteristics of such a ME device strongly depend on the molecule and the electrodes and their interfacial interactions.

Oligophenylenethiophene **30** self-assembled in a nanopore via thiol anchor-groups has been reported to have the potential of being used in molecular RAM cells between 260 and 190 K.<sup>[117]</sup> At lower temperature NDR behaviour becomes the prominent feature of the IV curve (see above). By comparison with other similar molecular rods with and without amino- and nitro-groups, it was concluded that a high and a low conductivity state, which can be read out between 0 – 1 V only appears, when the molecule has a nitro group attached to the middle aromatic ring. The exact mechanism of the storage effect is still under investigation.

### **2.3.4 Others**

Apart from the functions that have been presented in this chapter a couple of others including three-terminal devices have to be fulfilled by molecules, for instance logic gates, the function of a half-adder or of a (field-effect) transistor, to build ME computers based on current architectures. The synthesis of multi-terminated organic molecules has already been proposed and achieved.<sup>[118],[119]</sup> The biggest challenge at present, however, remains to assemble three-terminal devices, because it is very difficult to pattern three different electrodes at the nanometre scale using contemporary techniques.<sup>[4]</sup> The use of gate electrodes buried in the substrate has been proposed as one possible solution.<sup>[120],[121]</sup> While this approach does not allow for a third direct contact to the molecule, the gate electrode provides the opportunity to change the electrostatic potential inside the molecule by means of field effects.

## **2.4 Summary of Molecular (Scale) Electronics**

Several milestones of the emerging research area of ME have been presented in this chapter. Yet, most of the devices discussed herein should rather be considered as test systems at the basic research level to establish correlations between the molecular structure and the electron transport behaviour. Especially, problems of reproducibility and stability make the use of such devices in real-world quite unlikely. Maybe completely new, fault-tolerant architectures have

to be developed to overcome these problems. While the future applicability of ME devices still remains speculation, the concepts described underline the great potential for long-term applications due to the small, ultimate size of molecules, the low costs of production and the great variety of functionalised compounds accessible by organic synthesis.



### 3 Chemical and Physicochemical Methods

The following paragraphs will cover mainly aspects of reactions that were of central interest for the syntheses of the designed target structures. Especially metal–catalysed cross–coupling reactions for the assembly of rigid rod backbones will be discussed. Reactions required for the construction of carbon–sulphur bonds will also be described and additionally the rich chemistry of azo compounds, in particular their synthesis and some photophysical properties will be depicted. The chapter will close with a brief account on temperature–dependant (dynamic) NMR experiments as a tool for the determination of rotational barriers in organic compounds, for example aromatic amides or oligophenylenes.

#### 3.1 Metal–Catalysed Cross–Coupling Reactions

During the last thirty years cross coupling reactions (CCRs) of organic electrophiles **40** with organometallic reagents **41** (Figure 3–1) catalysed by transition metals have emerged as a very powerful tool to form carbon–carbon bonds as well as carbon–heteroatom bonds including C–nitrogen, C–oxygen and C–sulphur.<sup>[122]</sup> In this regard, the term cross coupling describes the reaction between two constitutionally different molecules to form a new cross–coupled product **42** as opposed to homo–coupling where two molecules of the same kind dimerise. Nowadays applications of this type of reaction can be found in various areas of chemistry.<sup>[123]</sup> While a couple of different transition metals can be employed as catalyst, like iron,<sup>[124]</sup> copper<sup>[125]</sup> and rhodium,<sup>[126],[127]</sup> the most prominent example found frequently in

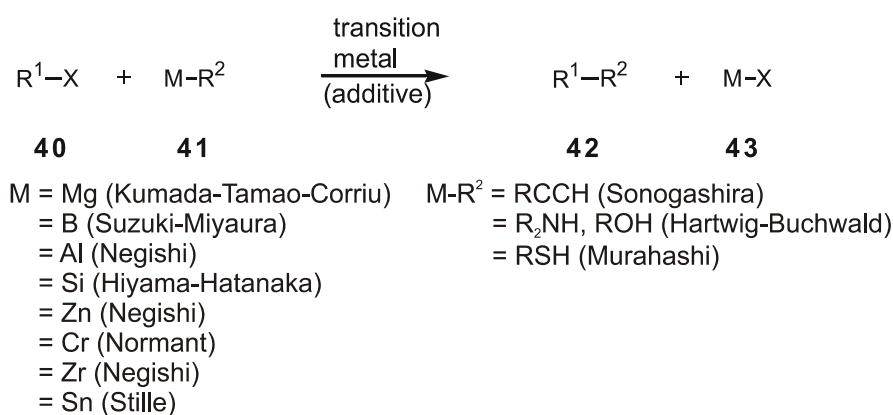


*Figure 3–1: Definition and overview of metal–catalysed cross–coupling procedures<sup>[123]</sup>*

literature is palladium followed by nickel.<sup>[128]</sup> Usually the yields in these reactions range between 70 to 100%. Figure 3–1 lists some of the most important metal–catalysed CCRs. Their classification has been done according to the nature of the organometallic species employed. The *Hartwig–Buchwald*–, the *Kumada–Tamao–Corriu*–, the *Negishi*–, the *Sonogashira*– and the *Suzuki–Miyaura* coupling were used in this work and will be described more comprehensively.

### 3.1.1 General Remarks

In 1972 the first reports about selective carbon–carbon bond formation using *Grignard* reagents and Nickel–catalysts were published almost simultaneously by *Kumada*<sup>[129]</sup> and by *Corriu*.<sup>[130]</sup> These discoveries are considered to mark the start of the field of metal–catalysed CCRs, because 1) the reactions were widely applicable due to the use of phosphine ligands, 2) cross–coupling products are favoured over homo–coupled species and 3) the idea of a catalytic cycle was proposed.<sup>[131]</sup> In the following years different researchers established that Mg can be exchanged for other metals, namely aluminium,<sup>[132]</sup> boron,<sup>[133]</sup> tin<sup>[134]</sup> or zinc.<sup>[135]</sup> Further studies suggested that palladium is somewhat superior to nickel, because less side–reactions were observed.<sup>[132]</sup> A lot of studies concerning the mechanism of this kind of reaction have been carried out in the last 30 years and as common sense CCRs follow a catalytic cycle that can be applied with minor changes to all types of reactions (Figure 3–2).<sup>[123],[128],[136]</sup>

Coordinatively unsaturated Pd(0) **44** is considered to be the catalytic active species in the cycle. If Pd(II) catalysts **45** are employed in the reaction, for example  $[\text{Pd}(\text{PPh}_3)_2\text{Cl}_2]$ , the catalytic active species is formed *in situ* by reduction with organometallics **41** (leading to homo–coupling products **46**) or with phosphines. In the next step Pd(0) inserts into the carbon–halogen (or –triflate) bond of the organic electrophile  $\text{R}^1\text{--X}$  (**40**) via oxidative addition giving a stable *trans*– $\sigma$ –palladium(II)–complex **47**. Transmetallation of the organometallic species  $\text{M--R}^2$  (**41**) leads to complex **48**. In the last step, reductive elimination produces the starting complex **44** and the desired cross–coupled product  $\text{R}^1\text{--R}^2$  **42**. The intermediates **47** and **48** have been isolated and characterised by spectroscopic analysis, respectively, proving their presence in the catalytic cycle. Besides, it has been deduced that either the oxidative addition or the transmetallation are the rate determining step.<sup>[137]</sup>

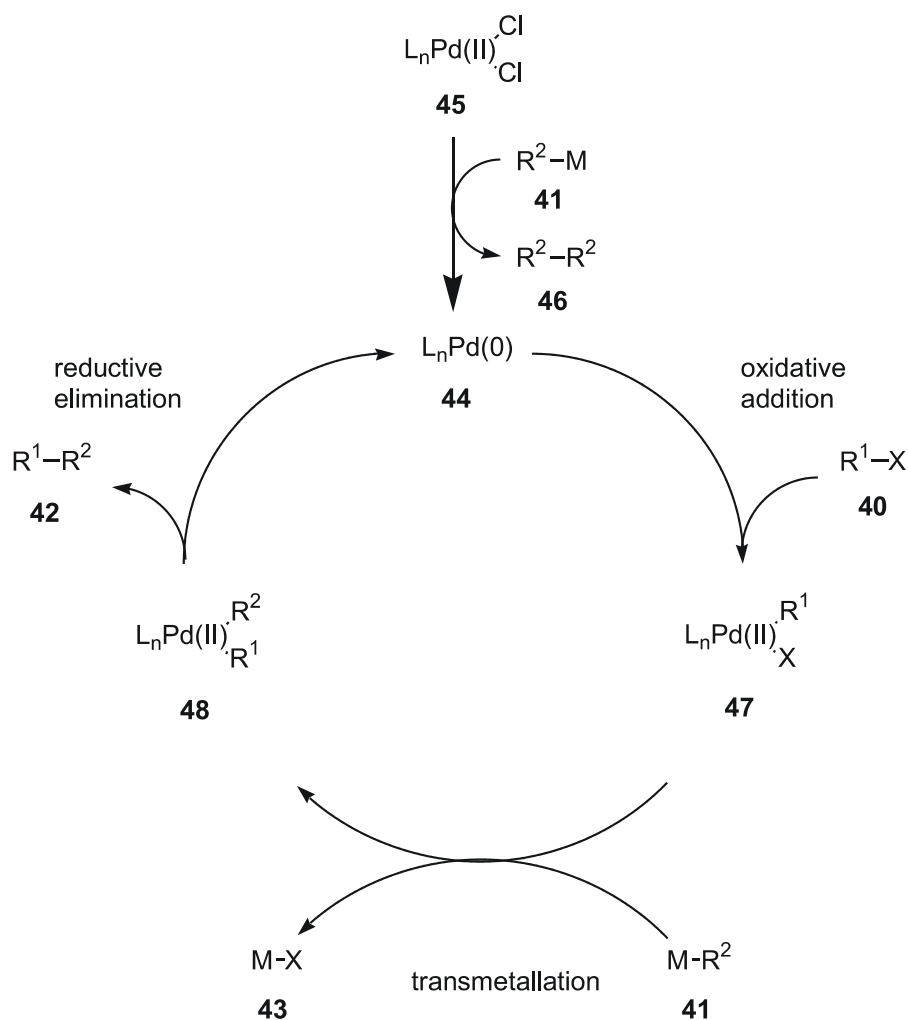


**Figure 3–2:** The proposed catalytic cycle for CCRs.<sup>[122]</sup>

The relative reactivity of the organic electrophile decreases in the order  $\text{I} > \text{OTf} > \text{Br} \gg \text{Cl}$  and electron-withdrawing groups near the reactive centre accelerate the reaction compared to electron-donating groups.<sup>[122]</sup> This observation has been mainly attributed to the considerably higher strength of the C–Cl bond (Table 3–1) hindering the oxidative addition to the Pd(0) species **44**. For the same reason electron-donating groups decrease the rate constant. Therefore, until recently, aryl chlorides were only employed in CCRs when electron-withdrawing groups or  $\pi$ -deficient heteroaromatics (called activated substrates) were present, although chlorides are usually cheaper and more readily available than other aryl halides.

Type of bond	Bond dissociation $D_{\text{Ph-X}}$ at 298 K kcal/mol	Bond dissociation $D_{\text{Ph-X}}$ at 298 K kJ/mol
Ph-F	126	528
Ph-Cl	96	402
Ph-Br	81	339
Ph-I	65	272

**Table 3–1:** Bond dissociation energies for halide substituted benzenes.<sup>[122]</sup>

However, the invention of new Pd–catalysts bearing sterically demanding phosphine–ligands facilitated the use of aryl chlorides as substrates.

In the following, the different kinds of cross–coupling reactions that were used during this work will be discussed largely ordered according to the reactivity of the organometallic species (Figure 3–3).<sup>[138]</sup>

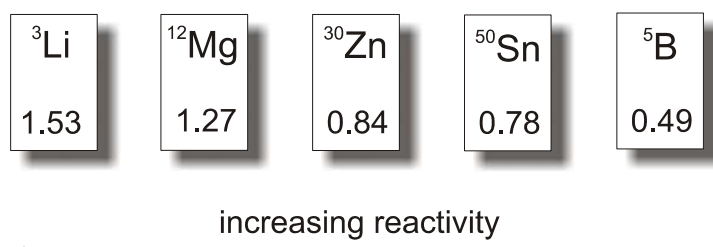


**Figure 3–3:** Typical metals used for the organometallic species of the CCR. The differences between the electronegativity of the metal and carbon are quoted (Allred–Rochow electronegativity scale).<sup>[138]</sup>

### 3.1.2 Kumada–Tamao–Corriu (KTC) Coupling

The reaction of *Grignard* reagents with organic halides under catalysis of various transition metal salts has long been known (*Kharasch* reaction), but was seldom used in organic synthesis, because it leads to mixtures of compounds including large amounts of homo–coupled products.<sup>[139]</sup> Therefore, it was not before the independent discoveries of *Kumada*<sup>[129]</sup> and *Corriu*<sup>[130]</sup> that this kind of reaction was considered as an interesting pathway for selective carbon–carbon bond formation. Reminding the discoverers this CCR is now called *Kumada–Tamao–Corriu (KTC)* coupling. It can be used for the cross–coupling of aryl and vinyl halides **40** to aryl, vinyl and alkyl *Grignard* reagents **49** using various nickel or palladium<sup>[140]</sup> catalysts (Figure 3–4). The rarely used reaction of Li–organic compounds with organic halides is also named *KTC* coupling. Irrespective of the use of nickel or palladium catalysis, the mechanism of this coupling reaction is believed to follow the general catalytic

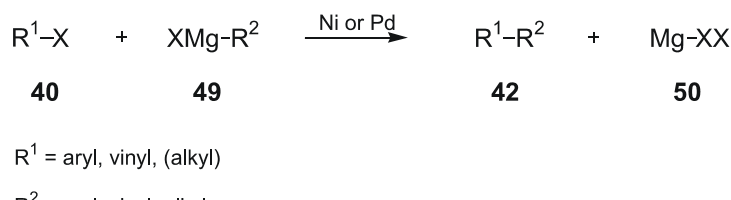
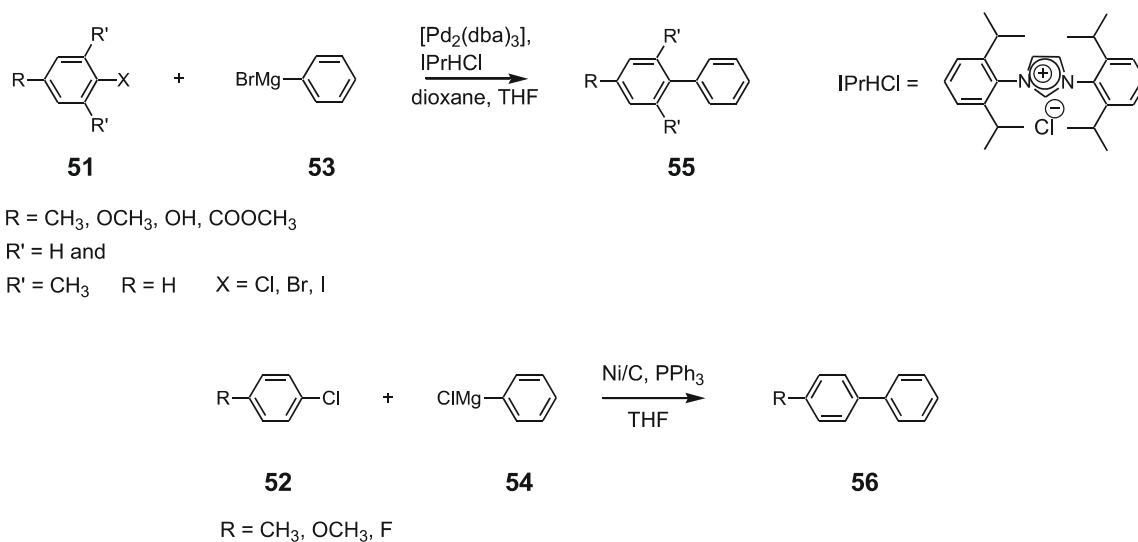


**Figure 3–4:** The Kumada–Tamao–Corriu Coupling.<sup>[128]</sup>

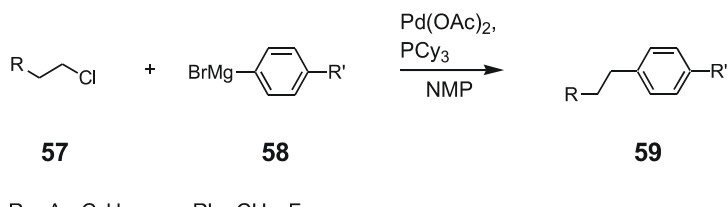
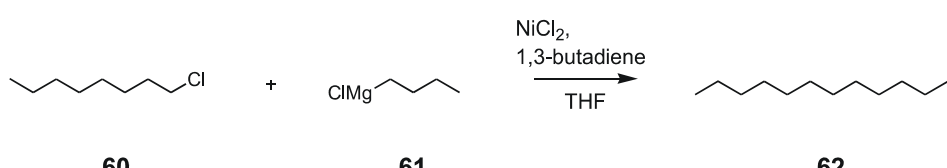
cycle (Figure 3–2) described earlier.

Interesting examples of the *KTC* coupling can be found in the synthesis of sterically hindered biaryls,<sup>[141]</sup> in the preparation of optically active compounds (by the use of chiral phosphine ligands)<sup>[142]</sup> and in the industrial application for the synthesis of *para*-substituted styrene derivatives.<sup>[143]</sup> The ease of synthesis of the *Grignard* substrate advantages the *KTC* protocol over other coupling reactions. Besides, compared to other CCRs it can readily be performed with chlorides as had already been shown in early work using nickel catalysis.<sup>[142]</sup> Sometimes even aryl fluorides can act as coupling partners.<sup>[144]</sup> In more recent work, fairly general procedures for the coupling of aryl halides **51** and **52** including unactivated aryl chlorides with aryl *Grignard* reagents **53** and **54** using a palladium/imidazolium chloride system<sup>[145]</sup> or nickel on charcoal<sup>[146]</sup> have been developed giving coupling products **55** and **56** in good yields (Figure 3–5). It is also possible to couple alkyl chlorides **57** to aryl *Grignard* reagents<sup>[147]</sup> **58** providing **59** and even to react alkyl chlorides **60** with alkyl *Grignards* **61** using 1,3-butadiene as ligand instead of phosphines with moderate to excellent yields (Figure 3–6).<sup>[148]</sup> However, at present there are no general methods for alkyl–alkyl coupling.<sup>[149]</sup>

The use of highly reactive and, hence less selective *Grignard* reagents represents the biggest disadvantage of the *KTC* coupling protocol, since it leads to a decreased tolerance of functional groups. Yet, work on highly functionalised organomagnesium reagents mainly done in the group of *Knochel* gives good indications that even this drawback can be overcome.<sup>[150]</sup> They showed that via halogen–metal exchange at low temperatures many more functional groups, like esters or nitro substituents, then previously thought seem to be



**Figure 3–5:** Examples of *KTC*–Coupling procedures using aryl chlorides(–bromides and –iodides) to form aryl–aryl bonds.<sup>[145],[146]</sup>

1) Alkyl-Aryl Coupling:2) Alkyl-Alkyl Coupling, eg:

**Figure 3–6:** Examples of alkyl–aryl and alkyl–alkyl couplings using the KTC protocol.<sup>[147],[148]</sup>

compatible with magnesium reagents opening the field for more general KTC couplings.

### 3.1.3 Negishi Coupling

The coupling of organic halides with zinc–organic substrates under the catalysis of nickel or palladium is called *Negishi* coupling.<sup>[123]</sup> Following the first report of *Negishi* and co-workers in 1977,<sup>[135]</sup> where only aryl– and benzylzinc derivatives were reacted with aryl bromides and iodides, the scope of the reaction has been extended to the coupling of alkynyl, aryl, vinyl and alkyl halides/triflates with alkynyl, aryl, vinyl and alkyl zinc substrates. Procedures using aluminium– and zirconium–organometallics are called *Negishi* coupling as well.

The main advantage of the *Negishi* coupling protocol compared to the KTC coupling is the tolerance of various functional groups on the organometallic species **63** and on the organic electrophile **64** providing the coupling product **65** (Figure 3–7).<sup>[151],[152]</sup> Besides, the synthesis of the zinc substrates can easily be achieved in different ways including the insertion into a

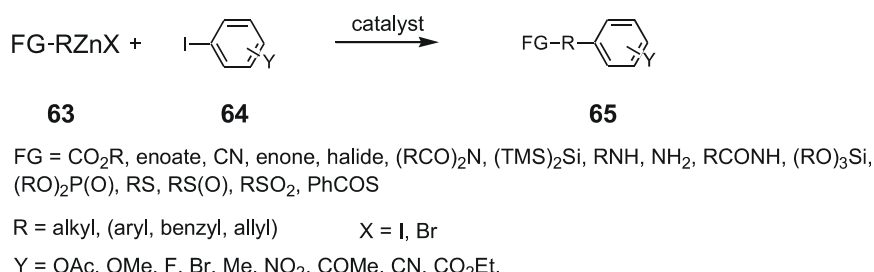


**Figure 3–7:** Variety of tolerated functional groups in the Negishi–cross coupling protocol.<sup>[151]</sup>

carbon–iodine bond using *Rieke* zinc<sup>[153]</sup> and the metathesis from *Grignard* derivatives<sup>[154]</sup> or organo–lithium compounds<sup>[155]</sup> with zinc–salts. Usually the organometallic species is not isolated, but used *in situ* for the CCR. Moreover, procedures employing Ni(0) as the catalytic active species, which is generally more reactive to unactivated aryl chlorides, are well established in literature. The low thermal and hydrolytic stability represents the main drawback of this cross–coupling protocol.<sup>[151]</sup>

Due to its high tolerance for functional groups the *Negishi* coupling is often used in the synthesis of natural products<sup>[151]</sup> or for applications in material chemistry, for example in the synthesis of polyphenylenes and –thiophenes.<sup>[156]</sup> Moreover, the *Negishi* coupling can sometimes be employed as a method superior to the *Sonogashira* coupling (see below) for the construction of polyethynyl–substituted aromatic compounds (Figure 3–8). In this case, the *Sonogashira* coupling protocol using hexaiodo–benzene **66** and TMS–acetylene **67** gave the desired hexa–coupled product **68** only in a yield of 1%, whereas the use of (less reactive) hexabromo–benzene **69** and an ethynylzinc species **70** using *Negishi* coupling procedures afforded the product in 64% yield. Hence the higher reactivity of the ethynylzinc derivative compared to ethynylcopper derivatives was utilised successfully.<sup>[157]</sup>

As for the *KTC* coupling, a lot of work has been devoted recently to the development of general procedures for coupling unactivated substrates such as aryl chlorides or alkyl chlorides or for establishing alkyl–alkyl coupling procedures (Figure 3–9). A rather general

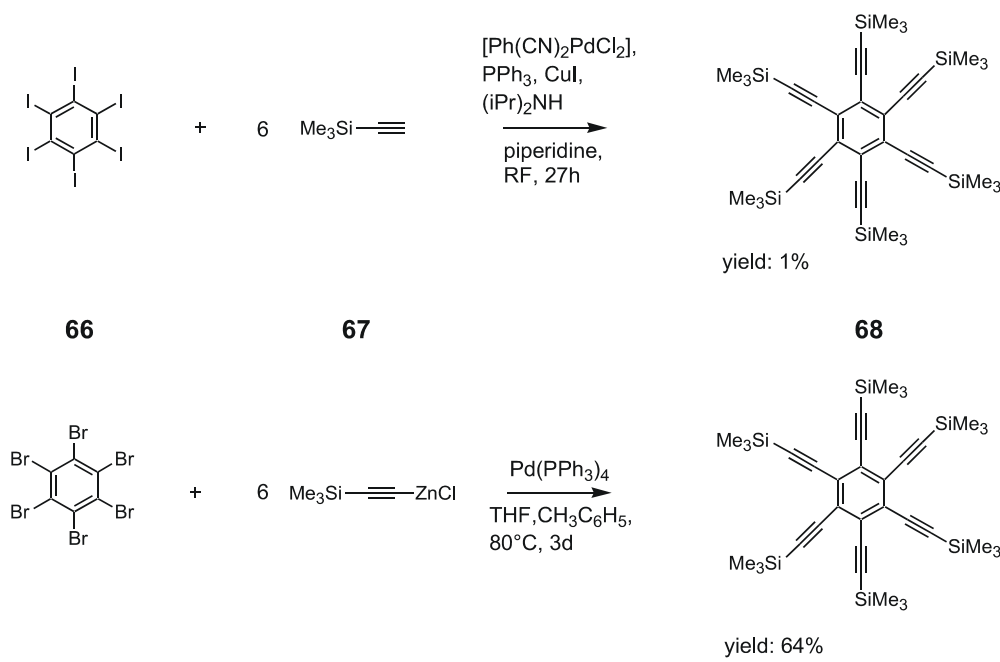
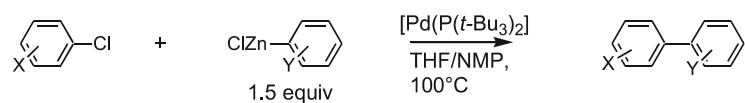


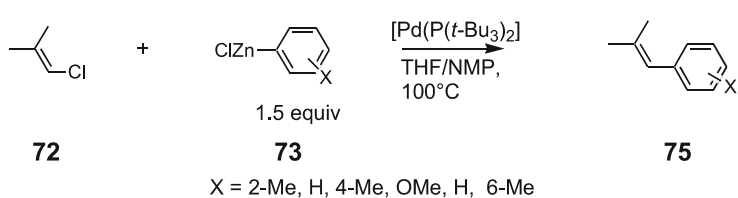
Figure 3–8: Superiority of the *Negishi*–cross coupling procedure over the *Sonogashira*–coupling.<sup>[157]</sup>

protocol developed by *Fu* and co-workers using the commercially available catalyst  $[\text{Pd}\{\text{P}(t\text{-Bu})_3\}_2]$  is now on hand and allows the coupling of aryl **71** and vinyl chlorides **72** to (sterically hindered) aryls **73** providing biphenyls **74** and vinyl substituted benzenes **75**, respectively.<sup>[154]</sup> Alkyl–alkyl couplings with alkylzinc iodides **76** and functionalised alkyl iodides **77** have been achieved with good yields using 4-fluorostyrene and tetrabutylammonium iodide as additives and Ni(0) as catalyst, which is assumed to be more effective in the reductive elimination step of the catalytic cycle.<sup>[138],[158]</sup> General palladium catalysed protocols for alkyl–alkyl coupling do not exist at present.<sup>[149]</sup>

(hindered) Aryl:



Vinyl:



Alkyl-Alkyl Coupling:

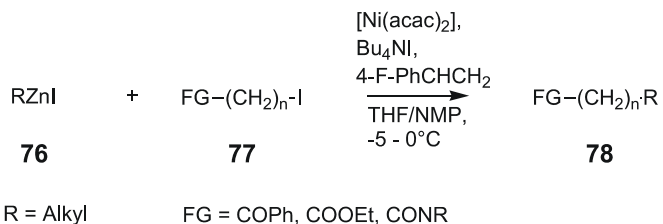


**Figure 3–9:** Examples of the Negishi–Coupling that allow the coupling of unactivated substrates.<sup>[154]</sup>

### 3.1.4 Stille Coupling

The reaction of aryl, vinyl or alkynyl halides/triflates with organotin compounds of alkynyls, aryls, vinyls or alkyls under palladium catalysis is called *Stille* coupling. It is mentioned here, because it has been widely used in organic synthesis due to the good functional group tolerance and the air and moisture stability of the organostannanes. Despite its frequent use in organic chemistry laboratories, the *Stille* coupling has not been applied on the industrial scale

owing to the extreme toxicity of organotin compounds.<sup>[159]</sup> No *Stille* couplings have been done during the course of this work.

### 3.1.5 Sonogashira Coupling

The *Sonogashira* Coupling, which can be considered as a hybrid of the *Stephens–Castro* and the *Heck* coupling protocol (figure 3–10), is routinely used for the reaction of substituted alkynyls with aryl iodides, bromides and triflates providing alkynyls **80**. The coupling to alkenyl electrophiles is also possible.<sup>[160]</sup>

The *Sonogashira* coupling differs slightly from the other procedures described above (Figure 3–11), because the organometallic species, here an organocopper compound, is produced *in situ* by using only catalytic amounts of copper(I) salts.<sup>[161]</sup> Consequently, the catalytic cycle is surrounded by additional cycles providing the activated copper species. However, the various roles of the copper(I) species are still under investigation.<sup>[162]</sup> Nevertheless, the proposed mechanism helps to explain various observations encountered in *Sonogashira* couplings. The main cycle A follows the general pattern found in all other CCRs consisting of a sequence of an oxidative addition to **82**, transmetallation of **83** with the organocopper species **84** and reductive elimination from **85** to give the product **80**. Presumably in a separate cycle B (and B'), the organocopper species **84** is produced. After transmetallation of **84** with **83** the copper(I) salt **86** is obtained, which can then be used again to yield the alkynylcopper. A base, usually an amine that has to be present in the reaction mixture traps the hydrogen halide that is produced during the formation of the organocopper compound giving **87**. Catalytic cycle B'

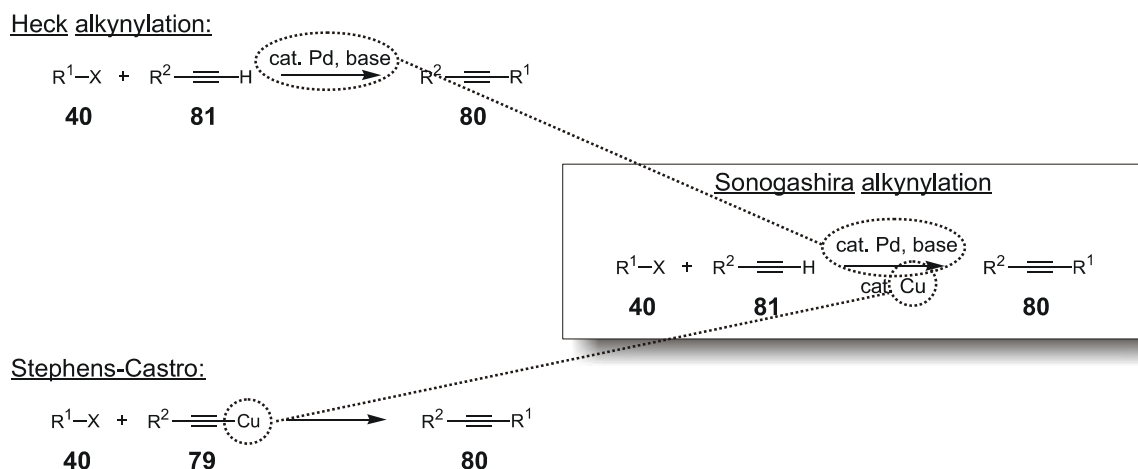


**Figure 3–10:** Development of the Sonogashira cross-coupling protocol from the Stephens–Castro– and the Heck alkynylation.<sup>[160]</sup>

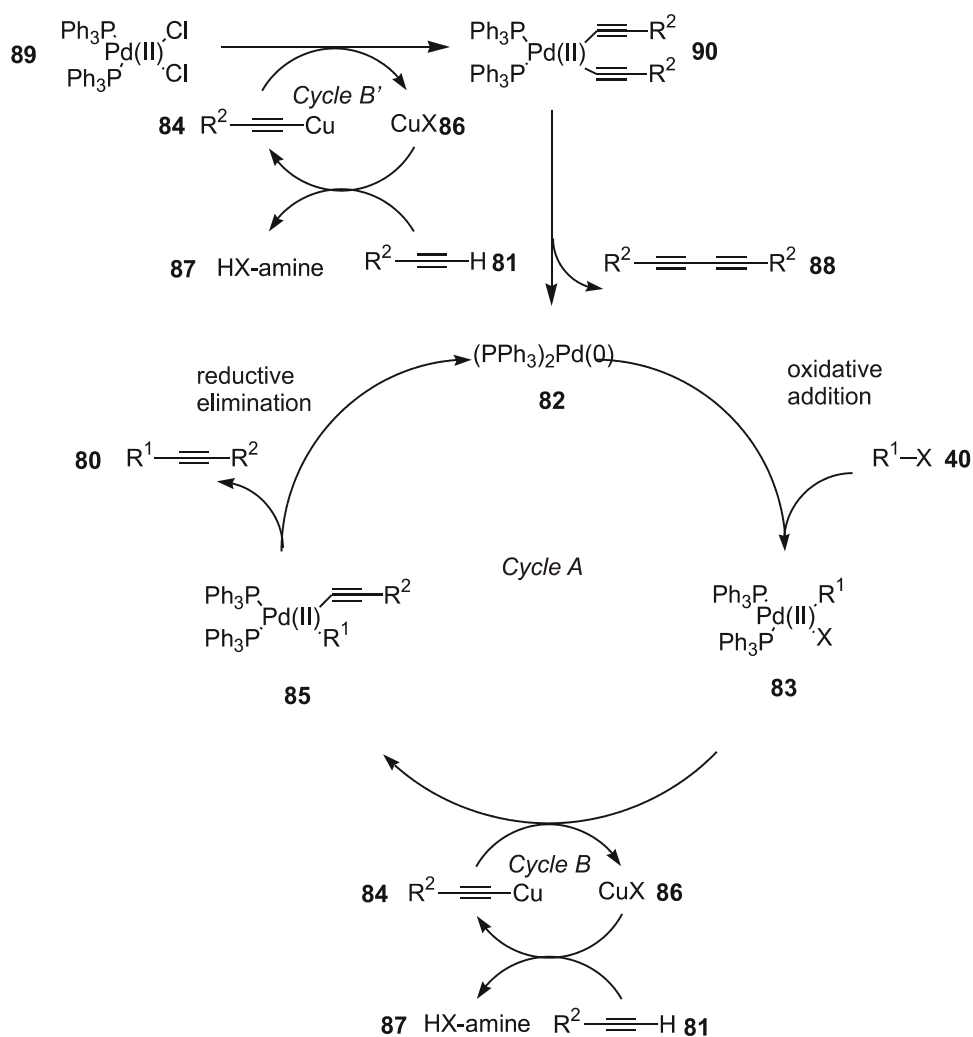


Figure 3–11: Proposed mechanism of the Sonogashira cross–coupling.<sup>[162]</sup>

explains the observation of homo–coupled dialkynes **88**, when Pd(II) **89** is employed as catalyst source via complex **90**. The reaction also proceeds without copper co–catalyst, but usually under more vigorous conditions.

The *Sonogashira* coupling has been extensively applied in the synthesis of molecular organic materials, especially molecular wires (see also Chapter 2) and of pharmaceutical products like antibiotics.<sup>[163]</sup> While other CCRs, for example the *Negishi* or the *Stille* coupling, also offer the opportunity to introduce functionalised alkynyls, the *Sonogashira* coupling is most widely used, because of usually good yields and easy application, which does not require isolation of organometallics.<sup>[160]</sup> A couple of limitations should, however, be mentioned. The *Sonogashira* coupling frequently fails when sterically demanding substrates are used (eg. Figure 3–8) and often gives low yields with alkynes bearing electron–withdrawing groups (Table 3–2).<sup>[160]</sup> Furthermore, a general protocol for *Sonogashira* couplings involving cheap and readily available (unactivated) aryl chlorides has not been developed yet, although some first examples of reactions with aryl chlorides **91** and **92** have been described (figure 3–

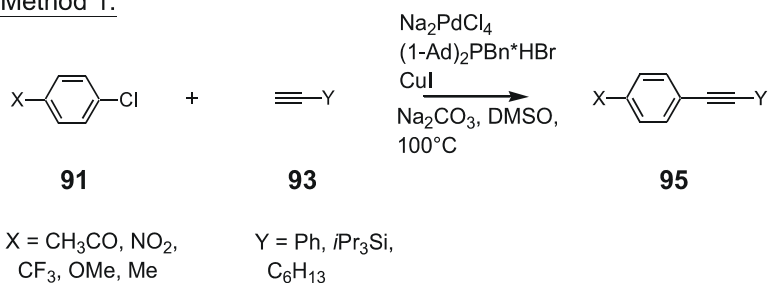
Alkyne	Organic Electrophile	yield (%) in	
		Sonogashira	Negishi
MeOOC—M	IPh	98	95
MeOOC—M	IC <sub>6</sub> H <sub>4</sub> Br- <i>m</i>	33	91
HexOC—M	IPh	65	82
EtOOCC—M	(E)-IHC—C(Me)Hex	23	84

Table 3–2: Examples where the Sonogashira coupling fails to get high yields.<sup>[162]</sup>

12).<sup>[163],[164]</sup> At present, the most general protocol for this purpose has been reported by *Buchwald* and co-workers.<sup>[164]</sup> Their procedure allows the coupling of electron-rich and, to some extent, sterically hindered aryl chlorides **92** with ethynyls **94**, albeit at elevated temperatures of 70 – 90 °C, affording **96** with reasonable yields. Interestingly, they observed that the copper co-catalyst actually inhibits the reaction of aryl chlorides with terminal alkynes.

Alkynyl–alkynyl couplings are normally not performed by *Sonogashira* coupling, but using alternative procedures like the copper catalysed *Glaser* coupling that allows the oxidative homo-coupling and the copper catalysed *Cadiot–Chodkiewicz* reaction, which yields heterocoupled product of alkynes and 1–haloalkynes.<sup>[165]</sup>

Method 1:



Method 2:

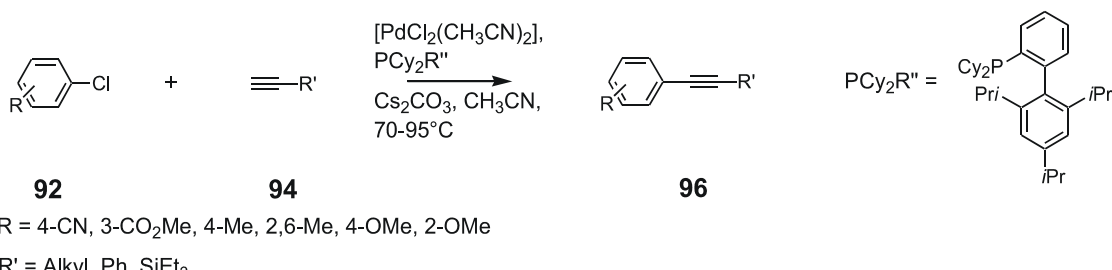


Figure 3–12: Examples of procedures employing aryl chlorides as substrates.<sup>[163],[164]</sup>

### 3.1.6 Suzuki–Miyaura (SM) Coupling

In 1979 the first publication of a *Suzuki–Miyaura (SM)* coupling named in honour of the discoverers appeared that describes the direct cross-coupling of an 1–alkenylboronic ester with 1–iodo–1–alkenes in the presence of a base.<sup>[166]</sup> Since then, the scope of the reaction has been extended to the coupling of various organic electrophiles including triflates and chlorides to a wide range of organoboron compounds (Figure 3–13).<sup>[137]</sup>

The main advantages of the *SM* coupling are seen in the properties of the organoboronic acids that are generally thermally stable, inert to water and oxygen and tolerate a lot of functional groups on the electrophile as well as on the organometallic species. Furthermore, organoboronic esters can also be employed in the coupling reaction. Due to the lower toxicity of organoboron species compared to organotin compounds the importance of *SM* coupling procedures in industrial processes is growing.<sup>[167]</sup>

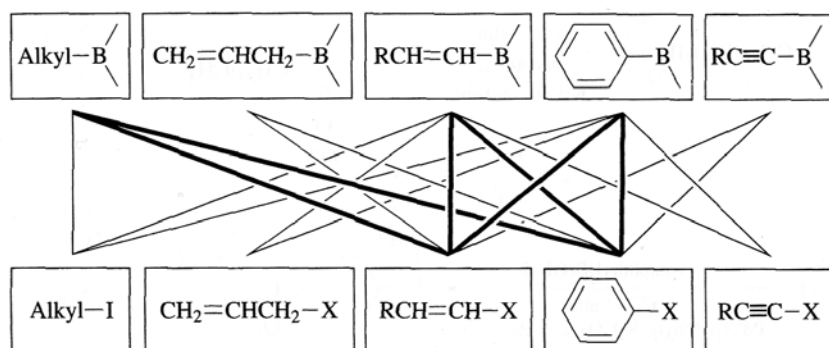


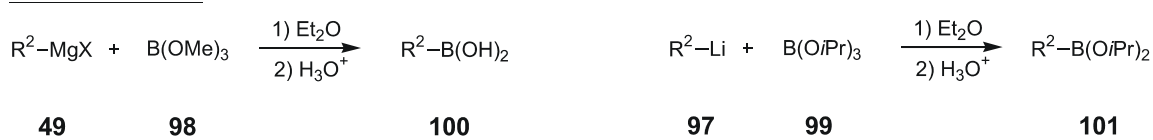
Figure 3–13: Scope of the Suzuki–Miyaura cross–coupling.<sup>[137]</sup>

#### 3.1.6.1 Preparation of Organoboron Compounds

The classical and generally efficient method for making boron compounds is based on the transmetallation of *Grignard* **49** or lithium reagents **97** with trialkylborates **98** or **99** giving organoboronic acids **100** (on acidification) or esters **101** (Figure 3–14). This protocol can be applied to organic compounds containing alkynyl–, alkenyl–, aryl– or alkyl–residues. Unfortunately, it does not tolerate a lot of functional groups.<sup>[168]</sup> Hydroboration of alkenes **102** and alkynes using 9–borabicyclo[3.3.1]nonane (9–BBN) (**103**) provides an alternative, usually very effective procedure to produce organoboron compounds **104** when alkyls or

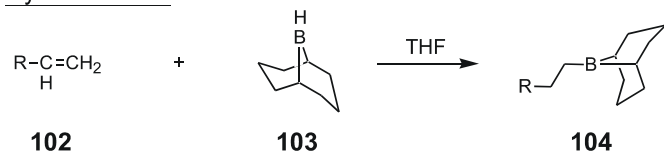
alkenyls are to be transferred in a CCR. An interesting procedure that allows the palladium catalysed borylation of alkynes using alkoxydiborons **105** has been first published by Suzuki and co-workers.<sup>[169]</sup> Later the reaction has been shown to work for alkenes and aryl halides **106** as well providing a one-step procedure for preparing aryl boronic esters **107**.<sup>[170]</sup> This approach is particularly useful, because a number of functional groups, for example esters, which are not compatible with *Grignard* or lithium reagents, can now be present in the organoboron compound, too. Besides, the alkoxydiborons are thermally stable and can be easily handled in air. Recently, a study has been published demonstrating the Pd-catalysed borylation of aryl halides and triflates using dialkoxyboranes **108**, which are more readily available than the diboron reagents.<sup>[171],[172]</sup> Apart from these synthetic pathways an increasing number of organoboronic acids becomes commercially available.<sup>[173]</sup>

Transmetallation:

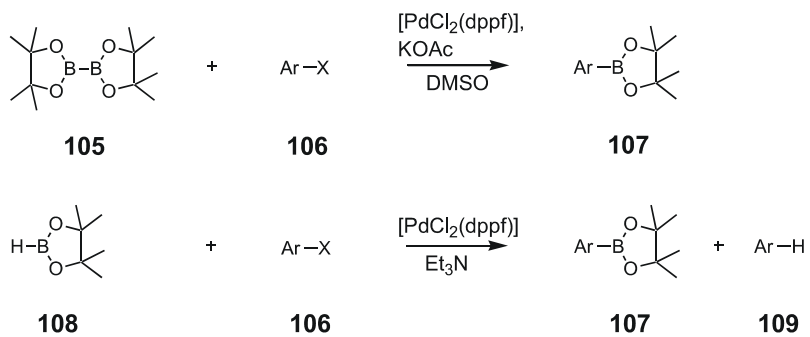


$\text{R}^2$  = alkynyl, alkenyl, aryl, alkyl

Hydroboration:



Palladium-catalysed Coupling, e.g.:



$\text{X} = \text{Br}, \text{I}, \text{OTf}$

**Figure 3–14:** Ways to prepare organo–boron compounds from different starting materials.<sup>[168],[170]</sup>

### 3.1.6.2 Mechanistic Considerations and Scope of the Reaction

The catalytic cycle of the *SM* coupling is assumed to comprise the usual oxidative addition–transmetallation–reductive elimination sequence.<sup>[174]</sup> However, organoboron compounds, which are quite inert to the organopalladium(II) halide **47**, only participate in the transmetallation step when a base is added to the reaction mixture. Three different processes, which seem to be highly dependant on organoboron reagents, bases and organic electrophiles used, have been proposed to explain this observation (Figure 3–15). According to path A the higher nucleophilicity of  $\text{RB}(\text{OH})_3^-$  (**110**) compared to  $\text{RB}(\text{OH})_2$  (**100**) allows the transmetallation with complex **47**. Path B assumes that **47** reacts with the base to give *in situ*  $\text{R-Pd(L}_n\text{-OR}$  (**111**), which is known to smoothly undergo transmetallation with organoboronic acids **100** forming complex **48** via a four-membered intermediate **112**. Path C proposes the direct formation of **111** from  $\text{Pd}(0)$  **44** and coupling partners like allyl phenoxides **113** in the absence of base.

The *SM* coupling is emerging as a favourite of the CCR<sup>[122]</sup> and has been widely used in the synthesis of organic electronic materials (see also Chapter 2),<sup>[77]</sup> natural product synthesis<sup>[175],[176]</sup> and even found industrial applications in the production of a *Merck* antihypertensive drug.<sup>[177]</sup> As for the others, recently a lot of attention has been paid to establish general procedures for the coupling to unactivated substrates like **114**. In 1999 two rather general protocols for the coupling of aryl boronic acids **115** have been published giving biphenyls **116** in yields higher than 90%.<sup>[178],[179]</sup> Furthermore, procedures for the reaction of organoboronic esters **105** with aryl chlorides bearing various functional groups exist (Figure 3–16).<sup>[180]</sup> The highly demanding coupling of two  $\text{sp}^3$ -centres has been achieved as well using a  $\text{Pd(OAc)}_2/\text{PCy}_3/\text{K}_3\text{PO}_4*\text{H}_2\text{O}$  system with yields between 66 – 93%.<sup>[181]</sup> Very recently, the

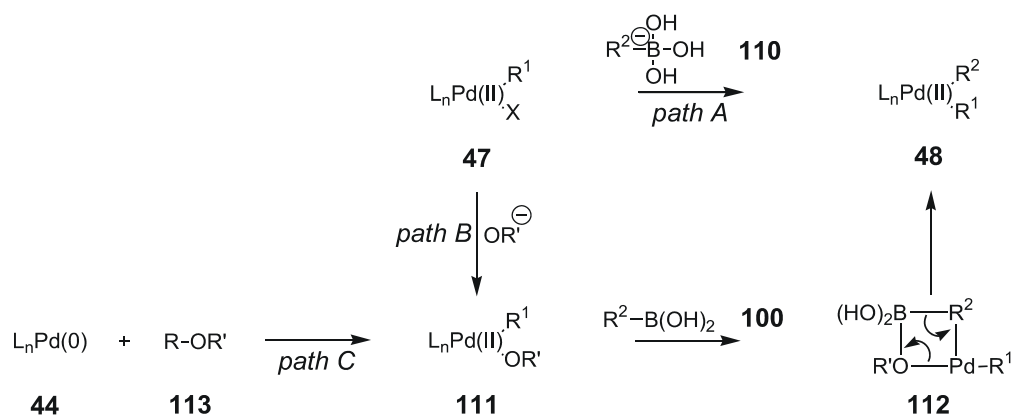


Figure 3–15: Proposed mechanisms for base–assisted transmetallation.<sup>[174]</sup>

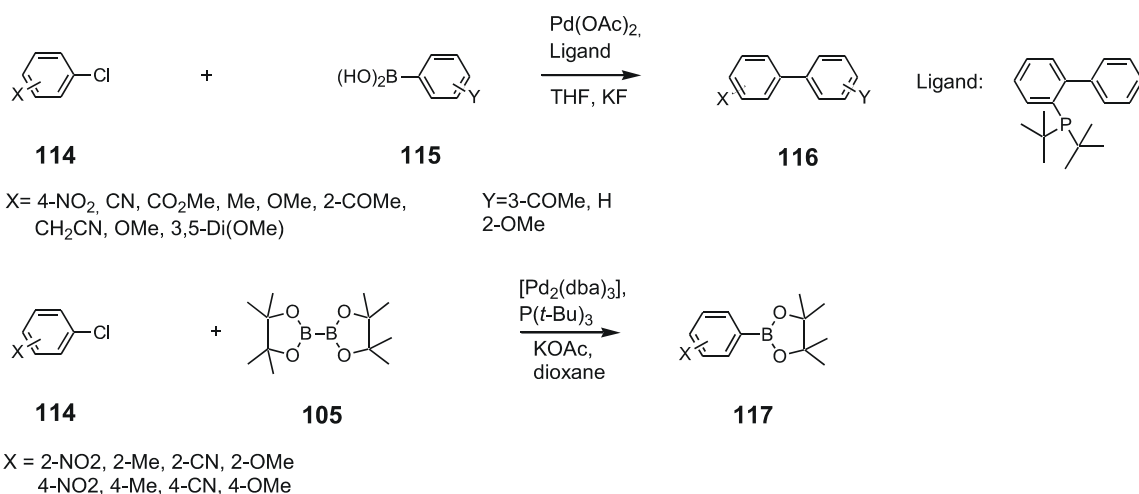


Figure 3–16: Examples of the Suzuki–Miyaura coupling using aryl chlorides as substrates.<sup>[178],[179]</sup>

SM coupling of unactivated secondary alkyl bromides and iodides could be shown, too.<sup>[182]</sup>

### 3.1.7 Hartwig–Buchwald (HB) Coupling

In 1983 *Migita* and co-workers reported the first palladium–catalysed formation of aryl C–N bonds.<sup>[183]</sup> But their synthetic protocol was limited by the use of thermally and moisture sensitive tributyltin amides. It was not before 1995 that the groups of *Hartwig*<sup>[184]</sup> and *Buchwald*<sup>[185]</sup> published results on tin–free amination of aryl halides using an alkoxide or silyl amide base, respectively. Since then, the scope of this reaction, which is now frequently called *Hartwig–Buchwald (HB)* coupling, has been expanded to the coupling of aryl halides and triflates to primary and secondary aliphatic and aromatic amines as well as certain ammonia equivalents and even amides and carbamates. Furthermore, the palladium–catalysed C–O bond formation giving aryl ethers is possible, though more challenging.<sup>[186]</sup>

Mechanistic studies that have been conducted hand–in–hand with the development of more versatile and efficient catalyst systems suggest a slightly different catalytic cycle as for the other CCRs (Figure 3–17).<sup>[136]</sup> The cycle starts with the oxidative addition of the aryl halide **106** to Pd (0) giving **118**. In path A direct displacement of the halide by the amide **119** affords the palladium(II) aryl amide **124** via intermediate **120**. Alternatively, **124** is formed via the intermediacy of a palladium (II) alkoxide **125** using **121**. Reductive elimination of the C–N bond, which was an unknown process prior the studies of *Hartwig* and *Buchwald*, yields the desired arylamine **126** and regenerates the Pd(0) species. Reduction of the aryl halide, that is

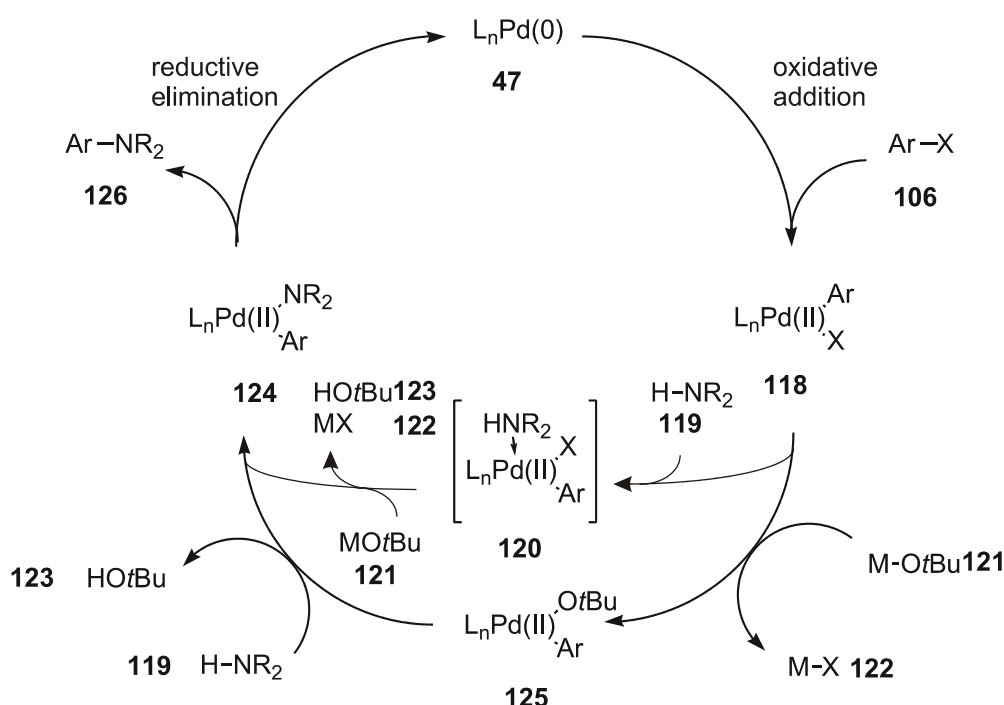
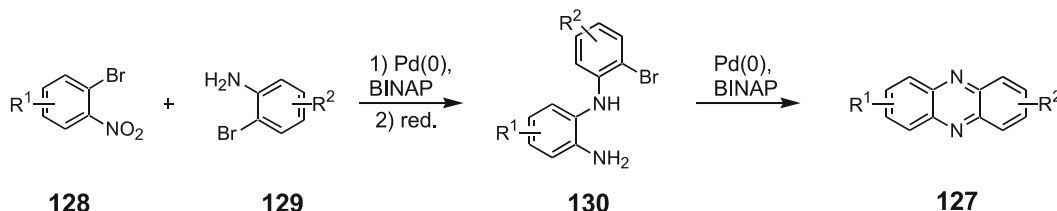
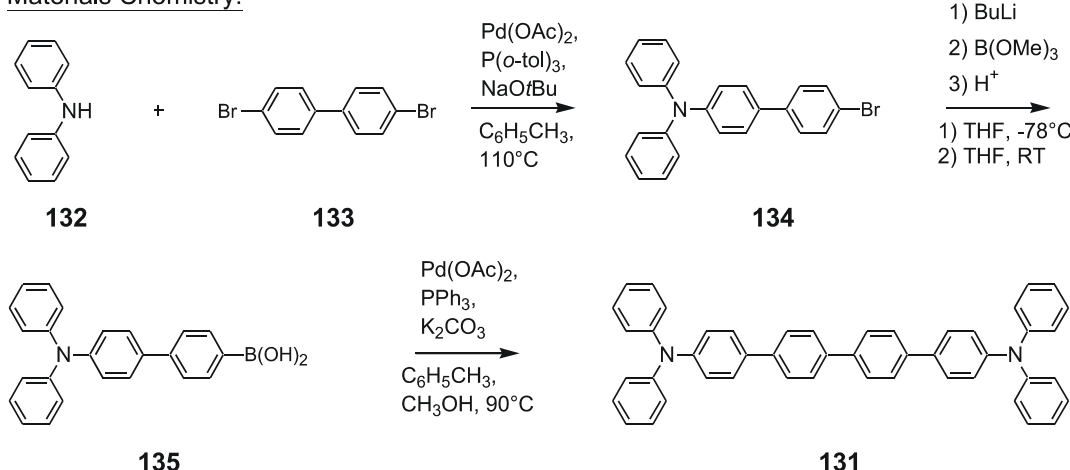


Figure 3–17: Mechanistic cycle of the Hartwig–Buchwald coupling procedure.<sup>[136]</sup>

formation of Ar–H, is the major side–product probably due to  $\beta$ –hydride elimination in the palladium amide.

Despite its rather recent invention the *HB* coupling has already found various applications in synthetic organic chemistry, because it tolerates more functional groups than the traditional pathways to alkylarylamines, that is reductive amination of aniline derivatives or arene nitration/reduction protocols.<sup>[186]</sup> For example, natural products<sup>[187],[188]</sup> such as **127** were prepared *via* a *HB* coupling of **128** with **129** or strongly luminescent oligophenylene<sup>[189]</sup> like **131** as an example from materials chemistry<sup>[190]</sup> were obtained (Figure 3–18). Here the pathway involved a *HB* coupling of amine **132** with **133** to give **134** followed by a *SM* coupling of boronic acid **135** to **134**. Particularly interesting is the arylation of ammonia equivalents to give unsubstituted primary anilines, which has first been reported by *Buchwald* in 1997, employing commercially available benzophenone imine.<sup>[191]</sup> Removal of the imine can be done by a transamination protocol, by hydrogenolysis using a palladium catalyst or by acidic hydrolysis. Alternative procedures to introduce –NH<sub>2</sub> exist as well.<sup>[192]</sup>

While the applicability of the *HB* coupling has been greatly improved in the last (almost) ten years, for instance to the use of aryl chlorides,<sup>[122],[178]</sup> mainly due to careful ligand design, continued efforts are necessary to widen the scope of the reaction further, for example to develop a general procedure for couplings at room temperature. It seems unlikely, though, that one ligand will be found that can effect the majority of important cross couplings.

Natural Products:Materials Chemistry:

**Figure 3–18:** Applications of the HB–coupling in natural products and materials chemistry.<sup>[188],[189]</sup>

### 3.1.8 Summary of Metal–Catalysed Cross–Coupling Reactions

This section portrayed some cross–coupling protocols that were the basis of syntheses carried out during this work to construct carbon–carbon as well as carbon–nitrogen bonds. Since almost 2000 publications in the last two years dealt with cross coupling procedures, a comprehensive coverage of the topic is impossible. Thus, this chapter focused on the procedures relevant for this work. Numerous CCRs of general importance like the *Hiyama–Hatanaka*, the *Heck* or the *Ullmann* coupling did not contribute in these investigations and are not discussed in detail. The palladium–catalysed cross coupling of organosilanes with organic halides and triflates, which has been described for the first time in 1988,<sup>[193]</sup> is commonly referred to as *Hiyama–Hatanaka* coupling. Furthermore, the *Heck* coupling, that is the palladium catalysed coupling of aryl and alkenyl halides with alkenes, has been extensively used in the preparation of novel polymers and especially natural products.<sup>[194],[195]</sup> The copper–catalysed *Ullmann* coupling, which can be used to form carbon–heteroatom bonds as well as carbon–carbon bonds<sup>[125]</sup> is another example.

## 3.2 Some Aspects of Organosulphur Chemistry

Generally, molecules containing one or more carbon–sulphur bonds are defined as organosulphur compounds.<sup>[196]</sup> Organosulphur compounds are used frequently in various areas of chemistry including agrochemicals such as the herbicide chlorsulfuron **136**,<sup>[197]</sup> pharmaceuticals like penicillin **137**,<sup>[198]</sup> additives in food chemistry, for example as sweeteners like saccharin **138** or dyes like Congo Red **139**<sup>[199]</sup> (Figure 3–19).<sup>[200]</sup> Furthermore, organosulphur compounds are of considerable biological significance occurring in many vital enzymes in plants and animals.<sup>[201]</sup> Owing to this great importance, the chemistry of organic molecules containing sulphur is well established and diverse. Here, only some selected aspects of this field of chemistry will be given focussing mainly on the syntheses of aromatic thiols ( $\text{R}-\text{SH}$ ), thioethers ( $\text{R}-\text{S}-\text{R}'$ ), sulphoxides ( $\text{R}-(\text{S}=\text{O})-\text{R}'$ ) and sulphylic acids ( $\text{R}-\text{SO}_3\text{H}$ ).

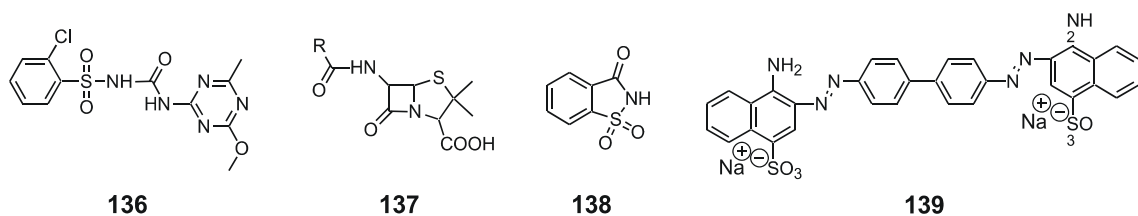


Figure 3–19: Some examples of organosulphur compounds.<sup>[196]</sup>

### 3.2.1 General Remarks

As sulphur lies just below oxygen in the periodic table, the chemistry of organosulphur compounds parallels that of the oxygen analogues in many aspects.<sup>[196]</sup> However, important differences exist. Due to the lowered electronegativity of sulphur compared to oxygen, the ionic character of organosulphur bonds is lessened accompanied by a reduced importance of hydrogen bonding. In addition, sulphur usually does not form “normal”  $\pi$ -bonds, that is  $\text{p}\pi-\text{d}\pi$  bonds are formed rather than  $\text{p}\pi-\text{p}\pi$  bonds.<sup>[202]</sup>

As a result of their expanded atomic structure, organosulphur compounds can react as nucleophiles and as electrophiles depending on the groups attached to the sulphur. Bearing electron-withdrawing groups like oxygen or halogen sulphur becomes an electrophilic centre, while alkyl-substituted sulphur-groups react as nucleophile. Generally, thiols are better

nucleophiles than alcohols. Sulphoxides can exist as optical enantiomers acting as directing groups in asymmetric synthesis.<sup>[203]</sup>

In the context of this work, the rather unique ability of sulphur–terminated molecules to self–assemble on noble metals, like e.g. gold was of great importance to provide an interface between molecular systems and nanoscale– or even macroscopic structures.<sup>[204],[205],[206]</sup> The success of this linkage is based on its ambivalence, the covalent Au–S bond is stable enough at room temperature for subsequent processing of the samples, but loose enough to allow dynamic processes like self–assembly on the surface.<sup>[38]</sup> However, only a limited number of functionalities like disulphides and acetyl–protected thiols, which are de–protected *in situ* on a gold surface, and free thiols can be used for self–assembly processes on gold.<sup>[61]</sup>

### 3.2.2 Synthesis of Thiols, Disulphides and Acetyl–protected Thiols

Thiols are sulphur analogues of alcohols and phenols.<sup>[196]</sup> Due to the larger size of sulphur and the decreased electronegativity compared to oxygen the strength of the bond between sulphur and hydrogen is lowered. Therefore, thiols are more acidic and form weaker hydrogen bonds. Of the various pathways to form thiols only the most important ones will be depicted here (Figure 3–20).<sup>[207]</sup> The first route, i.e. the reaction between organic halides **140** and metal thiolates **141**, can be employed to form alkyl and aryl thiols **142**, but the nucleophilic substitution of aromatic halides usually requires electron–withdrawing substituents.<sup>[208]</sup> The direct synthesis using sodium sulphide and subsequent acidic workup is possible.<sup>[207]</sup> However, side reactions can occur that lead to the formation of disulphides and symmetric thioethers. Thioether formation can be prevented when thiourea is used in the substitution reaction followed by hydrolysis. Tertiary thiols **146** are prepared more readily by addition of hydrogen sulphide **145** to a suitable alkene **144** (Figure 3–20 route 3). Route 2 describes a procedure that is normally applied to the synthesis of aromatic thiols starting from aryl–lithium or aryl *Grignard* **147** compounds.<sup>[209]</sup> It is important to use stoichiometric amounts of sulphur, because otherwise polysulfanes, that is compounds containing sulphur–sulphur chains, are obtained.<sup>[210]</sup> These S–S bonds have to be reduced in a second step using zinc in acidic media to get free thiols. Thiophenols **150** can also be produced very effectively by reduction of sulphonyl chlorides **149**,<sup>[211]</sup> which in turn can be prepared by electrophilic aromatic substitution (see below). Usually zinc or a reduction system consisting of zinc

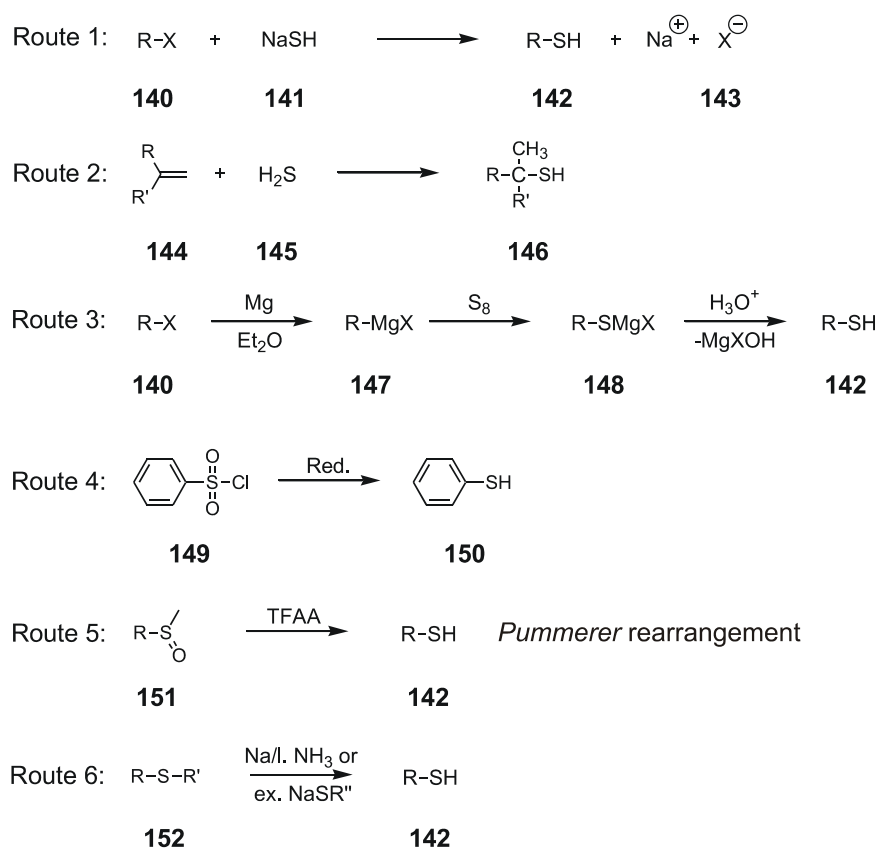


**Figure 3–20:** Most important pathways to thiols.

together with dichlorodimethylsilane–dimethylacetamide<sup>[212],[213]</sup> can be used for this purpose. Reduction of disulphides using zinc in acidic media, in particular acetic acid, or lithium aluminiumhydride also leads to the formation of thiols. Other methods include the use of diazonium salts with thiourea,<sup>[214]</sup> the *Pummerer* rearrangement of sulphoxides **151**,<sup>[215]</sup> the reaction of thioethers **152** with sodium in liquid ammonia<sup>[216],[217]</sup> or with an excess of sodium alkylthiolates (see below).<sup>[218]</sup>

Unfortunately, free thiols, especially thiophenol containing compounds, tend to the formation of disulphides in the presence of oxidation agents like traces of oxygen.<sup>[219],[220]</sup> Various methods for the controlled synthesis of disulphides exist in literature including oxidation agents like  $\text{H}_2\text{O}_2$ , iodine or iron(III)compounds.<sup>[219]</sup> Aromatic thiols oxidise more easily than primary alkyl thiols, and these easier than secondary and tertiary thiols. Molecules that are sulphur–functionalised on both ends like **153** have a tendency to form polymers **154** (Figure 3–21).

A very interesting alternative to free thiols are acetyl–protected thiols **155** that are formed by nucleophilic substitution at acid chlorides or anhydrides **156** (Figure 3–22).<sup>[221]</sup> Acetyl–protected thiols can be cleaved *in situ* on a gold–surface resulting in self–assembled monolayers.<sup>[61]</sup> However, S–acetyl derivatives do not tolerate harsh reaction conditions<sup>[222]</sup>

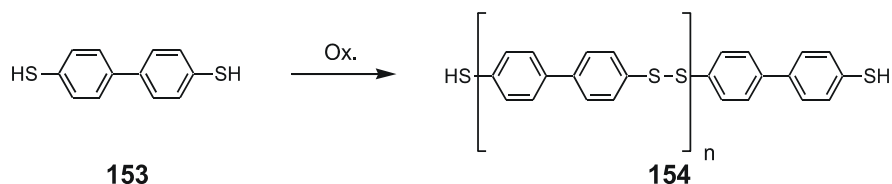


**Figure 3-21:** Polymerisation via S–S bond formation of compounds bearing two terminal thiol functionalities.

and consequently, synthetic strategies to exchange more stable protection groups for the acetyl protection group towards the end of a synthetic pathway are very promising. S-*tert.*-butyl groups are stable to acidic and basic reaction conditions and hence an ideal precursor of an acetyl-protected thiol.<sup>[223]</sup> Furthermore, *tert.*-butyl thiol groups can easily be introduced into target structures (see below). Two methods for the conversion S-*tert.*-butyl **157** to S-acetyl **155** have been reported, both being somewhat limited in application by the use of strong *Lewis* acids like AlCl<sub>3</sub><sup>[224]</sup> or BBr<sub>3</sub>.<sup>[225]</sup> Another method developed mainly by Blaszczyk uses bromine in acetic acid and acetyl chloride to convert the *tert*.-butyl-group to the acetyl-protection group.<sup>[226]</sup>

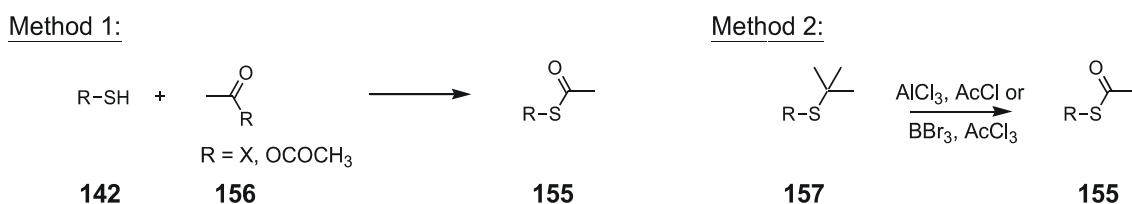


**Figure 3–22:** Methods for the preparation of acetyl-protected thiols.<sup>[225]</sup>

### 3.2.3 Synthesis of Thioethers

Thioethers or sulphides are sulphur analogues of ethers and like these can be either symmetrical ( $R_2S$ ) or unsymmetrical ( $R-S-R'$ ).<sup>[196]</sup>

Symmetrical alkyl or benzyl<sup>[227]</sup> thioethers **159** can be obtained by action of sodium sulphide **158** on the corresponding halides in yields of 70 – 90%, a reaction similar to the *Williamson* ether synthesis (Figure 3–23). Aromatic thioethers can only be synthesised using this pathway when electron-withdrawing groups like nitro-groups are present. However, nitro-groups can be substituted as well.<sup>[228]</sup> The alkylation of alkyl or aryl thiols with **160** is the most frequently used method to obtain unsymmetrical thioethers **152**. Of course this alkylation step can also be done instead of the hydrolytic step in route 2 of the described thiol syntheses.<sup>[196]</sup> Hence,

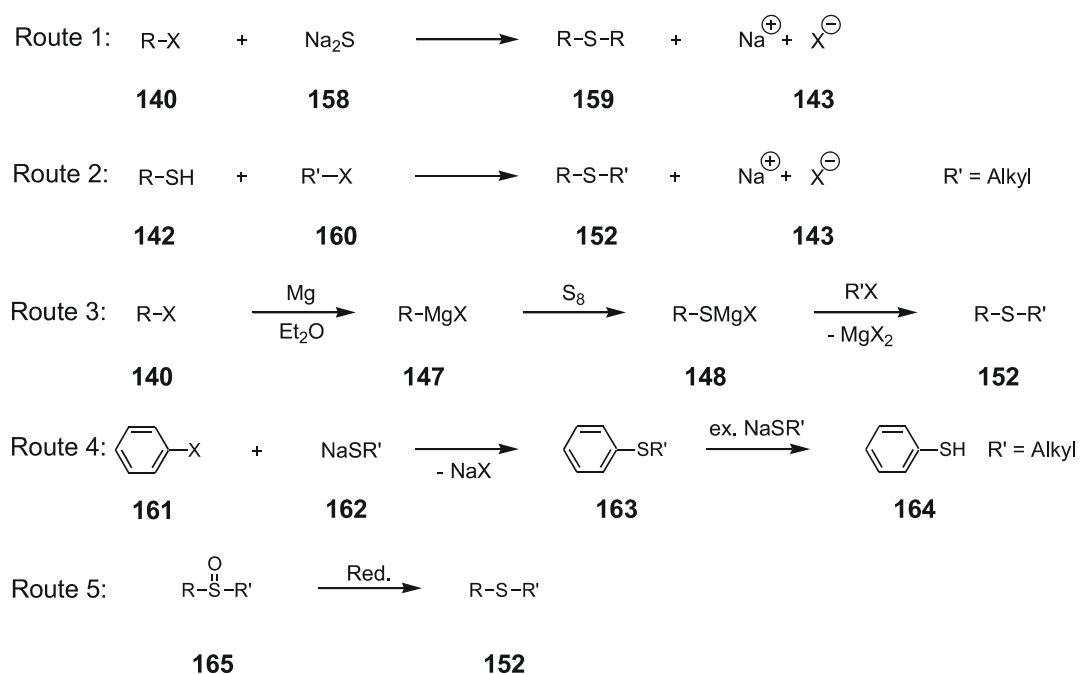


**Figure 3–23:** Most important synthetic procedures for thioethers.

Grignard compounds **147** can be employed as starting material to get thioethers **152** as well. Aromatic diazonium salts are converted to thioethers using sodium alkylthiolates, but care should be taken, because the intermediately formed diazosulphanes are often highly explosive.<sup>[229]</sup> This disadvantage can be overcome when arenediazonium *o*-benzenedisulphonimides in anhydrous methanol are used.<sup>[230]</sup>

Nucleophilic aromatic substitution reactions of unactivated aryl halides **161** with sodium thiolates **162** have to be performed in polar aprotic solvents like hexamethylphosphoric triamide (HMPTA),<sup>[231]</sup> dimethylformamide (DMF) or 1,3-dimethylimidazolidinone (DMI) at temperatures between 80 – 180 °C.<sup>[232]</sup> Usually good yields of alkyl aryl thioethers **163** between 70 – 90% are observed. In general in aromatic compounds, fluorine is displaced much more easily than bromine and iodine, and iodine is substituted faster than chlorine.<sup>[231]</sup> It was found that the reaction most probable proceeds by a classical S<sub>N</sub>Ar mechanism, because azobenzene did not have an effect on the reaction rate ruling out the S<sub>RN</sub>1 mechanism. Different alkyl thiolates including methyl-, isopropyl or *tert*.-butyl-thiolates can be employed. As mentioned above, aryl-*tert*.-butyl-sulfides are of particular interest, since the *tert*.-butyl group can be converted to the acetyl group in one step.<sup>[224],[225]</sup> Interestingly, an excess of NaSMe leads to the formation of thiols **164** in yields higher than 70% at high temperatures. The reaction proceeds in two steps: 1) the halogen of the aromatic ring is replaced by a SMe group following the pathway of a nucleophilic aromatic substitution; 2) the thiomethyl group is nucleophilically attacked by the excess of SMe<sup>−</sup> resulting in

demethylation.<sup>[233]</sup> Comparable results can be obtained using NaSiPr or NaStBu at temperatures of 160°C.<sup>[218]</sup> Often the substitution of aromatic halides with alkyl thiolates can be improved by adding catalytic amounts of Cu<sub>2</sub>O to the reaction mixture.<sup>[234]</sup> The copper-mediated formation of alkyl and aryl thioethers that tolerates a number of functional groups such as amino-, nitro-, methoxy- and ester-groups is called *Ullmann coupling*.<sup>[125]</sup> Usually good to excellent yields of the thioether compound can be obtained. An alternative synthetic strategy is the reduction of symmetric or unsymmetric sulphones **165** using reducing agents like palladium with H<sub>2</sub> or LiAlH<sub>4</sub> yielding the corresponding thioethers **152**.<sup>[196]</sup>

### 3.2.4 Synthesis of Sulphoxides, Sulphones and Sulphonic Acids

The valency of sulphur is not limited to two due to the presence of vacant 3d-orbitals in its outer shell. Hence, hypervalent compounds can be formed.<sup>[196]</sup> Furthermore, in oxidation reactions the oxidation site will be sulphur and not carbon.

Consequently, the classical and most widely used procedure to sulphoxides **165** involves oxidation of thioethers using highly selective oxidising agents, because otherwise over-oxidation to sulphones **166** will occur (Figure 3–24).<sup>[235]</sup> Old methods use hydrogen peroxide in the presence of different additives, nowadays sodium *meta*-periodate or *meta*-chloroperbenzoic acid (mCPBA) is most frequently employed.<sup>[236]</sup> However, care needs to be taken to avoid the formation of sulphones.<sup>[215]</sup> Very selective methods where the reaction stops on the stage of the sulphoxide, for example using benzyltriphenylphosphonium peroxyomonosulphate have been reported.<sup>[237]</sup> Chiral oxidation agents may give chiral sulphoxides.<sup>[203]</sup>

Sulphoxides containing at least one α-hydrogen like **151** can be converted to α-acetoxy sulphides via a *Pummerer* rearrangement using acetic anhydride (Figure 3–25).<sup>[91]</sup> First, an intermediate acylsulphonium ylide **168** is formed, which decomposes to a sulphur-stabilised



Figure 3–24: Possible routes to sulphoxides and sulphones.

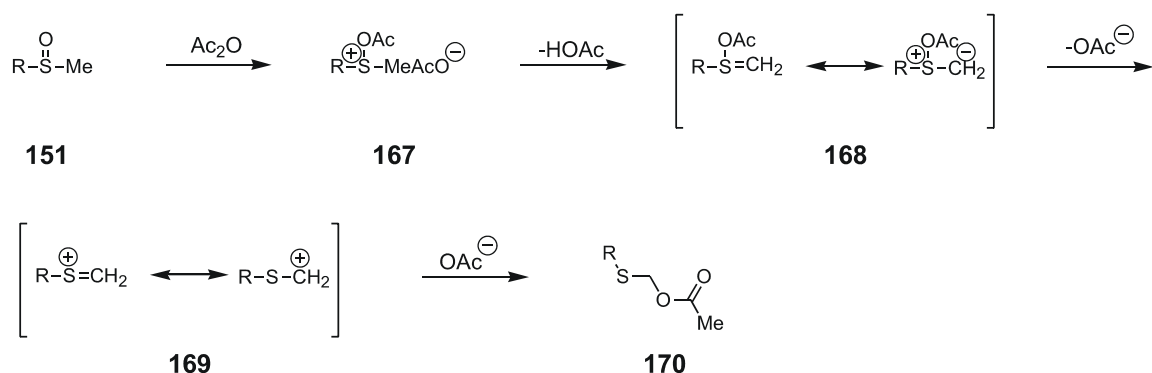


Figure 3–25: Mechanism of the Pummerer rearrangement.<sup>[196]</sup>

carbocation **169**. Then **169** is converted to the  $\alpha$ -acetoxy sulphide **170** resulting overall in a reduction of sulphur accompanied by an oxidation at the  $\alpha$ -carbon atom. When the rearrangement is performed with trifluoroacetic anhydride (TFAA) and methyl aryl sulphides the corresponding  $\alpha$ -acetoxy sulphide can readily be hydrolysed to the free thiol using a base such as triethylamine.<sup>[215]</sup> Hence, sulphoxides are interesting precursors for thiols.

As already mentioned sulphones are easily obtained by oxidation of thioethers using oxidizing agents like peroxycarboxylic acids (Figure 3–24).

Sulphonic acids **172** can be obtained by direct sulphonation of aromatic and sometimes of aliphatic substrates using sulphuric acid (Figure 3–26).<sup>[238]</sup> With arenes the reaction follows the pathway of an electrophilic aromatic substitution with  $\text{SO}_3$  as sulphonating agent.<sup>[196]</sup> The sulphonation reaction is reversible. An excess of chlorosulphonic acid as sulphonating agent will lead to the formation of sulphonyl chlorides **173**, which can also be obtained by the action of thionyl chloride on sulphonic acids.<sup>[239]</sup> These are interesting reactions to build carbon–sulphur bonds, because the obtained sulphonic acids or chlorides can easily be reduced to get free thiols.

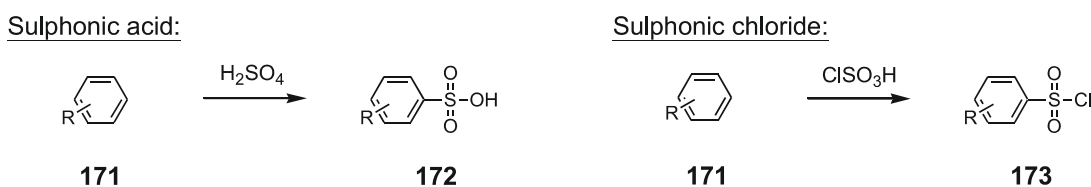


Figure 3–26: Possible routes to sulphonic acids and sulphonyl chlorides.

### 3.2.5 Others

Organosulphur compounds are known catalyst poisons due to their strong coordinating and adsorptive properties. Therefore, the metal–catalysed construction of carbon–sulphur bonds has been developed only recently.<sup>[240]</sup> The first palladium catalysed reaction between aryl bromides and iodides and alkyl and aryl thiols in the presence of sodium *tert*.–butoxide has been reported by *Migita* and co–workers.<sup>[241]</sup> Since then, the scope of the reaction has been extended to coupling to alkenes<sup>[242]</sup> and alkynes.<sup>[243]</sup> However, further research needs to be done to establish procedures for more general pathways. Besides, various other reactions exist to build carbon–sulphur bonds that were not used during this work.<sup>[196],[228],[219],[238]</sup>

### 3.2.6 Summary of Organosulphur Chemistry

A selection of reactions to build carbon–sulphur bonds has been described. In particular, the most widely used syntheses of thiols and acetyl–protected thiols have been depicted, because these groups are known to form covalent bonds when brought into contact with a gold surface. Thereby, organic molecules can be anchored on gold substrates providing a defined interface between nanostructures and macroscopic systems.

## 3.3 Chemistry and Physical Properties of Azo–Compounds

Azo compounds contain two symmetrically or asymmetrically substituted nitrogen atoms that are fused by a double or triple bond.<sup>[244]</sup> In 1834 *Mitscherlich* described the synthesis of red crystals by the action of alcoholic, caustic potash on nitrobenzene, which he analysed to be C<sub>12</sub>H<sub>10</sub>N<sub>2</sub>, that is azobenzene.<sup>[245]</sup> In the following years especially *Hantzsch*<sup>[246]</sup> and *Bamberger*<sup>[247]</sup> studied the properties and reactions of azo–compounds more thoroughly.

Azo compounds are extensively used as dyes for textiles and a lot of work has been devoted to the thermodynamics and kinetics of the dyeing process.<sup>[248]</sup> In addition, azo–compounds are employed as titration indicators in analytical chemistry. Furthermore, azo compounds can be found as colorants for ink–jet printers and are used as pigments, for instance in paint.<sup>[199]</sup>

More recently, research has been conducted to evaluate the potential of azo-compounds as functional components in catalysis,<sup>[249]</sup> in optical storage media,<sup>[250]</sup> in supramolecular chemistry<sup>[251],[112],[252]</sup> and in polymer chemistry.<sup>[253],[254]</sup>

### 3.3.1 Overview of Synthetic Procedures

The best known and most widely used method to build the azo functionality is the electrophilic substitution of aryl diazonium–ions with electron–rich aromatic compounds, the azo–coupling (Figure 3–27).<sup>[199]</sup> Due to steric hindrance the substitution mainly occurs in *para*–position to the activating group. Since the reaction follows the pathway of an electrophilic aromatic substitution, *ortho*–substitution can be found only when the *para*–position is blocked.<sup>[255],[239]</sup> In the first step, an aromatic or heteroaromatic primary amine **174** is reacted with sodium nitrite and mineral acid at 0 °C to give the corresponding diazonium salt **175**. It is essential to destroy any excess nitrite, because it tends to destabilise the diazonium ion or can induce subsequent coupling reactions. Usually nitrosamines are formed as intermediate in the reaction. In the second step, **175** attacks the coupling component **176** following the pathway of an electrophilic aromatic substitution (Figure 3–27). Unfortunately, since diazonium compounds are relatively weak electrophiles, only rather nucleophilic arenes can be employed, that is arenes bearing electron–releasing substituents.<sup>[199],[239]</sup>

In addition, several procedures to build azo-compounds **180** by oxidative methods starting from primary amines **178**<sup>[256],[257],[258]</sup> or by reductive methods starting from nitro compounds

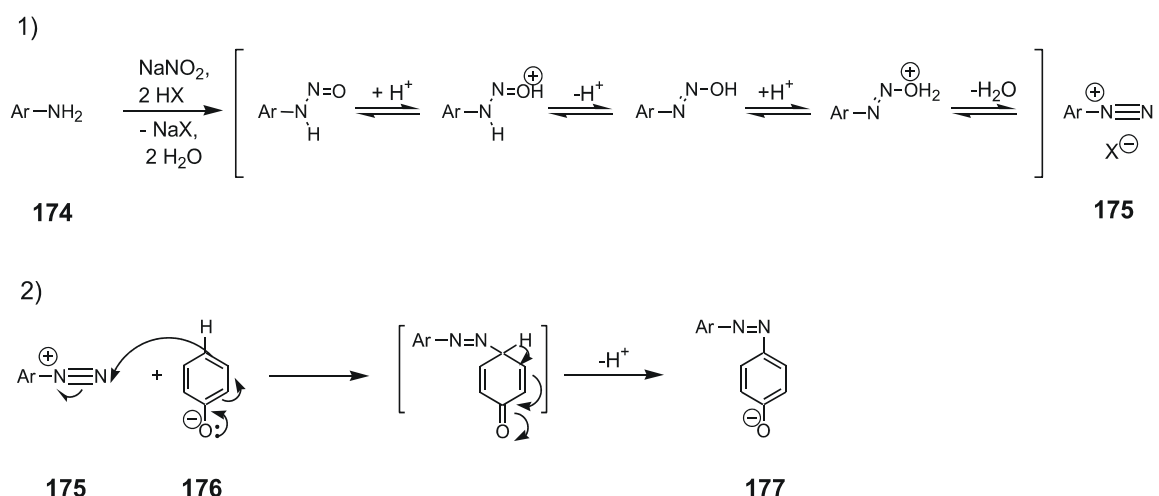


**Figure 3–27:** Mechanism of the azo-coupling including 1) the formation of the diazonium salt and 2) the electrophilic aromatic substitution.<sup>[239]</sup>

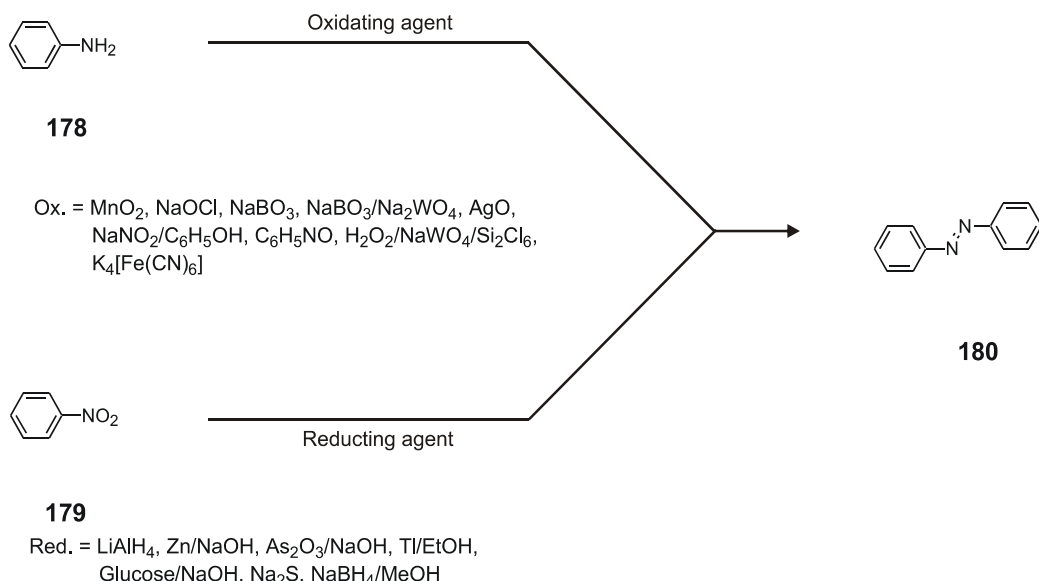


**Figure 3–28:** Oxidative and reductive methods to prepare azobenzene.<sup>[260]</sup>

**179** can be found in literature (Figure 3–28).<sup>[259],[260]</sup> It is complicated, though, to prepare asymmetrically substituted azo–compounds using these protocols.

In comparison, the reaction of aromatic primary amines with aromatic nitroso compounds in acidic media, normally glacial acetic acid, is particularly suitable for the synthesis of asymmetrically substituted azo compounds in good yields.<sup>[261],[262],[251]</sup> The mechanism of the reaction has been proven by kinetic studies (Figure 3–29).<sup>[263]</sup> In the first, rate-determining step the nitroso **181** or the protonated nitroso compound **181'** adds to the amino group of the aromatic coupling partner **182**. In the second step water is lost via **183** or **183'** providing the azo functionality of **185**. In accordance with the mechanism electron-releasing substituents in the amine accelerate the reaction, whereas electron withdrawing groups retard it. In the nitroso molecule the contrary effect is observed. This so-called *Mills* reaction tolerates a

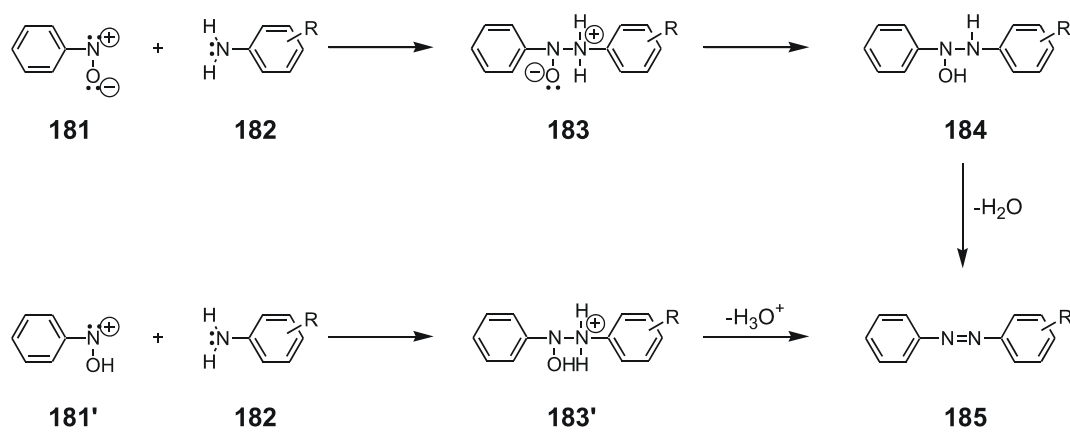


**Figure 3–29:** Mechanism of the Mills–reaction.<sup>[261]</sup>

number of functionalities like nitro-, protected amine-, alkoxy-groups, halides, acids and esters in the coupling partners.<sup>[261]</sup> It should be noted, though, that only one industrial application has been described that is not based on the azo coupling procedure.<sup>[199]</sup>

### 3.3.2 Photophysical Properties

Together with other groups of compounds like spiropyranes or diarylethenes azobenzene (and related compounds) belong to the class of photochromic compounds (see also chapter 2.3).<sup>[199]</sup> Interestingly, it was not until 1937 when Hartley discovered the influence of light on the configuration of the nitrogen–nitrogen double bond.<sup>[111]</sup> Since then, a lot of studies have been conducted dealing with this particular physical property of these structures.<sup>[244],[264],[265]</sup>

Azobenzene (and related compounds) exists in two distinct configurations, namely *E* and *Z* that can be inter-converted by irradiating or heating the sample. The *Z*-isomer is stable in the solid state, but isomerises to the thermodynamically favoured *E*-isomer in solution. The nitrogen–carbon bond length in azobenzene was determined to 1.41 Å in the *E*- and 1.46 Å in the *Z*-isomer, respectively (Figure 3–30). The distance between the two hydrogen atoms in *para*-position is 9 Å in the planar *E*-form, whereas in the *Z*-form, where the phenyl rings are rotated by 56° with respect to the N=N–C plane, the two hydrogens are only 5.5 Å apart from each other. The two stereoisomers can also be distinguished by their difference in dipole moment (*E*-isomer:  $\mu = 0$  D, *Z*-isomer:  $\mu = 3.5$  D).<sup>[264]</sup>

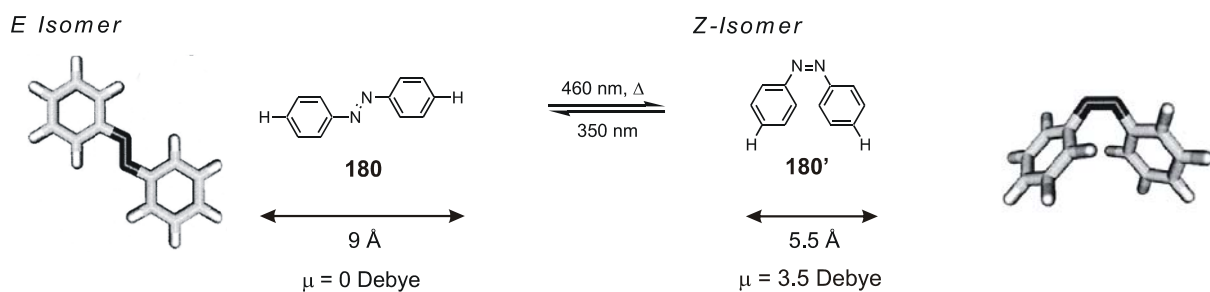
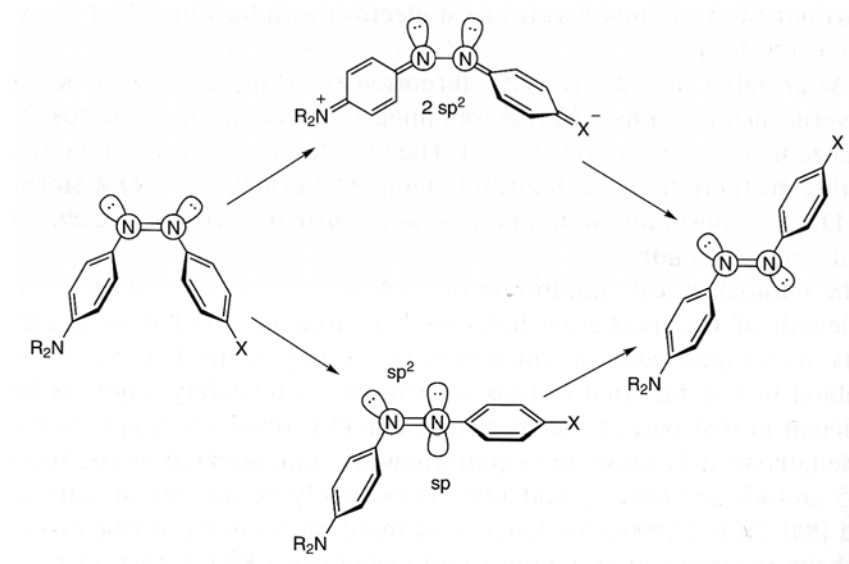


Figure 3–30: Properties of *E* and *Z*-isomer of azobenzene.<sup>[260],[264]</sup>

Two different mechanisms have been proposed for the *E*–*Z*-isomerisation (Figure 3–31).<sup>[266],[267],[268]</sup> The upper pathway where rotation around the N–N single bond takes place in a dipolar transition state was found, when azobenzene is substituted in 4– and/or 4’–position. This conclusion was drawn, since the isomerisation rates of 4–(dialkylamino)–4’–nitroazobenzenes are strongly influenced by solvent polarity and pressure. However, the inversion mechanism (lower pathway), where one of the azo nitrogen–atoms participates in a



**Figure 3-31:** Possible mechanisms for the isomerisation of azobenzene, taken from [199].

sp-hybridised linear transition state, seems to be favoured for the same compound in hexane. This pathway is also dominant in azobenzenes that lack electron-donating substituents in 4-position or that bear a strong electron donor in 4-, but no electron acceptor in 4'-position and in the gas phase.

In the absorption spectrum of *E*-azobenzene an intense  $\pi-\pi^*$ -transition around 350 nm and a weaker (forbidden)  $n-\pi^*$ -band at about 450 nm is observed (Figure 3-32).<sup>[269],[270]</sup> In contrast, the  $n-\pi^*$ -transition is allowed in the *Z*-isomer showing usually higher intensity. Therefore, azobenzene derivatives can be isomerised from *E* to *Z* by irradiating at the  $\pi-\pi^*$ -band around 350 nm and switched back from *Z* to *E* by utilising the  $n-\pi^*$ -transition around 450 nm. However, a photostationary equilibrium containing a maximum of 80% of *Z*-form is obtained, because irradiation with the  $\pi-\pi^*$ -transition wavelength will always induce re-isomerisation to the *E*-form as well. Drastic changes in the absorption spectra are observed when changing the substitution pattern. Hence, three different classes of azobenzenes were

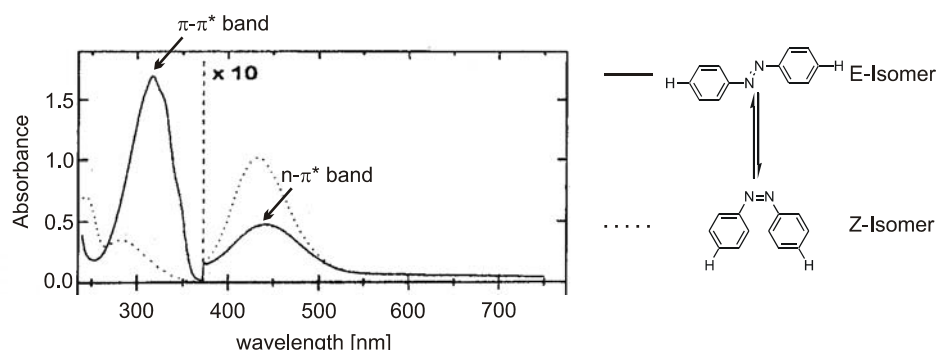


**Figure 3-32:** UVVis-spectrum of *E*- and *Z*-azobenzene in ethanol, taken from [270].

distinguished by *Rau*,<sup>[269]</sup> that is type I contains “normal” azobenzenes, type II comprises azobenzenes bearing electron–donors and type III (pseudo–stilbenes) includes azobenzenes having an electron–donor–acceptor–substitution. In type II compounds the  $n-\pi^*$ – and the  $\pi-\pi^*$ –bands overlap. In contrast, in pseudo–stilbenes the energy of the two transitions is exchanged as compared to type I.

Compared to UV/Vis spectroscopy, NMR measurements might be superior to investigate the *E*–*Z*–isomerisation of azobenzenes, because the spectra of the *E* and *Z* isomers are well resolved and can be unambiguously assigned.<sup>[271]</sup> Figure 3–33 shows NMR spectra that were recorded with laser radiation coupled into the sample within the NMR magnet. As anticipated, at time  $t = 0$  s (Figure 3–33 left a) when (almost) only the *E* isomer was present a doublet corresponding to four protons around 8.0 ppm arising from the protons at positions 2/6 and 8/12, a triplet around 7.2 ppm arising from the four protons at positions 3/5 and 9/11 and a triplet around 7.1 ppm arising from the two protons at positions 4 and 10 was found. The *Z*–isomer should consist of the same set of signals, but with different chemical shifts. The new

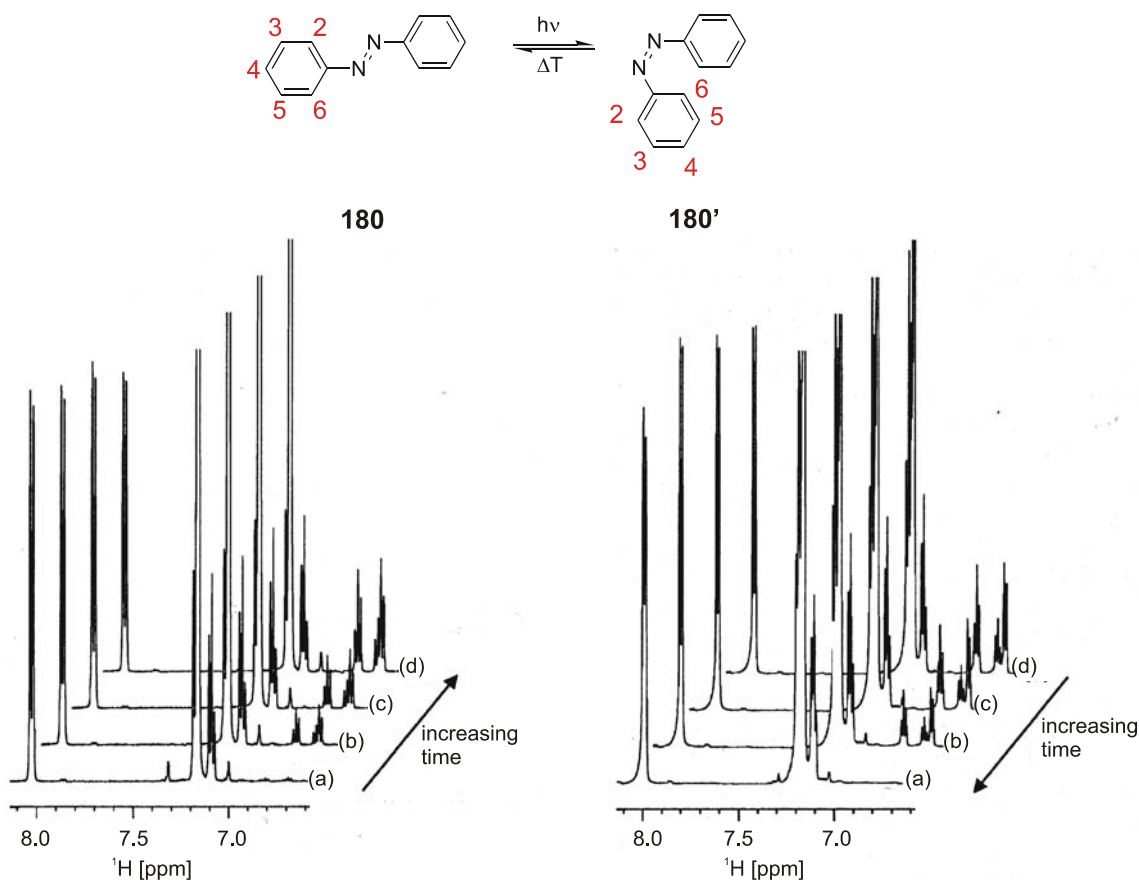


**Figure 3–33:** Left: NMR spectra of azobenzene and their development with time that were recorded with laser radiation coupled into the sample within the NMR magnet. Right: NMR spectra of previously irradiated azobenzene and their development with time when kept at 323 K.<sup>[271]</sup>

signals that appeared upon continuous laser irradiation were assigned as follows: a triplet resonated at 6.81 ppm corresponding to protons at positions 3/5 and 9/11, a triplet resonated at 6.70 ppm corresponding to protons at positions 4 and 10 and a doublet resonated at 6.68 ppm corresponding to protons at positions 2/6 and 8/12. The photostationary state was determined to contain 25% Z-isomer using peak integrals. Figure 3–33 right shows the development of the NMR spectra when a previously irradiated sample is kept at slightly elevated temperatures of 323 K in darkness for prolonged time, until after 50 h only *E*-azobenzene could be detected.

### 3.3.3 Summary of Chemistry and Physical Properties of Azo-Compounds

The most frequently used methods to produce symmetrically and asymmetrically substituted azo compounds have been depicted. From the discussion of their photophysical properties, it should be obvious that molecules containing one azo group can reversibly switched between two configurations (*E* to *Z*) by irradiating with a suitable wavelength and heating, respectively. A number of studies dealing with this photochromic behaviour have been published.

## 3.4 Dynamic NMR (DNMR) Spectroscopy

Usually NMR spectra are recorded to get information about the (static) structure and stereochemistry of molecules by looking at parameters like chemical shifts and coupling constants. But often further knowledge about dynamic relaxation- and exchange processes in molecules can be gathered by studying the effects of chemical exchange processes on NMR spectra in so-called dynamic NMR (DNMR) experiments.<sup>[272]</sup> By using these information about exchange of nuclei between sites with different chemical shifts and/or coupling constants, rate constants in the range of  $10^{-1}$  to  $10^5$  s<sup>-1</sup> can be obtained.<sup>[273]</sup> In 1956 the first DNMR study was done by Gutowsky and Holm,<sup>[274]</sup> which will be taken as an example to introduce the basic idea.

The study of dimethylformamide (DMF) represents one of the easiest cases to investigate chemical exchange processes with DNMR, that is a system with exchange between two equally populated sites that do not couple.<sup>[274]</sup> At room temperature the <sup>1</sup>H-NMR spectrum of

DMF showed two signals for the methyl groups, at  $\delta = 2.79$  and at  $\delta = 2.94$  ppm (Figure 3–34). When the temperature was increased, these two signals broadened until they eventually merged forming a broad signal at 120 °C. This temperature is called coalescence temperature  $T_C$ .<sup>[275]</sup> At even higher temperature one sharp signal was observed. The mesomeric structures of DMF can be taken to explain this behaviour, because the C–N bond can be considered as a partial double bond hindering rotation. Therefore, the methyl groups A and B are in a magnetically different environment (Figure 3–34).<sup>[276]</sup> When the temperature is increased, the rotational barrier can be overcome and, if the exchange between the two sites is fast enough, the methyl groups can no longer be distinguished any longer on the NMR time scale. Then only one signal is observed. In the case of DMF the process can be described as a reversible reaction having first-order kinetics (Figure 3–34) and the rate constant can be determined together with the activation parameters for rotation about the C–N bond (see below). The situation gets somewhat more complicated, when the rates of the two reactions are not equal anymore or when the nuclei couple.

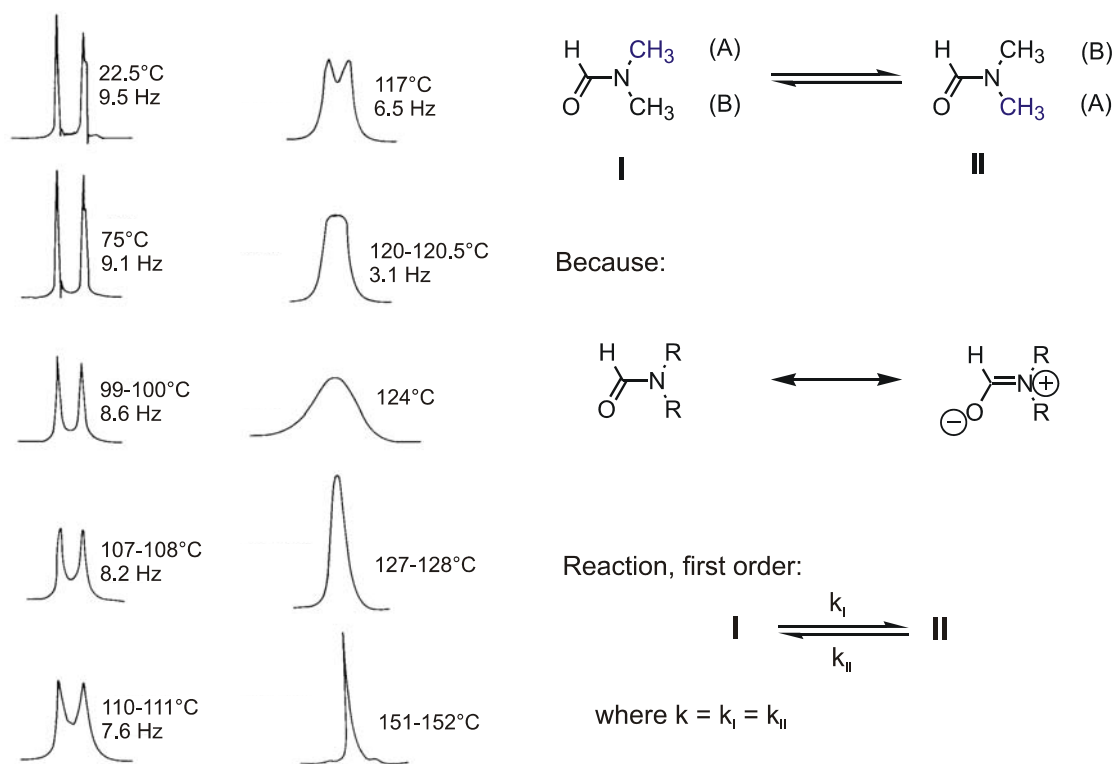


**Figure 3–34:** Left:  $^1\text{H}$ -NMR signals of the methyl-protons of DMF recorded at different temperatures. Right: Mesomeric structures of DMF that explain the observed temperature dependence and description of the kinetics of this process.<sup>[276]</sup>

### 3.4.1 Theoretical Background

The lineshape of a NMR spectrum, that is the functional dependence between intensity and frequency, is among other things a function of the rate constant.<sup>[273]</sup> Therefore, a theoretical calculation of NMR spectra and comparison with the measured ones for every temperature can provide the rate constant at different temperatures. This procedure is called Complete Lineshape Analysis (CLA).<sup>[276]</sup> In simple cases where exchange between non-coupling nuclei is investigated like in DMF, the spectra can be calculated using the classical *Bloch* equations (equation 3–1a–c).

$$\frac{dM_x}{dt} = -\frac{M_x}{T_2} \quad (3-1a)$$

$$\frac{dM_y}{dt} = -\frac{M_y}{T_2} \quad (3-1b)$$

$$\frac{dM_z}{dt} = -\frac{M_z - M_0}{T_1} \quad (3-1c)$$

Here  $T_1$  is the spin-lattice relaxation time used to describe, after transition, the relaxation of spins to their initial lower energy state affecting the  $z$ -component  $M_z$  of the magnetic field. The spin-spin relaxation time  $T_2$  characterises the relaxation of the magnetisation in the  $xy$ -plane to its equilibrium value.

The mathematical treatment of the process is greatly simplified when changing to a coordinate system in which the  $z$ -axis is parallel with the static magnetic field  $B_0$ , and in which the  $x$ - and  $y$ -axis rotate about the  $z$ -axis with the frequency of  $B_1$ , and in which  $B_1$  is in the  $x$ -direction. Equations (Figure 3–35 3–2a–c) are obtained where  $u$  and  $v$  denote the components of  $M$  in the directions of  $X$  and  $Y$ , the new axes. Assuming slow passage conditions and ruling out saturation effects it turns out that the magnetic moment in the  $xy$ -plane can be treated as a complex number. The imaginary part is closely related to  $v$  and contains information about the lineshape of a group of equivalent nuclei.

Now the effects of exchange between two equally populated sites A and B, which do not couple with each other, can be introduced. The exchange process is assumed to follow first-order kinetics (see above). The equation is separated into a real and imaginary part giving the final expression for the lineshape depending on the rate constant  $k_A$ , the fractional population

### Bloch equations

without exchange between sites

$$\frac{du}{dt} = 2\pi\nu(v_0 - v) - \frac{u}{T_2} \quad 3-2a$$

$$\frac{dv}{dt} = -2\pi u(v_0 - v) - \frac{v}{T_2} - \gamma B_1 M_z \quad 3-2b$$

$$\frac{dM_z}{dt} = -\frac{M_z - M_0}{T_1} + \gamma B_1 v \quad 3-2c$$

with exchange between sites

$$v = -C_0 \frac{\left\{ P \left[ 1 + \tau \left( \frac{P_B}{T_{2A}} + \frac{P_A}{T_{2B}} \right) \right] + QR \right\}}{P^2 + R^2}$$

$$\delta v = v_A - v_B, \Delta v = 0.5(v_A + v_B) - v \quad 3-3$$

$$P = \tau \left[ \frac{1}{T_{2A} T_{2B}} - 4\pi^2 \Delta v^2 + \pi^2 (\delta v)^2 \right] + \frac{P_A}{T_{2A}} + \frac{P_B}{T_{2B}}$$

$$Q = \tau [2\pi \Delta v - \pi \delta v (p_A - p_B)]$$

$$R = 2\pi \Delta v \left[ 1 + \tau \left( \frac{1}{T_{2A}} + \frac{1}{T_{2B}} \right) \right] + \pi \delta v \tau \left( \frac{1}{T_{2B}} - \frac{1}{T_{2A}} \right) + \pi \delta v (p_A - p_B)$$

$$\tau = \frac{P_A}{k_B} = \frac{P_B}{k_A}$$

**Figure 3–35:** Bloch equations, left: without exchange between sites, where  $u$  – component of  $M$  in direction of  $X$ ,  $v$  – component of  $M$  in direction of  $Y$ ,  $M_z$  – component of  $M$  in direction of  $z$ ,  $M_0$  – macroscopic magnetic moment,  $B_1$  – magnetic field in direction of  $X$ ,  $T_1$  – spin–lattice relaxation time,  $T_2$  – spin–spin relaxation time,  $\nu_0$  – Larmor frequency,  $\gamma$  – gyromagnetic constant; right: accounting for exchange between two sites, the indices A and B denote the two different sites.<sup>[273]</sup>

$p_A$ , the difference in chemical shift between A and B, and the relaxation time  $T_{2A}$  and  $T_{2B}$  (Figure 3–35 3–3).

Unfortunately, exchange between coupled sites cannot be treated with *Bloch* equations, but a quantum–mechanical approach based on the density matrix method is required. Fortunately, the spectra studied in this work can be calculated using the depicted simple approach. Hence, a detailed derivation of the quantum–mechanical equations is not required. However, as most computer programmes use the quantum–mechanical method developed by *Binsch*<sup>[277]</sup>, the functional dependence is shown (equation 3–4):

$$v = f(C, \nu, \nu_i, J_{ik}, T_{2i}, P_i, k_{ij}) \quad (3-4)$$

## 3.4.2 Experimental Technique

Apart from factors like purity of the compound and suitable concentration especially the choice of solvent and the method to measure the temperature are of great importance to obtain reliable data in temperature–dependent DNMR measurements.<sup>[273]</sup>

The solvent should have a melting point well below the lowest expected temperature, because usually the viscosity increases strongly near the melting point. Obviously, the boiling point

has to be in the range of the measurement as well, unless sealed sample tubes are employed provided pressure does not influence the process. Furthermore, the solvent has to dissolve the compound in the limits of the temperature measurements. The position of the chemical shifts of the solvent compared to the molecule under investigation and the influence of the solvent on the chemical shifts of the studied compounds, especially when a series of compounds is to be compared, have to be considered as well. At last, the solvent should be commercially available in its deuterated (or fluorinated) form. Table 3–3 gives a selection of potential solvents.

The precision of the determined rate constants depends directly on the accuracy of the control and measurement of the temperature. Unfortunately, the thermocouple found in commercial NMR spectrometers tends to be not very exact, but a variety of methods for calibration exist. The insertion of another thermocouple into the inside directly at the height of the receiver coil represents one possibility. The use of another sample tube containing a solvent with a known temperature-dependent change in chemical shifts, for instance methanol<sup>[278],[279]</sup> or ethylene glycol,<sup>[280]</sup> is also possible. The sample can be inserted into the machine at the same time like the tube with the compound studied or before and afterwards.

A number of temperature-dependent spectra has to be recorded, usually about three spectra in the region of slow exchange, i.e. low temperatures, five to ten around the coalescence temperature and about three at the fast exchange limit.

Solvent	Boiling point in °C (1 atm)	melting point in °C (1 atm)
CDCl <sub>3</sub>	61.2	-63.5
SO <sub>2</sub>	-10.0	-72.7
CD <sub>3</sub> C <sub>6</sub> D <sub>5</sub>	110.0	-95.0
(CD <sub>3</sub> ) <sub>2</sub> CO	56.0	-95.0
CD <sub>2</sub> Cl <sub>2</sub>	40.0	-97.0
m-F-toluene	116.0	-111.0
CS <sub>2</sub>	45.0	-111.5
SO <sub>2</sub> ClF	7.1	-124.7
CHCl <sub>2</sub> F	8.9	-135.0
SO <sub>2</sub> F <sub>2</sub>	-55.4	-136.7
(CD <sub>3</sub> ) <sub>2</sub> O	-24.8	-141.5
CCl <sub>2</sub> F <sub>2</sub>	-29.8	-158.0
Vinyl chloride	-13.9	-159.9
CHClF <sub>2</sub>	-40.9	-160.0
CBrF <sub>3</sub>	-57.8	-168.0
CClF <sub>3</sub>	-81.4	-181.0
propene	-47.7	-185.2

**Table 3–3:** Solvents for DNMR at low temperature, taken from [273].

### 3.4.3 Evaluation of Rate Constants

Apart from CLA approximate methods that due to certain suppositions use simplified equations based on expression 3–3 are known. The most popular one has already been derived by *Gutowsky* and co-workers (equation 3–5).<sup>[274]</sup>

$$k_c = \frac{\pi \delta v_c}{\sqrt{2}} \quad (3-5)$$

This so-called coalescence expression is based on the assumption that  $\delta v$  and  $k$  are much larger than the bandwidth in the absence of exchange.  $\delta v$  has to be determined from spectra at the slow exchange limit and extrapolated to the coalescence temperature. Although this approximation is only valid at  $T_c$ , it is often used to get a first estimate of  $k_c$ . There is a similar simple equation derived by *Kurland* and co-workers for the case of an AB spectrum.<sup>[281]</sup>

According to equation 3–4 the lineshape depends on several parameters, of which for the purpose of DNMR the rate constant is most important. When all other parameters are known, a NMR spectrum can be calculated by assuming a rate constant  $k$ . A visual comparison with the measured spectrum for this temperature reveals, whether the initial guess was correct. If not, further adjustment of the rate constant has to be achieved, until the calculated and the recorded spectrum match. Usually CLA is performed using programmes based on the quantum-mechanical code of DNMR5 that allow an iterative alteration of the parameters and comparison of recorded and calculated spectra.<sup>[282]</sup> In this work the programme WINDNMR71 was used.<sup>[283]</sup> Often an extrapolation of the chemical shifts  $v$  and the spin–spin relaxation time  $T_2$  from measurements at low temperatures to the region of coalescence is required to get matching spectra. Yet, in most cases a linear relationship is satisfactory. The temperature-dependence of  $T_2$  has to be obtained from a reference signal present in the spectrum, for example another signal of the compound that is not affected by the exchange process. As result from CLA, as many rate constants as spectra measured at different temperatures are obtained.

### 3.4.4 Evaluation of Activation Parameters

Two different possibilities, i.e. the *Arrhenius* and the *Eyring* equation, exist to determine activation parameters from the obtained rate constants (Figure 3–36). In recent years, however, the *Eyring* equation is preferred. Here  $\Delta G^\ddagger$ ,  $\Delta H^\ddagger$  and  $\Delta S^\ddagger$  are the standard activation parameters, that is they describe the differences per mol between the activated complex (transition state) and the reactants. It should be noted that only one rate constant is needed to calculate  $\Delta G^\ddagger$  at the coalescence temperature. Hence, the approximation of equation (3–5) often gives good results, especially because as a result of the logarithm an error in  $T_c$  of  $\pm 2$  K corresponds only to an error of  $\pm 0.5$  KJ/mol in  $\Delta G_c^\ddagger$ . In addition, the enthalpy of activation  $\Delta H^\ddagger$  as well as the entropy of activation  $\Delta S^\ddagger$  can be estimated from the slope of a plot of  $\log(k/T)$  against  $1/T$ . There is on-going discussion, though, about the accuracy of the entropies of activation obtained by DNMR.

Of course an analysis of errors has to be done to evaluate the reliability of data. Usually the temperature cannot be determined with a better precision than  $\pm 2$  K. Besides, errors in the measurement of  $T_2$  and  $\delta v$  can result in a variance of more than  $\pm 25\%$  in the rate constant.

#### Determination of Activation parameters

Arrhenius equation

$$k = A e^{-E_a/RT}$$

Eyring equation

$$k = \kappa \frac{k_B T}{h} e^{(\Delta H^\ddagger - T \Delta S^\ddagger)/RT}$$

$$\Delta G_c^\ddagger = 19.14 T_c \left( 10.32 + \log \frac{T_c}{k_c} \right) J mol^{-1}$$

$$\log \frac{k}{T} = 10.32 - \frac{\Delta H^\ddagger}{19.14 T} + \frac{\Delta S^\ddagger}{19.14}$$

**Figure 3–36:** Arrhenius and Eyring equation that allow to determine activation parameters from DNMR measurements.<sup>[276]</sup>

### 3.4.5 Selected Applications of DNMR

In the last decades DNMR studies have been used to investigate different dynamic processes found in organic compounds and only a small selection will be shown here.

### 3.4.5.1 Rotation About C–C Single Bonds

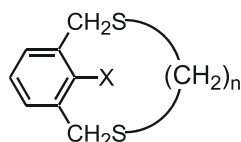
These processes are further subdivided into rotation about  $\text{C}(\text{sp}^3)\text{–C}(\text{sp}^3)$ ,  $\text{C}(\text{sp}^2)\text{–C}(\text{sp}^3)$  and  $\text{C}(\text{sp}^2)\text{–C}(\text{sp}^2)$  bonds.

Typical examples of  $\text{C}(\text{sp}^3)\text{–C}(\text{sp}^3)$  cases include rotation about the C–C single bond in butane and its derivatives.<sup>[284]</sup> Even when bulky substituents are used, the rotation remains so fast that the coalescence temperature usually is lower than  $-50\text{ }^\circ\text{C}$ . Hence,  $\Delta G^\ddagger$  values between  $30 – 50\text{ KJ/mol}$  are found.

The methyl group in toluene can be considered as one example of a rotation about a  $\text{C}(\text{sp}^2)\text{–C}(\text{sp}^3)$  bond.<sup>[276]</sup> However, even at temperatures lower than  $-150\text{ }^\circ\text{C}$  the rotation of the methyl group cannot be frozen. Bulkier substrates are required like substituted naphthalene derivatives.

More complex structures, where rotation about two  $\text{C}(\text{sp}^2)\text{–C}(\text{sp}^3)$  bonds occurs, have been investigated as well. For instance, studies of cyclophane derivatives mainly done by *Vögtle* and co-workers revealed rate constants for this rotational process between  $40 – 90\text{ KJ/mol}$  (Figure 3–37).<sup>[285]</sup> As anticipated,  $\Delta G^\ddagger$  seems to rise with increasing bulkiness of the substituent X.

The rotation about the single bond in biphenyl derivatives can be hindered by bulky



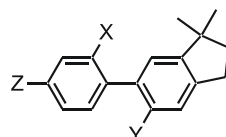
186

X	n	$\Delta G^\ddagger$ (kcal mol $^{-1}$ )	T (K)
H	7	> 10.3	211
F	7	> 10.9	223
Cl	9	11.6	238
Br	9	15.4	243
CH <sub>3</sub>	8	16.6	333
OCH <sub>3</sub>	9	17.9	363
CN	9	14.5	293
NO <sub>2</sub>	8	15.2	300
COOCH <sub>3</sub>	10	23.6	468
SCH <sub>3</sub>	10	17.4	358
SO <sub>2</sub> CH <sub>3</sub>	12	16.9	353

Figure 3–37: Barriers to rotation in substituted metacyclophanes.<sup>[286]</sup>

substituents giving rise to axially chiral biphenyl derivatives.<sup>[276]</sup> Since enantiomers cannot be distinguished in the NMR, the introduction of a prochiral group is required.<sup>[275]</sup>

The effects of substituents in *para*-position on the height of  $\Delta G^\ddagger$  have been studied by *Oki* and co-workers.<sup>[286]</sup> They found that electron-donating groups like methoxy lower the barrier, whereas electron-accepting groups like nitro have almost no effect on the barrier of rotation compared to hydrogen. Push-pull-systems bearing a methoxy-group at one and a nitro-group at the other *para*-position show a slightly lower barrier. This can be explained in terms of resonance stabilisation of the transition state. In all cases, the free energy of activation was in the range of 70 – 80 KJ/mol. Similar studies have been done with 5,7-dihydridobenzo[c,e]thiepins, but no consistent conclusions could be drawn due to the limited data set.<sup>[287]</sup> In summary, large changes in the electronic properties of the *para*-groups seem to have only a slight effect on the rotational barrier. Therefore, a biphenyl system could be designed to study steric effects of *ortho*-substituents.<sup>[288]</sup>  $\Delta G^\ddagger$  values between 50 – 100 KJ/mol have been found (Figure 3–38). Besides, it could be shown that both in the halogen series and in the series of  $-\text{OCH}_3$ ,  $-\text{SCH}_3$  and  $-\text{SiCH}_3$  substituents, when considering the *van-*



187

Y	X	Z	temp range, K	$\Delta G^\ddagger_{\text{m}}{}^a$ kJ mol <sup>-1</sup>	$\Delta H^\ddagger_{\text{m}}$ kJ mol <sup>-1</sup>	$\Delta S^\ddagger_{\text{m}}$ J mol <sup>-1</sup> K <sup>-1</sup>	$\Delta G^\ddagger_{\text{340}}{}^b$ kJ mol <sup>-1</sup>	$\Delta G^\ddagger_{\text{340}}{}^c$ kJ mol <sup>-1</sup>
1	CH <sub>3</sub>	I	H	356–415	89.9 ± 0.7	55.7 ± 1.3	-88 ± 3.5	85.8 ± 1.0
2	OCH <sub>3</sub>	I	H	299–325	69.8 ± 0.6	55.4 ± 1.5	-46 ± 5	71.1 ± 0.7
3	CH <sub>3</sub>	Br	H	335–367	83.8 ± 1.1	66.2 ± 1.5	-50 ± 4	83.3 ± 1.2
4	CH <sub>3</sub>	Cl	H	308–362	78.1 ± 1.0	49.4 ± 0.9	-86 ± 2.5	78.6 ± 1.0
5	CH <sub>3</sub>	F	H	210–273	51.8 ± 0.6	22.9 ± 2.0	-120 ± 2	63.6 ± 0.8
6	CH <sub>3</sub>	CH <sub>3</sub>	H	337–350	81.2 ± 1.0	—	—	80.9 ± 1.0
7	OCH <sub>3</sub>	CH <sub>3</sub>	H	258–308	62.3 ± 0.7	39.6 ± 0.4	-80 ± 1.5	66.8 ± 0.7
8	CH <sub>3</sub>	OCH <sub>3</sub>	H	259–281	61.4 ± 0.7	48.0 ± 3.5	-50 ± 5.5	64.9 ± 1.0
9	CH <sub>3</sub>	OH	H	256–269	61.4 ± 0.8	—	—	67.5 ± 2.7
10	CH <sub>3</sub>	OAc	H	275–290	65.3 ± 0.7	44.1 ± 1.5	-75 ± 5	69.6 ± 1.0
11	CH <sub>3</sub>	COOMe	H	297–322	70.8 ± 0.7	52.8 ± 0.9	-58 ± 3	72.6 ± 0.7
12	OCH <sub>3</sub>	COOMe	H	237–273	55.6 ± 0.5	37.2 ± 0.6	-73 ± 2	61.8 ± 0.7
13	CH <sub>3</sub>	COCH <sub>3</sub>	H	273,277	64.9 ± 0.7	—	—	70.0 ± 2.3
14	CH <sub>3</sub>	Ph	H	293–311	70.5 ± 0.7	40.6 ± 1.5	-99 ± 5	74.2 ± 0.9
15	CH <sub>3</sub>	CH <sub>3</sub> OH	H	336–364	82.4 ± 0.9	64.0 ± 1.4	-53 ± 4	81.9 ± 0.9
16	CH <sub>3</sub>	CH <sub>3</sub> OAc	H	333–404	84.6 ± 0.9	67.3 ± 1.0	-47 ± 2.5	83.2 ± 1.0
17	CH <sub>3</sub>	CH(CH <sub>3</sub> ) <sub>2</sub>	H	420–457	100.8 ± 0.7	51.5 ± 2.1	-113 ± 5	89.7 ± 1.9
18	CH <sub>3</sub>	CF <sub>3</sub>	H	392–422	97.3 ± 1.1	77.8 ± 3.7	-48 ± 9	94.1 ± 1.7
19	OCH <sub>3</sub>	CF <sub>3</sub>	H	307–332	74.3 ± 0.8	57.0 ± 1.7	-53 ± 5	75.4 ± 0.9
20	CH <sub>3</sub>	NO <sub>2</sub>	H	275–304	68.8 ± 1.0	—	—	72.8 ± 2.2
21	OCH <sub>3</sub>	NO <sub>2</sub>	H	233–253	55.3 ± 0.6	—	—	63.0 ± 3.0
22	CH <sub>3</sub>	NH <sub>2</sub>	H	323–361	80.8 ± 0.9	53.1 ± 1.3	-81 ± 4	80.7 ± 0.9
23	CH <sub>3</sub>	NHCH <sub>3</sub>	H	352–376	86.6 ± 0.8	52.7 ± 3.3	-93 ± 10	84.4 ± 1.1
24	CH <sub>3</sub>	N(CH <sub>3</sub> ) <sub>2</sub>	H	301–338	71.5 ± 0.6	44.5 ± 1.0	-84 ± 3	73.2 ± 0.7
25	CH <sub>3</sub>	N(CH <sub>3</sub> ) <sub>2</sub> *	H	>422	—	—	—	>94
26	CH <sub>3</sub>	NHC(O)CH <sub>3</sub>	H	284–308	67.6 ± 0.6	42.6 ± 0.3	-84 ± 1	71.3 ± 0.7
27	CH <sub>3</sub>	Si(CH <sub>3</sub> ) <sub>3</sub>	H	366–427	92.1 ± 0.8	53.6 ± 1.3	-97 ± 3.5	86.6 ± 1.0
28	CH <sub>3</sub>	SH	H	333–349	81.2 ± 0.9	45.9 ± 1.6	-103 ± 5	81.1 ± 0.9
29	CH <sub>3</sub>	SCH <sub>3</sub>	H	337–356	82.2 ± 0.8	53.1 ± 1.2	-84 ± 3.5	81.6 ± 0.9
30	CH <sub>3</sub>	CN	H	244–254	58.8 ± 0.8	—	—	66.0 ± 3.0
31	CH <sub>3</sub>	HgCl	H	320–351	73.7 ± 0.5	39.9 ± 1.6	-102 ± 5	74.6 ± 0.5
32	CH <sub>3</sub>	Cl	NO <sub>2</sub>	310–344	76.5 ± 0.9	56.2 ± 0.9	-62 ± 3	77.3 ± 0.9
33	CH <sub>3</sub>	F	NO <sub>2</sub>	213–243	48.6 ± 0.6	19.6 ± 0.8	-127 ± 3.5	62.9 ± 0.9

<sup>a</sup>  $\Delta G^\ddagger$  at the temperature at the center of the range over which kinetic data was obtained. <sup>b</sup>  $\Delta G^\ddagger$  at 340 K, calculated using  $\Delta G^\ddagger_{\text{m}}$  and  $\Delta S^\ddagger_{\text{m}}$ . <sup>c</sup>  $\Delta G^\ddagger$  at 340 K, calculated using  $\Delta G^\ddagger_{\text{m}}$  and  $\Delta S^\ddagger_{\text{av}}$ .

**Figure 3–38:** Activation parameters for differently substituted biphenyl derivatives obtained by DNMRA.<sup>[288]</sup>

der-Waals radii of the heteroatom, the barrier of activation rises with increasing radius. Assuming additivity of the steric effect of the two *ortho*-groups X and Y, values for individual bulkiness of one substituent could be calculated.

Other system with rotation about a C(sp<sup>2</sup>)–C(sp<sup>2</sup>) bond include chiral 1,3-butadienes<sup>[289]</sup> and aromatic ketones,<sup>[290]</sup> as well as related compounds. For 1,3-butadienes free activation energies in the range of 50 – 80 KJ/mol and for aromatic ketones and related compounds values between 70 to 90 KJ/mol have been determined.

### 3.4.5.2 Others

But not only rotation about a single bond can be studied using DNMR. The investigation of rotation about partial double bonds,<sup>[291]</sup> such as in DMF, or formal double bonds like in cumulenes<sup>[292]</sup> is also possible. Furthermore, ring inversion reactions in, for instance, cyclohexane<sup>[293]</sup> derivatives and keto–enol tautomerie<sup>[276]</sup> have been studied as well.

## 3.4.6 Summary of Dynamic NMR Spectroscopy

The recording of NMR spectra at different temperatures allows to study dynamic processes in organic compounds. The comparison between measured spectra and calculated spectra yields the rate constant of the exchange process for the respective temperature from which its activation parameters can be determined. Due to the time scale of the NMR measurement processes with *Gibbs* free energies in the order of 20 – 120 KJ/mol can be investigated.

## 4 Results and Discussion

This chapter comprises the results and a detailed discussion of the present work. The target compounds have been arranged according to the desired and designed ME functionality of the organic compound. A further subdivision has been done by means of the molecular structure of designed target compounds. First, in each section the motivation, the basic idea and the development of a suitable molecular structure to tackle the problem will be described. In the next step, the synthetic strategy that has been developed to obtain the target compound will be presented and discussed. After a comprehensive treatment of the synthetic pathway that was followed to realise the target structures, results of crystal structure analyses, UV/Vis spectroscopy and (dynamic) NMR measurements of the target compounds will be presented. Knowledge gained from these investigations will be discussed, in particular with regard to the electronic properties of the structure. If available, at the end of each section, first physical electronic transport investigations that were either obtained in the group of *H. Weber* at the Institut für Nanotechnologie (INT), Forschungszentrum Karlsruhe GmbH or the group of *M. Rampi* at the Università di Ferrara are shown.

### 4.1 Molecular Wires and Insulators

#### 4.1.1 Oligophenylenes

Poly- and oligophenylenes consist of phenylene-rings that are linked together by a single bond in *ortho*-, *meta*- or *para*-position. It was predicted that unsubstituted poly(*p*-phenylene) has an angle of rotation between neighbouring phenyls of about 23°.<sup>[294]</sup> Besides, X-ray analyses of various terphenyls and quaterphenyls that do not bear substituents in *ortho*-position to the ring connecting carbon gave angles of rotation between neighbouring phenyl-rings between 10 – 30°.<sup>[295],[296]</sup> Hence, it is assumed that the p<sub>z</sub>-orbitals of the neighbouring ring-connecting carbons can overlap by a large degree creating a delocalised π-system over the whole structure. When the rings are further rotated with respect to each other the overlap between the p<sub>z</sub>-orbitals will be reduced resulting in a breaking of the π-conjugation between the phenyl-rings. Such a rotation can be induced by sterical strain

caused by substituents in the *ortho*-position to the ring-connecting carbons.<sup>[297]</sup> Different poly(*p*-phenylenes) with and without additional *ortho*-substituents have already been synthesised, but a detailed structure–property analysis of poly(*p*-phenylene) has been hindered mainly due to the fact that most synthetic routes afford ill-defined, defect-rich polymeric products.<sup>[77]</sup> The defined build-up of oligophenylenes can help to establish such structure–property relationships, which are necessary for the successful development of molecular electronics.

In the present work, two different approaches have been developed to study the effect of reduced  $\pi$ -conjugation on the electronic transport behaviour of such compounds (Figure 4–1). First, a family of oligophenylenes **O1** – **O4** with increasing length has been designed. To disturb  $\pi$ -conjugation between the phenyl-rings methyl-groups were introduced in *ortho*-position to the ring-connecting carbons. Here, the correlation between the electronic transport behaviour and the number of such conjugation breaking units in the molecular rods is in the focus of interest. In a complementary study, it was envisaged to fix the angle between two adjacent phenyl-rings of a biphenyl (**B1** – **B3**) by the introduction of an alkyl-bridge in position 2 and 2'. By varying the length of the bridge different angles of rotation between the phenyl-rings will be attainable. Therefore, the influence of the degree of  $\pi$ -conjugation set by different angles on the electronic transport behaviour of these compounds can be investigated. All compounds were designed to allow the recording of current–voltage characteristics using the MCB technique. Thus, these stiff, rod-like molecules possess functionalities on both ends that allow a covalent binding of the molecule to the gold surface. For this purpose acetyl-protected sulphur functions have proven successful in earlier model compounds.<sup>[13],[62],[46]</sup> The protecting groups on both sides are cleaved by contact with the gold electrodes and the

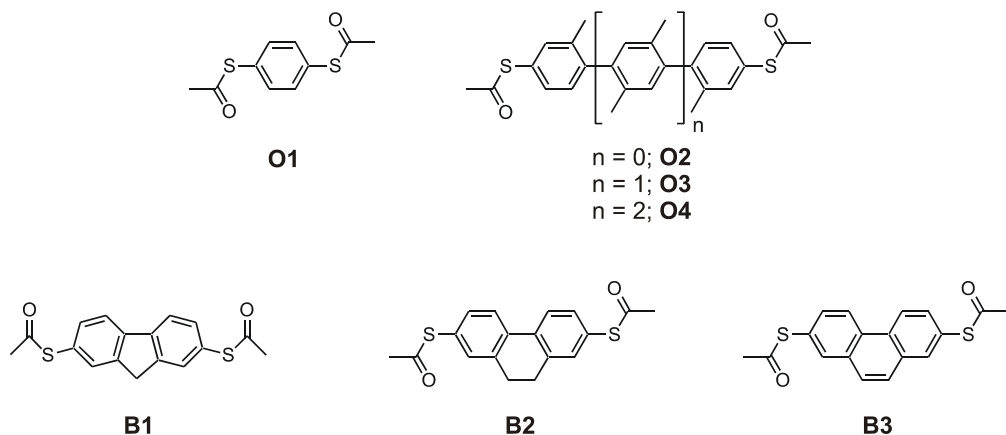


**Figure 4–1:** Target structures **O1** – **O4** and **B1** – **B3** with acetyl-protected sulphur anchor-groups for immobilisation between the electrodes of a MCB.

molecule bound covalently to the gold electrodes via the sulphur. For a detailed description of the immobilisation protocol see chapter 2.2.2.

#### 4.1.1.1 Synthetic Strategy

An approach involving metal–catalysed cross–coupling reaction (CCR) of a common outer building block to different inner moieties seemed to be most promising for the build–up of the oligomeric target compounds (Figure 4–2). To facilitate the synthesis it was planned to couple the outer building block **A** to both sides of the central building block **B** in one reaction step. The advantages of such a method are 1) the use of the same outer building block **A** for all target compounds; 2) the reduction of purification steps that have to be performed due to the coupling of three subunits (two **A** plus one **B**) at a time; 3) the terminal functionalities can be varied by changing only the outer building block **A**, the central part **B** will stay the same; 4) *vice versa*, the central building block **B** can easily be changed, while the outer part **A** remains; 5) the modular assembly probably requires only the development of one coupling procedure, which is utilisable for all following metal–catalysed CCRs.

In general, metal–catalysed CCRs need an organometallic reagent and an organic electrophile as substrate.<sup>[123]</sup> Aryl halides are commonly used as electrophiles, in which the reactivity drops from aryl iodides to bromides to chlorides. Aryl fluorides are usually unreactive in CCRs, which has been attributed to the high strength of the C–F bond.<sup>[122]</sup> For the synthesis of oligophenylenes the coupling of different phenyl–rings is required. Different cross coupling procedures exist for such type of reactions classified by the nature of the organometallic

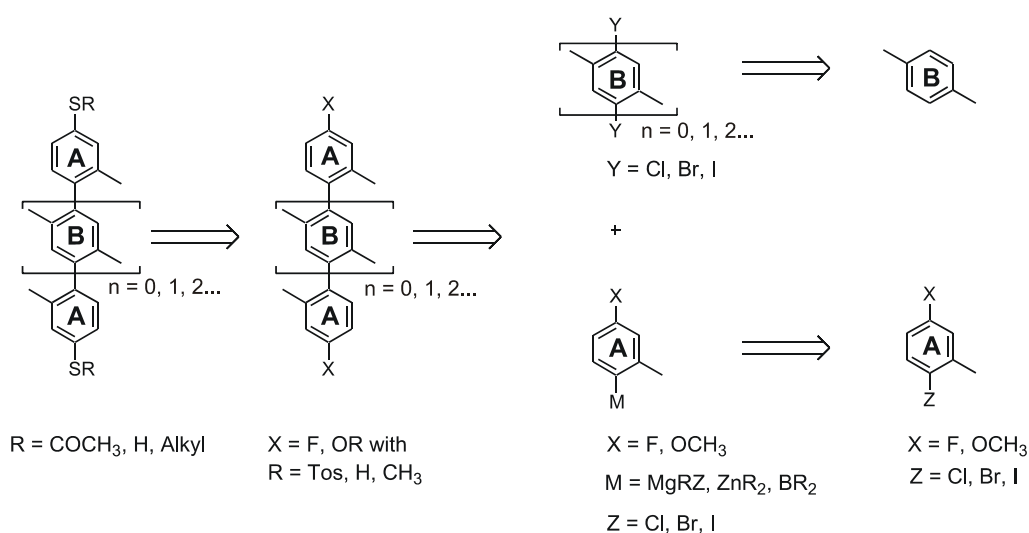


Figure 4–2: Synthetic strategy for the synthesis of the target compounds of the oligophenylene family.

reagent employed including the use of boron compounds (*Suzuki* coupling),<sup>[137]</sup> zinc-compounds (*Negishi* coupling)<sup>[151]</sup> or *Grignard*-compounds (*Kumada–Tamao–Corriu (KTC)* coupling).<sup>[142]</sup> Generally, *Negishi* or *KTC* procedures were favoured, because no isolation of organometallic species is required. However, sometimes the *Suzuki* coupling is superior when sterically demanding substrates are used.<sup>[137]</sup>

Organometallic substrates are usually obtained from aryl halides as well where the reactivity drops again from aryl iodides to bromides to chlorides. Since both the outer building block **A** and the central building block **B** need to have aryl halide bonds (Y and Z), in principle both could be used as organic electrophile or as organometallic reagent. However, the central building block **B** would require the introduction of two organometallic reaction centres per molecule. During the synthesis of such a building block the formation of polymeric products is quite likely due to self-coupling reactions of molecules that have been functionalised only once. Hence, it was more promising to use the outer building block **A** as organometallic species instead and the central building block as electrophile. In order to obtain good yields in the coupling procedure aryl iodides are the best choice for Y of the central building block **B**, as these are replaced more rapidly than other halogens.<sup>[122]</sup> The desired structures of the central part **B** have to bear methyl-groups that are in *para*-position with respect to each other and iodo-substituents in *ortho*-position to the methyl-groups to allow coupling at that position. Both groups can be introduced by electrophilic aromatic substitutions, the methyl-groups by a *Friedel–Crafts* alkylation and the iodo-groups by a halogenation reaction.<sup>[91]</sup> However, usually alkylated benzenes are commercially available, whereas only a limited number of iodo-compounds can be purchased. Besides, iodination will always require to introduce only two halogen-substituents while the number of alkylations that have to be performed will grow with the number of phenyl-rings present. Therefore, the pathway starting with alkylated products that are iodinated is preferred. Fortunately, the methyl-groups have an *ortho*- and *para*-directing effect in electrophilic aromatic substitutions<sup>[91]</sup> and hence, the required substitution pattern should be easily attainable. Furthermore, the first introduced iodo-substituent will be *ortho*- and *para*-directing, too. Because both methyl-groups will be in *para*-position with respect to each other, only the *ortho*-directing effect will play a role in the synthesis. Iodinated inner building blocks **B** can thus be obtained by electrophilic aromatic substitution of commercially available products following known literature procedures.<sup>[298],[299]</sup>

The outer common building block **A** has to have the following structure: One methyl-group has to be in *ortho*-position to a halogen-substituent Z, that is the position where the

organometallic centre will be and, thus coupling will occur. In addition, a sulphur–functionality or alternatively a substituent X that allows the introduction of the sulphur–functionality in a later step must be in *para*–position to the halogen–substituent Z. The available coupling procedures do either use highly reactive organometallic species (*Negishi* and *KTC* coupling) or strong basic conditions (*Suzuki* coupling). The final product has to have acetyl–protected sulphur anchor groups that will allow immobilisation on the gold–electrodes of an MCB. However, in the *KTC* coupling the carbonyl–group of the desired acetyl–protection group will be attacked by the organometallic species. Although procedures have been published that allow the use of carbonyl containing functional groups together with *Grignard* compounds, these methods are generally quite involved.<sup>[150]</sup> As the easiest way to prepare organzinc compounds is the employment of *Grignard* compounds as precursors, a similar situation is found for the *Negishi* coupling. In the *Suzuki* coupling the thioester will be cleaved due to the strong basic medium required. In summary, neither of these reactions can be applied to the synthesis of compounds already bearing an S–acetyl–group. Therefore, it is best to establish the acetyl–protection group after the CCR has been performed. However, no direct method to introduce the S–acetyl–group into an aromatic ring exists. Free thiols would allow the easy formation of an S–acetyl protected group by reaction with acetyl chloride or acetic anhydride. But free thiols cannot be used either in CCRs, because they will poison the catalyst. Two conceptually different strategies to prepare the desired organosulphur compounds are possible: 1) The sulphur functionality is present, before the CCR is performed. Then a protection group is needed, which tolerates the conditions of these protocols. 2) The carbon–sulphur bond is established after the build–up of the oligophenylene skeleton is finished. Here, the latter method was regarded as the more promising synthetic strategy, because coordination even of protected sulphur groups to the palladium catalyst might inhibit the CCR. Besides, no appropriate products containing a sulphur–functionality that would favour the first route were commercially available. As already mentioned, no routes for the direct preparation of acetyl–protected sulphur–groups on an aromatic ring are known. Hence, a substituent X on **A** that allows the easy formation of this protection group is needed. One possibility is the direct conversion of aryl bromides or iodides to free thiols by halogen–metal exchange with *tert*–butyllithium, quenching with elemental sulphur and *in situ* protection using acetanhydride in acetic acid. But when X and Z are two bromo– or iodo–substituents on the outer building block **A** CCRs might be complicated to perform selectively because of the various reaction sites present. While strategies that make use of the different reactivity of iodine, bromine and chlorine in CCRs to yield selectively coupled products have

been published,<sup>[300]</sup> such pathways are quite challenging and require more reaction steps. Therefore, such an approach was not followed. Instead substituents that could act like a mask for the sulphur functionality and that do not participate in CCRs were more promising. Tosyl- and halogen-groups can be reacted with sodium alkylthiolates to alkyl aryl thioethers in a nucleophilic aromatic substitution reaction.<sup>[231]</sup> Such thioethers can be converted to free thiols by a number of methods including a reductive procedure using sodium in liquid ammonia<sup>[216]</sup> or the use of an excess of sodium alkylthiolates giving a nucleophilic cleavage of the sulphur–alkyl bond, in particular when methyl-thioethers are used.<sup>[233]</sup> Alternatively, aryl methyl thioethers can be oxidised to sulphoxides, which can be transformed to free thiols via a series of reaction steps including a *Pummerer* rearrangement.<sup>[215]</sup>

The tosyl-group can not be present during the CCR, as it will react as well under these conditions forming cross-coupled products.<sup>[148]</sup> Therefore, it needs to be established after the coupling. Normally, tosylates are obtained by tosylation of phenolic OH-groups. Unfortunately, OH-group will inhibit the formation of highly reactive organometallic compounds due to their rather high acidity, but phenols can be obtained quite easily by ether cleavage from the robust methoxy groups.<sup>[239]</sup> Since 4-bromo-3-methylanisole is commercially available, it was used as outer building block **A** for the metal-catalysed cross-coupling reaction. In the next step, the aryl methyl ether can be cleaved to afford the phenol, which can then be tosylated. However, rather limited yields and troublesome isolation procedures in the tosylation step reduced the attraction of this synthetic pathway considerably. Therefore, an alternative strategy using halogen-substituents was developed as well. Only aryl fluorides were considered, because these are the only halides that will not participate in metal-catalysed cross-coupling reactions due to the high strength of the C–F bond.<sup>[122]</sup> Furthermore, due to the high electronegativity of fluorine aryl fluorides are the most reactive substrates in nucleophilic aromatic substitution reactions.<sup>[91]</sup> The alternative outer building block **A**, namely 2-bromo-5-fluorotoluene was also commercially available. Once the oligophenylene is formed, the sulphur functionality can be introduced by nucleophilic displacement using sodium alkylthiolates. These can then be converted to the desired acetyl-protected sulphur-groups by the methods mentioned above.

Within the developed synthetic strategy the biphenyl **O2** represents the easiest member, for which a CCR has to be performed. In this case, no central building block **B** is required, but only two outer building blocks **A** have to be dimerised. However, a very elegant synthetic procedure that allows the build-up of the biphenyl structure without the need of a metal-catalysed CCR has been known for a long time. The benzidine rearrangement will afford the

4,4'-diamino substituted biphenyl compound from cheap, commercially available 3-nitrotoluene. In a *Sandmeyer*-type reaction both amino-groups can be converted to halogen-substituents like bromine or iodine quite readily. As already mentioned above, these halides can easily be converted to sulphur functionalities by metal-halogen exchange reactions and subsequent quenching with sulphur. This synthetic path was considered as more reliable and efficient compared to CCR strategies and successful. Hence, another strategy to synthesise target compound **O2** was not developed.

In order to investigate the biphenyl unit in further detail a series of compounds comprising this structural motif has been considered. Biphenyl systems having an alkyl-bridge in position 2 and 2' allow to fix the torsion angle between two adjacent phenyl-rings. Furthermore, different angles of rotation between the phenyl-rings can be realised by varying the length of the bridge. For such bridged target compounds **B1** – **B3** two interesting bridged biphenyls were commercially available (Figure 4–3). 2,7-Dibromofluorene can be used to prepare the target having only one carbon in the bridge. It is known from literature that fluorene-compounds are essentially planar with an angle between the two phenyl-rings of almost 0°.<sup>[301]</sup> Even though the bridging carbon atom is not part of the delocalised π-system, fluorene has a high degree of π-conjugation, because the very short bridge forces the phenyl-rings to lie in plane. In principle, the same methods as described above for the conversion of aryl halides to organosulphur compounds can be applied. In this case, due to the experience gained during the synthesis of the oligophenylenes a route involving the nucleophilic

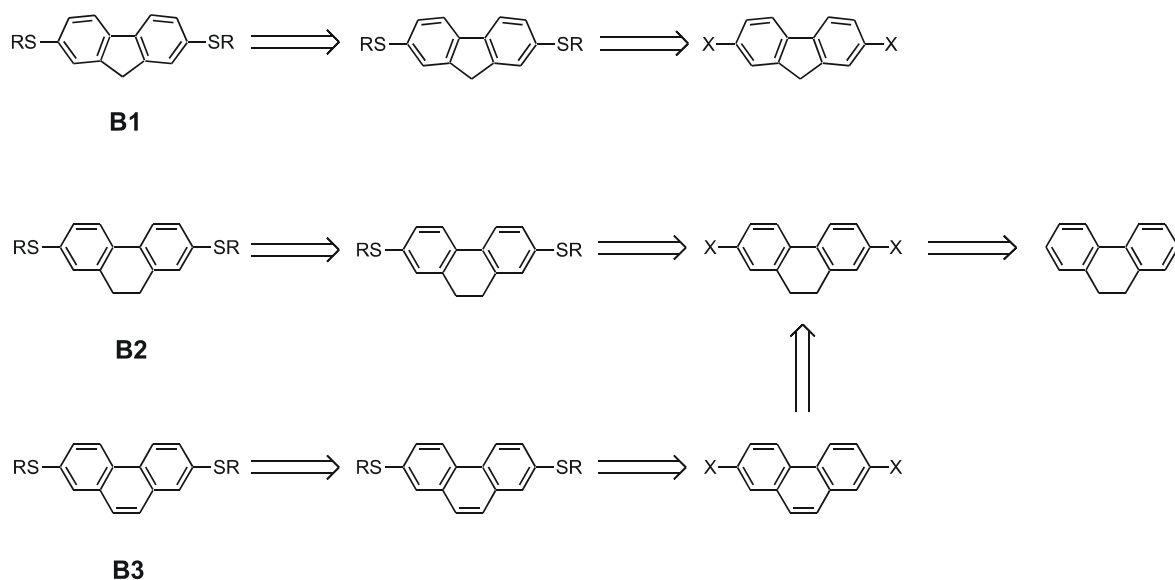


**Figure 4–3:** Synthetic strategy for the synthesis of the bridged biphenyls.

substitution of both bromines using sodium methylthiolate was preferred. Using an excess of sodium methylthiolate the formed aryl alkyl thioether can be cleaved and the obtained sodium salt converted to the acetyl-protected target compound by the use of acetyl chloride.

The next member of the series is an appropriately substituted 9,10-dihydrophenanthrene **B2**, that is a biphenyl with two carbons in the bridge. As determined by x-ray analysis such compounds will exhibit an angle of rotation of about 20°.<sup>[302]</sup> Hence, the overlap between the p<sub>z</sub>-orbitals of the two phenyl-rings is lowered resulting in a reduced π-conjugation as opposed to the fluorene **B1**. For comparison, a structure with a fully conjugated π-system was of interest as well. Target compound **O1** of the oligophenylene series has a π-system, which is not interrupted, but a quite shorter distance between the sulphur anchor-groups compared to the biphenyls **B1** and **B2**. For a more reliable estimation of the effect of changed π-conjugation a structure with a similar length seemed to be more attractive. Therefore, target compound **B3** comprising a phenanthrene moiety, which is essentially a biphenyl-compound with a conjugated bridge, was attractive. For target compounds **B2** and **B3** a strategy based on the same starting material, namely 9,10-dihydrophenanthrene was developed. Due to the positive experience made with the nucleophilic substitution reactions of aryl halides to get carbon-sulphur bonds, it was decided to use the same protocol to introduce the sulphur here as well. In a S<sub>N</sub>Ar reaction sodium methylthiolate is used to exchange both iodines for SMe-groups, which are cleaved in the same pot by an excess of sodium methylthiolate to afford the sodium salt of the free thiol. Subsequent addition of acetyl chloride affords the acetyl-protected sulphur functionality. Therefore, compounds that possess halogen-substituents in position 2 and 7 were needed. Fluorines would be an interesting choice, but are not easy to synthesise, because generally fluorine is too reactive to perform electrophilic aromatic substitutions.<sup>[91]</sup> Therefore, a known procedure for iodination of 9,10-dihydrophenanthrene was followed.<sup>[303]</sup> For **B3** phenanthrene, which has been iodinated in position 2 and 7, was needed as precursor. However, iodination of phenanthrene in these positions cannot be achieved easily, because the positions 9 and 10 are more reactive. Fortunately, an oxidation of the iodinated dihydro-compound, which is available from the synthesis of **B2** can yield the corresponding phenanthrene.<sup>[303]</sup> Again the sulphur functionality can be introduced by nucleophilic substitution with sodium methylthiolate affording the methyl aryl thioether as intermediate that can be cleaved in the same pot using an excess of sodium methylthiolate. The formed salt of the free dithiol can be converted to the acetyl-protected target compound using acetyl chloride.

### 4.1.1.2 Synthesis

1,4-bisacetylulfanyl–benzene **O1**, which has been synthesised prior to this work,<sup>[304]</sup> represents the simplest compound of this series. The synthetic pathway started from 1,4-dibromobenzene **O5**, on which both bromines were exchanged for ethylthio–groups by a nucleophilic substitution with sodium ethanethiolate in 1,3-dimethylimidazolidinone (DMI) similar to a literature procedure (Figure 4–4).<sup>[305]</sup> Compound **O6** was obtained as a white solid in 45% yield after column chromatography. Reduction of **O6** with sodium in liquid ammonia<sup>[216]</sup> and *in situ* protection of the formed thiol using acetanhydride afforded target compound **O1** as a white crystalline solid after column chromatography in a yield of 55%.

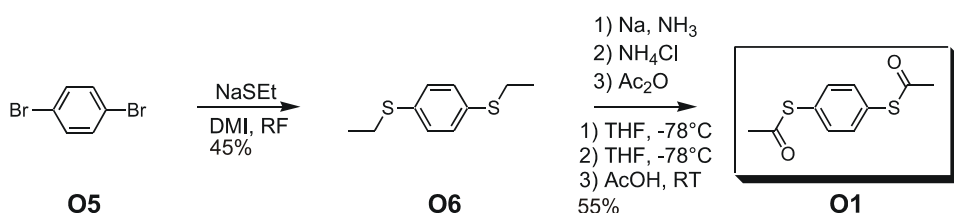


Figure 4–4: Synthesis of target molecule **O1**.

As mentioned in the synthetic strategy, the biphenyl skeleton of target compound **O2** is synthesised by the benzidine rearrangement reaction. Commercially available 3–nitrotoluene (**O7**) was reduced using zinc in sodium hydroxide to give an intermediate hydrazobenzene **O8** (Figure 4–5). This intermediate was not isolated, but converted further to the diamine **O9** using acidic conditions by a benzidine–rearrangement in a yield of 55%.<sup>[306]</sup> Diazotation and reaction with potassium iodide in a *Sandmeyer*–type reaction afforded **O10** as a white solid in

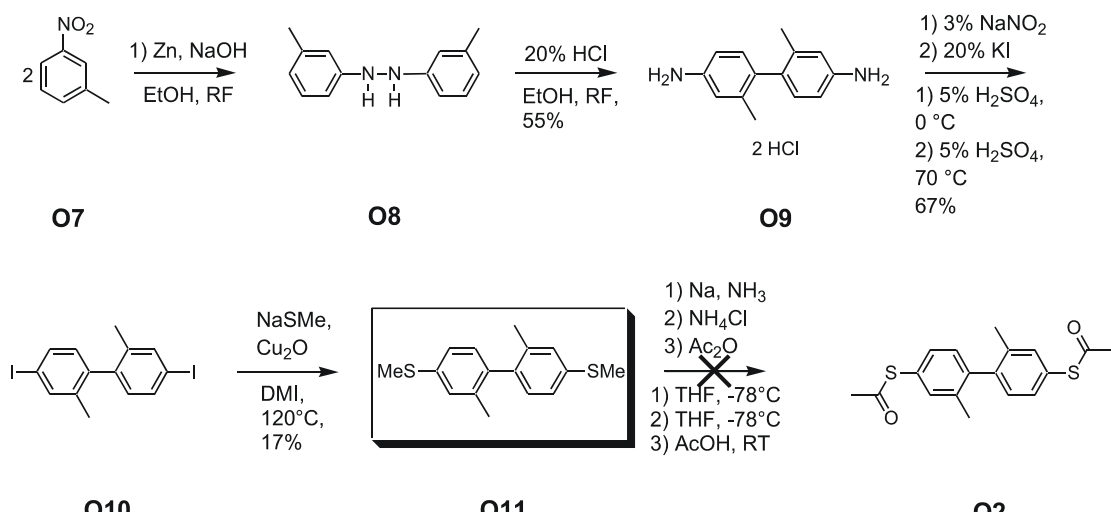
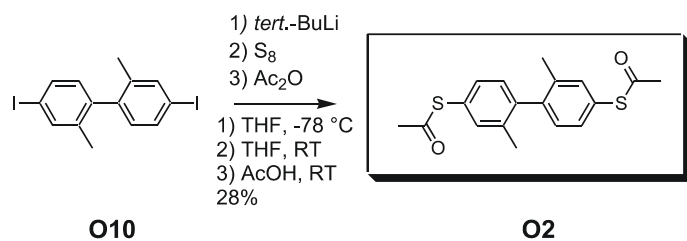


Figure 4–5: First, route for the preparation of **O2**.

67% yield.<sup>[307]</sup> It was planned to introduce the acetyl-protected sulphur-groups in a similar manner as for **O1**. But the yields of the nucleophilic displacement of the iodo-groups with sodium methanethiolate in DMI to give **O11** were consistently lower than 30%. Furthermore, the cleavage of the thioether using sodium in liquid ammonia could not be done successfully. Possibly, the relatively low solubility of compound **O11** in liquid ammonia/THF at -78 °C is one of the reasons for the failure of this reaction. Hence, another route which can be used due to the presence of iodo-substituents in **O10** was employed. This known one-pot three step procedure involves halogen-metal exchange with *tert*-butyllithium, quenching with elemental sulphur and *in situ* protection using acetanhydride in acetic acid (Figure 4–6).<sup>[209]</sup> This protocol provided target compound **O2** in an overall yield of 28% as a white solid after column chromatography.



**Figure 4–6:** Exchange of the iodo-groups for acetyl-protected sulphur-groups using a known literature procedure providing target compound **O2**.

The developed synthetic strategy consists of coupling of a common outer building block to a varying central moiety. This central building block **O13** for the synthesis of the terphenyl target compound **O3** was prepared by iodination of *p*-xylene (**O12**) with periodic acid and iodine in diluted acetic acid following a literature procedure (Figure 4–7). 2,5-Diido-*p*-xylene (**O13**) was obtained as a white solid in a yield of 65% after re-crystallisation.<sup>[298]</sup> In the first route **O13** was coupled to commercially available 4-bromo-3-methylanisole **O14** using *Kumada* conditions with  $[\text{NiCl}_2(\text{PPh}_3)_2]$  as catalyst giving **O15** as a white solid in 47% yield (Figure 4–8). Now the methylether was cleaved with  $\text{BBr}_3$  at  $-78\text{ }^\circ\text{C}$  affording the diol **O16** as a white solid after precipitation with conc. hydrochloric acid in a yield of 73%. It was sought to prepare the corresponding tosylated compound **O17**, which can then undergo

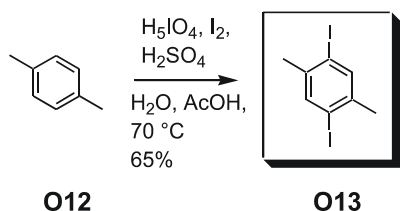


**Figure 4–7:** Synthesis of the central building block **O13** according to a literature procedure.

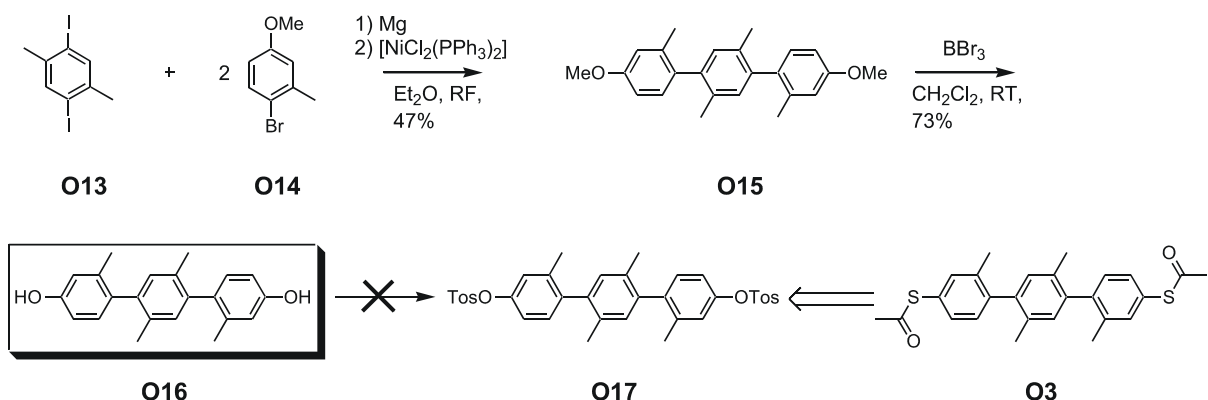


**Figure 4–8:** First route for the preparation of target compound **O3**.

nucleophilic aromatic substitution to give the sulphur–terminated compound. However, the reaction of *p*-toluenesulphonyl chloride with the diol **O16** in the presence of pyridine could not be performed successfully. Neither at 0 °C nor at room temperature the desired product could be obtained.

Therefore, the alternative pathway explained in detail in the synthetic strategy, where a fluoro–substituent is used as a mask for the future sulphur–functionality was followed. The required outer building block, namely 2–bromo–5–fluorotoluene (**O18**) was also commercially available. In a *Grignard* reaction **O18** was converted to (4–fluoro–2–methylphenyl)magnesium bromide, subsequent addition of  $\text{ZnCl}_2$  in dry THF yields the corresponding zinc organic compound. Cross–coupling of 2.5 equivalents of this zinc–organic species with the central building block **O13** employing a Nickel–catalysed cross–coupling protocol (*Negishi* reaction) afforded **O19** as a white solid in a yield of 65% after column chromatography (Figure 4–9).<sup>[135],[295]</sup> The metal–organic species was coupled directly without isolation. Now methyl–protected sulphur–groups were introduced on both ends of the molecular rod by a nucleophilic substitution of the fluorines using 2.5 equivalents of sodium methanethiolate in DMI at 90 °C. **O20** was obtained as a white solid in rather poor yield of 35% after column chromatography. The cleavage of the thiomethyl–groups with sodium in liquid ammonia was not considered this time, because the solubility of **O20** in liquid  $\text{NH}_3/\text{THF}$  is even lower than the one of **O11**. But already with **O11** this type of reaction could not be done successfully presumably due to solubility reasons. An alternative procedure involves the *Pummerer* rearrangement of sulphoxides to free thiols.<sup>[215]</sup> Hence, both thiomethyl–groups had to be oxidised selectively to the sulphoxide. However, oxidation of both sulphurs using 2 equivalents of 3–chloroperoxybenzoic acid (mCPBA) in  $\text{CH}_2\text{Cl}_2$  to get the corresponding sulphoxide **O21** gave only a low yield of 2%. The reaction with mCPBA can yield sulphoxides, but also sulphones.<sup>[235]</sup> These products can normally be separated quite

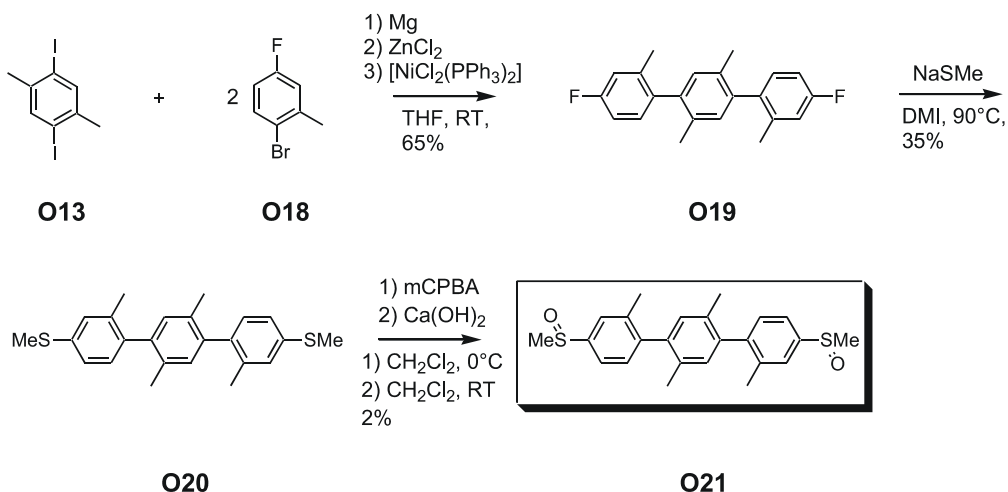


**Figure 4–9:** Second pathway for the synthesis of target compound **O3**.

easily, because they have very different  $R_F$ -values due to the big difference in polarity. However, molecules containing two sulphur-groups can give rise to mixtures of products that can bear sulphoxide— as well as sulphone—groups. In attempts at 0 °C and at –10 °C the yields of the desired sulphoxide **O21** could not be improved either. Besides, the yield of 35% for the previous step for the exchange of fluorine for SMe-groups was not very high either. Hence, alternative routes gained more attention.

During the introduction of the thiomethyl-group the cleavage of the methyl thioether is observed as side reaction and probably the reason for the low yields in the syntheses of **O11** and **O20**. After acidic work-up free thiols can be obtained. However, isolation of free thiols can sometimes pose serious problems, since aromatic thiols can easily be oxidised in the presence of oxygen giving disulphides.<sup>[219],[220]</sup> Dithiols may even lead to polymeric products with poor solubility. Protection of the free thiols without isolation can help to avoid these difficulties. The new protocol consists of a three steps including 1) nucleophilic aromatic substitution using sodium methanethiolate in DMI<sup>[305]</sup> at 120 °C to afford the intermediate (not isolated) compound **O20** bearing two terminal SMe-groups, 2) nucleophilic cleavage of the thiomethyl-groups using a 5-fold excess of sodium methanethiolate and long reaction time at 120 °C<sup>[233]</sup> producing presumably the sodium salt of the free dithiol **O22**, and 3) acetyl-protection of the free thiol-groups by careful addition of acetyl chloride at room temperature (Figure 4–10).<sup>[221]</sup> This three-step, one-pot procedure afforded the target compound **O3** as a white solid in an overall yield of 66% after column chromatography. Due to the salt formation the progress of the first two steps can easily be monitored by TLC, that is the acetyl chloride can be added to the reaction mixture when all starting compound has been converted. In the following paragraphs this developed procedure will be called halide-to-thioacetyl-conversion.

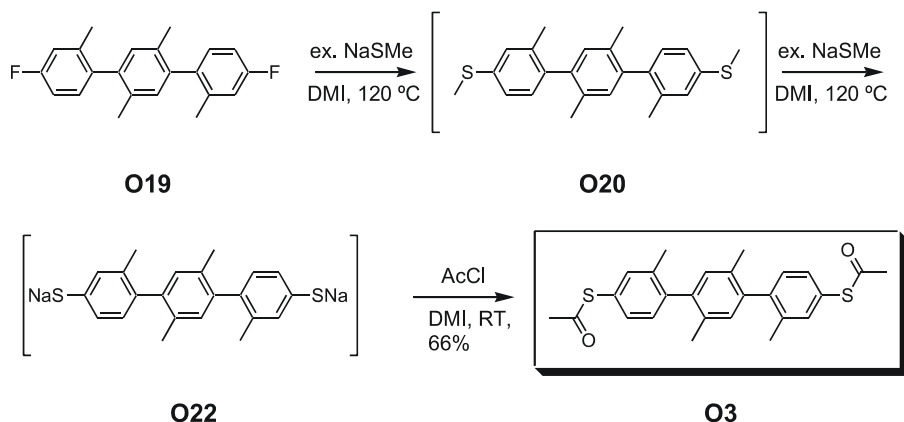


**Figure 4–10:** Protocol for the conversion of aryl fluoride to aryls having acetyl-protected sulphur groups affording target compound **O3**. Postulated possible intermediates that were not isolated are shown.

For the synthesis of target compound **O4** a different central building block, but the same outer building block **O18** was employed (Figure 4–11). In this case the organic electrophile was synthesised by iodination of 2,5,2',5'-tetramethyl-biphenyl (**O23**) with iodine, iodic acid and sulphuric acid in a mixture of acetic acid, water and carbon tetrachloride providing the iodinated central building block **O24** in a yield of 38%.<sup>[299]</sup> The same *Negishi* protocol as above allowed the coupling of 2.5 equivalents of **O18** with **O24**. The molecular rod **O25** was obtained as a white solid in a yield of 51% after column chromatography. The protocol for the halide-to-thioacetyl conversion gave the target **O4** in 50% yield after chromatography.

The developed synthetic strategy allows the synthesis of compounds with the same outer building block, but with different central parts. Of particular interest are chromophores to study the influence of light on the electron transport properties. A set-up that allows to study the influence using a MCB has been developed in the groups of *W. Pfeiffer* at the Universität Würzburg and of *H. Weber* at the INT. A compound having a central anthracene unit will

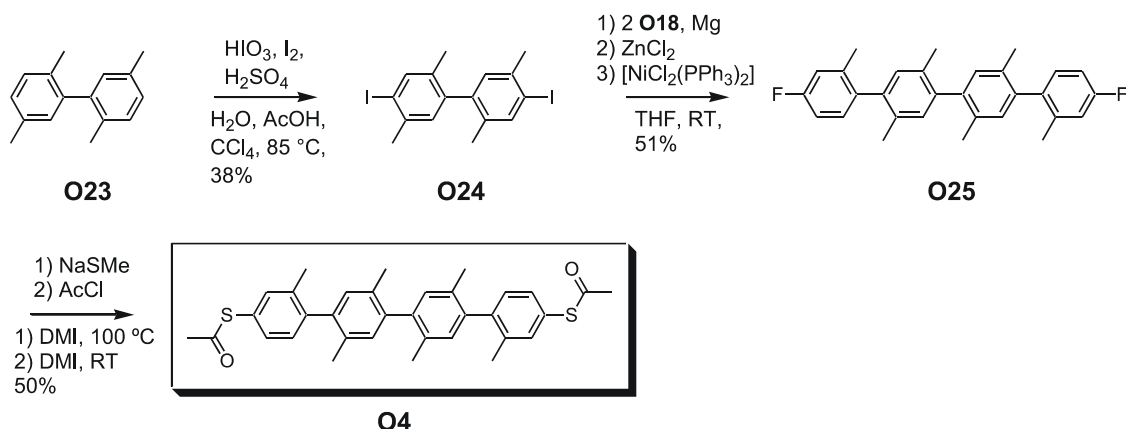


**Figure 4–11:** Reaction sequence for the preparation of **O4**.

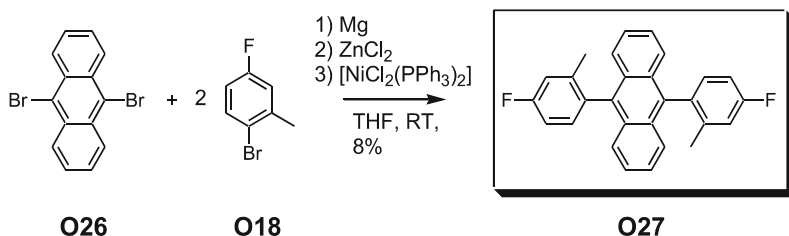


**Figure 4–12:** First route for the preparation of compound **O27**.

absorb light in the range of 400 nm. A similar *Negishi* cross coupling protocol as described above using 9,10-dibromoanthracene (**O26**) and **O18** as coupling partners afforded compound **O27** only in a yield of 8% (Figure 4–12).<sup>[295]</sup> The coupling of these two building blocks is sterically more demanding than other reactions that have been carried out so far because of the size of the anthracene ring system. Hence, it was decided to perform a *Suzuki* cross-coupling protocol, as this reaction is often superior to the *Negishi* coupling when sterically hindered substrates are used.<sup>[137]</sup> Suzuki coupling of the commercially available boronic acid **O28** to **O26** under Pd-catalysis in a solvent mixture of toluene/ethanol/water gave the fluoro-terminated molecule **O27** in a yield of 55% after re-crystallisation (Figure 4–13).<sup>[308]</sup> The target compound **O29** bearing two terminal acetyl-protected sulphur-groups was obtained as a white solid in a yield of 68% using the developed procedure for the halide-to-thioacetyl conversion.

Of particular interest are the NMR measurements of differently substituted terphenyls, as these compounds display atropisomerism at room temperature, that is they exits as rotational isomers about the single bond connecting the phenyl-rings.<sup>[273]</sup> To study the influence of different terminal groups on the energetics of the hindered rotation further terphenyls were designed. Due to the developed modular strategy only the outer building block needs to be

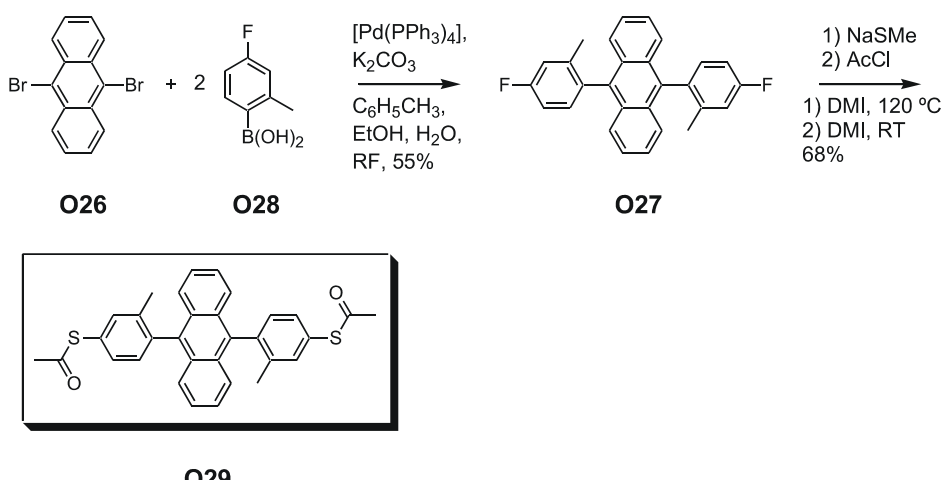


**Figure 4–13:** Second synthetic route to target compound **O29**.

changed, while the central part **O13** remains. It was hoped that dynamic NMR measurements (see below) will allow to establish correlations between the electronic effects of varying substituents in 4– and 4”–position and the barrier of rotation in these compounds. The simplest member of this series **O31** bears only hydrogen in 4– and 4”–position (Figure 4–14). Again different cross–coupling protocols for the coupling of the outer building block to the central part exist. Since in this case a suitable boronic acid **O30** could be purchased, a *Suzuki* cross–coupling protocol was favoured. The reaction of 2.6 equivalents of the boronic acid **O30** with **O13** using  $[\text{Pd}(\text{PPh}_3)_4]$  as catalyst in a solvent mixture toluene/ethanol/water afforded the target compound **O31** as a white solid in a yield of 98%.<sup>[308],[137]</sup> The synthesis of other compounds having strong electron–withdrawing–groups like  $\text{NO}_2$  or donor–substituents like  $\text{NR}_2$  is currently under way.

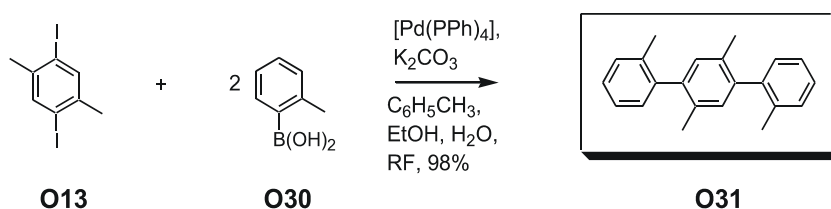


**Figure 4–14:** Synthesis of compound **O31** by a *Suzuki* cross–coupling protocol.

To investigate the effect of different angles of rotation between adjacent phenyl–rings on the electronic transport behaviour, alkyl–bridged biphenyls were synthesised. Target compound **B1** containing only one bridging C–atom was prepared starting from commercially available 2,7–dibromo–fluorene (Figure 4–15). The two bromines of **B4** were substituted by the developed protocol for the halide–to–thioacetyl conversion affording **B1** as a slightly yellow solid in a yield of 43% after column chromatography.

**B2** bearing two carbons in the bridge was obtained from 9,10–dihydrophenanthrene **B5** (Figure 4–16). First, iodination with iodine, iodic acid and sulphuric acid in a mixture of carbon tetrachloride, acetic acid and water gave compound **B6** having iodo–groups in position 2 and 7.<sup>[303]</sup> Biphenyl **B6** was obtained as a white solid in a yield of 56%. The preparation of **B2** using a known one–pot three step procedure involving halogen–metal exchange with *tert*–

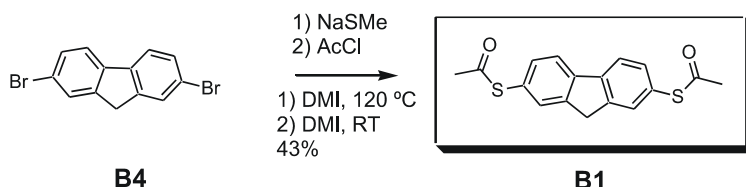


**Figure 4–15:** Synthesis of target compound **B1**.

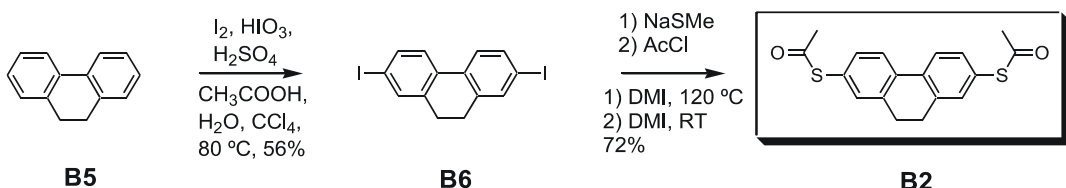


**Figure 4–16:** Synthetic pathway for the target compound **B2**.

butyllithium, quenching with sulphur and *in situ* protection using acetanhydride in acetic acid afforded only a yield of 10%.<sup>[209]</sup> Hence, the halide-to-thioacetyl conversion was employed again. By this method **B2** bearing two terminal acetyl-protected sulphur-groups was obtained as a white solid in 72% yield after column chromatography.

To compare a fully-conjugated  $\pi$ -systems of similar length with the biphenyls with rotated rings, the target compound **B3** was required (Figure 4–17). The diiodo compound **B6** was oxidised to the corresponding phenanthrene using N-bromosuccinimide (NBS) and dibenzoylperoxide affording **B7** as a white solid in 84% following a known literature procedure.<sup>[303]</sup> Again the thioacetyl-groups were introduced by the developed halide-to-thioacetyl conversion mentioned above. Target compound **B3** was obtained as white solid in 63% yield after column chromatography.

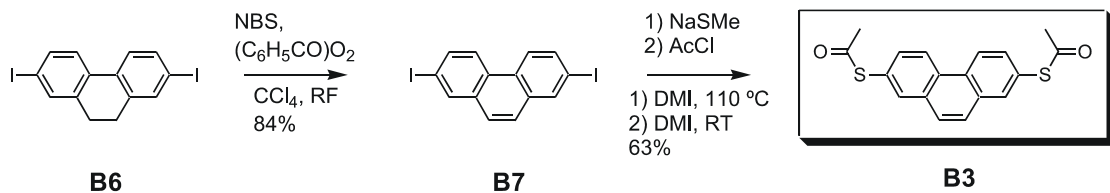


**Figure 4–17:** Preparation of a target compound **B3**.

#### 4.1.1.3 Characterisation and Structural Analysis

The identity of all new compounds has been proven by  $^1H$ –,  $^{13}C$ –NMR, mass spectrometry using either EI–MS or MALDI–TOF–MS and by elemental analysis. To gain further knowledge about the solid state structures of the target compounds **O2** – **O4**, **O29** and **B1** – **B3**, it was tried to obtain single crystals that are suitable for x-ray analysis. In particular, these investigations help to elucidate, whether the methyl-group in position 2 and 2' stabilise the rotation of the rings out of plane in the oligophenylene family. Hence, the angle of rotation

between two neighbouring rings was of special interest during the analysis. Besides, crystal structure analysis allows to determine the distance between the two terminal sulphur-functionalities. Depending on the prevalent electron transport mechanism the length of the molecule can be of great importance.

Single crystals of **O2** were grown by slow diffusion of hexane into a solution of diethylether. Compound **O2** crystallises in the orthorombic space group *Pbca*. The asymmetric unit is defined by the formula C<sub>18</sub>H<sub>18</sub>O<sub>2</sub>S<sub>2</sub>, that is the asymmetric unit contains one molecule. As there are eight asymmetric units in the unit cell, there are also eight molecules of **O2** in the unit cell. (Figure 4–18).<sup>[309]</sup> Both phenyl-rings of the biphenyl-structure are planar with the methyl-group in position 2 in the plane of the respective ring. The phenyl rings are rotated with respect to each other by an angle of 79.7(2)°. Due to the rotation of the phenyl-rings the molecular structure of **O2** does not have a centre of inversion. The bond length between the two phenyl rings (C(1)–C(10)) is 148.7(3) pm, which is close to the length of the C(sp<sup>2</sup>)–C(sp<sup>2</sup>) bond in unsubstituted biphenyl (148 pm).<sup>[91]</sup> The molecular axis of the molecule can be defined by the sulphur atoms S(1) and S(2) and the bond between both phenyl-rings, that is C(1)–C(10). The length along this molecular axis as defined by the distance between the two sulphurs was determined to 1.06(2) nm. The acetyl-protection groups on the terminal sulphurs do not lie in the plane of the phenyl-ring. The bond length between the sulphur and the aromatic carbon was determined to 177.6(3) pm for S(1)–C(4) and 177.0(2) for S(2)–C(13). This value lies between the length of a C(sp<sup>3</sup>)–S (182 pm) and C(sp<sup>2</sup>)–S (175 pm) bond.<sup>[91]</sup> The bond length between the carbonyl carbon and sulphur is with 179.0(3) pm (S(1)–C(8)) and 178.6(2) (S(2)–C(17)) slightly longer compared to the carbon–sulphur bond

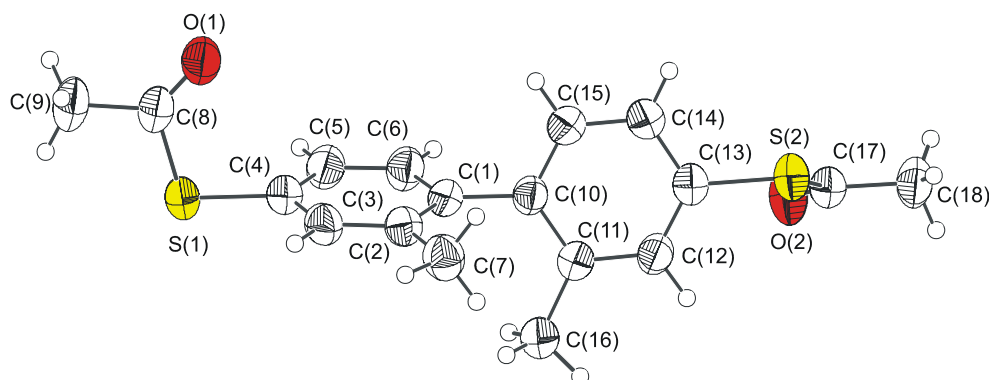


**Figure 4–18:** Molecular structure of **O2** (50% probability thermal ellipsoids). Selected bond lengths/pm and bond angles/°: S(1)–C(4) 177.6(3), S(1)–C(8) 179.0(3), S(2)–C(13) 177.0(2), S(2)–C(17) 178.6(2), O(1)–C(8) 118.3(3), O(2)–C(17) 119.2(3), C(1)–C(10) 148.7(3); C(4)–S(1)–C(8) 102.59(11), C(13)–S(2)–C(17) 103.93(11), O(1)–C(8)–C(9) 124.7(2), O(1)–C(8)–S(1) 123.31(19), O(2)–C(17)–C(18) 125.1(2), O(2)–C(17)–S(2) 124.03(19).

to the phenyl-ring.

A single crystal, which was suitable for x-ray analysis, of target **O3** was obtained by slow evaporation of a diethylether solution. **O3** crystallises in the monoclinic space-group  $P1\ 2_1/c$  (Figure 4–19).<sup>[309]</sup> The asymmetric unit comprises one molecule of **O3**, since the empirical formula was determined to  $C_{26}H_{26}O_2S_2$ . There are two asymmetric units per unit cell, thus, there are two molecules in the unit cell. The molecular structure has a centre of inversion, which is situated in the centre of the central phenyl-ring. All phenyl-rings are planar with the methyl-substituents in the plane of the respective phenyl-ring. The outer phenyl-rings are rotated by an angle of  $71.6(3)^\circ$  with respect to the central phenyl-ring. Due to the centre of inversion both outer rings lie in the same plane. The length of the carbon–carbon bond between the phenyl-rings ( $C(1)$ – $C(10)$ ) was measured to  $149.5(3)$  pm, which is slightly longer than in the case of the biphenyl target **O2**. The molecular axis of the molecule, which at the same time is an axis of reflection, is defined by the bonds  $S(1)$ – $C(4)$  and  $C(1)$ – $C(10)$ . The length of the molecule given by the intramolecular sulphur to sulphur distance was determined to  $1.49(8)$  nm. The acetyl-protection group on sulphur is situated below the plane of the outer phenyl-ring (or rather above the plane of the other outer phenyl-ring due to the inversion centre). The bond length between the aromatic carbon  $C(4)$  and sulphur  $S(1)$  was measured to  $177.4(3)$  pm, which is comparable to the length obtained in **O2**. The carbonyl–carbon  $C(8)$  sulphur  $S(1)$  bond has a length of  $178.2(3)$ , which is slightly elongated compared to a  $C(sp^2)$ – $S$  bond. Unfortunately, no single crystals of compound **O4** could be obtained so far.

From literature it is known that the torsion angles in differently 4 and 4'-substituted biphenyls

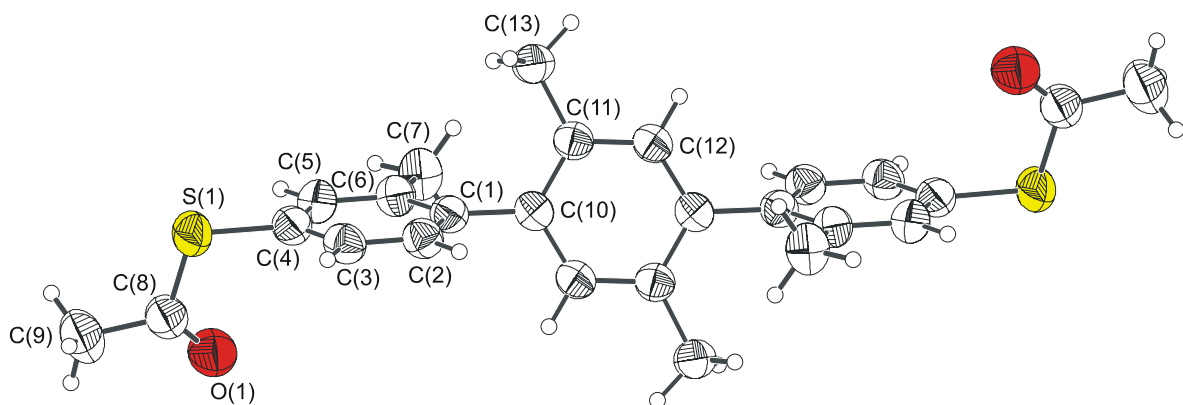


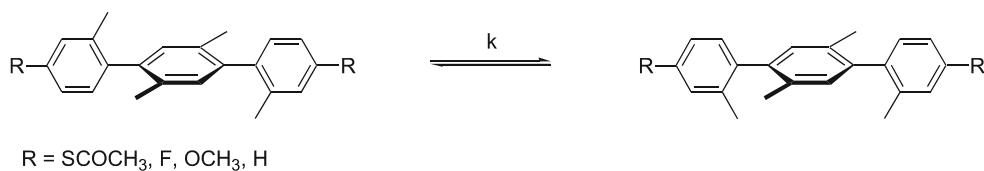
**Figure 4–19:** Molecular structure of **O3** (50% probability thermal ellipsoids). Selected bond lengths/pm and bond angles/ $^\circ$ :  $S(1)$ – $C(4)$   $177.4(3)$ ,  $S(1)$ – $C(8)$   $178.2(3)$ ,  $O(1)$ – $C(8)$   $120.1(4)$ ,  $C(1)$ – $C(10)$   $149.5(3)$ ;  $C(4)$ – $S(1)$ – $C(8)$   $101.80(12)$ ,  $O(1)$ – $C(8)$ – $C(9)$   $124.4(3)$ ,  $O(1)$ – $C(8)$ – $S(1)$   $122.9(2)$ ,  $C(9)$ – $C(8)$ – $S(1)$   $112.6(2)$ .

are between  $0^\circ$  and  $40^\circ$ .<sup>[310]</sup> X-ray analyses of various terphenyls and quaterphenyls that were not substituted in 2– or 2’– and 5 or 5’–position, respectively, gave angles of rotation between neighbouring phenyl–rings between  $10 - 30^\circ$ .<sup>[295],[296]</sup> Furthermore, it was predicted that unsubstituted poly(*p*–phenylene) has an angle of rotation between neighbouring phenyls of about  $23^\circ$ .<sup>[294]</sup> In comparison, the angles of target compounds **O2** and **O3** are considerably larger. This larger torsion angle between the phenyl–rings has probably been obtained due to steric hindrance induced by the methyl–groups in position 2 (and 5 for the terphenyl **O3**). Furthermore, an angle of rotation between  $70 - 80^\circ$  suggests that the overlap between the  $p_z$ –orbitals is greatly reduced. Hence, compound **O2** represents a structure consisting of two separated  $\pi$ –systems that are interrupted between the two phenyl–rings. Presumably, **O3** consists of three (almost) separate  $\pi$ –systems due to two conjugation breaking elements. Although no crystal structure of **O4** has been obtained so far, probably similar conclusions hold for this compound. Hence, the quaterphenyl comprises four distinct  $\pi$ –systems that are separated by three  $\pi$ –conjugation breaking elements.

Unfortunately, up to now no crystals of the target compounds **B1** – **B3** that were suitable for x–ray analysis could be obtained. However, known crystal structures obtained for the parent compounds fluorene, 9,10–dihydrophenanthrene and phenanthrene suggest the following angles of rotation: The fluorine **B1** should be essentially planar with an angle between the two phenyl–rings of almost  $0^\circ$ , but in fact the long axis, that is the one connecting positions 2 and 7, is probably not linear due to the large steric strain of the five–membered bridge.<sup>[301]</sup> X-ray analysis of 9,10–dihydrophenanthrene showed an angle of rotation of about  $20^\circ$  between the two phenyl–rings.<sup>[302]</sup> Therefore, the  $\pi$ –conjugation in this compound should be reduced somewhat compared to the fluorene compound. Crystal structure analysis revealed that the phenanthrene moiety is planar.<sup>[311]</sup> Hence,  $\pi$ –conjugation in this compound is not disturbed.

By x–ray analysis the torsion angle in these compounds can only be determined in the solid state. However, a different arrangement might be adopted in solution. Using NMR studies the rotation of the phenyl–rings in these compounds can be studied qualitatively and quantitatively. The  $^1\text{H}$ – and  $^{13}\text{C}$ –NMR spectra of different terphenyls that had been synthesised and the quaterphenyl compounds **O4** and **O25** indicate the existence of atropisomers, i.e. rotational isomers at room temperature. Figure 4–20 shows that in the terphenyl compounds the methyl groups of the two outer phenyl rings can either be situated on the same side of the plane of the central phenyl–ring or on opposite sides. In the quaterphenyl compounds a similar arrangement is possible. At elevated temperatures (about  $50^\circ\text{C}$ ) only one isomer can be detected suggesting that the phenyl–rings are rotating so fast

that they cannot be distinguished anymore on the NMR time-scale. Apart from this qualitative result a quantitative investigation of the process can be done as well using so-called dynamic NMR (DNMR) experiments.<sup>[272]</sup> As has been explained in more detail in chapter 3.4, the lineshape of a NMR spectrum is among other things a function of the rate constant, here it is the rate constant for the rotational process (Figure 4–20).<sup>[273]</sup> When all other parameters like chemical shift, relaxation time and population of the sites are known, a NMR spectrum can be calculated by assuming a rate constant k. Therefore, a theoretical calculation of NMR spectra and comparison with measured ones for every temperature can provide the rate constant at different temperatures. This procedure is called Complete Lineshape Analysis (CLA).<sup>[276]</sup> Using the obtained rate constants activation parameters of the investigated process can be calculated. As already shown in earlier work, different substituents can change the activation parameters of the rotational motion, for example in biphenyls.<sup>[288]</sup> At the same time different substituents might influence the angle of rotation between two phenyl-rings by steric and electronic effects.<sup>[312]</sup> Obviously, different angles of rotation will change the degree of  $\pi$ -conjugation of the system. Hence, it might be possible to establish correlations between different substitution patterns and the angle of rotation and, thereby the  $\pi$ -overlap in the studied systems using dynamic NMR measurements.



$R = \text{SCOCH}_3, \text{F}, \text{OCH}_3, \text{H}$

**Figure 4–20:** Rotational motion of the terphenyl compounds.

First, DNMR measurements of the target compounds **O3** and **O4** were performed to study the influence of the length of the molecule on the activation parameters. The spectra were recorded of ~25 mM solutions of **O3** and **O4** in  $\text{CDCl}_3$ . During these experiments a rough estimate of the temperature was provided by the thermocouple of the instrument, but the actual temperature was determined using the methanol and the ethylene glycol chemical shift thermometer, respectively.<sup>[278]</sup> Between –45 to 20 °C (thermocouple reading) 4% MeOH in  $[\text{D}_4]\text{-MeOH}$  was used, at temperatures higher than 20 °C (thermocouple reading) 80% ethylene glycol in  $[\text{D}_6]\text{-DMSO}$  was employed. The calibration tube was inserted into the machine after the measurement of the actual sample at the respective temperature had been performed. The calibration showed that the temperature reading of the thermocouple was wrong by up to 8 K, but different calibrations at the same thermocouple temperature deviated

only by  $\pm 0.5$  K. The interpretation of the obtained spectral data will be described using the measurements of **O3** as an example.

In principle, the development of two sets of signals with temperature could be followed, but the difference in chemical shift  $\Delta\nu$  of the  $\text{CH}_3$ -groups is rather small ( $\Delta\nu < 4.8$  Hz). In general, the bigger the difference in chemical shift the better (and more reliable) are the results obtained.<sup>[313]</sup> Therefore, it was decided to look at the temperature dependence of the chemical shifts of the protons in the middle ring, where the difference is a little bigger. First,  $\Delta\nu$  was read from the spectra at the slow exchange limit between  $-47.4$  °C to  $7.4$  °C. At higher temperatures approaching the coalescence temperature the difference in chemical shifts  $\Delta\nu$  cannot be determined from the recorded spectra anymore, because the different peaks will not be discernible. Hence, usually the difference at higher temperatures is estimated by extrapolation from a graph of  $\log(\Delta\nu)$  vs.  $1/T$ .<sup>[273]</sup> The same method was used here (Figure 4–21). At temperatures lower than  $-47$  °C spectra could not be recorded reproducibly probably due to the increased viscosity of the solvent  $\text{CDCl}_3$ . Therefore, these measurements were not used for the CLA. The required relaxation time  $T_2$  was determined for every temperature by band-fitting of a reference signal, in this case the  $\text{CH}_3$  of the acetyl-protection group, using the programme WINDNMR71.<sup>[283]</sup> The coalescence temperature was found to be  $T_C = (56.4 \pm 1.5)$  °C. With these data in hands spectra for different temperatures were calculated by changing the rate constant  $k$ , until the best fit between the calculated and the measured NMR

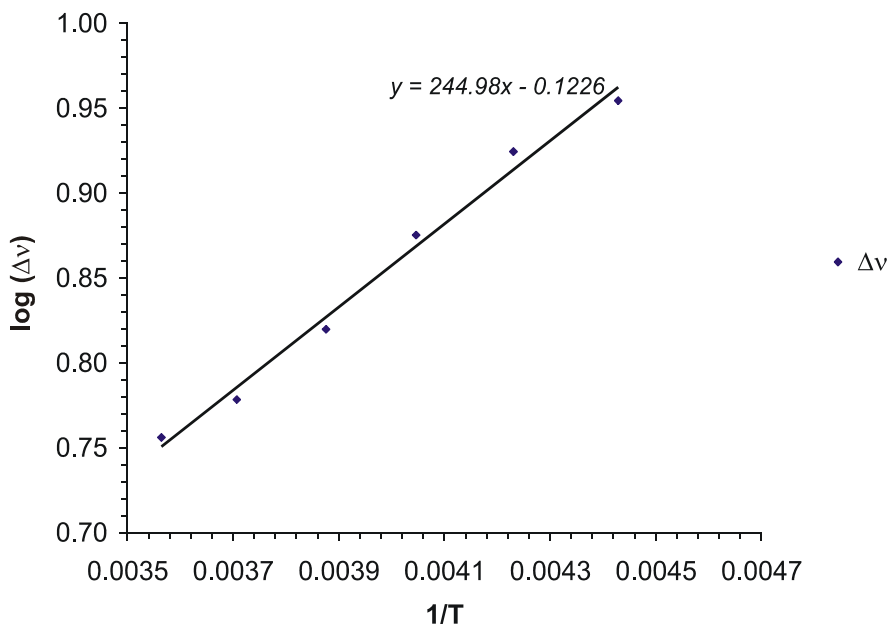


**Figure 4–21:** The temperature dependence of the apparent chemical shift difference of the protons in the middle ring of **O3**. The straight line fitted to the data points between  $-47.4$  °C and  $7.4$  °C is shown.

spectrum was obtained using the programme WINDNMR71 (Figure 4–22). In this way different rate constants for different temperatures were obtained allowing the determination of the free energy of activation  $\Delta G^\ddagger$  (Table 4–1).

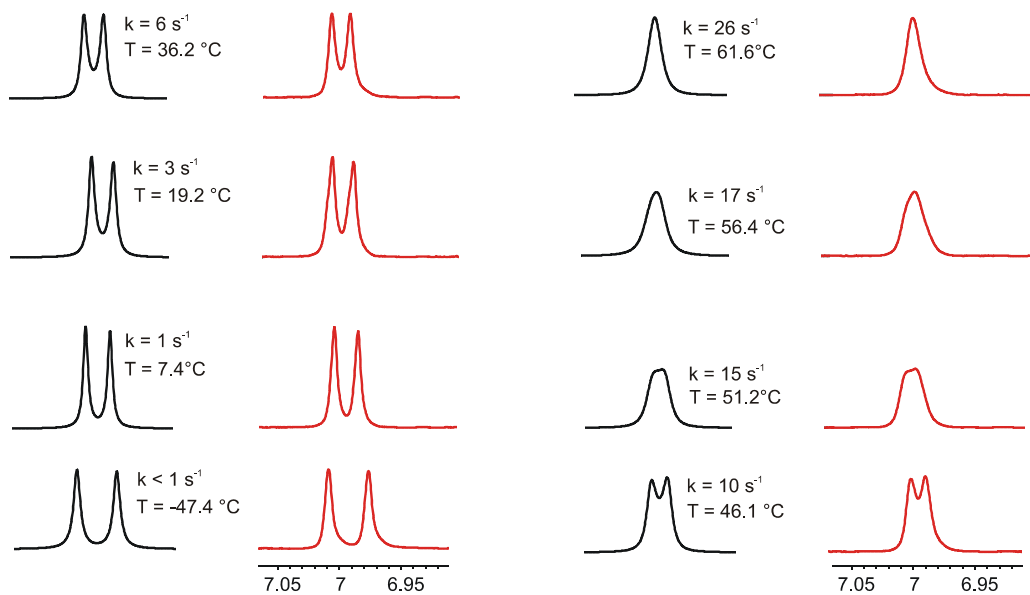


**Figure 4–22:** The temperature dependence of the signal of the protons in the middle ring of **O3**. A comparison between measured (red) and calculated (black) spectra together with the corresponding rate constant is shown.

By and large, the free energy of activation seems to be independent of temperature, as is often observed for processes like the one investigated.<sup>[314]</sup> Usually, the rate constant can be determined more accurately close to the coalescence temperature than at the region of slow exchange, because here the influence of  $k$  on the lineshape is bigger.<sup>[273]</sup> Therefore, only such values were considered. Using an *Eyring*–plot it would also be possible to determine  $\Delta H^\ddagger$  and  $\Delta S^\ddagger$ , however, reliable data can only be expected if the difference in chemical shift  $\Delta v$  is bigger than 50 Hz (here only 10 Hz at biggest!).<sup>[272]</sup> Hence, this separation was not attempted. Using line–shape analysis a free energy of activation at the coalescence temperature  $\Delta G_C^\ddagger =$

rate constant $k$ $s^{-1}$	Temperature in °C	Temperature in K	calculated $\Delta G^\ddagger$ in KJ/mol	error of $\Delta G^\ddagger$ in KJ/mol
6	36.2	309.4	71.3	0.7
10	46.1	319.3	72.3	0.7
15	51.2	324.4	72.4	0.7
17	56.4	329.6	73.2	0.7
26	61.6	334.8	73.2	0.8

**Table 4–1:** Calculated  $\Delta G^\ddagger$  values and errors at different temperatures for the terphenyl **O3**.

( $73.2 \pm 0.7$ ) KJ/mol for the target compound **O3** has been determined. The error was calculated assuming  $\Delta T = 1.5$  K and  $\Delta k = 25\%$ . The calibration of the thermocouple gave values that deviated only by  $\pm 0.5$  K, however, a bigger error in the temperature was supposed to account for inaccuracies in the exact determination of the point of coalescence. The rather large error in  $\Delta k$  was assumed, since a system with a relatively small difference in chemical shifts was investigated. The study of such systems can give rise to higher errors in the  $k$  values than systems with larger  $\Delta v$  values. Even for systems with  $\Delta v > 50$  Hz errors between 5 and 15 % are commonly observed.<sup>[273],[276],[272]</sup> Target compound **O4** has been investigated using the same approach (Table 4–2). The coalescence temperature is  $T_C = (51.2 \pm 1.5)^\circ\text{C}$ . Here, a free energy of activation of  $\Delta G_C^\ddagger = (72.1 \pm 0.7)$  KJ/mol was calculated. Figure 4–23 shows a comparison between measured and calculated spectra for this case.

rate constant $k$ $\text{s}^{-1}$	Temperature in $^\circ\text{C}$	Temperature in K	calculated $\Delta G^\ddagger$ in KJ/mol	error of $\Delta G^\ddagger$ in KJ/mol
6	36.2	309.4	71.3	0.7
9	41.2	314.4	71.5	0.7
12	46.1	319.3	71.8	0.7
16	51.2	324.4	72.1	0.7
25	56.4	329.6	72.2	0.7
32	61.6	334.8	72.6	0.7

**Table 4–2:** Calculated  $\Delta G^\ddagger$  values and errors at different temperatures for the quaterphenyl **O4**.

The determined free energies of activation  $\Delta G_C^\ddagger$  of **O3** and **O4** seem to be independent (in the error of the experiment) of the length of the oligophenylene and are in good agreement with values obtained for very similar terphenyl and quaterphenyl compounds<sup>[297]</sup> and with rotational barriers in various biphenyl compounds.<sup>[288]</sup> Compared to 2– and 5–substituted oligophenylenes,<sup>[297]</sup> where the substituents were varied from methyl to ethyl to hexyl ( $\Delta G^\ddagger = 76.5$  KJ/mol) somewhat lower rotational barriers have been calculated, which might be due to less steric hindrance in the target compounds **O3** and **O4**. Here, the independence of the rotational barrier of the oligomer length had also been observed.

In a second series of experiments the influence of different substitution R in 4 and 4''–position of a methyl–substituted terphenyl unit on the coalescence temperature was investigated. Since all molecular structures (**O3**, **O15**, **O19** and **O31**) are the same apart of the group in 4 and 4''–position, it was assumed that only electronic effects of the substituents cause different coalescence temperatures. In particular, a steric influence of these groups seemed to be unlikely, as they are too far away from the centre of rotation. Electronic effects of substituents can be quantified by their *Hammett* parameters. Thus, the *Hammett* parameters

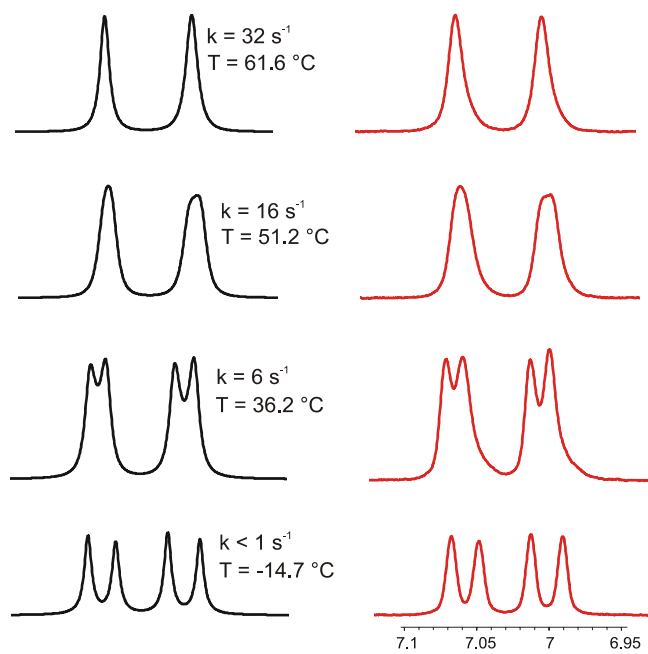


**Figure 4–23:** The temperature dependence of the two sets of signals of the protons in the middle rings of **O4**. A comparison between measured (red) and calculated (black) spectra together with the corresponding rate constant is shown.

were used to evaluate, whether a correlation between the electronic effect of the respective substituent and the coalescence temperature can be found.

Four different compounds with different substituents, namely R = S-acetyl **O3**, R = OCH<sub>3</sub> **O15**, R = F **O19** and R = H **O31** were used for this study. Table 4–3 lists the observed coalescence temperature for these four compounds and the *Hammett* parameter of the substituent.<sup>[315]</sup> Figure 4–24 shows a plot of measured coalescence temperature T<sub>C</sub> of the compound against *Hammett* parameter of the respective substituents. The assumed error of  $\pm 1.5$  K of the temperature measurement is also indicated. For compound **O3** bearing S-acetyl groups which have the highest *Hammett* parameter of  $\sigma_p = 0.45$  the lowest T<sub>C</sub> has been observed. The highest T<sub>C</sub>, that is 5.6 K higher than for **O3**, has been measured for compound **O31** having R = H with  $\sigma_p = 0$  (by definition). The coalescence temperature of compound **O19** bearing fluorine substituents lies with T<sub>C</sub> = 57.5 °C in between these two extremes. The

Compound	Group in 4-position	Coalescence T in °C	Hammett parameter $\sigma_p$
<b>O31</b>	H	62.0	0.00
<b>O19</b>	F	57.5	0.20
<b>O15</b>	OCH <sub>3</sub>	56.5	-0.15
<b>O3</b>	S-acetyl	56.4	0.45

**Table 4–3:** Different coalescence temperatures measured for differently substituted terphenyl compound together with Hammett parameter of the substituent.

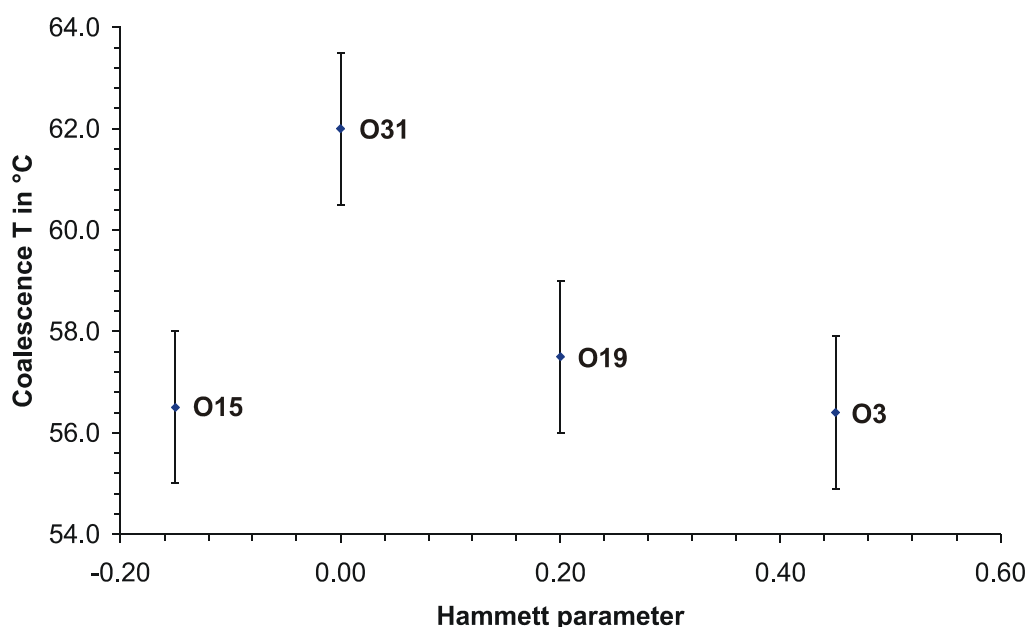


**Figure 4–24:** Correlation between Hammett parameters of the substituent in position 4 and 4'' and measured coalescence temperature for the compounds **O3**, **O15**, **O19**, **O31**.

substituent constant for fluorine (**O19**) is  $\sigma_p = 0.20$ , that is between the one of **O3** and **O31** as well. However,  $\text{OCH}_3$  substituents have the lowest  $\sigma_p = -0.15$ , while the coalescence temperature of the corresponding terphenyl **O15** differs only by 0.1 K from the lowest observed one of **O3**.

The available data does not allow to establish clear correlations between the coalescence temperature of the rotational motion of the investigated terphenyl-compounds and the Hammett parameters of the used substituents. In particular, the large deviation of the coalescence temperature of compound **O31** having hydrogen as substituent on one side and all other terphenyls on the other side prevents such a linear correlation. At present, it is not clear, why this compound shows this considerable increase in  $T_c$  compared to the others. In order to further investigate the influence of the substituents on the rotational motion other terphenyls having substituents with stronger electronic effects such as nitro-groups can be synthesised. Thereby, it could be possible to determine whether there is an electronic effect or not. Compounds having donor and acceptor substituents are assumed to have a different structure of the transition state.<sup>[286],[275]</sup> Hence, the synthesis and DNMR study of such compounds could help to investigate the influence of the structure of the transition state. The synthesis of such compounds is currently under way.

In a simple transport picture the frontier orbitals of the  $\pi$ -system are assumed to be dominating for electronic transport properties.<sup>[316],[46]</sup> UV/Vis spectra of organic compounds are associated with transitions between electronic energy levels. Electrons can be excited from

the occupied bonding  $\sigma$ - or  $\pi$ -orbitals or from the non-bonding  $n$ -orbitals (lone pairs) to the unoccupied, anti-bonding  $\pi^*$  - or  $\sigma^*$ -orbitals, that is transitions corresponding to  $\sigma \rightarrow \sigma^*$ ,  $\pi \rightarrow \pi^*$ ,  $n \rightarrow \pi^*$ ,  $n \rightarrow \sigma^*$  and so one can be observed. Hence, UV/Vis spectroscopy allows to obtain information about the electronic structure, in particular the frontier orbitals of organic compounds.

UV/Vis spectra of the rod like structures **O1 – O4** have been recorded as  $1 \times 10^{-5}$  M solutions in hexane (Figure 4–25). The simplest member of this series **O1** shows two featureless broad absorptions, one at 262.0 nm ( $\epsilon_{\max} = 18100$ ) and one at 200.0 nm ( $\epsilon_{\max} = 36800$ ), that is the spectrum resembles the one of the parent compound benzene (254 nm and 203 nm).<sup>[317]</sup> Usually, sulphur containing groups slightly red-shift the absorption maxima due to enhanced delocalisation resulting in a loss of the fine structure of the first maximum, for instance phenyl thioacetate exhibits a broad maximum in the region of 230 – 240 nm.<sup>[318]</sup> Consequently, the first absorption ( $\lambda = 262.0$  nm) of **O1** can probably be attributed to the alteration of the  $\pi$ -system by two S-acetyl-groups. The short-wavelength absorption ( $\lambda = 200$  nm) of higher intensity is probably the  $\beta$ -band, which arises from the  ${}^1E_{1u} \leftarrow {}^1A_{1g}$  transition. Target **O2** exhibits absorption maxima at 251.5 nm ( $\epsilon_{\max} = 20400$ ) and 208.0 nm ( $\epsilon_{\max} = 66500$ ). By comparison with literature known absorption spectra of differently substituted biphenyls the position of the first low-intensity absorption maximum of **O2** can be

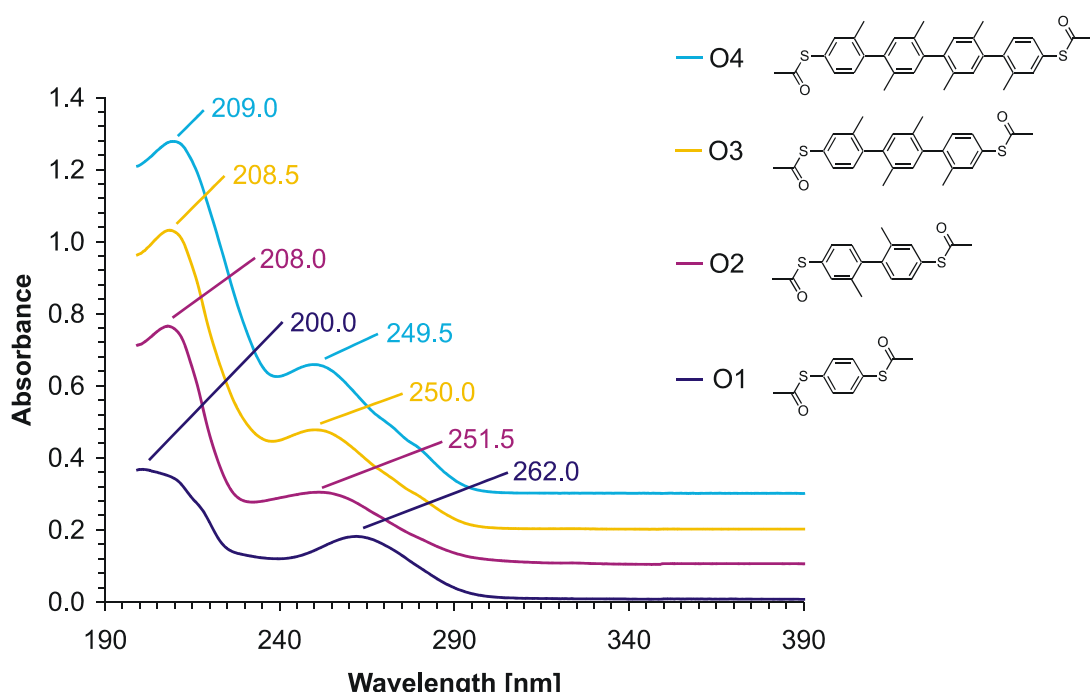


**Figure 4–25:** UV/Vis spectra of **O1 – O4** ( $1 \times 10^{-5}$  M solutions in hexane at room temperature). For clarity the spectra have been shifted by 0.1 units.

rationalised. The parent compound biphenyl shows an absorption at  $\lambda = 247.7$  nm, whereas 2,2'-dimethyl-biphenyl has an absorption maximum at  $\lambda = 227$  nm, that is the lowered  $\pi$ -conjugation of the substituted compound due to the rotation of the phenyl-rings compared to the unsubstituted one becomes apparent in the UV/Vis spectrum.<sup>[317],[319]</sup> The bathochromic shift of **O2** compared to 2,2'-dimethyl-biphenyl probably arises from the enlargement of the conjugated  $\pi$ -system due to substitution with lone-pairs containing S-acetyl-groups, as already observed for target compound **O1**.<sup>[318],[317]</sup> This absorption is commonly regarded as the p-band ( ${}^1B_{1u} \leftarrow {}^1A_{1g}$  transition).<sup>[320]</sup> The intense absorption at  $\lambda = 208$  nm is probably due to a transition, which corresponds to the benzene  $\beta$ -band. Hence, target **O2** exhibits an absorption spectrum closely related to the sum of two sulphur-substituted benzene moieties pointing at a divided  $\pi$ -system due to the torsion angle between both phenyl-rings. The terphenyl **O3** exhibits absorption maxima at  $\lambda = 250.0$  nm ( $\epsilon_{\max} = 27700$ ) and  $\lambda = 208.5$  nm ( $\epsilon_{\max} = 83100$ ), which can be assigned as the p-band and the  $\beta$ -band, respectively, as already described for the biphenyl compound. The quaterphenyl **O4** shows essentially the same spectrum as the terphenyl with bands at  $\lambda = 249.5$  nm ( $\epsilon_{\max} = 35900$ ) and  $\lambda = 209.0$  nm ( $\epsilon_{\max} = 97800$ ), albeit with a higher intensity. Again the assignment of the absorption maxima is the same as for the biphenyl compound **O2**.

In the unsubstituted oligophenylene series the absorption edge shifts towards longer wavelengths and increases in intensity with increasing number of benzene rings asymptotically approaching a limiting value,<sup>[320]</sup> the so-called effective conjugation length. In the spectrum of *p*-sexiphenyl the limit of about 308 nm was observed. A similar trend has been found in a series of 2 and 5-methyl substituted *p*-oligophenylenes, where saturation seems to be reached with the oligomer containing five rings.<sup>[297]</sup> In contrast, in the investigated family of oligophenylenes the spectra do not change considerably when going from the biphenyl **O2** to the quaterphenyl compound **O4** suggesting that isolated  $\pi$ -subunits have already been obtained in the biphenyl-compound.

When the  $\pi$ - $\pi$  interaction across a bond is eliminated almost completely due to an angle of rotation near 90°, the spectrum can be considered as the sum of the spectra of the modular parts of the molecule on either side of the bond.<sup>[317]</sup> A similar observation has been made in the present series of compounds. The target compounds **O2** to **O4** all exhibit absorption spectra closely related to the sum of two sulphur-substituted benzenes, that is the position of the absorption maxima changes only slightly compared to a S-acetyl substituted benzene, but the intensity of the peaks increases. When the extinction coefficient  $\epsilon_{\max}$  is divided by the number of phenyl-rings n present in the structure the following result is obtained for the p-

band:  $(\epsilon_{\max}/n) = 18100$  for **O1**,  $(\epsilon_{\max}/n) = 10200$  for **O2**,  $(\epsilon_{\max}/n) = 9200$  for **O3** and  $(\epsilon_{\max}/n) = 9000$  for **O4**. For the  $\beta$ -band the intensity per phenyl-ring shows the following development:  $(\epsilon_{\max}/n) = 36800$  for **O1**,  $(\epsilon_{\max}/n) = 33000$  for **O2**,  $(\epsilon_{\max}/n) = 27700$  for **O3** and  $(\epsilon_{\max}/n) = 24500$  for **O4**. The contribution of one phenyl-ring to the intensity of the p-band lies between 10000 to 9000 and to the intensity of the  $\beta$ -band between 33000 to 25000. Hence, excluding **O1** the contribution of one phenyl-ring to the intensity of the absorption band is comparable in target structures **O2 – O4**. Compound **O1** is probably an exception due to the presence of two sulphur-substituents on one aromatic system, which also has an effect on the intensity of absorption bands. This observations suggests that due to the methyl-substituents the phenyl-rings of the target compounds have a large torsion angle reducing  $\pi$ - $\pi$ -interaction between adjacent phenyl-rings.

The interpretation of the UV/Vis spectra allows for the following conclusions: 1)  $\pi$ - $\pi$  interaction seems to be reduced due to the introduction of the methyl-groups in appropriate position helping to rotate the phenyl-rings out of plane. 2) In this series the effective conjugation length seems to be reached with  $n = 2$ , that is with the biphenyl. Possibly, the benzene compound **O1** has a larger  $\pi$ -system due to the presence of two sulphur-endgroups on one phenyl-ring. 3) If the effective conjugation length is already reached with  $n = 2$ , the size of the  $\pi$ -system does not increase anymore, that is the  $\pi$ -electrons are not delocalised considerably over adjacent phenyl-rings. Hence, the electronic communication between the outer phenyl-rings of the higher homologues **O3** and **O4** is probably reduced by a large extent compared to unsubstituted oligophenylenes.

An UV/Vis spectrum of target compound **O29** which was designed to study the influence of light on the electron transport behaviour using a MCB has been recorded at room temperature ( $5 \times 10^{-6}$  M solution in hexane). Figure 4–26 shows the absorption spectrum of **O29**. The strongest absorption at  $\lambda = 258$  nm is the  $\beta$ -band and probably arises from the  ${}^1B_b \leftarrow {}^1A$  transition.<sup>[321]</sup> The longest wavelength absorption between 322.0 and 394.0 nm consists of five vibrational subbands and can probably be attributed to the  ${}^1L_\alpha \leftarrow {}^1A$  transition by comparison with the parent compound anthracene.<sup>[321]</sup> Both outer phenyl-rings give rise to the absorption maximum at 205.0 nm which corresponds to the  $\beta$ -band of benzene. A comparison with the UV/Vis spectrum of anthracene reveals that apparently substitution in 9 and 10 position does not change the spectrum considerably, only a slight bathochromic shift of all absorptions can be observed. Apparently, the addition of the two phenyl-rings in position 9 and 10 does not extend the  $\pi$ -system considerably suggesting an angle of rotation of the phenyl-rings out of the anthracene-plane of near  $90^\circ$ . In fact, compared to 9,10-

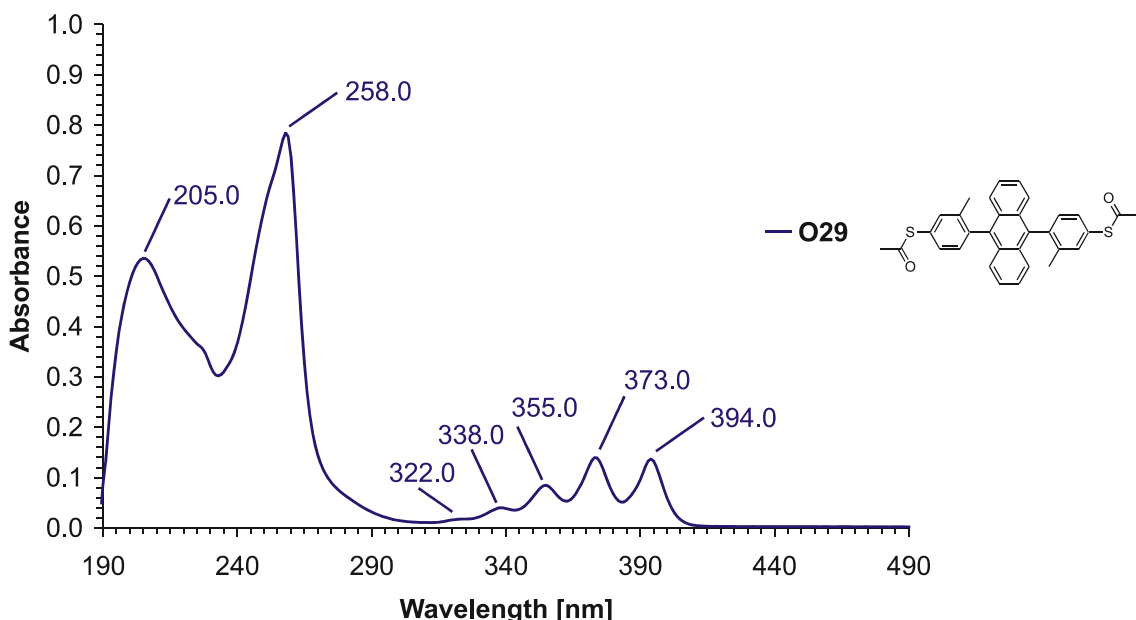


**Figure 4–26:** UV/Vis spectrum of **O29** ( $5 \times 10^{-6}$  M solution in hexane at room temperature).

diphenylanthracene a small hypsochromic shift of the longest wavelength absorption at  $\lambda = 394.0$  nm by  $\approx 4$  nm can be observed probably pointing at a divided  $\pi$ -system due to the angle of rotation between the phenyl-rings and the anthracene moiety. Therefore, **O29** can be described as a system of three (almost) separate  $\pi$ -systems, namely a central anthracene chromophore and two phenyl-rings connected by two conjugation breaking elements.

UV/Vis spectra of target compounds **B1** – **B3** have been recorded to study the influence of the length of the alkyl bridge between the two phenyl-rings on the  $\pi$ -conjugation of the system. For this purpose  $1 \times 10^{-5}$  M solutions in hexane of the three compounds have been prepared (Figure 4–27). The absorption spectra of **B1** and **B2** look rather comparable, as has already been described in the literature for the parent compounds fluorene and 9,10-dihydrophenanthrene.<sup>[317]</sup> Target compound **B1** shows two absorption maxima of almost equal intensity at 311.5 nm and 290.0 nm together with a broader more intense absorption at 211.5 nm. 2,7-Dimethylfluorene exhibits a similar spectrum with an intense absorption at 210 nm (the  $\beta$ -band), a weaker and broader absorption at 270 nm (the p-band) and an even weaker band with vibrational fine structure between 290 and 310 nm (the  $\alpha$ -band). The assignment mentioned has been done according to Clar.<sup>[322]</sup> These bands are known to shift bathochromically with extended  $\pi$ -conjugation.<sup>[323]</sup> Hence, an analogous assignment of the observed maxima of target compound **B1** can probably be done, that is the absorption at 211.5 corresponds to the  $\beta$ -band, the absorption at 290 nm is probably the p-band, which has been red-shifted due to the presence of two S-acetyl groups extending  $\pi$ -conjugation. The longest-wavelength absorption is probably the  $\alpha$ -band, but without vibrational fine structure.

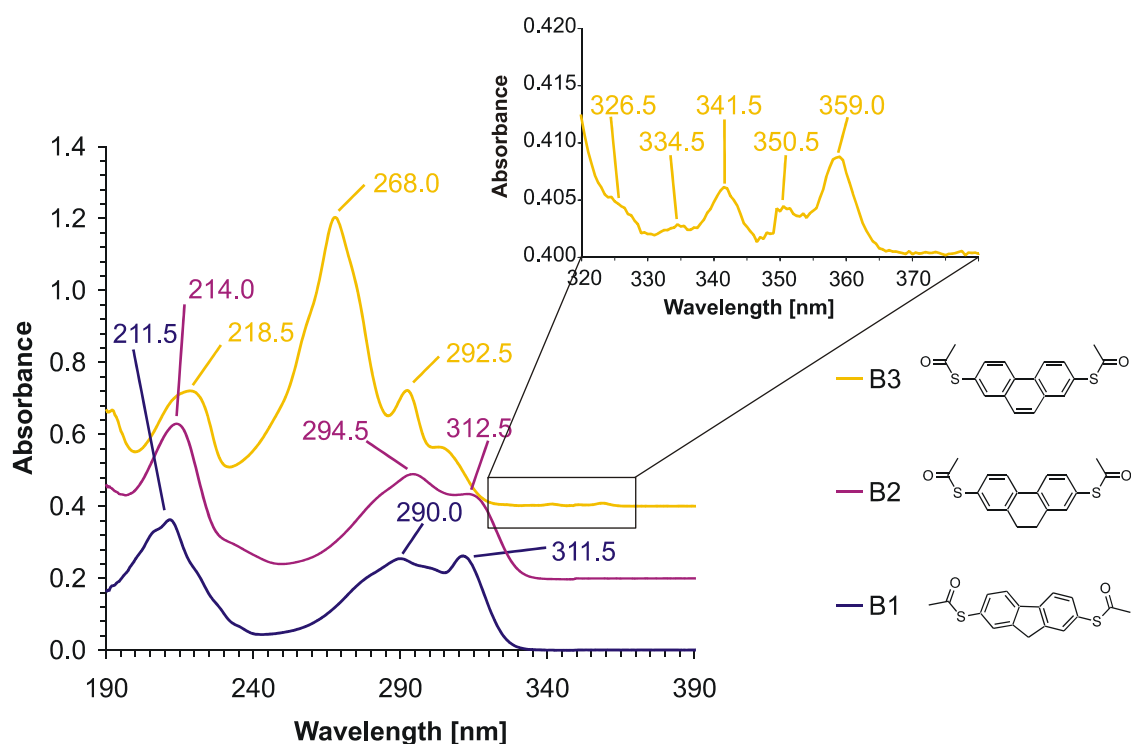


**Figure 4–27:** UV/Vis spectra of **B1 – B3**  $1 \times 10^{-5}$  M solutions in hexane. For clarity the spectra have been shifted by 0.2 units.

As already mentioned, the absorption spectrum of target compound **B2** is comparable to the one of **B1** showing three absorptions at 214.0, 294.5 and 312.5 nm. The parent compound 9,10-dihydrophenanthrene shows two broad absorption maxima at 210 nm ( $\beta$ -band) and 264 nm (p-band) together with a weak absorption at 300 nm ( $\alpha$ -band). These bands are known to red-shift with extended  $\pi$ -conjugation.<sup>[317]</sup> The  $\pi$ -system of target compound **B2** is probably altered due to the presence of two S-acetyl groups possessing lone pair electrons that can increase the  $\pi$ -system. Hence, the absorption maxima of **B2** can be assigned in the same way as has been done for the fluorene **B1**: 214.0 nm ( $\beta$ -band), 294.5 nm (p-band) and 312.5 ( $\alpha$ -band).

The last member of this series **B3** contains a phenanthrene-ring. Three absorption maxima are observed for this compound, namely a broad maximum at 218.5 nm, the most intense maximum at 268.0 nm and a weaker absorption at 292.5 nm. In addition, a fine structure consisting of five maxima between 326.0 – 359.0 nm is found. The parent compound phenanthrene shows a similar spectrum with a broad absorption at 210 nm (the  $\beta$ -band), the main broad absorption at 251 nm together with two minor peaks at 275 nm and 295 nm (the p-band) and a weak absorption between 310 and 350 nm (the  $\alpha$ -band) comprising a vibrational fine-structure of six distinct peaks.<sup>[317]</sup> Probably due to the presence of two acetyl-sulphur-groups the  $\pi$ -system of the target compound **B3** is extended compared to

phenanthrene. Hence, the absorption maxima of **B3** can be assigned accordingly: the  $\beta$ -band is at 218.5 nm, the p-band is made up of the intense absorption at 268.0 nm plus the one at 292.5 nm. The  $\alpha$ -band between 326.5 – 359.0 nm shows a similar vibrational fine-structure of five peaks. In fact, this fine-structure is often used to identify phenanthrene-containing compounds.

All investigated bridged biphenyls **B1** – **B3** show a pronounced red-shift of the longest wavelength absorption compared to biphenyls without an alkyl-bridging chain, for example target compound **O2**. This suggests that the degree of  $\pi$ -conjugation between the phenyl-rings can be increased by a bridge in position 2 and 2', because the rather short bridges used forces the phenyl-rings to adopt a more co-planar arrangement. From x-ray analysis (see above) it is known that fluorene shows an almost coplanar arrangement of the two phenyl rings, while dihydrophenanthrene has a torsion angle of about 20°. Hence, the overlap between the  $p_z$ -orbitals of the two phenyl rings in **B2** should be reduced slightly compared to **B1**. However, according to the UV/Vis spectra of **B1** and **B2** these two compounds have very similar degrees of  $\pi$ -conjugation suggesting that a torsion angle of 20° is not high enough to effect  $\pi$ -conjugation between the two phenyl-rings considerably. To further study the effect of the length of the bridge on the  $\pi$ -conjugation the synthesis of additional compounds with longer alkyl-bridges is required. Of particular interest will be that bridge length, at which the UV/Vis spectrum of the bridged compound and a corresponding non-bridged, but 2,2'-alkyl substituted one will match. From literature it is known that the spectrum of a compound having an alkyl-bridge consisting of five atoms can be superimposed on that of 2,2'-diethyl-biphenyl.<sup>[317]</sup> Here,  $\pi$ -conjugation in the bridged compound and the non-bridged biphenyl will presumably be equal. The synthesis of biphenyls bearing alkyl bridges with more than two carbon atoms is currently under way.

#### 4.1.1.4 Electron Transport Measurements

Before the results of the electron transport measurements done in the group of *H. Weber* at the INT are described in more detail, first some basic principles of electron transport through metal–molecule–metal junctions are presented, since these are necessary for an understanding and interpretation of the obtained data.

Different models dealing with electron transport through junctions containing molecules exist.<sup>[4]</sup> In general, such systems can be characterised by the electrochemical potential of the

metal electrodes, the electronic structure of the molecule between these electrodes and the coupling, in particular the strength of this coupling of the molecule to the metal electrodes. Two different pictures describing electron transport in such set-ups exist. In the first model the electron tunnels from an electrode into the molecule and remains there for a while, until it continues to tunnel to the opposite electrode. In this case, the electron dissipates energy while “on” the molecule. This model is called hopping model and commonly occurs in weakly coupled systems, for example quantumdots. Weak coupling is found, when the molecule is attached to the electrode surface only by weak *van der Waals* forces. In the second coherent transport model electrons are described as plane waves coming from one electrode. The wave is either transmitted through the molecular junction to the other electrode with a certain probability or it is reflected. Hence, the molecule acts as a scattering object. The scattering can be computed by a *Landauer*–type formula, when the wave function is known. Here no energy transfer between the electron and the molecule occurs. Strongly coupled systems are described best with this model. It should be noted, though, that due to the strong coupling between the molecule and the electrodes an independent treatment of the different parts of the metal–molecule–metal junctions is no longer possible. In particular, the molecular orbitals hybridise with the metallic states in the leads yielding a broadening of the energy levels.

Figure 4–28 shows schematically the electronic situation, when a molecule is placed between two metallic electrodes, which can be used as a simple model to explain the current–voltage characteristics observed in the experiments.<sup>[324],[325]</sup> For simplicity, the energy levels of the molecule are drawn as sharp levels, which is probably not completely correct (see above). Figure 4–28 left represents the situation when no voltage is applied. The electrochemical

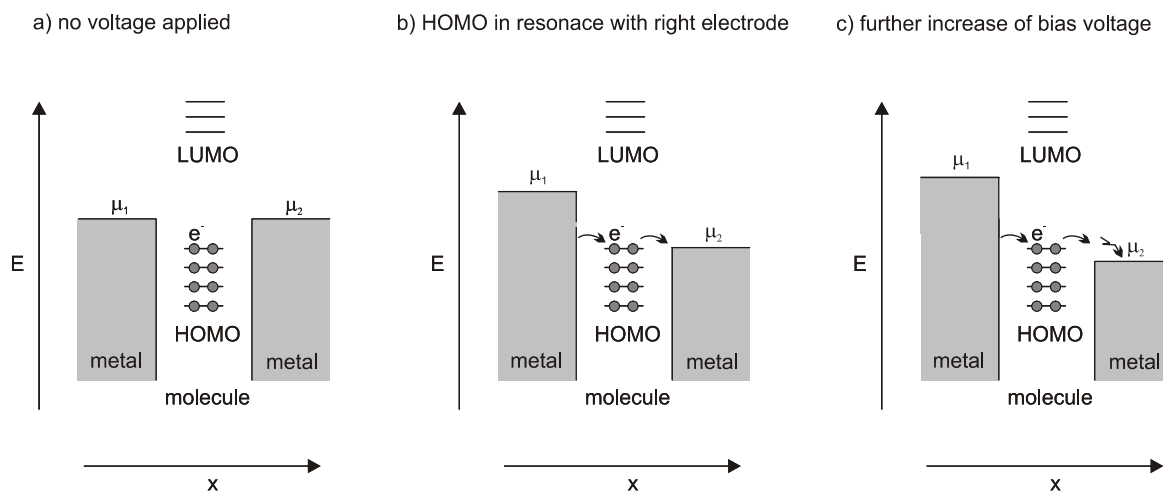


**Figure 4–28:** Simple model for electron transport. a) no voltage applied; b) HOMO comes in resonance with the electrochemical potential of the right electrode; c) further increase of the applied bias voltage.

potential  $\mu$  is shown on the left and on the right, in the middle the discrete energy levels, that is the HOMO and the LUMO, of the molecule are drawn. When no voltage is applied, the left and the right electrode will have the same electrochemical potential. The relative position of this compared to the energy levels of the molecule cannot be determined easily. However, it has been suggested that the electrochemical potential is closer to the HOMO than to the LUMO.<sup>[12],[326]</sup> When a voltage is applied, the electrochemical potentials of the metal electrodes  $\mu_1$  and  $\mu_2$  are shifted with respect to each other. Assuming a symmetrical coupling of the molecule to the electrode the potentials will shift symmetrically in reference to their original position. As long as both potentials fall in between the HOMO–LUMO–gap, the HOMO will be occupied and the LUMO will be unoccupied. Hence, no current will flow, because no molecular orbital lies within the energy window spanned by the two electrodes. When the HOMO comes in resonance with the electrochemical potential of one electrode, electron transport will start (Figure 4–28 middle). A further increase of the voltage will not result in a considerably increase of current, until the next molecular orbital comes into resonance with the electrode (Figure 4–28 right).

However, this simple model does not account for single-electron effects. Nanoscale objects like molecules or quantum dots have due to their small size very small capacities. Hence, the energy to charge such a nanoscale object can be very high.<sup>[324]</sup> If electron transport through a structure is suppressed, because there is not enough energy to charge the structure with a second electron, an effect called *Coulomb*–blockade is observed. The simple model described above does not account for this effect. If electron transport through an orbital is suppressed due to *Coulomb*–blockade, current will not flow until the *Coulomb*–blockade can be overcome. Hence, this effect can increase the onset voltage of electron transport through metal–molecule–metal junctions and has to be considered as well, when current–voltage characteristics of single–molecule junctions are studied.

The current–voltage characteristics of single molecules of **O1'** – **O4'** immobilised between two gold electrodes have been studied by *M. di Leo* in the group of *H. Weber* at the INT using the MCB technique (Figure 4–29).<sup>[324]</sup> All molecular rods have been immobilised on the gold electrodes of a MCB with a similar procedure from a solution of the respective molecule in THF.<sup>[324]</sup>

A freshly broken MCB was opened to about 10 nm. Then a  $5 \times 10^{-4}$  molar THF solution of the respective molecule bearing acetyl protected thiol groups on both ends was applied for 30s. After the application the MCB was rinsed with THF extensively. Acetyl–protected thiols have been used for several reasons. Acetyl–protected thiols can be cleaved *in situ* on the gold

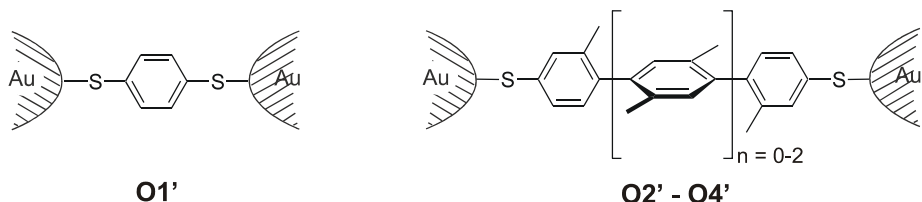


**Figure 4–29:** Target molecules **O1 – O4** immobilised between the electrodes of a MCB (schematic drawing).

surface allowing the formation of a Au–S bond. Presumably, this process happens due to hydrolysis of the thioester *via* trace amounts of water or enol forms of the thioester. However, the mechanism of this reaction is still not completely unravelled.<sup>[61]</sup> Free thiols tend to the formation of disulphides in the presence of oxygen. Since the investigated molecules bear sulphur on both ends, polymerisation of these molecules is possible *via* repeated disulphide formation. Hence, no individual molecules can be investigated anymore. The acetyl protection group prevents this reaction. Besides, acetyl-protected thiols require higher concentrations of compounds compared to free thiols to achieve monolayer coverage.<sup>[61]</sup> Because of this and due to the short application time the coverage of the surface of the electrode is expected to be far below a completed monolayer facilitating the measurement of individual molecules.

After the application, the individual molecules split of *in situ* one of their acetyl-protection groups and form a covalent bond between sulphur and gold. At this point of time, no molecule was bridging the electrode gap. Then, the whole set-up was transferred to the sample chamber that was evacuated. While a voltage was applied, the two electrodes were brought together again by releasing the bend of the MCB chip. The polarisable, rod-like molecules aligned themselves in the electric field towards the electrode on the opposite side. The current was monitored, and suddenly at a certain distance a sharp increase in current was observed that can be ascribed to the first molecule bridging the gap and, thereby, forming a metal–molecule–metal junction (lock-in situation). The ratio between the position of the motor, which is used to adjust the bend of the chip, and the electrode distance can be estimated geometrically only roughly, since the substrate does not bend homogeneously. Therefore, it is not clear, when the electrode gap reaches the size of the length of the molecule exactly. However, an equation describing the bending of a bar adopted from mechanics can give a first approximation of the distance between the electrodes. This has been confirmed further by measurements with a MCB without molecules, where the tunnelling current was used as an estimate for the electrode distance. Using these calculations the length of the electrode gap in the lock-in situation can be approximated. Usually the calculated length of the gap is comparable to the length of the investigated molecule that bridges the electrode gap. When

the electron transport measurements were done at room temperature, all current–voltage characteristics were recorded in this lock–in situation. A more thorough description of the MCB technique can be found in chapter 2.2.2.

In the present case, however, the investigations were done at lower temperatures of about 30 K to obtain a better data quality due to less thermal fluctuations of the metal–molecule–metal junction. In particular, the rather high mobility of gold atoms, which results in considerable fluctuations of the recorded current–voltage characteristics, can be reduced at lower temperatures.<sup>[62],[324]</sup> These measurements required a further development of the immobilisation protocol due to several reasons.<sup>[62]</sup> Cooling down an already established contact is probably not possible because of the different thermal expansion coefficients of the materials used, which results in a badly controlled drift of the electrode spacing. In first experiments a change of up to 1 nm in the spacing was observed when going from room temperature to 30 K, which is in the order of the length of the investigated molecules. An electronic feedback control of the electrode gap during cooling requires the knowledge of the absolute distance between the electrodes. This is rather difficult to obtain experimentally. To cool down an open junction and to establish the contact at low temperatures is probably not possible either. As already explained, the molecules possess acetyl–protection groups to prevent disulphide formation in the presence of oxygen. This protection group splits off *in situ* on the gold electrode at room temperature to form a covalent Au–S bond. However, this procedure is expected to work only at room temperature, since at lower temperatures there is probably not enough energy available for the deprotection reaction. Hence, a procedure that circumvents both described problems was developed. First, the usual immobilisation protocol depicted above was followed, until presumably a few molecules were bridging the electrode gap. Then the junction was opened again at room temperature (Figure 4–30). From molecular dynamic simulations<sup>[327]</sup> and experiments<sup>[328]</sup> it is known that all bonds in the molecule including the Au–S bond are more stable than a Au–Au bond. Hence, re–opening the junction probably resulted in an arrangement, where the molecule is covalently bonded to the electrode on one side via a Au–S bond, while the other side bears a sulphur group terminated by one or possibly a few gold atoms. Then the junction can be cooled down while it is open and re–established at low temperatures without any further organic reactions. The formation of a Au–Au bond is considered to have a negligible activation barrier. When the electrodes were approached to each other at low temperatures while a voltage was applied, a similar lock–in behaviour as at room temperature was observed. All current–voltage characteristics of molecule **O1' – O4'** presented below were recorded in this lock–in situation.<sup>[324]</sup>

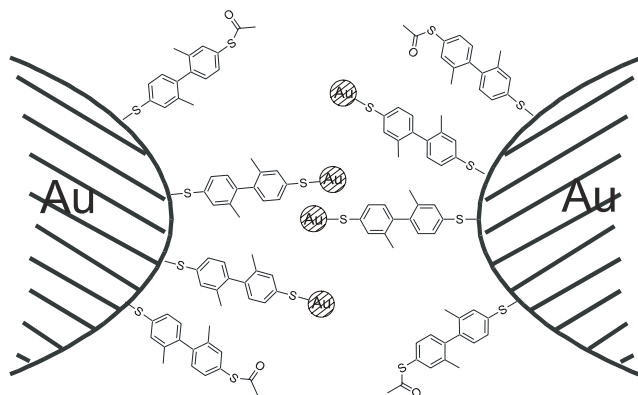


**Figure 4–30:** Scenario between the MCB after closing and re-opening at room temperature.

The recording of current–voltage characteristics was done in the same way for all described metal–molecule–metal junctions. Usually at about a third of the fabricated MCBs measurements with molecules in the gap could be performed. Sometimes the break–junction was damaged after the solution containing the molecule had been applied, sometimes the flexibility of the substrate was lost at low temperatures preventing the closing of the electrode gap. The measurements were done by changing the voltage, while the current was monitored. For every current–voltage (IV) curve the voltage was changed from 0 V to +1.5 V, then to –1.5 V and back to 0 V always in steps of 20 mV. The typical swept rate was 1 V/s. This way the IV–curves that are always shown in red were obtained (Figure 4–31 for example), the blue curves describe the numerical derivative  $dI/dU$ , that is the differential conductance. Different curves shown have been measured with the same molecule junction, but in different voltage sweeps. Often the junction became unstable after several voltage sweeps, which can probably be attributed to a change in the position of the molecule or the gold atoms of the electrodes. Then the electrodes had to be opened again and the protocol to contact a single molecule described above was repeated.

Figure 4–31 shows a typical set of IV curves obtained for a metal–molecule–metal junction of target compound **O1** at 30 K. They are clearly nonlinear, displaying some rounded step–like features. Although **O1** is a symmetric molecule, the recorded current–voltage characteristics of **O1** are asymmetric with respect to voltage inversion. In the area ranging from about +0.5 to –0.5 V the current is suppressed until a sharp increase is observed. The steps became more apparent as peaks in the first numerical derivative  $dI/dU$  of the current–voltage characteristic (shown in blue). At positive bias two peaks at 0.7 V and 1.3 V are observed, whereas at negative voltage a (hardly visible) double peak structure at –0.85 V and –1 V can be found. All peaks differ in their height considerably. Furthermore, the broadening of the peaks is different (0.2 V – 0.3 V). An interesting effect is observed at voltages beyond –1.55 V, where

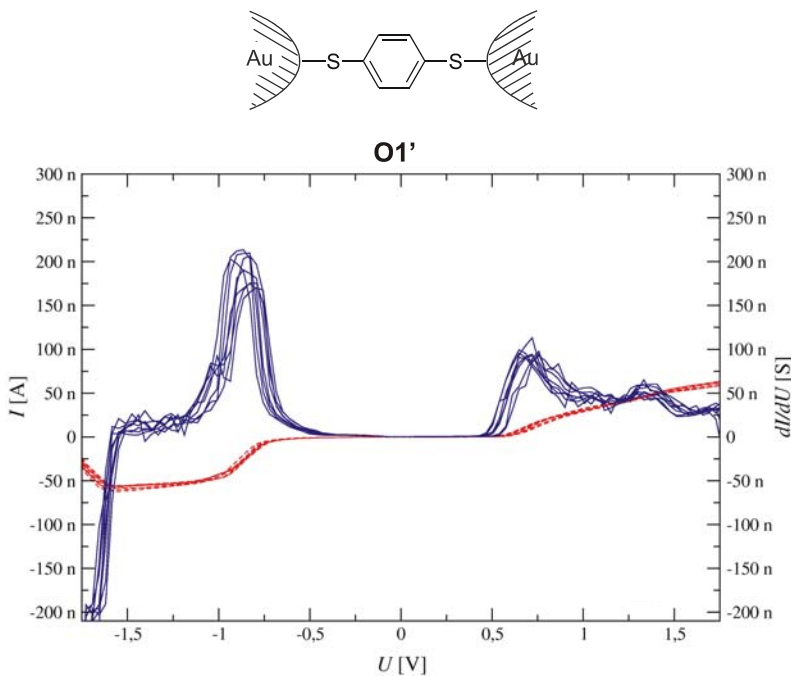


**Figure 4–31:** IV curves of **O1'** reproducibly recorded for a stable metal–molecule–metal junction in a MCB at 30 K (in red) and the numerical derivative  $dI/dU$  (in blue).

the current decreases with increasing voltage, that is a negative differential resistance is found.

Using the simple model explained above the detected steps (Figure 4–31) can probably be attributed to electron transport through the HOMO, which comes in resonance with the electrochemical potential of one of the electrodes. The numerical derivative  $dI/dU$  represents the differential conductance. Discrete energy levels of the molecule, as assumed in the model, should give rise to observed steps in the IV curve that look like a step function. However, more rounded steps are actually observed. Probably the molecular orbitals are not discrete any longer due to the coupling of the molecule to the electrodes giving rise to these more rounded-like steps. The suppression of current can maybe be attributed to Coulomb–blockade, where the Au–S bonds form the barrier in the system and the phenyl–ring is regarded as an island between these two contacts.

It had been anticipated that due to the symmetry plane of **O1**, which is perpendicular to the sulphur–sulphur axis, the observed IV curves will be symmetric with respect to voltage inversion. However, as already pointed out, no symmetric IV curves have been recorded for **O1'**. For immobilisation at low temperatures it was necessary to terminate the molecule with one or possibly more gold atoms on one sulphur–group (see above). After cooling the electrode gap was closed *via* formation of Au–Au bonds. Hence, the two electrodes attached to the molecule have a different history. While one contact was formed by self–assembly of

the acetyl-protected molecule on the gold, the other contact was essentially formed by formation of gold–gold bonds. This probably results in different contact arrangements on both sides, which can give rise to asymmetric IV curves. Furthermore, it has been shown in theoretical calculations that sulphur can bind covalently to gold in three different ways, namely to one gold atom, bridging two gold atoms or even three gold atoms. These configurations are energetically very similar, but differ considerably in their electronic structure.<sup>[46]</sup> When the structure of the molecular orbitals is different, different electron transport behaviour will be observed. In the experiment, the electrodes had to be adjusted very carefully after the described lock-in behaviour, because otherwise no stable IV curves could be recorded. Probably, this adjustment results in an asymmetric contact arrangement, that is the molecular orbitals are not exactly the same in the vicinity of both electrodes, giving rise to the recorded asymmetric current–voltage characteristics.

At voltages higher than  $-1.55$  V an effect called negative differential resistance has been found. Such an effect has already been observed in experiments<sup>[41]</sup> with a different molecular rod and proposed in theoretical work as well.<sup>[329]</sup> However, usually the molecular junctions became unstable at voltages higher than  $1.5$  V. Therefore, it is not clear, whether the observed effect is real or can maybe be attributed to the instability of the junction at this high bias voltage.

Despite the symmetry of target compound **O1** only asymmetric IV curves have been measured. As explained above, these asymmetries can probably be attributed to different contact arrangements of the molecule to the two electrodes. Furthermore, the measurement of **O1** turned out to be rather challenging, which can probably be assigned to the short length of the molecule of  $0.64$  nm. Due to this rather short length of **O1** the features of the microscopically rough and, thereby different electrodes probably influence the current–voltage characteristics considerably. Since the electric field between the two electrodes is inhomogeneous due to the microscopic roughness, an asymmetry is probably induced as well. In target compound **O2** the two phenyl rings of the biphenyl system are rotated with respect to each other by an angle of  $79.7(2)^\circ$ , as determined by x-ray analysis. Since this torsion angle reduces the overlap between the  $p_z$ -orbitals of the phenyl-rings, the conjugation between the rings is disturbed. The current–voltage characteristic of **O2** recorded at  $30$  K does not show a step-like behaviour, only a small suppression of the current between  $\pm 200$  mV is detected (Figure 4–32). At  $U = 1$  V a current of about  $10$  nA was measured, which is smaller by a factor of 3 to 6 compared to the measurements of the first target compound **O1**. A symmetric curve has been obtained suggesting a symmetric contact arrangement. Using again the simple

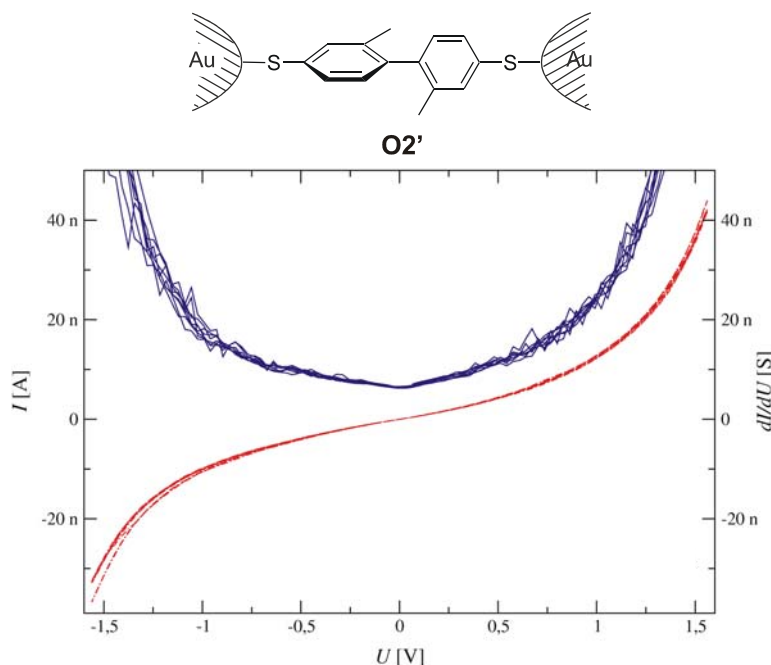


**Figure 4–32:** IV curves of **O2'** reproducibly recorded for a stable metal–molecule–metal junction in a MCB at 30 K (in red) and the numerical derivative  $dI/dU$  (in blue).

model for electron transport presented above a possible explanation for this observation can be found. The observation of peaks can be attributed to electron transport through a molecular orbital that comes in resonance with the electrochemical potential of one of the electrodes. If no peaks are observed, possibly no molecular orbital came in resonance with the electrode, that is the potential difference was not high enough to adjust to the HOMO–LUMO gap present in this compound. However, a comparison of the UV/Vis spectra of **O1** and **O2** points at different, but comparable HOMO–LUMO gaps in these two compounds. Therefore, possibly the position of the HOMO in **O2'** is different compared to **O1'** and a larger energy window has to be spanned by the electrodes to achieve an arrangement, where one molecular orbital comes in resonance with one of the electrodes. No Coulomb–blockade becomes apparent in this junction. The recorded IV curves rather resemble the characteristics of a tunnelling barrier,<sup>[4]</sup> which might be due to the conjugation breaking element between the two phenyl–rings. The reduced current level in this structure containing **O2** compared to **O1** can probably be attributed to the disturbed  $\pi$ –conjugation as well.

The measurements of **O2'** could be performed more reliably compared to **O1'**. In particular, no careful adjustment of the electrodes after lock-in was required to record stable current–voltage characteristics. The length, that is the sulphur–sulphur distance, of **O2** has been determined in the solid–state to 1.06 nm. Hence, **O2** is almost twice as long **O1**. Probably due to this increased size, the measurement of junctions containing **O2** turned out to be easier.

Especially, the influence of the microscopically rough electrodes on the current–voltage characteristics was probably reduced. Hence, rather symmetric curves could be recorded for this symmetric molecule.

Target compound **O3'** consists of three phenyl-rings that are separated by two conjugation breaking elements due to the torsion angle between the different phenyl-rings, as shown in the crystal structure. Therefore, the central phenyl-ring can probably be regarded as an island, which is electronically separated from the two outer rings. The current–voltage characteristics recorded at 30 K for junctions of **O3'** are not completely symmetric, but differ only slightly at positive and negative bias. An IV curve with two sharp peaks at  $-0.51$  V and at  $+0.47$  V, which are nearly of same height, has been obtained (Figure 4–33). At  $U = \pm 1.5$  V a current of  $I = \pm 20$  nA has been determined, which is comparable to the measurements of the junction containing the biphenyl **O2**. Assuming again the simple transport model explained above, the occurrence of peaks can probably be rationalised. However, the current was suppressed between  $-0.5$  to  $+0.5$  V. Since the structure of **O3'** bears an island in the centre, which is separated electronically from the outer phenyl-rings, possibly the suppression of current can be explained by Coulomb-blockade. Hence, additional energy is required to start electron transport through the structure resulting in the observed suppression and a shift of the onset-voltage for electron transport. In contrast to **O1**, in the structure of **O3'** the island is produced due to the conjugation breaking elements between the phenyl-rings. The current level of this

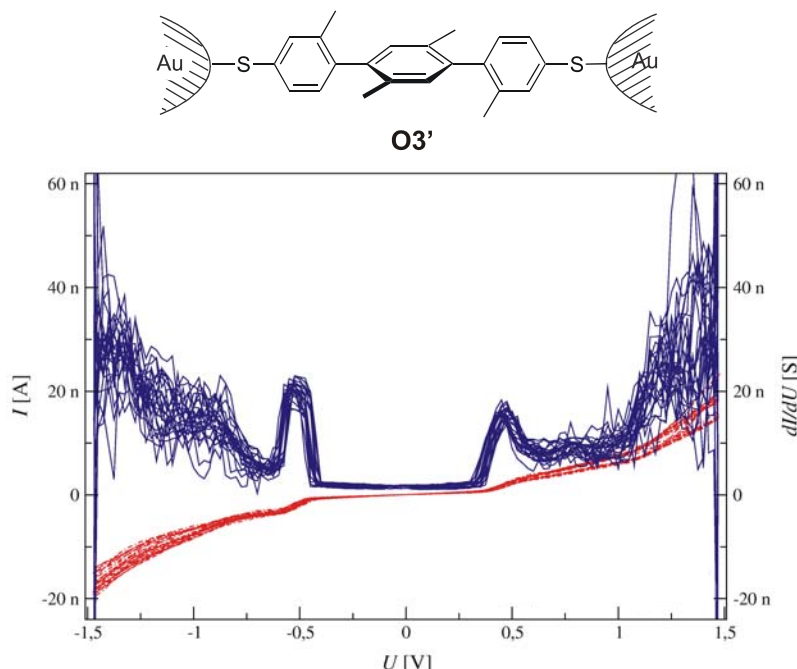


**Figure 4–33:** IV curves of **O3'** reproducibly recorded for a stable metal–molecule–metal junction in a MCB at 30 K (in red) and the numerical derivative  $dI/dU$  (in blue).

junction was reduced compared to **O1'**, but similar to **O2'**. The UV/Vis spectra of these compounds suggested that **O1** might have a larger  $\pi$ -system than the other two compounds **O2** and **O3**. The spectra of the latter two were comparable. Hence, possibly the difference in current level between **O1** on one side and **O2** and **O3** on the other side can be attributed to the different size of the  $\pi$ -systems in these compounds.

Junctions comprising target compound **O3** were considerably more stable than the other junctions, that is IV curves were recorded over a period of about one hour at 30 K. In the other measurements, current–voltage characteristics could be recorded only over a period of several minutes. Hence, it was possible to record more IV curves of one formed junction, that is more separate current–voltage characteristics are presented in figure 1–33 as compared to measurements of the other junctions containing **O1** and **O2**. The length of target compound **O3** as defined by the sulphur–sulphur distance was determined to 1.49 nm, which is about 0.4 nm longer than for the biphenyl **O2**. Possibly, this increase in length allowed for the better stability of these junctions. In particular, effects by the microscopically rough electrodes are probably reduced compared to the first two junctions of **O1'** and **O2'**.

Target compound **O4** consists of four phenyl–rings that are separated electronically by three conjugation breaking elements. Immobilisation of the quaterphenyl **O4** between the gold electrodes allows to record current–voltage characteristics, where the current is suppressed over a wide range from –0.9 up to +1.3 V (Figure 4–34). Then two peaks of about same height at –1 V and +1.4 V are observed. The recorded current–voltage characteristics are not completely symmetric with respect to voltage inversion. Again the current level at  $U = \pm 1.5$  V is within the error of the measurement comparable to the one observed in junctions of **O2** and **O3**. The UV/Vis spectrum of **O4** suggests that this compound has a similar size of the  $\pi$ -system as **O2** and **O3**. Therefore, the similar current levels in the junctions of **O2**, **O3** and **O4** can possibly be attributed to the similar size of the  $\pi$ -system in these structures. Interestingly, the onset voltage of electron transport through this junction is increased significantly compared to junctions containing **O3**. The influence of *Coulomb*–blockade is expected to decrease with increasing size of the system. Hence, the onset–voltage in **O4'** should be reduced compared to **O3'**. On the other hand, the number of conjugation breaking elements might play a role for *Coulomb*–blockade as well, because in **O4'** two islands are present as opposed to only one in **O3'**. It should be noted that the *Coulomb*–energy is in the order of the ionisation–energy of a free molecule. However, the determination of the capacity of a molecule, which is covalently bond to two electrodes, is complicated by the unknown influence of the electrodes on the capacity. Furthermore, the capacity of the investigated molecule can be influenced by

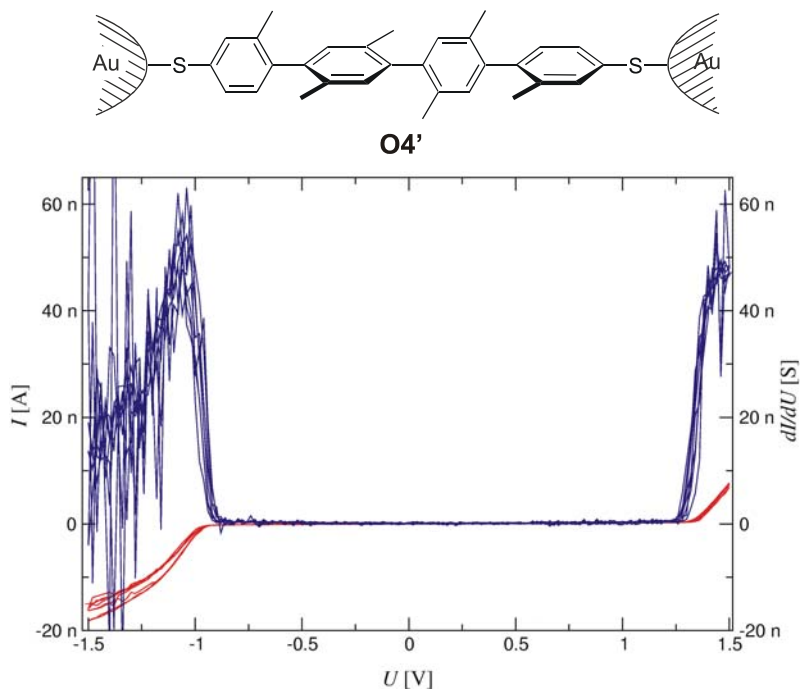


**Figure 4–34:** IV curves of **O4'** reproducibly recorded for a stable metal–molecule–metal junction in a MCB at 30 K (in red) and the numerical derivative  $dI/dU$  (in blue).

neighbouring molecules as well. Hence, a different observed Coulomb–blockade (if it is observed at all) might be caused by slightly different environments in the measurements due to other non–bridging molecules present or different arrangement on the electrode.

It turned out that the recording of IV curves of target compound **O4** was much more difficult than for **O3**. To form a junction the molecule has to align with the electric field applied while driving the electrodes together, that is the molecule has to “stand up”. However, the molecule can also interact with the surface of the gold electrodes by lying flat on this surface. The larger a  $\pi$ –systems is in the molecule, the better this interaction will be. Hence, the tendency of molecule **O4** to align with the electric field is probably reduced compared to **O3**, as it has one phenyl–ring more. This behaviour may be the reason for the more complicated formation of a metal–molecule–metal junction containing **O4**.

By comparison between the different obtained IV characteristics a few interesting results can be obtained. First, the current level of **O1'** was higher by a factor of 3 to 6 compared to the other three molecules. The target compound **O1** has a conjugated  $\pi$ –system between the two sulphur anchor–groups, whereas the other compounds **O2 – O4** have an interrupted  $\pi$ –system due to the rotation of the phenyl–rings out of plane. Different degrees of  $\pi$ –conjugation have been observed in the UV/Vis–spectra, where **O1** showed a bathochromic shift of the longest wavelength absorption compared to the other three oligophenylens. Hence, the higher current level of **O1** can probably be attributed to the higher degree of  $\pi$ –conjugation in this structure

as opposed to the others. Actually, this has been anticipated during the design of the target structures. Surprisingly, the current level of the other junctions containing **O2**, **O3** and **O4** is similar, that is the number of elements that break the  $\pi$ -conjugation does not seem to influence the current level. On the other hand, a comparison between **O3'** and **O4'** reveals that electron transport seems to start at higher voltages, when the number of conjugation breaking elements increases. Whether the observed effects can be explained by *Coulomb-blockade* or whether *Coulomb-blockade* can be observed in these metal–molecule–metal junctions at all, is not clear at present and further studies are required. Unfortunately, due to the difficulties encountered in the recording of current–voltage characteristics of **O4** molecules with more phenyl–rings will become increasingly challenging to immobilise between the electrodes of the MCB. Thus, no molecules with more phenyl–rings have been synthesised. Nevertheless, the presented results show that the shape of the current–voltage curves, that is the electron transport behaviour, can be influenced by changing the structure of the organic molecule.

Current–voltage characteristics of **B1 – B3** have not been measured yet.

#### 4.1.2 Phenyl–ethynyl–anthracene

The current–voltage characteristics of a metal–molecule–metal junction depend on the structure of the organic compound used as has been shown by various studies of self–assembled monolayers as well as of single molecules absorbed between two electrodes. For instance, the influence of the backbone of the molecule on the conductance properties could be shown by changing from alkyl–chains, that is presumably insulating structures, to oligophenylenes, that is  $\pi$ –conjugated molecules, of the same length using mercury drop electrodes.<sup>[9],[42]</sup> Crossed–wire junctions have been employed to study the difference in current–voltage characteristics of oligo(phenylene ethynylene)s and oligo(phenylene vinylene)s suggesting a better conductivity for the latter.<sup>[8]</sup> Between others single–molecule measurements have been done using a MCB device. Here, the difference in spatial symmetry of two molecules of the same length could be observed.<sup>[13],[46]</sup> A Pt–complex has been investigated in a MCB showing an increased resistance of this metal–molecule–metal junction compared to conjugated molecular wires of similar length.<sup>[15]</sup> This has been attributed to the pure  $\sigma$  character of the bond between the Pt(II) ion and the acetylene ligands.<sup>[89]</sup> The results described in the previous section display as well a dependence of the conductance

characteristics of a metal–molecule–metal junction on the length of the investigated oligophenylene.

All these measurements have been done with molecules that bear some kind of anchor–group, usually thiol–groups that allow a covalent binding of the molecule to the electrodes. The effects of different anchor–groups, that is selenium or sulphur, on the molecule have been investigated as well using STM measurements.<sup>[330]</sup> Investigations in crossed–wire junctions showed a dependence of the shape of the IV curves on different contact realisations, too.<sup>[7]</sup> In theoretical calculations different microscopic contact configurations of thiols bond to a gold surface have been proposed to alter the current–voltage characteristics of the junction.<sup>[46]</sup>

However, no experiment to study the influence of the position of the anchor–group in the molecular rod on the single–molecule level has been done so far. The lack of conjugation in the *meta*–position and therewith the reduced electronic communication compared to the *para*–position in rod–like  $\pi$ –systems is known and has been shown e.g. in electrochemical investigations<sup>[63]</sup> as well as in theoretical studies.<sup>[92]</sup> The rather strong covalent bonding to the atomistically disordered metallic electrode causes sample–to–sample fluctuations, which are undesired for both controlled scientific investigation and engineering of electronic properties. Due to reduced electronic communication in the *meta*–position compared to the *para*–position it might be possible to electronically decouple the molecular properties from the disordered electrodes. To demonstrate the validity of this concept for the anchor–groups of single immobilised molecular rods between two electrodes a molecular structure with anchor–groups in *meta*– and *para*–position has been designed (Figure 4–35).

Acetyl–protected sulphur–groups were chosen as anchor–groups, since these groups have proven successful in previous studies.<sup>[13],[15],[62]</sup> The anchor–groups will be attached to the outer building block on both ends of the molecule. An anthracene–ring was selected as the central building block of the structure for two reasons. First, anthracene can be substituted symmetrically in 9 and 10 position due to the higher reactivity of these positions.<sup>[91]</sup> A symmetric molecule was preferred, because the two anchor–groups that bind to both

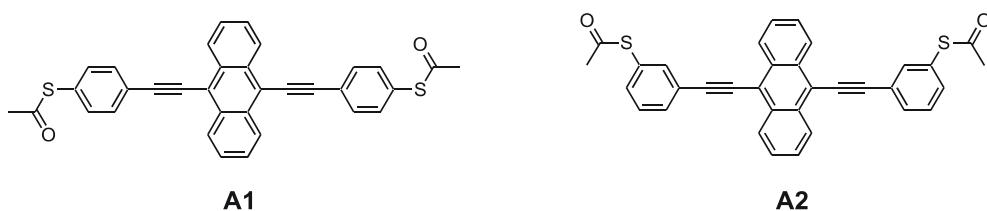


**Figure 4–35:** Target structures A1 and A2 that have been designed to study the influence of the position of the anchor–group.

electrodes should be essentially the same to facilitate the interpretation of the data. Due to the symmetry of the compound the current–voltage characteristics should be symmetric with respect to voltage inversion. Besides, the synthesis of a symmetric molecule will be easier. Second, anthracene has a larger  $\pi$ –system as opposed to, for example benzene. In general, the HOMO–LUMO–gap reduces with increasing size of the  $\pi$ –system.<sup>[91]</sup> Hence, the probability that the molecular orbitals fall into the energy window spanned by the electrodes in the MCB measurements is increased, when a central anthracene is used compared to a compound having a central benzene–ring. The anchor–groups were attached to a benzene ring in *meta*– or *para*–position relative to the ethynyl–linker between the phenyl–ring and the anthracene moiety. The outer phenyl–rings have to be connected to the anthracene ring without breaking the  $\pi$ –conjugation, because otherwise the interpretation of the data might become complicated due to effects of different degrees of  $\pi$ –conjugation in the inner part of the structure. Hence, a direct connection between the phenyl–rings and the central anthracene part is troublesome, because steric hindrance rotates the phenyl–rings out of plane. Therefore, acetylene linkers between the phenyl– and the anthracene–ring were chosen, because these allow electron transfer between two molecular entities and increase the distance between the phenyl–rings and the anthracene ring reducing steric hindrance.<sup>[331]</sup> Such structures consist exclusively of  $\pi$ –conjugated subunits allowing the study of the influence of the position of the anchor–group on the IV curves.

#### 4.1.2.1 Synthetic Strategy

The build–up of both molecular structures will be based on the same reaction sequence. Only the position of the sulphur–functionality R in the outer phenyl–ring **A** will be different (Figure 4–36). The synthesis of structures containing triple bonds is routinely performed by the metal–catalysed cross–coupling of (substituted) acetylenes to organic electrophiles, the so–called *Sonogashira* coupling.<sup>[161],[162]</sup> It was planned to connect both outer building blocks **A** to the inner moiety **B** in one reaction step to facilitate the synthesis and reduce purification steps. Two alternative routes exist for this stage. The acetylene–groups can either be attached to the outer building block **A** or to the central anthracene **B**. If the latter route is chosen, building block **B** has to bear two free acetylenes in 9 and 10 position. Anthracene is known to undergo thermal polymerisation and photo–polymerisation quite readily by irradiation with light of the wavelength of 350 nm.<sup>[332],[333]</sup> Extending the  $\pi$ –system by substitution with two

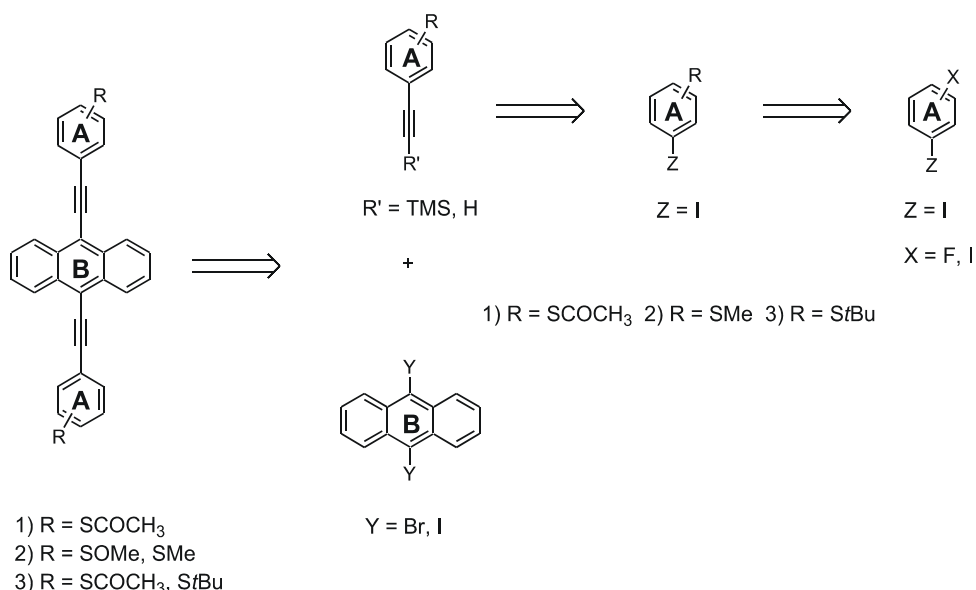


**Figure 4–36:** Synthetic strategy for the syntheses of target compounds **A1** and **A2**.

ethynyl-groups in position 9 and 10 will probably shift this wavelength into the region of the visible light. Hence, such a structure will probably polymerise even more easily leading to difficulties in the synthesis of such a building block. Thus, it was decided to attach the triple bonds to the outer building block **A** and use the central anthracene as electrophile in the *Sonogashira* coupling. A suitable starting compound, namely 9,10-dibromoanthracene can be purchased.

The outer building block will consist of a benzene ring, which is substituted by an acetylene group and a sulphur-group R in *meta* or *para*-position. However, the triple bond does not tolerate the harsh reaction conditions required for the nucleophilic substitution of halides, preferably fluorine using sodium alkylthiolate.<sup>[91]</sup> Hence, the strategy presented above for the synthesis of the oligophenylenes, where the CCR was done first followed by the introduction of the acetyl-protected sulphur by exchange of fluorine does not work for the present molecular structure. The sulphur functionality R needs to be introduced before the acetylene-group is present. Thiols cannot be used, because they will poison the catalyst<sup>[240]</sup> required for the subsequent *Sonogashira* coupling of the acetylene to the inner building block **B**. Acetyl-protected sulphur-groups can be used, but thioesters are pH-sensitive to some extent. The required outer building block **A** having R = S-acetyl and in *para*-position an acetylene-group can be synthesised following a literature procedure.<sup>[334]</sup> The procedure involves reduction of a sulfonyl chloride to a thiol group and *in situ* protection to get the acetyl-protected anchor-group. The acetylene is introduced by substitution of the halogen Z by using a TMS-protected acetylene under *Sonogashira* coupling conditions, which allows the selective coupling to only

one side of the triple bond.<sup>[162],[335]</sup> In the last step the TMS-group is removed providing the free acetylene. However, first attempts to couple this building block with R = S-acetyl to 9,10-dibromoanthracene **B** (Y = Br) using *Sonogashira* conditions could only be performed with rather low yields of about 5%. Presumably, the labile thioester in the outer building block **A** was cleaved by the rather basic amine required for the *Sonogashira* coupling to 9,10-dibromoanthracene in the high reaction temperature.

Two possible strategies exist to obtain higher yields of the target compound. First, the protection-group on sulphur of building block **A** can be changed to a group, which is more stable in the required reaction conditions. Second, the conditions for the *Sonogashira* coupling can be optimised. It was decided to first exchange the protection-group on the sulphur. As alkyl-protected sulphur-groups are more stable in the conditions applied for the *Sonogashira* coupling, such a protection-group was chosen for R. To obtain the target compound, the alkyl-protection-group needs to be exchanged for the acetyl-protection-group, after the *Sonogashira* coupling has been performed. Thiomethyl-groups can be converted to a free thiol in various ways as described above. Free thiols are easily protected by adding acetic anhydride or acetyl chloride. However, reduction with sodium in liquid ammonia<sup>[216]</sup> and nucleophilic cleavage of the alkyl thioether bond<sup>[233]</sup> to afford the free thiol cannot be done in the presence of triple bonds. A third pathway involving *Pummerer* rearrangement of sulphoxides is applicable in the presence of triple bonds.<sup>[215]</sup> Alternatively, *tert*.-Butyl-sulfanyl groups can be exchanged for the acetyl-sulfanyl group using boron tribromide to cleave the thioester and subsequent protection of the thiol with acetyl chloride.<sup>[223]</sup> However, traces of water react with BBr<sub>3</sub> to give hydrogen bromide, which might attack the electron-rich triple bond of the desired structure in an electrophilic addition reaction. Therefore, it was decided to follow the route using methyl as protection-group.

Both the nucleophilic substitution to obtain methyl aryl thioethers as well as the *Sonogashira* coupling requires aryl halide bonds (X and Z). In the nucleophilic displacement aryl fluorides react fastest,<sup>[91]</sup> whereas they do not participate in metal-catalysed CCRs.<sup>[122]</sup> These reactions are performed best with aryl bromides and iodides.<sup>[161]</sup> Therefore, a precursor having X = fluorine and Z = iodine in *para*-position is an interesting starting compound to synthesise the outer building block **A**. This compound, namely 1-fluoro-4-iodo-benzene was commercially available. The methyl thioether is formed first by nucleophilic substitution of the fluorine, then the acetylene is introduced by a *Sonogashira* coupling at the position of Z = iodine. For this purpose, commonly trimethylsilyl protected acetylene is used to allow selective coupling to one side of the acetylene. The protection-group can be removed in the next step to afford

the free acetylene<sup>[336],[335]</sup> that can participate in the next coupling reaction to the central building block **B**. After the *Sonogashira* coupling of the outer building block **A** bearing a stable methyl–sulfanyl group to the central building block **B**, the sulphur–groups have to be oxidised to the sulphoxides selectively. Unfortunately, the isolation procedures for this compound containing two sulphoxides turned out to be troublesome.

Hence, the second route using R = S–*tert*.–butyl was followed. As already mentioned, this protection–group can be converted to acetyl–protected sulphur–groups using BBr<sub>3</sub> in the presence of acetyl chloride.<sup>[223],[225]</sup> In similarity to the strategy developed for the thiomethyl–group, commercially available 1–fluoro–4–iodo–benzene can be used as starting compound. The *tert*.–butyl thioether is formed first by nucleophilic substitution of the fluorine, then the acetylene is introduced by a *Sonogashira* coupling at the position of Z = iodine. To allow selective coupling to one side of the acetylene trimethylsilyl protected acetylene can be used. Removal of this protection group in the next step affords the free acetylene<sup>[336],[335]</sup> that can participate in the next coupling reaction to the central building block **B**. Cleavage of the StBu–group using BBr<sub>3</sub> in the presence of acetyl chloride can give the target compound bearing acetyl–protected sulphur–groups on both ends of the molecular rod.

As mentioned above an alternative strategy is the optimisation of the *Sonogashira* coupling of the outer building block **A** having an acetyl–protected sulphur–group to the central building block **B**. In this way the exchange of the sulphur protection group in a letter step is not required. In first attempts to couple this building block **A** high reaction temperatures and long reaction times were required for the coupling to 9,10–dibromoanthracene. However, only rather low yields were obtained. Usually iodine is replaced more easily than bromine in *Sonogashira* coupling reactions due to the lower bond strength.<sup>[122]</sup> A suitable inner building block **B**, namely 9,10–diidoanthracene can be synthesised from commercially available 9,10–dibromoanthracene following a literature procedure.<sup>[337]</sup> *Sonogashira* coupling of the outer building block **A** bearing an acetyl–protected sulphur to this more reactive central moiety **B** can afford the target compound.

#### 4.1.2.2 Synthesis

The first revised route to the rigid rod comprising terminal sulphur anchor groups in *para*-position **A1** started from commercially available 1-fluoro-4-iodo-benzene (Figure 4–37). Making use of the higher reactivity of fluorine compared to iodine in S<sub>N</sub>Ar-reactions the fluoro-substituent of **A3** was substituted with a thiomethyl-group using 1.25 equivalents of sodium methanethiolate in DMI at 60 °C.<sup>[305]</sup> **A4** was obtained as a white solid after column chromatography in a yield of 68%. The iodine of **A4** was substituted at room temperature with trimethylsilylithiynyl using *Sonogashira* coupling conditions with [Pd(PPh<sub>3</sub>)<sub>2</sub>Cl<sub>2</sub>] and CuI as catalysts in diisopropylamine. The TMS-protected 4-methylsulfanyl-ethynylbenzene (**A5**) was obtained as a yellow liquid in 87% yield. Deprotection of the TMS-group with tetrabutylammoniumfluoride (TBAF) in THF at room temperature gave 4-methylsulfanyl-ethynylbenzene (**A6**) as a brown liquid in 99% yield. In a *Sonogashira* coupling reaction acetylene **A6** (2.75 equivalents) substituted both bromines of 9,10-dibromoanthracene (**O26**) with [Pd(PPh<sub>3</sub>)<sub>2</sub>Cl<sub>2</sub>] and CuI as catalysts in refluxing diethylamine. The strongly fluorescent compound **A7** was isolated as red solid after re-crystallisation from toluene in 61% yield. The oxidation of both sulphurs of **A7** to two sulphoxide groups giving **A8** was performed using mCPBA in dichloromethane. Attempts with 2.5 and 2.0 equivalents of oxidation agent at 0 °C were done. In both cases, mixtures of compounds containing starting compound, sulphoxides as well as sulphones as judged by TLC were obtained. These mixtures could not be separated

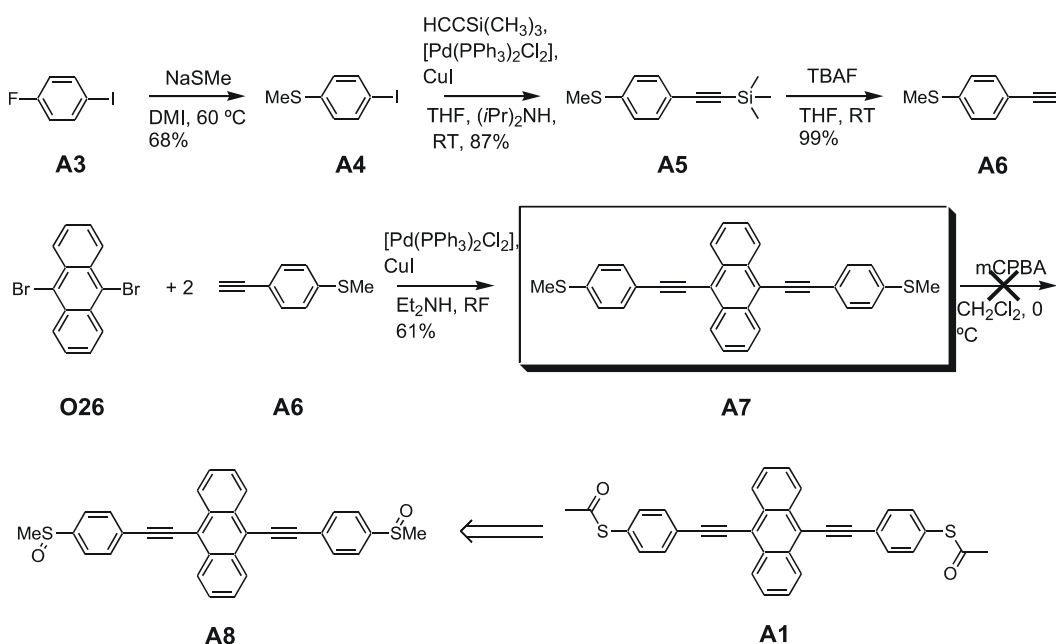
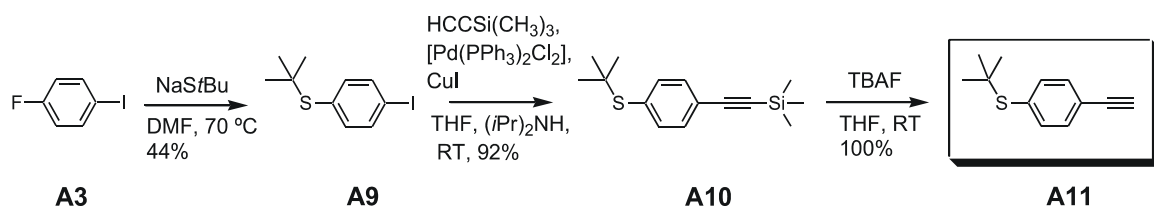
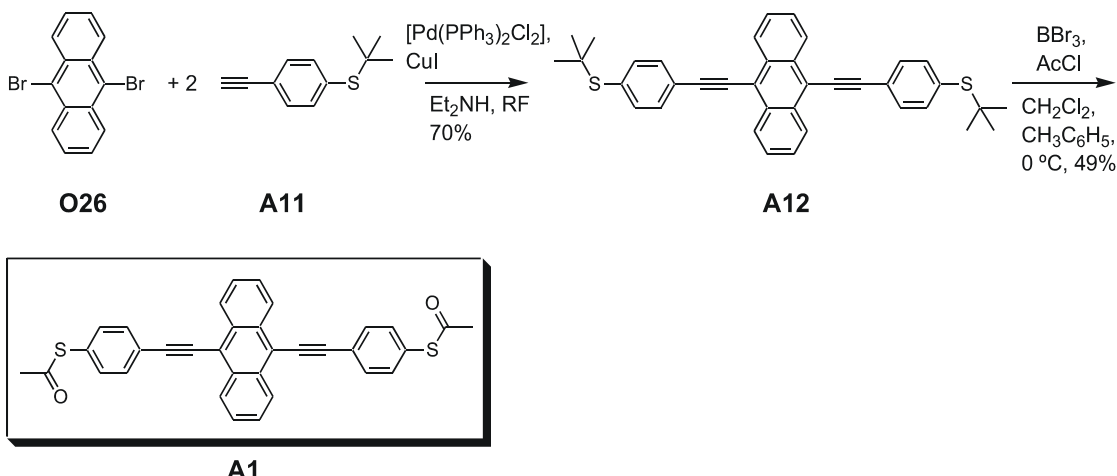


Figure 4–37: Route 1 for the preparation of **A1** using methyl-protected sulphur-groups.

by column chromatography possibly due to the rather low solubility of the obtained compounds. Hence, target compound **A1** could not be prepared *via* this route. Therefore, it was decided to use the second route using *tert*-butyl-protected sulphur-groups, which can be converted to acetyl-protected sulphur-groups using  $\text{BBr}_3$  in the presence of acetyl chloride. The route to the *tert*-butyl substituted outer building block started with the substitution of the fluorine of **A3** using 1.2 equivalents of sodium *tert*-butylthiolate in DMF at 70 °C. This reaction afforded compound **A9** as a white solid in 44% yield after column chromatography (Figure 4–38). Using similar reaction conditions as for **A6**, the TMS-protected acetylene was introduced and deprotected to yield in 4–*tert*.butylsulfanyl–ethynylbenzene (**A11**) as a brown liquid in a yield of 92% over both steps. The acetylene **A11** (2.75 equivalents) substituted both bromines of 9,10-dibromoanthracene (**O26**) with  $[\text{Pd}(\text{PPh}_3)_2\text{Cl}_2]$  and CuI as catalyst in refluxing diethylamine to afford the *tert*-butyl protected rod **A12** (Figure 4–39). The *tert*-butyl-protected molecular rod **A12** was obtained as a yellow–orange solid in 70% yield after column chromatography. In the last step, the transformation of the *tert*-butylsulfanyl– to acetylsulfanyl-groups with  $\text{BBr}_3$  in the presence of acetylchloride was done.<sup>[225],[223]</sup> Traces of water react with  $\text{BBr}_3$  resulting in the formation of HBr, that in turn can electrophilically attack the triple bond. Hence, it was necessary to work in thoroughly dry conditions using dried solvents and pre-dried glassware. This reaction seems to require solvent mixtures of dichloromethane and toluene. It has been proposed that toluene scavanges the *tert*-butyl group pulling the reaction in direction of the thiol suggesting that large amounts of toluene favour the reaction.<sup>[225]</sup> Furthermore, during attempts for the present reaction step, it was observed that the proportion of the solvents dichloromethane and toluene influences the speed of the reaction. While the presence of toluene is necessary to obtain the target compound, the use of mixtures having higher toluene contents (toluene/ $\text{CH}_2\text{Cl}_2$  > 2/1(v/v)) reduces the yield. Best results were obtained when mixtures of toluene/ $\text{CH}_2\text{Cl}_2$  1/1 (v/v) were used providing the target compound **A1** as a yellow–red solid in 49% yield after column chromatography. The overall yield over all steps starting from commercially available compounds is 14% as opposed to less than 4% for the original procedure, that is coupling of a building block having an acetyl-protected sulphur-group to 9,10-dibromoanthracene.



**Figure 4–38:** Synthesis of the building block **A11** having a *tert*-butyl-protected sulphur-group.



**Figure 4-39:** Route 2 for the preparation of target compound **A1**.

Target compound **A2** having the S-acetyl groups in *meta*-position of the outer building block was synthesised by a similar procedure as described above. Here, the first reaction step has been done with 1,3-diiodo-benzene (**A13**) affording the *tert*.-butyl substituted compound **A14** as a yellow oil in a yield of 53% (Figure 4-40). Due to the lower reactivity of iodine compared to fluorine in  $\text{S}_{\text{N}}\text{Ar}$ -reactions a slightly increased reaction temperature of  $80^\circ\text{C}$  compared to  $70^\circ\text{C}$  for the fluorine containing starting compound **A3** had to be used. The free acetylene **A16** was obtained using the same reaction sequence as described above for the *para*-compound as a yellow liquid in a yield over both steps of 79%. The acetylene **A16** (2.75 equivalents) substituted both bromines of 9,10-dibromoanthracene (**O26**) with  $[\text{Pd}(\text{PPh}_3)_2\text{Cl}_2]$  and  $\text{CuI}$  as catalyst in refluxing diethylamine to afford the *tert*.-butyl protected rod **A17** (Figure 4-41). Column chromatography and subsequent re-crystallisation from ethanol/toluene 5/1 gave the molecular rod **A17** as red solid in a yield of 63%. The conversion of the *tert*.-butylsulfanyl- to the acetyl sulfanyl-group was performed using  $\text{BBr}_3$  in the presence of acetyl chloride in a solvent mixture of toluene/ $\text{CH}_2\text{Cl}_2$  1/1 (v/v). Target compound **A2** having the anchor-groups in *meta*-position was obtained as an orange solid after column chromatography in 70% yield. Hence, a slightly increased overall yield for **A2** of

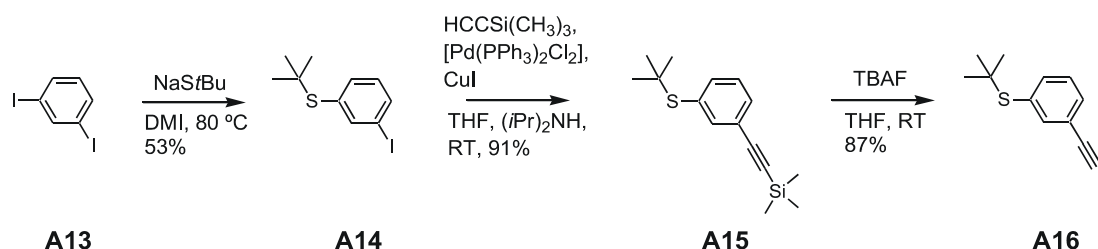


**Figure 4-40:** Synthesis of building block **A16** having a *tert*.-butyl-protected sulphur-group in *meta*-position.

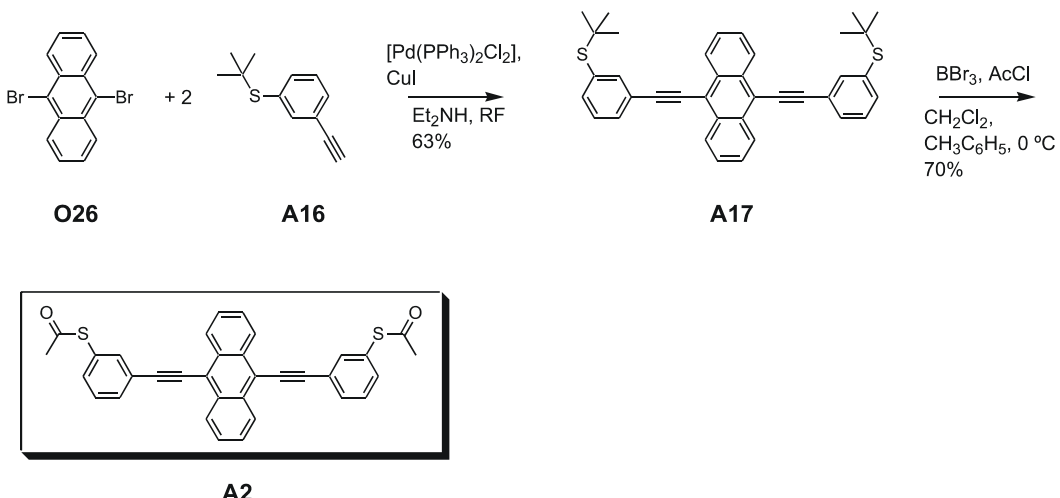


**Figure 4–41:** Alternative pathway for the synthesis of the meta–compound **A2**.

19% as opposed 14% for compound **A1** has been reached.

Surprisingly, the last reaction step for the conversion of the *tert*.–butyl– to the acetyl–group could not be scaled–up, that is the yields dropped dramatically with increasing amounts of starting compound. As described above, the success of the reaction seems to depend on the amount of toluene used. While solvent mixtures of toluene/CH<sub>2</sub>Cl<sub>2</sub> 1/1 (v/v) were suited best for reactions on small scale (about 0.04 mmol starting compound), attempts to adjust the solvent mixture for large scale reactions to get larger amounts of **A1** failed. Possibly, the mechanism of the reaction is more involved than currently assumed causing this puzzling observation.

Since the reaction for the conversion of the *tert*.–butyl to the acetyl–protection–group could not be scaled–up, another route was followed to obtain larger amounts of **A1**. This pathway involves the optimisation of the *Sonogashira* coupling protocol of an outer building block having an acetyl–protected sulphur–group to the central anthracene moiety. This outer building block **A21** can be synthesised from commercially available **A18** in three steps following a literature procedure in an overall yield of 62% (Figure 4–42).<sup>[334]</sup> Dichlorodimethylsilane–zinc–dimethylacetamide in non–aqueous conditions was used as a facile reduction system to convert the sulphonyl chloride **A18** to 4–iodo–benzenethiol, which was protected in the same pot using acetyl chloride to give **A19**. *Sonogashira* coupling of TMS–acetylene to **A19** under established conditions afforded the TMS–protected compound **A20** as a yellow liquid in a yield of 98% after column chromatography. In the last step the protection–group was cleaved by TBAF in THF and after re–protection of the thiol using acetic anhydride in acetic acid the desired building block **A21** bearing a free acetylene was obtained. Column chromatography provided pure **A21** as a yellow liquid in a yield of 69%. In

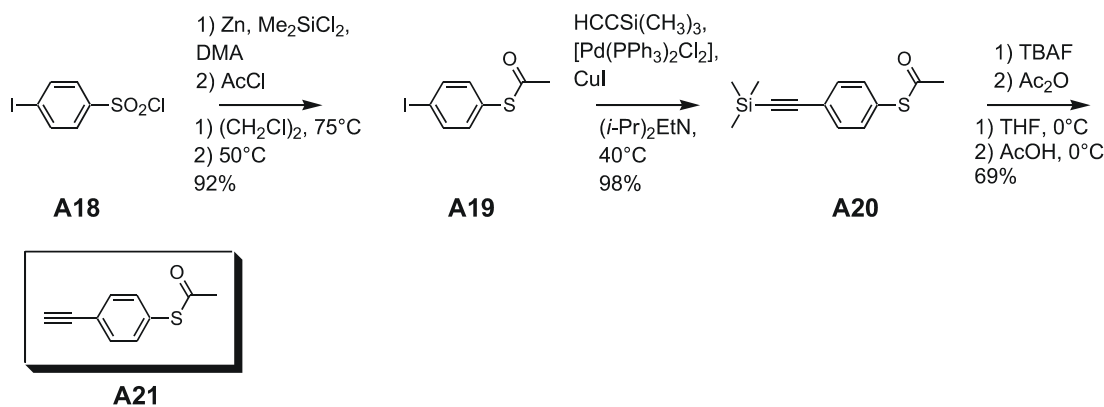


Figure 4–42: Synthesis of the building block **A21** according to a literature procedure.

earlier attempts this building block **A21** had been coupled to 9,10–dibromoanthracene using a *Sonogashira* protocol with high reaction temperature and long reaction time. These conditions probably resulted in a considerable cleavage of the pH-labile thioester giving rather low yields. To perform the cross coupling with less harsh conditions the two bromines of the inner building block can be exchanged for iodine, as iodine usually reacts more easily in CCRs.<sup>[122]</sup> The new central building block **A22** was synthesised from 9,10–dibromoanthracene following a literature procedure (Figure 4–43).<sup>[337]</sup> This reaction involves an exchange of both bromines of **O26** for lithium using 2.6 equivalents butyl–lithium followed by quenching with iodine at room temperature. 9,10–Diiodoanthracene (**A22**) was obtained as a yellow solid after re-crystallisation from carbon tetrachloride in a yield of 14%. The substitution of the two iodines of **A22** with **A21** was performed in a toluene/triethylamine mixture using *Sonogashira* coupling conditions with [Pd(PPh<sub>3</sub>)<sub>2</sub>Cl<sub>2</sub>] and CuI as catalyst at 50 °C. This revised protocol afforded target compound **A1** as yellow–red solid in a yield of 50% after column chromatography and subsequent re-crystallisation from toluene/methanol. Hence, in this way target compound **A1** was obtained in good yields and reasonable amounts.

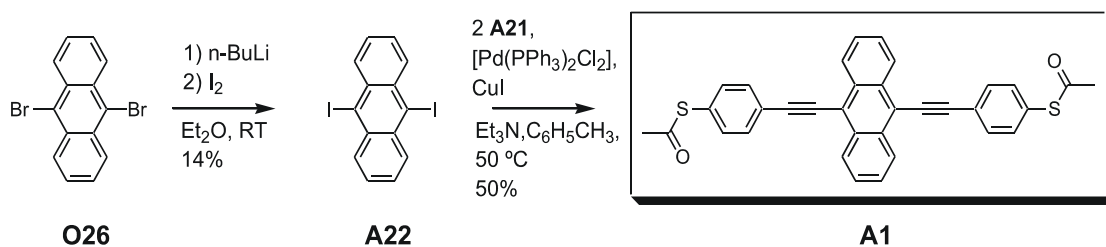
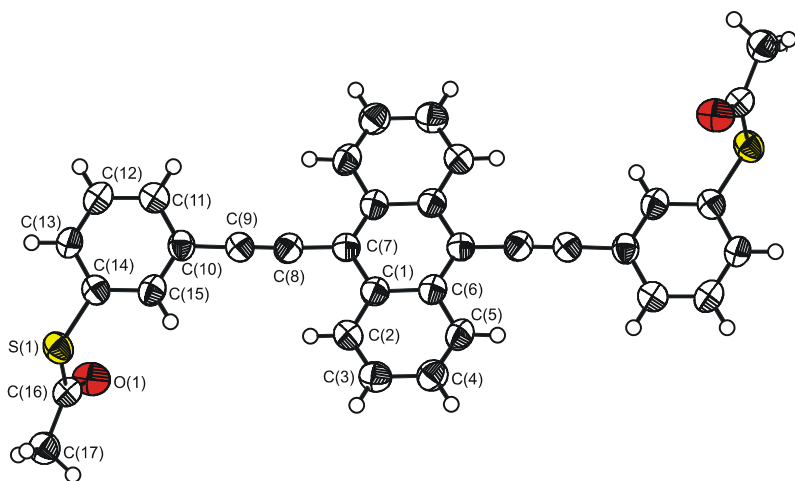


Figure 4–43: Route 3 for the preparation of **A1**.

#### **4.1.2.3 Characterisation and Structural Analysis**

All new compounds were characterised by mass spectroscopy,  $^1\text{H}$ - and  $^{13}\text{C}$ -NMR spectroscopy and elemental analysis. To gather information about the molecular structure of the synthesised molecular rods, it was tried to obtain single crystals of these compounds. The length of the molecule was of particular interest in the analysis of the molecular structure, since depending on the prevalent electron transport mechanism the length of the molecule can be of great importance.

Slow evaporation of a solution of **A2** in chloroform gave single crystals suitable for x-ray analysis (Figure 4–44). The inversion symmetric compound **A2** crystallises in the triclinic space group *P*–*1* with one molecule in the unit cell. The outer phenyl–rings and the central anthracene motif show an almost coplanar orientation, as judged by the angle of torsion between C(6)–C(7)–C(10)–C(11) of 9.1(1) $^{\circ}$ .<sup>[309]</sup> The C(sp<sup>2</sup>)–C(sp) bond between the anthracene moiety and the ethynyl–group has a length of 141.3(5) pm, that is it is slightly shorter than the average length of that type of bond (143 pm).<sup>[91]</sup> The acetylene bond between C(8)–C(9) is 119.7(5) pm long matching the typical length of C(sp)–C(sp) bonds. The second C(sp<sup>2</sup>)–C(sp) bond between the outer phenyl–ring and the acetylene part is with 142.8(5) close to the length commonly found for this type. The acetylene–bridge angles of 178.0(4) $^{\circ}$  (C(9)–C(8)–C(7)) and 179.5(4) $^{\circ}$  (C(8)–C(9)–C(10)) deviate from linearity only by a minor extent. The outer phenyl–ring is planar with the sulphur being in the plane of the ring. The



**Figure 4–44:** Molecular structure of A2. Selected bond lengths/pm and bond angles/ $^{\circ}$ : C(7)–C(8) 141.3(5), C(8)–C(9) 119.7(5), C(9)–C(10) 142.8(5), S(1)–C(14) 176.6(3), S(1)–C(16) 177.6(4); C(6)–C(7)–C(8) 120.4(3), C(9)–C(8)–C(7) 178.0(4), C(8)–C(9)–C(10) 179.5(4), C(14)–S(1)–C(16) 101.24(15)

intramolecular sulphur to sulphur distance in this compound was determined to 1.78(2) nm. The acetyl-*protection*-group lies beneath the plane of the phenyl-ring or rather above the plane of the other phenyl-ring due to the inversion centre in the middle of the anthracene-ring. Both C(sp<sup>2</sup>)–S bonds are with 176.6(3) pm (S(1)–C(14)) and 177.6(4) pm (S(1)–C(16)), respectively, slightly elongated compared to the average C(sp<sup>2</sup>)–S bond (175 pm).<sup>[91]</sup>

Crystallisation of target compound **A1** turned out to be rather challenging and success has been achieved only very recently (see below). Therefore, attempts were done to obtain single crystals suitable for x-ray analysis of the intermediates of the syntheses, namely **A7** and **A12**, instead. These two compounds have the desired inner molecular structure of the target compound **A1**, but differ in the protection-groups on the terminal sulphurs. Compound **A7** has methyl-protected sulphur-groups, whereas the molecular rod **A12** has *tert.*-butyl-protected sulphur-groups. As only the groups on the terminal sulphurs are different, the solid state structure is probably not influenced considerably by these different substituents. Hence, these compounds can be used as model compounds for **A1**.

Crystallisation of **A7** by slow evaporation of solutions of chloroform and of dichloromethane provided single crystals. In both cases very thin needles have been obtained. Unfortunately, these were not suitable for x-ray analysis due to the large difference in the dimension of the crystal in one direction compared to the other two. Single crystals suitable for x-ray analysis of compound **A12** having more bulky *tert.*-butyl protection-groups were obtained by slow evaporation of a solution in diethylether. Compound **A12** crystallises monoclinic (space group *C2/c*) with eight molecules in the unit cell (Figure 4–45).<sup>[309]</sup> Surprisingly, the molecular structure has no inversion centre and reveals two different *tBu*–S–phenyl-groups. While the phenyl-ring C(17)–C(22) is 78.2(1) $^{\circ}$  twisted relative to the anthracene fragment, the phenyl-

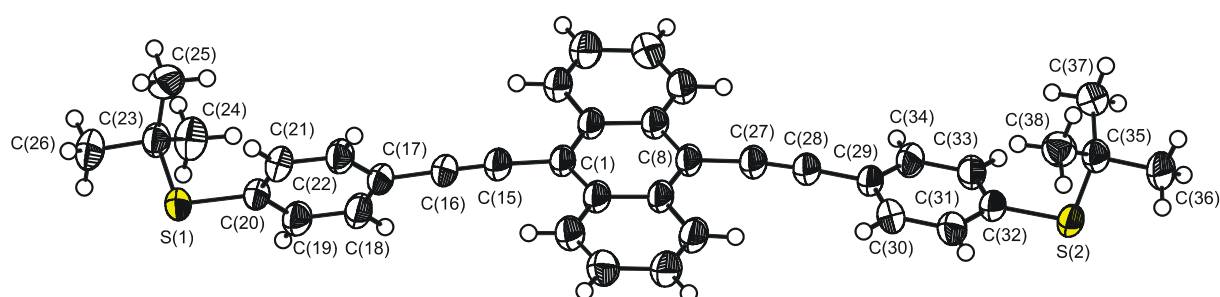


**Figure 4–45:** Molecular structures of **A12**. Selected bond lengths/pm and bond angles/ $^{\circ}$ : S(1)–C(20) 178.2(3), S(1)–C(23) 185.2(3), S(2)–C(32) 177.6(3), S(2)–C(35) 185.3(3) C(1)–C(15) 144.4(4), C(15)–C(16) 119.8(4), C(16)–C(17) 144.6(4), C(8)–C(27) 143.9(4), C(17)–C(28) 120.1(4), C(28)–C(29) 144.1(4); C(1)–C(15)–C(16) 175.1(3), C(15)–C(16)–C(17) 177.0(3), C(8)–C(27)–C(28) 173.6(3), C(27)–C(28)–C(29) 175.1(3).

ring C(29)–C(34) departs only  $8.1(1)^\circ$  from the anthracene plane. All  $\text{C}(\text{sp}^2)\text{—C}(\text{sp})$  bonds, that is the ones to the anthracene moiety C(1)–C(15) and C(8)–C(27) as well as the ones to the outer phenyl–rings C(16)–C(17) and C(28)–C(29), have a length commonly found for this type of bond.<sup>[91]</sup> Whereas on one side the acetylene bridge angles of  $175.1(3)^\circ$  (C(1)–C(15)–C(16)) and  $177.0(3)^\circ$  (C(15)–C(16)–C(17)) deviate only slightly from linearity, the other acetylene bond is bended to a larger extent, that is the angles are  $173.6(3)^\circ$  (C(8)–C(27)–C(28)) and  $175.1(3)^\circ$  (C(27)–C(28)–C(29)). Both outer phenyl–rings are planar with the sulphur–group residing in the plane of the ring. With both sulphur atoms on the molecules axis, the intramolecular sulphur to sulphur distance was measured to 1.99(2) nm. Both *tert.*–butyl protection groups are situated above the plane of the anthracene–ring. The  $\text{C}(\text{sp}^2)\text{—S}$  bonds, that is the ones to the phenyl–rings, were determined to 178.2(3) pm (S(1)–C(20)) and 177.6(3) pm (S(2)–C(32)). Thus, they are somewhat longer than the average bond lengths of 175 pm usually found for this kind.<sup>[91]</sup> The bond from sulphur to the carbon of the *tert.*–butyl group is with 185.2(3) pm (S(1)–C(23)) and 185.3(3) pm (S(2)–C(35)) slightly elongated compared to the average length of a  $\text{C}(\text{sp}^3)\text{—S}$ –bond.

The solid state structure of **A12** revealed two different *tert.*–butylsulfanyl groups. To find reasons for this arrangement the packing of **A12** in the solid state has been analysed in more detail using a packing diagram. Such diagrams show the orientation of molecules to each other in the unit cell and, thus allow to obtain information about intermolecular interactions between different molecules in the solid state. In particular, the influence of nondirectional forces such as  $\pi$ – $\pi$  stacking and directional interactions like hydrogen bonding can be studied.<sup>[338]</sup> Figure 4–46 shows the packing diagram of **A12**. To get these pictures all atoms in the unit cell were created and then the all molecular fragments completed to obtain the complete molecular structure of the compound. By this procedure all molecules that lie at least in parts inside the unit cell were generated. The diagram reveals four different kinds of stacks formed by **A12**. Always two stacks are related to each other by an inversion centre situated on the *c*–axis and in the centre of the unit cell, respectively. Within each stack, which is formed along the *b*–axis of the monoclinic unit cell, adjacent molecules are aligned approximately parallel, that is the central anthracene rings of two molecules fall almost on top of each other. Each stack is probably formed due to  $\pi$ – $\pi$ –interactions between the central anthracene–ring and the two outer phenyl–rings. Hydrogen bonding can be found between sulphur (S(2)) and hydrogen (at C(22)) between two different stacks that are related by a screw axis. Possibly the rotation of the outer phenyl–rings with respect to the central

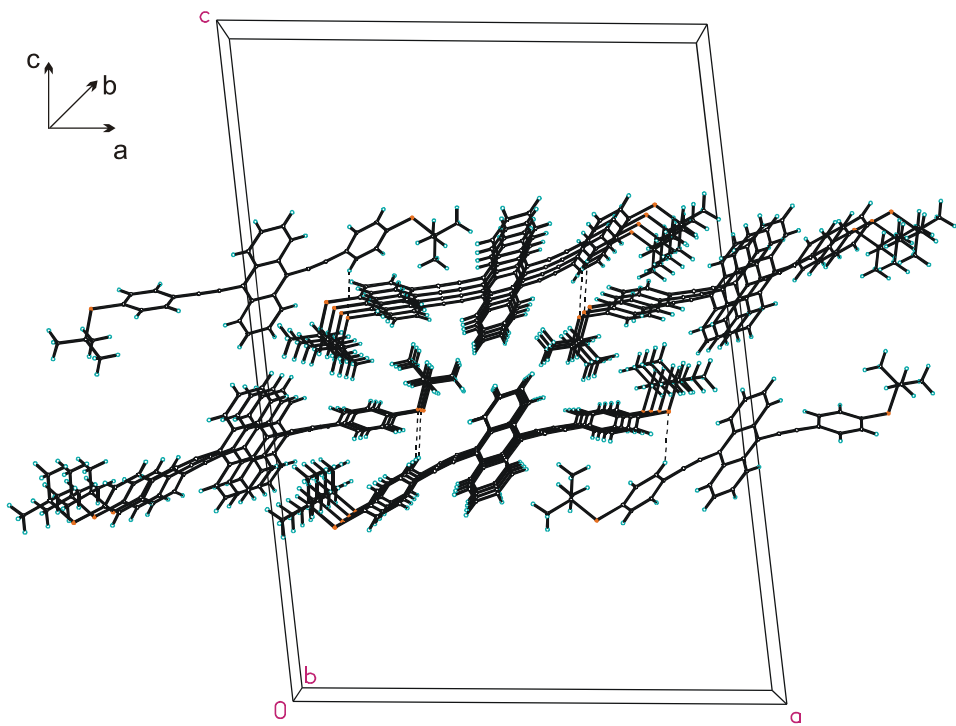


**Figure 4–46:** Packing of A12 in the crystal structure.

anthracene moiety can be attributed to this hydrogen bonding interactions, which requires a bonding angle between hydrogen–donor–acceptor of  $150 – 160^\circ$ .<sup>[338]</sup>

Very recently, it has been possible to obtain single crystals of target compound **A1** as well by slow evaporation of a solution of chloroform (Figure 4–47). This compound crystallises in the triclinic space group *P*ī with one molecule in the unit cell. The solid state structure shows an inversion centre situated in the middle of the anthracene unit. The torsion angle between C(6)–C(7)–C(11)–C(13) was measured to  $2.3(3)^\circ$ , that is the anthracene motif and the two

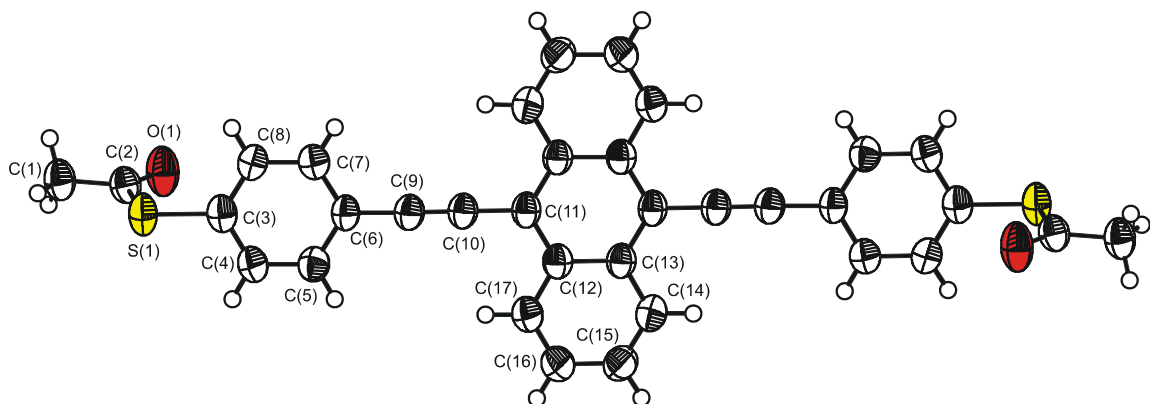


**Figure 4–47:** Molecular structure of **A1**. Selected bond lengths/pm and bond angles/ $^\circ$ : C(9)–C(10) 121.4(3), C(10)–C(11) 143.5(3), C(6)–C(9) 144.2(3), S(1)–C(3) 178.9(3), S(1)–C(2) 179.4(2); C(10)–C(9)–C(6) 179.0(2), C(9)–C(10)–C(11) 179.2(2), C(12)–C(11)–C(10) 119.6(2), C(3)–S(1)–C(2) 101.12(10).

phenyl–rings essentially reside in the same plane. The C(sp<sup>2</sup>)–C(sp) bond from the anthracene part to the triple bond is 143.5(3) pm long (C(10)–C(11)) and the one from the outer phenyl–ring to the triple bond is 144.2(3) long (C(6)–C(9)), which closely matches the typical length of a C(sp<sup>2</sup>)–C(sp) bond of 143 pm.<sup>[91]</sup> The acetylene (C(9)–C(10)) is with 121.4(3) pm slightly longer than the average value of 118 pm commonly found.<sup>[91]</sup> The acetylene bridge angles of 179.2(2) (C9)–C(10)–C(11) and 179.0(2) (C(10)–C(9)–C(6)) essentially show a linear arrangement. The outer phenyl–ring and the sulphur in *para*–position are situated in the same plane. The molecule’s axis runs through the atoms S(1)–C(3)–C(6)–C(9)–C(10)–C(11). With both sulphurs on this axis the sulphur–sulphur distance was determined to 2.02(3) nm. The acetyl–protecting group resides above the plane of the phenyl–ring and below the plane of the other phenyl–ring, respectively, due to the centre of inversion. With 178.9(3) pm (S(1)–C(3)) and 179.4(2) pm (S(1)–C(2)) the lengths of the bonds between sulphur and carbon are slightly elongated compared to the average value of 175 pm for C(sp<sup>2</sup>)–S.

The results of the crystal structure analysis suggest that (apart from the position of the anchor groups) the target compounds **A1** and **A2** have essentially the same molecular arrangement. In particular, the acetylene–linkers deviate from linearity only by a very small extent, that is an angle of nearly 180° is formed between the triple bond and the sp<sup>2</sup>–carbons on both sides. As the outer phenyl–rings are not rotated with respect to the central anthracene, both solid state structures reveal a basically planar arrangement in these compounds. Hence, the target compounds **A1** and **A2** have a comparable  $\pi$ –system, which is delocalised over the entire structure. The *para*–compound exhibits a sulphur–sulphur distance that is about 0.2 nm longer than in the *meta*–compound. In comparison, the molecular rod **A12** showed no co–planar arrangement of the different subunits. The *tert*.–butyl groups are more bulky than the acetyl–groups of compound **A1**. Therefore, these different orientations of the substituents probably result form packing effects in the crystal, as NMR investigations in solution show no evidence for distinguishable phenyl or *tert*.–butyl groups. The length of the molecule as defined by the intramolecular sulphur–sulphur–distance is only little affected by these packing effects and with 1.99(2) nm only 0.03 nm shorter than the one of the *para*–compound bearing acetyl protection groups.

As already discussed in the chapter before, in a simple transport picture the frontier orbitals of the  $\pi$ –system are assumed to be determining for electronic transport. UV/Vis spectra of organic compounds are associated with transitions between electronic energy levels. A comparison between the UV/Vis spectra of target compound **A1** and **A2** was of particular interest to study the influence of the position of the sulphur anchor–group on the  $\pi$ –system of

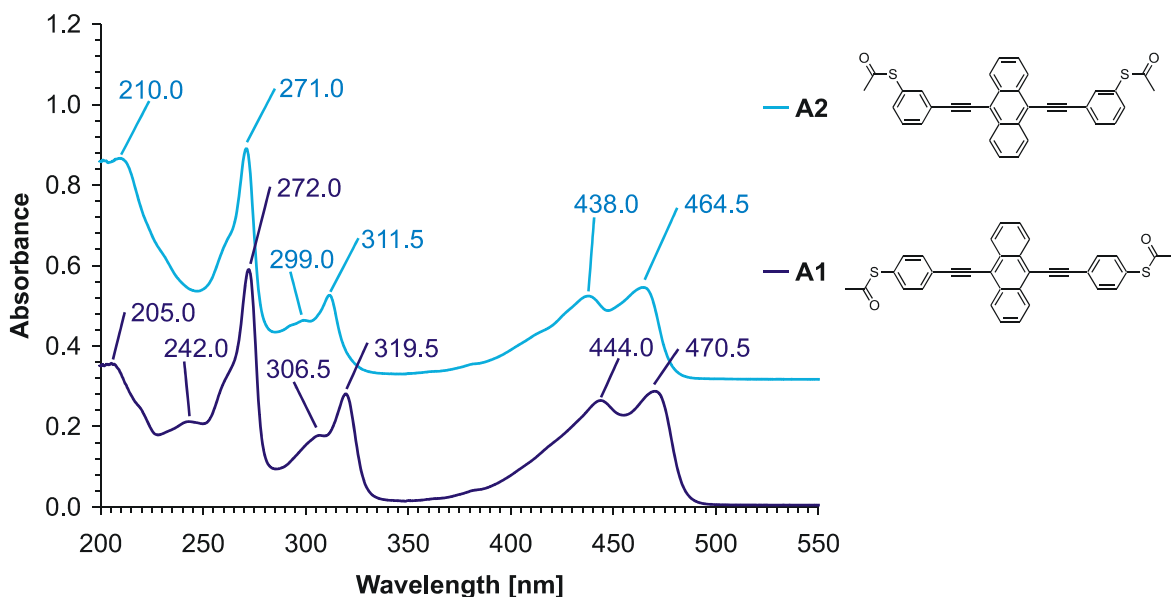


**Figure 4–48:** UV/Vis spectra of **A1** and **A2** ( $1 \times 10^{-5}$  M solutions in acetonitrile at room temperature. For clarity the spectra have been shifted by 0.3 units.

these two compounds. Both spectra were recorded of  $1 \times 10^{-5}$  M solutions in acetonitrile (Figure 4–48). The spectra of the *para*-compound **A1** and the *meta*-compound **A2** are comparable and resemble the one of unsubstituted bis(phenylethynyl)-anthracene.<sup>[339],[340]</sup> Target compound **A1** shows two rather broad absorptions in the visible region at 470.5 nm and 444.0 nm, which can probably be attributed to the anthracene  $S_0 - S_1$ -transition (p-band), but with less vibrational fine structure.<sup>[339]</sup> Compared to an unsubstituted bis(phenylethynyl)-anthracene as reference compound these absorptions are shifted bathochromically by about 5 to 10 nm, which can probably be explained by the presence of the sulphur endgroups extending the  $\pi$ -system.<sup>[318]</sup> Such a red-shift of the longest-wavelength band has already been described for *para*-methoxy- or *para*-diethylamino-substituted compounds.<sup>[341]</sup> A second sharper band can be found at 319.5 nm exhibiting a shoulder at 306.5. This absorption is red-shifted by about 10 nm as well compared to bis(phenylethynyl)-anthracene and presumably arises from the phenylethynyl-subunit.<sup>[342]</sup> The most intense sharp absorption band can be observed at 272.0 nm followed by a rather weak absorption at 242.0 nm. The band at 272.0 nm, which is probably due to the anthracene  $S_0 - S_3$  transition ( $\beta$ -band) is bathochromically shifted only by about 2 nm compared to bis(phenylethynyl)-anthracene.<sup>[339],[343]</sup> In addition, a rather broad absorption band can be found at 205.0 nm that is probably the  $\beta$ -band of the two outer phenyl-rings.

As already mentioned, the UV/Vis-spectrum of the *meta*-compound **A2** is similar to the one of the *para*-compound, but shows a hypsochromic shift of the three longest-wavelength absorptions. In comparison to **A1**, the first two bands are blue-shifted by 6 nm and the band

at 311.5 nm is hypsochromically shifted by 8 nm. Hence, these absorption bands are rather in the position of the ones of unsubstituted bis(phenylethynyl)-anthracene.<sup>[339]</sup> The assignment of these absorption bands can presumably be done according to **A1**. The most intense peak can be found at 271.0 nm, which is almost at the same wavelength as for **A2**. The  $\beta$ -band of the outer phenyl-rings can be seen at 210 nm as opposed to 205 nm for **A1**.

The results of the UV/Vis spectra suggest that target compounds **A1** and **A2** have a very comparable electronic structure, as the same absorption bands are present in both spectra. However, the *para*-compound **A1** shows a bathochromic shift of the longest-wavelength absorptions presumably indicating a slightly higher degree of  $\pi$ -conjugation in this system. Hence, the lack of conjugation of the sulphur-groups in *meta*-position to the ethynyl-linker compared to the *para*-position becomes apparent in the UV/Vis spectra of these two compounds. As discussed above, this lack of electronic communication has already been shown electrochemically<sup>[63]</sup> and theoretically,<sup>[92]</sup> too. The absorption at around 270 nm seems not to be influenced by the position of sulphur in the molecule. Interestingly, the  $\beta$ -band of the outer phenyl-rings of the *meta*-compound **A2** is red-shifted compared to **A1**.

#### 4.1.2.4 Electron Transport Measurements

The electronic transport properties of target compounds **A1** and **A2** have been investigated by *J. Reichert* in the group of *H. Weber* at the INT using the MCB technique.<sup>[325]</sup> Both acetyl-protected rods have been immobilised in different experiments between Au-electrodes from  $5 \times 10^{-4}$  M solutions in THF (Figure 4–49). Details of the protocol for immobilisation at room temperature and at low temperatures can be found in chapter 2.2.2 and the previous paragraphs of this section.

In these investigations the influence of the different position of the anchor-groups in the molecular rods **A1** and **A2** on the current-voltage characteristics was of particular interest. Figure 4–50 shows a typical example of IV characteristics of **A1'** that have been measured at

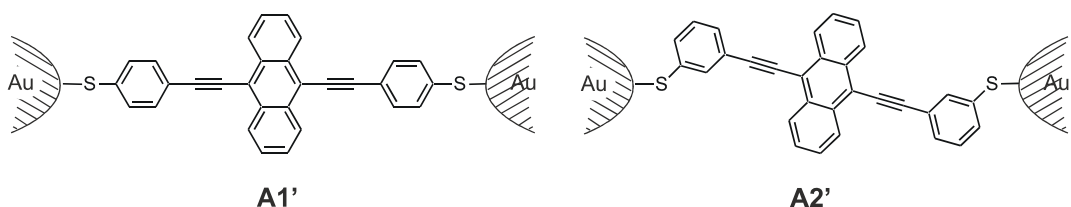


**Figure 4–49:** Target structures **A1** and **A2** immobilised in between two gold electrodes of a MCB (schematic drawing).

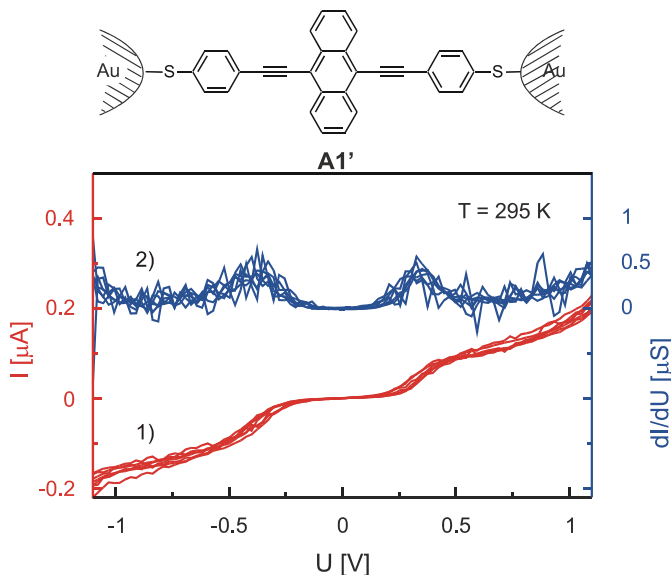


**Figure 4–50:** IV curves of **A1'** reproducibly recorded for a stable metal–molecule–metal junction in a MCB at room temperature (in red) and the numerical derivative  $dI/dU$  (in blue).

room temperature.<sup>[13],[93]</sup> Like in the measurements presented for the oligophenylenes the red curves describe the actual recorded current–voltage characteristics, while the blue curves represent the numerical derivative  $dI/dV$ , that is the differential conductance. Again different curves drawn were measured for the same metal–molecule–metal junction, but in different voltage sweeps. Here the voltage was swept between +1.2 V and –1.2 V. For clarity issues the curves have been shifted. As anticipated, the symmetric molecule **A1** gives rise to a current–voltage characteristic that is symmetric with respect to voltage inversion. In the IV curves some rounded step–like features are present that become more apparent as peaks in the first derivative (shown in blue). Two peaks at about  $\pm 0.4$  V of about same height have been found. The current level at  $U = 1$  V was determined to  $0.2$  μA. Beyond  $U \approx 1.2$  V the current rises strongly and if higher voltages were applied, the junction becomes unstable.

Immobilisation of **A2**, that is the *meta*–compound, between the Au electrodes of a MCB resulted in a stable configuration of **A2'** that allowed also to record reproducible IV curves at room temperature (Figure 4–51). As target compound **A2** also has a symmetric molecular structure like **A1**, in this case symmetric IV characteristics had been expected and have been obtained as well. The IV curves of **A2'** have a barely visible less–resolved step–like feature at  $U \approx 0.75$  V, which can better be visualised in the broad maximum of the first derivative (blue curve). The recorded currents for **A2'** were about 10 nA at  $U = 1$  V. At voltages higher than  $U \approx 1.2$  V a strong increase of the current level was noticed.

In addition, metal–molecule–metal junctions containing **A2'** have been measured at low temperatures of  $\approx 30$  K (Figure 4–51). These IV curves of **A2'** display a beautifully resolved

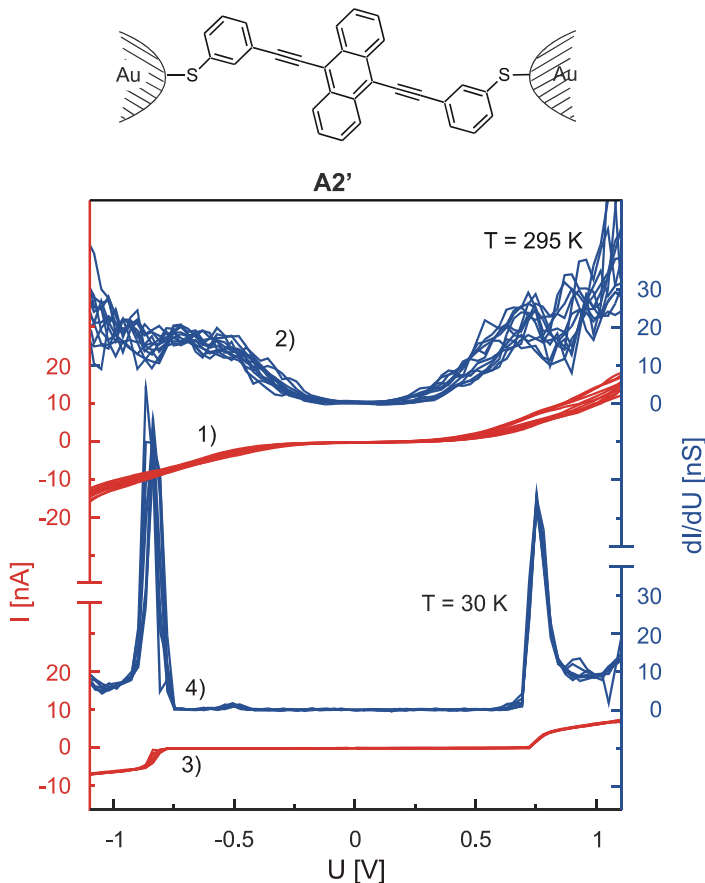


**Figure 4–51:** IV curves of Au–A2’–Au reproducibly recorded at room temperature 1) I/U (in red), 2)  $dI/dU$  (in blue); Au–A2’–Au at about 30 K 3) I/U (in red), 4)  $dI/dU$  (in blue)

step-like feature at  $U \approx 0.75$  V that becomes apparent as peaks in the first numerical derivative. The current–voltage characteristics are again rather symmetric with respect to voltage inversion, but the peak at negative bias is somewhat higher compared to the one at positive bias. The current level in these low temperature measurements was about 5 nA at  $U = 1$  V. The slight asymmetry of the recorded IV curves can probably be explained by different arrangements on the electrodes. In particular, the immobilisation protocol used for the low temperature measurements can give rise to asymmetries in the contact between gold and the molecule, as described above.

As explained in more detail in the section about the oligophenylenes, the observed peaks in the numerical derivative  $dI/dV$  can probably be attributed to electron transport through the HOMO of the molecule assuming a simple model.<sup>[324],[325]</sup> This has also been calculated in theoretical work for junctions of molecule **A1**<sup>[316]</sup> and can probably be transferred to target compound **A2**, since it has a comparable orbital structure due to the very similar molecular structure. The UV/Vis spectra shown above suggest that target compounds **A1** and **A2** have a very similar electronic structure as well. A comparison between the room and the low

temperature data of **A2** reveals that the observed conductance values are not exponentially suppressed, which indicates that probably not thermally activated hopping, but mainly tunnelling governs the electron transport. Besides, the measurements at low temperatures contain less noise and show a much better data quality, that is the position of the steps is clearly visible compared to room temperature experiments. This clear difference probably indicates that the molecule junction is fluctuating considerably at room temperature and the measurement averages over various microscopic configurations.

The difference of the IV curves between the *meta*- and the *para*-compound was of particular interest. In the room temperature measurements of **A1** and **A2** electron transport starts at similar values of about 0.3 – 0.4 V. However, junctions comprising the *meta*-compound **A2'** had an almost two orders of magnitude lower current level than junctions recorded for **A1'** under similar conditions. It has been shown e.g. in electrochemical investigations<sup>[63]</sup> as well as in theoretical studies<sup>[92]</sup> that the *meta*-position lacks conjugation to the  $\pi$ -system of a molecular system compared to the *para*-position. In the UV/Vis spectra measured of the target compounds **A1** and **A2** a similar effect has been observed. While both structures probably have very comparable orbital structures, the *para*-compound **A1** showed a slight bathochromic shift of the longest wavelength absorptions. This presumably indicates a somewhat higher degree of  $\pi$ -conjugation in this system compared to the *meta*-compound. Since both compounds differ only in the position of the anchor-groups, the increase of the size of the  $\pi$ -system can only be explained by the lack of  $\pi$ -conjugation in the *meta*-position compared to the *para*-position. Hence, the electronic communication is probably reduced resulting in a higher resistance for the *meta*-compound **A2'**. Furthermore, this finding suggests that the dominating current path is through the Au–S–C bonds (and not direct injection from the metal to the rod's  $\pi$ -system), because direct injection into the  $\pi$ -system does probably not depend on the position of the anchor-group on the aromatic system. Due to this lack of conjugation in the *meta*-position compared to the *para*-position molecule **A2** is probably electronically less coupled to the electrodes as opposed to the *para* compound **A1**. The obtained results illustrate that the conductance does depend on the structure of the molecule and can thus be intentionally altered on a molecular level by varying the position of the anchor-group in the synthesis of the molecules. Besides, the higher resistance for electron transport through junctions containing the *meta*-compound might be particularly useful for designing stable molecular junctions, because a reduced current level allows for a higher stability. According to the limited data set, also the reproducibility of the IV curves seems to be improved because the molecule is electronically less coupled to the disordered electrodes.

## 4.2 Molecular Rectifiers

The use of a molecular structure as a rectifier has already been put forward by *Aviram* and *Ratner* in 1974.<sup>[3]</sup> Only based on theoretical calculations, they proposed that a molecule comprising a donor  $\pi$ -system (D) and an acceptor  $\pi$ -system (A) linked together with a stiff, but not  $\pi$ -conjugated  $\sigma$ -spacer ( $\sigma$ ) behaves as a rectifier between two electrodes. Experimental current–voltage curves arising from such A– $\sigma$ –D molecular structure based rectifying devices, have been recorded on *Langmuir–Blodgett* films between two electrodes.<sup>[16],[344]</sup> Recently, block copolymers with a A– $\sigma$ –D structure displayed rectifier properties as self assembled monolayers in scanning probe experiments.<sup>[18]</sup> Rectification by a single molecule has been published recently using an STM.<sup>[19]</sup> A couple of other experiments demonstrated rectifying behaviour, too (see chapter 2.3.2). In these investigations, however, both electrodes and the molecule–electrode interfaces differ considerably, hence a contribution of the contact setup to the observed rectification cannot be ruled out.<sup>[96],[99]</sup> Hence, a molecule having such a D–spacer–A structure was designed to investigate the current–voltage characteristics of a single molecule between the electrodes of a MCB and to study whether rectification can be an inherent function of a molecular structure (Figure 4–52). To achieve the electronic asymmetry two aromatic building blocks with different electron densities have to be used. For this purpose, a fluorinated benzene core and a non–fluorinated benzene core were chosen. Fluorine will change the electron density in the phenyl–ring due to its –I–effect and its small +M–effect. To allow immobilisation in a MCB both ends of the molecule have to be functionalised with acetyl–protected sulphur–groups. Hence, both phenyl–rings have to bear one acetylsulfanyl–group. According to the *Aviram–Ratner* model these two building blocks have to be connected by an element that breaks the conjugation between them. As already explained in the section about oligophenylenes a biphenyl building block, where the benzene rings are rotated with respect to each other consists of two (almost)

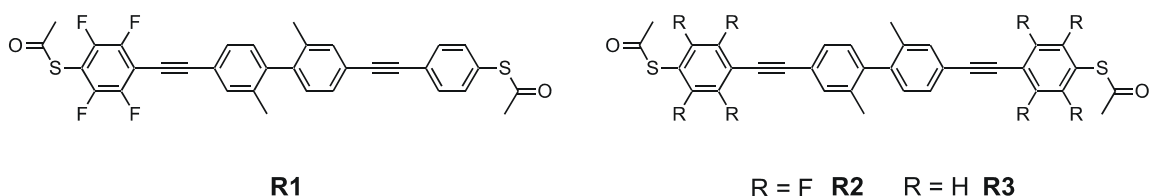


**Figure 4–52:** Target structures **R1 – R3**. The different electron density in the outer phenyl–rings of **R1** induces a strong electronic asymmetry that could give rise to rectification behaviour. The symmetric compounds **R2** and **R3** were required for control experiments.

separate  $\pi$ -systems. Hence, linking two (electronically different) outer building blocks to the biphenyl-spacer will probably result in two  $\pi$ -systems that are electronically separated. The conjugation breaking element is the bond between the two phenyl-rings of the biphenyl. Direct linkage of the two different outer building blocks to the biphenyl core would probably result in a torsion angle between these two rings due to steric hindrance introducing another  $\pi$ -conjugation breaking element. In order to prevent the formation of further interruptions of the  $\pi$ -system the connection will be done using acetylene-bonds, which are known to allow electronic communication.<sup>[331]</sup> Hence, the structure will consist of two  $\pi$ -system of different electron density, that is the two diphenylacetylene subunits, which are connected by a conjugation breaking element present in the central biphenyl core. Both outer phenyl-rings will bear sulphur functionalities in *para*-position to the acetylene linker. As the different electron density in the outer phenyl-rings induces a strong electronic asymmetry, the target **R1** immobilised between two electrodes should perform the function of a molecular rectifier. Apart from the MCB measurements it was planned to investigate the current–voltage characteristics of the target structure in a device based on a self-assembled monolayer (Figure 4–53). Such devices containing a larger ensemble of molecules might be more suitable for technological applications and might be integrated soon into existing circuitry.<sup>[4]</sup> Hence, it was interesting to fabricate such devices containing the rectifying molecule as well. It should be noted, though, that rectifying behaviour of a SAM can only be observed if all molecules are aligned in the same direction. However, self-assembly of a molecule bearing acetyl-protected sulphur anchor-groups on both ends will probably result in a random arrangement on the gold surface in terms of the direction of the molecule. Such a random order of the molecule would probably level out the asymmetric properties. Hence, a protocol to control the direction in the self-assembly process is required. One possibility to control the direction in

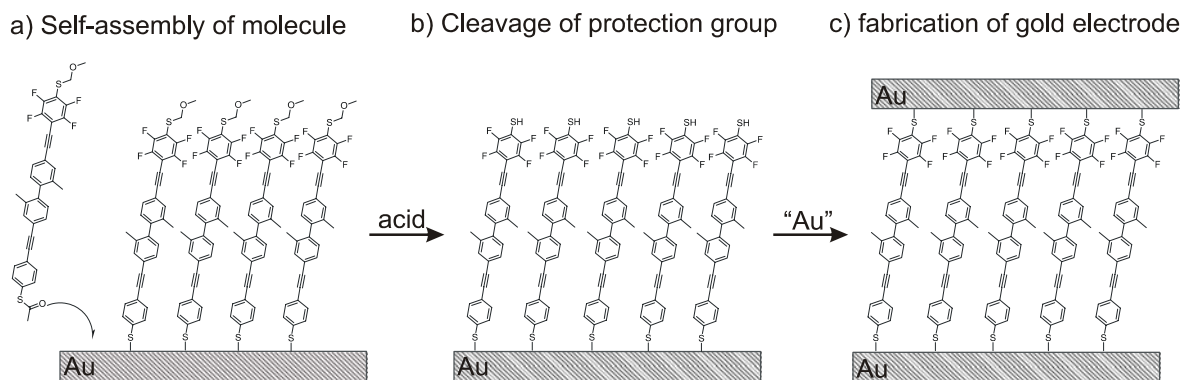


**Figure 4–53:** Formation of a device based on a SAM using a molecule with two different protection-groups on sulphur.

the self-assembly process is to use different protection-groups on the sulphur. One protection group should split off *in situ* on the gold surface, while the other one should be stable on self-assembly on gold and possible to remove by an additional chemical reaction after the monolayer has formed.<sup>[61]</sup> Such a reaction should not destroy the formed SAM. Therefore, the terminal sulphur functionalities of the molecule had to be protected with two different groups. On one side the acetyl-group, which can be cleaved *in situ* on a gold surface, was chosen while the other thiol group had to be protected by a different group. For this purpose, a methoxymethyl-group (MOM) was selected, because it is stable on self-assembly and can be cleaved in acidic conditions providing the free thiol.<sup>[345]</sup> As a result a well-ordered SAM should form by *in situ* cleavage of the S-acetyl group on the gold surface. In the next step the second stable protection group (MOM-group) can be cleaved in acidic conditions, for example by HCl gas, while the molecule has already been bond to the first gold electrode. Then the counterelectrode can be fabricated on top of the SAM. Hence, these manipulations should yield a monomolecular film device containing all molecules aligned in the same direction. For the MCB measurements this protection group has to be converted to the acetyl-group, because the procedure to obtain this junction relies on the presence of protection-groups on both terminal sulphur groups that can be cleaved *in situ*.

In order to prove further that the molecule's structure actually causes diode behaviour (and is not due to any other effects) two additional symmetric molecular rods have to be synthesised. In **R2** the central biphenyl core is substituted on both sides by the fluorinated part, while the second molecule **R3** bears the non-fluorinated phenyl-ring on both ends of the molecule. If rectification is really caused by the molecular structure, in a comparable experimental set-up these target compounds should show symmetric IV curves due to their symmetric structure (Figure 4-52).

#### 4.2.1 Synthetic Strategy

Molecular structures containing substituted acetylene moieties can be synthesised quite readily using the metal-catalysed *Sonogashira* coupling.<sup>[161],[162]</sup> This reaction requires an organic electrophile and a free acetylene, which are coupled in the presence of a copper and palladium catalyst together with a base, usually an amine. A suitable central building block **B** to obtain the desired structure, namely 4,4'-diiodo-2,2'-dimethyl-biphenyl (**O10**) has already been prepared during the syntheses of the oligophenylenes (see above).

Two strategies for the connection between this central building block **B** and the different outer building blocks **A** and **C** exist (Figure 4–54). For the first pathway the triple bonds will be introduced into the central building block first followed by a *Sonogashira* coupling of this free acetylene to the different outer building blocks **A** and **C**. The outer part will be the organic electrophile in this pathway. However, an outer building block **C** which has a free acetylene and a S–acetyl–group had already been obtained before during the syntheses of the anthracene structures (**A21**). Therefore, it was decided to follow the second strategy. Here, the central biphenyl **B** will be used as organic electrophile and the building blocks **A** and **C** having free acetylenes will be coupled in two subsequent steps to the inner building block. Since one outer building block **C** bearing a free acetylene and in *para*–position an acetyl–protected sulphur group was already available from prior work, a strategy had to be developed only for the second outer building block **A**. Like **C** it has to have a free acetylene and in *para*–position a sulphur–functionality. It was planned to investigate the current–voltage characteristics of the target structure both in a device based on a self–assembled monolayer and as a single molecule in a MCB. For this purpose, a molecular rod with two different protection groups on sulphur was required, namely and acetyl protection group and a MOM–group. Thus, the second outer part **A** has to have the other protection group. A MOM–group was selected for this

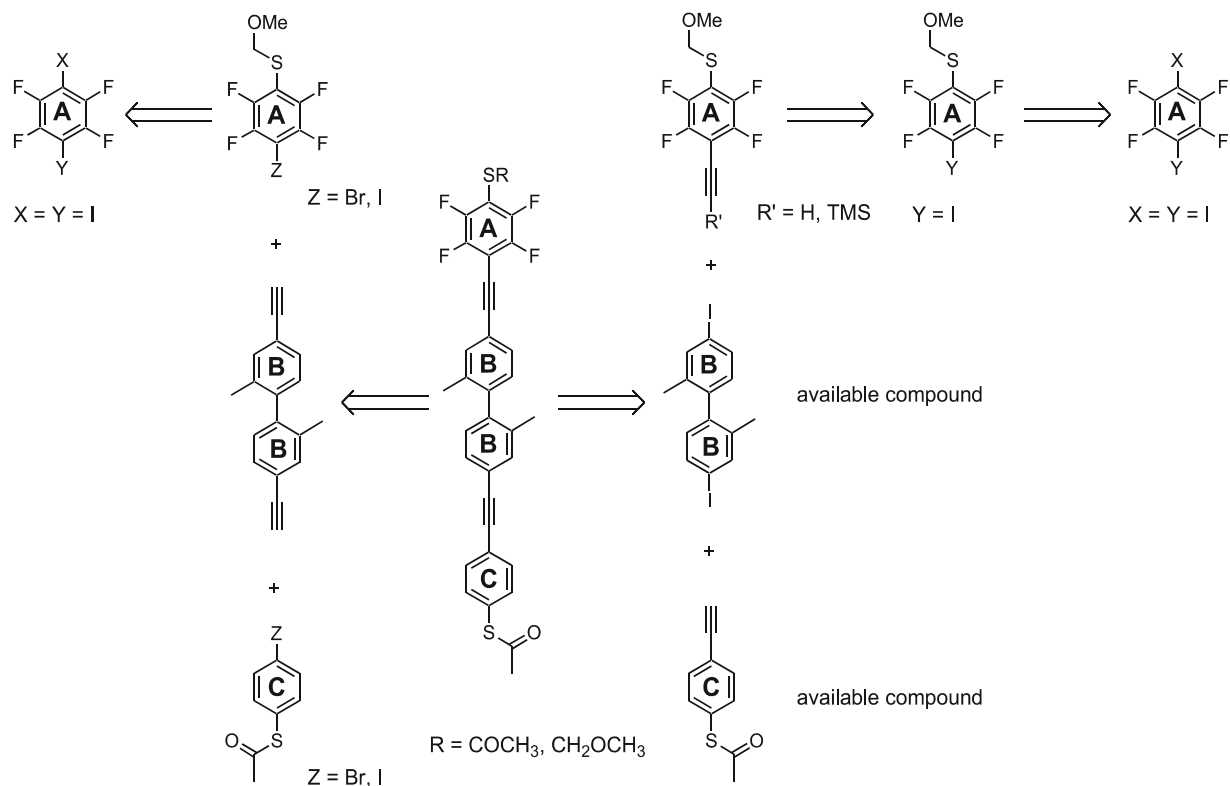


**Figure 4–54:** Synthetic strategy developed for the synthesis of target compound **RI**.

building block. It can be introduced quite readily, is stable in the conditions that are needed for the cross-coupling procedure and should be possible to cleave in acidic conditions providing the free thiol. The free thiol can be re-protected by addition of acetic anhydride or acetyl chloride. Hence, this strategy for the protection groups allows to obtain both required molecular rods using the same route.

Outer part **A** bears four fluorines. Furthermore, it needs to have the protected sulphur functionality and in *para*-position a free acetylene. Both groups can be introduced at positions where aryl halide bonds are present. It was decided to first introduce the sulphur and then the triple bond, because this order had already been successful for the build-up of the other outer building block **C**. A carbon–sulphur bond can be introduced in an elegant way by halogen–metal exchange and quenching with elemental sulphur.<sup>[209]</sup> The obtained free thiol can be protected using bromomethylmethylether to give the desired MOM–protection group. The halogen–metal exchange can be done with **X** = iodine and bromine, but not with **X** = fluorine. Therefore, the selective formation of one carbon–sulphur bond in the presence of four aryl fluoride bonds should be possible. The introduction of the acetylenic linker requires **Y** = iodine or bromine to obtain good results using the *Sonogashira* coupling as well. In the usual pathway a protected acetylene is formed followed by the cleavage of the protection group to give the free acetylene. Hence, a starting material with **X** and **Y** being iodo– or bromo–substituents in *para*-position and four fluorines is required. A suitable compound 2,3,5,6-tetrafluoro-1,4-diiodobenzene is commercially available.

Once both outer building blocks **A** and **C** having free acetylenes and sulphur functionalities are available, they have to be coupled one after another to the central building block **B**. It was decided to couple first building block **A** having a MOM–protected sulphur, because this protection group is more stable in the basic reaction conditions needed for the *Sonogashira* coupling. This way the acetyl–protection group of building block **C** will be exposed to the basic conditions only in one coupling reaction. Possibly, higher yields can be obtained using this order. To allow measurements in the MCB the MOM–protection group of **A** has to be cleaved to get the acetyl–protection group in the last step. It turned out that the protection groups is unusually stable in acidic conditions. Hence, a protocol using silver nitrate was used.<sup>[346]</sup> This method makes use of the high affinity of silver–ions to sulphur. The obtained silver salt can be reacted with acetyl chloride to get the S–acetyl group. Using this protocol probably both sulphurs are deprotected and subsequently protected again using acetyl chloride.

For control experiments, two symmetric rods, that is target compounds having building block **A** or **C** on both sides of the biphenylic linker, were envisaged. These can be synthesised from the available building blocks by *Sonogashira* couplings as well. In this case, both iodines of the central building block **B** will be substituted at once. For the fluorinated rod, the MOM–group has to be converted to the acetyl–group, which can be achieved with silver nitrate and subsequent addition of acetyl chloride.

#### 4.2.2 Synthesis

The fluorinated benzene subunit was assembled starting with commercially available 2,3,5,6–tetrafluoro–1,4–diiodobenzene (**R4**) (Figure 4–55). Treatment with 2.5 equivalents of *tert*–butyllithium at –78°C, subsequent quenching with stoichiometric amounts of elemental sulphur at room temperature followed by protection of the sulphide by addition of bromomethylmethylether after re–cooling to –78°C gave the methylmethoxy (MOM) protected 2,3,5,6–tetrafluoro–4–iodo–thiophenol **R5** as a yellowish oil in a yield of 77%. Palladium and copper–catalysed *Sonogashira* coupling with trimethylsilyl–acetylene in triethylamine at 40 °C gave **R6** as a yellow liquid in 69% yield after column chromatography. In the last step the trimethylsilyl (TMS) protection–group was cleaved using catalytic amounts of K<sub>2</sub>CO<sub>3</sub> in methanol at room temperature to afford building block **R7** bearing a free acetylene as a white solid after column chromatography in quantitative yield. In the following step this subunit was reacted with 4,4'–diido–2,2'–dimethyl–biphenyl (**O10**) that acts as the conjugation breaking element due to the twist of the phenyl–rings with respect

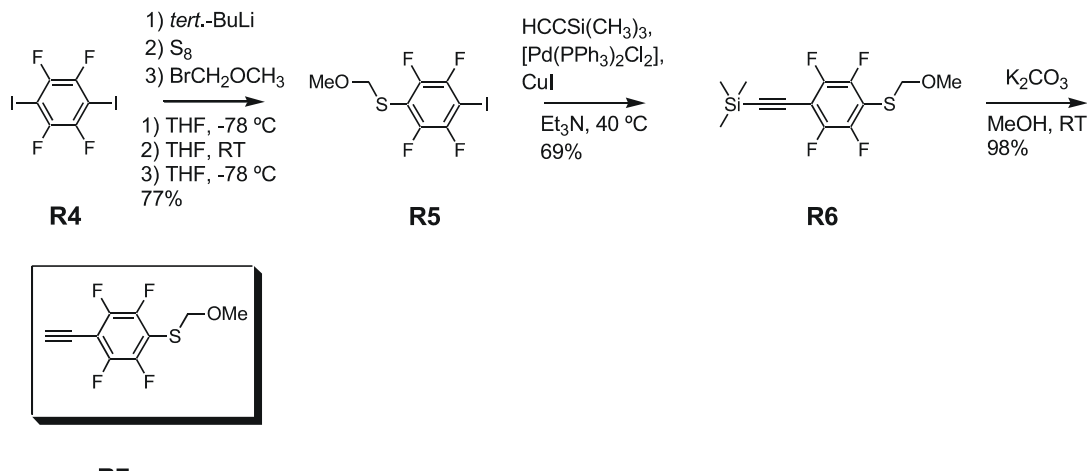
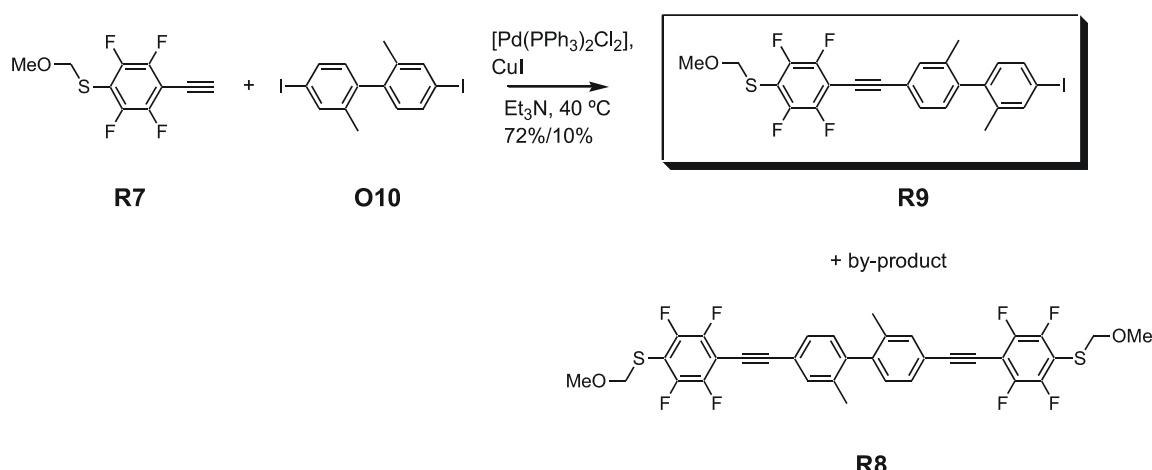


Figure 4–55: Synthetic pathway for the subunit **R7**.

to each other. The synthesis of compound **O10** has already been illustrated in the synthetic section about the oligophenylenes. In first attempts the *Sonogashira* coupling in triethylamine using  $[\text{Pd}(\text{PPh}_3)_2\text{Cl}_2]$  and CuI as catalysts was done only with a slight excess of **O10** over **R7** resulting mainly in structure **R8**, where both iodines on the biphenyl have been substituted. Therefore, the protocol had to be changed to achieve good yields of the mono-substituted product.

Now the acetylenic building block **R7** dissolved in triethylamine was dropped into a solution of a five-fold excess of **O10** in triethylamine over the period of 20 min. After stirring at 40 °C for 18 h **R9** was obtained as a white solid after column chromatography in a yield of 72% by this alteration of the synthetic procedure (Figure 4–56). Besides, still the product, in which **R8** has substituted both iodines of **O10**, was isolated as a slightly yellow solid, but now only in about 10% yield. For the next step (4–ethynyl)phenyl thioacetate (**A21**) was needed, which had been synthesised according to the procedure described above for the anthracene compounds (Figure 4–42). Palladium– and copper–catalysed *Sonogashira* coupling of the acetylene building block **A21** to the biphenyl containing intermediate **R9** in a THF/ethyl-diisopropylamine mixture at room temperature gave compound **R10** as a white solid in a yield of 67% after column chromatography (Figure 4–57). Here, ethyl-diisopropylamine was used as base, because it is known to give better yields in CCR when an acetyl–protection group is present.<sup>[347]</sup> Presumably, this can be attributed to the bulkiness of the amine compared to, for example triethylamine. Compound **R10** already comprises the structure of the electronically asymmetric molecular rod bearing terminal sulphur anchor–groups which are protected by an acetyl and a MOM group, respectively. While two different protection–groups are of particular interest to obtain a defined orientation of the asymmetric molecular rod in a self–



**Figure 4–56:** *Sonogashira* coupling of **R7** to the spacer part, 4,4'-diido-2,2'-dimethyl-biphenyl resulting in two products **R8** and **R9**.

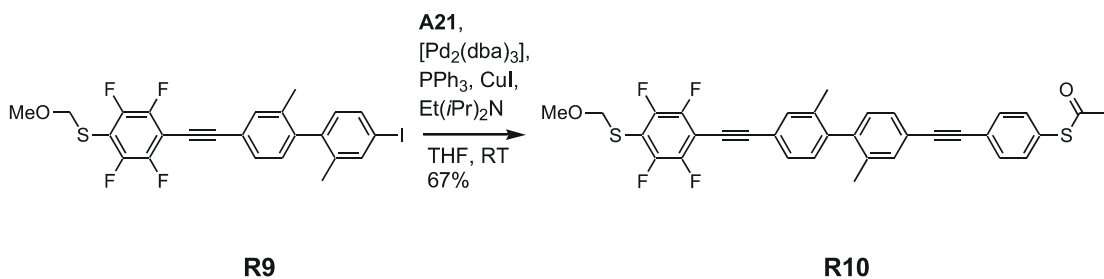


**Figure 4–57:** Synthesis of the molecular rod **R10**.

assembled monolayer, acetyl protected terminal sulphur anchor-groups turned out to be the best choice for single molecule investigations in a MCB.<sup>[13]</sup>

Compound **R8**, which had been obtained as a by–product in the formation of **R9**, was used as a model compound to test the transformation of the MOM–group to the acetyl–group. First, it was attempted to cleave the MOM protection–group using trifluoroacetic acid in CH<sub>2</sub>Cl<sub>2</sub> at room temperature. However, no conversion was observed. In the next attempt conc. hydrochloric acid in ethanol was employed at room temperature and at reflux. Again, the cleavage could not be achieved. The cleavage of the MOM protection–group in acidic conditions is probably hampered due to the four fluorine atoms on the aromatic ring lowering the electron density. Therefore, another method, which makes use of the high affinity of silver–ions to sulphur, was employed. In analogy to a procedure described by Topolski **R8** was treated with 2.5 equivalents of silver nitrate in ethanol at room temperature in the dark (Figure 4–58).<sup>[346]</sup> The obtained yellowish silver salt was then suspended in pentane and acetyl chloride was added at room temperature affording target compound **R2** as a white solid in a yield of 90%.

Now this method was used to obtain target compound **R1**. When exactly the same protocol as for **R8** was used, only low yields were obtained. In particular, it was more complicated to achieve the conversion to the silver salt, but the use of a mixture of ethanol and dichloromethane as solvents helped to solve this problem probably due to the better solubility of compound **R10** in this mixture. Hence, **R10** was dissolved in a CH<sub>2</sub>Cl<sub>2</sub>/ethanol–mixture and 3.0 equivalents of silver nitrate were added (Figure 4–59). The use of 3.0 equivalents of

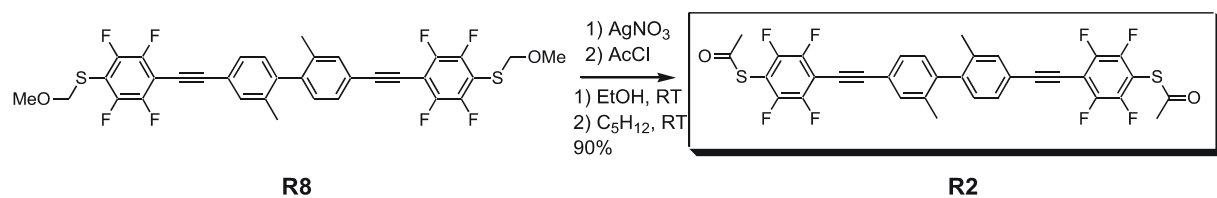


**Figure 4–58:** Cleavage of the MOM protection group using silver nitrate and in situ protection of the thiol with acetyl chloride giving **R2**.

$\text{AgNO}_3$  probably results in a cleavage of the acetyl protection–group as well. After stirring at room temperature in the dark, a white solid was obtained which was suspended in toluene and acetic anhydride. At this point no conversion of the silver–salt is observed, the subsequent addition of acetyl chloride starts the reaction. Probably, the driving force for this reaction is the formation of very insoluble  $\text{AgCl}$ , which can only be formed if acetyl chloride and traces of water are present. If only acetyl chloride is used for the last reaction step, low yields have been obtained as well. Possibly, high concentrations of acetyl chloride, can cleave the acetyl–protection group again, as has been described in literature.<sup>[348]</sup> Therefore, the addition of acetic anhydride probably helps to keep high levels of protection agent and stabilise the desired compound. The observed differences for target compounds **R1** and **R2** can probably attributed to different reactivities of the acid–induced thioester cleavage. In particular, the thioester group, which is present on the non–fluorinated phenyl–ring of **R1** will be more prone to an acidic attack, as it has a higher electron density on sulphur. Using the modified procedure target compound **R1** has been obtained as a white solid in a yield of 37% after column chromatography.

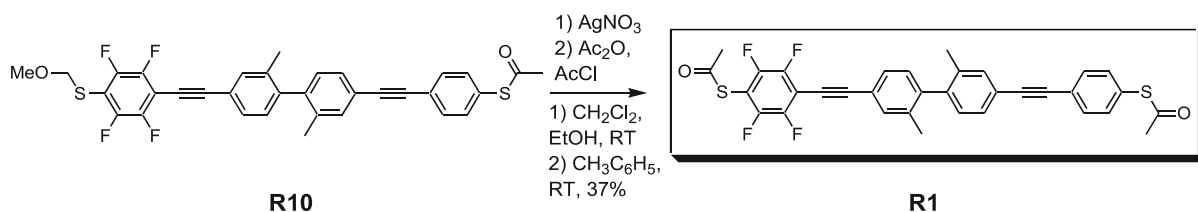


Figure 4–59: Synthesis of the molecular rod **R1** via cleavage of the MOM–group with silver nitrate.

In addition, two symmetric compounds **R2** and **R3** were synthesised for control experiments. The fluorinated rod **R8** has already been obtained as side product during the synthesis of **R9**. To improve the yield 2.4 equivalents of the fluorinated acetylene **R7** and the diiodine **O10** have been exposed to similar coupling conditions as described for compound **R9** above. The rod **R8** with two terminal MOM protected sulphur–groups was obtained as slightly yellow solid in 93% yield (Figure 4–60). Deprotection of both MOM groups has been mentioned above. Target compound **R2** was prepared by treatment with silver nitrate in ethanol and

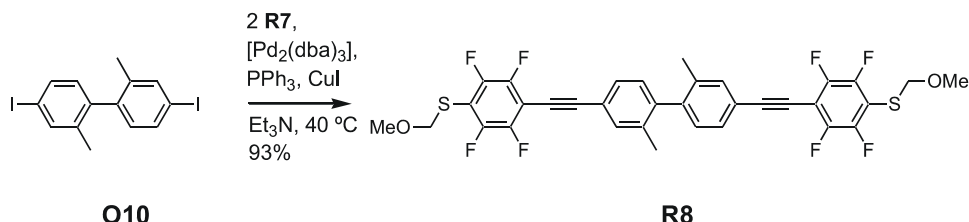
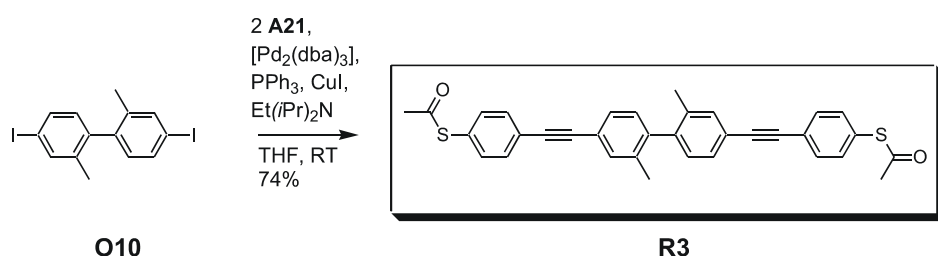


Figure 4–60: Synthesis of fluorinated rod **R8** having two MOM–protection groups.

subsequent cleavage of the silver salt suspended in pentane with acetyl chloride. The fluorinated rod **R2** with acetyl-protected terminal anchor-groups was obtained as white solid in 90% yield. The unfluorinated symmetric rod **R3** was obtained by a *Sonogashira* coupling of 2.4 equivalents of (4–ethynyl)phenyl thioacetate (**A21**) to **O10** in THF at room temperature using ethyl-diisopropylamine as base (Figure 4–61). Purification by column chromatography provided target **R3** bearing two acetyl protected terminal sulphur-groups as a white solid in 74% yield.



**Figure 4–61:** *Sonogashira* coupling of **A21** to biphenyl **O10** to get the molecular rod **R3**.

### 4.2.3 Characterisation and Structural Analysis

All new compounds were characterised by  $^1\text{H}$  and  $^{13}\text{C}$ –NMR, elemental analysis and EI–MS and MALDI–TOF–MS, respectively. Besides, single crystals suitable for x–ray analysis could be obtained from compounds **R3**, **R8** and **R10**. Despite several attempts no single crystals that were suitable for x–ray analysis could be obtained from target compounds **R1** and **R2**. However, compound **R10** has the same molecular structure as **R1** except of a MOM protection–group on the sulphur of the fluorinated ring and **R8** has the same molecular structure as **R2**. Here, both sulphurs are protected by MOM–groups instead of acetyl–groups. Two parameters were of particular interest in the analysis of the solid–state structures of these compounds. First, the length of the molecule as defined by the intramolecular sulphur–sulphur distance was important, because it can have a pronounced influence depending on the prevalent electron transport mechanism. Second, the torsion angle between the two phenyl–rings of the common biphenyl core was measured as well, as the degree of  $\pi$ –conjugation in the molecular structure, which is altered by different angles, is likely to effect the electronic transport behaviour, too. Both properties are probably not changed considerably by different protection–groups on sulphur. Therefore, **R10** can be regarded as model compound for **R1** and **R8** as model compound for **R2**. However, crystal structure analysis can only give the

spatial arrangement of the molecular subunits with respect to each other in the solid-state, which can be influenced by packing effects in the crystal. Hence, the determined arrangement can be different from the one in solution or of single-molecules immobilised between two electrodes.

Slow diffusion of pentane into a dichloromethane solution of **R10** gave single crystals suitable for X-ray analysis (Figure 4–62). Compound **R10** crystallises in the triclinic space group  $P\bar{1}$ .<sup>[309]</sup> There are two asymmetric units per unit cell that have the empirical formula  $C_{34}H_{24}F_4O_2S_2$ , that is the molecular formula. Hence, there are two molecules per unit cell. The torsion angle between both phenyl-rings of the central 2,2'-dimethyl-biphenyl unit was measured to  $75.0(8)^\circ$ . The  $C(sp^2)$ – $C(sp^2)$ -bond between these rings was determined to 150.1(3) pm, which is slightly longer than the average value of 148 pm commonly observed for that kind of bond.<sup>[91]</sup> The phenyl-rings of both diphenylacetylene  $\pi$ -systems are almost coplanar. However, the acetylene linker angles of  $179.0(3)^\circ$  ( $C(6)$ – $C(9)$ – $C(10)$ ) and  $175.6(3)^\circ$  ( $C(9)$ – $C(10)$ – $C(11)$ ), that is the ones to the fluorinated phenyl-ring, deviate from linearity by a small extent. Hence, these two rings are slightly bended out of plane. The  $C(sp^2)$ –F bonds on this ring are between 134.3(3)–135.4(3) pm, which matches the average bond length of this kind.<sup>[91]</sup> Compared to the values commonly found both carbon–sulphur bonds, that is  $C(sp^2)$ –S to the phenyl-ring and  $C(sp^3)$ –S to the MOM-protection group, are elongated a little. The carbon–sulphur bonds on the other end of the molecule are 178.2(3) pm ( $S(2)$ – $C(30)$ ) and 178.6(4) pm ( $S(2)$ – $C(33)$ ), which is slightly longer than the average  $C(sp^2)$ –S bond. The length of the molecular rod given by the intramolecular sulphur to sulphur distance was determined to 2.43(4) nm.

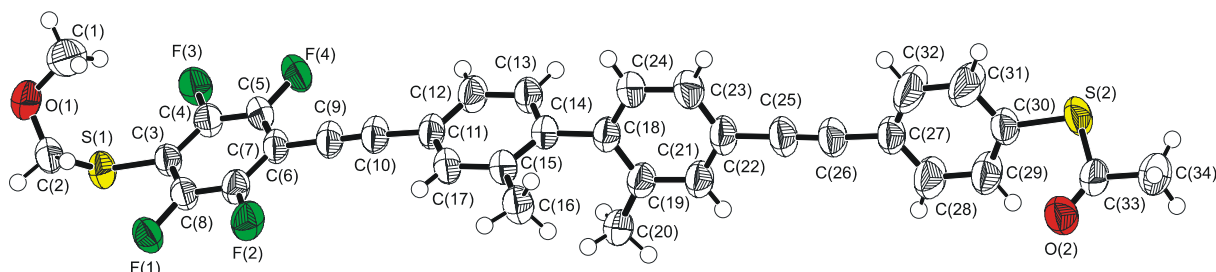


**Figure 4–62:** Molecular structure of compound **R10**. Selected bond lengths/pm and bond angles/ $^\circ$ :  $S(1)$ – $C(2)$  183.1(3),  $S(1)$ – $C(3)$  177.1(3),  $S(2)$ – $C(30)$  178.2(3),  $S(2)$ – $C(33)$  178.6(4),  $F$ – $C$  134.3(3)–135.4(3),  $O(1)$ – $C(1)$  142.6(5),  $O(1)$ – $C(2)$  139.9(4),  $O(2)$ – $C(33)$  118.7(4),  $C(9)$ – $C(10)$  120.0(4),  $C(14)$ – $C(18)$  150.1(3),  $C(25)$ – $C(26)$  120.1(5);  $C(2)$ – $S(1)$ – $C(3)$  102.6(2),  $C(30)$ – $S(2)$ – $C(33)$  103.8(2),  $C(1)$ – $O(1)$ – $C(2)$  112.3(2),  $C(6)$ – $C(9)$ – $C(10)$  179.0(3),  $C(9)$ – $C(10)$ – $C(11)$  175.6(3),  $C(22)$ – $C(25)$ – $C(26)$  178.6(4),  $C(25)$ – $C(26)$ – $C(27)$  176.7(4).

In order to further investigate the spatial arrangement of **R10** in the solid state the packing diagram of this compound has been analysed. Such diagrams show the orientation of molecules to each other in the unit cell and, thus allow to obtain information about intermolecular interactions between different molecules in the solid state. In particular, the influence of nondirectional forces such as  $\pi$ - $\pi$  stacking and directional interactions like hydrogen bonding can be studied.<sup>[338]</sup> Figure 4–63 presents the packing of **R10**, that is the asymmetric compound, in the crystal together with the unit cell. The diagram reveals two kinds of stacks formed by the asymmetric molecule. Within each stack, which is formed along the *a*-axis of the triclinic unit cell, adjacent molecules are approximately parallel. Target compound **R10** contains three phenyl-rings and one fluorinated phenyl-ring. From literature it is known that often arene and perfluoroarene units tend to stack on each other by  $\pi$ - $\pi$ -interactions due to their rather different electron densities.<sup>[338],[349]</sup> While the stacks in the present compound are probably formed due to  $\pi$ - $\pi$ -interactions between the phenyl-rings, interestingly no  $\pi$ - $\pi$  forces between fluorinated and non-fluorinated rings can be observed, that is the molecules pack in a completely parallel fashion and fluorinated and non-fluorinated rings do not reside on each other. The two different stacks observed are related to each other by an inversion centre situated at *c*/2. Hydrogen bonding interactions were found between F(1) (cf. Figure 4–62) and hydrogen of the acetyl-protection group. Due to this

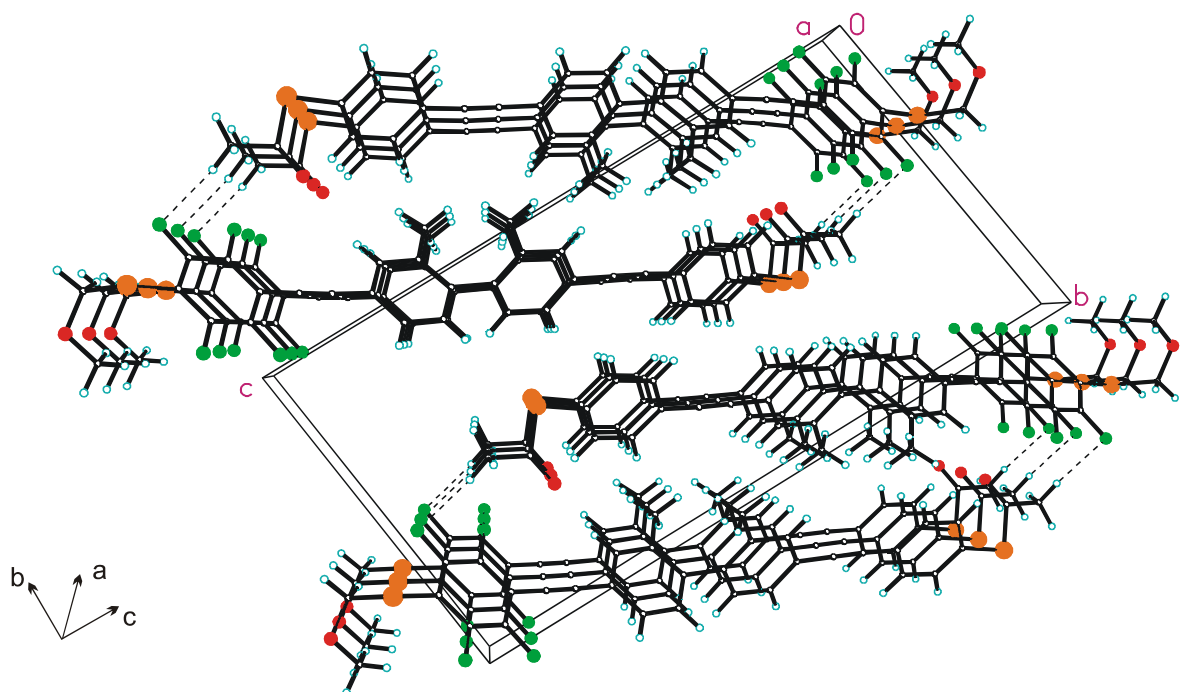


**Figure 4–63:** Packing of **R10** in the crystal structure.

hydrogen bonding pseudo-dimers are formed of the two different stacks of molecules.

A crystal structure of compound **R8** was obtained from single crystals grown by slow diffusion of hexane into a solution of **R8** in diethylether (Figure 4–64). This molecular rod crystallises in the monoclinic space group  $P2_1/n$  with four molecules in the unit cell.<sup>[309]</sup> The angle of rotation between the two phenyl-rings of the biphenyl core was determined to  $60.6(4)^\circ$  which is somewhat smaller than in **R10**. The bond length between the two phenyl-rings is  $149.8(3)$  pm ( $C(15)-C(18)$ ), which is comparable to the length found in **R10**. Only on one side the phenyl-rings in the diphenylacetylene subunit are coplanar, on the other side the two phenyl-rings are rotated by an angle of  $63.2(3)^\circ$  with respect to each other. In the diphenylacetylene subunits the acetylene bridge angles of  $177.4(3)^\circ$  ( $C(10)-C(9)-C(6)$ ),  $177.4(3)^\circ$  ( $C(9)-C(10)-C(11)$ ) in the coplanar subunit as well as the angles of  $178.0(2)^\circ$  ( $C(26)-C(25)-C(22)$ ) and  $176.3(3)^\circ$  ( $C(25)-C(26)-C(27)$ ) in the non-planar part deviate from linearity only by a minor extent. Due to the torsion angle in one of the diphenylacetylene units both outer, fluorinated phenyl-rings reside almost in the same plane. The  $C(sp^2)-F$  bonds lie in the range between  $133.5(2) - 134.8(2)$  pm, which closely matches the average length of this kind of bond.<sup>[91]</sup> The  $C(sp^2)-S$  bond length of  $176.5(2)$  pm ( $S(1)-C(3)$ ) and  $176.9(2)$  ( $S(2)-C(30)$ ) as well as the  $C(sp^3)-S$  bond length of  $181.3(3)$  pm ( $S(1)-C(2)$ ) and  $182.2(2)$  ( $S(2)-C(33)$ ) are comparable on both ends of the molecule. The intramolecular sulphur sulphur distance was determined to be  $2.43(1)$  nm showing the same length as the rod **R10**.

Compound **R8** shows a different solid state structure compared to **R10**, in particular a

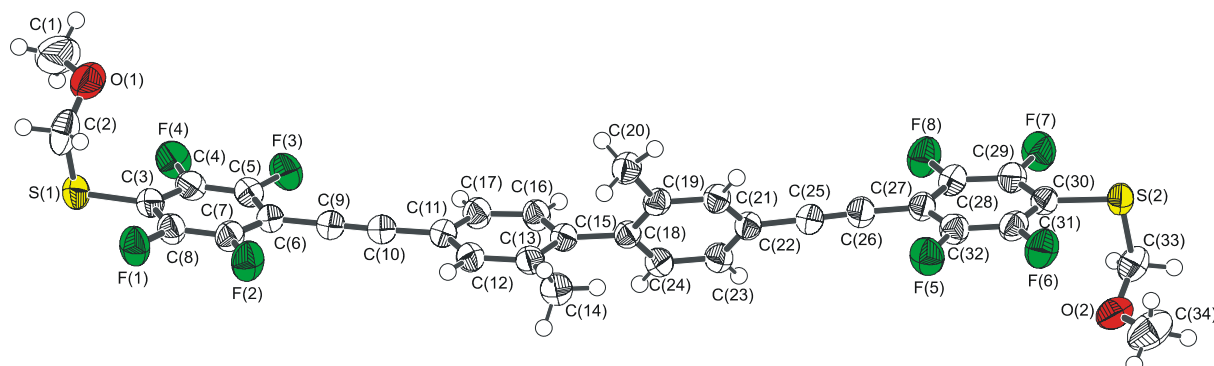


**Figure 4–64:** Molecular structure of compound **R8** having two MOM–protection groups. Selected bond lengths/pm and bond angles/°:  $S(1)-C(3)$  176.5(2),  $S(1)-C(2)$  181.3(3),  $S(2)-C(30)$  176.9(2),  $S(2)-C(33)$  182.2(2),  $F-C$  133.5(2)–134.8(2),  $O(1)-C(2)$  138.6(4),  $O(1)-C(1)$  141.5(4),  $O(2)-C(33)$  138.7(3),  $O(2)-C(34)$  142.5(3),  $C(9)-C(10)$  120.2(3),  $C(15)-C(18)$  149.8(3),  $C(15)-C(16)$  139.7(3),  $C(25)-C(26)$  119.3(3);  $C(3)-S(1)-C(2)$  99.36(11),  $C(30)-S(2)-C(33)$  98.37(10),  $C(2)-O(1)-C(1)$  113.5(2),  $C(33)-O(2)-C(34)$  113.7(2),  $C(10)-C(9)-C(6)$  177.4(3),  $C(9)-C(10)-C(11)$  177.4(3),  $C(26)-C(25)-C(22)$  178.0(2),  $C(25)-C(26)-C(27)$  176.3(3).

different spatial arrangement of the two diphenylacetylene subunits has been observed. To investigate, whether these differences arise from packing effects, the packing diagram of this compound has been analysed as well. Figure 4–65 shows the packing diagram of **R8**, the completely fluorinated molecule. Different stacks of molecule **R8** are organised in a layer type structure reminding of the so-called herringbone arrangement often found for aromatic hydrocarbons.<sup>[350]</sup> Between these two different layers hydrogen bonding interactions between F(6) and the hydrogen at C(23) have been found, that is the hydrogen bonding occurs between two diphenylacetylene subunits, which show a non-planar arrangement. Both different layers consist of two different kinds of stacks that are probably formed due to  $\pi$ – $\pi$ –interactions between different molecules along the *a*–axis. No  $\pi$ – $\pi$ –stacking between fluorinated and non-fluorinated rings is present. The different  $\pi$ – $\pi$ –stacks are related to each other by an inversion centre situated on the *c*–axis. Besides, directional forces between these different stacks exist. Fluorine–fluorine interactions are found between F(3) and F(5) of molecules of the same kind of stack, but between the distinct diphenylacetylene subunits. Sulphur–oxygen interactions are present between O(1) and S(2) of molecules of different stacks, this interaction occurs between the protection–groups at the different ends of the molecule as well.

Single crystals of target compound **R3** were obtained by slow evaporation of a solution of dichloromethane (Figure 4–66). This compound crystallises monoclinic as well, but in the space group  $P2_1/c$ .<sup>[309]</sup> The asymmetric unit has the empirical formula  $C_{34}H_{26}O_2S_2$ , hence, there are four molecules in the unit cell. The angle of rotation in the central biphenyl core of **R3** is  $64.2(4)^\circ$ . The bond length between the two phenyl–rings was measured to  $149.2(3)$  (C15)–C(18)), which is close to the ones observed in **R10** and **R8**. The phenyl–rings of the

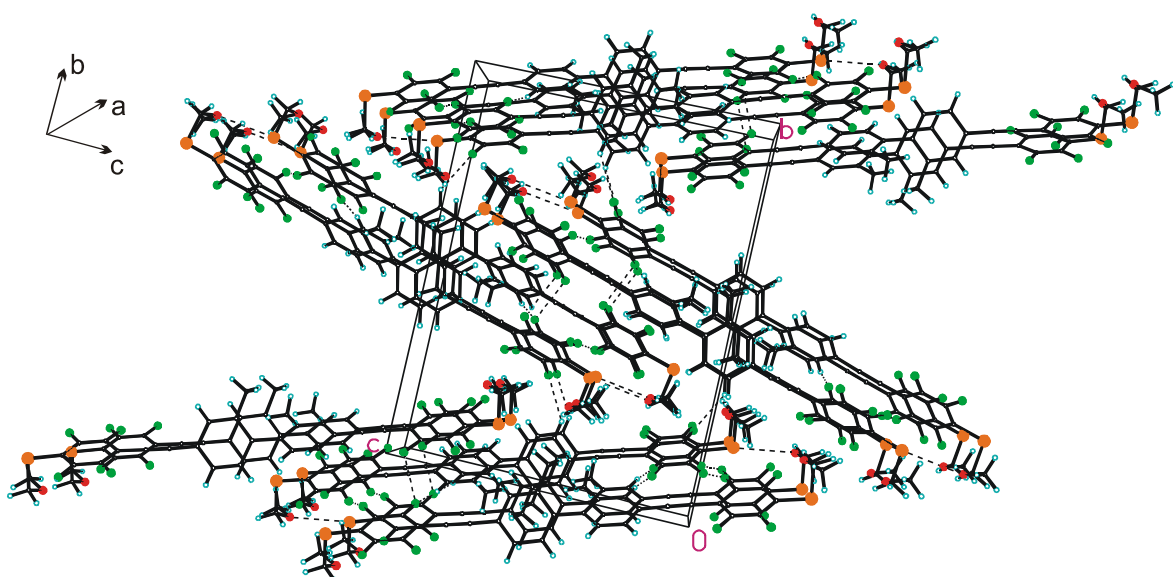


**Figure 4–65:** Packing of **R8** in the crystal structure.

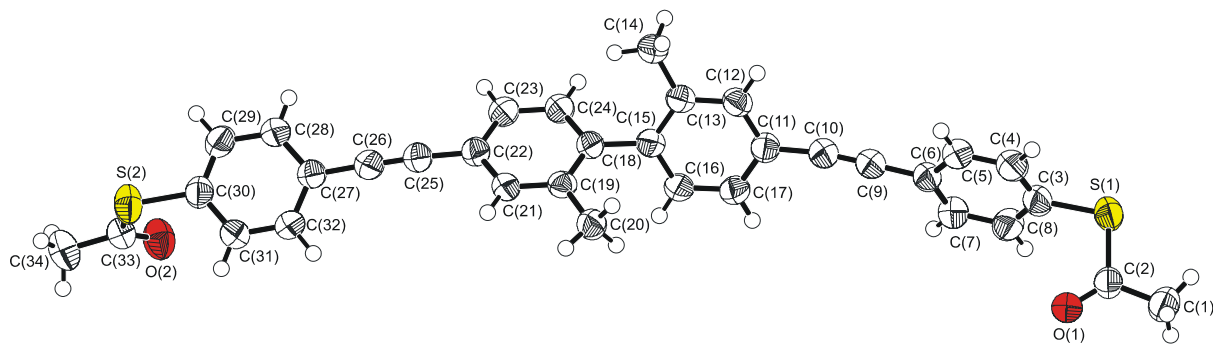


**Figure 4–66:** Molecular structure of target **R3**. Selected bond lengths/pm and bond angles/ $^{\circ}$ : S(1)–C(3) 177.8(3), S(1)–C(2) 177.9(3), S(2)–C(30) 177.2(3), S(2)–C(33) 177.5(3), O(1)–C(2) 119.9(3), O(2)–C(33) 120.0(3), C(9)–C(10) 119.7(4), C(15)–C(18) 149.2(3), C(25)–C(26) 120.5(4); C(3)–S(1)–C(2) 101.66(13), C(30)–S(2)–C(33) 100.74(13), O(1)–C(2)–C(1) 124.7(3), O(1)–C(2)–S(1) 122.1(2), C(26)–C(25)–C(22) 177.2(3), C(25)–C(26)–C(27) 179.1(3), C(10)–C(9)–C(6) 179.1(3), C(9)–C(10)–C(11) 172.5(3).

diphenylacetylene subunit are rotated with respect to each other by an angle of 25.2(3) $^{\circ}$  and 24.6(3) $^{\circ}$ , respectively. Hence, both diphenylacetylene subunits are not planar. Whereas the acetylene linker angles of 177.2(3) $^{\circ}$  (C(26)–C(25)–C(22)) and 179.1(3) $^{\circ}$  (C(25)–C(26)–C(27)) deviate only slightly from linearity on one side (Figure 4–66 left), the acetylene bond is bended to a larger extent on the other side (179.1(3) $^{\circ}$  for C(10)–C(9)–C(6) and 172.5(3) for C(9)–C(10)–C(11)). Due to the different rotations all phenyl–rings of **R3** lie in different planes. All C(sp<sup>2</sup>)–S bonds have a very similar length and are slightly elongated compared to the average value of 175 pm commonly found.<sup>[91]</sup> The length of the molecule measured by the sulphur to sulphur distance was determined to 2.41(4) nm.

In target compound **R3** both diphenylacetylene subunits are not co–planar, which is in marked contrast to the solid state structures of the other two compounds **R10** and **R8**. The analysis of a packing diagram of **R3** can probably help to find out, whether these different arrangements result from packing effects in the crystal. Figure 4–67 shows the packing diagram of **R3**, the last member of this family of compounds. As already mentioned, this compound crystallised in the monoclinic space–group *P2<sub>1</sub>/c*, which comprises a 180° screw axis and an axial glide plane along the *c*–axis. No  $\pi$ – $\pi$ –stacking forces become apparent between different molecules in this solid state structure. However, hydrogen bonding interactions and sulphur–sulphur interactions between different molecules exist. One hydrogen bond can be found between oxygen of the acetyl protection and the methyl group of the acetyl protection group of a second molecule. At the same time, this oxygen is hydrogen–bonded to hydrogen of an outer phenyl ring of the diphenylacetylene subunit. An additional hydrogen bond exists between the oxygen of a different acetyl protection–group and hydrogen of an outer phenyl–ring of the

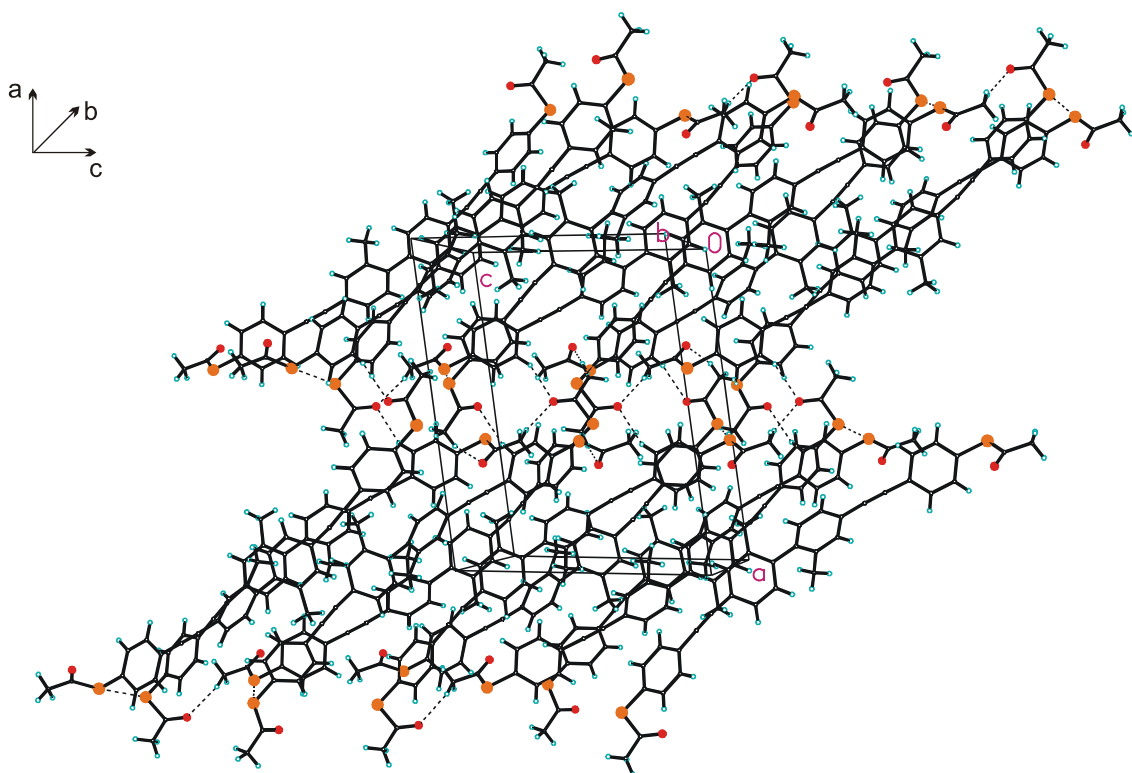


**Figure 4–67:** Packing of **R3** in the crystal structure.

diphenylacetylene unit. Due to the symmetry elements present in the structure, the hydrogen bonding interactions are arranged in the crystal structure almost in a zip-like fashion. Furthermore, sulphur–sulphur interactions between two molecules that are related to each other by a screw axis can be observed.

All molecular structures measured exhibit a large torsion angle (from  $60.6(4)^\circ$  to  $75.0(8)^\circ$ ) between the two phenyl–rings of the biphenyl core. The smallest angle was found in the fluorinated compound **R8** and the largest in **R10** where only one phenyl–ring is substituted by fluorines. The rather large torsion angles suggest a breaking of the  $\pi$ –conjugation due to the presence of the biphenyl core, that is the molecular units on both sides of the biphenylic linker are separated electronically, as was the aim of the design of the different molecular structures. Since the angles are comparable in **R3**, **R8** and **R10**, the degree of  $\pi$ –conjugation between the two diphenylacetylene subunits probably does not differ considerably in these three compounds. However, different arrangements for the subunits left and right of the linker have been observed. In **R10**, that is the asymmetric structure, the phenyl–rings of both diphenylacetylene  $\pi$ –systems are almost coplanar. Hence, here the diphenylacetylene subunits are  $\pi$ –conjugated. In the fluorinated compound **R8** only one diphenylacetylene subunit is

coplanar, on the other side the phenyl-rings are rotated by 63.2(3) $^{\circ}$ . In the crystal structure of **R3** all four phenyl-rings lie in different planes. However, due to the cylindrical shape of the  $\pi$ -system of the acetylene the rotation of the phenyl-rings with respect to each other will not hamper the formation of a delocalised,  $\pi$ -conjugated system. Only the torsion angle in the biphenyl moiety will result in a breaking of the  $\pi$ -conjugation, the diphenylacetylene subunits probably do not have different degrees of  $\pi$ -conjugation. Hence, differences in the current-voltage characteristics caused by different degrees of  $\pi$ -conjugation are unlikely. Furthermore, the length of the molecule between the two terminal sulphur groups was measured to 2.43(4) nm for **R10**, 2.43(1) nm for **R8** and 2.41(4) nm for **R3**, that is only a small difference of 0.02 nm was observed. Hence, the influence of the length of the molecule on the electronic transport behaviour should be negligible.

In general, hydrogen bonding interactions are stronger than nondirectional forces such as  $\pi$ - $\pi$ -stacking.<sup>[338]</sup> If both kinds of interactions are present, usually the packing in a crystal will be governed by the stronger one, because these are energetically more favourable. In the solid state structure of **R10** only one type of hydrogen bonding was found, whereas in the other two different kinds of directional forces are present. On the other hand  $\pi$ - $\pi$ -stacking seems to play a role in the solid state arrangement found for **R10** and also for **R8**, but not for **R3**. The packing of **R3** seems to be governed solely by hydrogen bonding interactions. The formation of hydrogen bonding requires a certain spatial arrangement, because these are directional forces which commonly show bonding angles between hydrogen-donor-acceptor between 150 to 160 $^{\circ}$ .<sup>[338]</sup> In the present molecular structures a spatial adjustment can be achieved by rotation of the molecular subunits with respect to each other due to the presence of single bonds. This can result in an arrangement where the different units are not coplanar anymore, as seen for example in **R3**. Hence, possibly the different kinds of hydrogen bonding that can be formed in these three molecules can result in the different spatial arrangements of the subunits that were observed in the solid state structures of **R3**, **R8** and **R10**.

As already mentioned, in a simple transport model the frontier orbitals of the  $\pi$ -system are assumed to be determining for electronic transport properties. Therefore, UV/Vis spectra of the rod like structures **R1 – R3**, **R8** and **R10** have been recorded as  $1 \times 10^{-5}$  M solutions in acetonitrile as well to obtain information about the frontier orbitals in these structures.

All spectra are comparable and show an absorption maximum between 300 and 320 nm and a slightly lower absorptivity at 204 nm (Figure 4–68). By comparison with the absorption studies of the oligophenylenes presented above the latter band, which does not shift with

different substitution, can be attributed to the common central building block of all compounds. This is the  $\beta$ -band of the phenyl-rings of the central biphenyl core.

At longer wavelengths all five rods display an intense peak with a hypsochromic shoulder shifted by 12 – 14 nm. This double peak is probably due to both, the individual delocalised diphenylacetylene  $\pi$ -systems and the whole rod-like backbone. The intense peak is observed at 317.5 nm for the unfluorinated rod **R3** and is bathochromically shifted to 323 nm for both symmetrical fluorinated rods **R2** and **R8**. Both asymmetric fluorinated rods **R1** and **R10** display this peak in between at 319.5 nm and 320 nm, respectively. Furthermore, the fluorinated symmetric rod **R2** and the asymmetric target structure **R1** display a broad weak shoulder up to 395 nm. However, as these shoulders are only observed for the structures with acetyl protected terminal sulphurs **R1** and **R2**, while the corresponding structures with MOM protection groups **R10** and **R8** do not display comparable features, these additional long wavelength absorptions can presumably be assigned to enlarged delocalisation due to the acetyl-group on the fluorinated thiophenol. All UV/Vis spectra taken together suggest comparable relative positions of the frontier orbitals.

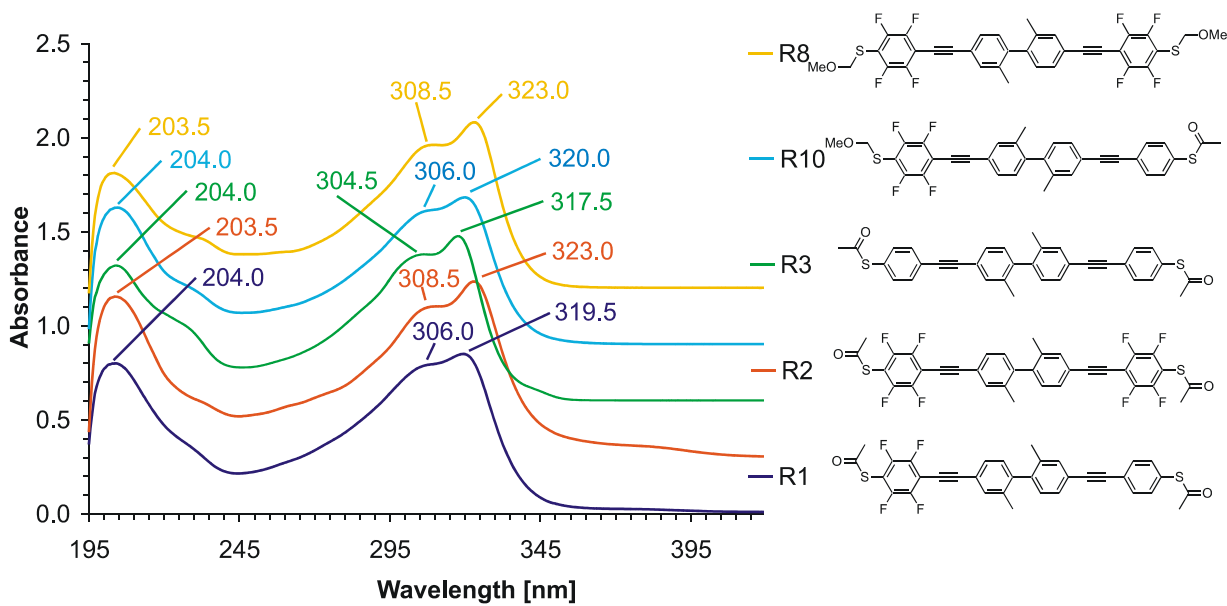


**Figure 4–68:** UV/Vis-spectra of compounds **R1 – R3, R8** and **R10** ( $1 \times 10^{-5}$  M solutions in acetonitrile at room temperature). For clarity the spectra have been shifted by 0.3 units.

#### 4.2.4 Electron Transport Measurements

The electronic transport properties of the molecular rods **R1** – **R3** have been studied by *R. Ochs* in the group of *H. Weber* at the INT using the MCB technique.<sup>[351]</sup> As usual, the molecules were immobilised as single molecules **R1'**, **R2'** and **R3'** in different experiments in between Au–electrodes of a MCB from a  $5 \times 10^{-4}$  M solution in THF (Figure 4–69). Details of the protocol can be found in chapter 2.2.2. and the previous paragraphs of this section. Considerable sample–to–sample fluctuations have been observed for these junctions at room temperature, due to the single molecule nature of the experiment. To increase the data quality and to reduce these fluctuations, the junctions were cooled to  $\approx 30$  K. At low temperature, stable junctions have been obtained reproducibly with all three immobilised rods.

Figure 4–70 depicts a typical example for the asymmetric rod **R1**. The actual measured IV curves are shown in red. Here, the numerical derivative  $dI/dV$  drawn in blue was calculated from the average of the measured IV curves. Hence only one derivative  $dI/dV$ , that is the differential conductance can be seen. In these measurements the voltage was swept between –1.5 V to +1.5 V. Different IV curves shown were measured with the same metal–molecule–metal junction, but in consecutive voltage sweeps. All presented experiments were done at about 30 K. The recorded IV curves of a single asymmetric molecular rod **R1'** immobilised between the Au–electrode pair of a MCB are non–linear and clearly asymmetric with respect to voltage inversion. The IV curves display several step like features of different intensities, which become more apparent as peaks in the first derivative. Between about + 0.6 V and – 0.4 V the current is suppressed. Assuming the simple transport picture described in the section about the oligophenylenes, the peaks in the differential conductance can probably be

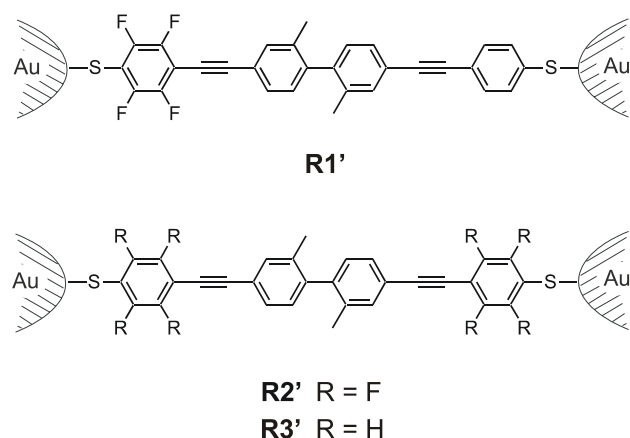


**Figure 4–69:** Target structures **R1** – **R3** immobilised in between two gold electrodes of a MCB (schematic drawing).

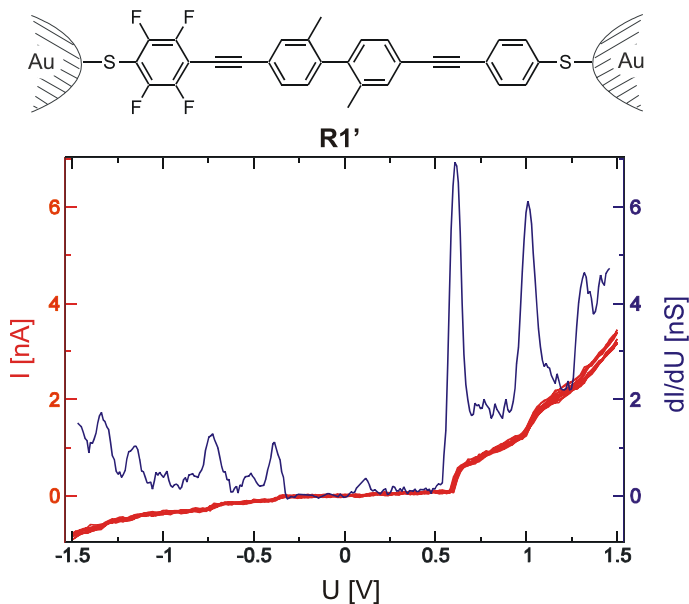


**Figure 4–70:** IV curves of **R1'** reproducibly recorded for a stable metal/molecule/metal junction in a MCB at  $T \approx 30$  K (in red) and the numerical derivative  $dI/dV$  (in blue).

attributed to electron transport through the HOMO of the molecule. Probably the suppression of current results from the orbital structure of the immobilised molecule, that is at low bias no molecular orbital came in resonance with the electrodes. Possibly, the suppression can also result from *Coulomb*–blockade. However, as already mentioned in the section about the oligophenylenes, it is not completely clear, whether *Coulomb*–blockade contributes to the electron transport behaviour in the investigated metal–molecule–metal junctions. Eye-catching are two particularly intense steps at about +0.6 V and +1 V, respectively, which were observed solely in one current direction, while in the opposite current direction only smaller steps were recorded, but at lower absolute voltage values of about –0.4 V and –0.75 V, respectively. At negative bias two to three further steps can be observed beyond  $U = -1$  V. All peaks in the numerical derivative are of different height. The current level at  $U = 1.5$  V is about 3.5 nA, whereas at  $U = -1.5$  V only a current of about 0.7 nA was observed.

Control experiments with the symmetric molecular rods **R2'** and **R3'** were of particular interest to find out, whether the observed asymmetries in the IV curves of **R1'** are due to the molecular structure or due to any other effects. Figure 4–71 shows a typical set of recorded current voltage characteristics for the completely fluorinated, symmetric target compound **R2'**. As usual, the actual recorded IV curves are drawn in red, while the blue curve represents the numerical derivative  $dI/dU$  of the average of the recorded IV curves. The IV characteristics shown were recorded over the period of about ten minutes. The recorded IV curves are rather symmetric with respect to voltage inversion showing pronounced rounded–

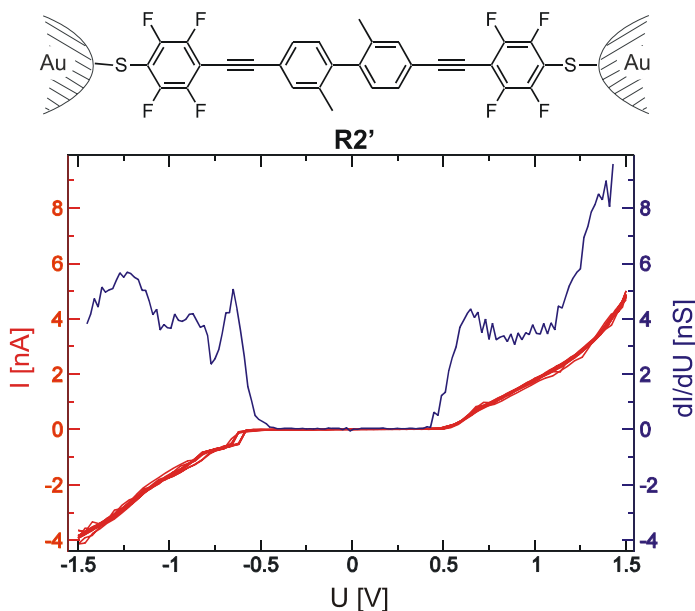


**Figure 4–71:** IV curves of **R2'** reproducibly recorded for a stable metal/molecule/metal junction in a MCB at  $T \approx 30\text{ K}$  (in red) and the numerical derivative  $dI/dV$  (in blue).

like steps at voltages higher  $U = \pm 0.5\text{ V}$ , which can be visualised better in the first derivative. Between about  $-0.5\text{ V}$  to  $+0.5\text{ V}$  the current is suppressed. In both current directions peaks of similar height are observed at about  $U = \pm 0.65\text{ V}$  in the first derivative. Assuming the simple transport picture, the peaks can probably be attributed to electron transport through the HOMO of the molecule. Hence, the current is probably suppressed at low voltages, because there was no molecular orbital close to the *Fermi* energy of the electrodes at this low bias. Coulomb-blockade can also lead to a suppression of current. At higher voltages the curves become slightly asymmetric with respect to voltage inversion, that is at negative voltage two less prominent steps can be seen, whereas at positive bias the current rises strongly beyond  $U \approx 1.2\text{ V}$ . These small asymmetries are probably caused by the different history of the contacts between the molecule and the electrode on both sides due to the immobilisation protocol at low temperature. A somewhat different coupling to the electrode can induce asymmetries to the molecular orbitals resulting in asymmetric IV curves. The current level at  $U = 1.5\text{ V}$  is about 5 nA at positive and negative bias.

Figure 4–72 shows a typical set of recorded current–voltage characteristics of the second symmetric rod **R3** without fluorinated phenyl–rings. Again, the red curves depict the actual recorded IVs, whereas the blue curve describes the numerical derivative of the average of the recorded IV characteristics. These curves were recorded over the period of about 10 min. The obtained rounded–like curves are clearly non–linear. They are also pretty symmetric with respect to voltage inversion, as had been expected for this symmetric molecule. No clear

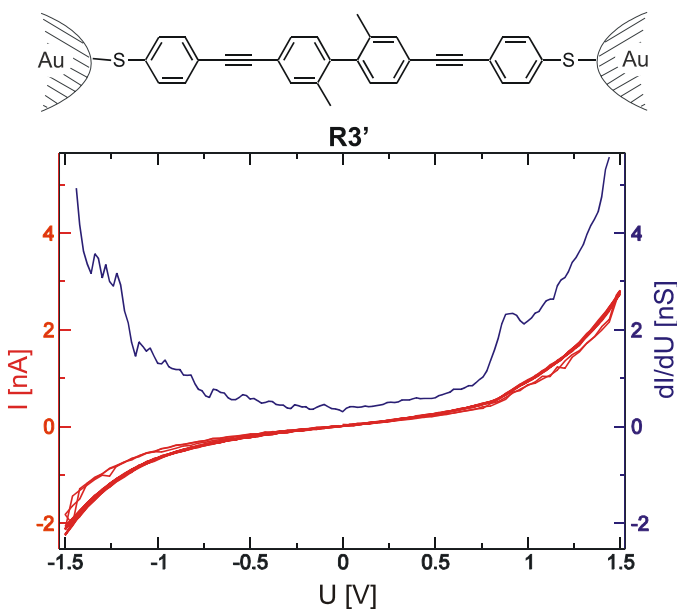


**Figure 4–72:** IV curves of **R3'** reproducibly recorded for a stable metal/molecule/metal junction in a MCB at  $T \approx 30\text{ K}$  (in red) and the numerical derivative  $dI/dV$  (in blue).

suppression of current at low bias can be observed and no distinct peaks become apparent in the first derivative, which is in marked contrast to the IV curves of the other two compounds **R1'** and **R2'**. The UV/Vis spectra presented above suggested comparable relative positions of the frontier orbital in the three target compounds **R1**, **R2** and **R3**. However, the energy of the HOMO can be different in these compounds. Hence, different bias voltages can be required to obtain electron transport through a molecular orbital. The absence of peaks in the differential conductance suggests that in this structure there were no orbitals in the energy window spanned by the two electrodes at the used voltages. The slight asymmetries observed can probably be attributed to an asymmetric coupling of the molecule to the electrodes due to the immobilisation protocol at low temperatures. The current level at  $U = 1.5\text{ V}$  is about 3 nA at positive and negative bias.

All three investigated molecular rods **R1'** – **R3'** showed comparable current levels between 3 to 5 nA at  $+1.5\text{ V}$ . This is consistent with the UV/Vis spectra of these compounds shown above that suggested a comparable size of the  $\pi$ -system in these compounds. However, metal–molecule–metal junctions containing the asymmetric molecule **R1** had a reduced current level at  $U = -1.5\text{ V}$  of about 0.7 nA, whereas junctions comprising the two symmetric molecules **R2** and **R3** showed the same current as at positive bias. Apparently, the transparency for current of **R1'** strongly depends on the current direction, that is the setup shows the electronic function of a rectifier. The rectification ratio  $RR$ , defined by  $RR = (\text{current at } V_0)/(\text{current at } -V_0)$ , where  $V_0$  is the highest positive bias used,<sup>[39]</sup> is  $\sim 4$  to 5 at  $1.5\text{ V}$ . Common silicon-based rectifiers have a rectification ratio of several orders of magnitude.

Hence, the observed on–off–ratio is small compared to semiconductor diodes, but notable for a single–molecule arrangement. Obviously, the electronic asymmetry in the IV characteristics originates in the asymmetry of the molecular structure of **R1'**, as control experiments with the symmetric rods **R2'** and **R3'** displayed rather symmetric curves with respect to voltage inversion.

The asymmetric molecule **R1** had been designed based on the proposal by *Aviram* and *Ratner*. They predicted rectifying behaviour for an organic molecule comprising a D– $\pi$ –system and an A– $\pi$ –system fused together by a stiff, but not  $\pi$ –conjugated spacer.<sup>[3]</sup> Therefore, for a detailed understanding of the presented results, one may first consider the *Aviram–Ratner* picture, which operates in the incoherent transport regime. As explained in more detail in chapter 2.3.2, in this model the asymmetry in the current–voltage characteristics arises from different onset voltages for forward bias and reverse bias of the metal–molecule–metal–junction. At forward bias, that is the direction of higher current levels, electron transport starts at lower voltage than at reverse bias, that is the direction of low current levels (Figure 4–73). In the recorded current–voltage characteristics of the asymmetric molecule **R1'** the forward bias is at positive voltage, because here higher current levels were observed. However, the onset voltage of electron transport at positive bias is increased compared to the onset voltage at negative bias. Hence, the similarity of the recorded IV curves to diode characteristics does not arise from the position of the steps in the IVs, but rather from the height of these steps suggesting that the *Aviram–Ratner* model might not be valid here. The observation of a very comparable sequence of steps independent of the voltage direction in the data rather points towards a nonlinear picture, where the same electronic levels rule the electronic transport, but change their shape (and their transparency) due to polarisation effects when the voltage is inverted. Hence, to understand the data in detail, a more advanced theoretical model is

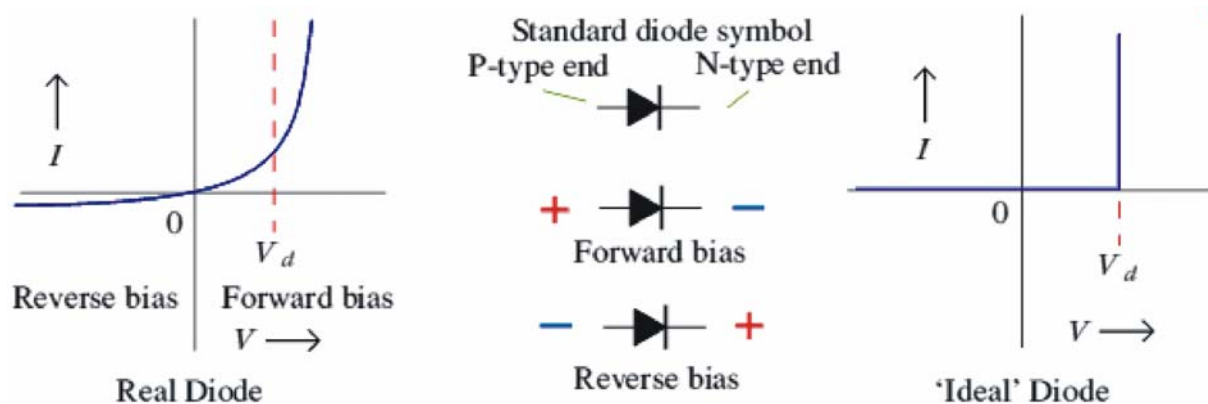


**Figure 4–73:** Current–voltage characteristics of a typical semiconductor diode.

needed, which is currently developed by *M. Köntopp* in the group of *F. Evers* at the INT. The entirety of the presented investigations demonstrates 1) that IV characteristics strongly depend on the molecules' structure and hence, can be designed and tailored by chemical synthesis; 2) that even single molecules bear inherent electronic functions. Here rectification behaviour with a rectification ratio of about 4 to 5 at  $U = 1.5$  V was observed; 3) that presumably single molecules are investigated in the MCB experiments, as the asymmetry of the immobilised molecular structure would be randomised in an assembly comprising larger numbers of molecules.<sup>[13]</sup>

### 4.3 Molecular Switches

Switches form an integral part of electronic circuits.<sup>[4]</sup> Hence, for the successful development of ME molecular counterparts of switches have to be designed and studied. In order to show switching behaviour the used compounds have to exist in (at least) two different states, that must be possible to inter-convert by means of a driving force. In principle, different driving forces such as electrical energy or light can be used.<sup>[103]</sup> A large number of organic molecules that show switching in solution induced by light have been published over the years including compounds based on azo–benzene building blocks and diarylethenes.<sup>[352]</sup> Electrochemical switching and switching by the addition of oxidation/reduction agents has been studied for a [2]catenane in solution extensively.<sup>[116],[21]</sup> However, only a limited number of publications dealing with switching in solid-state devices based on organic molecules have appeared. It has been shown that the catenane mentioned above can probably be used to build switching devices where the crossing between the different states is induced by different voltage bias.<sup>[20]</sup> Recent studies demonstrated that switching can also occur with more simple molecules in the same electrode set-up suggesting that the observed mechanism of switching is more involved.<sup>[24]</sup> In particular, it has been proposed that switching in these devices depends on the structure of the molecule and the electrodes and their interfacial interactions.<sup>[24]</sup> In addition, a diarylethene-based compound has been studied using a MCB. The light-induced switching of these compounds is well-known. However, in the measurements in a MCB light-induced switching could only be performed from the closed to the open state.<sup>[23]</sup>

As part of the European LIMM project (Light-Induced Molecular Movements) a photo-switchable molecule has been designed meeting the requirements for an investigation of its electronic properties and switching behaviour using a mercury drop electrode (Figure 4–75).

The measurements with this technique will be done in the group of *M. Rampi* at the Università di Ferrara. Furthermore, it was sought to study the switching behaviour of the target compound in solution and on the surface of gold–nanoparticles using UV/Vis spectroscopy to get a first insight into the characteristics of the *E*– to *Z*–isomerisation (also *Rampi*–group).

The set–up of the experiment for the mercury drop electrode consists of a, in this case translucent gold electrode, on which a self–assembled monolayer of the studied compound has been absorbed *via* thiol anchor–groups. A small mercury–drop with a diameter of ~ 1 mm is expressed into a solution of hexadecanethiol (HDT) in hexadecane from a microsyringe connected to a reservoir of mercury. This way a SAM of HDT can form on the surface of the mercury drop that serves as counterelectrode in this set–up. The SAM on the mercury drop is required to prevent amalgamation of the gold electrode, when the two electrodes are brought together very closely using a micromanipulator. These manipulations are done with the gold electrode placed in a beaker and covered with a solution of hexadecane containing HDT. The area of contact was estimated to be between  $1.5 \times 10^{-3}$  and  $3 \times 10^{-3} \text{ cm}^2$ . IV curves are recorded by applying a potential across the junction. It has been shown experimentally and in theoretical calculations that in this set–up electron transport occurs due to superexchange tunnelling through the molecular bridge. A more detailed description of this technique can be found in chapter 2.2.1.

For the investigation of switching behaviour in this set–up a molecule that can self–assemble on the gold electrode is required. For this purpose thiol anchor–groups are suited best, because they allow the immobilisation of the molecule on the gold electrode due to the formation of a covalent bond between sulphur and gold. Alternatively, an acetylsulfanyl–group like in the measurements in a MCB can be used that can be cleaved *in situ* on a gold surface forming a Au–S bond. However, the free thiol was favoured, because usually acetyl–protected thiols require higher concentrations of compounds to achieve monolayer coverage.<sup>[61]</sup> Besides, the molecule has to have a structure that allows to obtain two different states. Switching between these two different forms has to be possible by shining light through the translucent gold electrode. The azo–group, which can be switched reversibly between its *E* and *Z*–form by light of different wavelengths, was chosen as the photoactive unit. The device will be in its ON–state when the molecule is bridging the gap between the two electrodes (Figure 4–74 left) Hence, current can flow. Since a tunnelling contact is established between the top of the molecule and the mercury electrode, the measured currents show a pronounced dependence on the size of the gap between the molecule and the top

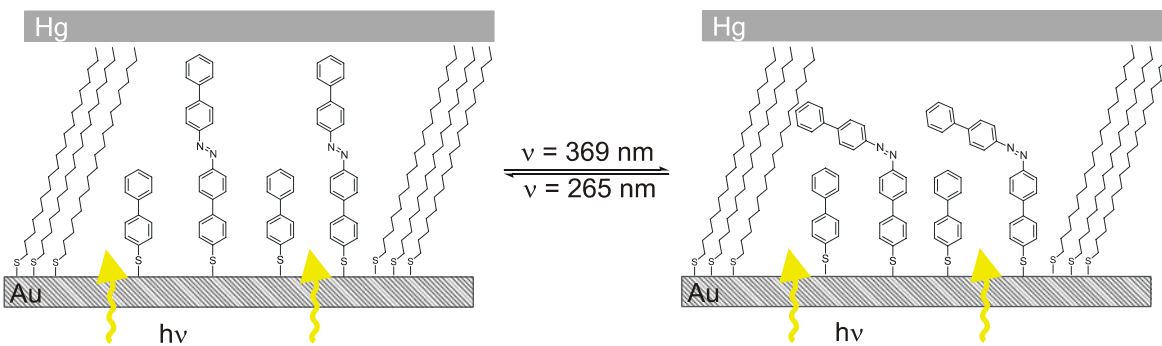


**Figure 4–74:** Schematic experimental set-up for the current–voltage measurement of the switching molecule S1.

electrode. Therefore, the OFF-state of the device is reached when the gap between the molecule and the electrode is considerably bigger than in the ON-state (Figure 4–74 right). To allow an easy detection of these two states a rod-like molecule has to be used, where the two different forms differ significantly in length. Due to the experimental set-up insulating alkanethiols have to be present in the set-up of the experiment as well (see below). Therefore, the studied molecular structure has to have a comparably higher conductivity than these insulating alkanethiols to allow differentiation between these two components of the SAM, that is it has to act as a molecular wire. Aromatic systems are known to have a higher transparency for electron transport as opposed to alkyl chains due to the presence of a delocalised  $\pi$ -system.<sup>[9]</sup> Hence, the azo-functionality was substituted by a biphenyl moiety on both sides providing a rod-like structure with a delocalised  $\pi$ -system. A biphenyl substituted azo-group was preferred, as such a compound has a bigger difference in length between the *E*- and *Z*-form compared to, for example a phenyl substituted one. This way, a bigger drop in tunnelling current when going from the *E* to the *Z*-configuration can occur facilitating the detection of switching. The formation of well-ordered SAMs is favoured, when the angle of rotation between the phenyl-rings of the biphenyl units is small. Besides, the investigations done in the family of oligophenylanes presented above suggested that biphenyls having a rather large torsion angle between the two phenyl-rings due to a substitution in position 2 and 2' show a breaking of  $\pi$ -conjugation. Hence, such structures show a higher resistance for electron transport compared to unsubstituted ones. For this experiment, a molecular structure with a rather high conductivity was preferred to facilitate the interpretation of the data. Therefore, no further substituents were introduced in 2- and 2'-position to obtain a comparably small angle of rotation in the biphenyl subunits. As mentioned above, a thiol-group has to be present in the structure to allow self-assembly on the gold-surface. This was placed on one end of the molecular rod, that is in position 4' of one biphenyl subunit.

However, when only the target compound is present in the SAM, the mercury drop probably follows the movement of the molecule, that is there is no difference in the gap between the two states. Therefore, a mixed SAM together with a second molecule of very similar length as the target compound has to be employed. In order to not interfere with the measurements of the target compound an insulating molecule has to be used, for example an alkanethiol. The alkanethiol acts like a column holding the mercury drop in place, when switching occurs. The gold surface is pre-structured with a SAM of the alkanethiol using nano-imprinting, before the target molecule is absorbed. Then in the confined space delimited by the SAMs of alkanethiol the studied molecule can be self-assembled. When the molecule is switched from its *E* to the *Z*-form, the length of the molecule decreases, but at the same time the lateral dimension will increase. In a closely packed monolayer consisting only of the target compound there is no space available for the extension of the lateral dimension. Hence, the isomerisation from the *E* to the *Z*-form in the SAM on the gold surface is hindered, as has already been described in literature.<sup>[353]</sup> The required separation between two target compounds can be obtained by employing a mixed SAM together with 4-biphenylthiol, which has roughly half the length of the target compound. Assuming a statistical distribution in the monolayer, 4-biphenylthiol acts as a spacer between two target compounds. In this way, the space next to the upper biphenyl subunit of the target compound is not occupied by another biphenyl moiety, but there is a gap that can be filled due to the lateral extension when going from the *E*- to the *Z*-form.

Following the described needs of the experiments the target molecule **S1** has been designed. It consists of an azo-functionality that is substituted on both sides by a biphenyl unit. One of the biphenyls bears a thiol group in 4'-position to allow self-assembly. Alternatively, target compound **S2** can be used, that only differs in the acetyl protection-group on the sulphur. Essentially, the target compound will have an asymmetric substitution on the azo-group.



**Figure 4–75:** Target Structure **S1** bearing a free thiol and alternative structure **S2** having an acetyl-protected thiol.

### 4.3.1 Synthetic Strategy

The key step of the synthetic pathway will be the formation of the azo–functionality. Two conceptually different approaches exist for this reaction. The first symmetric build–up is based on the formation of an azo–compound using either reductive methods to couple nitro–compounds<sup>[259],[260]</sup> or oxidative methods to couple amino–compounds.<sup>[256],[257],[258]</sup> These reactions will yield compounds that are symmetric with respect to the substitution on the azo–group. Hence, the desired asymmetry of the target compound has to be introduced by a further functionalisation once the azo–compound has been prepared. The second approach uses an asymmetric coupling procedure to give asymmetrically substituted molecules. Since this method requires the synthesis of suitable asymmetrically substituted starting compounds, the symmetric azo–coupling was more attractive.

In principle, two different approaches exist for the symmetric build–up. The desired sulphur functionality can be present before the azo–group is formed or afterwards. When the sulphur functionality is present in the structure, before the azo–group is formed, compounds with sulphur groups on both ends will be obtained. Hence, this route affords compounds that do not meet the requirements of the target structure and was ruled out. The introduction of the sulphur functionality after the build–up can, in principle be done in different ways. Carbon–sulphur bonds can be formed by S<sub>N</sub>Ar reactions of sodium alkylthiolates with aryl halides.<sup>[231]</sup> Another procedure involving metal–halide exchange using *tert*–butyllithium followed by quenching with sulphur can be used with aryl iodides and bromides to give sulphur–substituted aromatic structures. However, due to the envisaged symmetric build–up of the azo–group a precursor with a halogen on one and a nitro or amino–group on the other end has to be used then. Hence, an azo–compound with halogens on both terminal positions is obtained. This does not meet the requirements of the designed target compound either. Furthermore, such an azo–dye is probably quite insoluble. Therefore, these two reactions for the introduction of sulphur into an azo–compound were not considered further. Sulphur can also be introduced into a phenyl–ring using an electrophilic aromatic substitution, that is a sulphonation or chlorosulphonation reaction (Figure 4–76).<sup>[238]</sup> Such a route does not require any substituents other than hydrogen on the aromatic ring and is widely used in the chemistry of azo–dyes.<sup>[199]</sup> The obtained chlorosulphonic acid or sulphonic acid can be reduced to the free thiol using a literature procedure.<sup>[334]</sup> As already mentioned the azo–group can be built starting from an amino–compound by oxidative methods or from a nitro–compound by reductive methods. When a sulphonation or chlorosulphonation reaction is used after the

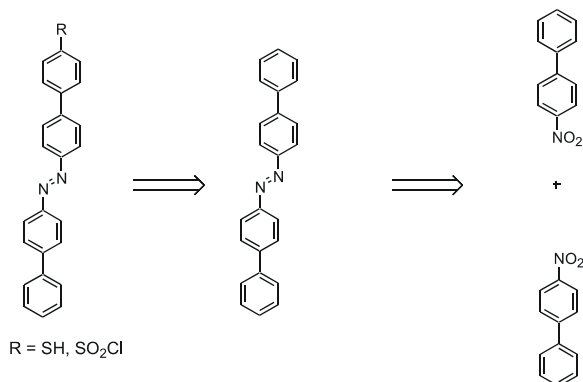


**Figure 4–76:** First synthetic strategy for the synthesis of the target compound **S1** based on a symmetric assembly of the azo–functionality.

build-up of the azo–group, biphenyl precursors bearing only an amino– or nitro–group in position 4 are required. Since 4–nitro–biphenyl was commercially available, the reductive route was chosen. After the formation of the azo–compound bis–biphenyl–4–yl–diazene, the electrophilic substitution using chlorosulphonic acid to obtain the carbon–sulphur bond can be done. However, this reaction step was not successful. Therefore, an alternative strategy based on an asymmetric azo–coupling of two different precursors was developed.

In these methods the carbon–sulphur bond can be established, before the azo–functionality is build. In general, three different routes for the formation of asymmetric azo–compounds exist. In principle, similar oxidative or reductive conditions as for the symmetric azo–forming reactions can be applied. However, the coupling of two different building blocks using these methods will give rise to mixtures of three different compounds (two homo–coupled and one cross–coupled product). The selectivity of the reaction will be difficult to control. Hence, such an approach was not considered further. Asymmetric azo–compounds can also be obtained by the azo–coupling procedure involving the electrophilic substitution of aryldiazonium–ions, that is essentially an amine, with electron–rich aromatic compounds.<sup>[199]</sup> However, apart from the thiol–functionality on one end of the molecule there are no further electron–donating substituents in the target compound. If the reaction is done with a sulphur substituted aryldiazonium–ion, an unsubstituted biphenyl has to be used as the electron–rich part. Presumably, the electron–density of this system is not high enough, to afford good yields of the azo–coupling. If the reaction is performed the other way around, the aryldiazonium ion has to be coupled to a biphenyl bearing a sulphur functionality. Alkyl–protected sulphur groups are probably stable in the required reaction conditions, but they increase the electron density of the phenyl–ring they are attached to. Hence, the diazonium ion attacks this phenyl–ring preferably. However, this way the desired azo–dye cannot be obtained. Acetyl–protected

thiols cannot be present either, because then the electron density of the aromatic system is probably not high enough to allow the coupling of the diazonium salt in good yields. Therefore, the third possibility for an asymmetric build-up of the azo-compound was more attractive (Figure 4–77).

The key step of this synthetic strategy is the so-called *Mills* reaction, that allows the formation of azo-compounds by the reaction of an amino- with a nitroso-precursor.<sup>[261],[251]</sup>

To get the desired compound one of these precursors has to have a sulphur-group. Nitroso-compounds are commonly prepared by a procedure involving reduction of a nitro-group followed by selective oxidation to obtain the nitroso-group.<sup>[354]</sup> Such a protocol can probably not be applied to compounds having a sulphur-group, because the sulphur can be oxidised as well. Furthermore, 4-nitro-biphenyl, that is a suitable starting compound for 4-nitroso-biphenyl, can be purchased. Hence, it was decided to perform the *Mills* reaction with 4-nitroso-biphenyl and a biphenyl having an amino- and a sulphur-group.

The target compound has a free thiol (or an acetyl-protected thiol) on one end of the molecule. The reaction between the amino-precursor bearing the sulphur functionality and the nitroso-precursor is usually performed in strong acidic conditions at elevated temperatures.<sup>[261]</sup> Probably, neither the thiol nor the thioester, which can be cleaved in acidic media, are stable in these conditions required for the *Mills* reaction. Therefore, a sulphur protection group has to be used that is stable in acidic conditions and that can be converted to a free thiol or acetyl-protected thiol in the presence of an azo-group. Alkyl-protected thiols tolerate strong acidic conditions and can be converted to free or acetyl-protected thiols in

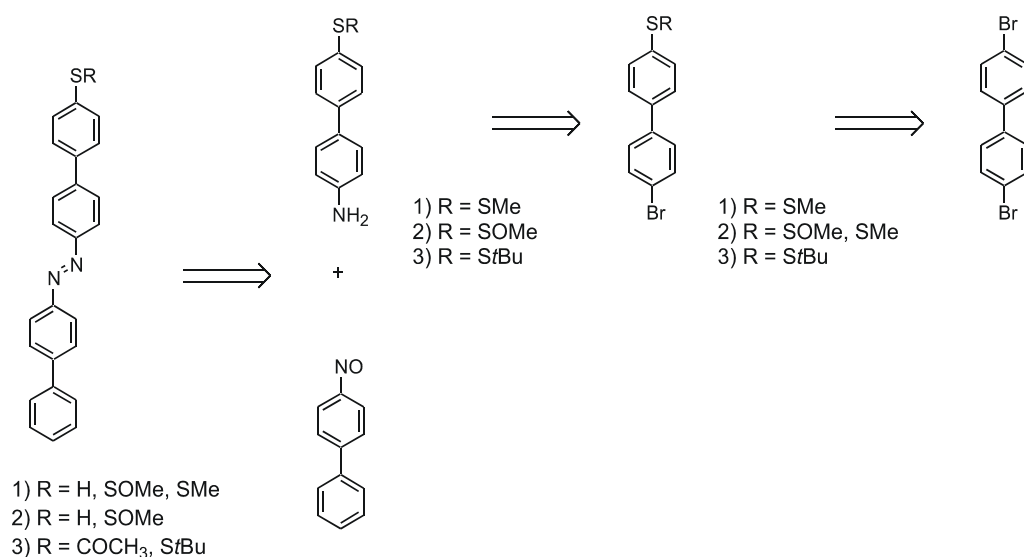


**Figure 4–77:** Synthetic strategy for the synthesis of target compound S1. Here an asymmetric build-up of the azo-compound was chosen.

various ways. Methylsulfanyl-groups can be transformed to a free thiol by nucleophilic cleavage with sodium alkylthiolates,<sup>[231]</sup> by a reductive method using sodium in liquid ammonia<sup>[216]</sup> and by a reaction sequence involving a *Pummerer* rearrangement.<sup>[215]</sup> The nucleophilic cleavage requires harsh reaction conditions that are probably not applicable in the presence of an azo-group. The reductive method using sodium in liquid ammonia is likely to yield a reduction of the azo-group. Besides, the biphenyl-substituted azo-dye is probably not soluble in liquid ammonia. Therefore, these two routes were not followed. For the *Pummerer* rearrangement the thiomethyl-group has to be oxidised to the corresponding sulphoxide, which can then be converted to the free thiol. Sulphoxides are stable in acidic conditions. Thus, this oxidation can be done before or after the azo-group has been formed.

Apart from methylsulfanyl-groups *tert*-butyl protected thiols can be used as well, because they are moderately stable in acidic conditions and can be transformed to acetyl-protected thiols in two different ways.  $\text{BBr}_3$  in the presence of acetyl chloride<sup>[223]</sup> or bromine in a mixture of acetyl chloride and acetic acid<sup>[226]</sup> can be used to obtain the S-acetyl group from this alkyl-protection group. Both methods yield acetyl-protected thiols, but the target compound having a free thiol was preferred to an acetyl-protected one for the experiment. Therefore, the route using a methylsulfanyl-group that can be converted to free thiol was more attractive.

The  $\text{SMe}$ -group is commonly introduced by a nucleophilic aromatic substitution on aryl halides using sodium methylthiolate.<sup>[231]</sup> A free amine does not tolerate the strong nucleophilic conditions required in this reaction step. Hence, the sulphur-group has to be present, before the amino-group is formed. The amino-group can be introduced in different ways including the reduction of a nitro-group<sup>[91]</sup> and the palladium-catalysed *Hartwig-Buchwald (HB)* coupling.<sup>[191]</sup> When a reductive method is chosen, a biphenyl precursor having a nitro-group in position 4 and a methylsulfanyl-group in position 4' is required. Such a compound can be synthesised from simpler starting materials using a palladium-catalysed build-up of the biphenyl skeleton similar to a literature procedure.<sup>[355]</sup> Suitable starting compounds, namely 1-iodo-4-nitro-benzene and 4-(methylsulfanyl)-phenylzinc bromide to perform a *Negishi*-coupling can be purchased. However, low yields of the cross-coupling reduced the attraction of this route involving a reduction of a nitro-substituted biphenyl to obtain the amino-precursor. Therefore, a strategy involving *HB*-coupling to obtain the amino-precursor was developed.

In the palladium-catalysed *HB*-coupling aryl halides are reacted with lithium bis(trimethylsilyl)amide or with commercially available benzophenone imine to prepare a

protected amine.<sup>[191]</sup> In the latter method a diphenyl ketimine is obtained that can be cleaved to obtain a free amine by transamination, by hydrogenolysis using a palladium catalyst or by acidic hydrolysis, that is the reaction conditions for the cleavage of the amino–protection group can be adjusted to the structure of the target compound.<sup>[191]</sup> Therefore, this protocol was regarded superior to the other. The *HB*–coupling is performed best with aryl bromides or iodides.<sup>[136]</sup> As mentioned above, the thiomethyl–group is commonly introduced by a nucleophilic substitution using aryl halides as substrate. Hence, a starting compound bearing halogen–substituents in position 4 and 4' was required. A suitable compound, namely 4,4'–dibromobiphenyl can be purchased. The nucleophilic substitution to obtain the thiomethyl–group has to be done before the amino–group is present, because a free amine does not tolerate the required reaction conditions. Therefore, the developed strategy starts with the introduction of the sulphur–group by a  $S_NAr$  reaction using sodium methylthiolate followed by a *HB*–coupling including removal of the amine protection group by transamination to provide the amino–precursor. This precursor, 4'–methylsulfanyl–biphenyl–4–ylamine, is reacted with 4–nitroso–biphenyl giving the thiomethyl substituted azo–compound under *Mills* conditions. As explained above, the sulphur needs to be oxidised to the corresponding sulphoxide to perform the *Pummerer* rearrangement in the next step. Using *mCPBA* this reaction was done successfully, but the yields were rather low and the isolation procedures troublesome. Hence, the developed synthetic strategy was revised slightly.

Now the sulphur was oxidised directly after the introduction of the thiomethyl–group to the biphenyl. The obtained sulphoxide was used for the *HB*–coupling providing the amino–precursor. This was reacted with 4–nitroso–biphenyl to give the azo–compound, but this time with a sulphoxide group. Using the reaction sequence involving a *Pummerer* rearrangement this compound was transformed into the target compound bearing a free thiol. While this synthetic strategy afforded the desired compound, the yields of the last step were only moderate probably due to the ease of oxidation of the thiol group to give disulphides. Therefore, an additional synthetic route to get better yields was developed. This time the methyl–protection groups on sulphur were exchanged for *tert*.–butyl groups. These groups can be converted to acetyl–protection groups by two different methods mentioned above. Using these methods no free thiol is obtained, that is the compound is not prone to oxidation. In general, the synthetic pathway stayed the same, that is the *tert*.–butylsulfanyl group was introduced first to the biphenyl skeleton using 4,4'–dibromobiphenyl. Then the *HB*–coupling was performed to afford the *tert*.–butylsulfanyl substituted amino precursor, that was reacted

with nitroso–biphenyl giving the corresponding azo–compound. Unfortunately, first attempts to exchange the *tert*–butyl group for the acetyl–group were not successful.

### 4.3.2 Synthesis

The first synthetic route is based on a symmetric build–up of the azo–functionality by a reduction of a suitable nitro–compound. Commercially available 4–nitro–biphenyl (**S3**) was treated with lithium aluminiumhydride in dry THF<sup>[356]</sup> at room temperature affording the already known azo–biphenyl compound **S4** in moderate yield of 35% as a red solid after re-crystallisation from toluene (Figure 4–78). In the next step, **S4** was reacted with three equivalents of chlorosulphonic acid to form the required carbon–sulphur bond. However, attempts at 0 °C and at room temperature using chlorosulphonic acid without an additional solvent did not afford the desired product. Only, starting compound was recovered from the reaction mixture. Probably, the low solubility of **S4** is one of the reasons for the failure of this reaction step.

Since the synthetic strategy involving a symmetric build–up of the azo–compound could not be performed successfully, a new strategy based on an asymmetric procedure, namely the *Mills* reaction, has been developed. This reaction, which requires a nitroso compound and an amino moiety, has proven to be very useful in the synthesis of asymmetrically substituted azo–dyes.<sup>[251]</sup> The necessary 4–nitroso–biphenyl (**S6**) was obtained by a reduction of **S3** with zinc in a solvent mixture of methoxyethanol and water containing ammonium chloride at 30 °C and subsequent selective oxidation using iron(III)chloride in a mixture of water and ethanol at –5 °C. (Figure 4–79).<sup>[354]</sup> Re-crystallisation of the crude product from ethanol afforded the nitroso–precursor **S6** as an orange solid in a yield of 63%.<sup>[357]</sup>

Apart from the nitroso–compound a second biphenyl precursor bearing a sulphur–group and

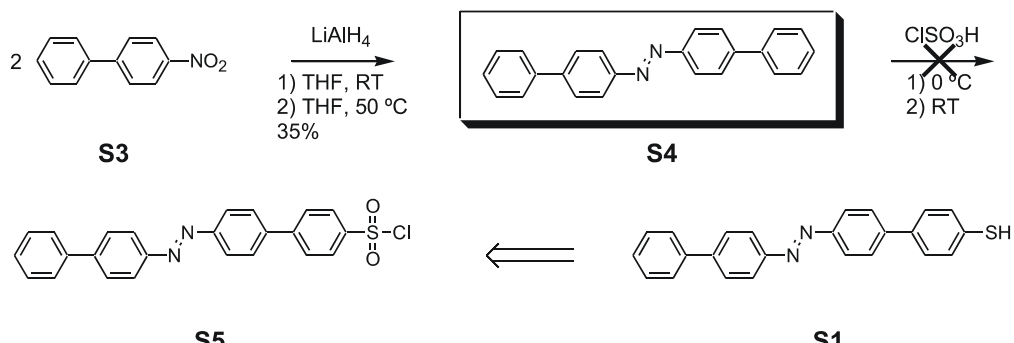


**Figure 4–78:** First route to target compound **S1** based on a symmetric build–up of the azo–group.

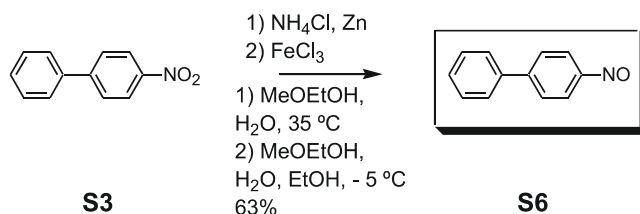


**Figure 4–79.** Synthesis of the nitroso-precursor **S6** following a literature procedure.

an amino-group is required for the build-up of the target compound using the *Mills* reaction. Following the first developed strategy such an amino-compound can be prepared from the corresponding nitro-compound by reduction. The nitro-compound **S9** was synthesised following a literature procedure (Figure 4–80). In a *Negishi* cross-coupling protocol using  $[\text{Pd}(\text{PPh}_3)_4]$  as catalyst commercially available **S7** was coupled with the zinc-organic compound **S8** at room temperature to give the biphenyl **S9** bearing a nitro-group and a methylsulfanyl-group. This compound was obtained as a yellow solid in a yield of 30% after column chromatography. However, due to the low yield of this *Negishi* coupling in the first step of the developed route, this synthetic pathway was not continued further.

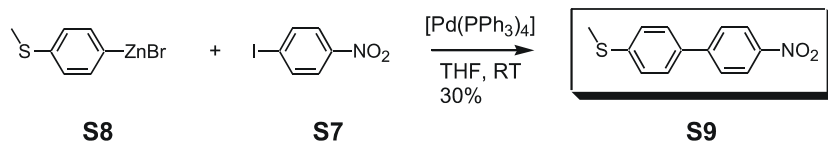


**Figure 4–80:** Synthesis of the biphenyl **S9** by a Negishi coupling.

Instead a different synthetic route involving a *Hartwig–Buchwald* (*HB*) coupling to obtain the necessary amino-precursor was followed. As explained in more detail in the synthetic strategy, the methyl protected thiol-group has to be introduced, before the *HB* coupling is performed. In a  $\text{S}_{\text{N}}\text{Ar}$  reaction using sodium methanethiolate in DMI at  $150^\circ\text{C}$  one bromine of commercially available 4,4'-dibromo-biphenyl (**S10**) was replaced by a methylsulfanyl-group affording the biphenyl **S11** as a white solid after column chromatography in a yield of 60%. (Figure 4–81).<sup>[305]</sup> Using a *HB* protocol with  $[\text{Pd}_2(\text{dba})_3]^*\text{CHCl}_3$  as catalyst, BINAP as phosphine ligand and  $\text{KO}t\text{Bu}$  as base the bromine of **S11** was reacted with benzophenone imine in dry toluene at  $80^\circ\text{C}$ . The diphenyl ketimine **S12** was obtained as a yellow solid after re-crystallisation from methanol in a yield of 79%.<sup>[191]</sup> Transamination with hydroxylamine in methanol at room temperature to cleave the protection group on the amine afforded amine **S13** as a white solid in quantitative yield. In the key step one equivalent of the amino-precursor **S13** was reacted with 1.04 equivalents of 4-nitroso-biphenyl (**S6**) under *Mills* conditions in glacial acetic acid/ $\text{CH}_2\text{Cl}_2$  2/1 (v/v) at room temperature for 72 h (Figure 4–82).

## Results and Discussion

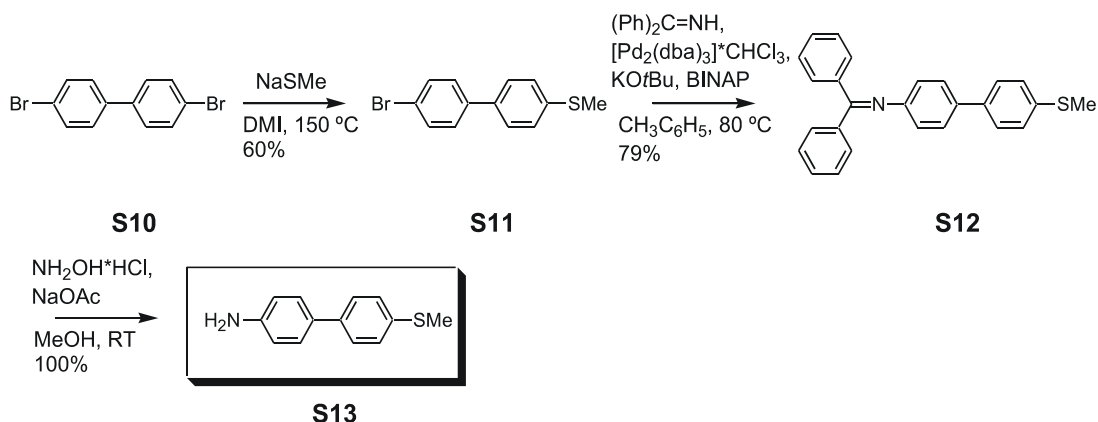


**Figure 4–81:** Preparation of the amino–precursor **S13**.

Re-crystallisation from toluene afforded the desired azo-dye **S14** as a red solid in a yield of 80%. In the next step the methylsulfanyl-group was oxidised to the corresponding sulphoxide using 1.3 equivalents of *m*CPBA in  $\text{CHCl}_3$  at 0 °C. The azo-dye **S15** bearing a SOMe-group was obtained as a red–brown solid after column chromatography in a yield of 36%. Using *m*CPBA sulphone formation is possible as well. Usually sulphoxides and sulphones can be separated quite readily by column chromatography due to the big difference in polarity of these compounds. However, in the present case the purification turned out to be troublesome presumably due to the very low solubility of the azo-compounds, that is the starting compound **S14**, the desired compound **S15** with a SOMe and the by-product with a  $\text{SO}_2\text{Me}$ -group.

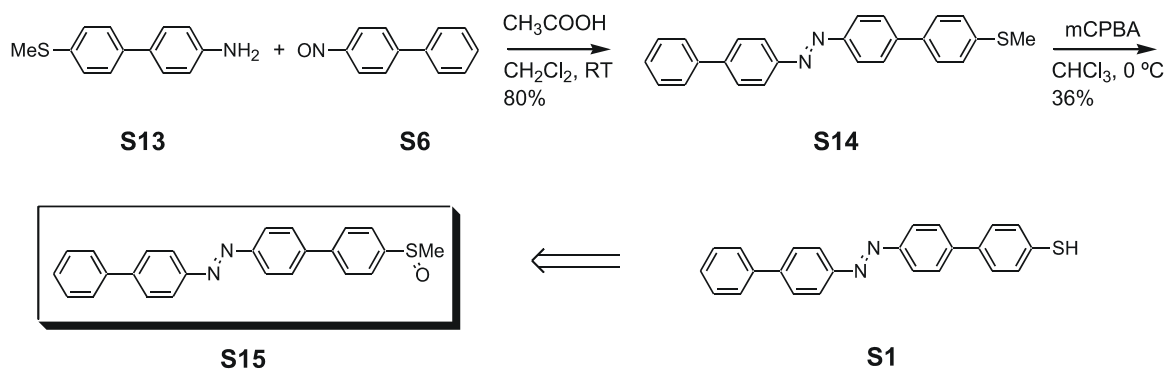


**Figure 4–82:** Second synthetic route to the target compound **S1**.

Due to the difficulties encountered in the oxidation step from the SMe- to the SOMe-group on the already formed azo-compound, the synthetic strategy was changed and the oxidation was done at an earlier stage, before the rather insoluble azo-dye had been formed. Reaction of **S11** with 1.3 equivalents of *m*CPBA in  $\text{CH}_2\text{Cl}_2$  at 0 °C gave the corresponding sulphoxide **S16** as a white solid after column chromatography in 89% yield (Figure 4–83). Using the same *HB* coupling procedure as above with  $[\text{Pd}_2(\text{dba})_3]^*\text{CHCl}_3$  as catalyst, BINAP as

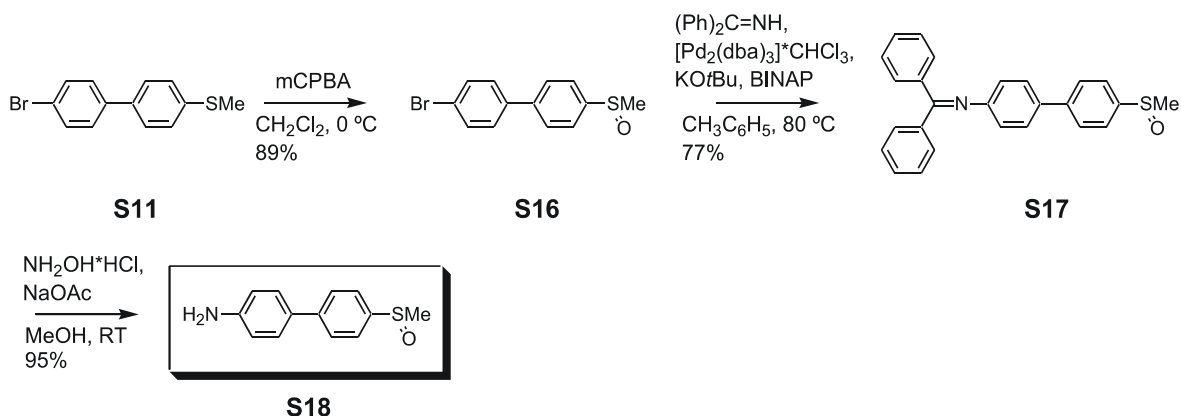


**Figure 4–83:** Synthesis of the amino-precursor **S18** bearing a SOMe-group.

phosphine ligand and KOtBu as base the bromine of **S16** was substituted affording the diphenyl ketimine **S17** as a yellow solid after re-crystallisation from methanol in 77% yield. The amine protection-group was cleaved by transamination in methanol to give the amino-precursor **S18** bearing a SOMe-group as a yellowish solid after column chromatography in a yield of 95%. Now the key-step was performed where **S18** was reacted with 4-nitro-biphenyl (**S6**) under *Mills* conditions in glacial acetic acid/CH<sub>2</sub>Cl<sub>2</sub> 2/1 (v/v) at 65 °C for 67 h (Figure 4–84). Re-crystallisation from toluene afforded the desired azo-dye **S15** as a red-brown solid in a yield of 83%.

According to a literature procedure for the conversion of a SOMe-group to a free thiol, **S15** was dissolved in dichloromethane and treated with ten equivalents of trifluoroacetic anhydride (TFAA) at room temperature for 2 h.<sup>[215]</sup> Subsequent hydrolysis with triethylamine in refluxing methanol afforded the target compound **S1** as an orange solid in a yield of less than 10% after re-crystallisation from toluene. Probably, the low solubility of the compounds **S15** and **S1** in the used solvents is one of the reasons for this rather low yield. In the following attempts the synthetic procedure was optimised to obtain higher yields. Toluene turned out to

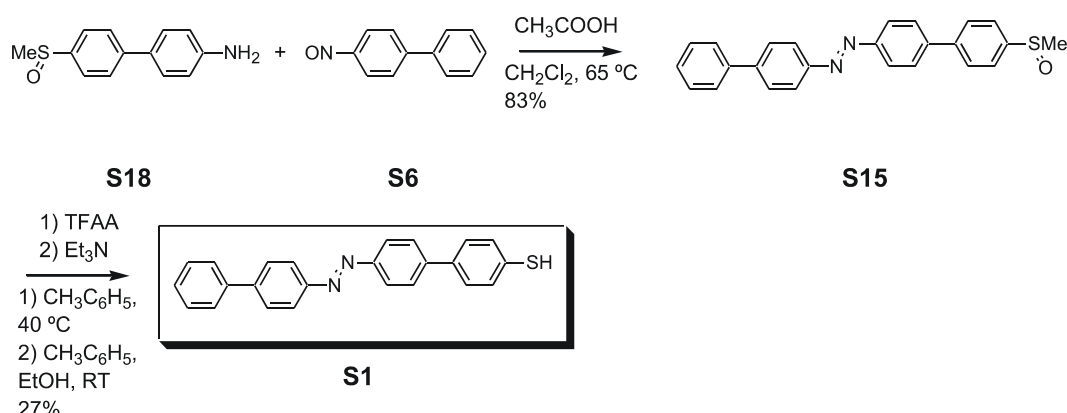


**Figure 4–84:** Third synthetic route to the target compound **S1**.

be the best solvent for the sulfoxide **S15** and was used in all further reactions.

In the optimised protocol **S15** was treated with 11.6 equivalents of TFAA in dry toluene at 40 °C for 2.5 h giving a dark–red intermediate after *Pummerer* rearrangement. This α–acetoxy sulphide was hydrolysed using triethylamine in toluene/ethanol ~3/1 (v/v) at room temperature to afford the crude target compound **S1**. Long reaction times (> 3 days) were required for this step, because due to the low solubility of the azo–compounds large amounts of solvent resulting in diluted solutions were needed. Besides, it was essential to use dry toluene in the first step, because due to the mechanism of the *Pummerer* rearrangement traces of water can probably yield in the formation of a by–product bearing a thiomethyl–group.<sup>[196]</sup> It turned out that the separation of this by–product from the desired compound by column chromatography is troublesome due to the low solubility of these compounds. Re–crystallisation does not differ between the target compound bearing a free thiol and the by–product having a thiomethyl–group. After the hydrolytic step with triethylamine, the crude product was purified by filtration over a small column with silica gel and subsequent re–crystallisation from toluene/ethanol 3/1 (v/v) affording **S1** as an orange solid in a yield of 27% (Figure 4–84). The moderate yield of this reaction can probably be attributed to the low solubility of the compound and the ease of oxidation of free thiols in the presence of oxygen giving disulphides. Disulphides of **S1** are essentially insoluble due to the presence of four (almost) planar biphenyls in such a compound.

Hence, a third strategy that gives acetyl–protected thiols, that is target compound **S2**, was developed. Acetyl–protected thiols can be obtained from *tert*–butyl–protected thiols by two different methods. Hence, this alkyl–protection groups was used in this strategy. Reaction of sodium 2–methyl–2–propanethiolate with **S10** in DMI at 160 °C afforded the biphenyl **S19** as a white solid in a yield of 43% after column chromatography (Figure 4–85). The same *HB* coupling in dry toluene at 80 °C as described above afforded the diphenyl ketimine **S20** as a yellow solid after re–crystallisation from methanol in 71% yield. Using the same transamination protocol as above the amino–compound **S21** was obtained as a white solid in a yield of 97% after column chromatography. Now the *Mills* reaction was performed using the amino–precursor **S21** bearing a *tert*–butylsulfanyl group and 1.1 equivalent of the nitroso–precursor **S6** in glacial acetic acid/CH<sub>2</sub>Cl<sub>2</sub> 3/1 (v/v) at 65 °C. The azo–compound **S22** was obtained as a red–solid in a yield of 84% after re–crystallisation from toluene. Conversion of the *tert*–butyl–group of **S22** to the acetyl–group using BBr<sub>3</sub><sup>[223]</sup> in CH<sub>2</sub>Cl<sub>2</sub>/toluene 2/1 (v/v) at 0 °C apparently destroyed the azo–group of **S22** resulting in a colourless solution. Possibly, the *Lewis*–acid BBr<sub>3</sub> reacts with the electron–rich azo–group to form a complex instead of

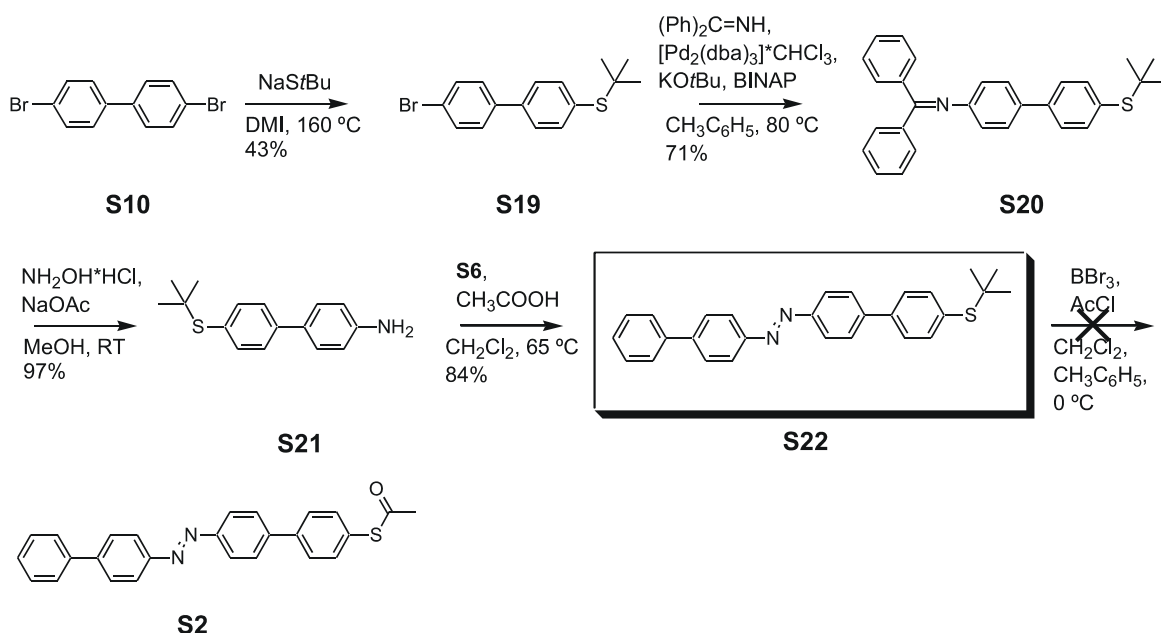


**Figure 4–85:** Synthetic route to obtain the target compound **S2**.

cleaving the thioether. Hence, a second protocol for this conversion, which has been developed mainly by A. Blaszczyk, was followed.<sup>[226]</sup> **S22** was dissolved in a mixture of  $\text{CH}_2\text{Cl}_2$ /acetyl chloride 3/2 (v/v) and bromine dissolved in acetic acid/acetyl chloride 1/1 (v/v) was added dropwise at room temperature (Figure 4–86). No target compound **S2** could be isolated after column chromatography using this procedure either. This protocol requires high concentrations of acetyl chloride to protect the formed thiol *in situ* providing the acetyl-protected thiol. If the level of acetyl chloride is too low, large amounts of disulphides are commonly obtained. In the present reaction relatively large amounts of dichloromethane had to be used to dissolve the azo-compound **S22** resulting in comparably low levels of acetyl chloride in the reaction mixture. Hence, probably considerable amounts of the disulphide of **S1**, which is essentially insoluble, have been obtained. Thus, the failure of this reaction can probably be attributed to the low solubility of the azo-compound **S22** in the used solvents.

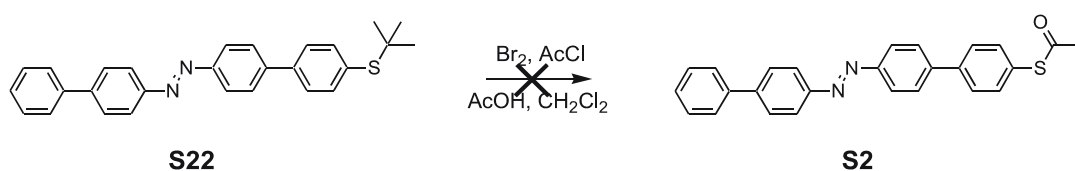


**Figure 4–86:** Conversion of the tert.-butylsulfanly-group to the acetyl sulfanly-group to obtain target compound **S2**.

### 4.3.3 Characterisation and Structural Analysis

New compounds were characterised by  $^1\text{H}$ - and  $^{13}\text{C}$ -NMR, elemental analysis and EI-MS and MALDI-TOF-MS, respectively. To obtain further information about the molecular structure of the synthesised azo-compounds it was attempted to obtain single crystals that are suitable for x-ray analysis. The arrangement of the two biphenyl subunits was of particular interest in these investigations. However, it turned out that due to the sensitivity of the target compound **S1** to oxygen, slow crystallisation of this compound was troublesome. Besides, the solubility of this compound was rather low. Hence, it was decided to use the azo-compounds **S14**, **S15** and **S22** as model compounds for the target structure. These compounds differ only in the protection group on sulphur compared to the target compound **S1** bearing a free thiol. **S14** bears a methyl-group, **S15** has a methyl-substituted sulphoxide-group and **S22** bears a *tert*-butyl-group. Since the solid state structure of these compounds is presumably governed by  $\pi$ - $\pi$ -interactions between the biphenyl subunits, these compounds probably show a comparable solid state arrangement like the target compound. Hence, they can be regarded as model compounds. These compounds had to be crystallised from hot solutions for two reasons. At room temperature in daylight azo-compound usually exist as a mixture of *E*- and *Z*-isomer. However, at elevated temperatures only the thermally more stable *E*-form is found. Hence, the crystallisation from hot solution is probably easier due to the presence of only one isomer. Besides, these compounds have a rather low solubility at room temperature resulting in rather diluted solutions. Higher concentrations facilitate crystallisation. At present only single crystals of compound **S15** could be obtained that were suitable for x-ray analysis.

This compound was crystallised from a hot solution of toluene (about 100 °C) by slow cooling of the solution. For this purpose a dewar filled with boiling water was used. **S15** crystallises azcentric in the orthorhombic space group *Pna* 2<sub>1</sub> with four asymmetric units in the unit cell (Figure 4–87). Since the empirical formula of the asymmetric unit was determined to C<sub>25</sub>H<sub>20</sub>N<sub>2</sub>OS, that is the molecular formula, there are four molecules per unit cell. The azcentric arrangement has been taken into account when solving the structure (see flack-parameter).<sup>[309]</sup> Both biphenyl subunits are essentially planar, in the biphenyl subunit bearing the sulphur-group a torsion angle of 2.2(3) $^\circ$  and in the other biphenyl an angle of 2.5(3) $^\circ$  was determined between the two phenyl-rings. The bond length between the two phenyl rings is 150.3(3) pm (C(5)–C(8)) and 151.0(3) pm (C(17)–C(20)), respectively, which is slightly longer than the length of the C(sp<sup>2</sup>)–C(sp<sup>2</sup>) bond in unsubstituted biphenyls (148 pm).<sup>[91]</sup> Due to the planer N=N-group both biphenyl subunits reside in the same plane. The carbon sulphur bond (S(1)–

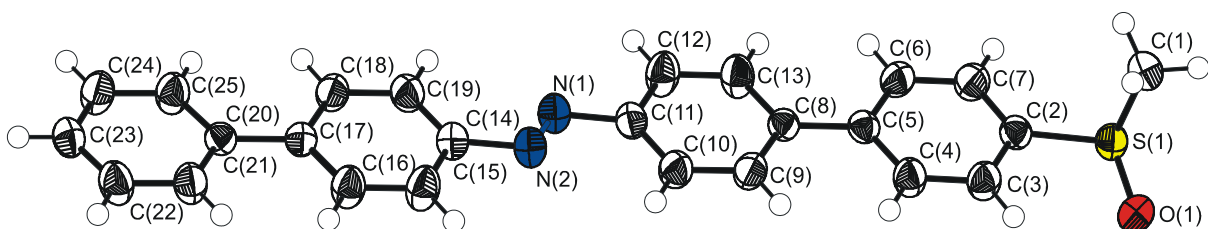


**Figure 4–87:** Molecular structure of compound **S15** bearing a SOMe-group. Selected bond lengths/pm and bond angles/ $^{\circ}$ : S(1)–C(1) 180.9(3), S(1)–C(2) 181.6(3), N(1)–N(2) 125.8(3), N(1)–C(11) 144.7(3), N(2)–C(14) 144.9(3), C(5)–C(8) 150.3(3), C(17)–C(20) 151.0(3); C(13)–C(8)–C(5) 121.7(2), C(4)–C(5)–C(8) 121.5(2), C(21)–C(20)–C(17) 121.3(2), C(25)–C(20)–C(17) 122.0(2).

C(2) is 181.6(3) pm, which is closer to the average bond length of a C(sp<sup>3</sup>)–S bond than to a C(sp<sup>2</sup>)–S bond.<sup>[91]</sup> With 180.9(3) pm the C(sp<sup>3</sup>)–S bond (C(1)–S(1)) is shortened compared to the average C(sp<sup>3</sup>)–S bond length of 182 pm.

Apart from the methyl–group of the SOMe–group compound **S15** shows an almost completely coplanar arrangement. Apparently, almost no steric hindrance of the hydrogen in position 2 and 2' of the biphenyl rings is present in this structure allowing such a coplanar arrangement. This plane structure gives rise to  $\pi$ – $\pi$ –stacking interactions between two different molecules in the solid state. As the compound comprises two biphenyl subunits such  $\pi$ – $\pi$ –stacking interactions can result in a rather low solubility of the compound, as noticed during the synthesis.

Target compound **S1** has been designed to study light–induced switching due to the *E*– to *Z*–isomerisation of the azo–functionality. In the group of *M. Rampi* at the Università di Ferrara an advanced set–up of the mercury–drop electrode described above will be used to investigate this switching behaviour in the solid state. To gain a first insight into the characteristics of the *E*–*Z*–isomerisation of the target compound experiments in solution and on gold surfaces were of particular interest. In principle, two different methods to study this behaviour exist, that is UV/Vis spectroscopy and NMR–spectroscopy<sup>[271]</sup> (see also chapter 3.3). In the NMR spectrum the *E*– and the *Z*–isomer can be distinguished, because the two isomers have a different spatial arrangement. Therefore, the two substituents on the azo–functionality are in different magnetic environments in the two isomers resulting in different chemical–shifts of the *E*– and the *Z*–isomer. In the UV/Vis spectrum the *E*–isomer usually shows an intense  $\pi$ – $\pi^*$ –transition and a weaker (forbidden) n– $\pi^*$ –band, whereas in *Z*–isomer the n– $\pi^*$ –transition is allowed showing usually higher intensity. The exact position of these bands depends on the substitution on the azo–compound, but usually the differences in the n– $\pi^*$ –transition of the *E*– and the *Z*–form can be used to distinguish these two isomers. The UV/Vis technique has a

higher sensitivity than the NMR technique. However, it is often limited by poor resolution resulting in overlapping of spectra of the two isomers. In NMR spectroscopy, in contrast, the assignment of the spectra of the *E* and *Z* compound is usually straightforward. Therefore, first preliminary investigations were performed using  $^1\text{H}$ -NMR spectroscopy.

These experiments have been done with two different intermediates from the synthesis, namely with the SMe-substituted azo-compound **S14** and with the SOMe-substituted azo-dye **S15**. These compounds can probably be used as model compounds for the target compound **S1** to investigate the light-induced *E*-*Z*-isomerisation, because they have the same molecular structure, but only different protection-groups on sulphur. While these different groups might slightly change the absorption maxima in these compounds as opposed to the target compound, they probably do not have a pronounced effect on the isomerisation behaviour. In particular, any steric or electronic effects are probably negligible, since the (protected) thiol group is not close to the centre where isomerisation occurs. The study has not been performed with the target molecule **S1**, because it has a very low solubility hampering the interpretation of the NMR-spectra and it oxidises quite readily to the corresponding (completely insoluble) disulphide in the presence of traces of oxygen.

Figure 4–88 shows the  $^1\text{H}$ -NMR spectrum of **S14** as measured after re-crystallisation of the compound from toluene. A few peaks are of particular interest in this spectrum. In the aliphatic region two single peaks are present, one intense peak at 2.54 ppm and a rather small one at 2.51 ppm. The peak at 2.54 ppm can be assigned to the methyl-group on the sulphur in position 4' of the aromatic ring. In the aromatic region an intense doublet around 8.00 ppm

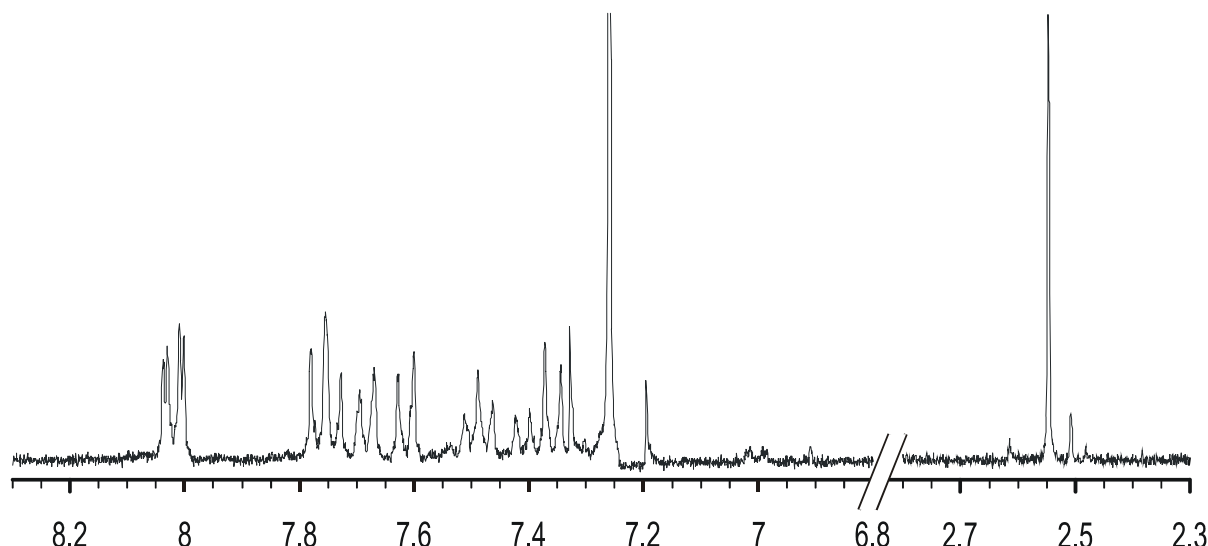
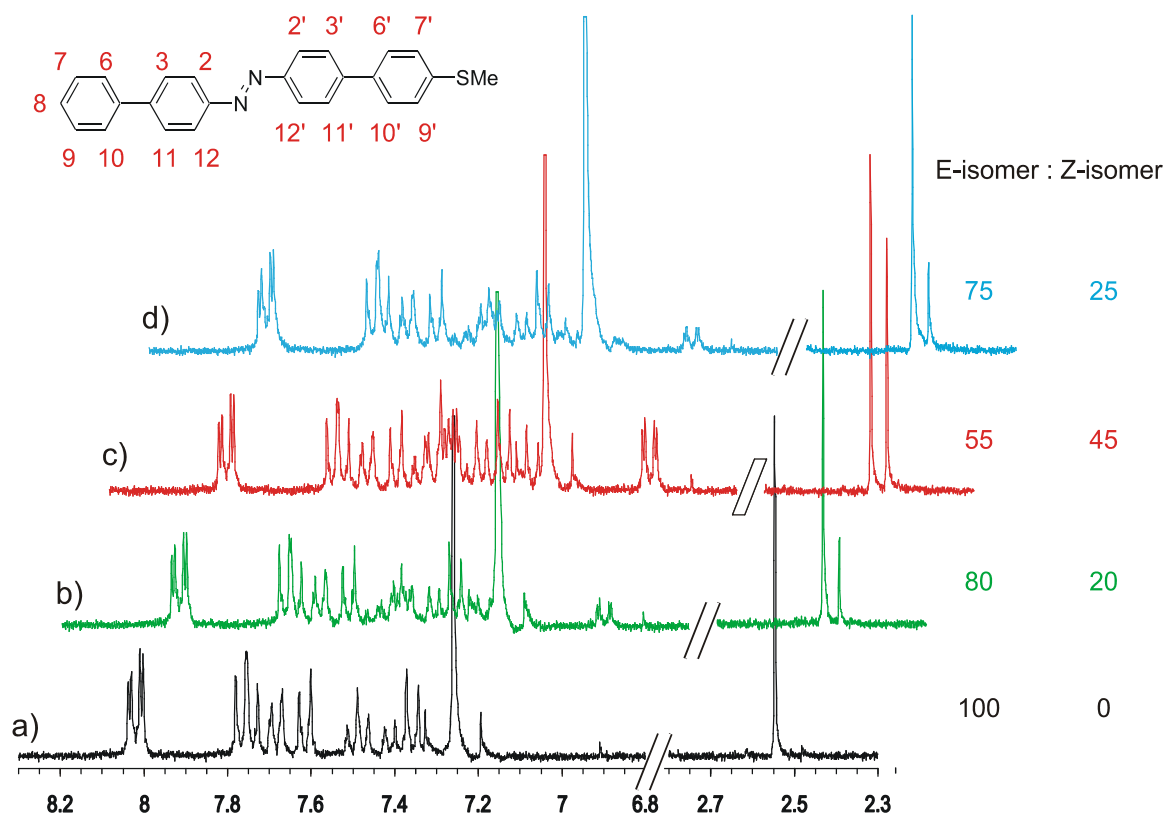


Figure 4–88:  $^1\text{H}$ -NMR spectrum of the azo-compound **S14** as measured after re-crystallisation from hot toluene.

and a smaller one of the same structure between 6.99 – 7.01 ppm have been found. A comparison with the spectrum of azo–benzene known from literature suggests that the small doublet in the aromatic region probably arises from the Z–isomer of **S14**.<sup>[271]</sup> If this is true, the small peak in the aliphatic region probably results from the Z–isomer as well, especially because a mixture of an E– and Z–isomer of dimethylamino–substituted azobenzene shows a similar pattern in the aliphatic region.<sup>[271]</sup> To prove this assumption, the sample tube was kept at 48 °C for 18 h in the dark, because the Z–isomer of azo–compounds can be converted to the E–isomer at elevated temperatures, that is the E–isomer is the thermally more stable one.

Figure 4–89a depicts the spectrum measured after heating the sample. Here, the peaks can be assigned as follows: double doublet around 8.00 ppm of intensity four arises from the protons in 2, 12 and 2', 12'–position, the triplet of intensity four at 7.8 ppm corresponds to protons at 3, 11 and 3', 11', the doublet at 7.7 ppm of intensity two comes from the protons at position 6 and 10, the doublet at 7.6 ppm of intensity two corresponds to positions 6' and 10', the triplet at 7.5 ppm of intensity two arises from the protons at position 7 and 9. The doublet of intensity two at 7.3 ppm that corresponds to the protons at 7' and 9' position overlaps slightly



**Figure 4–89:**  $^1\text{H}$ –NMR spectra of **S14** measured a) after keeping the sample tube at 48°C for 18 h (black); b) after keeping the same sample tube at daylight for 12 h (green); c) after irradiating the sample with light of the wavelength 366 nm for 16 h (red) and d) after keeping the same sample tube again at daylight for 12 h (blue). The spectra have been shifted by 0.1 ppm for clarity.

with the triplet of intensity one at 7.4 ppm coming from the proton at position 8. In particular, no peaks at 2.51 ppm and at 6.99 – 7.01 ppm are visible in this NMR-spectrum. Hence, this NMR proves that a clean compound has been obtained (100 % *E*-isomer) and that the other peaks that vanished in this spectrum are most probably due to the thermally unstable *Z*-isomer. To confirm this further, the sample tube was kept at room temperature in daylight for 12 h. Now a different spectrum can be recorded again (Figure 4–89b). Here, the peaks supposed to arise from the *Z*-isomer are present again. This corroborates that the first spectrum measured after re-crystallisation probably arose from a mixture of the *E*- and *Z*-form of **S14**. Assuming that the peak at 2.51 ppm arises from the *Z*-isomer the composition of the sample can be calculated. The sample contains about 80% *E*- and 20% *Z*-isomer as measured by the peak integrals of the SMe-group. To further prove the *E*- to *Z*-isomerisation the sample tube was irradiated with light of the wavelength of 366 nm for 16 h giving rise to spectrum c) (Figure 4–89). The wavelength of 366 nm usually induces the isomerisation to the *Z*-form, as known from literature.<sup>[260],[115]</sup> Here, the *E*- to *Z*-ratio was determined to 55:45 by using the peak integrals. Standing in daylight for about 12 h again results in a composition of *E*- to *Z*-isomer of 75% to 25% (Figure 4–89 d).

These preliminary experiments allow for the following conclusions to be drawn: 1) The small peaks are not due to impurities present, but arise from the nature of the compound; 2) It is possible to switch in solution from the *E*- to the *Z*-isomer by irradiating with light of the wavelength of 366 nm and, in principle, to switch back using daylight. However, a photostationary state seems to be reached at room temperature in daylight containing between 20 to 25% *Z*-isomer. In these first experiments, it has not been attempted to obtain pure *Z*-isomer by irradiating with light of a defined wavelength; 3) Heating the sample to 48 °C for prolonged time afforded the thermally more stable, pure *E*-configuration of **S14**.

A similar series of experiments has been conducted with the azo-compound **S15** having a SOMe- instead of the SMe-endgroup. Essentially, the same results have been obtained confirming again that it is possible to switch in solution between the two isomers by irradiating with light (Figure 4–90). In this case, the equilibrium state comprises 84% *E*- and 16% *Z*-form.

While these preliminary studies using NMR spectroscopy, were useful as a proof-of-principle of the *E*- to *Z*-isomerisation of the obtained azo-compounds, further experiments were required to characterise the isomerisation behaviour in more detail. In particular, it is difficult to follow the development of the spectra with time, because for this purpose an additional light source needs to be coupled into the NMR machine, which is not a standard

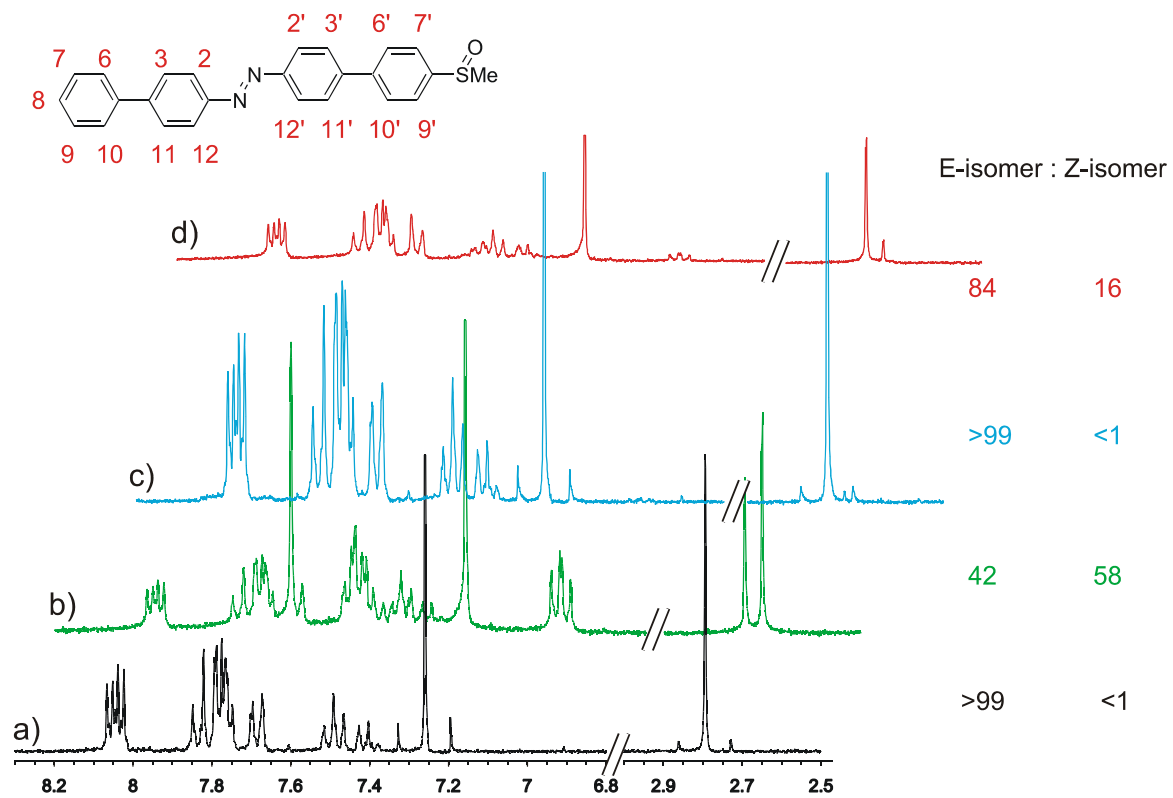


**Figure 4–90:** Change of the  $^1\text{H}$ -NMR spectra of compound S15. a) after re-crystallisation from hot toluene (black); b) irradiating with light of the wavelength of 366 nm overnight (green); c) after keeping the sample tube at 45°C for 16 h (blue) and d) after keeping the sample at daylight for several days (red). The spectra have been shifted by 0.1 ppm for clarity.

experimental procedure. Hence, almost no kinetic data about the *E*– to *Z*–isomerisation can be obtained using  $^1\text{H}$ –NMR spectroscopy. In comparison, UV/Vis spectroscopy allows to record absorption spectra and to induce the isomerisation by light of a certain wavelength using the same experimental set–up. Besides, the UV/Vis spectra allow to determine the exact wavelengths required for the *E*–*Z*–isomerisation and *vice versa*, since these wavelengths are equal to the recorded absorption maxima of the compounds. As already mentioned above, the *E*– and the *Z*–form of azo–compounds can be distinguished by their UV/Vis spectra due to different intensities of the  $\text{n}–\pi^*$ –transition and the different positions of the  $\pi–\pi^*$ –band. The following UV/Vis investigations were done by *B. Long* in the group of *M. Rampi* at the Università di Ferrara.

The experiments were done with about  $10^{-5}$  M solutions of **S1** in chloroform. The spectrum of **S1** at thermal equilibrium in the dark, i.e. the *E*-isomer, is drawn in dark red colour (Figure 4–91). The intense absorption at  $\lambda = 375$  nm can be attributed to the  $\pi-\pi^*$ -band of the *E*-isomer, in addition a weak absorption at about  $\lambda = 450$  nm is visible, that can probably be assigned to the forbidden  $n-\pi^*$ -transition of the *E*-isomer of **S1**. Published results of a similar

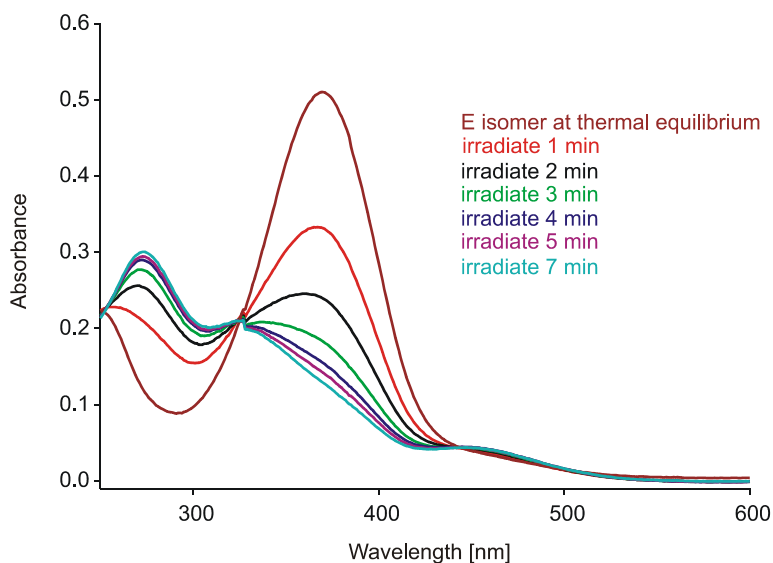


**Figure 4–91:** Development of the UV/Vis spectrum of a  $10^{-5}$  M solution of **S1** in chloroform over time when irradiating with light of the wavelength 369 nm.

structure suggest that this is 100 % *E*–isomer.<sup>[45]</sup> The cyan line is the photostationary state of the *Z*–isomer after irradiation at 369 nm for 7 minutes. Here, the absorption at  $\lambda = 265$  nm can be attributed to the  $\pi-\pi^*$ –transition and the band at  $\lambda = 450$  nm to the  $n-\pi^*$ – transition of the *Z*–isomer of **S1**. The other spectra show the development over time as cited when irradiating the sample at 369 nm. In the spectra bleaching of the  $\pi-\pi^*$  band of the *E*–isomer and an increase of the  $\pi-\pi^*$  absorption at 265 nm and of the  $n-\pi^*$  band at 450 nm of the *Z*–isomer is visible. The photostationary state seems to be reached after about 7 min. When the obtained *Z*–form is irradiated with light of the wavelength 265 nm for 10 min the photostationary state of the *E*–isomer of **S1** is reached again. If the structure is allowed to thermally equilibrate, it will take more than five hours to reach the thermally equilibrated system. These UV/Vis experiments suggest that target compound **S1** can be switched reversibly between its two isomers in solution. Besides, these investigations show that the isomerisation occurs within minutes when irradiating with light of a suitable wavelength.

Target compound **S1** has been designed to observe isomerisation in a solid state device comprising a self–assembled monolayer of this compound. While the investigations presented up to now show that isomerisation and thereby switching is possible in solution, possibly these results cannot be transferred without alteration to a monolayer of **S1** absorbed on gold. In particular, inhibition of the isomerisation of azo–compounds in well–ordered self–assembled monolayers due to the close–packing has already been reported.<sup>[353]</sup> Therefore, it was interesting to study the conversion from the *E*– to the *Z*–form of the target compound **S1** absorbed on a gold surface as well. In addition, it was sought to study the isomerisation of **S1**

absorbed on gold nano-particles. First preliminary results indicate, that switching is not possible in SAMs on thin gold films that consist only of the target compound **S1**.<sup>[45]</sup> The *E*– to *Z*–isomerisation is associated with a lateral expansion of the *Z*–isomer compared to the *E*–isomer. Hence, possibly close-packed SAMs of the azo–compound cannot be isomerised, because there is not enough space available for this lateral expansion. There are also first indications that mixed SAMs of target compound **S1** and octanethiol absorbed on gold nanoparticles show reversible switching induced by light of different wavelengths. However, further experiments to study the isomerisation on gold surfaces in more detail need to be done. This work is currently conducted by *B. Long* at the Università di Ferrara.

At present, no current–voltage characteristics of **S1** could be recorded using the advanced set-up of the mercury drop electrode described above. Thus, no switching in such a device was observed up to now. However, further investigations are currently done by *C. Grave* at the Università di Ferrara.

The available results allow for the following conclusions: 1) *E* to *Z*–isomerisation of **S1** is possible in solution as shown by UV/Vis experiments; 2) Isomerisation of similar compounds having a protected sulphur–group instead of a free thiol, namely **S14** and **S15** using light and heat could be shown by <sup>1</sup>H–NMR studies. 3) First preliminary results suggest that SAMs of **S1** formed on thin gold films cannot be isomerised, but mixed monolayers with octanethiol on gold nanoparticle might show reversible switching.



## 5 Concluding Remarks

In the present work different molecular structures have been designed and synthesised to achieve distinct electronic properties. Physical characterisations of these compounds have been done in collaboration with experimental physics groups to determine correlations between the structure of the organic compound and its electronic transport behaviour. In particular, the influence of the degree of  $\pi$ -conjugation and the coupling to the electrodes, that is the position of the anchor-groups, has been addressed. Furthermore, different functionalities of electronic circuits including rectification and, in principle switching have been found for different molecular structures.

The presented results indicate that electronic properties of organic molecules can be tailored by carefully planned organic synthesis stressing the importance of organic chemistry for the successful development of the field of molecular electronics. Furthermore, insights gained during this work can contribute to the understanding of electron transport through molecular structures. However, these studies are still at the basic research level and many challenges have to be met, until molecule-based electronic circuits can become reality. In particular, the accurate prediction of certain electronic properties requires a much deeper understanding of the effects of the molecular structure and the electrodes and the interaction between these on the electron transport behaviour of such molecule-based junctions.

The potential of the concept of molecular electronics for long-term applications lies in the small, ultimate size of molecules, the low costs of fabrication and the plethora of functional molecular building blocks accessible by organic synthesis. However, at present the future applicability of such devices still remains speculation and further investigations are required to allow to verify (or dismiss) the concept.



## 6 Experimental Part

### 6.1 General remarks

All chemicals were used as received from the supplier, solvents were p.a. quality and used without further purification. If necessary the solvents were dried by standard literature procedures, THF, diethylether and toluene with Na/benzophenone, CH<sub>2</sub>Cl<sub>2</sub> and all amines over CaH, ethanol using magnesium turnings.<sup>[239]</sup> If not mentioned otherwise all reactions were carried out under an atmosphere of nitrogen or argon. TLC was performed on Merck silica gel 60 F<sub>254</sub> plates and column chromatography using Merck silica gel 60 (0.040–0.063 mm). The R<sub>f</sub> values are quoted for the solvents used for column chromatography.

### 6.2 Analytics

#### NMR-spectroscopy

<sup>1</sup>H NMR and <sup>13</sup>C NMR spectra were recorded on a Bruker Ultra Shield 300 MHz in CDCl<sub>3</sub> as internal standard at room temperature if not stated otherwise at the Institute for Nanotechnology, Forschungszentrum Karlsruhe. If temperatures other than room temperature were used, the reading of the thermocouple of the instrument is quoted. The chemical shift δ is cited in ppm. The following abbreviations were used in the assignment of spin multiplicity: s – single peak, d – doublet, t – triplet, m – multiplet, dd – doublet of doublet etc., br – broad. During the dynamic NMR measurements a rough estimate of the temperature was provided by the thermocouple of the instrument, but the actual temperature was determined using the methanol and the ethylene glycol chemical shift thermometer, respectively.<sup>[278]</sup> Between –45 to 20°C (thermocouple reading) 4% MeOH in [D<sub>4</sub>]–MeOH was used, at temperatures higher than 20°C (thermocouple reading) 80% ethylene glycol in [D<sub>6</sub>]–DMSO was employed. The calibration tube was inserted into the machine after the measurement of the actual sample at the respective temperature had been performed.

**Mass spectrometry**

MALDI–TOF spectra were measured on a PerSeptive Biosystems Voyager –DE PRO time-of-flight mass spectrometer at the Institute for Nanotechnology, Forschungszentrum Karlsruhe, EI–MS on a LKB–9000S at Service de Spectrometrie de Masse, Strasbourg. If not mentioned otherwise 1,8,9–anthracenetriol was used as matrix for the MALDI–TOF–measurements.

**Melting points**

Melting points were measured with a Büchi Melting Point B–540 apparatus and are uncorrected.

**Elemental analysis (EA)**

Elemental analyses were performed using the ThermoQuest FlashEA 1112 N/Protein Analyzer at the Institute for Nanotechnology. I am very grateful to Matthias Fischer for these measurements.

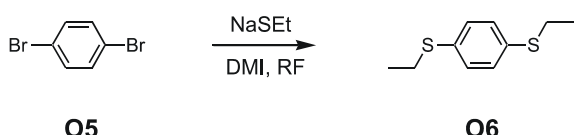
**UV/Vis–spectroscopy**

UV/Vis spectra were recorded on a Varian Cary 500Scan UV–Vis–NIR–spectrophotometer using 1 cm cuvettes at the Institute for Nanotechnology. The concentration of the sample solution and the solvents used are mentioned together with the measurement. The wavelength is cited in nm, the extinction coefficient in  $\text{lmol}^{-1}\text{cm}^{-1}$ .

## 6.3 Synthetic procedures

### 6.3.1 Oligophenylenes

#### 1,4-Bis-ethylsulfanyl-benzene O6



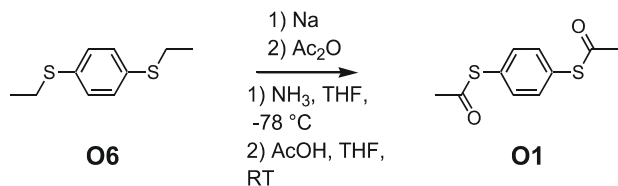
Sodium ethanethiolate (20.00 g, 0.24 mol) and 1,4-dibromobenzene **O5** (23.70 g, 0.10 mol) were dissolved in dry DMI (180 ml) and the mixture heated to reflux for 18 h. The reaction mixture was poured on ice/water and extracted with toluene. The combined organic extracts were dried over  $\text{MgSO}_4$ , and the solvent removed by rotary evaporation. Column chromatography (silica gel, hexane/toluene, 4/1) provided **O6** as a white solid (8.83 g, 44.52 mmol; 45%). M.p.: 46.5 – 47.5 °C (lit.:<sup>[305]</sup> 46 – 47°C).

$R_f = 0.33$ .

$^1\text{H}$ -NMR (300 MHz,  $\text{CDCl}_3$ ):  $\delta = 1.30$  (t,  $^3J(\text{H},\text{H}) = 8$  Hz, 6 H), 2.92 (q,  $^3J(\text{H},\text{H}) = 8$  Hz, 4 H), 7.25 (s, 6 H).

$^{13}\text{C}$ -NMR (75 MHz,  $\text{CDCl}_3$ ):  $\delta = 14.40$  ( $\text{CH}_3$ ), 28.00 ( $\text{CH}_3\text{CO}$ ), 129.81 (C2, C3), 134.13 (C1, C4).

#### 1,4-Bis-acetylthio-benzene O1



In an oven-dried two-necked flask equipped with  $\text{NH}_3$ -condenser sodium (0.50 g, 21.70 mmol) was dissolved in liquid ammonia at -78 °C. A solution of 1,4-bis-ethylsulfanyl-benzene **O6** (1.00 g, 5.04 mmol) in dry THF (2 ml) was added. After refluxing for 30 min the reaction was quenched with ammonium chloride (3.00 g, 56.10 mmol) and warmed to room

temperature. N<sub>2</sub>-saturated acetic acid (20 ml) and acetic anhydride (4 ml) was added and the resulting suspension stirred at room temperature for 30 min. The reaction mixture was poured on ice/water, extracted with toluene, the combined organic phases washed with saturated NaCl-solution and dried over MgSO<sub>4</sub>. Evaporation of the solvents in vacuo and purification by column chromatography (silica gel, toluene) afforded **O1** as a white solid (0.62 g, 2.74 mmol; 55 %). M.p.: 130 – 131 °C (Lit.<sup>[304]</sup>: 126 °C).

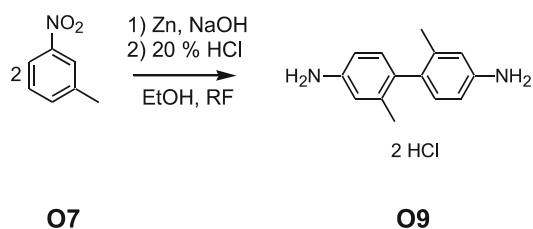
R<sub>f</sub> = 0.09.

<sup>1</sup>H-NMR (300 MHz, CDCl<sub>3</sub>): δ = 2.43 (s, 6 H), 7.45 (s, 4 H)

<sup>13</sup>C-NMR (75 MHz, CDCl<sub>3</sub>): δ = 30.30 (CH<sub>3</sub>), 129.60 (C1, C4), 134.74 (C2, C3), 193.07 (CO).

UV/Vis (1 × 10<sup>-5</sup> n-hexane): λ<sub>max</sub> (ε) = 200.0 (36800), 262.0 (18100).

**m-Tolidine dihydrochloride O9** following the procedure by W. Wenner<sup>[306]</sup>

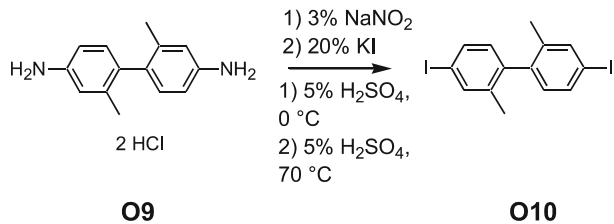


3-Nitrotoluene (80.00 g, 0.58 mol) was heated to reflux in ethanol (80 ml). The heating bath was removed and zinc dust (60.00 g, 0.92 mol) was added in small portions. After completion a solution of sodium hydroxide (12.00 g, 0.30 mol) in 68% ethanol (60 ml) was cautiously dropped in. Then zinc dust (60.00 g, 0.92 mol) was added again in portions and the resulting mixture was refluxed for 2 h. The solution was acidified with about 960 ml of 20% hydrochloric acid and heated to reflux for another hour. After the reaction mixture had cooled to room temperature stirring was continued overnight. The formed solid was collected, re-dissolved in hot water (1000 ml) and filtered. **O9** was precipitated as its hydrochloride using conc. hydrochloric acid (250 ml). After filtration and drying a grey solid was obtained that was sufficiently pure for the next step (46.14 g, 0.16 mol; 55%).

<sup>1</sup>H-NMR (300 MHz, [D<sub>6</sub>]DMSO): δ = 2.05 (s, 6 H), 7.22 (d, <sup>3</sup>J(H,H) = 8 Hz, 2 H), 7.30 (dd, <sup>3</sup>J(H,H) = 8 Hz, <sup>4</sup>J(H,H) = 2 Hz, 2 H), 7.33 (d, <sup>4</sup>J(H,H) = 2 Hz, 2 H).

<sup>13</sup>C-NMR (75 MHz, [D<sub>6</sub>]DMSO): δ = 19.98 (CH<sub>3</sub>), 121.30, (C5), 125.01 (C3), 130.85 (C6), 131.52 (C1), 137.61 (C2), 140.13 (C4)

**4,4'-Diiodo-2,2'-dimethyl-biphenyl O10** following the procedure by K. Fuji et al.<sup>[307]</sup>



A 3% solution of NaNO<sub>2</sub> (7.590 g, 110.00 mmol) was dropped to a solution of **O9** (15.160 g, 50.00 mmol) dissolved in 5% sulphuric acid (1500 ml) over a period of about 90 min at 0 °C. Then a 10% solution of urea was added to decompose the excess of NaNO<sub>2</sub>. After addition of a 20% solution of potassium iodide (70.500 g, 424.67 mmol) the reaction was allowed to come to room temperature and then heated to 70 °C for 15 min. The reaction mixture was extracted with CH<sub>2</sub>Cl<sub>2</sub>, the organic layers were washed with a solution of sodium thiosulphate and dried over MgSO<sub>4</sub>. After rotary evaporation the product was purified by column chromatography (silica gel, hexane/toluene 15/1) to give a white solid (14.53 g, 33.47 mmol; 67%). M.p. 96.5 – 98.0 °C (Lit.<sup>[307]</sup>: 62.0 – 63.0 °C).

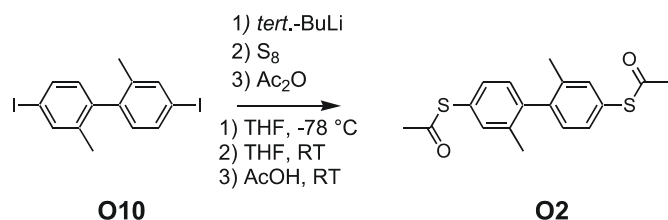
$$R_f = 0.47.$$

<sup>1</sup>H-NMR (300 MHz, CDCl<sub>3</sub>): δ = 1.99 (s, 6 H), 6.79 (d, <sup>3</sup>J(H,H) = 8 Hz, 2 H), 7.55 (dd, <sup>3</sup>J(H,H) = 8 Hz, <sup>4</sup>J(H,H) = 1 Hz, 2 H), 7.63 (d, <sup>4</sup>J(H, H) = 1 Hz, 2 H).

<sup>13</sup>C-NMR (75 MHz, CDCl<sub>3</sub>): δ = 19.51 (CH<sub>3</sub>), 93.16 (C4), 130.89 (C6), 134.83 (C5), 138.25 (C1), 138.77 (C3), 140.00 (C2).

MS (EI):  $m/z$  (%) = 434.3 (77) [ $M^+$ ], 180.2 (36) [ $M^+ - 2 I$ ], 165.2 (100) [ $M^+ - 2 I, - CH_3$ ], 152.3 (15) [ $M^+ - 2 I, - 2 CH_3$ ], 89.3 (37), 76.3 (17).

Elemental analysis calcd. (%) for C<sub>14</sub>H<sub>12</sub>I<sub>2</sub> (434.05): C 38.74, H 2.79; found C 38.98, H 2.79.

**4,4'-Bis(acetylsulfanyl)-2,2'-dimethyl-biphenyl O2**

In a two-necked flask 4,4'-diiodo-2,2'-dimethyl-biphenyl **O10** (2.170 g, 5.00 mmol) was dissolved in dry THF (20 ml). The solution was cooled to  $-78^\circ\text{C}$  using dry ice/acetone and treated with *tert*.-butyllithium (10.670 g of a 15% solution in pentane, 25.00 mmol). After stirring for 20 min sulphur (0.321 g, 10.00 mmol) was added, the dry ice/acetone bath removed and the mixture stirred for another 90 min at room temperature. After rotary evaporation of the solvents Ar-saturated acetic acid (20 ml) and zinc dust (1.310 g, 20.00 mmol) were used to reduce any formed disulfide. After 20 min the zinc was filtered off and acetic acid anhydride (5.100 g, 50.00 mmol) added to the filtrate and stirring continued overnight. The reaction mixture was poured on ice/water, the aqueous phase extracted with toluene, the organic layers dried over  $\text{MgSO}_4$  and the solvents removed in vacuo. Column chromatography (silica gel, hexane/diethylether 7/3) afforded **O2** as a white solid (0.460 g, 1.39 mmol; 28%). M.p.: 101.0 – 102.5 °C.

$R_f = 0.36$

$^1\text{H-NMR}$  (300 MHz,  $\text{CDCl}_3$ ):  $\delta = 2.08$  (s, 6 H), 2.44 (s, 6 H), 7.16 (d,  $^3J(\text{H,H}) = 8$  Hz, 2 H), 7.30 (dd,  $^3J(\text{H,H}) = 8$  Hz,  $^4J(\text{H,H}) = 1$  Hz, 2 H), 7.34 (d,  $^4J(\text{H,H}) = 1$  Hz, 2 H).

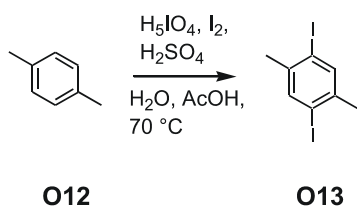
$^{13}\text{C-NMR}$  (75 MHz,  $\text{CDCl}_3$ ):  $\delta = 19.82$  ( $\text{CH}_3$ ), 30.27 ( $\text{CH}_3\text{CO}$ ), 126.79 (C5), 130.02 (C6), 131.66 (C3), 135.74 (C4), 137.01 (C1), 142.00 (C2), 194.315 ( $\text{COCH}_3$ ).

MS (EI):  $m/z$  (%) = 330.1 (21) [ $\text{M}^+$ ], 288.1 (21) [ $\text{M}^+ - \text{CH}_3\text{CO}$ ], 246.1 (100) [ $\text{M}^+ - 2 \text{CH}_3\text{CO}$ ], 179.1 (13) [ $\text{M}^+ - 2 \text{SCOCH}_3$ ], 165.1 (10) [ $\text{M}^+ - 2 \text{SCOCH}_3 - \text{CH}_3$ ].

Elemental analysis calcd. (%) for  $\text{C}_{18}\text{H}_{18}\text{O}_2\text{S}_2$  (330.47): C 65.42, H 5.49; found C 65.40, H 5.26.

UV/Vis ( $1 \times 10^{-5}$  n-hexane):  $\lambda_{\text{max}}$  ( $\varepsilon$ ) = 208.0 (66500), 251.5 (20400).

**2,5-Diiodo-*p*-xylene O13** following the procedure by K. L. Platt et al.<sup>[298]</sup>



*p*-Xylene **O12** (13.27 g, 125.00 mmol), periodic acid (11.40 g, 50.00 mmol) and iodine (25.38 g, 100.00 mmol) were added subsequently to a solution of conc. sulphuric acid (7.5 ml) and water (50 ml) in glacial acetic acid (250 ml). The resulting purple solution was stirred at 70 °C for 3 h, then cooled to 0 °C and the precipitate collected by filtration. Recrystallisation from methanol/chloroform yielded **O13** as a white solid (28.940 g, 80.85 mol; 65%). M.p.: 102.5 – 103.0 °C (Lit.<sup>[298]</sup>: 103.0 °C)

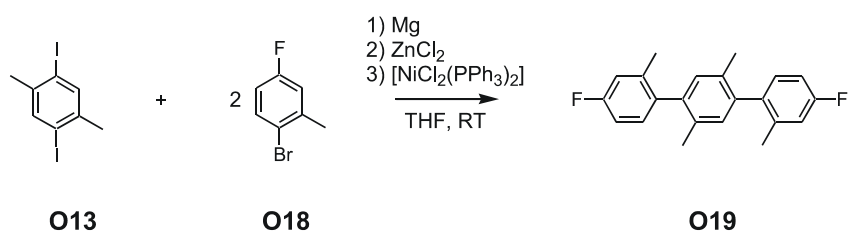
$^1\text{H}$ -NMR (300 MHz,  $\text{CDCl}_3$ ):  $\delta$  = 2.34 (s, 6 H), 7.65 (s, 2 H).

$^{13}\text{C}$ -NMR (75 MHz,  $\text{CDCl}_3$ ):  $\delta$  = 26.87 ( $\text{CH}_3$ ), 100.62 (C2, C5), 139.29 (C3, C6), 140.67 (C1, C4).

MS (EI):  $m/z$  (%) = 358 (100) [ $\text{M}^+$ ], 230.9 (39) [ $\text{M}^+ - \text{I}$ ], 104.1 (38) [ $\text{M}^+ - 2\text{I}$ ], 78.1 (17).

Elemental analysis calcd. (%) for  $\text{C}_8\text{H}_8\text{I}_2$  (357.96): C 26.84, H 2.25; found C 26.83, H 2.24.

#### 4,4''-Difluoro-2,2',5',2''-tetramethyl-[1,1';4',1'']terphenyl O19



Magnesium turnings (1.094 g, 45.00 mmol) suspended in dry THF (6 ml) were treated with a solution of 2-bromo-5-fluorotoluene **O18** (8.506 g, 45.00 mmol) in dry THF (25 ml). The resulting mixture was stirred at room temperature for 1 h. Then dry zinc chloride (6.132 g, 45.00 mmol) suspended in dry THF was added to the solution and stirring continued at room temperature for another hour.  $[\text{NiCl}_2(\text{PPh}_3)_2]$  (0.276 g, 0.42 mmol) and a solution of 2,5-diiodo-*p*-xylene **O13** (6.450 g, 18 mmol) in dry THF (48 ml) were added subsequently. After stirring the reaction mixture at room temperature for 64 h the grey suspension was poured on

ice (about 450 g) and acidified with H<sub>2</sub>O /conc. hydrochloric acid (45 ml/45 ml). The aqueous phase was extracted with CH<sub>2</sub>Cl<sub>2</sub>, the organic phases washed with water and dried over MgSO<sub>4</sub>. After rotary evaporation a yellow residue was obtained which was purified by column chromatography (silica gel, hexane/toluene 15/1) affording **O19** as a white solid (3.780 g, 11.72 mmol, 65%). M.p.: 140.0 – 142.0 °C.

R<sub>f</sub> = 0.31.

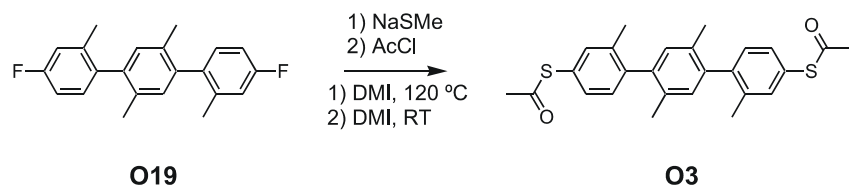
<sup>1</sup>H-NMR (300 MHz, CDCl<sub>3</sub>): δ = 2.02 (d, due to different isomers, 6 H), 2.11 (d, due to different isomers, 6 H), 6.94 (ddd, <sup>3</sup>J(H,F) = 9 Hz, <sup>3</sup>J(H,H) = 8 Hz, <sup>4</sup>J(H,H) = 2 Hz, 2 H), 6.97 (d, due to different isomers, 2H), 6.99 (dd, <sup>3</sup>J(H,F) = 9 Hz, <sup>4</sup>J(H,H) = 2 Hz, 2 H), 7.12 (dd, <sup>3</sup>J(H,H) = 8 Hz, <sup>4</sup>J(H,F) = 7 Hz, 2 H).

<sup>1</sup>H-NMR (300 MHz, CDCl<sub>3</sub>, T = 51 °C): δ = 2.03 (s, 6 H), 2.11 (d, due to different isomers, 6 H), 6.93 (ddd, <sup>3</sup>J(H,F) = 9 Hz, <sup>3</sup>J(H,H) = 8 Hz, <sup>4</sup>J(H,H) = 2 Hz), 6.97 (s, 2 H), 6.99 (dd, <sup>3</sup>J(H,F) = 9 Hz, <sup>4</sup>J(H,H) = 2 Hz, 2 H), 7.12 (dd, <sup>3</sup>J(H,H) = 8 Hz, <sup>4</sup>J(H,F) = 7 Hz, 2 H).

<sup>13</sup>C-NMR (75 MHz, CDCl<sub>3</sub>): δ = 19.29 (CH<sub>3</sub>), 19.99 (d, <sup>4</sup>J(F,C) = 2 Hz), 20.15 (d, <sup>4</sup>J(F,C) = 2 Hz, two peaks due to different isomers, CH<sub>3</sub>), 112.27, 112.34 (d, <sup>2</sup>J(F,C) = 21 Hz, due to different isomers, C5, C5''), 116.33 (d, <sup>2</sup>J(F,C) = 21 Hz, C3, C3''), 130.71, 130.80 (d, <sup>3</sup>J(F,C) = 8 Hz, due to different isomers, C6, C6''), 130.94, 130.96 (due to different isomers, C3''), 133.01, 133.13 (due to different isomers, C2''), 137.33, 137.39 (d, <sup>4</sup>J(F,C) = 3 Hz, due to different isomers, C1, C1''), 138.28, 138.36 (d, <sup>3</sup>J(F,C) = 7 Hz, due to different isomers, C2, C2''), 139.55, 139.61 (due to different isomers, C1''), 161.91 (d, <sup>1</sup>J(F,C) = 243 Hz, C4, C4''). MS (EI): m/z (%) = 322.3 (100) [M<sup>+</sup>], 307.2 (35) [M<sup>+</sup> – CH<sub>3</sub>], 292.1 (15) [M<sup>+</sup> – 2 CH<sub>3</sub>], 197.2 (12), 183.2 (10), 161.2 (11), 146.2 (12), 135.2 (12).

Elemental analysis calcd. (%) for C<sub>22</sub>H<sub>20</sub>F<sub>2</sub> (322.39): C 81.96, H 6.25; found C 82.09, H 6.27.

#### 4,4''-Bis(acetylsulfanyl)-2,2',5',2''-tetramethyl-[1,1';4',1''] terphenyl **O3**



4,4''-Difluoro-2,2',5',2''-tetramethyl-[1,1';4',1'']terphenyl **O19** (0.322 g, 1.00 mmol) was dissolved in dry, N<sub>2</sub>-saturated DMI (5 ml) and the mixture heated to 120 °C. Now sodium methanethiolate (0.701 g, 10.00 mmol) was added at once. The reaction was kept at this

temperature for 13 h and then cooled to room temperature. After addition of acetyl chloride (0.785 g, 10.00 mmol) the solution was stirred at room temperature for 3 h and then poured on ice/water. The aqueous phase was extracted with toluene, the organic extracts were dried over MgSO<sub>4</sub>, and the solvent removed by rotary evaporation. Purification using column chromatography (silica gel, toluene/diethylether 40/1) provided **O3** as a white solid (0.288 g, 0.66 mmol; 66%). M.p.: 182.5 – 183.5 °C.

*R*<sub>f</sub> = 0.31.

<sup>1</sup>H-NMR (300 MHz, CDCl<sub>3</sub>): δ = 2.03 (s, 6 H), 2.13 (d, due to different isomers, 6 H), 2.45 (s, 6 H), 6.99 (d, due to different isomers, 2 H), 7.21 (d, <sup>3</sup>J(H,H) = 8 Hz, 2 H), 7.28 (d, <sup>3</sup>J(H,H) = 8 Hz, 2 H), 7.34 (s, 2 H).

<sup>1</sup>H-NMR (300MHz, [D<sub>6</sub>]DMSO): δ = 2.04 (s, 6 H), 2.12 (s, 6 H), 2.50 (s, 6 H), 7.10 (s, 2 H), 7.27 (d, <sup>3</sup>J(H,H) = 8 Hz, 2 H), 7.35 (d, <sup>3</sup>J(H,H) = 8 Hz, 2 H), 7.43 (s, 2 H).

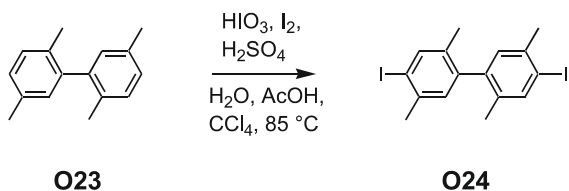
<sup>13</sup>C-NMR (75 MHz, CDCl<sub>3</sub>): δ = 19.33, 19.80, 19.95 (different isomers, CH<sub>3</sub>), 30.26 (CH<sub>3</sub>CO), 126.30, 130.28, 130.36, 130.56, 131.51, 131.56, 132.70, 132.81, 135.62, 137.22, 137.31, 139.68, 139.73, 142.83, 142.89 (Ar, sometimes two peaks due to different isomers), 194.53 (CO).

MALDI-TOF MS: 434.29 [M<sup>+</sup>], 406.26.

Elemental analysis calcd. (%) for C<sub>26</sub>H<sub>26</sub>O<sub>2</sub>S<sub>2</sub> (434.62): C 71.85, H 6.03; found: C 71.59, H 6.06.

UV/Vis (1 × 10<sup>-5</sup> n-hexane): λ<sub>max</sub> (ε) = 208.5 (83100), 250.0 (27700).

**4,4'-Diiodo-2,5,2',5'-tetramethyl-biphenyl O24** following the procedure by H. O. Wirth et al.<sup>[299]</sup>



Tetramethylbiphenyl **O23** (2.103 g, 10.00 mmol), iodic acid (0.774 g, 4.40 mmol) and iodine (2.00 g, 7.88 mmol) were added to a solution of glacial acetic acid (18 ml), water (1.4 ml), conc. sulphuric acid (1 ml) and carbon tetrachloride (1.5 ml). The reaction mixture was heated to 85 °C and kept at this temperature for 6 h. The reaction was quenched by adding water and the resulting mixture extracted with chloroform. The organic extracts were washed

subsequently with sodiumthiosulfate–solution, 2 N sodium hydroxide solution and water and then dried over  $\text{Na}_2\text{SO}_4$ . After rotary evaporation of the solvent a yellow oil was obtained which was stirred with methanol at 60 °C for 3 h. The solid was collected by filtration and recrystallised from diethylether providing **O24** as a white solid (1.758 g, 3.80 mmol; 38.0%). M.p.: 95.0 °C (Lit.<sup>[299]</sup>: 110.0 °C).

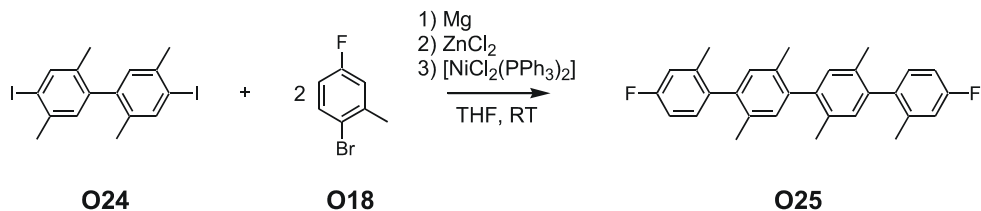
<sup>1</sup>H-NMR (300 MHz,  $\text{CDCl}_3$ ):  $\delta$  = 1.97 (s, 6 H), 2.39 (s, 6 H), 6.92 (s, 2 H), 7.71 (s, 2 H).

<sup>13</sup>C-NMR (75 MHz,  $\text{CDCl}_3$ ):  $\delta$  = 19.19 ( $\text{CH}_3\text{C}$ ), 27.84 ( $\text{CH}_3\text{C}$ ), 100.15 (C4), 130.62 (C6), 135.54 (C2), 138.94 (C3), 140.32 (C1), 141.12 (C5).

MS (EI):  $m/z$  (%) = 462.0 (74) [ $\text{M}^+$ ], 336.0 (49) [ $\text{M}^+ - \text{I}$ ], 208.0 (34) [ $\text{M}^+ - 2\text{I}$ ], 193.0 (100) [ $\text{M}^+ - 2\text{I}, \text{CH}_3$ ], 178.0 (62) [ $\text{M}^+ - 2\text{I}, 2\text{CH}_3$ ], 165.0 (25), 152.0 (16), 128.0 (11), 96.0 (13).

Elemental analysis calcd. (%) for  $\text{C}_{16}\text{H}_{16}\text{I}_2$  (462.11): calcd. C 41.59, H 3.49; found C 41.72, H 3.51.

#### 4,4'''-Difluoro-2,2',5',2'',5'',2'''-hexamethyl-[1,1';4',1'';4'',1''']quaterphenyl **O25**



Magnesium turnings (0.182 g, 7.50 mmol) suspended in THF (1 ml) were treated with a solution of 2-bromo-5-fluorotoluene **O18** (1.418 g, 7.50 mmol) in dry THF (5 ml). The resulting mixture was stirred at room temperature for 1 h. Then dry zinc chloride (1.022 g, 7.50 mmol) dissolved in dry THF (20 ml) was added to the solution and stirring continued at room temperature for another hour.  $[\text{NiCl}_2(\text{PPh}_3)_2]$  (0.046 g, 0.07 mmol) and a solution of 4,4'-diiodo-2,5,2',5'-tetramethyl-biphenyl **O24** (1.386 g, 3.00 mmol) in dry THF (8 ml) were added subsequently. After stirring at room temperature for 48 h the grey suspension was poured on ice (about 75 g) and acidified with  $\text{H}_2\text{O}/\text{conc. hydrochloric acid}$  (7.5 ml/7.5 ml). The aqueous phase was extracted with  $\text{CH}_2\text{Cl}_2$ , the combined organic phases washed with water and dried over  $\text{MgSO}_4$ . After rotary evaporation a white solid was obtained which was purified by column chromatography (silica gel, hexane/toluene 20/1) affording **O25** as a white solid (0.647 g, 1.52 mmol; 51%). M.p.: 197.0 – 198.5 °C.

$R_f = 0.46$ .

$^1\text{H}$ -NMR (300 MHz,  $\text{CDCl}_3$ ):  $\delta = 2.03$  (s, 6 H), 2.09 (d, due to different isomers, 6 H), 2.12 (d, due to different isomers, 6 H), 6.94 (ddd,  $^3J(\text{H},\text{F}) = 9$  Hz,  $^3J(\text{H},\text{H}) = 8$  Hz,  $^4J(\text{H},\text{H}) = 2$  Hz, 2 H), 6.97 (s, 2 H), 6.99 (dd,  $^3J(\text{H},\text{F}) = 9$  Hz,  $^4J(\text{H},\text{H}) = 2$  Hz, 2 H), 7.05 (d, due to different isomers, 2 H), 7.13 (dd,  $^3J(\text{H},\text{H}) = 8$  Hz,  $^4J(\text{H},\text{F}) = 6$  Hz, 2 H).

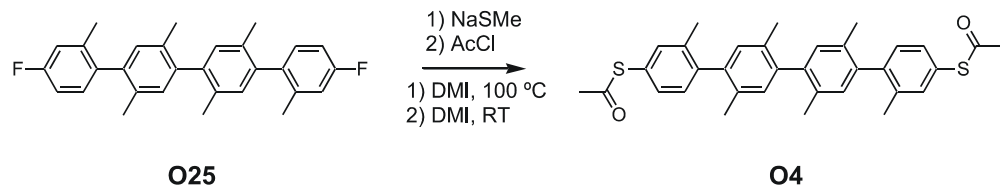
$^1\text{H}$ -NMR (300 MHz,  $\text{CDCl}_3$ ,  $T = 53$  °C):  $\delta = 2.04$  (s, 6 H), 2.09 (s, 6 H), 2.12 (s, 6 H), 6.94 (ddd,  $^3J(\text{H},\text{F}) = 9$  Hz,  $^3J(\text{H},\text{H}) = 8$  Hz,  $^4J(\text{H},\text{H}) = 2$  Hz, 2 H), 6.97 (s, 2 H), 6.99 (dd,  $^3J(\text{H},\text{F}) = 9$  Hz,  $^4J(\text{H},\text{H}) = 2$  Hz, 2 H), 7.06 (s, 2 H), 7.13 (dd,  $^3J(\text{H},\text{H}) = 8$  Hz,  $^4J(\text{H},\text{F}) = 6$  Hz, 2 H).

$^{13}\text{C}$ -NMR (75 MHz,  $\text{CDCl}_3$ ):  $\delta = 19.27$ , 19.31, 19.44, (two peaks due to different isomers,  $\text{CH}_3$ ), 20.02, 20.16 (d,  $^4J(\text{F},\text{C}) = 2$  Hz,  $\text{CH}_3$ , due to different isomers), 112.25, 112.30 (d,  $^2J(\text{F},\text{C}) = 21$  Hz, due to different isomers, C5, C5'''), 116.30 (d,  $^2J(\text{F},\text{C}) = 21$  Hz, C3, C3'''), 130.76, 130.85 (d,  $^3J(\text{F},\text{C}) = 8$  Hz, due to different isomers, C6, C6'''), 130.77, 130.86 (due to different isomers, C3', C6', C3'', C6''), 132.84, 132.93, 132.95, 133.03 (due to different isomers, C2', C5', C2'', C5'') 137.48, 137.53 (d,  $^4J(\text{F},\text{C}) = 3$  Hz, due to different isomers, C1, C1'''), 138.34, 138.40 (d,  $^3J(\text{F},\text{C}) = 7$  Hz, due to different isomers, C2, C2'''), 139.24, 139.27, 139.30, 139.33, 140.45, 140.51, 140.56 (due to different isomers, C1', C4', C1'', C4''), 161.89 (d,  $^1J(\text{F},\text{C}) = 243$  Hz, C4, C4'''').

MALDI-TOF MS: 450.87 [ $\text{M}^+ + \text{Na}$ ], 425.96 [ $\text{M}^+$ ].

Elemental analysis calcd. (%) for  $\text{C}_{30}\text{H}_{28}\text{F}_2$  (426.54): C 84.48, H 6.62; found C 84.49, H 6.74.

#### 4,4'''-Bis(acetylsulfanyl)-2,2',5',2",5",2'''-hexamethyl-[1,1';4',1";4",1'']quaterphenyl **O4**



4,4'''-Difluoro-2,2',5',2",5",2'''-hexamethyl-[1,1';4',1";4",1'']quaterphenyl **O25** (0.213 g, 0.50 mmol) was dissolved in dry,  $\text{N}_2$ -saturated DMI (5 ml) and the mixture heated to 100 °C. Now sodium methanethiolate (0.351 g, 5.00 mmol) was added at once. The reaction mixture was kept at this temperature for 20 h and then cooled to room temperature. After addition of acetyl chloride (0.730 g, 9.30 mmol) the solution was stirred at room temperature for 4 h and then poured on ice/water. The aqueous phase was extracted with toluene, the organic extracts were dried over  $\text{MgSO}_4$  and the solvent removed by rotary evaporation. The crude oily substance

was purified by column chromatography (silica gel, toluene/diethylether 40/1) followed by re-crystallisation from diethylether/hexane to afford **O4** as a white solid (0.132 g, 0.25 mmol; 50%). M.p.: 178.0 °C.

$R_f = 0.32$ .

$^1\text{H}$ -NMR (300 MHz,  $\text{CDCl}_3$ ):  $\delta = 2.05$  (s, 6 H), 2.09 (d, due to different isomers, 6 H), 2.14 (d, due to different isomers, 6 H), 2.45 (s, 6 H), 7.00 (d, due to different isomers, 2 H), 7.06 (d, due to different isomers, 2 H), 7.23 (d,  $^3J(\text{H},\text{H}) = 8$  Hz, 2 H), 7.31 (d,  $^3J(\text{H},\text{H}) = 8$  Hz, 2 H), 7.34 (s, 2 H).

$^1\text{H}$ -NMR (300 MHz,  $[\text{D}_6]\text{DMSO}$ , T = 41 °C):  $\delta = 1.99$  (s, 6 H), 2.05 (s, 6 H), 2.08 (s, 6 H), 2.44 (s, 6 H), 7.03 (s, 2 H), 7.07 (s, 2 H), 7.22 (d,  $^3J(\text{H},\text{H}) = 8$  Hz, 2 H), 7.31 (d,  $^3J(\text{H},\text{H}) = 8$  Hz, 2 H), 7.38 (s, 2 H).

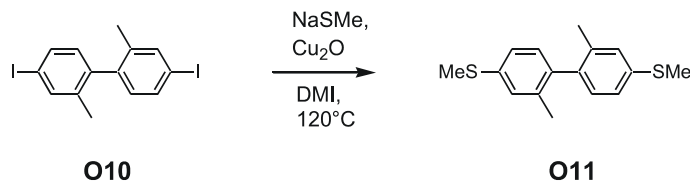
$^{13}\text{C}$ -NMR (75 MHz,  $\text{CDCl}_3$ ):  $\delta = 19.68, 19.86, 20.22, 20.35$  (different isomers,  $\text{CH}_3,$ ), 30.64 ( $\text{CH}_3\text{CO}$ ), 126.54, 126.59, 130.73, 130.82, 131.19, 131.26, 131.87, 131.92, 132.84, 132.89, 132.95, 133.00, 133.27, 133.37, 133.46, 135.98, 137.69, 137.74, 139.63, 139.67, 139.69, 139.72, 140.91, 140.97, 141.03, 143.40, 143.47 (Ar, often several peaks due to different isomers), 194.95 (CO).

MALDI-TOF MS (9-Nitroanthracene): 537.94 [ $\text{M}^+$ ], 412.88, 399.88, 370.90, 369.89.

Elemental analysis calcd. (%) for  $\text{C}_{34}\text{H}_{34}\text{O}_2\text{S}_2$  (538.76): C 75.80, H 6.36; found C 75.52, H 6.12.

UV/Vis ( $1 \times 10^{-5}$  n-hexane):  $\lambda_{\text{max}} (\varepsilon) = 209.0$  (97800), 249.5. (35900).

### 2,2'-Dimethyl-4,4'-bis-methylsulfanyl-biphenyl **O11**



Sodium methanethiolate (1.402 g, 20.00 mmol) was dissolved in dry DMI (80 ml) and 4,4'-diiodo-2,2'-dimethyl-biphenyl **O10** (2.170 g, 5.00 mmol) and copper(I)oxide (0.358 g, 2.50 mmol) added. The reaction mixture was heated to 120 °C for 2 h and then poured into sat.  $\text{NaCl}$ -solution. The aqueous phase was extracted with toluene, the combined toluene layers washed with water once, dried over  $\text{MgSO}_4$  and the solvents removed in vacuo. Column

chromatography (silica gel, hexane/toluene 2/1) afforded **O11** as a white solid (0.231 g, 0.84 mmol; 17%). M.p.: 57.5 – 58.5 °C.

$R_f = 0.50$ .

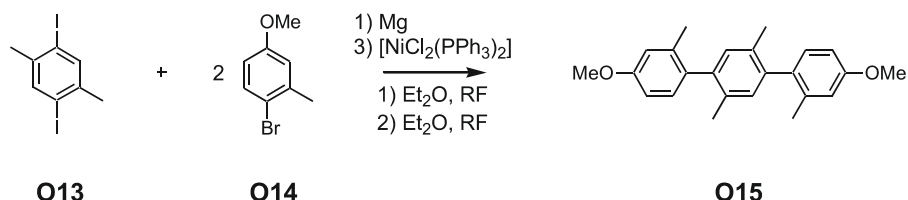
$^1\text{H}$ -NMR (300 MHz,  $\text{CDCl}_3$ ):  $\delta = 2.04$  (s, 6 H), 2.52 (s, 6 H), 7.01 (d,  $^3J(\text{H},\text{H}) = 8$  Hz, 2 H), 7.12 (dd,  $^3J(\text{H},\text{H}) = 8$  Hz,  $^4J(\text{H},\text{H}) = 2$  Hz, 2 H), 7.16 (d,  $^4J(\text{H},\text{H}) = 2$  Hz, 2 H).

$^{13}\text{C}$ -NMR (75 MHz,  $\text{CDCl}_3$ ):  $\delta = 15.87$  ( $\text{CH}_3$ ), 19.91 ( $\text{SCH}_3$ ), 123.75 (C5), 127.92 (C6), 129.97 (C3), 136.71 (C1), 136.97 (C4), 138.01 (C2).

MS (EI):  $m/z$  (%) = 274.0 (100) [ $\text{M}^+$ ], 259.0 (10) [ $\text{M}^+ - \text{CH}_3$ ], 180.0 (10) [ $\text{M}^+ - 2 \text{SCH}_3$ ].

Elemental analysis calcd. (%) for  $\text{C}_{16}\text{H}_{18}\text{S}_2$  (274.45): C 70.02, H 6.61; found C 70.28, H 6.52.

#### 4,4''-Dimethoxy-2,2',5',2''-tetramethyl-[1,1';4',1'']terphenyl **O15**



Magnesium turnings (0.850 g, 34.96 mmol) suspended in dry diethylether (3.5 ml) were treated with a solution of 4-bromo-3-methylanisole **O14** (7.040 g, 35.00 mmol) in dry diethylether (15 ml). The resulting mixture was heated to reflux for 2 h and then allowed to come to room temperature.  $[\text{NiCl}_2(\text{PPh}_3)_2]$  (0.210 g, 0.32 mmol) and a solution of 2,5-diido-*p*-xylene **O13** (5.010 g, 14.00 mmol) in dry diethylether (48 ml) were added subsequently. After stirring the reaction mixture at reflux for 16 h the grey suspension was poured on ice (about 200 g) and acidified with  $\text{H}_2\text{O}/\text{conc. hydrochloric acid}$  (17.5 ml/17.5 ml). The aqueous phase was extracted with diethylether, the organic phases washed with water and dried over  $\text{MgSO}_4$ . After rotary evaporation a brown solid was obtained which was purified by column chromatography (silica gel, toluene/hexane 2/1) affording **O15** as a white solid (2.290 g, 6.61 mmol; 47%). M.p. 182.0 – 184.5 °C.

$R_f = 0.40$ .

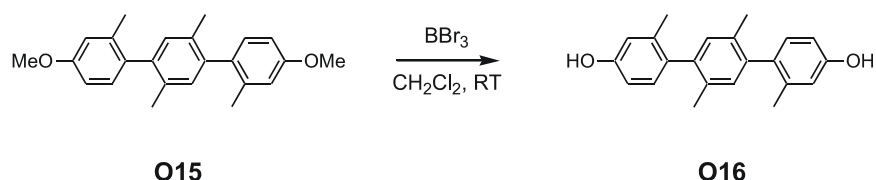
$^1\text{H}$ -NMR (300 MHz,  $\text{CDCl}_3$ ):  $\delta = 2.03$  (s, 6 H), 2.10 (d, due to different isomers, 6 H), 3.85 (s, 6 H), 6.79 (dd,  $^3J(\text{H},\text{H}) = 9$  Hz,  $^4J(\text{H},\text{H}) = 2$  Hz, 2 H), 6.83 (d,  $^4J(\text{H},\text{H}) = 2$  Hz, 2 H), 6.97 (d, due to different isomers, 2 H), 7.09 (dd, due to different isomers,  $^3J(\text{H},\text{H}) = 9$  Hz, 2 H).

<sup>1</sup>H-NMR (300 MHz, CDCl<sub>3</sub>, T = 53 °C): δ = 2.03 (s, 6 H), 2.10 (s, 6 H), 3.85 (s, 6 H), 6.79 (dd, <sup>3</sup>J(H,H) = 9 Hz, <sup>4</sup>J(H,H) = 2 Hz, 2 H), 6.84 (d, <sup>4</sup>J(H,H) = 2 Hz, 2 H), 6.97 (s, 2 H), 7.08 (d, <sup>3</sup>J(H,H) = 9 Hz, 2 H).

<sup>13</sup>C-NMR (75 MHz, CDCl<sub>3</sub>): δ = 19.39, 20.14, 20.30 (different isomers, CH<sub>3</sub>), 55.23 (CH<sub>3</sub>O), 110.77, 115.20, 130.35, 130.45, 131.11, 131.13, 133.06, 133.18, 134.22, 134.29, 137.34, 137.41, 139.87, 139.93 (Ar, sometimes two peaks due to different isomers), 158.57 (COCH<sub>3</sub>). MALDI-TOF MS: 371.85, 345.84 [M<sup>+</sup>].

Elemental analysis calcd. (%) for C<sub>24</sub>H<sub>26</sub>O<sub>2</sub> (346.46): C 83.20, H 7.56; found C 83.10, H 7.55.

## 2,2',5',2''-Tetramethyl-[1,1';4',1'']terphenyl-4,4''-diol O16



**4,4"-Dimethoxy-2,2',5',2"-tetramethyl-[1,1';4',1"]terphenyl** **O15** (1.606 g, 4.64 mmol) was dissolved in dry CH<sub>2</sub>Cl<sub>2</sub> and the mixture cooled to -78 °C using a dry ice/acetone bath. Then boron tribromide (1 M solution in CH<sub>2</sub>Cl<sub>2</sub>; 11.00 ml, 11.00 mmol) was slowly dropped in via syringe. The reaction mixture was allowed to come to room temperature and stirred at this temperature for 28 h. Now it was poured into ice/water (about 150 ml) and the white precipitate that formed was collected. It was dissolved in 2 M potassium hydroxide (about 100 ml) and then precipitated again with conc. hydrochloric acid. **O16** was obtained as a white solid (1.074 g, 3.37 mmol; 73%). M.p.: 197.0 – 199.0 °C.

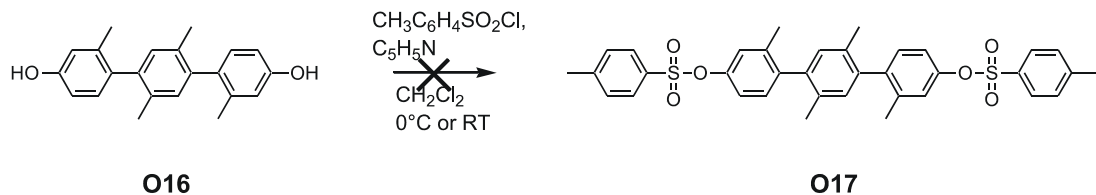
<sup>1</sup>H-NMR (300 MHz, CDCl<sub>3</sub>): δ = 2.02 (s, 6 H), 2.07 (d, due to different isomers, 6 H), 6.71 (dd, <sup>3</sup>J(H,H) = 8 Hz, <sup>4</sup>J(H,H) = 3 Hz, 2 H), 6.76 (d, <sup>4</sup>J(H,H) = 3 Hz, 2 H), 6.95 (d, due to different isomers, 2 H), 7.03 (dd, due to different isomers, <sup>3</sup>J(H,H) = 8 Hz, 2 H).

<sup>13</sup>C-NMR (75 MHz, [D<sub>6</sub>]DMSO): δ = 19.96, 20.49, 20.70 (different isomers, CH<sub>3</sub>), 113.38 (C5, C5''), 117.19 (C3, C3''), 130.83, 130.84, 131.75, 131.79, 132.59, 133.43, 137.11, 137.16, 140.52 (Ar, sometimes two peaks due to different isomers), 157.10 (C4, C4'').

MALDI-TOF MS: 317.83 [M<sup>+</sup>].

Elemental analysis calcd. (%) for C<sub>22</sub>H<sub>22</sub>O<sub>2</sub> (318.41): C 82.99, H 6.96; found C 82.69, H 7.08.

**Toluene-4-sulphonic acid 4-toluenesulphonyloxy-2,2',5',2''-tetramethyl-[1,1';4',1'']ter-phenyl-4''-yl ester O17**



**2,2',5',2"-Tetramethyl-[1,1';4',1"]terphenyl-4,4"-diol (O16** (0.048 g, 0.15 mmol) and toluenesulphonyl chloride (0.086 g, 0.45 mmol) was dissolved in CH<sub>2</sub>Cl<sub>2</sub> (1 ml). and pyridine (0.048 g, 0.60 mmol) was added at 0 °C. The resulting mixture was stirred at this temperature for 2 h. The solution was allowed to come to room temperature and stirred for an additional 24 h. The mixture was poured into ice/water/conc. HCl (100 ml/2 ml) and extracted with CH<sub>2</sub>Cl<sub>2</sub>. The organic layers were washed with NaHCO<sub>3</sub>-solution and with water, dried over MgSO<sub>4</sub> and evaporated to dryness. No pure compound could be obtained after column chromatography (silica gel, dichloromethane/5% methanol). The reaction was also repeated at room temperatures without better result.

## 2,2',5',2''-Tetramethyl-4,4''-bis-methylsulfanyl-[1,1';4',1'']terphenyl O20



4,4"-Difluoro-2,2',5',2"-tetramethyl-[1,1';4',1"]terphenyl **O19** (0.097 g, 0.30 mmol) was dissolved in dry DMI (10 ml) and the mixture heated to 90 °C. Now sodium methanethiolate (0.074 g, 1.05 mmol) was added and the reaction kept at 90 °C for 6 h. It was poured into sat. NaCl-solution, the aqueous phase was extracted with toluene, the combined organic phases dried over MgSO<sub>4</sub> and the solvent removed by rotary evaporation. Column chromatography (silica gel, hexane/toluene 2/1) afforded **O20** as a white solid (0.040 g, 0.11 mmol; 35%). M.p.: 143.5 – 145.0°C.

$$R_f = 0.38.$$

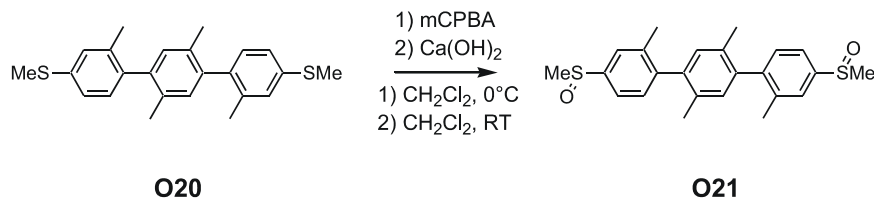
<sup>1</sup>H-NMR (300 MHz, CDCl<sub>3</sub>): δ = 2.02 (s, 6 H), 2.09 (d, due to different isomers, 6 H), 2.53 (s, 6 H), 6.96 (d, due to different isomers, 2 H), 7.09 (dd, due to different isomers, <sup>3</sup>J(H,H) = 8 Hz, 2 H), 7.14 (d, <sup>3</sup>J(H,H) = 8 Hz, 2 H), 7.18 (s, 2 H).

<sup>13</sup>C-NMR (75 MHz, CDCl<sub>3</sub>): δ = 15.93, 19.36, 19.86, 20.02 (different isomers, CH<sub>3</sub>), 123.74, 127.92, 129.91, 130.00, 130.82, 132.86, 132.98, 136.64, 136.72, 138.61, 139.86 (Ar, sometimes two peaks due to different isomers).

MALDI-TOF MS: 377.80 [M<sup>+</sup>].

Elemental analysis calcd. (%) for C<sub>24</sub>H<sub>26</sub>S<sub>2</sub> (378.60): C 76.14, H 6.92; found C 75.99, H 7.06.

#### 4,4"-Bis-methanesulfinyl-2,2',5',2"-tetramethyl-[1,1';4',1"]terphenyl O21



A solution of 2,2',5',2"-Tetramethyl-4,4"-bis-methysulfanyl-[1,1';4',1"]terphenyl **O20** (0.223 g, 0.59 mmol) in dry CH<sub>2</sub>Cl<sub>2</sub> (25 ml) was cooled to 0 °C using an ice/water bath. To the cooled solution was added 3-chloroperoxybenzoic acid (mCPBA) (0.204 g, 1.18 mmol) in three portions and the mixture stirred at 0 °C for 30 min. Then Ca(OH)<sub>2</sub> was added and stirred for an additional 30 min at room temperature. The reaction mixture was filtered, washed with toluene and the solvents removed *in vacuo*. The crude product was purified by column chromatography (silica gel, acetone/hexane 1/1 increasing to acetone) giving **O21** as a white solid (0.041 g, 0.01 mmol; 2%). M.p.: 212.0 – 215.0 °C.

Repetition of the reaction at –10°C did not give better yields.

R<sub>f</sub> = 0.30 (acetone).

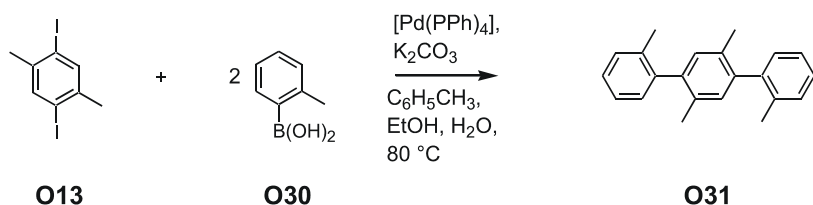
<sup>1</sup>H-NMR (300 MHz, CD<sub>2</sub>Cl<sub>2</sub>): δ = 2.03 (s, 6 H), 2.18 (d, due to different isomers, 6 H), 2.80 (s, 6 H), 6.98 (d, due to different isomers, 2 H), 7.29 – 7.35 (m, 2 H), 7.49 (dd, due to different isomers, <sup>3</sup>J(H,H) = 8 Hz, 2 H), 7.60 (d, due to different isomers, 2 H).

<sup>13</sup>C-NMR (75 MHz, CDCl<sub>3</sub>): δ = 19.28, 19.98, 20.12 (CH<sub>3</sub>), 43.90, 43.92 (SOCH<sub>3</sub>), 120.81, 120.88, 120.95, 121.00, 124.72, 124.84, 130.28, 130.37, 130.43, 130.53, 132.78, 132.87, 137.73, 137.79, 137.90, 137.97, 139.59, 139.64, 144.24, 144.52, 144.56 (Ar, sometimes two peaks due to different isomers).

MALDI-TOF MS: 410.71 [M<sup>+</sup>], 394.73 [M<sup>+</sup> – CH<sub>3</sub>].

Elemental analysis calcd. (%) for C<sub>24</sub>H<sub>26</sub>O<sub>2</sub>S<sub>2</sub> (410.59): C 70.20, H 6.38; found C 70.30, H 6.48.

### 2,2',5',2''-Tetramethyl-[1,1';4',1'']terphenyl O31



A two-necked flask was successively charged with 2,5-diodo-*p*-xylene **O13** (0.179 g, 0.50 mmol), 2-methylbenzeneboronic acid **O30** (0.177 g, 1.30 mmol), toluene (6.5 ml), tetrakis(triphenylphosphine)palladium (0.046 g, 0.04 mmol), ethanol (1.3 ml), potassium carbonate (0.556 g, 4.00 mmol) and H<sub>2</sub>O (2.5 ml). The mixture was stirred vigorously while heating to 80 °C for 3 h and then at room temperature overnight. The reaction mixture was poured into sat. NH<sub>4</sub>Cl-solution, the aqueous phase extracted with diethylether, the ethereal phases washed with water, dried over MgSO<sub>4</sub> and the solvents removed by rotary evaporation. The crude product was absorbed on silica gel and added to a column (silica gel, hexane/toluene 20/1) giving **O31** as a white solid (0.140 g, 0.49 mmol; 98 %). M.p.: 169.0 – 171.0 °C.

R<sub>f</sub> = 0.47.

<sup>1</sup>H-NMR (300 MHz, CD<sub>2</sub>Cl<sub>2</sub>): δ = 2.03 (s, 6 H), 2.13 (d, due to different isomers, 6 H), 7.00 (s, 2 H), 7.15 – 7.17 (m, 2 H), 7.22 – 7.32 (m, 6 H).

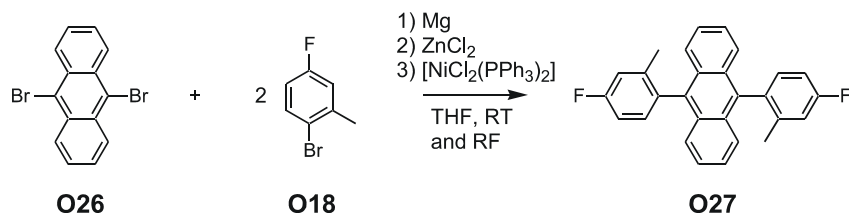
<sup>13</sup>C-NMR (75 MHz, CDCl<sub>3</sub>): δ = 19.33, 19.83, 20.00 (CH<sub>3</sub>, different isomers), 125.47, 125.53, 127.05, 127.08, 129.41, 129.52, 129.79, 130.62, 130.64, 132.64, 132.76, 135.95, 136.03, 140.36, 141.63, 141.69 (Ar, sometimes two peaks due to different isomers).

MALDI-TOF MS: 285.86 [M<sup>+</sup>], 241.77 [M<sup>+</sup> – 3 CH<sub>3</sub>].

Elemental analysis calcd. (%) for C<sub>22</sub>H<sub>22</sub> (286.41): C 92.26, H 7.74; found C 92.09, H 7.59.

**9,10-Bis-(4-fluoro-2-methyl-phenyl)-anthracene O27**

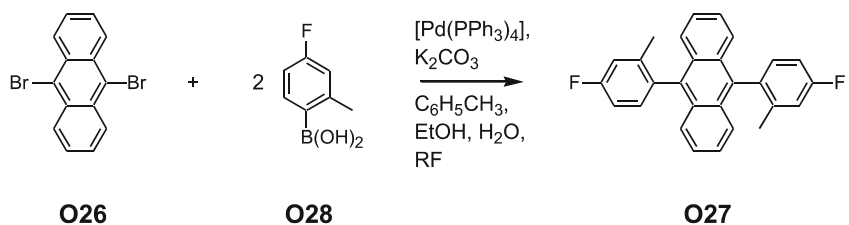
Method 1:



Magnesium turnings (0.182 g, 7.50 mmol) suspended in THF (1 ml) were treated with a solution of 2-bromo-5-fluorotoluene **O18** (1.418 g, 7.50 mmol) in dry THF (5 ml). The resulting mixture was stirred at room temperature for 1 h. Then dry zinc chloride (1.022 g, 7.50 mmol) dissolved in dry THF (20 ml) was added to the solution and stirring continued at room temperature for another hour.  $[\text{NiCl}_2(\text{PPh}_3)_2]$  (0.046 g, 0.07 mmol) and a solution of 9,10-dibromoanthracene **O26** (1.008 g, 3.00 mmol) in dry THF (50 ml) were added subsequently. After stirring at room temperature for 44 h no reaction could be detected on TLC. Therefore, the reaction mixture was heated to reflux for 52 h. The yellow suspension was poured on ice (about 75 g) and acidified with  $\text{H}_2\text{O}/\text{conc. hydrochloric acid}$  (7.5 ml/7.5 ml). The aqueous phase was extracted with toluene, the combined organic phases washed with water and dried over  $\text{MgSO}_4$ . After rotary evaporation a yellow solid was obtained which was absorbed on silica gel and purified by column chromatography (silica gel, hexane/toluene 50/1) affording **O27** as a white solid (0.090 g, 0.23 mmol; 8%). M.p.: 333.0 – 335.0 °C.

$^1\text{H-NMR}$  (300 MHz,  $\text{CD}_2\text{Cl}_2$ ):  $\delta = 1.91$  (s, 6 H), 7.12 (ddd,  ${}^3J(\text{H},\text{F}) = 9$  Hz,  ${}^3J(\text{H},\text{H}) = 8$  Hz,  ${}^4J(\text{H},\text{H}) = 3$  Hz, 2 H), 7.19 (dd,  ${}^3J(\text{H},\text{F}) = 9$  Hz,  ${}^4J(\text{H},\text{H}) = 3$  Hz, 2 H), 7.25 – 7.29(m, 2 H), 7.33 – 7.37 (m, 4 H), 7.52 – 7.55 (m, 4 H).

Method 2:



A two-necked flask was successively charged with 9,10-dibromoanthracene **O26** (0.840 g, 2.50 mmol), 4-fluoro-2-methylbenzeneboronic acid **O28** (1.026 g, 6.66 mmol), toluene (32.5 ml), tetrakis(triphenylphosphine)palladium (0.231 g, 0.20 mmol), ethanol (6.5 ml), potassium carbonate (2.764 g, 20.00 mmol) and H<sub>2</sub>O (12.5 ml). The mixture was stirred vigorously while heating to reflux for 18 h. After cooling a white solid precipitated, which was collected and washed with water and ethanol giving **O27** as a white solid (0.489 g, 1.24 mmol; 50%) without further purification. The filtrate was extracted with CH<sub>2</sub>Cl<sub>2</sub>, the combined organic phases filtered over silica gel and the solvents removed by rotary evaporation. The residue was re-crystallised from ethanol providing **O27** as a white solid (0.055 g; 0.14 mmol; combined yields: 55 %). M.p.: 334.0 – 336.0 °C.

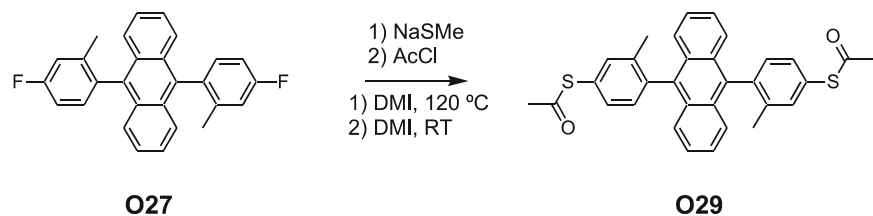
<sup>1</sup>H-NMR (300 MHz, CD<sub>2</sub>Cl<sub>2</sub>): δ = 1.91 (s, 6 H), 7.15 (ddd, <sup>3</sup>J(H,F) = 9 Hz, <sup>3</sup>J(H,H) = 8 Hz, <sup>4</sup>J(H,H) = 3 Hz, 2 H), 7.22 (dd, <sup>3</sup>J(H,F) = 9 Hz, <sup>4</sup>J(H,H) = 3 Hz, 2 H), 7.30 (dd, <sup>3</sup>J(H,H) = 8 Hz, <sup>4</sup>J(H,F) = 7 Hz, 2 H), 7.35 – 7.39 (m, 4 H), 7.52 – 7.56 (m, 4 H).

<sup>13</sup>C-NMR (75 MHz, CDCl<sub>3</sub>, T = 40°C): δ = 19.96 (d, <sup>4</sup>J(F,C) = 2 Hz), 112.80 (d, <sup>2</sup>J(F,C) = 21 Hz, C5), 116.75 (d, <sup>2</sup>J(F,C) = 21 Hz, C3), 125.38 (C2), 126.56 (C1), 129.58, 132.73 (d, <sup>3</sup>J(F,C) = 8 Hz, C6), 134.12 (d, <sup>4</sup>J(F,C) = 3 Hz, C1), 135.42, 140.40 (d, <sup>3</sup>J(F,C) = 8 Hz, C2), 162.57 (d, <sup>1</sup>J(F,C) = 245 Hz, C4).

MALDI-TOF MS: 393.77 [M<sup>+</sup>].

Elemental analysis calcd. (%) for C<sub>28</sub>H<sub>20</sub>F<sub>2</sub> (394.46): C 85.26, H 5.11; found C 85.11, H 5.25.

### 9,10-Bis-(4-acetylsulfanyl-2-methyl-phenyl)-anthracene **O29**



9,10-Bis-(4-fluoro-2-methyl-phenyl)-anthracene **O27** (0.489 g, 1.24 mmol) was dissolved in dry, N<sub>2</sub>-saturated DMI (17 ml) and the mixture heated to 120 °C. Now sodium methanethiolate (0.869 g, 12.40 mmol) was added at once. The reaction mixture was kept at this temperature for 17 h and then cooled to room temperature. After addition of acetyl chloride (0.973 g, 12.40 mmol) the solution was stirred at room temperature for 4 h and then poured on ice/water. The aqueous phase was extracted with toluene, the organic extracts were

dried over  $\text{MgSO}_4$  and the solvent removed by rotary evaporation. The crude product was purified by column chromatography (silica gel, toluene/diethylether 40/1) affording **O29** as a white solid (0.429 g, 0.85 mmol; 68%). M.p.: 254.0 – 256.0 °C.

$R_f = 0.34$ .

$^1\text{H}$ -NMR (300 MHz,  $\text{CDCl}_3$ ):  $\delta = 1.94$  (s, 6 H), 2.53 (s, 6 H), 7.34 – 7.40 (m, 6 H), 7.48 (dd,  $^3J(\text{H},\text{H}) = 8$  Hz,  $^4J(\text{H},\text{H}) = 2$  Hz, 2 H), 7.54 – 7.57 (m, 6 H).

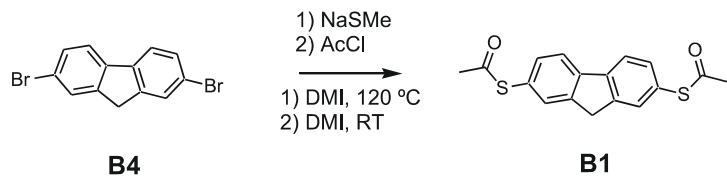
$^{13}\text{C}$ -NMR (75 MHz,  $\text{CDCl}_3$ ):  $\delta = 19.78$ , 19.89 ( $\text{CH}_3$ ), 30.40 ( $\text{CH}_3\text{S}$ ), 125.59, 126.63, 127.32, 129.49, 131.80, 131.85, 132.11, 132.17, 135.43, 135.46, 135.87, 139.17, 139.27, 139.87 (Ar, sometimes two peaks due to different isomers), 194.36 ( $\text{COCH}_3$ ).

MALDI-TOF MS (9-Nitroanthracene): 505.69 [ $\text{M}^+$ ], 477.70 [ $\text{M}^+ - \text{CO}$ ], 463.70 [ $\text{M}^+ - \text{COCH}_3$ ].

Elemental analysis calcd. (%) for  $\text{C}_{32}\text{H}_{26}\text{O}_2\text{S}_2$  (506.68): C 75.86, H 5.17; found C 75.55, H 5.15.

UV/Vis ( $5 \times 10^{-6}$  n-hexane):  $\lambda_{\text{max}} (\varepsilon) = 205.0$  (107000), 258.0 (157000), 322.0 (3400), 338.0 (8000), 355.0 (17000), 373.0 (27900), 394.0 (27400).

### 2,7-Bis-(acetylsulfanyl)-fluorene **B1**



2,7-Dibromofluorene **B4** (0.486 g, 1.50 mmol) was dissolved in dry,  $\text{N}_2$ -saturated DMI (15 ml) and the mixture heated to 120 °C. Now sodium methanethiolate (1.052 g, 15.00 mmol) was added at once. The reaction mixture was kept at this temperature for 18 h and then cooled to room temperature. After addition of acetyl chloride (1.178 g, 15.00 mmol) the solution was stirred at room temperature for 3 h and then poured on ice/water. The aqueous phase was extracted with toluene, the organic extracts were dried over  $\text{MgSO}_4$  and the solvent removed by rotary evaporation. The dark oily product was purified by column chromatography (silica gel, toluene/diethylether 40/1) affording **B1** as a yellow solid (0.203 g, 0.65 mmol; 43%). M.p.: 145.5 – 147.0 °C.

$R_f = 0.20$ .

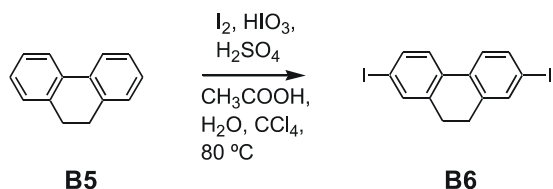
<sup>1</sup>H-NMR (300 MHz, CDCl<sub>3</sub>): δ = 2.45 (s, 6 H), 3.93 (s, 4 H), 7.43 (dd, <sup>3</sup>J(H,H) = 8 Hz, <sup>4</sup>J(H,H) = 1 Hz, 2 H), 7.59 (d, <sup>4</sup>J(H,H) = 1 Hz, 2 H), 7.81 (d, <sup>3</sup>J(H,H) = 8 Hz, 2 H).

<sup>13</sup>C-NMR (75 MHz, CDCl<sub>3</sub>): δ = 30.28 (CH<sub>3</sub>), 36.74 (CH<sub>2</sub>), 120.94 (C3, C6), 126.55 (C4, C5), 131.28 (C2, C7), 133.31 (C1, C8), 142.16 (C4a, C4b), 144.37 (C8a, C9a), 194.581 (CO) MS (EI): *m/z* (%) = 314.1 (26) [M<sup>+</sup>], 272.0 (23) [M<sup>+</sup> - CH<sub>3</sub>CO], 230.0 (100) [M<sup>+</sup> - 2 CH<sub>3</sub>CO], 197 (33) [M<sup>+</sup> - CH<sub>3</sub>CO, - S CH<sub>3</sub>CO], 152 (15).

Elemental analysis calcd. (%) for C<sub>17</sub>H<sub>14</sub>O<sub>2</sub>S<sub>2</sub> (314.42): C 64.94, H 4.49; found: C 64.89, H 4.23.

UV/Vis (1 × 10<sup>-5</sup> n-hexane): λ<sub>max</sub> (ε) = 211.5 (36300), 290.0 (25400), 311.5 (26200).

**2,7-Diodo-9,10-dihydro-phenanthrene B6** following the procedure by H. O. Wirth et al.<sup>[303]</sup>



9,10-Dihydrophenanthrene **B5** (9.013 g; 50.00 mmol), iodine (10.152 g, 40.00 mmol) and iodic acid (4.750 g, 27.00 mmol) were added subsequently to a solution of glacial acetic acid (60 ml), H<sub>2</sub>O (10 ml) and conc. sulphuric acid (2.5 ml) and CCl<sub>4</sub> (5 ml). Then the reaction mixture was heated to 80°C and kept at this temperature for 4 h. After quenching with water, the solid was collected by filtration and dried overnight. The crude product was stirred with diethylether:methanol 1:1 (about 100 ml) at room temperature for 2 h. The resulting light orange solid was re-crystallised from ethyl acetate to provide **B6** as light yellow crystals (12.042 g, 27.87 mmol; 56%). M.p.: 177.5 °C (Lit.<sup>[303]</sup>: 175.0 °C).

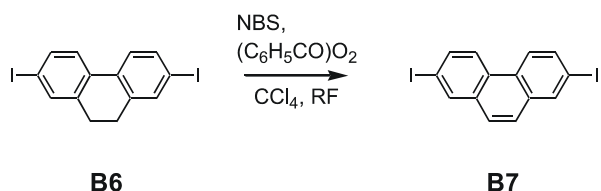
<sup>1</sup>H-NMR (300 MHz, CDCl<sub>3</sub>): δ = 2.80 (s, 4H), 7.42 (d, <sup>3</sup>J(H,H) = 8 Hz, 2 H), 7.58 (d, <sup>4</sup>J(H,H) = 2 Hz, 2 H), 7.62 (dd, <sup>3</sup>J(H,H) = 8 Hz, <sup>4</sup>J(H,H) = 2 Hz, 2 H).

<sup>13</sup>C-NMR (75 MHz, CDCl<sub>3</sub>): δ = 28.33 (CH<sub>2</sub>), 93.41 (CI), 125.34 (C4, C5), 133.29 (C4a, C4b), 136.18 (C3, C6), 137.08 (C1, C8), 139.34 (C8a, C10a).

MS (EI): *m/z* (%) = 432.1 (100) [M<sup>+</sup>], 178.1 (83) [M<sup>+</sup> - 2 I], 176.1 (34), 152.0 (12), 151.0 (13), 89.1 (25), 88.1 (17), 76.2 (14).

Elemental analysis calcd. (%) for C<sub>14</sub>H<sub>10</sub>I<sub>2</sub> (432.04): C 38.92, H 2.33; found: C 39.24, H 2.36.

**2,7-Diido-phenanthrene B7** following the procedure by H. O. Wirth et al.<sup>[303]</sup>



2,7-Diido-9,10-dihydro-phenanthrene **B6** (2.160 g, 5.00 mmol) was dissolved in  $\text{CCl}_4$  (35 ml). Then N-bromosuccinimide (0.900 g, 5.00 mmol) and a trace of dibenzoylperoxide were added and the reaction refluxed for 4 h. The formed solid was collected by filtration and dried overnight. The crude orange product was stirred with 50 ml of ethanol at room temperature for 3 h. After filtration a white solid was obtained (1.807 g, 4.20 mmol; 84%). M.p.: 229.5 – 230.5 °C (Lit.<sup>[303]</sup>: 231.0 °C).

$^1\text{H}$ -NMR (300 MHz,  $\text{CDCl}_3$ ):  $\delta$  = 7.62 (s, 2 H), 7.91 (dd,  $^3J(\text{H},\text{H})$  = 9 Hz,  $^4J(\text{H},\text{H})$  = 2 Hz, 2H), 8.25 (d,  $^4J(\text{H},\text{H})$  = 2 Hz, 2 H), 8.34 (d,  $^3J(\text{H},\text{H})$  = 9 Hz, 2 H).

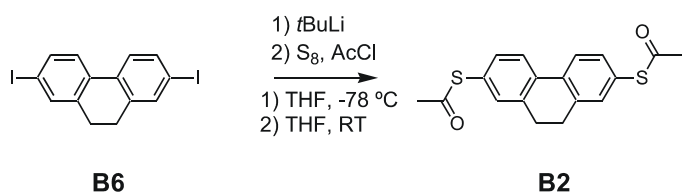
$^{13}\text{C}$ -NMR (75 MHz,  $\text{CDCl}_3$ ):  $\delta$  = 92.73 (CI), 124.21 (C4, C5), 126.69 (C9, C10), 129.08 (C4a, C4b), 133.68 (C8a, C10a), 135.53 (C3, C6), 137.31 (C1, C8).

MS (EI):  $m/z$  (%) = 430.0 (57) [ $\text{M}^+$ ], 176.0 (100) [ $\text{M}^+ - 2 \text{I}$ ], 150.0 (14), 88.1 (17).

Elemental analysis calcd. (%) for  $\text{C}_{14}\text{H}_8\text{I}_2$  (430.02): C 39.10, H 1.88; found: C 38.91, H 1.87.

### 2,7-Bis-(acetylsulfanyl)-9,10-dihydro-phenanthren **B2**

Method 1:



In a two-necked flask 2,7-diido-9,10-dihydro-phenanthrene **B6** (1.080 g, 2.50 mmol) was dissolved in dry THF (15 ml). The solution was cooled to –78 °C using dry ice/acetone and treated with *tert*-butyllithium (5.34 g of a 15% solution in pentane, 12.50 mmol). After stirring for 45 min sulphur (0.160 g, 5.00 mmol) was added, the dry ice/acetone bath removed

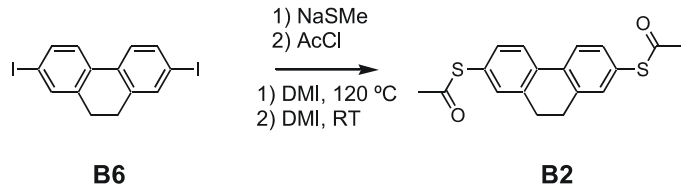
and the mixture stirred for another 90 min. Now acetyl chloride (1.104 g, 14.06 mmol) was carefully dropped in while cooling with a dry ice/acetone bath, the cooling was removed and the reaction mixture stirred at room temperature for 17 h. The mixture was poured into ice/water, the aqueous phase extracted with toluene, the combined organic extracts washed with water once, dried over  $\text{MgSO}_4$  and the solvents removed in vacuo. Column chromatography (silica gel, hexane/diethylether 7/3) afforded **B2** as a yellow solid which was re-crystallised from diethylether/hexane giving a white solid (0.081 g, 0.25 mmol; 10%). M.p.: 137.0 °C.

$R_f = 0.20$ .

$^1\text{H}$ -NMR (300 MHz,  $\text{CDCl}_3$ ):  $\delta = 2.44$  (s, 6H), 2.90 (s, 4H), 7.302 (d,  $^4J(\text{H},\text{H}) = 2$  Hz, 2 H), 7.35 (dd,  $^3J(\text{H},\text{H}) = 8$  Hz,  $^4J(\text{H},\text{H}) = 2$  Hz, 2 H), 7.77 (d,  $^3J(\text{H},\text{H}) = 8$  Hz, 2 H).

$^{13}\text{C}$ -NMR (75 MHz,  $\text{CDCl}_3$ ):  $\delta = 28.61$  ( $\text{CH}_3\text{CO}$ ), 30.28 ( $\text{CH}_2$ ), 124.79 (C3, C6), 127.20 (C4, C5), 133.04 (C1, C8), 134.01 (C2, C7), 134.96 (C4a, C4b), 138.45 (C8a, C10a), 194.25 (CO).

Route 2:



2,7-Diido-9,10-dihydro-phenanthrene **B6** (0.648 g, 1.50 mmol) was dissolved in dry,  $\text{N}_2$ -saturated DMI (5 ml) and the mixture heated to 120°C. Now sodium methanethiolate (1.052 g, 15.00 mmol) was added at once. The reaction mixture was kept at this temperature for 17 h and then cooled to room temperature. After addition of acetyl chloride (1.178 g, 15.00 mmol) the solution was stirred at room temperature for 3 h and then poured on ice/water. The aqueous phase was extracted with toluene, the organic extracts were dried over  $\text{MgSO}_4$  and the solvent removed by rotary evaporation. The red liquid was purified by column chromatography (silica gel, toluene/diethylether 40/1) giving **B2** as a white solid (0.354 g, 1.08 mmol; 72%). M.p.: 137.5 °C.

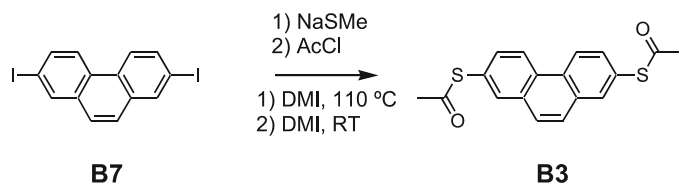
$^1\text{H}$ -NMR (300 MHz,  $\text{CDCl}_3$ ):  $\delta = 2.44$  (s, 6H), 2.90 (s, 4H), 7.302 (d,  $^4J(\text{H},\text{H}) = 2$  Hz, 2 H), 7.35 (dd,  $^3J(\text{H},\text{H}) = 8$  Hz,  $^4J(\text{H},\text{H}) = 2$  Hz, 2 H), 7.77 (d,  $^3J(\text{H},\text{H}) = 8$  Hz, 2 H).

MS (EI):  $m/z$  (%) = 328.2 (23) [ $M^+$ ], 286.1 (23) [ $M^+ - \text{CH}_3\text{CO}$ ], 244.1 (100) [ $M^+ - 2 \text{CH}_3\text{CO}$ ], 209.0 (13), 178.1 (15), 165.1 (18).

Elemental analysis calcd. (%) for  $\text{C}_{18}\text{H}_{16}\text{O}_2\text{S}_2$  (328.45): C 65.82, H 4.91; found: C 65.76, H 4.89.

UV/Vis ( $1 \times 10^{-5}$  n-hexane):  $\lambda_{\text{max}} (\varepsilon)$  = 214.0 (52500), 294.5 (35500), 312.5 (28700),

### 2,7-Bis-(acetylsulfanyl)-phenanthrene **B3**



2,7-Diodophenanthrene **B7** (0.645 g, 1.50 mmol) was dissolved in dry,  $\text{N}_2$ -saturated DMI (5 ml) and the mixture heated to 110 °C. Now sodium methanethiolate (1.052 g, 15.00 mmol) was added at once. The reaction mixture was kept at this temperature for 15 h and then cooled to room temperature. After addition of acetyl chloride (1.178 g, 15.00 mmol) the solution was stirred at room temperature for 3 h and then poured on ice/water. The aqueous phase was extracted with toluene, the organic extracts were dried over  $\text{MgSO}_4$  and the solvent removed by rotary evaporation. The red solid was purified by column chromatography (silica gel, toluene/diethylether 40/1) providing **B3** as a white solid (0.307 g, 0.94 mmol; 63%). M.p.: 197.0 – 198.5 °C.

$R_f$  = 0.21.

$^1\text{H-NMR}$  (300 MHz,  $\text{CDCl}_3$ ):  $\delta$  = 2.49 (s, 6 H), 7.68 (dd,  $^3J(\text{H,H})$  = 9 Hz,  $^4J(\text{H,H})$  = 2 Hz, 2 H), 7.75 (s, 2 H), 7.99 (d,  $^4J(\text{H,H})$  = 2 Hz, 2 H), 8.70 (d,  $^3J(\text{H,H})$  = 9 Hz, 2 H).

$^{13}\text{C-NMR}$  (75 MHz,  $\text{CDCl}_3$ ):  $\delta$  = 30.39 ( $\text{CH}_3$ ), 123.90 (C4, C5), 126.82 (C4a, C4b), 127.38 (C9, C10), 130.33 (C8a, C10a), 132.12 (C3, C6), 132.83 (C1, C8), 134.62 (C2, C7), 193.98 (CO).

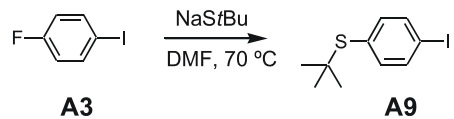
MS (EI):  $m/z$  (%) = 326.1 (26) [ $M^+$ ], 284.1 (26) [ $M^+ - \text{CH}_3\text{CO}$ ], 242 (100) [ $M^+ - 2 \text{CH}_3\text{CO}$ ], 208 (29) [ $M^+ - 2 \text{CH}_3\text{CO}, - \text{S}$ ].

Elemental analysis calcd. (%) for  $\text{C}_{18}\text{H}_{14}\text{O}_2\text{S}_2$  (326.43): C 66.23, H 4.32; found: C 66.02, H 4.34.

UV/Vis ( $1 \times 10^{-5}$  n-hexane):  $\lambda_{\text{max}} (\varepsilon)$  = 218.5 (32100), 268.0 (80400), 292.5 (32200), 326.5 (430), 334.5 (290), 341.5 (610), 350.5 (450), 359.0 (880).

### 6.3.2 Phenyl–ethynyl–anthracene

#### 1-*tert.*-Butylsulfanyl-4-iodo-benzene A9



1-Fluoro-4-iodo-benzene **A3** (2.220 g, 10.00 mmol) was dissolved in dry DMF (30 ml) and the mixture heated to 70 °C. Then sodium-2-methyl-2-propanethiolate (1.346 g, 12.00 mmol) was added in portions. After 4 h at this temperature the mixture was poured into saturated NaCl-solution. The aqueous phase was extracted with diethylether, the ethereal layers washed with water, dried over MgSO<sub>4</sub> and the solvents removed *in vacuo*. The crude product was purified by column chromatography (silica gel, hexane/toluene 20/1) providing **A9** (1.276 g, 4.37 mmol; 44%) as a white solid. M.p.: 60.0 – 61.0 °C.

$R_f = 0.52$ .

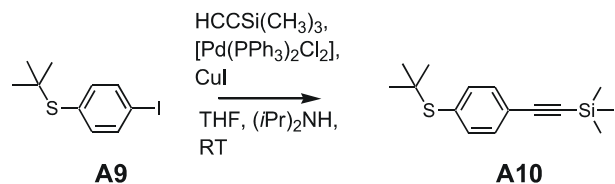
<sup>1</sup>H-NMR (300 MHz, CDCl<sub>3</sub>):  $\delta = 1.23$  (s, 9 H), 7.25 (d, <sup>3</sup>J(H,H) = 8 Hz, 2 H), 7.66 (d, <sup>3</sup>J(H,H) = 8 Hz, 2 H).

<sup>13</sup>C-NMR (75 MHz, CDCl<sub>3</sub>):  $\delta = 30.92$  (CH<sub>3</sub>), 46.24 (C(CH<sub>3</sub>)<sub>3</sub>), 95.34 (C4), 132.60 (C1), 137.67 (C3), 139.16 (C2).

MS (EI): *m/z* (%) = 292.1 (19) [M<sup>+</sup>], 236 (100) [M<sup>+</sup> – *t*Bu], 134 (15), 109.1 (25) [M<sup>+</sup> – *t*Bu, – I], 57.2 (40) [*t*Bu].

Elemental analysis calcd (%) for C<sub>10</sub>H<sub>13</sub>IS (292.18): C 41.11, H 4.48; found: C 41.22, H 4.38.

#### 1-*tert.*-Butylsulfanyl-4-(trimethylsilylethynyl)-benzene A10



1-*tert.*-Butylsulfanyl-4-iodo-benzene **A9** (0.450 g, 1.54 mmol) was dissolved in Ar-saturated, dry THF (20 ml). Then trimethylsilylacetylene (0.227 g, 2.31 mmol) and dry diisopropylamine (0.35 ml) were added and the mixture stirred at RT for 1 h. After the

addition of trans–bis(triphenylphosphane)platinum(II) chloride (0.055 g, 0.08 mmol) and copper(I) iodide (0.002 g, 0.008 mmol) the solution was stirred at RT for 48 h. Then the reaction mixture was poured into H<sub>2</sub>O (about 50 ml), the aqueous phase extracted with diethylether, the ethereal layers dried over MgSO<sub>4</sub> and evaporated to dryness. Column chromatography (silica gel, hexane/toluene 20/1) provided **A10** (0.374 g, 1.42 mmol; 92%) as a yellow liquid.

$R_f = 0.49$ .

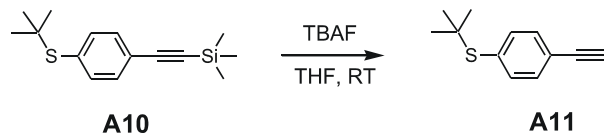
<sup>1</sup>H–NMR (300 MHz, CDCl<sub>3</sub>):  $\delta = 0.25$  (s, 9 H), 1.27 (s, 9 H), 7.41 (d, <sup>3</sup>J(H,H) = 8 Hz, 2 H), 7.46 (d, <sup>3</sup>J(H,H) = 8 Hz, 2 H).

<sup>13</sup>C–NMR (75 MHz, CDCl<sub>3</sub>):  $\delta = -0.03$  ((CH<sub>3</sub>)<sub>3</sub>Si), 30.98 (CH<sub>3</sub>), 46.46 (C(CH<sub>3</sub>)<sub>3</sub>), 95.92, 104.46, (C≡C), 123.46 (C4), 131.88 (C3), 133.48 (C1), 137.16 (C2).

MS (EI):  $m/z$  (%) = 262.2 (18) [M<sup>+</sup>], 206.1 (83) [M<sup>+</sup> – tBu], 191.0 (100) [M<sup>+</sup> – TMS], 115.1 (14), 57.2 (23) [tBu].

Elemental analysis calcd (%) for C<sub>15</sub>H<sub>22</sub>SSi (262.49): C 68.64, H 8.45; found: C 68.76, H 8.15.

### 1–*tert*.–Butylsulfanyl–4–ethynyl–benzene **A11**



1–*tert*.–Butylsulfanyl–4–(trimethylsilylethynyl)–benzene **A10** (0.7875 g, 3.00 mmol) was dissolved in THF (15 ml) and tetrabutylammonium fluoride trihydrate (1.420 g, 4.50 mmol) added in two portions at 0 °C. The ice bath was removed and the mixture stirred at RT for 2 h. Then the reaction mixture was filtered through a plug of silica gel, washed with CH<sub>2</sub>Cl<sub>2</sub> several times and the solvents removed *in vacuo* affording **A11** (0.571 g, 3.00 mmol; 100%) as a brown liquid without further purification.

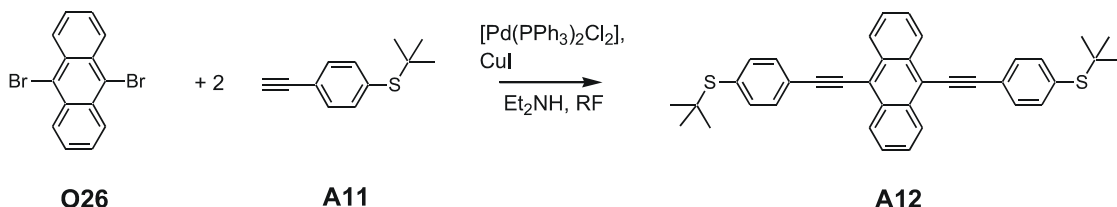
<sup>1</sup>H–NMR (300 MHz, CDCl<sub>3</sub>):  $\delta = 1.28$  (s, 9 H), 3.15 (s, 1 H), 7.44 (d, <sup>3</sup>J(H,H) = 8 Hz, 2 H), 7.49 (d, <sup>3</sup>J(H,H) = 8 Hz, 2 H).

<sup>13</sup>C–NMR (75 MHz, CDCl<sub>3</sub>):  $\delta = 30.99$  (CH<sub>3</sub>), 46.54 (C(CH<sub>3</sub>)<sub>3</sub>), 78.65, 83.12 (C≡C), 122.45 (C4), 132.07 (C3), 133.92 (C1), 137.22 (C2).

MS (EI):  $m/z$  (%) = 190.1 (10) [M<sup>+</sup>], 134 (100) [M<sup>+</sup> – tBu], 89.1 (15), 57.2 (16) [tBu].

Elemental analysis calcd (%) for C<sub>12</sub>H<sub>14</sub>S (190.31): C 75.74, H 7.42; found: C 75.44, H 7.04.

**9,10-Bis-(4-*tert*-butylsulfanyl-phenylethyynyl)-anthracene A12**



9,10-Dibromoanthracene (0.510 g, 1.52 mmol) was suspended in dry, Ar-saturated diethylamine (23 ml). Then copper iodide (0.023 g, 0.12 mmol), trans-bis(triphenylphosphane)platinum(II) chloride (0.042 g, 0.60 mmol) and 1-*tert*-butylsulfanyl-4-ethynylbenzene **A11** (0.794 g, 4.17 mmol) were added subsequently. The reaction mixture was heated to reflux under an Ar-atmosphere for 6 h. Filtration and washing with CH<sub>2</sub>Cl<sub>2</sub> followed by column chromatography (silica gel, hexane/toluene 2/1) provided **A12** (0.595 g, 1.07 mmol; 70%) as a yellow-orange solid. M.p.: 222.0 – 223.0 °C (decomp.).

R<sub>f</sub> = 0.38

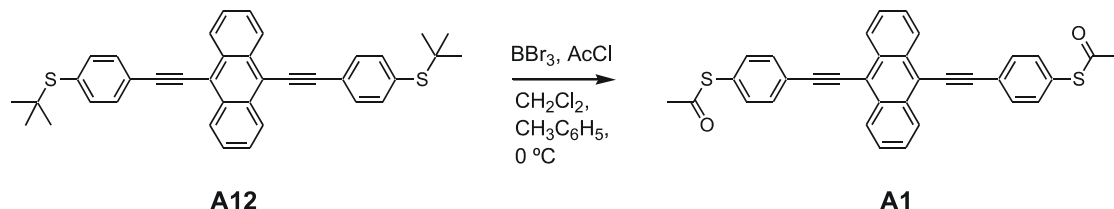
<sup>1</sup>H-NMR (300 MHz, CDCl<sub>3</sub>): δ = 1.35 (s, 18 H), 7.61 – 7.68 (m, 8 H), 7.74 (d, J(H,H) = 6 Hz, 4 H), 8.67 – 8.70 (m, 4 H).

<sup>13</sup>C-NMR (75 MHz, CDCl<sub>3</sub>): δ = 31.42 (CH<sub>3</sub>), 47.11 (C(CH<sub>3</sub>)<sub>3</sub>), 88.37, 102.38 (C≡C), 118.81, 124.11, 127.36, 127.62, 131.97, 132.49, 134.20, 137.87 (Ar).

MALDI-TOF-MS: 553.95 [M<sup>+</sup>], 497.88 [M<sup>+</sup> - tBu], 330.91 [M<sup>+</sup> - tBu, - PhStBu].

Elemental analysis calcd (%) for C<sub>38</sub>H<sub>34</sub>S<sub>2</sub> (554.81): C 82.26, H 6.18; found: C 81.89, H 6.27.

**9,10-Bis-(4-acetylsulfanyl-phenylethyynyl)-anthracene A1**



9,10-Bis-(4-*tert*-butylsulfanyl-phenylethyynyl)-anthracene **A12** (0.023 g, 0.042 mmol) was dissolved in a mixture of dry Ar-saturated CH<sub>2</sub>Cl<sub>2</sub> (1.5 ml) and dry Ar-saturated toluene (1.5 ml). The mixture was cooled to 0 °C and acetyl chloride (0.126 g, ca. 0.12 ml, 1.60 mmol)

added and after that boron tribromide (1.0 M solution in CH<sub>2</sub>Cl<sub>2</sub>, 0.09 ml, 0.09 mmol) dropped in. After removal of the ice bath the reaction was stirred at room temperature for 3 h and then poured in ice–water (about 100 ml). The aqueous phase was extracted with diethylether, the ethereal layers washed with water until neutral, dried over MgSO<sub>4</sub> and evaporated to dryness. Column chromatography (silica gel, CH<sub>2</sub>Cl<sub>2</sub>/hexane 2/1) and subsequent washing with diethylether afforded **A1** (0.011 g, 0.02 mmol; 49%) as a yellow–red solid. M.p.: 248.0 – 249.0 °C.

R<sub>f</sub> = 0.30.

<sup>1</sup>H-NMR (300 MHz, CDCl<sub>3</sub>): δ = 2.48 (s, 6 H), 7.51 (d, <sup>3</sup>J(H,H) = 8 Hz, 4 H), 7.65 – 7.68 (m, 4 H), 7.81 (d, <sup>3</sup>J(H,H) = 8 Hz, 4 H), 8.65 – 8.69 (m, 4 H).

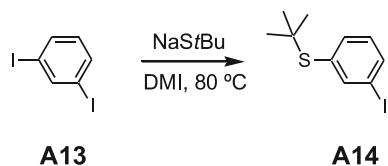
<sup>13</sup>C-NMR (75 MHz, CDCl<sub>3</sub>): δ = 30.38 (CH<sub>3</sub>), 88.14, 101.74 (C≡C), 118.41, 124.57, 127.06, 127.21, 128.63, 132.17, 132.26, 134.47 (Ar), 193.43 (CO).

MALDI-TOF-MS: 525.91 [M<sup>+</sup>], 452.80 [M<sup>+</sup> – SAc].

Elemental analysis (%) calcd. for C<sub>34</sub>H<sub>22</sub>O<sub>2</sub>S<sub>2</sub> (526.67) C 77.54, H 4.21; found: C 77.38, H 4.32.

UV/Vis (1 × 10<sup>-5</sup> acetonitrile): λ<sub>max</sub> (ε) = 205.0 (35700), 242.0 (21200), 271.0 (59000), 306.5 (17800), 319.5 (28100), 444.0 (26500), 470.5 (28800).

### 1-*tert*.-Butylsulfanyl-3-iodo-benzene **A14**



1,3-Diiodobenzene **A13** (3.311 g, 10.40 mmol) was dissolved in dry DMI (50 ml), sodium-2-methyl-2-propanethiolate (1.126 g, 10.40 mmol) was added and the reaction stirred at 80 °C for 9 h. The mixture was poured into saturated NaCl-solution. The aqueous phase was extracted with diethylether, the ethereal layers washed with water, dried over Na<sub>2</sub>SO<sub>4</sub> and the solvents removed *in vacuo*. The crude product was purified by column chromatography (silica gel, hexane/toluene 20/1) providing **A14** (1.610 g, 5.51 mmol; 53%) as a yellowish oil.

R<sub>f</sub> = 0.50.

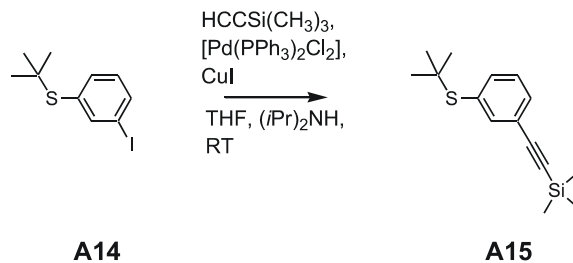
<sup>1</sup>H-NMR (300 MHz, CDCl<sub>3</sub>): δ = 1.29 (s, 9 H), 7.07 (t, <sup>3</sup>J(H,H) = 8 Hz, 1 H), 7.50 (td, <sup>3</sup>J(H,H) = 8 Hz, <sup>4</sup>J(H,H) = 2 Hz, 1 H), 7.69 (td, <sup>3</sup>J(H,H) = 8 Hz, <sup>4</sup>J(H,H) = 2 Hz, 1 H), 7.91 (t, <sup>4</sup>J(H,H) = 2 Hz, 1 H).

<sup>13</sup>C-NMR (75 MHz, CDCl<sub>3</sub>): δ = 30.96 (CH<sub>3</sub>), 46.45 (C(CH<sub>3</sub>)<sub>3</sub>), 93.86 (C3), 129.99 (C5), 135.07 (C1), 136.59 (C6), 137.65 (C4), 145.62 (C2).

MS (EI): *m/z* (%) = 291.8 (42) [M<sup>+</sup>], 235.8 (100) [M<sup>+</sup> - *t*Bu], 109.1 (10) [M<sup>+</sup> - *t*Bu, -I], 57.2 (32) [*t*Bu].

Elemental analysis (%) calcd. for C<sub>10</sub>H<sub>13</sub>IS (292.18): C 41.11, H 4.48; found: C 41.30, H 4.32.

### 1-*tert*.-Butylsulfanyl-3-(trimethylsilylethynyl)-benzene A15



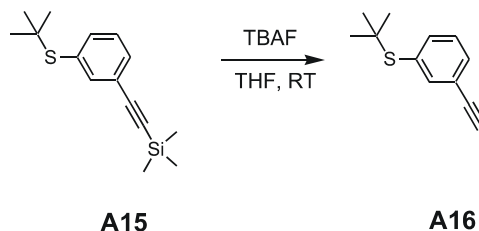
This compound was prepared from 1-*tert*.-butylsulfanyl-3-iodo-benzene **A14** (0.438 g, 1.50 mmol) following the procedure described for 1-*tert*.-Butylsulfanyl-4-(trimethylsilylethynyl)-benzene **A10**. **A15** was obtained as a yellow liquid (0.360 g, 1.37 mmol; 91%).

R<sub>f</sub> = 0.49.

<sup>1</sup>H-NMR (300 MHz, CDCl<sub>3</sub>): δ = 0.25 (s, 9 H), 1.29 (s, 9 H), 7.26 (t, <sup>3</sup>J(H,H) = 8 Hz, 1 H), 7.44 – 7.49 (m, 2H), 7.64 (dd, <sup>4</sup>J(H,H) = 2 Hz, <sup>4</sup>J(H,H) = 2 Hz, 1 H).

<sup>13</sup>C-NMR (75 MHz, CDCl<sub>3</sub>): δ = -0.01 ((CH<sub>3</sub>)<sub>3</sub>Si), 31.03 ((CH<sub>3</sub>)<sub>3</sub>C), 46.13 (C(CH<sub>3</sub>)<sub>3</sub>), 94.83, 104.37 (C≡C), 123.56 (C3), 128.30 (C5), 132.20 (C4), 132.94 (C1), 137.60 (C6), 140.55 (C2). MS (EI): *m/z* (%) = 262.0 (44) [M<sup>+</sup>], 205.0 (98) [M<sup>+</sup> - *t*Bu], 190.9 (100) [M<sup>+</sup> - TMS], 57.2 (13) [*t*Bu].

Elemental analysis (%) calcd. for C<sub>15</sub>H<sub>22</sub>SSi (262.49): C 68.64, H 8.45; found: C 68.94, H 8.57.

**1-*tert.*-Butylsulfanyl-3-ethynyl-benzene A16**

This compound was synthesised from 1-*tert.*-butylsulfanyl-3-(trimethylsilylethynyl)-benzene **A15** (0.354 g, 1.35 mmol) according to the procedure shown for 1-*tert.*-butylsulfanyl-4-ethynyl-benzene **A11**. **A16** was obtained as a yellowish liquid (0.223 g, 1.17 mmol; 87%) after column chromatography (silica gel, hexane/toluene 20/1).

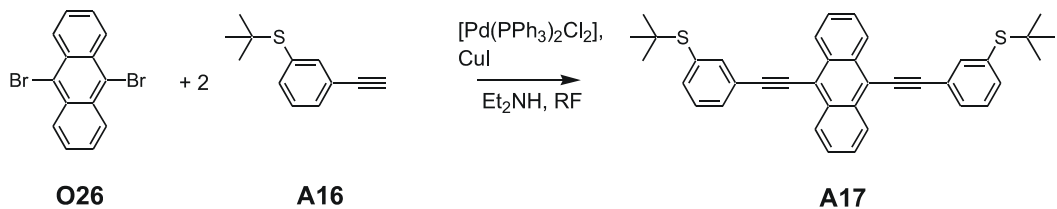
$R_f = 0.41$ .

$^1\text{H}$ -NMR (300 MHz,  $\text{CDCl}_3$ ):  $\delta = 1.29$  (s, 9 H), 3.10 (s, 1 H), 7.29 (t,  $^3J(\text{H},\text{H}) = 8$  Hz, 1 H), 7.47 – 7.54 (m, 2 H), 7.67 (dd,  $^4J(\text{H},\text{H}) = 2$  Hz,  $^4J(\text{H},\text{H}) = 2$  Hz, 1 H).

$^{13}\text{C}$ -NMR (75 MHz,  $\text{CDCl}_3$ ):  $\delta = 30.98$  ( $(\text{CH}_3)_3\text{C}$ ), 46.21 ( $\text{C}(\text{CH}_3)_3$ ), 77.81, 83.02 ( $\text{C}\equiv\text{C}$ ), 122.50 (C3), 128.43 (C5), 132.35 (C4), 133.11 (C1), 137.93 (C6), 140.75 (C2).

MS (EI):  $m/z$  (%) = 190.0 (41) [ $\text{M}^+$ ], 134 (100) [ $\text{M}^+ - t\text{Bu}$ ], 57.2 (18) [ $t\text{Bu}$ ].

Elemental analysis (%) calcd. for  $\text{C}_{12}\text{H}_{14}\text{S}$  (190.31): C 75.74, H 7.42; found: C 75.59, H 7.06.

**9,10-Bis-(3-*tert.*-butylsulfanyl-phenylethyynyl)-anthracene A17**

Starting from 1-*tert.*-Butylsulfanyl-3-ethynyl-benzene **A16** (0.223 g, 1.17 mmol) **A17** was prepared following the synthetic protocol described for 9,10-Bis-(4-*tert.*-butylsulfanyl-phenylethyynyl)-anthracene **A12**. Column chromatography (silica gel, hexane/toluene 2/1) and subsequent re-crystallisation from ethanol/toluene (5/1) afforded **A17** as a red solid (0.149 g, 0.27 mmol; 63%). M.p.: 209.0–210.0 °C.

$R_f = 0.27$ .

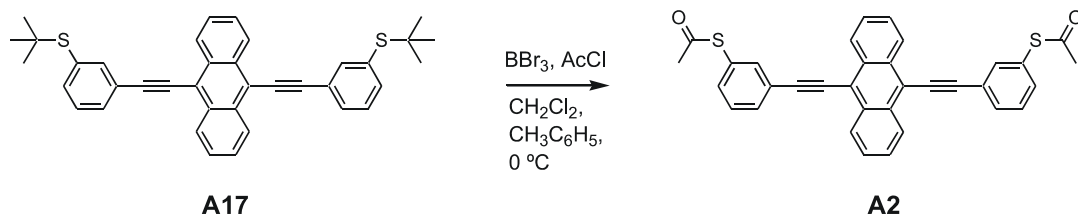
<sup>1</sup>H-NMR (300 MHz, CDCl<sub>3</sub>): δ = 1.37 (s, 18 H), 7.44 (t, <sup>3</sup>J(H,H) = 8 Hz, 2 H), 7.60 (ddd, <sup>3</sup>J(H,H) = 8 Hz, <sup>4</sup>J(H,H) = 2 Hz, <sup>4</sup>J(H,H) = 2 Hz, 2 H), 7.65 – 7.69 (m, 4 H), 7.78 (ddd, <sup>3</sup>J(H,H) = 8 Hz, <sup>4</sup>J(H,H) = 2 Hz, <sup>4</sup>J(H,H) = 2 Hz, 2H), 7.95 (dd, <sup>4</sup>J(H,H) = 2 Hz, <sup>4</sup>J(H,H) = 2 Hz, 2 H), 8.68 – 8.71 (m, 4 H).

<sup>13</sup>C-NMR (75 MHz, CDCl<sub>3</sub>): δ = 31.09 (CH<sub>3</sub>)<sub>3</sub>C), 46.40 (C(CH<sub>3</sub>)<sub>3</sub>), 87.07, 101.80 (C≡C), 118.41, 123.84, 127.01, 127.25, 128.71, 131.92, 132.15, 133.36, 137.76, 140.23 (Ar).

MALDI-TOF-MS: 719.76 [M<sup>+</sup> – tBu, +matrix], 553.81 [M<sup>+</sup>], 497.76 [M<sup>+</sup> – tBu], 441.70 [M<sup>+</sup> – 2 tBu].

Elemental analysis (%) calcd. for C<sub>38</sub>H<sub>34</sub>S<sub>2</sub> (554.81): C 82.26, H 6.18; found: C 82.20, H 5.90.

### 9,10-Bis-(3-acetylsulfanyl-phenylethyynyl)-anthracene A2



This compound was prepared according to the synthetic procedure described for 9,10-Bis-(4-acetylsulfanyl-phenylethyynyl)-anthracene **A1** starting from 9,10-Bis-(3-*tert*-butylsulfanyl-phenylethyynyl)-anthracene **A22** (0.021 g, 0.038 mmol). Column chromatography (silica gel, CH<sub>2</sub>Cl<sub>2</sub>/Hexane 2/1) provided **A2** as an orange solid (0.014 g, 0.027 mmol; 70%). M.p.: 203.0 – 205.0 °C (decomp.).

R<sub>f</sub> = 0.28.

<sup>1</sup>H-NMR (300 MHz, CDCl<sub>3</sub>): δ = 2.49 (s, 6 H), 7.46 – 7.54 (m, 4 H), 7.64 – 7.67 (m, 4 H), 7.80 – 7.83 (m, 4 H), 8.65 – 8.68 (m, 4 H).

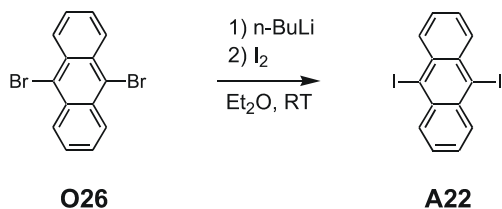
<sup>13</sup>C-NMR (75 MHz, CDCl<sub>3</sub>): δ = 30.36 (CH<sub>3</sub>CO), 87.53, 101.31 (C≡C), 118.36, 124.64, 127.03, 127.22, 128.57, 129.41, 132.15, 132.65, 134.76, 137.33 (Ar), 193.57 (COCH<sub>3</sub>).

MALDI-TOF-MS: 525.81 [M<sup>+</sup>], 514.75, 505.75, 451.70 [M<sup>+</sup>-SAcetyl], 409.70.

Elemental analysis (%) calcd. for C<sub>34</sub>H<sub>22</sub>O<sub>2</sub>S<sub>2</sub> (526.67) C 77.54, H 4.21; found: C 77.17, H 4.35.

UV/Vis (1 × 10<sup>-5</sup> acetonitrile): λ<sub>max</sub> (ε) = 210.0 (56700), 271.0 (59100), 299.0 (16400), 311.5 (22600), 438.0 (22400), 464.5 (24600).

**9,10-Diidoanthracene A22** following the protocol from B. F. Duerr et al. [337]



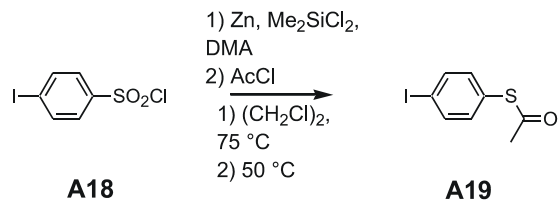
9,10-Dibromoanthracene **O26** (33.602 g, 100.00 mmol) was dissolved in dry diethylether (330 ml) and n–butyllithium (103.2 ml of a 2.5 M solution in hexane, 262.00 mol) dropped in *via* syringe over the course of 30 min. Then the resulting mixture was stirred at RT for an additional 30 min. Now iodine crystals (85.280 g, 336.00 mol) were added through the top of the reflux condenser over the course of 15 min and the mixture stirred for 30 min. When the dark mixture was washed with 20% Na<sub>2</sub>S<sub>2</sub>O<sub>4</sub>–solution several times an orange solid precipitated that was collected and dried. Re–crystallisation from CCl<sub>4</sub> afforded **A22** as a yellow solid (6.194 g, 14.40 mmol; 14%). M.p. : 252.0 – 253.0 °C (Lit.<sup>[337]</sup>: 254.0 – 255.0 °C).

<sup>1</sup>H–NMR (300 MHz, CDCl<sub>3</sub>): δ = 7.59 – 7.62 (m, 4 H), 8.53 – 8.57 (m, 4 H).

<sup>13</sup>C–NMR (75 MHz, CDCl<sub>3</sub>): δ = 108.76, 127.99, 134.16, 134.44.

MS (EI): *m/z* (%) = 429.7 (100) [M<sup>+</sup>], 303.9 (62) [M<sup>+</sup> – I], 176.0 (67) [M<sup>+</sup> – 2 I].

**1–Acetylsulfanyl–4–iodo–benzene A19** following the protocol from D. T. Gryko et al.<sup>[334]</sup>



To a stirred suspension of zinc powder (22.690 g, 0.347 mol) and dichlorodimethylsilane (44.790 g, 0.347 mol) in 1,2–dichloroethane (750 ml) was added a solution of 4–iodobenzenesulfonyl chloride **A18** (30.000 g, 0.099 mol) and *N,N*–dimethylacetamide (25.91 g, 0.297 mol) in 1,2–dichlorethane (750 ml). The mixture was stirred at 75 °C for 2 h until the zinc powder was no longer visible. Then the reaction mixture was cooled to 50 °C and acetyl chloride (10.060 g, 9.14 ml, 0.128 mol) was added. After 15 min the mixture was poured into water. The aqueous layer was extracted with CH<sub>2</sub>Cl<sub>2</sub> and the combined organic layers were

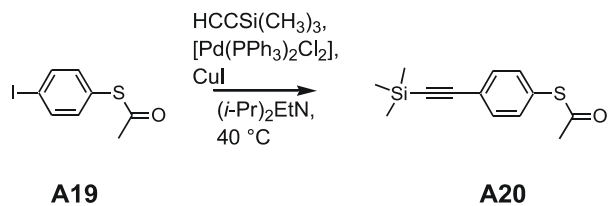
dried over  $\text{Na}_2\text{SO}_4$ . After removal of the solvents by rotary evaporation a colourless liquid was obtained that was purified by column chromatography (silica gel, Hexane/ $\text{CH}_2\text{Cl}_2$  4/1) providing **A19** as a white solid (25.250 g, 0.091 mol; 92%).

$R_f = 0.25$ .

$^1\text{H}$ -NMR (300 MHz,  $\text{CDCl}_3$ ):  $\delta = 2.43$  (s, 3 H), 7.13 (d,  $^3J(\text{H},\text{H}) = 8$  Hz, 2 H), 7.74 (d,  $^3J(\text{H},\text{H}) = 8$  Hz, 2 H).

$^{13}\text{C}$ -NMR (75 MHz,  $\text{CDCl}_3$ ):  $\delta = 29.22$  ( $\text{CH}_3\text{CO}$ ), 94.95 (C4), 126.63 (C1), 134.86 (C2), 137.23 (C3), 192.06 (CO).

### 1-Acetylsulfanyl-4-(trimethylsilylethyynyl)-benzene **A20**<sup>[334]</sup>

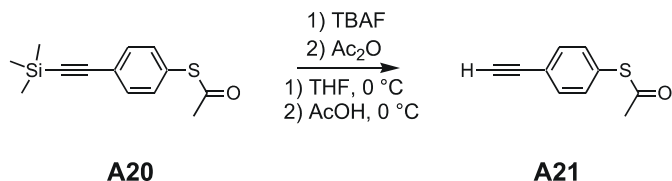


1-Acetylsulfanyl-4-iodo-benzene **A19** (30.00 g, 0.108 mol) was dissolved in dry, Ar-saturated ethyl-diisopropylamine (300 ml).  $[\text{Pd}(\text{PPh}_3)_2\text{Cl}_2]$  (3.020 g, 4.30 mmol) was added and the mixture stirred for 10 min at room temperature. Then copper(I) iodide (1.640 g, 8.61 mmol) and trimethylsilylacetylene (21.190 g, 0.216 mol) were added and the mixture heated to 40 °C for 20 h. The solution was poured into 2N hydrochloric acid/ice and extracted with diethylether. The organic phases were washed with sat.  $\text{NaHCO}_3$ -solution once, with sat.  $\text{NaCl}$ -solution twice and then the organic phase were dried over  $\text{Na}_2\text{SO}_4$ . After rotary evaporation of the solvents the crude product was purified by column chromatography (silica gel, hexane/diethylether 7/3) providing **A20** as a dark oil (26.30 g, 0.106 mol; 98%).

$R_f = 0.44$ .

$^1\text{H}$ -NMR (300 MHz,  $\text{CDCl}_3$ ):  $\delta = 0.25$  (s, 9 H), 2.42 (s, 3 H), 7.34 (dd,  $^3J(\text{H},\text{H}) = 8$  Hz,  $^4J(\text{H},\text{H}) = 2$  Hz, 2 H), 7.48 (dd,  $^3J(\text{H},\text{H}) = 8$  Hz,  $^4J(\text{H},\text{H}) = 2$  Hz, 2 H).

$^{13}\text{C}$ -NMR (75 MHz,  $\text{CDCl}_3$ ):  $\delta = -0.06$  ( $\text{CH}_3\text{Si}$ ), 30.32 ( $\text{CH}_3\text{CO}$ ), 96.24, 104.19 (C≡C), 124.38 (C4), 128.33 (C1), 132.55 (C2), 134.12 (C3), 193.39 (CO)

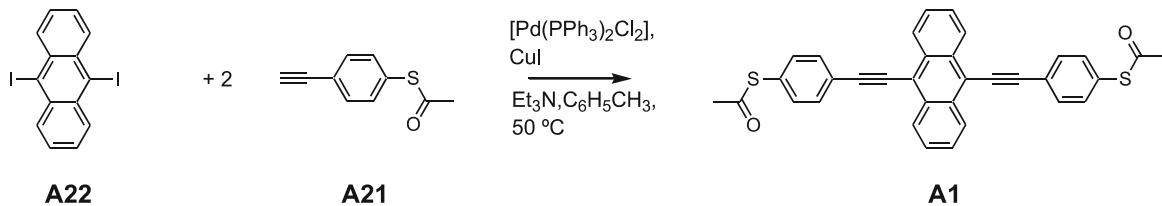
**1-Acetylsulfanyl-4-ethynyl-benzene A21<sup>[334]</sup>**

1-Acetylsulfanyl-4-(trimethylsilyl)ethynyl-benzene **A20** (26.30 g, 0.106 mol) and acetic anhydride (6 ml) were dissolved in THF (500 ml) and acetic acid (3 ml) and the solution cooled to 0 °C using an ice bath. Now TBAF (120.00 g, 0.380 mol) dissolved in THF (500 ml) was added. After the addition the ice bath was removed and the solution stirred at room temperature for 20 min. Then acetic anhydride (94 ml) was added at once and the mixture stirred for another 20 min at room temperature. The reaction mixture was filtered over silica gel and washed with THF. After removal of the solvents by rotary evaporation the crude product was purified by column chromatography (silica gel, hexane/diethylether 7/3) affording **A21** as a yellow oil (12.77 g, 0.072 mol; 69%).

$R_f = 0.42$ .

$^1\text{H}$ -NMR (300 MHz,  $\text{CDCl}_3$ ):  $\delta = 2.44$  (s, 3 H), 3.15 (s, 1 H), 7.37 (dd,  $^3J(\text{H},\text{H}) = 8$  Hz,  $^4J(\text{H},\text{H}) = 2$  Hz, 2 H), 7.52 (dd,  $^3J(\text{H},\text{H}) = 8$  Hz,  $^4J(\text{H},\text{H}) = 2$  Hz, 2 H).

$^{13}\text{C}$ -NMR (75 MHz,  $\text{CDCl}_3$ ):  $\delta = 30.34$  ( $\text{CH}_3\text{CO}$ ), 78.88, 82.86 ( $\text{C}\equiv\text{C}$ ), 123.35 (C4), 128.79 (C1), 132.75 (C2), 134.21 (C3), 193.32 (CO).

**9,10-Bis-(4-acetylsulfanyl-phenylethyynyl)-anthracene A1**

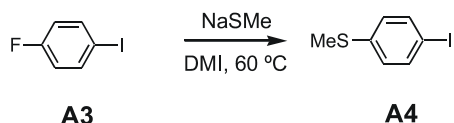
9,10-Diidoanthracene **A22** (0.256 g, 0.60 mmol) was dissolved in Ar-saturated triethylamine (1 ml) and toluene (15 ml). Then *trans*-bis(triphenylphosphane)platinum(II) chloride (0.069 g, 0.098 mmol), copper iodide (0.017 g, 0.09 mmol) and (4-ethynyl)phenyl thioacetate **A21** (0.262 g, 1.49 mmol) were added subsequently. The reaction mixture was heated to 50 °C for 4 h and, after cooling, poured on 2N hydrochloric acid/ice. The aqueous

phase was extracted with  $\text{CH}_2\text{Cl}_2$ , the organic layers dried over  $\text{MgSO}_4$  and evaporated to dryness leaving a dark solid. Column chromatography (silica gel,  $\text{CH}_2\text{Cl}_2/\text{Hexane}$  2/1) and subsequent re-crystallisation from toluene/methanol yielded **A1** as a yellow-red solid (0.155 g, 0.295 mmol; 50%). M.p.: 248.0 – 249.0 °C.

$^1\text{H}$ -NMR (300 MHz,  $\text{CDCl}_3$ ):  $\delta$  = 2.48 (s, 6 H), 7.51 (d,  $^3J(\text{H},\text{H})$  = 8 Hz, 4 H), 7.65 – 7.68 (m, 4 H), 7.81 (d,  $^3J(\text{H},\text{H})$  = 8 Hz, 4 H), 8.65 – 8.69 (m, 4 H).

$^{13}\text{C}$ -NMR (75 MHz,  $\text{CDCl}_3$ ):  $\delta$  = 30.37 ( $\text{CH}_3$ ), 88.15, 101.73 ( $\text{C}\equiv\text{C}$ ), 118.41, 124.58, 127.04, 127.21, 128.64, 132.17, 132.27, 134.47 (Ar), 193.44 (CO).

### 1-Iodo-4-methylsulfanyl-benzene **A4**



1-Fluoro-4-iodo-benzene **A3** (11.100 g, 50.00 mmol) was dissolved in dry DMI (30 ml). The solution was heated to 60 °C and then sodium methanethiolate (4.380 g, 62.48 mmol) suspended in dry DMI (20 ml) was added and the reaction kept at this temperature for 15 h. The mixture was poured into sat.  $\text{NaCl}$ -solution, the aqueous phase extracted with toluene, the collected toluene phases washed twice with sat.  $\text{NaCl}$ -solution and then dried over  $\text{MgSO}_4$ . After removal of the solvents by rotary evaporation a yellow liquid was obtained that was purified by column chromatography (silica gel, hexane/toluene 15/1) providing **A4** as a white solid. M.p.: 45.0 – 46.0 °C (Lit.<sup>[358]</sup>: 45 °C)

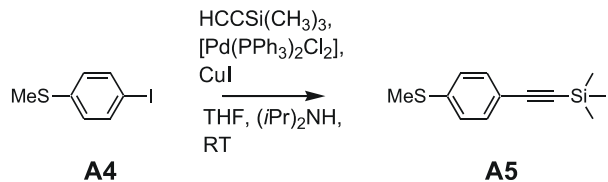
$R_f$  = 0.29.

$^1\text{H}$ -NMR (300 MHz,  $\text{CDCl}_3$ ):  $\delta$  = 2.46 (s, 3 H), 6.99 (td,  $^3J(\text{H},\text{H})$  = 9 Hz,  $^4J(\text{H},\text{H})$  = 2 Hz, 2 H), 7.58 (td,  $^3J(\text{H},\text{H})$  = 9 Hz,  $^4J(\text{H},\text{H})$  = 2 Hz, 2 H).

$^{13}\text{C}$ -NMR (75 MHz,  $\text{CDCl}_3$ ):  $\delta$  = 15.71 ( $\text{CH}_3$ ), 89.25 (C1), 128.28 (C3), 137.67 (C2), 138.67 (C4).

MS (EI):  $m/z$  (%) = 249.9 (100) [ $\text{M}^+$ ], 234.8 (9) [ $\text{M}^+ - \text{CH}_3$ ].

Elemental analysis (%) calcd. for  $\text{C}_7\text{H}_7\text{IS}$  (250.10): C 33.62, H 2.82; found: C 33.64, H 2.71.

**1-(Trimethylsilylethynyl)-4-methylsulfanyl-benzene A5**

This compound was prepared following the procedure described for 1-*tert.*-butylsulfanyl-4-(trimethylsilylethynyl)-benzene **A10** earlier starting from 1-iodo-4-methylsulfanyl-benzene **A4** (0.938 g, 3.75 mmol). After column chromatography (silica gel, hexane/toluene 20/1) **A5** was obtained as a yellow liquid (0.720 g, 3.27 mmol; 87 %).

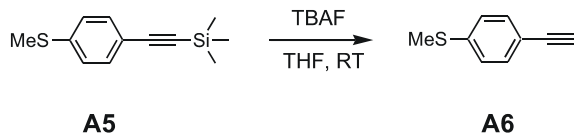
$R_f = 0.36$ .

$^1\text{H}$ -NMR (300 MHz,  $\text{CDCl}_3$ ):  $\delta = 0.25$  (s, 9 H), 2.47 (s, 3 H), 7.14 (td,  $^3J(\text{H,H}) = 9$  Hz,  $^4J(\text{H,H}) = 2$  Hz, 2 H), 7.37 (td,  $^3J(\text{H,H}) = 9$  Hz,  $^4J(\text{H,H}) = 2$  Hz, 2 H).

$^{13}\text{C}$ -NMR (75 MHz,  $\text{CDCl}_3$ ):  $\delta = 0.02$  ( $(\text{CH}_3)_3\text{Si}$ ), 15.33 ( $\text{CH}_3\text{S}$ ), 94.17, 104.89 (C=C), 119.36 (C1), 125.63 (C3), 132.26 (C2), 139.61 (C4).

MS (EI):  $m/z$  (%) = 220.0 (79) [ $\text{M}^+$ ], 205 (100) [ $\text{M}^+ - \text{CH}_3$ ], 189.9 (10) [ $\text{M}^+ - 2\text{CH}_3$ ].

Elemental analysis (%) calcd. for  $\text{C}_{12}\text{H}_{16}\text{SSi}$  (220.41): C 65.39, H 7.32; found: C 65.70, H 7.28.

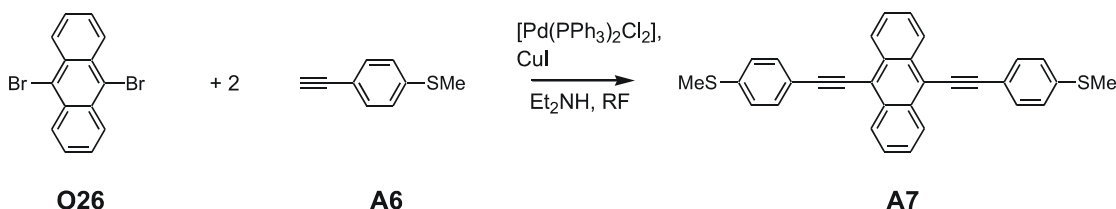
**1-Ethynyl-4-methylsulfanyl-benzene A6<sup>[359]</sup>**

1-Ethynyl-4-methylsulfanyl-benzene **A6** was synthesised starting from 1-(trimethylsilylethynyl)-4-methylsulfanyl-benzene **A5** (0.720 g, 3.26 mmol) according to the procedure described for 1-*tert.*-butylsulfanyl-4-ethynyl-benzene **A11**. A dark-brown liquid was obtained (0.480 g, 3.24 mmol; 99%).

$^1\text{H}$ -NMR (300 MHz,  $\text{CDCl}_3$ ):  $\delta = 2.49$  (s, 3 H), 3.07 (s, 1 H), 7.17 (td,  $^3J(\text{H,H}) = 8$  Hz,  $^4J(\text{H,H}) = 2$  Hz, 2 H), 7.40 (td,  $^3J(\text{H,H}) = 8$  Hz,  $^4J(\text{H,H}) = 2$  Hz, 2 H).

<sup>13</sup>C-NMR (75 MHz, CDCl<sub>3</sub>): δ = 15.31 (CH<sub>3</sub>), 77.21, 83.47 (C≡C), 118.28 (C1), 125.72 (C3), 132.42 (C2), 140.08 (C4).

### 9,10-Bis-(4-methylsulfanyl-phenylethyynyl)-anthracene A7



This compound was prepared according to the synthetic procedure described for 9,10-bis-(4-*tert*-butylsulfanyl-phenylethyynyl)-anthracene **A12** using 1-ethynyl-4-methylsulfanyl-benzene **A6** (0.480 g, 3.23 mmol). The crude product was purified by re-crystallisation from toluene affording **A7** as a red solid (0.344 g, 0.73 mmol; 61%). M.p.: 276.0–278.0°C.

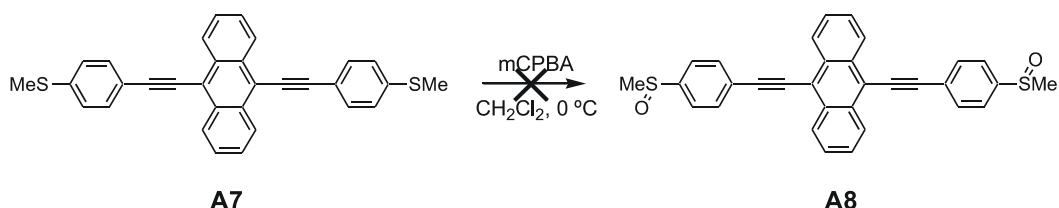
<sup>1</sup>H-NMR (300 MHz, CDCl<sub>3</sub>): δ = 2.56 (s, 6 H), 7.32 (td, <sup>3</sup>J(H,H) = 9 Hz, <sup>4</sup>J(H,H) = 2 Hz, 4 H), 7.63 – 7.66 (m, 4 H), 7.69 (td, <sup>3</sup>J(H,H) = 9 Hz, <sup>4</sup>J(H,H) = 2 Hz, 4 H), 8.66 – 8.70 (m, 4 H).

<sup>13</sup>C-NMR (75 MHz, CDCl<sub>3</sub>): δ = 15.59 (CH<sub>3</sub>), 86.76, 102.30 (C≡C), 119.84, 126.01, 126.30, 126.73, 127.20, 131.92, 132.11, 140.03 (Ar).

MALDI-TOF-MS: 469.70 [M<sup>+</sup>], 454.69 [M<sup>+</sup> – CH<sub>3</sub>].

Elemental analysis (%) calcd. for C<sub>32</sub>H<sub>22</sub>S<sub>2</sub> (470.65): C 81.66, H 4.71; found: C 81.53, H 4.65.

### 9,10-Bis-(4-methanesulfinyl-phenylethyynyl)-anthracene A8



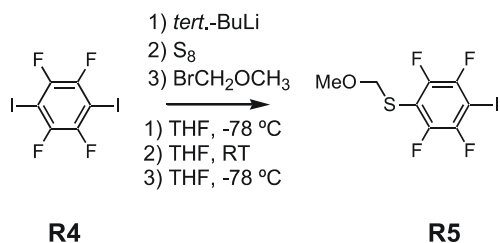
9,10-Bis-(4-methylsulfanyl-phenylethyynyl)-anthracene **A7** (0.037 g, 0.08 mmol) was dissolved in dry CH<sub>2</sub>Cl<sub>2</sub> (15 ml) and the mixture cooled to 0 °C. Then mCPBA (0.035 g, 0.20 mmol) was added in portions and the mixture monitored by TLC. The reaction was stopped by quenching with Ca(OH)<sub>2</sub>, the solid filtered off and washed with CH<sub>2</sub>Cl<sub>2</sub> several times. The filtrate was evaporated to dryness *in vacuo* yielding an orange solid. No separation of the

mixture of compounds could be obtained neither by column chromatography nor by preparative TLC.

The reaction was also repeated with 2.0 equivalents of mCPBA, but without success.

### 6.3.3 Molecular Rectifiers

#### 1,2,4,5-Tetrafluoro-3-iodo-6-methoxymethylsulfanyl-benzene R5



In a two necked flask equipped with a mechanical stirrer and septum 1,4-diiodotetrafluorobenzene **R4** (16.470 g, 40.98 mmol) was dissolved in dry, Ar-saturated THF (200 ml) and the solution cooled to  $-78^\circ\text{C}$  using a dry ice/acetone bath. *tert*.-Butyllithium (68.35 ml, 0.102 mol of 15% solution in pentane) was carefully dropped in via syringe. After stirring for 20 min sulphur (1.310 g, 40.98 mmol) was added and the cooling bath removed. Stirring was continued until all sulphur has disappeared (about 2.5 h) and the mixture then cooled again to  $-78^\circ\text{C}$ . Bromomethylmethylether (12.800 g, 0.10 mol) was added and the dry ice/acetone-bath removed again. The reaction was stirred for another hour and then the solvents were removed by rotary evaporation while absorbing on silica gel. Column chromatography (silica gel, toluene/hexane 1/1) yields **R5** as a yellow oil (11.11 g, 31.55 mmol; 77%).

$$R_f = 0.44$$

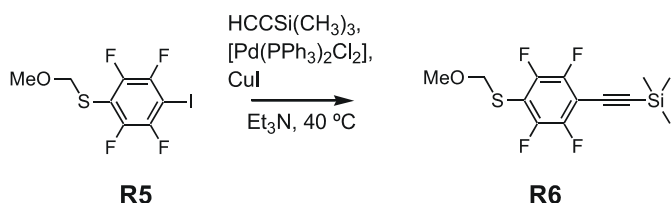
$^1\text{H-NMR}$  (300 MHz,  $\text{CDCl}_3$ ):  $\delta = 3.45$  (s, 3 H), 4.90 (s, 2 H).

$^{13}\text{C-NMR}$  (75 MHz,  $\text{CDCl}_3$ ):  $\delta = 56.51$  ( $\text{CH}_3\text{O}$ ), 73.56 (t,  $^2J(\text{C},\text{F}) = 32$  Hz, C3), 77.72 (t,  $^4J(\text{C},\text{F}) = 2$  Hz,  $\text{CH}_2\text{O}$ ), 113.29 (t,  $^2J(\text{C},\text{F}) = 23$  Hz, C6), 146.93 (m,  $^1J(\text{C},\text{F}) = 246$  Hz,  $^2J(\text{C},\text{F}) = 16$  Hz), 147.21 (m,  $^1J(\text{C},\text{F}) = 245$  Hz,  $^2J(\text{C},\text{F}) = 16$  Hz).

MS (EI):  $m/z$  (%) = 352.0 (100) [ $\text{M}^+$ ], 321.0 (29) [ $\text{M}^+ - \text{CH}_3\text{O}$ ], 307.0 (41) [ $\text{M}^+ - \text{CH}_2\text{OCH}_3$ ], 262.9 (29), 180.0 (75) [ $\text{M}^+ - \text{CH}_2\text{OCH}_3, -\text{I}$ ], 136.0 (19), 117.0 (53), 111 (43), 98 (18), 87 (27).

Elemental analysis calcd. (%) for C<sub>8</sub>H<sub>5</sub>F<sub>4</sub>IOS (352.09): C 27.29 H 1.43; found: C 27.41, H 1.44.

**1,2,4,5-Tetrafluoro-3-methoxymethylsulfanyl-6-(trimethylsilyl-ethynyl)-benzene R6**



1,2,4,5-Tetrafluoro-3-iodo-6-methoxymethylsulfanyl-benzene **R5** (4.000 g, 11.36 mmol) was dissolved in dry, Ar-saturated triethylamine (320 ml). [Pd(PPh<sub>3</sub>)<sub>2</sub>Cl<sub>2</sub>] (0.800 g, 1.14 mmol) was added and the mixture stirred for 15 min at room temperature. Then copper(I) iodide (0.217 g, 1.14 mmol) and trimethylsilylacetylene (1.680 g, 17.10 mol) were added and the mixture heated to 40 °C for 18 h. The solution was filtered over a plug of silica gel, washed with toluene, the filtrate washed several times with 12% hydrochloric acid, then twice with water and the organic phase dried over Na<sub>2</sub>SO<sub>4</sub>. After rotary evaporation of the solvents a dark liquid was obtained that was absorbed on silica gel and purified by column chromatography (silica gel, hexane/diethylether 30/1) providing **R6** as a yellow liquid (2.520 g, 7.82 mmol; 69%).

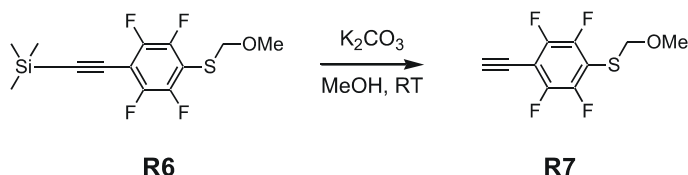
R<sub>f</sub> = 0.24.

<sup>1</sup>H-NMR (300 MHz, CDCl<sub>3</sub>): δ = 0.29 (s, 9 H), 3.43 (s, 3 H), 4.91 (s, 2 H).

<sup>13</sup>C-NMR (75 MHz, CDCl<sub>3</sub>): δ = -0.49 (CH<sub>3</sub>Si), 56.44 (CH<sub>3</sub>O), 77.78 (t, <sup>4</sup>J(C,F) = 2 Hz, CH<sub>2</sub>O), 88.59 (t, <sup>3</sup>J(C,F) = 4 Hz, C≡C), 105.12 (tt, <sup>2</sup>J(C,F) = 18 Hz, <sup>3</sup>J(C,F) = 3 Hz, C6), 110.10 (t, <sup>4</sup>J(C,F) = 4 Hz, C≡C), 113.39 (t, <sup>2</sup>J(C,F) = 21 Hz, C3), 147.07 (m, <sup>1</sup>J(C,F) = 253 Hz, <sup>2</sup>J(C,F) = 16 Hz), 147.23 (m, <sup>1</sup>J(C,F) = 244 Hz, <sup>2</sup>J(C,F) = 13 Hz).

MS (EI): m/z (%) = 322.1 (25) [M<sup>+</sup>], 307.1 (22) [M<sup>+</sup> - CH<sub>3</sub>], 218.0 (100) [M<sup>+</sup> - TMS, - OCH<sub>3</sub>], 199.9 (13), 181.0 (11), 103.0 (11), 73.1 (17) [TMS].

Elemental analysis calcd. (%) for C<sub>13</sub>H<sub>14</sub>F<sub>4</sub>OSSi (322.39): C 48.43 H 4.38; found: C 48.14, H 4.60.

**1–Ethynyl–2,3,5,6–tetrafluoro–4–methoxymethylsulfanyl–benzene R7**

1,2,4,5–Tetrafluoro–3–methoxymethylsulfanyl–6–(trimethylsilyl–ethynyl)–benzene (**R6**) (0.589 g, 1.83 mmol) was dissolved in methanol (40 ml) and  $K_2CO_3$  (0.028 g, 0.20 mmol) added. After stirring at room temperature for 15 h the crude product was absorbed on silica gel and purified by column chromatography (silica gel, hexane/diethylether 9/1) affording **R7** as a white solid (0.447 g, 1.79 mmol; 98%). M.p.: 36.5–37.5°C.

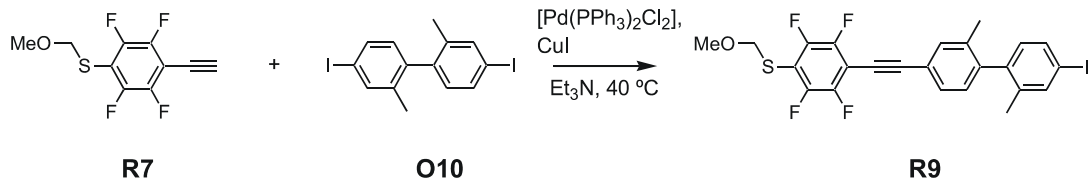
$R_f = 0.33$ .

$^1H$ -NMR (300 MHz,  $CDCl_3$ ):  $\delta = 3.44$  (s, 3 H), 3.67 (s, 1 H), 4.92 (s, 2 H).

$^{13}C$ -NMR (75 MHz,  $CDCl_3$ ):  $\delta = 56.54$  ( $CH_3O$ ), 68.82 (t,  $^3J(C,F) = 4$  Hz,  $C\equiv C$ ), 77.75 (t,  $^4J(C,F) = 3$  Hz,  $CH_2O$ ), 90.53 (t,  $^4J(C,F) = 4$  Hz,  $C\equiv C$ ), 103.88 (tt,  $^2J(C,F) = 18$  Hz,  $^3J(C,F) = 3$  Hz, C1), 114.29 (t,  $^2J(C,F) = 21$  Hz, C4), 147.28 (m,  $^1J(C,F) = 245$  Hz,  $^2J(C,F) = 16$  Hz), 147.46 (m,  $^1J(C,F) = 254$  Hz,  $^2J(C,F) = 13$  Hz).

MS (EI):  $m/z$  (%) = 249.9 (100) [ $M^+$ ], 219.9 (67) [ $M^+ - OCH_3$ ], 204.9 (25) [ $M^+ - CH_2OCH_3$ ], 161.0 (30) [ $M^+ - CH_2OCH_3, - F, - CCH$ ].

Elemental analysis calcd. (%) for  $C_{10}H_6F_4OS$  (250.21): C 48.00 H 2.42; found: C 47.69, H 2.42.

**4'–Iodo–2,2'–dimethyl–4–(2,3,5,6–tetrafluoro–4–methoxymethylsulfanyl–phenylethynyl)–biphenyl R9**

4,4'-Diiodo–2,2'–dimethyl–biphenyl **O10** (5.339 g, 12.30 mmol) was dissolved in dry, Ar-saturated triethylamine (120 ml).  $[Pd(PPh_3)_2Cl_2]$  (0.086 g, 0.12 mmol) was added and the mixture stirred for 15 min at room temperature. After addition of copper(I) iodide (0.023 g, 0.12 mmol) the mixture was heated to 40 °C. Now, 1–Ethynyl–2,3,5,6–tetrafluoro–4–

methoxymethylsulfanyl–benzene **R7** (0.615 g, 2.46 mmol) dissolved in dry, Ar-saturated triethylamine (30 ml) was dropped in over a period of about 20 min and allowed to react at 40 °C for 18 h. The mixture was filtered over a plug of silica gel, washed with diethylether and the solvents removed by rotary evaporation. Column chromatography (silica gel, hexane/diethylether 9/1) provided **R9** as a white solid (0.979 g, 1.76 mmol; 72%). M.p.: 91.5–92.5°C.

$R_f = 0.37$ .

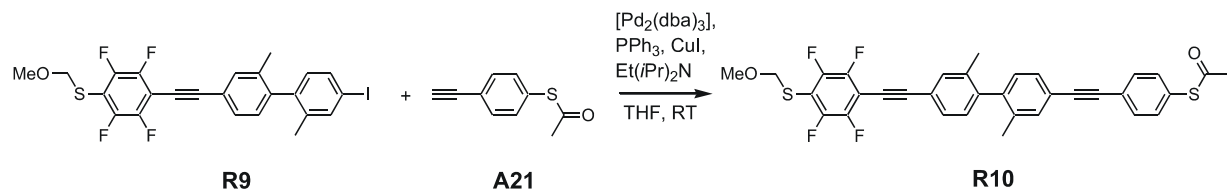
$^1\text{H}$ -NMR (300 MHz,  $\text{CDCl}_3$ ):  $\delta = 2.01$  (s, 3 H), 2.06 (s, 3 H), 3.47 (s, 3 H), 4.94 (s, 2 H), 6.82 (d,  $^3J(\text{H},\text{H}) = 8$  Hz, 1 H), 7.09 (d,  $^3J(\text{H},\text{H}) = 8$  Hz, 1 H), 7.46 (d,  $^3J(\text{H},\text{H}) = 8$  Hz, 1 H), 7.51 (s, 1 H), 7.58 (d,  $^3J(\text{H},\text{H}) = 8$  Hz, 1 H), 7.65 (s, 1 H).

$^{13}\text{C}$ -NMR (75 MHz,  $\text{CDCl}_3$ ):  $\delta = 19.49$ , 19.69 ( $\text{CH}_3$ ), 56.55 ( $\text{CH}_3\text{O}$ ), 74.41 (t,  $^3J(\text{C},\text{F}) = 4$  Hz,  $\text{C} \equiv \text{C}$ ), 77.89 ( $\text{CH}_2\text{O}$ ), 93.26 ( $\text{C}4'$ ), 102.52 (t,  $^4J(\text{C},\text{F}) = 4$  Hz,  $\text{C} \equiv \text{C}$ ), 105.49 (tt,  $^2J(\text{C},\text{F}) = 18$  Hz,  $^3J(\text{C},\text{F}) = 3$  Hz), 112.91 (t,  $^2J(\text{C},\text{F}) = 21$  Hz), 120.74, 129.41, 129.44, 130.76, 133.44, 134.84, 136.34, 138.17, 138.80, 140.21, 142.17 (Ar), 146.67 (m,  $^1J(\text{C},\text{F}) = 252$  Hz,  $^2J(\text{C},\text{F}) = 16$  Hz), 147.39 (m,  $^1J(\text{C},\text{F}) = 244$  Hz,  $^2J(\text{C},\text{F}) = 13$  Hz).

MALDI-TOF-MS (caffeic acid): 554.60 [ $\text{M}^+$ ], 524.60 [ $\text{M}^+ - \text{CH}_3\text{O}$ ], 504.71 [ $\text{M}^+ - \text{CH}_3\text{O}, - \text{F}$ ], 472.75 [ $\text{M}^+ - \text{CH}_2\text{OCH}_3, - 2 \text{ F}$ ], 382.73 [ $\text{M}^+ - \text{CH}_2\text{OCH}_3, - \text{I}$ ], 278.79, 226.79.

Elemental analysis calcd. (%) for  $\text{C}_{24}\text{H}_{17}\text{F}_4\text{IOS}$  (556.36): C 51.81, H 3.08; found: C 51.89, H 2.72.

#### 4'-(4-Acetylsulfanyl-phenylethyynyl)-2,2'-dimethyl-4-(2,3,5,6-tetrafluoro-4-methoxymethylsulfanyl-phenylethyynyl)-biphenyl **R10**



4'-Iodo-2,2'-dimethyl-4-(2,3,5,6-tetrafluoro-4-methoxymethylsulfanyl-phenylethyynyl)-biphenyl **R9** (0.620 g, 1.11 mmol) and triphenylphosphine (0.291 g, 1.11 mmol) were dissolved in dry, Ar-saturated tetrahydrofuran (11 ml). Then ethyl-diisopropylamine (2.87 g, 22.20 mmol) and  $[\text{Pd}_2(\text{dba})_3]*\text{CHCl}_3$  (0.228 g, 0.22 mmol) were added and the mixture stirred at room temperature for 30 min. After the addition of copper(I) iodide (0.084 g, 0.44 mmol) and 1-ethynyl-4-acetylsulfanyl-benzene **A21** (0.236 g, 1.34 mmol) the reaction mixture was

stirred at room temperature for 18 h. Then it was filtered over a plug of silica gel, washed with diethylether, the filtrate washed with saturated NH<sub>4</sub>Cl–solution, the organic phase dried over Na<sub>2</sub>SO<sub>4</sub> and the solvents removed by rotary evaporation. Column chromatography (silica gel, toluene/hexane 2/1) provided **R10** as a white solid (0.447 g, 0.74 mmol; 67%). M.p.: 102.0–104.0°C.

*R*<sub>f</sub> = 0.22.

<sup>1</sup>H-NMR (300 MHz, CDCl<sub>3</sub>): δ = 2.07 (s, 3 H), 2.08 (s, 3 H), 2.44 (s, 3 H), 3.47 (s, 3 H), 4.94 (s, 2 H), 7.09 (d, <sup>3</sup>J(H,H) = 8 Hz, 1 H), 7.13 (d, <sup>3</sup>J(H,H) = 8 Hz, 1 H), 7.39 – 7.42 (m, <sup>3</sup>J(H,H) = 8 Hz, 3 H), 7.46 – 7.48 (m, 2 H), 7.53 (s, 1 H), 7.57 (d, <sup>3</sup>J(H,H) = 8 Hz, 2 H).

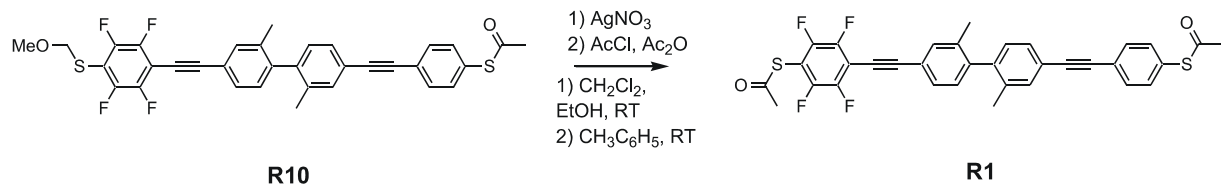
<sup>13</sup>C-NMR (75 MHz, CDCl<sub>3</sub>): δ = 19.68 (CH<sub>3</sub>), 30.33 (CH<sub>3</sub>CO), 56.53 (CH<sub>3</sub>O), 74.40 (t, <sup>3</sup>J(C,F) = 4 Hz, C≡C), 77.90 (CH<sub>2</sub>O), 88.69, 91.02 (C≡C), 102.62 (t, <sup>4</sup>J(C,F) = 4 Hz, C≡C), 105.51 (tt, <sup>2</sup>J(C,F) = 18 Hz, <sup>3</sup>J(C,F) = 3 Hz), 112.91 (t, <sup>2</sup>J(C,F) = 21 Hz), 120.66, 122.11, 124.60, 128.03, 129.08, 129.19, 129.38, 129.45, 132.23, 133.20, 133.43, 134.29, 136.00, 136.38, 141.17, 142.65 (Ar), 146.68 (m, <sup>1</sup>J(C,F) = 250 Hz, <sup>2</sup>J(C,F) = 16 Hz), 147.39 (m, <sup>1</sup>J(C,F) = 244 Hz, <sup>2</sup>J(C,F) = 13 Hz), 193.56 (COCH<sub>3</sub>).

MALDI-TOF-MS: 648.72 [M<sup>+</sup> + CO<sub>2</sub>], 604.71 [M<sup>+</sup>], 574.71 [M<sup>+</sup> – OCH<sub>3</sub>], 562.70 [M<sup>+</sup> – CH<sub>3</sub>CO].

Elemental analysis calcd. (%) for C<sub>34</sub>H<sub>24</sub>F<sub>4</sub>O<sub>2</sub>S<sub>2</sub> (604.68): C 67.53 H 4.00; found: C 67.75, H 4.21.

UV/Vis (1 × 10<sup>-5</sup> acetonitrile): λ<sub>max</sub> (ε) = 204.0 (72800), 320.0 (78300).

#### 4'-(4-Acetylsulfanyl-phenylethynyl)-4-(4-acetylsulfanyl-2,3,5,6-tetrafluoro-phenylethynyl)-2,2'-dimethyl-biphenyl **R1**



To a solution of 4'-(4-acetylsulfanyl-phenylethynyl)-2,2'-dimethyl-4-(2,3,5,6-tetrafluoro-4-methoxymethylsulfanyl-phenylethynyl)-biphenyl **R10** (0.033 g, 0.05 mmol) in dry, Ar-saturated CH<sub>2</sub>Cl<sub>2</sub>/ethanol (1/1.5 ml) was added silver nitrate (0.023 g, 0.14 mmol) and the mixture stirred at room temperature for 17 h in the dark. The white solid was filtered off, washed several times with ethanol and then added to dry, Ar-saturated toluene (10 ml). Ar-

saturated acetic anhydride (0.165 g, ca. 0.150 ml, 1.62 mmol) was dropped in and the mixture stirred at room temperature for 15 min. The solution was cooled to 0 °C using an ice/water bath and acetyl chloride (0.011 g, 0.15 mmol) was carefully added. After 1.5 h of stirring the reaction mixture was poured on ice/water, the aqueous phase extracted with diethylether, the collected organic phases washed with water a few times, dried over Na<sub>2</sub>SO<sub>4</sub> and the solvents removed by rotary evaporation at room temperature. Column chromatography (silica gel, toluene/hexane 4/1) afforded **R1** as a white solid (0.012 g, 0.02 mmol; 37%). M.p.: 145.0–146.0°C.

*R*<sub>f</sub> = 0.40.

<sup>1</sup>H-NMR (300 MHz, CDCl<sub>3</sub>): δ = 2.07 (s, 3 H), 2.09 (s, 3 H), 2.45 (s, 3 H), 2.53 (s, 3 H), 7.09 (d, <sup>3</sup>J(H,H) = 8 Hz, 1 H), 7.14 (d, <sup>3</sup>J(H,H) = 8 Hz, 1 H), 7.39 – 7.43 (m, <sup>3</sup>J(H,H) = 8 Hz, 3 H), 7.46 – 7.48 (m, 2 H), 7.54 (s, 1 H), 7.57 (d, <sup>3</sup>J(H,H) = 8 Hz, 2 H).

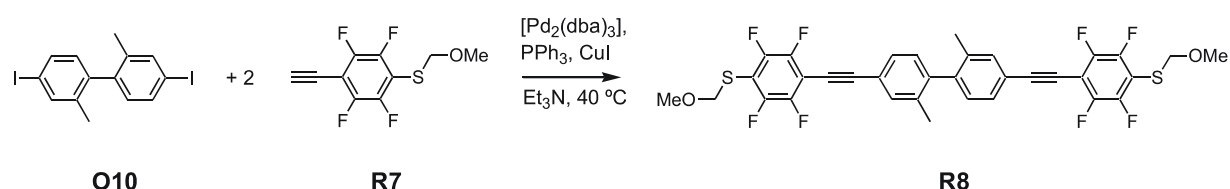
<sup>13</sup>C-NMR (75 MHz, [D8]toluene): δ = 19.51, 19.59 (CH<sub>3</sub>), 29.04, 29.61 (CH<sub>3</sub>CO), 74.93 (t, <sup>3</sup>J(C,F) = 4 Hz, C≡C), 89.54, 91.61 (C≡C), 104.04 (t, <sup>4</sup>J(C,F) = 4 Hz, C≡C), 107.41 (tt, <sup>2</sup>J(C,F) = 18 Hz, <sup>3</sup>J(C,F) = 3 Hz), 108.89 (t, <sup>2</sup>J(C,F) = 21 Hz), 121.17, 123.04, 129.49, 129.56, 129.79, 129.84, 132.42, 133.72, 133.90, 134.61, 136.19, 136.66, 141.48, 143.16 (Ar), 145.13 – 145.72 (m), 148.25 – 149.04 (m, C2, C3, C5, C6), 187.33, 191.24 (COCH<sub>3</sub>).

MALDI-TOF-MS (nicotinic acid): 602.96 [M<sup>+</sup>], 574.95 [M<sup>+</sup> – CO], 560.93 [M<sup>+</sup> – COCH<sub>3</sub>], 531.91 [M<sup>+</sup> – CO, COCH<sub>3</sub>], 517.90 [M<sup>+</sup> – 2 COCH<sub>3</sub>], 454.90.

Elemental analysis calcd. (%) for C<sub>34</sub>H<sub>22</sub>F<sub>4</sub>O<sub>2</sub>S<sub>2</sub> (602.66): C 67.76, H 3.68; found: C 67.36, H 3.95.

UV/Vis (1 × 10<sup>-5</sup> acetonitrile): λ<sub>max</sub> (ε) = 204.0 (80000), 319.5 (85100).

### 2,2'-Dimethyl-4,4'-bis-(2,3,5,6-tetrafluoro-4-methoxymethylsulfanyl-phenylethyynyl)-biphenyl **R8**



4,4'-Diiodo-2,2'-dimethyl-biphenyl **O10** (0.182 g, 0.42 mmol), triphenylphosphine (0.055 g, 0.21 mmol) and [Pd<sub>2</sub>(dba)<sub>3</sub>] (0.019 g, 0.02 mmol) were dissolved in dry, Ar-saturated triethylamine (10 ml) and the mixture stirred at room temperature for 15 min. After the

addition of copper(I) iodide (0.016 g, 0.084 mmol) and 1–ethynyl–2,3,5,6–tetrafluoro–4–methoxymethylsulfanyl–benzene **R7** (0.250 g, 1.00 mmol) the reaction mixture was stirred at 40 °C for 3 h. Then saturated NH<sub>4</sub>Cl (about 20 ml) was poured into the reaction mixture, the resulting solution extracted with diethylether, the organic phases washed once with saturated NH<sub>4</sub>Cl, once with water, the organic phases dried over Na<sub>2</sub>SO<sub>4</sub> and evaporated to dryness. The crude product was absorbed on silica gel and purified by column chromatography (silica gel, hexane/diethylether 9/1) affording **R8** as a slightly yellow solid (0.264 g, 0.39 mmol; 93%). M.p.: 106.0–107.0 °C.

$$R_f = 0.20.$$

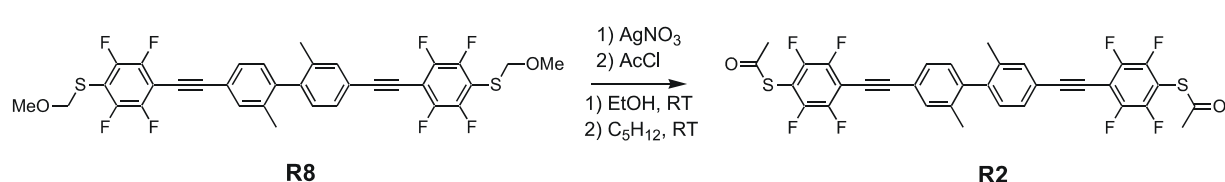
<sup>1</sup>H-NMR (300 MHz, CDCl<sub>3</sub>): δ = 2.08 (s, 6 H), 3.47 (s, 6 H), 4.94 (s, 4 H), 7.13 (d, <sup>3</sup>J(H,H) = 8 Hz, 2 H), 7.48 (d, <sup>3</sup>J(H,H) = 8 Hz, 2 H), 7.53 (s, 2 H).

<sup>13</sup>C-NMR (75 MHz, CDCl<sub>3</sub>): δ = 19.62 (CH<sub>3</sub>), 56.54 (CH<sub>3</sub>O), 74.45 (t, <sup>3</sup>J(C,F) = 4 Hz, C≡C), 77.90 (CH<sub>2</sub>O), 102.51 (t, <sup>4</sup>J(C,F) = 4 Hz, C≡C), 105.47 (tt, <sup>2</sup>J(C,F) = 18 Hz, <sup>3</sup>J(C,F) = 3 Hz), 112.96 (t, <sup>2</sup>J(C,F) = 21 Hz), 120.84, 129.32, 129.41, 133.47, 136.26, 142.37 (Ar), 146.68 (m, <sup>1</sup>J(C,F) = 252 Hz, <sup>2</sup>J(C,F) = 16 Hz), 147.38 (m, <sup>1</sup>J(C,F) = 244 Hz, <sup>2</sup>J(C,F) = 13 Hz).

MALDI-TOF-MS (caffeic acid): 676.74 [ $M^+$ ], 646.73 [ $M^+ -CH_3O$ ], 614.75 [ $M^+ -CH_2OCH_3$ ,  $-F$ ].

Elemental analysis calcd. (%) for C<sub>34</sub>H<sub>22</sub>F<sub>8</sub>O<sub>2</sub>S<sub>2</sub> (678.66): C 60.17, H 3.25.

**4,4'-Bis-(4-acetylulfanyl-2,3,5,6-tetrafluoro-phenylethynyl)-2,2'-dimethyl-biphenyl**



To a solution of 2,2'-dimethyl-4,4'-bis-(2,3,5,6-tetrafluoro-4-methoxymethylsulfanyl-phenylethynyl)-biphenyl **R8** (0.028 g, 0.04 mmol) in Ar-saturated ethanol (1 ml) was added silver nitrate (0.017 g, 0.10 mmol) and the mixture stirred at room temperature for 15 h in the dark. The white solid was filtered off, washed several times with ethanol and then added to Ar-saturated pentane (2.5 ml). After careful addition of acetyl chloride (0.047 g, 0.60 mmol)

the reaction mixture was stirred at room temperature for 1.5 h and then poured on ice/water. The aqueous phase was extracted with diethylether, the collected organic extracts washed with water a few times, dried over  $\text{Na}_2\text{SO}_4$  and the solvents removed by rotary evaporation. Column chromatography (silica gel, hexane/dichloromethane 2/1) of the crude product provided **R2** as a white solid (0.024 g, 0.036 mmol; 90%). M.p.: 173.0–175.0 °C.

$R_f = 0.12$ .

$^1\text{H}$ -NMR (300 MHz,  $\text{CDCl}_3$ ):  $\delta = 2.09$  (s, 6 H), 2.54 (s, 6 H), 7.13 (d,  $^3J(\text{H},\text{H}) = 8$  Hz, 2 H), 7.50 (d,  $^3J(\text{H},\text{H}) = 8$  Hz, 2 H), 7.54 (s, 2 H).

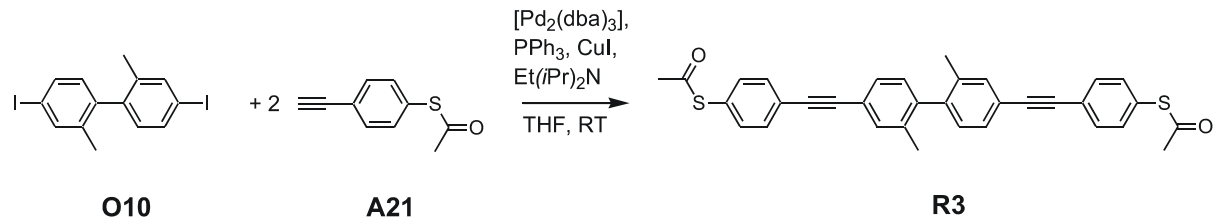
$^{13}\text{C}$ -NMR (75 MHz, [D8]toluene):  $\delta = 19.41$  ( $\text{CH}_3$ ), 28.99 ( $\text{CH}_3\text{CO}$ ), 74.96 (t,  $^3J(\text{C},\text{F}) = 4$  Hz,  $\text{C}\equiv\text{C}$ ), 103.83 (t,  $^4J(\text{C},\text{F}) = 4$  Hz,  $\text{C}\equiv\text{C}$ ), 107.41 (tt,  $^2J(\text{C},\text{F}) = 18$  Hz,  $^3J(\text{C},\text{F}) = 3$  Hz), 108.89 (t,  $^2J(\text{C},\text{F}) = 21$  Hz), 121.25, 129.55, 129.81, 133.88, 136.47, 142.73 (Ar), 146.88 (m,  $^1J(\text{C},\text{F}) = 246$  Hz,  $^2J(\text{C},\text{F}) = 17$  Hz), 147.19 (m,  $^1J(\text{C},\text{F}) = 252$  Hz,  $^2J(\text{C},\text{F}) = 14$  Hz), 187.33 (CO).

MALDI-TOF-MS (Nicotinic acid): 674.68 [ $\text{M}^+$ ], 646.68 [ $\text{M}^+ - \text{CO}$ ], 632.67 [ $\text{M}^+ - \text{COCH}_3$ ], 618.68 [ $\text{M}^+ - 2 \text{CO}$ ], 603.67 [ $\text{M}^+ - \text{COCH}_3, \text{CO}$ ], 589.65 [ $\text{M}^+ - 2 \text{COCH}_3$ ], 454.71.

Elemental analysis calcd. (%) for  $\text{C}_{34}\text{H}_{18}\text{F}_8\text{O}_2\text{S}_2$  (674.62): C 60.53, H 2.69; found: C 60.71, H 3.05.

UV/Vis ( $1 \times 10^{-5}$  acetonitrile):  $\lambda_{\text{max}} (\varepsilon) = 203.5$  (85600), 323.0 (93600).

#### 4,4'-Bis-(4-acetylsulfanyl-phenylethynyl)-2,2'-dimethyl-biphenyl **R3**



4,4'-Diiodo-2,2'-dimethyl-biphenyl **O10** (0.434 g, 1.00 mmol), triphenylphosphine (0.131 g, 0.50 mmol),  $[\text{Pd}_2(\text{dba})_3]$  (0.046 g, 0.05 mmol) and copper iodide (0.038 g, 0.20 mmol) were dissolved in dry, Ar-saturated tetrahydrofuran (10 ml) and the mixture stirred at room temperature for 15 min. After the addition of ethyl-diisopropylamine (1.29 g, 10 mmol) and 1-acetylsulfanyl-4-ethynyl-benzene **A21** (0.423 g, 2.40 mmol) the reaction mixture was stirred at room temperature for 24 h. It was poured into saturated  $\text{NH}_4\text{Cl}$ -solution and extracted with diethylether. The organic phases were washed once with saturated  $\text{NH}_4\text{Cl}$ , once with water, dried over  $\text{Na}_2\text{SO}_4$  and the solvents removed by rotary evaporation. Purification

using column chromatography (silica gel, dichloromethane/hexane 2/1) provided **R3** as a white solid (0.395 g, 0.74 mmol; 74%). M.p.: 139.5 – 140.5 (decomp.).

$R_f = 0.29$ .

$^1\text{H}$ -NMR (300 MHz,  $\text{CDCl}_3$ ):  $\delta = 2.07$  (s, 6 H), 2.44 (s, 6 H), 7.09 (d,  $^3J(\text{H},\text{H}) = 8$  Hz, 2 H), 7.41 (m,  $^3J(\text{H},\text{H}) = 8$  Hz, 6 H), 7.47 (s, 2 H), 7.57 (d,  $^3J(\text{H},\text{H}) = 8$  Hz, 4 H).

$^{13}\text{C}$ -NMR (75 MHz,  $\text{CDCl}_3$ ):  $\delta = 19.66$  ( $\text{CH}_3$ ), 30.31 ( $\text{CH}_3\text{CO}$ ), 88.58, 91.08 ( $\text{C}=\text{C}$ ), 121.97, 124.67, 128.01, 129.02, 129.30, 132.21, 133.16, 134.26, 136.10, 141.46 (Ar), 193.50 (CO).

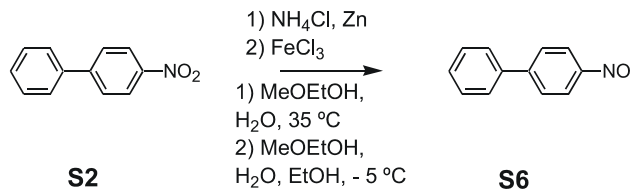
MALDI-TOF-MS: 529.31 [ $\text{M}^+$ ], 501.35 [ $\text{M}^+ - \text{CO}$ ], 488.38 [ $\text{M}^+ - \text{COCH}_3$ ], 459.43 [ $\text{M}^+ - \text{CO,} - \text{COCH}_3$ ], 445.44 [ $\text{M}^+ - 2 \text{COCH}_3$ ], 278.48.

Elemental analysis calcd. (%) for  $\text{C}_{34}\text{H}_{26}\text{O}_2\text{S}_2$  (530.70): C 76.95, H 4.94; found: C 76.93, H 4.80.

UV/Vis ( $1 \times 10^{-5}$  acetonitrile):  $\lambda_{\text{max}} (\varepsilon) = 204.0$  (72000), 317.5 (87600).

### 6.3.4 Molecular Switches

#### 4-Nitroso-biphenyl **S9**

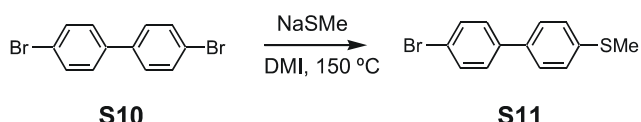


4-Nitro-biphenyl **S2** (15.936 g, 80.00 mmol) was dissolved in methoxyethanol (400 ml) and a solution of  $\text{NH}_4\text{Cl}$  (6.793 g, 127.00 mmol) in  $\text{H}_2\text{O}$  (100 ml) added. The reaction mixture was warmed to 30 °C and finely powdered zinc (20.384 g, 311.72 mmol) added in portions over a period of 30 min maintaining the temperature between 30 – 35 °C while stirring vigorously using mechanical stirring. The mixture was allowed to react at 35 °C for 2 h and then filtered and washed with methoxyethanol. The filtrate was added to a solution of  $\text{FeCl}_3$  (25.200 g, 155.37 mmol) in  $\text{H}_2\text{O}$  (300 ml) and ethanol (120 ml) over the course of 90 min while the temperature was kept at –5 °C. After 1 h the mixture was poured into water (ca. 800 ml) and the yellow precipitate collected. It was dried and then dissolved in  $\text{CH}_2\text{Cl}_2$  and filtered over silica gel. After evaporation of the solvents a dark orange solid was obtained that

was purified by re-crystallisation from ethanol affording **S6** as an orange solid (9.266 g, 50.58 mmol; 63%). M.p.: 73.0 – 74.0 °C (Lit.<sup>[360]</sup>: 74 °C).

<sup>1</sup>H-NMR (300 MHz, CDCl<sub>3</sub>): δ = 7.45 – 7.54 (m, 3 H), 7.68 (td, <sup>3</sup>J(H,H) = 8 Hz, <sup>4</sup>J(H,H) = 2 Hz, 2 H), 7.83 (dd, <sup>3</sup>J(H,H) = 9 Hz, <sup>4</sup>J(H,H) = 1 Hz, 2 H), 7.98 (d, <sup>3</sup>J(H,H) = 9 Hz, 2 H).  
<sup>13</sup>C-NMR (75 MHz, CDCl<sub>3</sub>): δ = 121.70 (C3), 127.51 (C2'), 127.89 (C3'), 128.67 (C4'), 129.16 (C2), 148.13 (C1), 165.00 (C4).

### **4'-Bromo-4-methylsulfanyl-biphenyl S11**



Sodium methanethiolate (4.110 g, 0.059 mol) was dissolved in dry DMI (310 ml) and 4,4'-dibromo-biphenyl **S10** (13.104 g, 0.042 mol) added at once. The mixture was heated to 150 °C for 41 h. It was allowed to cool to room temperature, poured into sat. NaCl-solution (ca. 1200 ml), the aqueous phase extracted with diethylether, the ethereal layers washed once with water, dried over Na<sub>2</sub>SO<sub>4</sub> and then the solvent removed by rotary evaporation. Column chromatography (silica gel, starting with hexane/toluene 15/1 increasing to hexane/toluene 4/1) yielded **S11** as a white solid (7.038 g, 0.025 mol; 60%). M.p.: 148.0 – 149.5°C (Lit.:<sup>[361]</sup> 148.0–150.0).

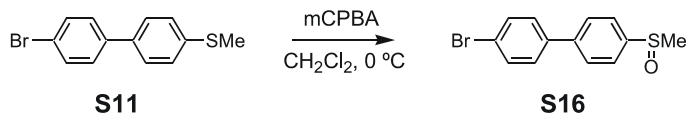
$R_f = 0.16$  (hexane/toluene 15/1).

<sup>1</sup>H-NMR (300 MHz, CDCl<sub>3</sub>): δ = 2.52 (s, 3 H), 7.32 (td, <sup>3</sup>J(H,H) = 9 Hz, <sup>4</sup>J(H,H) = 2 Hz, 2 H), 7.43 (td, <sup>3</sup>J(H,H) = 9 Hz, <sup>4</sup>J(H,H) = 2 Hz, 2 H), 7.48 (td, <sup>3</sup>J(H,H) = 9 Hz, <sup>4</sup>J(H,H) = 2 Hz, 2 H), 7.55 (td, <sup>3</sup>J(H,H) = 9 Hz, <sup>4</sup>J(H,H) = 2 Hz, 2 H).

<sup>13</sup>C-NMR (75 MHz, CDCl<sub>3</sub>): δ = 16.19 (CH<sub>3</sub>S), 121.80 (C4'), 127.30 (C3), 127.65 (C2), 128.80 (C2'), 132.31 (C3'), 137.11 (C1), 138.62 (C4), 139.85 (C1').

MS (EI): m/z (%) = 279.9, 277.9 (100) [ $M^+$ ], 264.9, 262.9 (30) [ $M^+ - CH_3$ ], 184.0 (15) [ $M^+ - Br - CH_3$ ], 152.1 [ $M^+ - Br - SCH_3$ ].

Elemental analysis calcd. (%) for C<sub>13</sub>H<sub>11</sub>BrS (279.20): C 55.92, H 3.97; found C 55.96, H 3.92.

**4'-Bromo-4-methanesulfinyl-biphenyl S16**

A solution of 4'-bromo-4-methanesulfonyl-biphenyl **S11** (5.026 g, 18.00 mmol) in dry  $\text{CH}_2\text{Cl}_2$  was cooled to 0 °C using an ice/water bath. To the cooled solution was added 3-chloroperoxybenzoic acid (mCPBA) (4.038 g, 23.40 mmol) in three portions and the mixture stirred at 0 °C for 1 h. Then  $\text{Ca}(\text{OH})_2$  (2.222 g, 30.00 mmol) was added and stirred for an additional 30 min at room temperature. The reaction mixture was filtered, washed with  $\text{CH}_2\text{Cl}_2$  and the solvents removed *in vacuo*. The crude product was purified by column chromatography (silica gel, ethyl acetate/toluene 9/1) giving **S16** as a white solid (4.732 g, 16.03 mmol; 89%). M.p.: 144.0 – 145.0 °C.

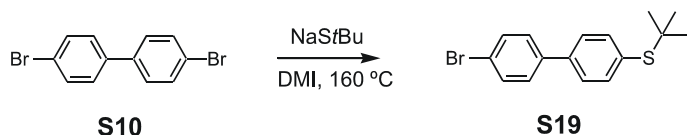
$R_f = 0.20$ .

$^1\text{H}$ -NMR (300 MHz,  $\text{CDCl}_3$ ):  $\delta = 2.77$  (s, 3 H), 7.47 (td,  $^3J(\text{H},\text{H}) = 9$  Hz,  $^4J(\text{H},\text{H}) = 2$  Hz, 2 H), 7.60 (td,  $^3J(\text{H},\text{H}) = 9$  Hz,  $^4J(\text{H},\text{H}) = 2$  Hz, 2 H), 7.71 (s, 4 H).

$^{13}\text{C}$ -NMR (75 MHz,  $\text{CDCl}_3$ ):  $\delta = 44.02$  ( $\text{CH}_3\text{SO}$ ), 122.58 ( $\text{C}4'$ ), 124.22 ( $\text{C}3$ ), 127.92 ( $\text{C}2$ ), 128.86 ( $\text{C}2'$ ), 132.17 ( $\text{C}3'$ ), 138.70 ( $\text{C}1'$ ), 142.94 ( $\text{C}1$ ), 144.89 ( $\text{C}4$ ).

MS (EI):  $m/z$  (%) = 295.9, 293.9 (55) [ $\text{M}^+$ ], 280.8, 278.8 (100) [ $\text{M}^+ - \text{CH}_3$ ], 246.9 (21) [ $\text{M}^+ - \text{SCH}_3$ ], 152 (21) [ $\text{M}^+ - \text{Br}, - \text{SOCH}_3$ ].

Elemental analysis calcd. (%) for  $\text{C}_{13}\text{H}_{11}\text{BrOS}$  (295.20): C 52.89, H 3.76; found: C 52.79, H 3.73.

**4-Bromo-4'-*tert*-butylsulfanyl-biphenyl S19**

In a two-necked flask sodium-2-methyl-2-propanethiolate (2.692 g, 0.02 mmol) was dissolved in dry DMI (50 ml), then 4,4'-dibromo-biphenyl **S10** (6.240 g, 0.02 mmol) was added and the mixture heated to 160 °C for 130 h. The reaction mixture was poured into sat.  $\text{NaCl}$ -solution, the aqueous phase extracted with diethylether, the ethereal phases washed with water and then dried over  $\text{Na}_2\text{SO}_4$ . After rotary evaporation a brownish solid was

obtained which was purified by column chromatography (silica gel, hexane/toluene 6/1) affording **S19** as a white solid (2.767 g, 8.61 mmol; 43%). M.p.: 81.0 – 83.0°C.

$R_f = 0.29$ .

$^1\text{H}$ -NMR (300 MHz,  $\text{CDCl}_3$ ):  $\delta = 1.32$  (s, 9 H), 7.46 (d,  $^3J(\text{H},\text{H}) = 8$  Hz), 7.51 (d,  $^3J(\text{H},\text{H}) = 8$  Hz), 7.56 – 7.61 (m, 4 H).

$^{13}\text{C}$ -NMR (75 MHz,  $\text{CDCl}_3$ ):  $\delta = 31.03$  ( $(\text{CH}_3)_3\text{C}$ ), 46.21 ( $\text{C}(\text{CH}_3)_3$ ), 121.95 (C4), 126.94 (C2'), 128.71 (C2), 132.00 (C3), 132.24 (C4'), 137.96 (C3'), 139.29, 140.27 (C1, C1').

MS (EI):  $m/z$  (%) = 321.9, 319.9 (29) [ $\text{M}^+$ ], 265.8, 263.8 (100) [ $\text{M}^+ - t\text{Bu}$ ], 185.1 (23) [ $\text{M}^+ - t\text{Bu} - \text{Br}$ ].

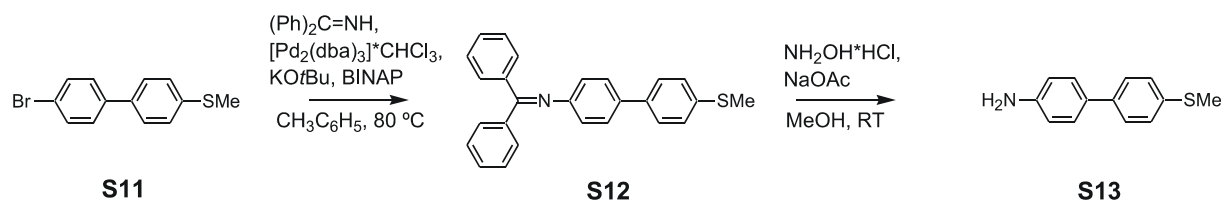
Elemental analysis calcd. (%) for  $\text{C}_{16}\text{H}_{17}\text{BrS}$  (321.28): C 59.81, H 5.33; found: C 59.88, H 5.03.

### General Procedure for Hartwig–Buchwald–Coupling:

A pre-dried two necked flask was successively charged with  $[\text{Pd}_2(\text{dba})_3]^*\text{CHCl}_3$ , BINAP, the biphenyl compound, benzophenone imine,  $\text{NaOtBu}$  and dry toluene and the mixture heated to 80 °C and the progress of the reaction monitored by TLC. Then the reaction mixture was poured into diethylether, filtered over a plug of silica gel and washed with diethylether and with ethyl acetate in the case of **S18**, respectively. The solvents were removed by rotary evaporation and the obtained solid re-crystallised from methanol.

The diphenyl ketimine was suspended in methanol and sodium acetate and hydroxylamine hydrochloride were added and the reaction stirred at room temperature for 2 h. It was poured into 0.1 M NaOH-solution, the aqueous phase extracted with  $\text{CH}_2\text{Cl}_2$ , the collected organic phases dried over  $\text{Na}_2\text{SO}_4$  and evaporated to dryness. Purification by column chromatography afforded the respective amino-biphenyl.

### 4'-Methylsulfanyl-biphenyl-4-ylamine **S13**



From

[Pd<sub>2</sub>(dba)<sub>3</sub>]\*CHCl<sub>3</sub> (0.041 g, 0.04 mmol) BINAP (0.075 g, 0.12 mmol)  
benzophenone imine (0.870 g, 4.80 mmol) NaOtBu (0.538 g, 5.60 mmol)  
**S11** (1.117 g, 4.00 mmol) and dry toluene (16 ml).

Reaction time: 5 h.

After re-crystallisation the diphenyl ketimine was obtained as a yellow solid (1.192 g, 3.14 mmol; 79%).

## Cleavage of protection group from

Purification by column chromatography (silica gel, hexane/diethylether 1/1) afforded **S13** as a white solid (0.618 g, 2.87 mmol; 100%). M.p.: 130.0 – 131.0 °C (Lit.<sup>[362]</sup>: 108.0–109.0 °C)

$$R_f = 0.17.$$

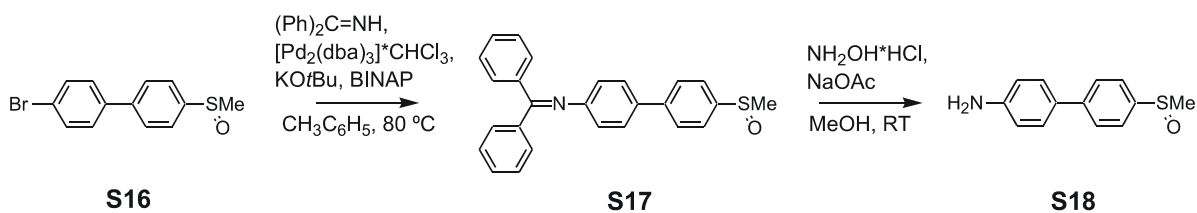
<sup>1</sup>H-NMR (300 MHz, CDCl<sub>3</sub>): δ = 2.51 (s, 3 H), 3.73 (br, 2 H), 6.75 (d, <sup>3</sup>J(H,H) = 8 Hz, 2 H), 7.30 (d, <sup>3</sup>J(H,H) = 8 Hz, 2 H), 7.39 (d, <sup>3</sup>J(H,H) = 6 Hz, 2 H), 7.47 (d, <sup>3</sup>J(H,H) = 6 Hz, 2 H).

<sup>13</sup>C-NMR (75 MHz, CDCl<sub>3</sub>): δ = 16.21 (CH<sub>3</sub>S), 115.43 (C3), 126.78, 127.21 (C2',C3'), 127.76 (C2), 130.89 (C1), 136.08 (C1'), 138.20 (C4'), 145.84 (C4).

MS (EI):  $m/z$  (%) = 215.0 (100) [ $M^+$ ], 200 (50) [ $M^+ - CH_3$ ].

Elemental analysis calcd. (%) for C<sub>13</sub>H<sub>13</sub>NS (215.32): C 72.52, H 6.09, N 6.51; found: C 72.77, H 6.48, N 6.58.

## **4'-Methanesulfinyl-biphenyl-4-ylamine S18**



From

[Pd<sub>2</sub>(dba)<sub>3</sub>]\*CHCl<sub>3</sub> (0.083 g, 0.08 mmol) BINAP (0.149 g, 0.24 mmol)  
benzophenone imine (1.740 g, 9.60 mmol) NaOtBu (1.076 g, 11.20 mmol)  
**S16** (2.362 g, 8.00 mmol) and dry toluene (30 ml).

Reaction time: 12 h.

After re-crystallisation the diphenyl ketimine was obtained as a yellow solid (2.444 g, 6.18 mmol; 77%).

## Cleavage of protection group from

Diphenyl ketimine (1.187 g, 3.00 mmol) NaOAc (0.591 g, 7.20 mmol)

H<sub>2</sub>NOH\*HCl (0.375 g, 5.40 mmol) and methanol (30 ml)

Purification by column chromatography (silica gel, ethyl acetate/toluene 9/1) afforded **S18** as a yellowish solid (0.657 g, 2.84 mmol; 95%). M.p.: 191.0 – 192.0 °C.

$$R_f = 0.12.$$

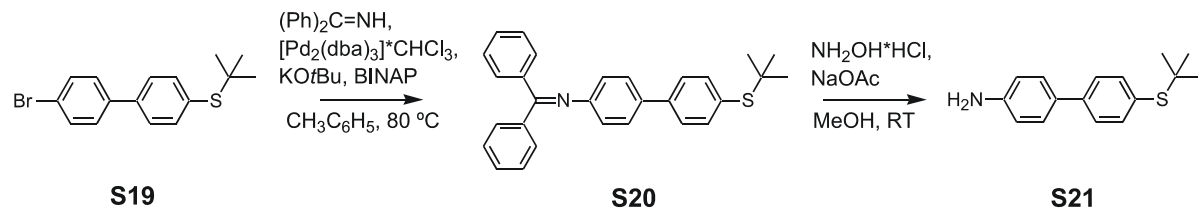
<sup>1</sup>H-NMR (300 MHz, CDCl<sub>3</sub>): δ = 2.75 (s, 3 H), 3.82 (br, 2 H), 6.82 (td, <sup>3</sup>J(H,H) = 9 Hz, <sup>4</sup>J(H,H) = 2 Hz, 2 H), 7.43 (td, <sup>3</sup>J(H,H) = 9 Hz, <sup>4</sup>J(H,H) = 2 Hz, 2 H), 7.67 (s, 4 H).

<sup>13</sup>C-NMR (75 MHz, CDCl<sub>3</sub>): δ = 44.03 (CH<sub>3</sub>SO), 115.41 (C3), 124.03 (C3'), 127.14, 128.21 (C2', C2), 129.83 (C1), 143.05 (C1'), 144.18 (C4'), 146.71 (C4).

MS (EI):  $m/z$  (%) = 231 (60) [ $M^+$ ], 216 (100) [ $M^+ - CH_3$ ], 184.0 (10) [ $M^+ - SCH_3$ ].

Elemental analysis calcd. (%) for C<sub>13</sub>H<sub>13</sub>NOS (231.31): C 67.50, H 5.66, N 6.06; found: C 67.58, H 5.88, N 5.92.

### **4'-*tert.*-Butylsulfanyl-biphenyl-4-ylamine S21**



From

[Pd<sub>2</sub>(dba)<sub>3</sub>]\*CHCl<sub>3</sub> (0.031 g, 0.03 mmol) BINAP (0.056 g, 0.09 mmol)  
benzophenone imine (0.652 g, 3.60 mmol) NaOtBu (0.404 g, 4.20 mmol)  
**S19** (0.964 g, 3.00 mmol) and dry toluene (12 ml).

Reaction time: 24 h.

After re-crystallisation the diphenyl ketimine was obtained as a yellow solid (0.902, 2.14 mmol; 71%).

### Cleavage of protection group from

H<sub>2</sub>NOH\*HCl (0.268 g, 3.86 mmol) and methanol (23 ml)

Purification by column chromatography (silica gel, hexane/diethylether 1/1) afforded **S21** as a white solid (0.534 g, 2.07 mmol; 97%). M.p.: 153.0 – 155.0 °C.

$R_f = 0.25$ .

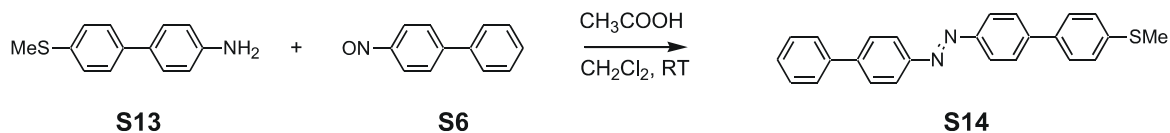
$^1\text{H}$ -NMR (300 MHz,  $\text{CDCl}_3$ ):  $\delta = 1.31$  (s, 9 H), 3.83 (br, 2 H), 6.77 (td,  $^3J(\text{H},\text{H}) = 9$  Hz,  $^4J(\text{H},\text{H}) = 2$  Hz, 2 H), 7.43 (td,  $^3J(\text{H},\text{H}) = 9$  Hz,  $^4J(\text{H},\text{H}) = 2$  Hz, 2 H), 7.49 (td,  $^3J(\text{H},\text{H}) = 9$  Hz,  $^4J(\text{H},\text{H}) = 2$  Hz, 2 H), 7.54 (td,  $^3J(\text{H},\text{H}) = 9$  Hz,  $^4J(\text{H},\text{H}) = 2$  Hz, 2 H).

$^{13}\text{C}$ -NMR (75 MHz,  $\text{CDCl}_3$ ):  $\delta = 30.98$  ( $(\text{CH}_3)_3\text{C}$ ), 45.98 ( $\text{C}(\text{CH}_3)_3$ ), 115.65 (C3), 126.31 (C2'), 128.02 (C2), 130.35 (C4'), 130.89 (C1), 137.83 (C3'), 141.41 (C1'), 145.69 (C4).

MS (EI):  $m/z$  (%) = 257.0 (70) [ $\text{M}^+$ ], 201 (100) [ $\text{M}^+ - t\text{Bu}$ ].

Elemental analysis calcd. (%) for  $\text{C}_{16}\text{H}_{19}\text{NS}$  (257.39): C 74.66, H 7.44, N 5.44; found: C 74.89, H 7.36, N 5.09.

### Biphenyl-4-yl-(4'-methylsulfanyl-biphenyl-4-yl)-diazene **S14**



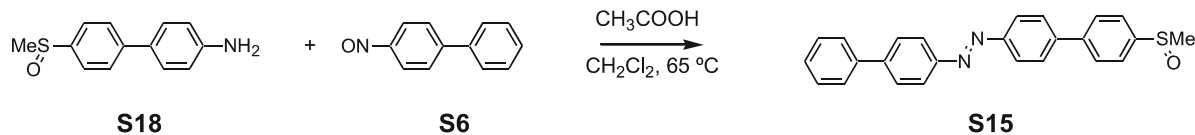
4-Nitroso-biphenyl **S6** (0.339 g, 1.85 mmol) and 4'-methylsulfanyl-biphenyl-4-ylamine **S13** (0.383 g, 1.78 mmol) were dissolved in  $\text{CH}_2\text{Cl}_2$  (14 ml) and glacial acetic acid (28 ml) and the reaction mixture stirred at room temperature for 72 h. The solvents were removed by rotary evaporation leaving a dark red solid which was re-crystallised from toluene affording **S14** as a red solid (0.540 g, 1.42 mmol; 80%). M.p.: 277.0 – 279.0 °C.

$^1\text{H}$ -NMR (300 MHz,  $\text{CDCl}_3$ , T = 48 °C):  $\delta = 2.54$  (s, 3 H), 7.36 – 7.41 (m, 3 H), 7.48 (tt,  $^3J(\text{H},\text{H}) = 7$  Hz,  $^4J(\text{H},\text{H}) = 2$  Hz, 2 H), 7.61 (td,  $^3J(\text{H},\text{H}) = 7$  Hz,  $^4J(\text{H},\text{H}) = 2$  Hz, 2 H), 7.67 (td,  $^3J(\text{H},\text{H}) = 7$  Hz,  $^4J(\text{H},\text{H}) = 1$  Hz, 2 H), 7.73 (d,  $^3J(\text{H},\text{H}) = 7$  Hz, 2 H), 7.76 (d,  $^3J(\text{H},\text{H}) = 8$  Hz, 2 H), 7.99 – 8.03 (m, 4 H).

$^{13}\text{C}$ -NMR (75 MHz,  $\text{CDCl}_3$ , T = 48 °C):  $\delta = 15.88$  ( $\text{CH}_3\text{S}$ ), 123.36, 123.43, 127.17, 127.37, 127.47, 127.75, 127.83, 128.85, 137.09, 138.67, 140.32, 143.05, 152.07 (Ar).

MALDI-TOF-MS: 380.72 [ $\text{M}^+$ ].

Elemental analysis calcd. (%) for  $\text{C}_{25}\text{H}_{20}\text{N}_2\text{S}$  (380.51): C 78.91, H 5.30, N 7.36; found: C 78.71, H 5.53, N 7.16.

**Biphenyl-4-yl-(4'-methanesulfinyl-biphenyl-4-yl)-diazene S15**

## Route 1:

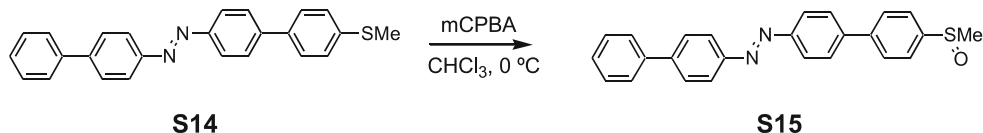
4-Nitroso-biphenyl **S6** (0.572 g, 3.12 mmol) and 4'-methanesulfinyl-biphenyl-4-ylamine **S18** (0.657 g, 2.84 mmol) were dissolved in  $\text{CH}_2\text{Cl}_2$  (25 ml) and glacial acetic acid (75 ml) and the reaction mixture heated to 65 °C for 67 h. The solvents were removed by rotary evaporation leaving a dark orange solid which was re-crystallised from toluene affording **S15** as a red-brown solid (0.935 g, 2.36 mmol; 83%). M.p.: 270.0 – 272.0°C.

$^1\text{H}$ -NMR (300 MHz,  $\text{CDCl}_3$ , T = 48 °C):  $\delta$  = 2.78 (s, 3 H), 7.39 (t,  $^3J(\text{H},\text{H})$  = 8 Hz, 1 H), 7.48 (t,  $^3J(\text{H},\text{H})$  = 8 Hz, 2 H), 7.68 (d,  $^3J(\text{H},\text{H})$  = 8 Hz, 2 H), 7.75 – 7.79 (m, 6 H), 7.83 (d,  $^3J(\text{H},\text{H})$  = 8 Hz, 2 H), 8.02 – 8.06 (m, 4 H).

$^{13}\text{C}$ -NMR (75 MHz,  $\text{CDCl}_3$ , T = 48 °C):  $\delta$  = 44.03 ( $\text{CH}_3\text{SO}$ ), 123.45, 123.52, 124.16, 127.18, 127.79, 127.91, 127.94, 128.09, 128.88, 140.25, 142.13, 143.22, 144.03, 145.55, 151.98, 152.55 (Ar).

MALDI-TOF-MS: 396.77 [ $\text{M}^+$ ].

Elemental analysis calcd. (%) for  $\text{C}_{25}\text{H}_{20}\text{N}_2\text{OS}$  (396.51): C 75.73, H 5.08, N 7.07; found: C 75.57, H 5.26, N 6.80.



## Route 2:

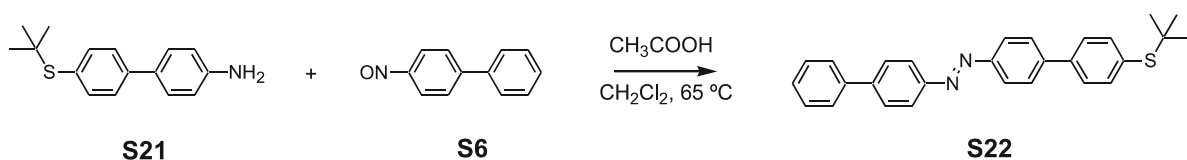
A suspension of biphenyl-4-yl-(4'-methylsulfanyl-biphenyl-4-yl)-diazene **S14** (0.160 g, 0.42 mmol) in dry  $\text{CHCl}_3$  (17 ml) was cooled to 0 °C using an ice/water bath. To the cooled suspension was added mCPBA (0.095 g, 0.55 mmol) in three portions and the mixture stirred at 0 °C for 15 min. Then  $\text{Ca}(\text{OH})_2$  (0.075 g, 1.00 mmol) was added and stirred for an additional 15 min at room temperature. The reaction mixture was filtered, washed with toluene and the solvents removed *in vacuo*. The crude product was purified by column

chromatography (silica gel, toluene/methanol 10/1) giving **S15** as a red–brown solid (0.061 g, 0.15 mmol; 36%). M.p.: 270.5 – 272.0 °C.

<sup>1</sup>H-NMR (300 MHz, CDCl<sub>3</sub>): δ = 2.80 (s, 3 H), 7.40 (t, <sup>3</sup>J(H,H) = 7 Hz, 1 H), 7.49 (t, <sup>3</sup>J(H,H) = 8 Hz, 2 H), 7.69 (d, <sup>3</sup>J(H,H) = 8 Hz, 2 H), 7.75 – 7.79 (m, 6 H), 7.84 (d, <sup>3</sup>J(H,H) = 9 Hz, 2 H), 8.02 – 8.06 (m, 4 H).

MALDI-TOF-MS: 418.65 [M<sup>+</sup> + Na], 396.68 [M<sup>+</sup>].

### Biphenyl-4-yl-(4'-*tert*.-butylsulfanyl-biphenyl-4-yl)-diazene **S22**



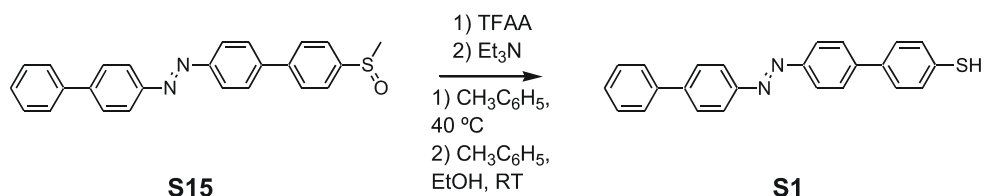
4-Nitroso-biphenyl **S6** (0.302 g, 1.65 mmol) and 4'-*tert*.-butylsulfanyl-biphenyl-4-ylamine **S21** (0.386 g, 1.50 mmol) were dissolved in CH<sub>2</sub>Cl<sub>2</sub> (13 ml) and glacial acetic acid (39 ml) and the reaction mixture heated to 65 °C for 48 h. The solvents were removed by rotary evaporation leaving a red–brown solid which was re-crystallised from toluene affording **S22** as a red solid (0.531 g, 1.26 mmol; 84%). M.p.: 271.0 – 273.0 °C.

<sup>1</sup>H-NMR (300 MHz, CDCl<sub>3</sub>, T = 48 °C): δ = 1.34 (s, 9 H), 7.40 (t, <sup>3</sup>J(H,H) = 8 Hz, 1 H), 7.49 (t, <sup>3</sup>J(H,H) = 7 Hz, 2 H), 7.64 (s, 4H), 7.67 (d, <sup>3</sup>J(H,H) = 7 Hz, 2 H), 7.77 (dd, <sup>3</sup>J(H,H) = 8 Hz, <sup>4</sup>J(H,H) = 2 Hz, 4 H), 8.03 (d, <sup>3</sup>J(H,H) = 9 Hz, 4 H).

<sup>13</sup>C-NMR (75 MHz, CDCl<sub>3</sub>, T = 48 °C): δ = 31.07 (CH<sub>3</sub>), 46.14 (C(CH<sub>3</sub>)<sub>3</sub>), 123.39, 123.43, 127.09, 127.18, 127.71, 127.77, 127.86, 128.87, 132.87, 137.75, 140.29, 140.47, 142.84, 143.86, 152.22 (Ar).

MALDI-TOF-MS: 422.83 [M<sup>+</sup>], 366.78 [M<sup>+</sup> - *t*Bu].

Elemental analysis calcd. (%) for C<sub>28</sub>H<sub>26</sub>N<sub>2</sub>S (422.59): C 79.58, H 6.20, N 6.63; found: C 79.22, H 5.83, N 6.30.

**4'-(Biphenyl-4-ylazo)-biphenyl-4-thiol S1**

Biphenyl-4-yl-(4'-methanesulfinyl-biphenyl-4-yl)-diazene **S15** (0.119 g, 0.30 mmol) was dissolved in dry, Ar-saturated toluene (170 ml) and the mixture heated to 40°C. Then trifluoroacetic anhydride (0.752 g, 0.5 ml, 3.5 mmol) was dropped in and the reaction kept at 40 °C for 2.5 h. The volatiles were removed by rotary evaporation and the residue co-evaporated with dry toluene (2x 20 ml) to remove residual trifluoroacetic acid and anhydride. The obtained dark red solid was dried at HV for 1 h. Then dry, Ar-saturated toluene (200 ml) and dry, Ar-saturated ethanol (60 ml) was added followed by triethylamine (3.5 ml) and the mixture stirred at room temperature for 88 h. The solvents were removed *in vacuo*, the residue dissolved in CH<sub>2</sub>Cl<sub>2</sub>, the organic phase washed twice with Ar-saturated, sat. NH<sub>4</sub>Cl-solution, once with Ar-saturated H<sub>2</sub>O, dried over Na<sub>2</sub>SO<sub>4</sub> and then filtered over a small column (silica gel, CH<sub>2</sub>Cl<sub>2</sub>). After rotary evaporation an orange solid was obtained which was re-crystallised from toluene/ethanol 3/1 to give **S1** as an orange solid (0.030 g, 0.08 mmol; 27%). M.p.: 290.0 (decomp.).

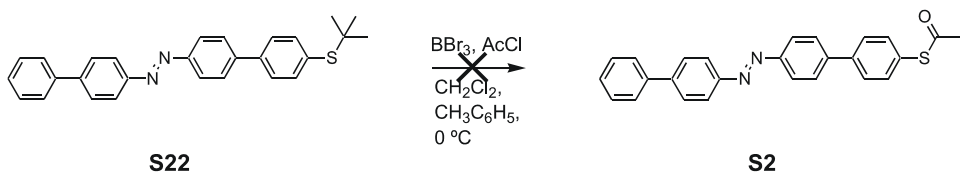
<sup>1</sup>H-NMR (300 MHz, CDCl<sub>3</sub>, T = 48 °C): δ = 3.53 (s, 1 H), 7.37 – 7.39 (m, 3 H), 7.48 (t, <sup>3</sup>J(H,H) = 7 Hz, 2 H), 7.56 (t, <sup>3</sup>J(H,H) = 8 Hz, 2 H), 7.67 – 7.78 (m, 6 H), 8.00 – 8.04 (m, 4 H).

MALDI-TOF-MS: 366.75 [M<sup>+</sup>].

Elemental analysis calcd. (%) for C<sub>24</sub>H<sub>18</sub>N<sub>2</sub>S (366.48): C 78.66, H 4.95, N 7.64; found: C 78.36, H 5.18, N 7.26.

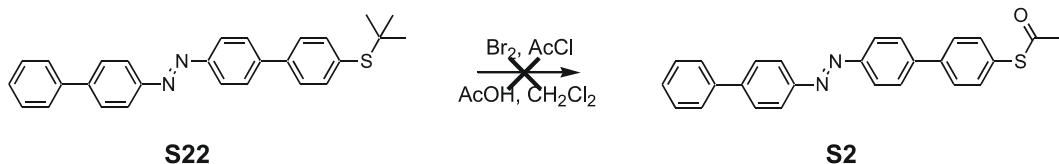
**Biphenyl-4-yl-(4'-acetylsulfanyl-biphenyl-4-yl)-diazene S2**

Route 1:

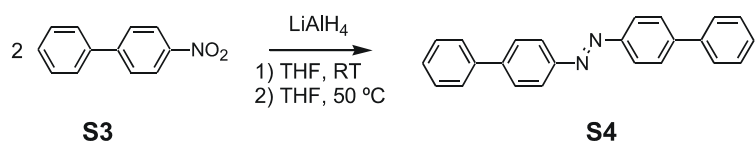


Biphenyl-4-yl-(4'-*tert.*-butylsulfanyl-biphenyl-4-yl)-diazene **S22** (0.020 g, 0.048 mmol) was dissolved in a mixture of dry Ar-saturated  $\text{CH}_2\text{Cl}_2$  (18 ml) and dry Ar-saturated toluene (9 ml). The mixture was cooled to 0°C and acetyl chloride (0.098 g, ca. 0.10 ml, 1.25 mmol) added and after that boron tribromide (1.0 M solution in  $\text{CH}_2\text{Cl}_2$ , 0.05 ml, 0.05 mmol) dropped in and the reaction monitored by TLC. All starting material disappeared after 3 h, but the solution turned colourless. No more azo-compound could be detected.

Route 2:



Biphenyl-4-yl-(4'-*tert.*-butylsulfanyl-biphenyl-4-yl)-diazene **S22** (0.006 g, 0.015 mmol) was dissolved in acetyl chloride (5 ml) and  $\text{CH}_2\text{Cl}_2$  (8 ml) and a bromine solution (0.1 ml in  $\text{CH}_3\text{COOH}/\text{CH}_3\text{COCl}$  10 ml/10 ml) slowly added dropwise. After 3 h all solvents were removed by rotary evaporation. The crude product was purified by column chromatography (silica gel,  $\text{CH}_2\text{Cl}_2$ ). No desired compound could be detected.

**Bis-biphenyl-4-yl-diazene S4**

4-Nitro-biphenyl **S3** (0.996 g, 5.00 mmol) was dissolved in dry THF (5 ml) and treated with lithium aluminium hydride (1 M solution in THF, 20.00 ml, 20.00 mmol) very carefully. The

reaction mixture was kept at room temperature for 1 h, then heated to 50 °C for 15 min. Now water was added very cautiously, filtered and washed with CH<sub>2</sub>Cl<sub>2</sub>. The phases were separated and the aqueous phase extracted with CH<sub>2</sub>Cl<sub>2</sub>, washed with water once, the combined organic phases dried over MgSO<sub>4</sub> and evaporated to dryness leaving a red solid. Re-crystallisation from toluene gave **S4** as a red solid (0.293 g, 0.88 mmol; 35%). M.p.: 254.0 – 255.0°C (Lit.:<sup>[363]</sup> 248.0 – 250.0°C).

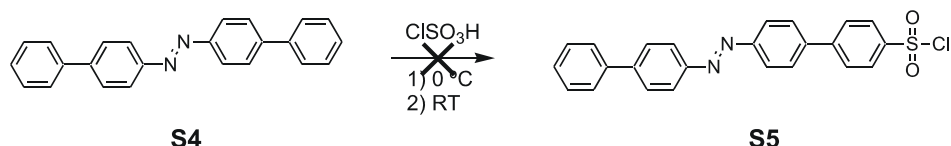
<sup>1</sup>H-NMR (300 MHz, CDCl<sub>3</sub>): δ = 7.40 (t, <sup>3</sup>J(H,H) = 7 Hz, 2 H), 7.46 – 7.52 (m, 4 H), 7.69 (d, <sup>3</sup>J(H,H) = 8 Hz, 4 H), 7.77 (d, <sup>3</sup>J(H,H) = 8 Hz, 4 H), 8.03 (d, <sup>3</sup>J(H,H) = 8 Hz, 4 H).

<sup>13</sup>C-NMR (75 MHz, CDCl<sub>3</sub>): δ = 123.43 (C2), 127.24, 127.83 (C3, C6), 127.93 (C8), 128.94 (C7), 140.25, 143.76 (C4, C5), 151.92 (C1).

MALDI-TOF-MS (9-Nitroanthracene): 334.78 [M<sup>+</sup>].

Elemental analysis calcd. (%) for C<sub>24</sub>H<sub>18</sub>N<sub>2</sub> (334.41): C 86.20, H 5.43, N 8.38; found: C 86.25, H 5.21, N 8.26.

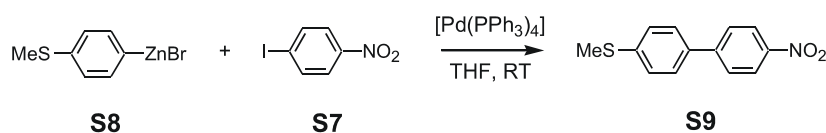
#### 4'-(Biphenyl-4-ylazo)-biphenyl-4-sulfonyl chloride **S5**



Chlorosulphonic acid (0.10 ml, 0.175 g, 1.50 mmol) was placed in a flask and cooled to 0 °C and bis-biphenyl-4-yl-diazene **S4** (0.167 g, 0.50 mmol) was carefully added. The mixture turned black, the ice bath was removed and the reaction stirred at room temperature for 1 h. Re-crystallisation from toluene afforded only starting compound.

The reaction was also repeated at room temperatures without result.

4-Methylsulfanyl-4'-nitro-biphenyl **S7** following the protocol from C. Amatore et al.<sup>[355]</sup>



1-Iodo-4-nitro-benzene **S7** (1.245 g, 5.00 mmol) and tetrakis(triphenylphosphine)palladium (0.578 g, 0.50 mmol) were dissolved in dry, Ar-saturated THF (5 ml) and the mixture stirred

for 15 min at room temperature. Now 4-(methylsulfanyl)-phenylzinc bromide **S8** (0.50 M solution in THF, 12.00 ml, 6.00 mmol) was added via syringe and the reaction kept at room temperature for 50 h. Then it was poured into 10% hydrochloric acid/ice, the aqueous phase extracted with CH<sub>2</sub>Cl<sub>2</sub>, the organic phases washed with water once, dried over MgSO<sub>4</sub> and evaporated to dryness leaving an orange solid. The residue was dissolved again in CH<sub>2</sub>Cl<sub>2</sub>, absorbed on silica gel and added to a column (silica gel, hexane/ethyl acetate 9/1). **S9** was obtained as a yellow solid (0.371 g, 1.51 mmol; 30%). M.p.: 141.0 – 143.0°C (Lit.<sup>[355]</sup>: 128 °C).

R<sub>f</sub> = 0.26.

<sup>1</sup>H-NMR (300 MHz, CDCl<sub>3</sub>): δ = 2.54 (s, 3 H), 7.36 (td, <sup>3</sup>J(H,H) = 8 Hz, <sup>4</sup>J(H,H) = 2 Hz, 2 H), 7.56 (td, <sup>3</sup>J(H,H) = 9 Hz, <sup>4</sup>J(H,H) = 2 Hz, 2 H), 7.72 (td, <sup>3</sup>J(H,H) = 8 Hz, <sup>4</sup>J(H,H) = 2 Hz, 2 H), 8.29 (td, <sup>3</sup>J(H,H) = 9 Hz, <sup>4</sup>J(H,H) = 2 Hz, 2 H).

<sup>13</sup>C-NMR (75 MHz, CDCl<sub>3</sub>): δ = 15.46 (CH<sub>3</sub>S), 124.23, 126.66, 127.35, 127.66, 135.15, 140.33, 146.96 (Ar).

MS (EI): *m/z* (%) = 245 (100) [M<sup>+</sup>], 152.1 (26) [M<sup>+</sup> – NO<sub>2</sub>, – SCH<sub>3</sub>].

Elemental analysis calcd. (%) for C<sub>13</sub>H<sub>11</sub>NO<sub>2</sub>S (245.30): C 63.65, H 4.52, N 5.71; found: C 63.53, H 4.32, N 5.61.

## 7 Bibliography

- [1] *The International Roadmap for Semiconductors*, **2003**.
- [2] H. Kuhn, D. Möbius, *Angew. Chem.* **1971**, *83*, 672–676; *Angew. Chem. Int. Ed.* **1971**, *10*, 460–464.
- [3] A. Aviram, M. A. Ratner, *Chem. Phys. Lett.* **1974**, *29*, 277–283.
- [4] M. Mayor, H. B. Weber, R. Waser, in *Nanoelectronics and Information Technology* (Ed.: R. Waser), Wiley–VCH, Weinheim, **2003**, pp. 501–525.
- [5] G. Binning, H. Rohrer, C. Gerber, E. Weibel, *Phys. Rev. Lett.* **1982**, *49*, 57–61.
- [6] F.–R. F. Fan, J. Yang, S. M. Dirk, D. W. Price, D. Kosynkin, J. M. Tour, A. J. Bard, *J. Am. Chem. Soc.* **2001**, *123*, 2454–2455.
- [7] J. G. Kushmerick, D. B. Holt, J. C. Yang, J. Naciri, M. H. Moore, R. Shashidhar, *Phys. Rev. Lett.* **2002**, *89*, 086802/1–086802/4.
- [8] J. G. Kushmerick, D. B. Holt, S. K. Pollack, M. A. Ratner, J. C. Yang, T. L. Schull, J. Naciri, M. H. Moore, R. Shashidhar, *J. Am. Chem. Soc.* **2002**, *124*, 10654–10655.
- [9] R. E. Holmlin, R. F. Ismagilov, R. Haag, V. Mujica, M. A. Ratner, M. A. Rampi, G. M. Whitesides, *Angew. Chem.* **2001**, *113*, 2378–2382; *Angew. Chem. Int. Ed.* **2001**, *40*, 2316–2320.
- [10] L. A. Bumm, J. J. Arnold, M. T. Cygan, T. D. Dunbar, T. P. Burgin, L. J. II, D. L. Allara, J. M. Tour, P. S. Weiss, *Science* **1996**, *271*, 1705–1707.
- [11] M. A. Reed, C. Zhou, C. J. Muller, T. P. Burgin, J. M. Tour, *Science* **1997**, *278*, 252 – 254.
- [12] C. Kergueris, J.–P. Bourgoin, S. Palacin, D. Esteve, C. Urbina, M. Magoga, C. Joachim, *Phys. Rev. B* **1999**, *59*, 12505–12513.
- [13] J. Reichert, R. Ochs, D. Beckmann, H. B. Weber, M. Mayor, H. v. Löhneysen, *Phys. Rev. Lett.* **2002**, *88*, 176804/1–176804/4.
- [14] N. Robertson, C. A. McGowan, *Chem. Soc. Rev.* **2003**, *32*, 96–103.
- [15] M. Mayor, C. v. Hänisch, H. B. Weber, J. Reichert, D. Beckmann, *Angew. Chem.* **2002**, *114*, 1228–1231; *Angew. Chem., Int. Ed.* **2002**, *41*, 1183–1186.
- [16] R. M. Metzger, B. Chen, U. Höpfner, M. V. LakshmiKantham, D. Vuillaume, T. Kawai, X. Wu, H. Tachibana, T. V. Hughes, H. Sakurai, J. W. Baldwin, C. Hosch, M. P. Cava, L. Brehmer, G. J. Ashwell, *J. Am. Chem. Soc.* **1997**, *119*, 10455–10466.
- [17] T. Xu, I. R. Peterson, M. V. LakshmiKantham, R. M. Metzger, *Angew. Chem.* **2001**, *113*, 1799–1802; *Angew. Chem. Int. Ed.* **2001**, *40*, 1749–1752.
- [18] M.–K. Ng, L. Yu, *Angew. Chem.* **2002**, *114*, 3750–3753; *Angew. Chem.* **2002**, *41*, 3598–3601.
- [19] P. Jiang, G. M. Morales, W. You, L. Yu, *Angew. Chem.* **2004**, *116*, 4571–4575; *Angew. Chem. Int. Ed.* **2004**, *34*, 4471–4475.
- [20] C. P. Collier, G. Mattersteig, E. W. Wong, Y. Luo, K. Beverly, J. Sampaio, F. M. Raymo, J. F. Stoddart, J. R. Heath, *Science* **2000**, *289*, 1172–1175.
- [21] V. Balzani, A. Credi, G. Mattersteig, O. A. Matthews, F. M. Raymo, J. F. Stoddart, M. Venturi, A. J. P. White, D. J. Williams, *J. Org. Chem.* **2000**, *65*, 1924–1936.
- [22] C. P. Collier, E. W. Wong, M. Belohradsky, F. M. Raymo, J. F. Stoddart, P. J. Kuekes, R. S. Williams, J. R. Heath, *Science* **1999**, *285*, 391–394.
- [23] D. Dulic, S. J. v. d. Molen, T. Kudernac, H. T. Jonkman, J. J. D. d. Jong, T. N. Bowden, J. v. Esch, B. L. Feringa, B. J. v. Wees, *Phys. Rev. Lett.* **2003**, *91*, 207402/1–207402/4.

- [24] D. R. Stewart, D. A. A. Ohlberg, P. A. Beck, Y. Chen, R. S. Williams, J. O. Jeppesen, K. A. Nielsen, J. F. Stoddart, *Nano Lett.* **2004**, *4*, 133–136.
- [25] G. E. Moore, *Digest of the 1975 International Electron Devices Meeting*, IEEE, New York, **1975**.
- [26] G. Maruccio, R. Cingolani, R. Rinaldi, *J. Mater. Chem.* **2004**, *14*, 542–554.
- [27] P. Packan, *Science* **199**, 285, 2079–2081.
- [28] C. Joachim, J. K. Gimzewski, A. Aviram, *Nature* **2000**, *408*, 541–548.
- [29] M. Mayor, H. B. Weber, *Angew. Chem.* **2004**, *116*, 2942–2944; *Angew. Chem. Int. Ed.* **2004**, *43*, 2882–2884.
- [30] R. L. Carroll, C. B. Gorman, *Angew. Chem.* **2002**, *114*, 4556–4579; *Angew. Chem. Int. Ed.* **2002**, *41*, 4378–4400.
- [31] D. Demus, J. Goodby, G. W. Gray, H.-W. Spiess, V. Vill, *Handbook of Liquid Crystals, Fundamentals*, Wiley–VCH, Weinheim, **1998**.
- [32] R. H. Friend, R. W. Gymer, A. B. Holmes, J. H. Burroughes, R. N. Marks, C. Taliani, D. D. C. Bradley, D. A. D. Santos, J. L. Bredas, M. Lögdlund, W. R. Salaneck, *Nature* **1999**, *397*, 121–128.
- [33] J. M. Tour, *Acc. Chem. Res.* **2000**, *33*, 791–804.
- [34] B. Mann, H. Kuhn, *J. Appl. Phys.* **1971**, *42*, 4398–4405.
- [35] M. Mayor, H. B. Weber, *Nachr. aus der Chemie* **2002**, *50*, 1212–1217.
- [36] R. F. Bunshah, *Handbook of Deposition Technologies for Films and Coatings*, Noyes Publ., Park Rdige, **1994**.
- [37] A. Ulman, *An Introduction to Ultrathin Organic Films, from Langmuir Blodgett to Self-Assembling*, Academic Press, Boston, **1991**.
- [38] A. Ulman, *Chem. Rev.* **1996**, *96*, 1533–1554.
- [39] R. M. Metzger, *J. Mater. Chem.* **2000**, *10*, 55–62.
- [40] C. Zhou, M. R. Deshpande, M. A. Reed, L. J. II, J. M. Tour, *Appl. Phys. Lett.* **1997**, *71*, 611–613.
- [41] J. Chen, M. A. Reed, A. M. Rawlett, J. M. Tour, *Science* **1999**, *286*, 1550–1552.
- [42] R. E. Holmlin, R. Haag, M. L. Chabinyc, R. F. Ismagilov, A. E. Cohen, A. Terfort, M. A. Rampi, G. M. Whitesides, *J. Am. Chem. Soc.* **2001**, *123*, 5075–5085.
- [43] M. A. Rampi, O. J. A. Schueller, G. M. Whitesides, *Appl. Phys. Lett.* **1998**, *72*, 1781–1783.
- [44] R. Haag, M. A. Rampi, R. E. Holmlin, G. M. Whitesides, *J. Am. Chem. Soc.* **1999**, *121*, 7895–7906.
- [45] C. Grave, B. Long, M. A. Rampi, personal communication, **2004**.
- [46] H. B. Weber, J. Reichert, F. Weigend, R. Ochs, D. Beckmann, M. Mayor, R. Ahlrichs, H. v. Löhneysen, *Chem. Phys.* **2002**, *281*, 113–125.
- [47] M. F. Crommie, C. P. Lutz, D. M. Eigler, *Science* **1993**, *262*, 218–220.
- [48] P. Ebert, K. Szot, A. Roelofs, in *Nanoelectronics and Information Technology* (Ed.: R. Waser), Wiley–VCH, Weinheim, **2003**, pp. 299–320.
- [49] R. Wiesendanger, U. D. Schwarz, in *Handbook of Microscopy* (Eds.: S. Amelinckx, D. v. Dyck, J. v. Landuyt, G. v. Tendeloo), VCH, Weinheim, **1997**, pp. 805–884.
- [50] E. Meyer, H. J. Hug, R. Bennewitz, *Scanning Probe Microscopy – The Lab on a Tip*, Springer–Verlag, Berlin, **2004**.
- [51] J. Tersoff, D. R. Hamann, *Phys. Rev. B* **1985**, *31*, 805–813.
- [52] J. Y. Park, Y. Yaish, M. Brink, S. Rosenblatt, P. L. McEuen, *Appl. Phys. Lett.* **2002**, *80*, 4446–4448.
- [53] S.–W. Hla, L. Bartels, G. Meyer, K.–H. Rieder, *Phys. Rev. Lett.* **2000**, *85*, 2777–2780.
- [54] X. D. Cui, A. Primak, X. Zarate, J. Tomfohr, O. F. Sankey, A. L. Moore, T. A. Moore, D. Gust, G. Harris, S. M. Lindsay, *Science* **2001**, *294*, 571–574.

- [55] A. M. Rawlett, T. J. Hopson, L. A. Nagahara, R. K. Tsui, G. K. Ramachandran, S. M. Lindsay, *Appl. Phys. Lett.* **2002**, *81*, 3043–3045.
- [56] G. K. Ramachandran, J. K. Tomfohr, J. Li, O. F. Sankey, X. Zarate, A. Primak, Y. Terazono, T. A. Moore, A. L. Moore, D. Gust, L. A. Nagahara, S. M. Lindsay, *J. Phys. Chem. B* **2003**, *107*, 6162–6169.
- [57] B. Xu, N. J. Tao, *Science* **2003**, *301*, 1221–1223.
- [58] C. J. Muller, J. M. Krans, T. N. Todorov, M. A. Reed, *Phys. Rev. B* **1996**, *53*, 1022–1025.
- [59] E. Scheer, *Spektrum der Wissenschaft* **1999**, *95*, 95–98.
- [60] E. Scheer, P. Joyez, D. Esteve, C. Urbina, M. H. Devoret, *Phys. Rev. Lett.* **1997**, *78*, 3535–3538.
- [61] J. M. Tour, L. J. II, D. L. Pearson, J. J. S. Lamba, T. P. Burgin, G. M. Whitesides, D. L. Allara, A. N. Parikh, S. V. Atre, *J. Am. Chem. Soc.* **1995**, *117*, 9529–9534.
- [62] J. Reichert, H. B. Weber, M. Mayor, H. v. Löhneysen, *Appl. Phys. Lett.* **2003**, *82*, 4137–4139.
- [63] M. Mayor, M. Büschel, K. M. Fromm, J.-M. Lehn, J. Daub, *Ann. N. Y. Acad. Sci.* **2002**, *960*, 16–28.
- [64] W. B. Davis, W. A. Svec, M. A. Ratner, M. R. Wasielewski, *Nature* **1998**, *396*, 60–63.
- [65] P. F. Barbara, T. J. Meyer, M. A. Ratner, *J. Phys. Chem.* **1996**, *100*, 13148–13168.
- [66] S. Creager, C. J. Yu, C. Bamdad, S. O'Connor, T. MacLean, E. Lam, Y. Chong, G. T. Olsen, J. Luo, M. Gozin, J. F. Kayyem, *J. Am. Chem. Soc.* **1999**, *121*, 1059–1064.
- [67] C. Z. Li, N. J. Tao, *Appl. Phys. Lett.* **1998**, *72*, 894–896.
- [68] S. Boussaad, N. J. Tao, *Appl. Phys. Lett.* **2002**, *80*, 2398–2400.
- [69] H. Park, A. K. L. Lim, A. P. Alivisatos, J. Park, P. L. McEuen, *Appl. Phys. Lett.* **1999**, *75*, 301–303.
- [70] R. Kuhn, *Angew. Chem.* **1937**, *50*, 703–708.
- [71] R. Eastmond, T. R. Johnson, D. R. M. Walton, *Tetrahedron* **1972**, *28*, 4601–4616.
- [72] W. Steinkopf, R. Leitsmann, K.-H. Hofmann, *Lieb. Ann. Chem.* **1941**, *546*, 180–199.
- [73] W. Kern, M. Seibel, H. O. Wirth, *Makromol. Chemie* **1959**, *29*, 164–189.
- [74] G. Drefahl, G. Plötner, *Chem. Ber.* **1961**, *94*, 907–914.
- [75] G. Drefahl, G. Plötner, *Chem. Ber.* **1958**, *91*, 1274–1280.
- [76] A. Nitzan, M. A. Ratner, *Science* **2003**, *300*, 1384–1389.
- [77] K. Müllen, G. Wegner, *Electronic Materials: The Oligomer Approach*, Wiley–VCH, Weinheim, **1998**.
- [78] P. Liess, V. Hensel, A.–D. Schlüter, *Liebigs Ann. Org. Bioorg. Chem.* **1996**, *7*, 1037–1040.
- [79] L. Jones, J. S. Schumm, J. M. Tour, *J. Org. Chem.* **1997**, *62*, 1388–1410.
- [80] A. C. Benniston, A. Harriman, P. Li, C. A. Sams, *Tetrahedron Lett.* **2003**, *44*, 4167 – 4169.
- [81] A. Tsuda, A. Osuka, *Science* **2001**, *293*, 79–82.
- [82] J. R. Reimers, L. E. Hall, M. J. Crossley, N. S. Hush, *J. Phys. Chem. A* **1999**, *103*, 4385–4397.
- [83] A. J. Storm, J. v. Noort, S. d. Vries, C. Dekker, *Appl. Phys. Lett.* **2001**, *79*, 3881–3883.
- [84] L. Cai, H. Tabata, T. Kawai, *Appl. Phys. Lett.* **2000**, *77*, 3105–3106.
- [85] H.–W. Fink, C. Schönenberger, *Science* **1999**, *398*, 407–410.
- [86] P. M. Ajayan, *Chem. Rev.* **1999**, *99*, 1787–1799.
- [87] R. Krupke, F. Hennrich, H. v. Löhneysen, M. M. Kappes, *Science* **2003**, *301*, 344–347.
- [88] D. Tasis, N. Tagmatarchis, V. Georgakilas, M. Prato, *Chem. Eur. J.* **2003**, *9*, 4000–4008.
- [89] C. Elschenbroich, A. Salzer, *Organometallchemie*, Teubner, Stuttgart, **1993**.

- [90] T. L. Schull, J. G. Kushmerick, C. H. Patterson, C. George, M. H. Moore, S. K. Pollack, R. Shashidhar, *J. Am. Chem. Soc.* **2003**, *125*, 3202–3203.
- [91] J. March, *Advanced Organic Chemistry*, 4 ed., Wiley–Interscience, New York, **1992**.
- [92] S. N. Yaliraki, M. A. Ratner, *Ann. N. Y. Acad. Sci.* **2002**, *960*, 153–162.
- [93] M. Mayor, H. B. Weber, J. Reichert, M. Elbing, C. v. Hänisch, D. Beckmann, M. Fischer, *Angew. Chem.* **2003**, *115*, 6014–6018; *Angew. Chem. Int. Ed.* **2003**, *42*, 5834–5838.
- [94] K. Stokbro, J. Taylor, M. Brandbyge, *J. Am. Chem. Soc.* **2003**, *125*, 3674–3675.
- [95] A. S. Martin, J. R. Sambles, G. J. Ashwell, *Phys. Rev. Lett.* **1993**, *70*, 218–221.
- [96] A. Stabel, P. Herwig, K. Müllen, J. P. Rabe, *Angew. Chem.* **1995**, *107*, 335–339; *Angew. Chem. Int. Ed.* **1995**, *34*, 303–307.
- [97] K. Müllen, J. P. Rabe, *Ann. N. Y. Acad. Sci.* **1998**, *852*, 205–218.
- [98] A. Dhirani, P.–H. Lin, P. Guyot–Sionnest, R. W. Zehner, L. R. Sita, *J. Chem. Phys.* **1997**, *106*, 5249–5253.
- [99] C. Krzeminski, C. Delerue, G. Allan, D. Vuillaume, R. M. Metzger, *Phys. Rev. B* **2001**, *64*, 085405/1–085405/6.
- [100] G. J. Ashwell, R. Hamilton, L. R. H. High, *J. Mater. Chem.* **2003**, *13*, 1501–1503.
- [101] G. J. Ashwell, D. S. Gandolfo, R. Hamilton, *J. Mater. Chem.* **2002**, *12*, 416–420.
- [102] J. W. Baldwin, R. R. Amaresh, I. R. Peterson, W. J. Shumate, M. P. Cava, M. A. Amiri, R. Hamilton, G. J. Ashwell, R. M. Metzger, *J. Phys. Chem. B* **2002**, *106*, 12158–12164.
- [103] V. Balzani, M. Venturi, A. Credi, *Molecular Devices and Machines*, Wiley–VCH, Weinheim, **2003**.
- [104] F. M. Raymo, J. F. Stoddart, in *Molecular Switches* (Ed.: B. L. Feringa), Wiley–VCH, Weinheim, **2001**, pp. 219–248.
- [105] K. Matsuda, M. Irie, *Chem. Eur. J.* **2001**, *7*, 3466–3473.
- [106] H. Schroeder, A. Kingon, in *Nanoelectronics and Information Technology* (Ed.: R. Waser), Wiley–VCH, Weinheim, **2003**, pp. 541–563.
- [107] M. Irie, in *Molecular Switches* (Ed.: B. L. Feringa), Wiley–VCH, Weinheim, **2001**, pp. 37–62.
- [108] I. Willner, B. Willner, in *Molecular Switches* (Ed.: B. L. Feringa), Wiley–VCH, Weinheim, **2001**, pp. 165–218.
- [109] M. Irie, *Chem. Rev.* **2000**, *100*, 1685–1716.
- [110] S. H. Kawai, S. L. Gilat, R. Posinet, J.–M. Lehn, *Chem. Eur. J.* **1995**, *1*, 285–293.
- [111] G. S. Hartley, *Nature* **1937**, *140*, 281–282.
- [112] F. Vögtle, *Supramolekulare Chemie*, Teubner–Studienbücher, Stuttgart, **1992**.
- [113] S. Tsuchiya, *J. Am. Chem. Soc.* **1999**, *121*, 48–53.
- [114] B. Jousselme, P. Blanchard, N. Gallego–Planas, J. Delaunay, M. Allain, P. Richomme, E. Levillain, J. Roncali, *J. Am. Chem. Soc.* **2003**, *125*, 2888–2889.
- [115] S. Yasuda, T. Nakamura, M. Matsumoto, H. Shigekawa, *J. Am. Chem. Soc.* **2003**, *125*, 16430–16433.
- [116] M. Asakawa, P. R. Ashton, V. Balzani, A. Credi, C. Hamers, G. Mattersteig, M. Montalti, A. N. Shipway, N. Spencer, J. F. Stoddart, M. S. Tolley, M. Venturi, A. J. P. White, D. J. Williams, *Angew. Chem.* **1998**, *110*, 357–361; *Angew. Chem. Int. Ed.* **1998**, *37*, 333–337.
- [117] M. A. Reed, J. Chen, A. M. Rawlett, D. W. Price, J. M. Tour, *Appl. Phys. Lett.* **2001**, *78*, 3735–3737.
- [118] D. W. Price, S. M. Dirk, F. Maya, J. M. Tour, *Tetrahedron* **2003**, *59*, 2497–2518.
- [119] J. C. Ellenbogen, J. C. Love, *Proc. IEEE* **2000**, *88*, 386–426.
- [120] W. Liang, M. P. Shores, M. Bockrath, J. R. Long, H. Park, *Nature* **2002**, *417*, 725–729.

- [121] J. Park, A. N. Pasupathy, J. I. Goldsmith, C. Chang, Y. Yaish, J. R. Petta, M. Rinkoski, J. P. Sethna, H. D. Abruna, P. L. McEuen, D. C. Ralph, *Nature* **2002**, *417*, 722–725.
- [122] A. F. Littke, G. C. Fu, *Angew. Chem.* **2002**, *114*, 4350–4386; *Angew. Chem. Int. Ed.* **2002**, *41*, 4176–4211.
- [123] F. Diederich, P. J. Stang, *Metal–Catalyzed Cross–coupling Reactions*, Wiley–VCH, Weinheim, **1998**.
- [124] B. Scheiper, M. Bonnekessel, H. Krause, A. Fürstner, *J. Org. Chem.* **2004**, *69*, 3943–3949.
- [125] S. V. Ley, A. W. Thomas, *Angew. Chem.* **2003**, *115*, 5558–5607; *Angew. Chem. Int. Ed.* **2003**, *42*, 5400–5449.
- [126] K. Fagnou, M. Lautens, *Chem. Rev.* **2003**, *103*, 169–196.
- [127] M. Lautens, J. Mancuso, *J. Org. Chem.* **2004**, *69*, 3478–2487.
- [128] K. Tamao, N. Miyaura, *Top. Curr. Chem.* **2002**, *219*, 1–9.
- [129] K. Tamao, K. Sumitani, M. Kumada, *J. Am. Chem. Soc.* **1972**, *94*, 4374–4376.
- [130] R. J. P. Corriu, J. P. Masse, *J. Chem. Soc. Chem. Commun.* **1972**, 144a–144a.
- [131] E. Negishi, *J. Organomet. Chem.* **2002**, *653*, 34–40.
- [132] S. Baba, E. Negishi, *J. Am. Chem. Soc.* **1976**, *98*, 6729–6731.
- [133] K. Kondo, S.-I. Murahashi, *Tetrahedron Lett.* **1979**, *20*, 1237–1240.
- [134] M. Kosugi, K. Sasazawa, Y. Shimizu, T. Migita, *Chem. Lett.* **1977**, 301–302.
- [135] E. Negishi, A. O. King, N. Okukado, *J. Org. Chem.* **1977**, *42*, 1821–1823.
- [136] J. F. Hartwig, *Angew. Chem.* **1998**, *110*, 2154–2177; *Angew. Chem. Int. Ed.* **1998**, *37*, 2046–2067.
- [137] A. Suzuki, in *Metal–Catalyzed Cross–coupling Reactions* (Eds.: F. Diederich, P. J. Stang), Wiley–VCH, Weinheim, **1998**, pp. 49–97.
- [138] A. Boudier, L. O. Bromm, M. Lotz, P. Knochel, *Angew. Chem.* **2000**, *112*, 4584–4606; *Angew. Chem. Int. Ed.* **2000**, *39*, 4414–4435.
- [139] M. S. Kharasch, E. K. Fields, *J. Am. Chem. Soc.* **1941**, *63*, 2316–2320.
- [140] M. Yamamura, I. Moritani, S.-I. Murahashi, *J. Organomet. Chem.* **1975**, *91*, C39–C42.
- [141] V. P. W. Böhm, T. Weskamp, C. W. K. Gstöttmayr, W. A. Herrmann, *Angew. Chem.* **2000**, *112*, 1672–1674; *Angew. Chem. Int. Ed.* **2000**, *39*, 1602–1604.
- [142] M. Kumada, *Pure Appl. Chem.* **1980**, *52*, 669–679.
- [143] T. Banno, Y. Hayakawa, M. Umeno, *J. Organomet. Chem.* **2002**, *653*, 288–291.
- [144] F. Mongin, L. Mojovic, B. Guillamet, F. Trécourt, G. Quéguiner, *J. Org. Chem.* **2002**, *67*, 8991–8994.
- [145] J. Huang, S. P. Nolan, *J. Am. Chem. Soc.* **1999**, *121*, 9889–9890.
- [146] S. Tasler, B. H. Lipshutz, *J. Org. Chem.* **2003**, *68*, 1190–1199.
- [147] A. C. Frisch, N. Shaikh, A. Zapf, M. Beller, *Angew. Chem.* **2002**, *114*, 4218–4221; *Angew. Chem. Int. Ed.* **2002**, *41*, 4056–4059.
- [148] J. Terao, H. Watanabe, A. Ikumi, H. Kuniyasu, N. Kambe, *J. Am. Chem. Soc.* **2002**, *124*, 4222–4223.
- [149] D. J. Cardenas, *Angew. Chem.* **2003**, *115*, 398–401; *Angew. Chem. Int. Ed.* **2003**, *42*, 384–387.
- [150] P. Knochel, W. Dohle, N. Gommermann, F. F. Kneisel, F. Kopp, T. Korn, I. Sapountzis, V. A. Vu, *Angew. Chem.* **2003**, *115*, 4438–4456; *Angew. Chem. Int. Ed.* **2003**, *42*, 4302–4320.
- [151] E. Negishi, F. Liu, in *Metal–Catalyzed Cross–coupling Reactions* (Eds.: F. Diederich, P. J. Stang), Wiley–VCH, Weinheim, **1998**, pp. 1–48.
- [152] P. Knochel, R. D. Singer, *Chem. Rev.* **1993**, *93*, 2117–2188.
- [153] L. Zhu, R. M. Wehmeyer, R. D. Rieke, *J. Org. Chem.* **1991**, *56*, 1445–1453.

- [154] C. Dai, G. C. Fu, *J. Am. Chem. Soc.* **2001**, *123*, 2719–2724.
- [155] C. E. Tucker, T. N. Majid, P. Knochel, *J. Am. Chem. Soc.* **1992**, *114*, 3983–3985.
- [156] T. A. Chen, R. A. O'Brien, R. D. Rieke, *Macromolecules* **1993**, *26*, 3462–3463.
- [157] M. Sonoda, A. Inaba, K. Itahashi, Y. Tobe, *Org. Lett.* **2001**, *3*, 2419–2421.
- [158] A. E. Jensen, P. Knochel, *J. Org. Chem.* **2002**, *67*, 79–85.
- [159] T. N. Mitchell, in *Metal-Catalyzed Cross-coupling Reactions* (Eds.: F. Diederich, P. J. Stang), Wiley–VCH, Weinheim, **1998**, pp. 167–202.
- [160] E. Negishi, L. Anastasia, *Chem. Rev.* **2003**, *103*, 1979–2017.
- [161] K. Sonogashira, in *Metal-Catalyzed Cross-coupling Reactions* (Eds.: F. Diederich, P. J. Stang), Wiley–VCH, Weinheim, **1998**, pp. 203–229.
- [162] K. Sonogashira, *J. Organomet. Chem.* **2002**, *653*, 46–49.
- [163] A. Köllhofer, T. Pullmann, H. Plenio, *Angew. Chem.* **2003**, *115*, 1086–1088; *Angew. Chem. Int. Ed.* **2003**, *42*, 1056–1058.
- [164] D. Gelman, S. L. Buchwald, *Angew. Chem.* **2003**, *115*, 6175–6178; *Angew. Chem. Int. Ed.* **2003**, *42*, 5993–5996.
- [165] P. Siemsen, R. C. Livingston, F. Diederich, *Angew. Chem.* **2000**, *112*, 2740–2767; *Angew. Chem. Int. Ed.* **2000**, *39*, 2632–2657.
- [166] N. Miyaura, K. Yamada, A. Suzuki, *Tetrahedron Lett.* **1979**, *20*, 3437–3440.
- [167] N. Yasuda, *J. Organomet. Chem.* **2002**, *653*, 279–287.
- [168] N. Miyaura, A. Suzuki, *Chem. Rev.* **1995**, *95*, 2457–2483.
- [169] T. Ishiyama, N. Matsuda, N. Miyaura, A. Suzuki, *J. Am. Chem. Soc.* **1993**, *115*, 11018–11019.
- [170] T. Ishiyama, M. Murata, N. Miyaura, *J. Org. Chem.* **1995**, *60*, 7508–7510.
- [171] M. Murata, S. Watanabe, Y. Masuda, *J. Org. Chem.* **1997**, *62*, 6458–6459.
- [172] M. Murata, T. Oyama, S. Watanabe, Y. Masuda, *J. Org. Chem.* **2000**, *65*, 164–168.
- [173] see for example: Lancaster catalogue 2002–2003 or lancastersynthesis.com.
- [174] N. Miyaura, *J. Organomet. Chem.* **2002**, *653*, 54–57.
- [175] A. Suzuki, *J. Organomet. Chem.* **1999**, *576*, 147–168.
- [176] Z. Ahmed, P. Langer, *J. Org. Chem.* **2004**, *69*, 3753–3757.
- [177] G. B. Smith, G. C. Dezeny, D. L. Hughes, A. O. King, T. R. Verhoeven, *J. Org. Chem.* **1994**, *59*, 8151–8156.
- [178] J. P. Wolfe, S. L. Buchwald, *Angew. Chem.* **1999**, *111*, 2570–2573; *Angew. Chem. Int. Ed.* **1999**, *38*, 2413–2416.
- [179] A. F. Littke, G. C. Fu, *Angew. Chem.* **1998**, *110*, 3586–3587; *Angew. Chem. Int. Ed.* **1998**, *37*, 3387–3388.
- [180] T. Ishiyama, K. Ishida, N. Miyaura, *Tetrahedron* **2001**, *57*, 9813–9816.
- [181] M. R. Netherton, C. Dai, K. Neuschütz, G. C. Fu, *J. Am. Chem. Soc.* **2001**, *123*, 10099–10100.
- [182] J. S. Zhou, G. C. Fu, *J. Am. Chem. Soc.* **2004**, *126*, 1340–1341.
- [183] M. Kosugi, M. Kameyama, T. Migita, *Chem. Lett.* **1983**, 927–928.
- [184] J. Louie, J. F. Hartwig, *Tetrahedron Lett.* **1995**, *36*, 3609–3612.
- [185] A. S. Guram, R. A. Rennels, S. L. Buchwald, *Angew. Chem.* **1995**, *107*, 1456–1459; *Angew. Chem. Int. Ed.* **1995**, *34*, 1348–1350.
- [186] A. R. Muci, S. L. Buchwald, *Top. Curr. Chem.* **2002**, *219*, 131–209.
- [187] J. B. Laursen, J. Nielsen, *Chem. Rev.* **2004**, *104*, 1663–1685.
- [188] A. J. Peat, S. L. Buchwald, *J. Am. Chem. Soc.* **1996**, *118*, 1028–1030.
- [189] Z. H. Li, M. S. Wong, Y. Tao, M. D'Iorio, *J. Org. Chem.* **2004**, *69*, 921–927.
- [190] S. Becker, A. Böhm, K. Müllen, *Chem. Eur. J.* **2000**, *6*, 3984–3990.
- [191] J. P. Wolfe, J. Ahman, J. P. Sadighi, R. A. Singer, S. L. Buchwald, *Tetrahedron Lett.* **1997**, *38*, 6367–6370.
- [192] S. Lee, M. Jorgensen, J. F. Hartwig, *Org. Lett.* **2001**, *3*, 2729–2732.

- [193] Y. Hatanaka, T. Hiyama, *J. Org. Chem.* **1988**, *53*, 918–920.
- [194] S. Bräse, A. d. Meijere, in *Metal-Catalyzed Cross-coupling Reactions* (Eds.: F. Diederich, P. J. Stang), Wiley–VCH, Weinheim, **1998**, pp. 99–166.
- [195] J. T. Link, L. E. Overman, in *Metal-Catalyzed Cross-coupling Reactions* (Eds.: F. Diederich, P. J. Stang), Wiley–VCH, Weinheim, **1998**.
- [196] R. J. Cremlin, *An Introduction to Organosulfur Chemistry*, Wiley, Chichester, **1996**.
- [197] H. M. Brown, *Pestic. Sci.* **1990**, *29*, 263–281.
- [198] A. Fleming, *Br. J. Exper. Path.* **1929**, *10*, 226–236.
- [199] H. Zollinger, *Color Chemistry – Syntheses, Properties and Applications of Organic Dyes and Pigments*, 3 ed., Verlag Helvetica Chimica Acta, Zürich, **2003**.
- [200] J. G. Lombardino, *J. Org. Chem.* **1971**, *36*, 1843–1845.
- [201] S. Oae, T. Okuyama, *Organic Sulfur Chemistry: Biochemical Aspects*, CRC Press, Boca Raton, **1992**.
- [202] E. Riedel, *Anorganische Chemie*, 3. ed., Walter deGruyter, Berlin, **1994**.
- [203] M. C. Carreno, *Chem. Rev.* **1995**, *95*, 1717–1760.
- [204] C. A. Mirkin, R. L. Letsinger, R. C. Mucic, J. J. Storhoff, *Nature* **1996**, *382*, 607–609.
- [205] A. P. Alivisatos, K. P. Johnsson, X. Peng, T. E. Wilson, C. J. Loweth, M. P. Bruchez, P. G. Schultz, *Nature* **1996**, *382*, 609–612.
- [206] M. Boncheva, D. A. Bruzewicz, G. M. Whitesides, *Pure Appl. Chem.* **2003**, *75*, 621–631.
- [207] K. D. Gundermann, K. Hümke, in *Houben–Weyl, Methoden der organischen Chemie*, Vol. E11, 4 ed., Thieme, Stuttgart, **1985**, pp. 32–63.
- [208] H. Gilman, G. C. Gainer, *J. Am. Chem. Soc.* **1949**, *71*, 1747–1751.
- [209] D. L. Pearson, J. M. Tour, *J. Org. Chem.* **1997**, *62*, 1376–1387.
- [210] E. Jones, I. M. Moodie, *Org. Synth.* **1970**, *50*, 104–106.
- [211] R. Adams, C. S. Marvel, *Org. Synth. Coll. Vol. I* **1964**, 504–506.
- [212] D. T. Gryko, C. Clausen, J. S. Lindsey, *J. Org. Chem.* **1999**, *64*, 8635–8647.
- [213] H. Uchiyo, S. Kobayashi, *Tetrahedron Lett.* **1999**, *40*, 3179–3182.
- [214] T. Schaefer, J. D. Baleja, G. H. Penner, *Can J. Chem.* **1984**, *63*, 2471–2475.
- [215] R. N. Young, J. Y. Gauthier, W. Coombs, *Tetrahedron Lett.* **1984**, *25*, 1753–1756.
- [216] W. E. Truce, D. P. Tate, D. N. Burdge, *J. Am. Chem. Soc.* **1960**, *82*, 2872–2876.
- [217] W. E. Truce, J. J. Breiter, *J. Am. Chem. Soc.* **1962**, *84*, 1621–1622.
- [218] A. Pinchart, C. Dallaire, M. Gingras, *Tetrahedron Lett.* **1998**, *39*, 543–546.
- [219] K. D. Gundermann, K. Hümke, in *Houben–Weyl, Methoden der organischen Chemie*, Vol. E11, 4 ed., Thieme, Stuttgart, **1985**, pp. 129–141.
- [220] T. J. Wallace, A. Schriesheim, *J. Org. Chem.* **1962**, *27*, 1514–1516.
- [221] H. K. Oh, S. Y. Woo, C. H. Shin, Y. S. Park, I. Lee, *J. Org. Chem.* **1997**, *62*, 5780–5784.
- [222] B. Zeysing, C. Gosch, A. Terfort, *Org. Lett.* **2000**, *2*, 1843–1845.
- [223] N. Stuhr-Hansen, J. B. Christensen, N. Harrit, T. Bjornholm, *J. Org. Chem.* **2002**, *68*, 1275–1282.
- [224] I. A. Aliev, G. A. Kalabin, N. Ghelis, *Sulfur Lett.* **1991**, *12*, 123–132.
- [225] N. Stuhr-Hansen, *Synth. Commun.* **2003**, *33*, 641–645.
- [226] A. Blaszczyk, M. Elbing, M. Mayor, *Org. Biomol. Chem.* **2004**, *2*, 2722–2724.
- [227] C. Barkenbus, E. B. Friedman, R. K. Flege, *J. Am. Chem. Soc.* **1927**, *49*, 2549–2553.
- [228] K. D. Gundermann, K. Hümke, in *Houben–Weyl, Methoden der organischen Chemie*, Vol. E11, 4 ed., Thieme, Stuttgart, **1985**, pp. 158–187.
- [229] J. H. Ziegler, *Chem. Ber.* **1890**, *23*, 2469–2472.
- [230] M. Barbero, I. Degani, N. Diulgheroff, S. Dughera, R. Fochi, M. Migliaccio, *J. Org. Chem.* **2000**, *65*, 5600–5608.

- [231] P. Cogolli, F. Maiolo, L. Testaferri, M. Tingoli, M. Tiecco, *J. Org. Chem.* **1979**, *44*, 2642–2646.
- [232] L. Testaferri, M. Tiecco, M. Tingoli, D. Chianelli, M. Montanucci, *Synthesis* **1983**, 751–755.
- [233] L. Testaferri, M. Tiecco, M. Tingoli, *J. Org. Chem.* **1980**, *45*, 4376–4380.
- [234] R. G. R. Bacon, H. A. O. Hill, *J. Chem. Soc.* **1964**, 1108–1112.
- [235] M. Madesclaire, *Tetrahedron* **1986**, *42*, 5459–5495.
- [236] G. Kresze, in *Houben–Weyl, Methoden der organischen Chemie*, Vol. E11, 4 ed., Thieme, Stuttgart, **1985**, pp. 669–886.
- [237] A. R. Hajipour, S. E. Mallakpour, H. Adibi, *J. Org. Chem.* **2002**, *67*, 8666–8668.
- [238] S. Pawlenko, in *Houben–Weyl, Methoden der organischen Chemie*, Vol. E11, 4 ed., Thieme, Stuttgart, **1985**, pp. 1055–1073.
- [239] Autorenkollektiv, *Organikum*, Wiley–VCH, Weinheim, **2001**.
- [240] T. Kondo, T. Mitsudo, *Chem. Rev.* **2000**, *100*, 3205–3220.
- [241] T. Migita, T. Shimizu, Y. Asami, J. Shiobara, Y. Kato, M. Kosugi, *Bull. Chem. Soc. Jpn.* **1980**, *53*, 1385–1389.
- [242] A. Ogawa, J. Kawakami, N. Sonoda, T. Hirao, *J. Org. Chem.* **1996**, *61*, 4161–4163.
- [243] J.–E. Bäckvall, A. Ericsson, *J. Org. Chem.* **1994**, *59*, 5850–5851.
- [244] H. Zollinger, *Azo and Diazo Chemistry*, Interscience, New York, **1961**.
- [245] E. Mitscherlich, *Ann. Pharm.* **1834**, 311–314.
- [246] A. Hantzsch, *Ber. Dtsch. Chem. Ges.* **1895**, *28*, 1734–1758.
- [247] E. Bamberger, *Ber. Dtsch. Chem. Ges.* **1895**, *28*, 444–449.
- [248] A. Johnson, in *The Theory of Coloration of Textiles* (Ed.: A. Johnson), Dyers Comp. Publ. Trust, Bradford, **1989**.
- [249] F. Würthner, J. Rebek, *Angew. Chem.* **1995**, *107*, 503–505; *Angew. Chem. Int. Ed.* **1995**, *34*, 446–448.
- [250] N. Tamaoki, S. Song, M. Moriyama, H. Matsuda, *Adv. Mater.* **2000**, *12*, 94–97.
- [251] A. Archut, F. Vögtle, L. d. Cola, G. C. Azzellini, V. Balzani, P. S. Ramanujam, R. H. Berg, *Chem. Eur. J.* **1998**, *4*, 699–706.
- [252] H. B. Mekelburger, F. Vögtle, K. Rissanen, *Chem. Ber.* **1993**, *126*, 1161–1169.
- [253] F. Agolini, F. P. Gay, *Macromolecules* **1970**, *3*, 349–351.
- [254] J. A. Delaire, K. Nakatani, *Chem. Rev.* **2000**, *100*, 1817–1845.
- [255] S. M. Parmerter, *Org. React.* **1959**, *10*, 1–142.
- [256] E. Haselbach, *Helv. Chim. Acta* **1970**, *53*, 1526–1543.
- [257] B. Ortiz, P. Villanueva, F. Walls, *J. Org. Chem.* **1972**, *37*, 2748–2750.
- [258] M. Hedayatullah, L. Denivelle, J. P. Dechatre, *Tetrahedron Lett.* **1975**, *35*, 2039–2042.
- [259] E. Tauer, R. Machinek, *Liebigs Ann.* **1996**, 1213–1216.
- [260] P. Dragut, PhD thesis, Rheinische Friedrich–Wilhelms–Universität (Bonn), **2004**.
- [261] K. H. Schündehütte, in *Houben–Weyl, Methoden der organischen Chemie*, Vol. 10/3, 1 ed., Thieme, Stuttgart, **1965**, pp. 213–466.
- [262] G. Lin, C.–I. Hwang, J.–Y. Chouhwang, H.–J. Tsai, *J. Chin. Chem. Soc.* **2000**, *47*, 449–454.
- [263] Y. Ogata, Y. Takagi, *J. Am. Chem. Soc.* **1958**, *80*, 3591–3595.
- [264] H. Basch, T. Hoz, in *The chemistry of the hydrazo, azo and azoxy groups*, Vol. 2 (Ed.: S. Patai), John Wiley & Sons Ltd., **1997**, pp. 1–795.
- [265] A. M. Makushenko, B. S. Neporent, O. V. Stolbova, *Opt. Spectrosc.* **1971**, *31*, 397–401.
- [266] T. Asano, T. Yano, T. Okada, *J. Am. Chem. Soc.* **1982**, *104*, 4900–4904.
- [267] T. Asano, T. Okada, *J. Org. Chem.* **1984**, *49*, 4387–4391.

- [268] N. J. Bunce, G. Ferguson, C. L. Forber, G. J. Stachnyk, *J. Org. Chem.* **1987**, *52*, 394–398.
- [269] H. Rau, *Angew. Chem.* **1973**, *85*, 248–258; *Angew. Chem. Int. Ed.* **1973**, *12*, 224–235.
- [270] T. Nägele, R. Hoche, W. Zinth, J. Wachtveitl, *Chem. Phys. Lett.* **1997**, *727*, 489–495.
- [271] K. M. Tait, J. A. Parkinson, S. P. Bates, W. J. Ebenezer, A. C. Jones, *J Photoch Photobio A* **2003**, *154*, 179–188.
- [272] G. Binsch, H. Kessler, *Angew. Chem.* **1980**, *92*, 445–463; *Angew. Chem. Int. Ed.* **1980**, *19*, 411–428.
- [273] J. Sandström, *Dynamic NMR Spectroscopy*, Academic Press, London, **1982**.
- [274] H. S. Gutowsky, C. H. Holm, *J. Chem. Phys.* **1956**, *25*, 1228–1234.
- [275] M. Oki, *Applications of Dynamic NMR Spectroscopy to Organic Chemistry*, VCH, Weinheim, **1985**.
- [276] H. Friebolin, *Ein- und zweidimensionale NMR-Spektroskopie – Eine Einführung*, VCH, Weinheim, **1992**.
- [277] G. Binsch, *J. Am. Chem. Soc.* **1969**, *91*, 1304–1309.
- [278] S. Braun, H. O. Kalinowski, S. Berger, *150 and More Basic NMR Experiments*, Wiley–VCH, Weinheim, **1998**.
- [279] A. L. v. Geet, *Anal. Chem.* **1970**, *42*, 679–680.
- [280] D. S. Raiford, C. L. Fisk, E. D. Becker, *Anal. Chem.* **1979**, *51*, 2050–2051.
- [281] R. J. Kurland, M. B. Rubin, W. B. Wise, *J. Chem. Phys.* **1964**, *40*, 2426–2427.
- [282] D. S. Stephenson, G. Binsch, *Quantum Chemistry Program Exchange* **1978**, *11*, 365.
- [283] H. J. Reich, <http://www.chem.wisc.edu/areas/reich/plt/windnmr.htm>.
- [284] J. D. Roberts, B. L. Hawkins, W. Bremser, S. Borcic, *J. Am. Chem. Soc.* **1971**, *93*, 4472–4479.
- [285] F. Vögtle, *Tetrahedron Lett.* **1969**, *10*, 3193–3196.
- [286] M. Oki, G. Yamamoto, *Bull. Chem. Soc. Jpn.* **1971**, *44*, 266–270.
- [287] M. Oki, H. Iwamura, G. Yamamoto, *Bull. Chem. Soc. Jpn.* **1971**, *44*, 262–265.
- [288] G. Bott, L. D. Field, S. Sternhell, *J. Am. Chem. Soc.* **1980**, *102*, 5618–5626.
- [289] L. W. Jelinski, E. F. Kiefer, *J. Am. Chem. Soc.* **1976**, *98*, 281–282.
- [290] W. Walter, T. Fleck, J. Voss, M. Gerwin, *Justus Liebigs Ann. Chem.* **1975**, 275–294.
- [291] R. A. Olsen, L. Liu, N. Ghaderi, A. Johns, M. E. Hatcher, L. J. Mueller, *J. Am. Chem. Soc.* **2003**, *125*, 10125–10132.
- [292] K. Bertsch, J. C. Jochims, *Tetrahedron Lett.* **1977**, *18*, 4379–4382.
- [293] D. L. Hasha, T. Eguchi, J. Jonas, *J. Am. Chem. Soc.* **1982**, *104*, 2290–2296.
- [294] R. H. Baughman, J. L. Bredas, R. R. Chance, E. L. Elsenbaumer, L. W. Shacklette, *Chem. Rev.* **1982**, *82*, 209–222.
- [295] H. Saitoh, K. Saito, Y. Yamamura, H. Matsuyama, K. Kikuchi, M. Iyoda, I. Ikemoto, *Bull. Chem. Soc. Jpn.* **1993**, *66*, 2847–2853.
- [296] H. M. Rietveld, E. N. Maslen, C. J. B. Clews, *Acta Cryst. B* **1970**, *26*, 693–706.
- [297] S. T. Pasco, G. L. Baker, *Synth. Met.* **1997**, *84*, 275–276.
- [298] K. L. Platt, F. Setiabudi, *J. Chem. Soc. Perkin. Trans. I* **1992**, 2005–2009.
- [299] H. O. Wirth, F. U. Herrmann, W. Kern, *Makromol. Chemie* **1964**, *80*, 120–140.
- [300] V. Hensel, A.–D. Schlüter, *Liebigs Ann. Org. Bioorg. Chem.* **1997**, *2*, 303–309.
- [301] G. M. Brown, M. H. Bortner, *Acta Crystallogr.* **1954**, *7*, 139–140.
- [302] R. Cosmo, T. W. Hambley, S. Sternhell, *J. Org. Chem.* **1987**, *52*, 3119–3123.
- [303] H. O. Wirth, K. H. Gönner, W. Kern, *Makromol. Chemie* **1963**, *63*, 53–68.
- [304] T. Zincke, W. Frohneberg, *Chem. Ber.* **1910**, *48*, 840–848.
- [305] P. Cogolli, L. Testaferri, M. Tingoli, M. Tiecco, *J. Org. Chem.* **1979**, *44*, 2636–2642.
- [306] W. Wenner, *J. Org. Chem.* **1952**, *17*, 523–528.
- [307] K. Fuji, T. Yamada, E. Fujita, *Org. Magn. Res.* **1981**, *17*, 250–256.
- [308] Y. Teki, S. Miyamoto, M. Nakatsuji, Y. Miura, *J. Am. Chem. Soc.* **2001**, *123*, 294.

- [309] confer, appendix for details.
- [310] S. Ando, T. Hironaka, H. Kurosu, I. Ando, *Magn. Reson. Chem.* **2000**, *38*, 241–250.
- [311] J. Trotter, *Acta Crystallogr.* **1963**, *16*, 605–608.
- [312] A. Almenningen, O. Bastiansen, L. Fernholz, B. N. Cyvin, S. J. Cyvin, S. Samdal, *J. Mol. Struct.* **1985**, *128*, 59–76.
- [313] H. Kessler, *Angew. Chem.* **1970**, *82*, 237–253; *Angew. Chem. Int. Ed.* **1970**, *9*, 219–235.
- [314] S. Grilli, L. Lunazzi, A. Mazzanti, M. Pinamonti, *Tetrahedron* **2004**, *60*, 4451–4458.
- [315] N. B. Chapman, J. Shorter, *Correlation Analysis in Chemistry*, Plenum Press, New York, **1978**.
- [316] J. Heurich, J. C. Cuevas, W. Wenzel, G. Schön, *Phys. Rev. Lett.* **2002**, *88*, 256803/1–256803/4.
- [317] H. Suzuki, *Electronic Absorption Spectra and Geometry of Organic Molecules*, Academic Press, New York, **1967**.
- [318] F. G. Bordwell, P. J. Boutan, *J. Am. Chem. Soc.* **1956**, *78*, 854–860.
- [319] P. J. Wagner, B. J. Scheve, *J. Am. Chem. Soc.* **1977**, *99*, 2888–2892.
- [320] N. I. Nijegorodov, W. S. Downey, M. B. Danailov, *Spectrochim. Acta Part A* **2000**, *56*, 783–795.
- [321] H. H. Jaffe, M. Orchin, *Theory and Applications of Ultraviolet Spectroscopy*, John Wiley and Sons, New York, **1964**.
- [322] D. Schweitzer, M. W. Haenel, *Chem. Ber.* **1985**, *118*, 163–175.
- [323] J. Lewis, P. R. Raithby, W.-Y. Wong, *J. Organomet. Chem.* **1998**, *556*, 219–228.
- [324] M. d. Leo, Diplom thesis, Fachhochschule München (München), **2002**.
- [325] J. Reichert, PhD thesis, Universität (TH) Karlsruhe (Karlsruhe), **2003**.
- [326] P. S. Damle, A. W. Gosh, S. Datta, *Phys. Rev. B* **2001**, *64*, 201403/1–201403/4.
- [327] D. Krüger, H. Fuchs, R. Rousseau, D. Marx, M. Parrinello, *Phys. Rev. Lett.* **2002**, *89*, 186402/1–186402/4.
- [328] B. Xu, X. Xiao, N. J. Tao, *J. Am. Chem. Soc.* **2003**, *125*, 16164–16165.
- [329] M. H. Hettler, H. Schoeller, W. Wenzel, *Europhys. Lett.* **2002**, *57*, 571–577.
- [330] L. Patrone, S. Palacin, J. P. Bourgoin, *Appl. Surf. Sci.* **2003**, *212–213*, 446–451.
- [331] M. Mayor, M. Büschel, K. M. Fromm, J.-M. Lehn, J. Daub, *Chem. Eur. J.* **2001**, *7*, 1266–1272.
- [332] M. A. Fox, M. D. Wooten, *Langmuir* **1997**, *13*, 7099–7105.
- [333] F. D. Greene, S. L. Misrock, J. R. Wolfe, *J. Am. Chem. Soc.* **1955**, *77*, 3852–3855.
- [334] D. T. Gryko, C. Clausen, K. M. Roth, N. Dontha, D. F. Bocian, W. G. Kuhr, J. S. Lindsey, *J. Org. Chem.* **2000**, *65*, 7345–7355.
- [335] J. M. Tour, A. M. Rawlett, M. Kozaki, Y. Yao, R. C. Jagessar, S. M. Dirk, D. W. Price, M. A. Reed, C.-W. Zhou, J. Chen, W. Wang, I. Campbell, *Chem. Eur. J.* **2001**, *7*, 5118–5134.
- [336] J. Suffert, R. Ziessel, *Tetrahedron Lett.* **1991**, *32*, 757–760.
- [337] B. F. Duerr, Y.-S. Chung, A. W. Czarnik, *J. Org. Chem.* **1988**, *53*, 2120–2122.
- [338] G. R. Desiraju, *Angew. Chem.* **1995**, *107*, 2541–2558; *Angew. Chem. Int. Ed.* **1995**, *34*, 2311–2327.
- [339] I. B. Berlin, *Handbook of fluorescence spectra of aromatic molecules*, Academic Press, New York, **1971**.
- [340] M. Levitus, M. A. Garcia-Garibay, *J. Phys. Chem. A* **2000**, *104*, 8632–8637.
- [341] S. Nakatsuji, K. Matsuda, Y. Uesugi, K. Nakashima, S. Akiyama, W. Fabian, *J. Chem. Soc. Perkin Trans. I* **1992**, 755–758.
- [342] E. Birckner, U.-W. Grummt, A. H. Göller, T. Pautzsch, D. A. M. Egbe, M. Al-Higari, E. Klemm, *J. Phys. Chem. A* **2001**, *105*, 10307–10315.

- [343] P. N. Taylor, A. P. Wylie, J. Huuskonen, H. L. Anderson, *Angew. Chem.* **1998**, *110*, 1033–1037; *Angew. Chem. Int. Ed.* **1998**, *37*, 986–989.
- [344] C. M. Fischer, M. Burghard, S. Roth, K. v. Klitzing, *Appl. Phys. Lett.* **1995**, *66*, 3331–3333.
- [345] T. W. Greene, P. G. M. Wuts, *Protective Groups in Organic Synthesis*, John Wiley & Sons, New York, **1999**.
- [346] M. Topolski, *J. Org. Chem.* **1995**, *60*, 5588–5594.
- [347] R. P. Hsung, J. R. Babcock, C. E. D. Chidsey, L. R. Sita, *Tetrahedron Lett.* **1995**, *36*, 4525–4528.
- [348] D. I. Gittins, D. Bethell, R. J. Nichols, D. J. Schiffrian, *J. Mater. Chem.* **2000**, *10*, 79–83.
- [349] S. W. Watt, C. Dai, A. J. Scott, J. M. Burke, R. L. Thomas, J. C. Collings, C. Viney, W. Clegg, T. B. Marder, *Angew. Chem.* **2004**, *116*, 3123–3125; *Angew. Chem. Int. Ed.* **2004**, *43*, 3061–3063.
- [350] J. J. Wolff, *Angew. Chem.* **1996**, *108*, 2339–2341; *Angew. Chem. Int. Ed.* **1996**, *35*, 2195–2197.
- [351] R. Ochs, PhD thesis, Universität (TH) Karlsruhe (Karlsruhe), **2004**.
- [352] B. L. Feringa, *Molecular Switches*, Wiley–VCH, Weinheim, **2001**.
- [353] S. Sortino, S. Petralia, S. Conoci, S. D. Bella, *J. Mater. Chem.* **2004**, *14*, 811–813.
- [354] S. Wang, R. C. Advincula, *Org. Lett.* **2001**, *3*, 3831–3834.
- [355] C. Amatore, A. Jutand, S. Negri, J.–F. Fauvarque, *J. Organomet. Chem.* **1990**, *390*, 389–398.
- [356] J. F. Corbett, P. F. Holt, *J. Chem. Soc.* **1963**, 2385–2387.
- [357] W. J. Mijs, S. E. Hoekstra, R. M. Ullmann, E. Havinga, *Recl. Trav. Chim. Pays-Bas* **1958**, *77*, 746–752.
- [358] L. Gattermann, *Lieb. Ann. Chem.* **1912**, *393*, 224–230.
- [359] A. Fürstner, K. Nikolakis, *Lieb. Ann. Chem.* **1996**, 2107–2113.
- [360] T. Haack, L. Erdinger, G. Boche, *Mutat. Res.* **2001**, *491*, 183–194.
- [361] M. Janczewski, W. Charmas, *Chem. Abstr.* **1967**, *66*, 37570z.
- [362] H. Niwa, *Chem. Abstr.* **1958**, *52*, 7234e.
- [363] J.–D. Cheng, H. J. Shine, *J. Org. Chem.* **1975**, *40*, 703–710.



## 8 Acknowledgement

I would like to thank Dr. M. Mayor for the interesting topic, fruitful discussions and his support and help, in particular during the last days of writing of this thesis. Furthermore, I would like to thank Prof. Dr. M. Kappes for his support and for the reading of this work as first examiner and Prof. Dr. S. Bräse for reading this work as a co-examiner.

In addition, I am very grateful to the following people (in alphabetical order):

- Dr. Alfred Blaszczyk* for (almost) three years in the same lab, help with synthetic problems, discussions about our work and a short introduction to the (challenging) Polish language (dziękuję bardzo!).
- Dr. Martin Chadim* for interesting discussions about organic chemistry and his never-ending interest in football.
- Dr. Dale Cave* for help with the packing diagrams, discussions about these and his support during the writing of this thesis by telling about his own experience.
- Prof. Dr. L. de Cola* for the organisation of the LIMM-meetings.
- Dr. Patrick Dragut* for helpful discussions about chemistry, in particular azo-chemistry at the LIMM-meetings.
- Matthias Fischer* for help with some of the syntheses, in particular for the molecular rectifier and the “*meta*-“ and “*para*-molecule”, for keeping the organic labs running and a very special thanks for the elemental analyses.
- Dr. Keir Foster* for the organisation of the INT football matches.
- Dr. Christian Grave* for an introduction to the technique of the mercury drop electrode during the LIMM-meetings.
- Dr. Carsten von Hänisch* for the crystal structure analyses presented in this work and special advices about crystal structure analysis.
- Max Köntopp* for trying to introduce to me concepts of theoretical physics and for his three(!) Christmas parties every year.
- Dr. Aitor Landa* for the weekends in the organic chemistry labs and the Champions League.

---

<i>Dr. Brenda Long</i>	for discussions about the switching behaviour of the azo-compounds during LIMM-meetings, the UV/Vis spectra of the azo-compound and support during the writing of this thesis.
<i>Michelle di Leo</i>	for the measurements of the oligophenylenes, discussions about these and a “tour” of the experimental physics labs.
<i>Dr. Rolf Ochs</i>	for the measurements of the single-molecule rectifier.
<i>Prof. Dr. M. Rampi</i>	for discussions about the mercury drop electrode and the structure of the required azo-compound during LIMM-meetings.
<i>Dr. Joachim Reichert</i>	for the measurements of the “meta-“ and “para-molecule”, interesting discussions about molecular electronics and his ambitious efforts to explain the <i>Kondo</i> -effect to three organic chemists in the middle of the night.
<i>Dr. Christophe Stroh</i>	for interesting discussions about organic chemistry and his sympathy during the writing of this thesis.
<i>Dr. Lijin Shu</i>	for interesting discussions about chemistry and keeping calm in every situation of life.
<i>Prof. Dr. F. Vögtle</i>	for discussions about azo-chemistry and sulfoxide-chemistry at the LIMM-meetings and for his kind support.
<i>Dr. Heiko Weber</i>	for discussions about electron transport through molecular junctions and his patience when explaining physical models to an organic chemist.
<i>Dr. Olaf Wollersheim</i>	for help in all organisational problems during my time at the INT, in particular money issues.
<i>Jan Würfel</i>	for discussions about the MCB and electron transport models at (almost) any time of the day and for the nice time in Mühlburg.

At the end, I would like to thank all my friends in Karlsruhe and elsewhere for being how they are and what they are and for a nice, enjoyable time outside the chemistry lab.

Last but not least,

Danke ich meinen Eltern, die mir das Studium ermöglicht haben und mich in allen Entscheidungen auch finanziell unterstützt haben, sowie Susan Mau, die mich den manchmal frustrierenden Laboralltag hat vergessen lassen und mich immer wieder von neuem motiviert hat. Ein Dank auch für das Korrekturlesen von Teilen dieser Arbeit.

To err is human, if I have forgotten someone in this list, I would like to apologise for it.

## 9 Appendix

### Crystal Structure Data of 4,4'-Bis(acetylsulfanyl)-2,2'-dimethyl-biphenyl O2

Empirical formula	$C_{18}H_{18}O_2S_2$	
Formula weight	330.44	
Temperature	180(2) K	
Wavelength	0.71073 Å	
Crystal system	orthorhombic	
Space group	<i>Pbca</i>	
Unit cell dimensions	$a = 18.257(4)$ Å	alpha = 90 deg.
	$b = 9.826(2)$ Å	beta = 90 deg.
	$c = 18.866(4)$ Å	gamma = 90 deg.
Volume	$3384.4(12)$ Å <sup>3</sup>	
Z	8	
Density (calculated)	1.297 Mg/m <sup>3</sup>	
Absorption coefficient	0.318 mm <sup>-1</sup>	
F(000)	1392	
Theta range for data collection	2.43 to 25.95 deg.	
Index ranges	-22<=h<=16, -11<=k<=12, -20<=l<=23	
Reflections collected	10686	
Independent reflections	3254 [ $R_{int} = 0.0531$ ]	
Observed reflections	2405	
[I>2sigma(I)]		
Refinement method	Full-matrix least-squares on F <sup>2</sup>	
Data/restraints/parameters	3254/0/199	
Goodness-of-fit on F <sup>2</sup>	1.115	
Final R indices [I>2sigma(I)]	$R_1 = 0.0490, wR_2 = 0.1466$	
R indices (all data)	$R_1 = 0.0651, wR_2 = 0.1588$	
Largest diff. peak and hole	0.509 and -0.294 e. Å <sup>-3</sup>	

**Crystal Structure Data of 4,4''-Bis(acetylsulfanyl)-2,2',5',2''-tetramethyl-[1,1';4',1'']-terphenyl O3**

Empirical formula	C <sub>26</sub> H <sub>26</sub> O <sub>2</sub> S <sub>2</sub>
Formula weight	434.59
Temperature	200(2) K
Wavelength	0.71073 Å
Crystal system	monoclinic
Space group	P2 <sub>1</sub> /c
Unit cell dimensions	a = 6.3197(13) Å      alpha = 90 deg. b = 14.774(3) Å      beta = 98.35(3) deg. c = 12.466(3) Å      gamma = 90 deg.
Volume	1151.6(4) Å <sup>3</sup>
Z	2
Density (calculated)	1.253 Mg/m <sup>3</sup>
Absorption coefficient	0.251 mm <sup>-1</sup>
F(000)	460
Theta range for data collection	2.15 to 25.96 deg.
Index ranges	-6<=h<=7, -18<=k<=18, -15<=l<=12
Reflections collected	5326
Independent reflections	2115 [R <sub>int</sub> = 0.0608]
Observed reflections	1827
[I>2sigma(I)]	
Refinement method	Full-matrix least-squares on F <sup>2</sup>
Data/restraints/parameters	2115/0/136
Goodness-of-fit on F <sup>2</sup>	1.071
Final R indices [I>2sigma(I)]	R <sub>1</sub> = 0.0595, wR <sub>2</sub> = 0.1794
R indices (all data)	R <sub>1</sub> = 0.0647, wR <sub>2</sub> = 0.1849
Largest diff. peak and hole	0.370 and -0.451 e.Å <sup>-3</sup>

**Crystal Structure Data of 9,10-Bis-(4-acetylsulfanyl-phenylethynyl)-anthracene A1**

Empirical formula	C <sub>34</sub> H <sub>22</sub> O <sub>2</sub> S <sub>2</sub>
Formula weight	526.64

---

Temperature	200(2) K
Wavelength	0.71073 Å
Crystal system	triclinic
Space group	$P\bar{1}$
Unit cell dimensions	$a = 5.1023(10)$ Å      alpha = 98.03(3) deg.
	$b = 9.6642(19)$ Å      beta = 91.47(3) deg.
	$c = 14.065(3)$ Å      gamma = 101.70(3) deg.
Volume	671.4(2) Å <sup>3</sup>
Z	1
Density (calculated)	1.302 Mg/m <sup>3</sup>
Absorption coefficient	0.228 mm <sup>-1</sup>
F(000)	274
Theta range for data collection	1.46 to 25.95 deg.
Index ranges	-5<=h<=6, -11<=k<=11, -17<=l<=17
Reflections collected	4784
Independent reflections	2439 [ $R_{int} = 0.0546$ ]
Observed reflections	1860
[I>2sigma(I)]	
Refinement method	Full-matrix least-squares on F <sup>2</sup>
Data/restraints/parameters	2439/0/172
Goodness-of-fit on F <sup>2</sup>	1.043
Final R indices [I>2sigma(I)]	$R_1 = 0.0572$ , $wR_2 = 0.1612$
R indices (all data)	$R_1 = 0.0691$ , $wR_2 = 0.1696$
Largest diff. peak and hole	0.242 and -0.380 e. Å <sup>-3</sup>

### Crystal Structure Data of 9,10-Bis-(3-acetylsulfanyl-phenylethynyl)-anthracene A2

Empirical formula	C <sub>34</sub> H <sub>22</sub> O <sub>2</sub> S <sub>2</sub>
Formula weight	526.64
Temperature	200(2) K
Wavelength	0.71073 Å
Crystal system	triclinic
Space group	$P\bar{1}$
Unit cell dimensions	$a = 6.2973(13)$ Å      alpha = 85.83(3) deg.

---

	b = 9.0895(18) Å	beta = 89.55(3) deg.
	c = 11.085(2) Å	gamma = 79.36(3) deg.
Volume	621.9(2) Å <sup>3</sup>	
Z	1	
Density (calculated)	1.406 Mg/m <sup>3</sup>	
Absorption coefficient	0.247 mm <sup>-1</sup>	
F(000)	274	
Theta range for data collection	1.84 to 22.50 deg.	
Index ranges	-6<=h<=6, -9<=k<=9, -11<=l<=11	
Reflections collected	2929	
Independent reflections	1542 [R <sub>int</sub> = 0.0733]	
Observed reflections	1827	
[I>2sigma(I)]		
Refinement method	Full-matrix least-squares on F <sup>2</sup>	
Data/restraints/parameters	1542/0/172	
Goodness-of-fit on F <sup>2</sup>	1.057	
Final R indices [I>2sigma(I)]	R <sub>1</sub> = 0.0602, wR <sub>2</sub> = 0.1752	
R indices (all data)	R <sub>1</sub> = 0.0664, wR <sub>2</sub> = 0.1806	
Largest diff. peak and hole	0.305 and -0.267 e. Å <sup>-3</sup>	

**Crystal Structure Data of 9,10-Bis-(4-*tert*.-butylsulfanyl-phenylethynyl)-anthracene****A12**

Empirical formula	C <sub>38</sub> H <sub>34</sub> S <sub>2</sub>	
Formula weight	554.77	
Temperature	200(2) K	
Wavelength	0.71073 Å	
Crystal system	monoclinic	
Space group	C2/c	
Unit cell dimensions	a = 26.918(5) Å	alpha = 90 deg.
	b = 5.9472(12) Å	beta = 96.88(3) deg.
	c = 37.799(8) Å	gamma = 90 deg.
Volume	6007(2) Å <sup>3</sup>	
Z	8	

---

Calculated density	1.227 Mg/m <sup>3</sup>
Absorption coefficient	0.203 mm <sup>-1</sup>
F(000)	2352
Theta range for data collection	2.17 to 23.94 deg.
Limiting indices	-19<=h<=30, -6<=k<=6, -42<=l<=43
Reflections collected/unique	9082/4476 [ $R_{\text{int}} = 0.0661$ ]
Refinement method	Full-matrix least-squares on F <sup>2</sup>
Data/restraints/parameters	4476/0/361
Goodness-of-fit on F <sup>2</sup>	0.928
Final R indices [I>2sigma(I)]	$R_1 = 0.0540$ , $wR_2 = 0.1334$
R indices (all data)	$R_1 = 0.0739$ , $wR_2 = 0.1438$
Largest diff. peak and hole	0.262 and -0.432 e. Å <sup>-3</sup>

### Crystal Structure Data of 4,4'-Bis-(4-acetylsulfanyl-phenylethynyl)-2,2'-dimethyl-biphenyl R3

Empirical formula	C <sub>34</sub> H <sub>26</sub> O <sub>2</sub> S <sub>2</sub>		
Formula weight	530.67		
Temperature	200(2) K		
Wavelength	0.71073 Å		
Crystal system	monoclinic		
Space group	<i>P</i> 2 <sub>1</sub> /c		
Unit cell dimensions	a = 17.632(4) Å	alpha = 90 deg.	
	b = 11.770(2) Å	beta = 98.05(3) deg.	
	c = 13.711(3) Å	gamma = 90 deg.	
Volume	2817.5(10) Å <sup>3</sup>		
Z	4		
Density (calculated)	1.251 Mg/m <sup>3</sup>		
Absorption coefficient	0.218 mm <sup>-1</sup>		
F(000)	1112		
Theta range for data collection	2.09 to 26.09 deg.		
Index ranges	-19<=h<=21, -11<=k<=14, -16<=l<=16		
Reflections collected	9695		
Independent reflections	5235 [ $R_{\text{int}} = 0.0374$ ]		

---

Observed reflections	4027
[I>2sigma(I)]	
Refinement method	Full-matrix least-squares on $F^2$
Data/restraints/parameters	5235/0/343
Goodness-of-fit on $F^2$	1.100
Final R indices [I>2sigma(I)]	$R_1 = 0.0602, wR_2 = 0.1739$
R indices (all data)	$R_1 = 0.0742, wR_2 = 0.1863$
Largest diff. peak and hole	0.605 and -0.518 e. $\text{\AA}^{-3}$

**Crystal Structure Data of 2,2'-Dimethyl-4,4'-bis-(2,3,5,6-tetrafluoro-4-methoxymethylsulfanyl-phenylethyanyl)-biphenyl R8**

Empirical formula	$\text{C}_{34}\text{H}_{22}\text{F}_8\text{O}_2\text{S}_2$		
Formula weight	678.64		
Temperature	200(2) K		
Wavelength	0.71073 $\text{\AA}$		
Crystal system	monoclinic		
Space group	$P2_1/n$		
Unit cell dimensions	$a = 9.2374(18) \text{\AA}$	$\alpha = 90$ deg.	
	$b = 20.948(4) \text{\AA}$	$\beta = 100.13(3)$ deg.	
	$c = 16.456(3) \text{\AA}$	$\gamma = 90$ deg.	
Volume	$3134.8(11) \text{\AA}^3$		
Z	4		
Density (calculated)	1.438 Mg/m <sup>3</sup>		
Absorption coefficient	$0.248 \text{ mm}^{-1}$		
F(000)	1384		
Theta range for data collection	1.59 to 26.17 deg.		
Index ranges	$-11 \leq h \leq 10, -25 \leq k \leq 25, -20 \leq l \leq 20$		
Reflections collected	22301		
Independent reflections	6194 [ $R_{\text{int}} = 0.0350$ ]		
Observed reflections	4434		
[I>2sigma(I)]			
Refinement method	Full-matrix least-squares on $F^2$		
Data/restraints/parameters	6194/0/415		

---

Goodness-of-fit on $F^2$	1.042
Final R indices [ $I > 2\sigma(I)$ ]	$R_1 = 0.0440, wR_2 = 0.1257$
R indices (all data)	$R_1 = 0.0611, wR_2 = 0.1332$
Largest diff. peak and hole	0.356 and -0.388 e. $\text{\AA}^{-3}$

**Crystal Structure Data of 4'-(4-Acetylsulfanyl-phenylethynyl)-2,2'-dimethyl-4-(2,3,5,6-tetrafluoro-4-methoxymethylsulfanyl-phenylethynyl)-biphenyl R10**

Empirical formula	$C_{34}H_{24}F_4O_2S_2$	
Formula weight	604.65	
Temperature	200(2) K	
Wavelength	0.71073 $\text{\AA}$	
Crystal system	triclinic	
Space group	$P\bar{1}$	
Unit cell dimensions	$a = 5.2098(10) \text{\AA}$	alpha = 96.58(3) deg.
	$b = 12.387(3) \text{\AA}$	beta = 90.77(3) deg.
	$c = 23.095(5) \text{\AA}$	gamma = 97.75(3) deg.
Volume	1466.4(5) $\text{\AA}^3$	
Z	2	
Density (calculated)	1.369 Mg/m <sup>3</sup>	
Absorption coefficient	0.237 mm <sup>-1</sup>	
F(000)	624	
Theta range for data collection	1.78 to 26.08 deg.	
Index ranges	$-5 \leq h \leq 6, -10 \leq k \leq 15, -28 \leq l \leq 28$	
Reflections collected	6316	
Independent reflections	4591 [ $R_{\text{int}} = 0.0301$ ]	
Observed reflections	3232	
[ $I > 2\sigma(I)$ ]		
Refinement method	Full-matrix least-squares on $F^2$	
Data/restraints/parameters	4591/0/379	
Goodness-of-fit on $F^2$	1.067	
Final R indices [ $I > 2\sigma(I)$ ]	$R_1 = 0.0567, wR_2 = 0.1616$	
R indices (all data)	$R_1 = 0.0747, wR_2 = 0.1737$	
Largest diff. peak and hole	0.238 and -0.252 e. $\text{\AA}^{-3}$	

**Crystal Structure Data of Biphenyl-4-yl-(4'-methanesulfinyl-biphenyl-4-yl)-diazene**  
**S15**

Empirical formula	C <sub>25</sub> H <sub>20</sub> N <sub>2</sub> OS
Formula weight	396.49
Temperature	200(2) K
Wavelength	0.71073 Å
Crystal system	orthorhombic
Space group	<i>Pna2</i> <sub>1</sub>
Unit cell dimensions	a = 8.1562(16) Å alpha = 90 deg. b = 5.5776(11) Å beta = 90 deg. c = 43.966(9) Å gamma = 90 deg.
Volume	2000.1(7) Å <sup>3</sup>
Z	4
Density (calculated)	1.317 Mg/m <sup>3</sup>
Absorption coefficient	0.181 mm <sup>-1</sup>
F(000)	832
Theta range for data collection	3.91 to 25.91 deg.
Index ranges	-9<=h<=10, -5<=k<=6, -53<=l<=53
Reflections collected	6869
Independent reflections	3603 [R <sub>int</sub> = 0.0519]
Observed reflections	3221
[I>2sigma(I)]	
Refinement method	Full-matrix least-squares on F <sup>2</sup>
Data/restraints/parameters	3603/1/263
Goodness-of-fit on F <sup>2</sup>	1.074
Final R indices [I>2sigma(I)]	R <sub>1</sub> = 0.0431, wR <sub>2</sub> = 0.1195
R indices (all data)	R <sub>1</sub> = 0.0473, wR <sub>2</sub> = 0.1218
Absolute structure parameter	0.42(9) (Flack parameter)
Largest diff. peak and hole	0.192 and -0.254 e. Å <sup>-3</sup>

## Publications

M. Mayor, H. B. Weber, M. Elbing, J. Reichert, D. Beckmann, R. Ochs, M. Fischer, C. von Hänisch, M. Di Leo

“*Single molecules in electronic circuits – Structure property correlations*”

*Abs. Pap. Amer. Chem. Soc.* **2003**, 226: U423-U423

M. Mayor, H. B. Weber, J. Reichert, M. Elbing, C. von Hänisch, D. Beckmann, M. Fischer

“*Electric Current through a Molecular Rod – Relevance of the Position of the Anchor Group*”

*Angew. Chem. Int. Ed.* **2003**, 42, 5834 – 5838; *Angew. Chem.* **2003**, 115, 6014 – 6018.

A. Blaszczyk, M. Elbing, M. Mayor

“*Bromine catalyzed conversion of S-tert-butyl groups into versatile and, for self-assembly processes accessible, acetyl-protected thiols*”

*Org. Biomol. Chem.* **2004**, 2, 2722 – 2724

## Talks

KOPO’03 – Von der Synthese zur elektronischen Funktion, Blaubeuren, Germany, 02. – 05. November 2003

“*Single Oligophenylene Rods – Synthesis and Current-Voltage Characteristics*”

## Poster Presentations

7<sup>th</sup> European Conference on Molecular Electronics, Avignon, France, 10. – 14. September 2003

“*Electric current through single oligophenylene rods*”

5<sup>th</sup> International Wilhelm and Else Heraeus Summerschool, Wittenberg, Germany, 02. – 13. August 2004

“*A Single-Molecule Rectifier*”